A STUDY OF THE COMPRESSIVE STRENGTH AND BEHAVIOUR OF CONCRETE BLOCKWORK MASONRY WITH SPECIAL REFERENCE TO REINFORCED COLUMNS

BY

Fouad M. Khalaf

Thesis submitted for the
Degree of
Doctor of Philosophy

Department of Civil Engineering and Building Science
University of Edinburgh

April 1991

PREFACE

This thesis is the result of research work undertaken in the Department of Civil Engineering and Building Science, University of Edinburgh, for the Degree of Doctor of Philosophy.

I declare that the work in this thesis is the result of original research which has been, unless otherwise stated, carried out by myself, and have not been submitted for a higher degree to any other University or Institution.

During the period of research seven papers have been published. The titles and place of publication are as follows:

1. "Concrete Blocks Compressed Parallel to Bed Face: A Theoretical Study," Masonry Inter., Vol. 1, No. 2, 1987, pp. 64-70.

2. "The Performance of Concrete Blocks Loaded Parallel to the Bed Face," Masonry Inter., Vol. 2, No. 1, 1988, pp. 20-24.

3. "An Investigation Into the Capacity and Behaviour of Concrete Block Specimens Loaded Parallel to the Bed Face," Proc. of the 8th Inter. Brick/Block Masonry Conf. (IBMAC), Ireland, 1988, pp. 752-763.

4. "Concrete Block Masonry Prisms Compressed Normal and Parallel to the Bed Face," Proc. of the 5th North Amer. Masonry Conf., University of Illinois at Urbana-Champaign, 1990, pp. 595-614.

5. "Compressive Strength of Concrete Block Masonry Prisms Tested Concentrically and Eccentrically Normal and Parallel to the Bed Face," Proc. of the 3rd Inter. Seminar on Struc. Masonry for the Developing Countries, Mauritius, 1990, pp. 123-135.

6. "Effect of Bed-Face Preparation in Compressive Testing of Masonry Units," Proc. of the 2nd Inter. Masonry Conf., British Masonry Society Proc. No. 4, 1990, pp. 129-130.

7. "Behaviour of Concrete Blockwork Prisms Compressed Parallel to the Unit Bed Face," Presented at the Inter. Symp. on Computer Methods in Struc. Masonry, Swansea, 3-5 April 1991.

Also the following papers are being prepared and will be submitted for publication in referred journals. The titles are as follows:

1. "Concrete Block Masonry Prisms Compressed Parallel to the Unit Bed Face," (To be published in the Structural Engineers).

2. "Concrete Block Masonry Prisms Compressed Normal to the Bed Face," (To be published in the ACI Journal).

3. "Behaviour of Concrete Blockwork Prisms Compressed Normal to the Bed Face," (To be published in the ACI Journal).

4. "The Strength of Blockwork Prisms Compressed Parallel to the Bed Face with Reference to the Method of Construction," (To be published in the ACI Journal).

5. "Mechanical Properties of Materials Used in Blockwork Construction," (To be published in the Masonry International).

6. "Factors Affecting Compressive Strength of Blockwork Masonry," (To be published in the Masonry International).

7. "Finite Element Analysis of Blockwork Masonry Prisms," (To be published in the Masonry International).

8. "The Ultimate Strength and Behaviour of Blockwork Masonry Columns Subjected to Axial Load," (To be published in the Masonry International).

Edinburgh, April 1991

F. M. Khalaf

ABSTRACT

In recent years great advances have taken place in the use of masonry in building construction. Where as the number of storeys has increased substantially, the thickness of the wall has decreased.

An important factor in the development of masonry structures was the introduction of the concrete block in the early 1900's. This added a new dimension to the construction and design of masonry structures. Greater flexibility was provided by the use of hollow, filled and solid blocks utilising different colours, shapes and texture for interior and exterior masonry elements. The use of hollow blocks provided the advantage of using reinforced concrete filled masonry elements without the need for formwork.

Reinforced blockwork masonry consists of four component materials, namely the concrete block, mortar, concrete infill and reinforcement. These four materials give masonry non-homogeneous properties compared to those of concrete. Differences in the mechanical properties of the four materials, the wide variety of block units available of different shapes and geometry, and the direction in which the masonry element is loaded all have an affect on the strength and behaviour of the masonry structure.

This present investigation consists of experimental and theoretical studies of the effects of masonry non-homogeneity and of using different concrete infill and mortar types on the compressive strength and behaviour of blockwork masonry prisms compressed axially in two directions, normal and parallel to the bed face. Methods are suggested to determine the ultimate compressive

strength of blockwork masonry f'_m. Finally the study investigates the effect of using different percentages of lateral and vertical reinforcement on the ultimate strength and behaviour of reinforced concrete blockwork masonry columns. A new method of predicting the ultimate strength of reinforced concrete blockwork masonry columns subjected to axial compression is proposed.

ACKNOWLEDGEMENTS

The author wishes to thank Professor A. W. Hendry and Dr. D. R. Fairbairn for their valuable advice, encouragement, understanding and assistance during the experimental and theoretical parts of this investigation and in preparing this thesis.

The author wish to express his appreciation and thanks to FORTICRETE CONCRETE MASONRY Ltd, Bootle, Merseyside, for supplying the materials for the experimental part of this investigation.

Thanks also to my wife, daughter, family and all my friends for their encouragement and support especially to Khaled, Nabeel, Sabah and Martin.

TABLE OF CONTENTS

LIST OF FIGURES

Chapter 3

LIST OF TABLES

NOTATION

The notation presented herein are only for those used in this investigation. The notation for any other previous work reported in this thesis are given in the text.

A_c Cross-sectional area of concrete infill, mm^2

A_g Gross cross-sectional area of specimen, mm^2

A_n Net cross-sectional area of specimen, mm^2

A_s Area of vertical reinforcement, mm^2

E_{bs} Secant modulus of elasticity of concrete block, for three unfilled half-blocks specimen, as derived experimentally in chapter 3 (see Table 3.7), N/mm^2

E_{cs} Secant modulus of elasticity of concrete, for three steel moulded cubes specimen, as derived experimentally in chapter 3 (see Table 3.7), N/mm^2

E_{js} Secant modulus of elasticity of mortar joint, as derived experimentally in chapter 3 (see Table 3.7), N/mm^2

E_m Short term static modulus of elasticity of masonry, N/mm^2

E_{mrs} Secant modulus of elasticity of mortar, for three steel moulded cubes specimen, as derived experimentally in chapter 3 (see Table 3.7), N/mm^2

f_b Cube compressive strength of block material, N/mm^2

f_{bb} Tensile bond strength between block and concrete, N/mm^2

f_{bnf} Compressive strength of filled full-block compressed normal to bed face, N/mm^2

f_{bpf} Compressive strength of filled full-block compressed parallel to bed face, N/mm^2

f_{bt} Tensile strength of filled concrete block, N/mm^2

f_{bv} Shear bond strength between block and concrete, N/mm^2

f_c Cube compressive strength of concrete, N/mm^2

f_{ct} Tensile strength of concrete, N/mm^2

f_{cv}	Shear strength of concrete, N/mm^2
f_{hnf}	Compressive strength of filled half-block, compressed normal to the bed face, N/mm^2
f_k	Characteristic compressive strength of masonry, N/mm^2
f_{mr}	Cube compressive strength of mortar, N/mm^2
f'_m	Ultimate compressive strength of blockwork masonry, N/mm^2
f_s	Stress in the reinforcement, N/mm^2
f_y	Yield strength of reinforcement, N/mm^2
h	Height of specimen, mm
h_b	Height of block, mm
h_j	Height of mortar joint, mm
l	Length of specimen, mm
P_u	Ultimate load of blockwork masonry column, KN
r	Correlation coefficient
t	Thickness of specimen, mm
α	E_{js}/E_{mrs}
Γ	The contribution of concrete infill to the modulus of elasticity of blockwork masonry
μ_b	Poisson's ratio of block
μ_c	Poisson's ratio of concrete
ϕ	Diameter of reinforcement, mm
ρ	A_s/A_g percent
δ	$\frac{h_b}{h_b + h_j}$

CHAPTER 1

INTRODUCTION

Masonry has been used as a load bearing material for centuries. Many of the ancient masonry structures are still standing today. The craftsmanship and ingenuity of the ancient Egyptians, for example, as demonstrated in the pyramids, were truly wonders in themselves. At about the same time that the Egyptians were constructing their monuments in stone, fired bricks were being used in mesopotamia with a bonding agent of asphalt. By the sixth century B.C., brick construction in Babylon was well-developed. The Tower of Babel had walls eighty feet high and wide enough at the top to accommodate chariot races.

Through the Minoan, Mycenaean, Greek and Roman periods, further developments in masonry are observed. The Romans, in particular, elaborated on the use of the arch and produced such impressive structures as the Coliseum and the Aqueducts. Their use of mortar and concrete was unsurpassed until the nineteenth century.

Concrete has a long history. It has been used since ancient times and was known to the Ancient Egyptians and even earlier civilizations. The first all-concrete house was built in 1835 in Kent. The first concrete blocks were made in the United Kingdom in about 1850 by JOSEPH GIBBS[1]. The blocks were hollow with moulded faces which imitated the dressed stone of that period. It was not until about 1910, coinciding with the significant growth in the production of cement, that the concrete block industry became properly established. Major growth took place between 1918 and 1939 with the establishment of many small block manufacturers throughout the United Kingdom. Many concrete block houses were built entirely of concrete and

were the first in this country to be built in metric units.

After the Second World War, the demand for concrete blocks began to increase and both solid and hollow blocks became widely accepted for all purposes. This, in turn, brought about the introduction of autoclaved aerated blocks which, at that time, were probably appreciated more for their operational advantages on site than for their thermal insulation properties. Concurrent with developments in the United Kingdom, many were also taking place in the United States of America, and it is here that the evolution of high quality facing concrete masonry, and machines associated with its production, can be discovered. The seismic problems, associated with certain areas of the country, having also fostered the development of reinforced masonry[1].

In recent years great advances have taken place in the use of masonry in building construction, where the number of storeys has increased substantially while the thickness of the wall has similarly decreased[1,2,3,4,5,6,7,8,9].

The use of concrete blocks added a new dimension to the construction and design of masonry structures with the flexibility provided by the use of hollow, filled and solid blocks with different colour, shapes and texture for the interior and exterior masonry elements[1,10]. Hollow blocks provided the advantage of using reinforced concrete filled masonry elements without the need for a frame. The presence of reinforcement increased the axial and eccentric load bearing strength of the masonry elements and also allowed the use of smaller cross-sections as an alternative to the thicker unreinforced elements[11,12]. This method of constructing blockwork masonry has been designed largely through the adaptation of early theories for the design of reinforced concrete.

Reinforced blockwork masonry consists of four component materials, namely the concrete block, mortar, concrete infill and reinforcement. These four materials give masonry non-homogeneous properties compared to those for concrete. The differences in the mechanical properties of the four materials, the wide variety of block units available, of different shapes and geometry, and the direction in which the masonry element is loaded will all effect the strength and behaviour of the masonry structure.

Since masonry is used primarily in wall construction, a considerable amount of research has been directed toward the behaviour of blockwork masonry walls[13,14,15,16,17]. However, the "Masonry Bibliography 1900-1977"[18] reveals that little published work exists on blockwork masonry columns. Most current codes[19,20], handbooks[3] and books[2,4,6,7] advocate the use of a working stress design which is based on elastic theory and no guide is given to ultimate strength design principles. To the knowledge of the author, the British Code of Practice, BS 5628: Parts 1, 2 and 3[21] and the Australian Masonry Code SAA 3700[22], are the only standards which adopted the use of limit state philosophy. The use of this philosophy enables the degree of risk to be varied by the choice of different partial safety factors.

Reinforced concrete blockwork masonry columns can be used as a structural elements in buildings where concrete masonry is used. Blockwork columns can be constructed from special, large blocks, similar to the pilaster block, U-block and standard hollow block shown in Figs 1.1 (i, ii, iii) respectively as separate structural elements, or may be incorporated into a blockwork masonry wall as shown in Figs 1.1 (iv, v).

On the design of masonry columns subjected to axial loading, the British Standard, BS 5628: Part 2: 1985,

states that reinforced masonry walls or columns, subjected to axial loading or vertical loading having a resultant eccentricity not exceeding 0.05 times the thickness of the member in the direction of the eccentricity, may be designed without taking the reinforcement into account. It is well established in the ultimate design theories for reinforced concrete columns, however, that the reinforcement contributes to the ultimate strength of the column. There is a clear need therefore for further study of the behaviour and method of design of blockwork masonry columns.

Recently FOSTER[23] showed that, where blockwork columns could be integrated into the design of blockwork buildings incorporating walls that were adequate to sustain wind loading when propped by floors, (probably, but not necessarily, of in-situ concrete) the problem of differential vertical movements of dissimilar materials was greatly reduced or eliminated.

The study presented herein provides additional information to confirm, extend, or adapt existing theory and procedures. The main objectives and scope of this study are:

1. To review our current understanding of the behaviour of blockwork masonry prisms compressed axially in two directions normal and parallel to the unit bed face with review of the methods used in determining the ultimate compressive strength of blockwork masonry f'_m.

2. To review our current understanding of the behaviour of brickwork and blockwork reinforced masonry columns and the method used to determine their ultimate strength.

3. To determine the mechanical properties of the materials used in blockwork masonry construction and suggests the mathematical expressions to determine their values.

4. To study experimentally and theoretically the differences in the compressive strength and behaviour of blockwork masonry prisms compressed axially normal and parallel to the unit bed face with the suggestion of the best expressions to determine f'_m.

5. To examine the effect of using different mortar types and concrete infill strengths on the compressive strength and behaviour of blockwork masonry prisms compressed axially normal and parallel to the unit bed face.

6. To study experimentally and theoretically the effect of the following factors: prism height-to-thickness ratio (h/t), aspect ratio (prism length-to-thickness) (l/t), mortar thickness, shrinkage in 28 days and bond between block and concrete infill affecting the compressive strength and behaviour of blockwork masonry prisms, compressed axially normal to the unit bed face.

7. To determine the effect of the changing the percentage of lateral ties and vertical bars on the strength and behaviour of axially loaded reinforced blockwork masonry columns.

8. To develop a new method of predicting the ultimate strength of reinforced blockwork masonry columns subjected to axial load.

The structure layout of the thesis can be summarised as follows:

CHAPTER 1: Introduction, scope and aim of the present investigation.

CHAPTER 2: Literature review of previous investigations of the compressive strength of masonry, brickwork masonry columns and blockwork masonry columns.

CHAPTER 3: An experimental determination of the mechanical properties of the materials used in blockwork masonry construction.

CHAPTER 4: An experimental and theoretical investigations of the compressive strength and behaviour of blockwork masonry prisms compressed parallel to the unit bed face.

CHAPTER 5: An experimental and theoretical investigations of the compressive strength and behaviour of blockwork masonry prisms compressed normal to the unit bed face.

CHAPTER 6: A study of the factors, other than the mortar types and concrete strengths, affecting the compressive strength and behaviour of blockwork masonry prisms.

CHAPTER 7: An experimental investigation of reinforced blockwork masonry columns with proposals for design rules.

CHAPTER 8: A general summary and conclusion with recommendations for further research.

The units used in this project are SI units of Newton (N) and millimetre (mm). The results of several research papers which had been presented in Imperial units were converted to SI units.

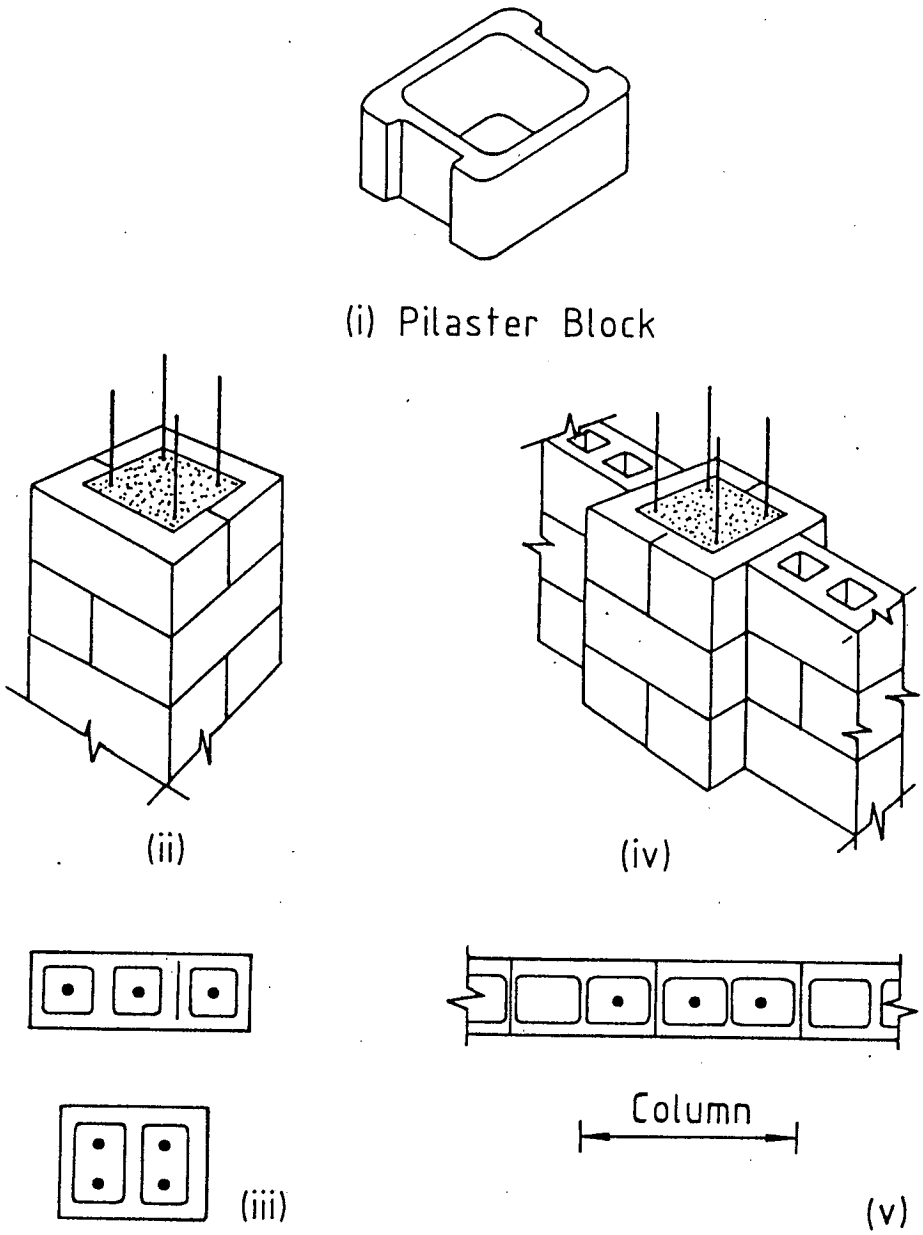

Fig. 1.1 - Various methods of constructing blockwork masonry columns.

CHAPTER 2

LITERATURE REVIEW

2.1 INTRODUCTION

This chapter provides a review of previous work on blockwork masonry prisms compressed normal and parallel to the unit bed face, as a standard test for determining the ultimate compressive strength of blockwork masonry, f'_m. The review also includes studies of the ultimate strength and behaviour of brickwork and blockwork masonry columns.

2.2 ULTIMATE COMPRESSIVE STRENGTH OF BLOCKWORK MASONRY, f'_m

The ultimate compressive strength of blockwork masonry f'_m, is according to North American Codes and Standards[19,20], found from tables relating unit strength and mortar types to masonry strength or, alternatively, by testing stack-bonded masonry prisms[24,25], with a prism height-to-thickness ratio (h/t) between 2.0 and 5.0, made of the same materials used in actual construction, and compressed normal to the bed face. The British Code of Practice BS 5628: Part 2: 1985[21] gives a procedure for determining the strength of brick masonry by testing prisms built with different brick orientations, and in some cases with concrete infill, but does not provide for corresponding tests on concrete filled hollow blockwork. For this case it is suggested that the filled block may, under certain conditions, be treated as a solid block and the masonry strength derived from the tables and graphs relate to mortar type.

Without doubt many studies have been carried out to determine the ultimate compressive strength of blockwork

masonry, f'_m. The present review will deal only with investigations carried out recently and with special reference to the differences in f'_m found by testing blockwork masonry prisms normal and parallel to the unit bed face.

ROBERTS in 1973[26], reported results for the indicated compressive strength of concrete blocks obtained from different test procedures. Six forms of specimen were considered in the investigation, using two types of prism, each two blocks high with 10 mm mortar joint between, one mortar capped and the other board capped. Other specimens tested consisted of a single block, but varied as follows:

1. Mortar-capped blocks tested wet.

2. Mortar-capped blocks tested dry.

3. Board-capped blocks tested wet.

4. Board-capped blocks tested dry.

In addition to these small specimens, wall panels were tested to relate the results of test on the small specimens to the performance of concrete blockwork walls. The wall panels, each 12 or 13 courses high by 4.5 blocks wide, were subjected to axial loading under flat-end conditions.

The aim of the investigation was, first to compare various methods of capping, and second to examine the relationship between the strength of a concrete block wall and the strength of the control specimen.

The blocks used in the investigation were of different types (solid, cellular and hollow). The blocks were supplied by seven manufacturers with different types of

aggregate (aerated, lightweight and dense). The mortar mix used to construct the wall panels and the two blocks prisms was 1:0.25:3 (cement:lime:sand) by volume. Mortar used for capping consisted of equal parts by weight of rapid-hardening Portland cement and fine sand. A nominal 10 mm thick mortar joint was used for both the prisms and the walls, with the exception of some specimens in which joint thicknesses of 3 and 25 mm were used to assess the effect of joint thickness upon prism strength. Five different fibre-boards were used in capping, consisting of three types of soft-board, a medium hardboard and a hardboard.

The results showed that board-capped specimens produced a lower indicated strength than mortar-capped specimens. The use of fibre-board with wet and dry blocks gave results which were as consistent as the 10 mm mortar capped specimens. The type of capping board employed had a small effect upon the mean indicated block strength. All types gave similarly consistent results, except that the use of 10 mm hardboard did yield somewhat larger coefficients of variation. It further appears that the relationship between the results of tests on mortar-capped and board-capped blocks depends upon the type of blocks used (i.e. whether solid, cellular or hollow). The effect of changing the thickness of the mortar cap from 10 mm to 3 or 6 mm was small.

The author observed a typical mode of failure for all blocks and prisms tested, regardless of the capping. This was by vertical splitting of the specimen, although some of the solid blocks exhibited a combination of crushing and splitting.

A comparison between the results showed that a good linear relationship was obtained for mortar-capped blocks tested wet and dry. A similar relationship was obtained for

board-capped blocks tested wet and dry. In general, it may be assumed that an indicated increase in strength of some 15% will result from testing the blocks in a dry condition. Another good linear relationship was obtained between the indicated strengths for mortar- and board-capped single blocks, both tested wet. Fig. 2.1 shows that a good linear relationship was obtained between the results yielded by tests on the two forms of prism specimen.

Considering the relationship between wall and specimen strengths, the results for 100 and 150 mm thick blocks gave a reasonably good linear relationships between the wall and specimen strengths for all specimens (Fig. 2.2). The relationship with wall strength seems to be dependent upon block thickness for the three mortar-capped specimens, and upon whether the block is solid or hollow for the three board-capped specimens.

The results for 200 mm thick blocks were considered separately from the other sizes because block shape has a very significant effect. A better correlation with wall strength for 200 mm thick blocks is provided by the board-capped prism.

The author also explained that the ratio of wall strength to control strength for 200 mm thick hollow blocks is lower than for 100 and 150 mm thick blocks since, when laid in running bond, the cross-webs of the blocks do not align vertically and, therefore, do not effectively carry load.

With regard to mortar strength, the results of tests on sets of 50 prisms, each set jointed with a different grade of mortar, suggest that changing the mortar grade has little effect on the indicated strength. Walls tested with the strongest and weakest mortar grades also confirm these

results.

With regard to the effect of joint thickness upon prism strength, the results showed that changing the thickness of the mortar within the range 3 to 25 mm has apparently little effect upon the prism indicated strength.

The author concluded that the use of prisms as a limited form of design test offers no significant advantage over the use of a single block control specimen, since mortar strength has little effect upon the load-bearing performance of blockwork walls. For both control and compliance tests, there seems no reason why board capping should not be used instead of mortar capping.

BOULT[27] in 1979, presented the results of an experimental investigation carried out by the New Zealand Concrete Masonry Association and the New Zealand Portland Cement Association on the compressive properties of filled concrete masonry prisms. Masonry units used in this work had the following differences:

Materials: Units made of normal weight concrete and of lightweight concrete.

Geometry: Blocks with different external dimensions and different internal configuration.

Sets of stack-bonded masonry prisms with height-to-thickness ratios (h/t) of 2.0 to 5.0 were constructed from each masonry unit type and tested normal to the bed face after grout filling. Storey height columns, with h/t = 12.0, were also tested to study the effect of height on the compressive strength. The mortar used was a nominal 1:4 (cement: sand) by weight. The grout used was a highly fluid infill material with nominal 1:3:2 mix (cement: sand: 10 mm

stone) by weight.

Concerning the effect of block geometry on the prism compressive strength, the results showed that the web thickness has little influence on the variation of prism strength to height. To explain the reduction in filled prism strength as the height increases beyond a value of h/t = 3.0, BOULT related the reduction to the effect of core shape (i.e. the tapering of the block shells) and to the texture of the interior face of the block cores. The core shape was responsible for significant changes in the prism net cross-sectional area. In addition to that, the mortar intrusion to the inner face of the prism, left after levelling and bedding down the blocks caused a further reduction in the prism net cross-sectional area. These excessive cross-sectional changes restrict the shrinkage settlement which occurs over the full height of the grouted column and results in plastic cracking as shrinkage proceeds. The severity of the plastic cracking increases with prism height.

In combining block and grout for filled masonry the author suggested that the individual material characteristics should be considered to obtain optimum results. It appears that if the modulus and limiting strain of both block and grout are similar the resulting prism has ultimate properties in excess of the individual elements. The results showed also that platen restraint has little effect on prism strength above a value of h/t = 2.0. Also there was no significant difference in strength between a full storey height column and prisms with h/t between 3.0 to 5.0.

Unfortunately, BOULT did not present a formula for determining the strength of ungrouted and grouted prism strengths.

DRYSDALE and HAMID[28] in 1979, reported the results of an experimental investigation on concrete block masonry prisms compressed axially in a direction normal to the bed face. Autoclaved concrete blocks were used to keep the properties as constant as possible. Three types of mortar mix, viz. 1:0.5:4, 1:0.5:3.38 and 1:1.25:6.75 (cement: lime: sand) and five different grout mixes were used to give a wide range of strength and deformational properties. The cylinder compressive strength of the grout mixes were 7.58, 13.72, 17.58, 20.75 and 41.09 N/mm^2. 3-block height prisms were constructed with a nominal 9.5 mm mortar joint thickness.

The mode of failure observed by the authors for almost all the prisms tested was by tensile splitting which initiated in the shells of the central block. Bond pattern was proved to have no effect on either the mode of failure or the capacity. The results of the half-block prisms were essentially identical to the results for the full-block prisms. Hence the authors decided that all remaining tests would be carried out using half-block prisms.

The results showed that the compressive strength of ungrouted blockwork masonry prisms was not very sensitive to the type of mortar used. A decrease in mortar strength of 69% resulted in a corresponding decrease in prism strength of less than 10%.

Although the grout occupied approximately 40% of the gross area its contribution to the prism strength was very small. Large increases in grout strength resulted in only relatively small increases in prism capacity. The authors gave an equation relating the compressive strength of a grouted concrete block masonry prism to an ungrouted prism and the grout strength was expressed as follows:

$$f'_{mg} = \cap(1 - K(1-\cap))(\sigma_{cg}/f'_{mu})f'_{mu} + (1-\cap)\sigma_{cg} \quad \ldots(2.1)$$

Where

f'_{mg} Average compressive strength of grouted concrete block masonry based on gross area, N/mm^2

f'_{mu} Average compressive strength of ungrouted concrete block masonry based on net area, N/mm^2

K A coefficient which reflects the interaction between the block shell and the grouted core under axial compression

$\cap$ Net to gross area ratio of the block

σ_{cg} Grout compressive strength as calculated from block moulded prisms tested under axial compression, N/mm^2

The above equation was based on the results of half-block prisms and the authors believed that the equation conforms that, in the extreme, the strength of a 100% solid will be f'_{mu} and of a 0% solid will be σ_{cg}.

With regard to the effect of mortar joint thickness, the authors tested prisms with joint thicknesses of 0, 9.5 and 19 mm for both ungrouted and grouted prisms. For zero joint thickness, a layer of cement paste was placed between the blocks which were then pressed together under a low load. The results showed that increasing the mortar joint thickness from 9.5 to 19 mm resulted in the prism compressive strength decreasing by 16% for ungrouted masonry whereas for grouted masonry the decrease was only 3%.

The results for prisms built with different block geometry (percentage solid ($\cap$) and shell thickness-to-block width ratio (t_s/w)) showed that, for ungrouted prisms, the percentage solid and shape did not appear to have much effect within the range tested. However, for grouted prisms with increased percentage solid, the compressive strength

increased toward the compressive strength of the ungrouted prisms. The ratio of the strength of a grouted prism to a similar ungrouted prism increased from about 0.70 to 0.91 as the percentage solid increased from about 0.61 to 0.73. It was also observed that the shell thickness-to-block width ratio (t_s/w) is not a significant parameter for the range tested.

On the effect of joint reinforcement, the results showed that No. 9 gauge wire joint reinforcement placed at the centre of the shells had no significant effect on prism strength nor was there evidence of any detrimental effect due to stress concentrations caused by the presence of such reinforcement. As an extreme of joint reinforcement, 2.8 mm thick confining plates were cut to fit the half-block cross-section and were inserted at the mid height of 13 mm thick mortar joints. The results showed an increase in strength of 8% and 18% for the ungrouted and grouted respectively. Also the mode of failure changed from splitting to shear failure, indicating the effect of confinement on reducing the lateral expansion which resulted in an increased compressive strength.

The authors also presented an explanation for the failure mechanism for ungrouted and grouted prisms. In the case of ungrouted prisms, the lateral expansion of the weaker mortar joint had a lower tension effect on the concrete blocks as compared to brickwork masonry. The reasons given by the authors for the reduction in the mortar effect in blockwork masonry were the greater compatibility between the materials and the fact that the ratio of unit height to mortar thickness is much greater for blocks than for bricks. In grouted prisms, the grout approaches its capacity first, the grout undergoes large lateral expansion due to an increased Poisson's ratio near ultimate strength. These large lateral expansions in turn

create tension in the shells of the block. As a result of this behaviour the block fails in tension at relatively low compressive stresses. The average compressive strength is therefore considerably less than the strength of either the ungrouted prism or the grout.

The authors concluded that the 2-course high prism does not properly represent the strength of a full scale blockwork masonry wall and that a 3-course high half-block prism was more representative. The compressive strength of grouted masonry was considerably lower than would be predicted using a superposition approach. Basing values for masonry compressive strength, f'_m, on block strength and mortar type does not seem to be appropriate for grouted concrete block masonry.

Unfortunately, the work of the authors was based on half-block prisms where the effect of the aspect ratio (l/t) (prism length-to-thickness) was not considered. This ratio would definitely have some influence on the mode of failure. Also, the presence of the block mid-webs would result in increasing the area of the weak mortar joint and consequently influence the compressive strength and behaviour of the ungrouted and grouted prisms.

Based on the above experimental work HAMID and DRYSDALE[29] in 1979, suggested failure criteria for grouted concrete masonry under axial compression. The criteria accounted for the interaction of the block, mortar and grout under multiaxial states of stress. The authors believed that the formulation could be developed in a generalized form and therefore able to account for any strength or geometric characteristics, such as the ratio of net to gross area of the block, tapering of the grout cores, joint thickness and even ungrouted masonry. In developing the failure criteria, the strength approach was

adopted due to its advantage in dealing with the strength values of the constituent materials which are readily and accurately measurable quantities. Alternatively, the strain approach would have require the determination of stress vs strain relationships of the component materials which are difficult to measure accurately near ultimate load especially considering that the component materials are under a state of multiaxial stress.

In developing the failure criteria the following assumptions were introduced:

1. Perfect bond was assumed at the interfaces between the block, mortar and grout.

2. Vertical stresses were assumed to be distributed between the shell (block and mortar joint) and the grouted cores in proportion to their axial stiffness.

3. The lateral stresses created in the block shells due to the lateral deformation of the grout and mortar was assumed to be uniformly distributed.

4. MOHR's theory of failure can be applied to the failure of concrete blocks under a bi-axial compression-tension state of stress.

5. Grout was assumed to have the same strength characteristics as normal concrete under triaxial compression.

Two failure cases were considered for grouted masonry under axial compression depending on whether the shell (block and mortar joint) or the grouted core reaches its unconfined compressive strength first.

Case I: When the grout has a lower strain level than the block shell at maximum stress, its unconfined compressive strength will be reached first. At this stage large lateral expansion occurs in the grout due to inelastic deformations and microcracking. The shell will tend to confine the grout and the resulting tensile stresses in the shell, when added to the tensile stresses due to confinement of the mortar, will cause a premature splitting failure of the block shell under a compression-tension state of stress.

In order to derive an expression for the average compressive strength of blockwork masonry assemblage the authors considered the following assumptions and factors:

1. The compatibility of deformation in the vertical direction.

2. MOHR's theory for the failure criterion of block under bi-axial stresses.

3. The mortar and grout under a triaxial compression state of stress.

4. The consideration of block tapering by using a magnifying factor to the grout stress representing the ratio of the maximum to minimum areas of the grout core.

5. The consideration of discrepancy caused by either some non-uniformity of the block geometry or due to the fact that the vertical stresses were distributed between the shell and the grouted core according to stiffness obtained from uniaxial stress condition corresponding to strain of 0.002.

Based on all the above conditions the authors

suggested the following equation for the average compressive strength of the masonry assemblage:

$$f'_{mg} = \frac{[4.1\ \sigma_{tb} + 1.14\ \alpha\ \sigma_{cm} + \beta\ \sigma_{cg}]\quad \sigma_{cb}}{[4.1\ \sigma_{tb} + (1.14\ \alpha + c\ \beta/n)\ \sigma_{cb}]\ n\ \phi\ K} \quad \ldots(2.2)$$

Where

c	Ratio of maximum to minimum cross-sectional area of the grouted core
E_{bs}	Secant modulus of elasticity of the shell at 0.002 strain, N/mm^2
E_g	Secant modulus of elasticity of the grout at 0.002 strain, N/mm^2
f'_{mg}	Average compressive strength of grouted masonry, N/mm^2
K	Stress adjustment coefficient
n	Modular ratio, E_{bs}/E_g
t_b	Height of the block, mm
t_m	Thickness of the mortar joint, mm
α	Mortar thickness-to-block height ratio, t_m/t_b
β	$= (1 - \cap)^{1/2}/(1 - (1 - \cap)^{1/2})$
$\cap$	Minimum net area-to-gross area ratio of the block
ϕ	$= 1/(1 + (n - 1)\ \cap)$
σ_{cb}	Uniaxial compressive strength of the block, N/mm^2
σ_{cg}	Unconfined compressive strength of the grout, N/mm^2
σ_{cm}	Unconfined compressive strength of the mortar, N/mm^2
σ_{tb}	Tensile strength of the block, N/mm^2

This equation was only valid when the vertical stress acting on the grout at failure was higher than its unconfined compressive strength.

Case II: The block shell reaches its maximum compressive stress at a lower strain than the grout. The grout in this case was assumed not to be confined and the capacity is controlled by either failure of the block under a compression-tension state of stress or the capacity of the grouted core under axial compression after failure of the shell. The block shell will act to confine the mortar only.

In order to derive an equation for the average compressive strength of blockwork masonry assemblage for Case II, the authors considered the following assumptions and factors:

1. MOHR's theory for the failure criterion of block under bi-axial stresses.

2. The mortar under a triaxial compression state of stress.

3. Same as assumption 5 for Case I.

Based on all the above conditions the following equation was proposed for the average compressive strength of grouted masonry:

$$f'_{mg} = \frac{[3.6\ \sigma_{tb} + \alpha\ \sigma_{cm}]\quad \sigma_{cb}}{[3.6\ \sigma_{tb} + \alpha\ \sigma_{cb}]\quad n\ \phi\ K} \qquad \ldots(2.3)$$

For large cores or for very strong grout, it was suggested that the grout could sustain higher loads than those corresponding to failure of the block shell. In this case the authors suggested an expression for the average compressive strength (based on the gross area of the assemblage) as follows:

$$f'_{mg} = (1 - \cap_m)\ \sigma_{cg} \qquad \ldots(2.4)$$

Where

$\cap_m$ Maximum net area-to-gross area ratio of the block

For Case II, the governing compressive strength, f'_{mg}, will be the larger value from either Eqn. 2.3 or 2.4.

Examination of the proposed expressions indicates that the most significant parameter is the block strength. Also, the compressive strength of grouted masonry increases with increasing net-to-gross area ratio, increasing the stiffness of the block or decreasing the stiffness of the grout and decreasing the thickness of the mortar.

STURGEON et al[30] in 1980, reported work carried out at the University of Alberta on blockwork masonry columns and prisms. Four block high prisms were built using 400 x 400 x 200 mm single core pilaster units. Some of the prisms were ungrouted and some were grouted with one of five different mixes of varying cylinder compressive strength (38.6, 35.2, 29.0, 17.7 and 10.3 N/mm^2) and slump (100 - 150 mm). Two of the mixes represented strengths in excess of block unit strength, and the other mixes provided strengths below block unit strength. Some of the prisms were subsequently stripped to permit testing of the cores alone. The actual dimension of all prisms were 397 x 397 x 803 mm and their h/t ratio equal to 2.0.

Failure of all the ungrouted prisms was sudden, complete and explosive. Grouted prism failures were characterized by two typical modes. Type A failure was described by the authors as a simultaneous splitting of the block shell and crushing of the prism core. Failure was gradual and shell cracking was noted in advance of the prism ultimate load. Vertical splitting of the prisms

tended to originate at block face centres in the upper or lower course. Type B failure was characterized by gradual splitting, with subsequent separation from the prism core, and spitting of the block shell before core crushing. Shell cracking was normally observed before shell spitting. All prism cores, irrespective of failure mode, showed a typical conical shear failure similar to that observed in standard concrete test cylinders.

Based on these results, the authors proposed an equation relating the ultimate load of a grouted masonry prism to grout strength and ungrouted prism strength as follows:

$$P_{um} = [0.75\ f'_c\ A_c + 0.62\ f'_{mpn}\ A_{sh}]/1000 \qquad ...(2.5)$$

Where

A_c Core area of block unit, mm^2

A_{sh} Masonry shell area, mm^2

f'_c Standard concrete cylinder compressive strength, N/mm^2

f'_{mpn} Ungrouted prism net area compressive strength, N/mm^2

P_{um} Ultimate load of grouted masonry prism, KN

The authors emphasized that the above empirical equation had been obtained using one block size and only one block strength.

The authors also recommended that since the designer cannot guarantee that sufficient bond will exist between the shell and the core to ensure shell contribution at ultimate load, a more conservative approach be adopted until the relationship is better understood, and that the second term in Eqn. 2.5, which is of secondary importance for pilaster units with the dimensions tested in this

investigation, be neglected in ultimate strength calculations.

The authors concluded that the superposition concept of grout strength and block strength was not valid and it may be more appropriate to match the deformational characteristics of the grout to those of the block rather than matching the strengths.

High slump concretes cast in columns and prisms built with pilaster units having large core areas produced extensive shrinkage cracking in the upper region of the core. Tests showed that they do not have a detrimental effect on the structural performance of masonry subjected to concentric compression.

Unfortunately, all the blockwork masonry prisms were of a single core pilaster unit which limits the use of the above formula to this type of block. It was also noted that the mode of failure for all the prisms built with the pilaster units were characterized by premature splitting of the block shell at low loads.

MAURENBRECHER[31] in 1980, presented work carried out by the National Research Council of Canada to study the effect of the following: prism height-to-thickness ratio (h/t); capping material; face-shell and full mortar bedding; workmanship; stack versus running bond and age (7- vs 28-day strength); on the compressive strength of blockwork and brickwork masonry prisms.

In this review work carried out on brickwork prisms has not been discussed. Two types of hollow concrete blocks, 140 and 190 mm thick, 2-core, autoclaved, with 79% and 84% solid, were used in the investigation. The mortar used had a compressive strength of 6.6 N/mm^2. Blockwork

prisms with face-shell bedding were capped with fiber-board strips placed on the face-shell area.

The results showed that the ultimate strength of the prisms increases as the h/t ratio decreases. The correction factors given for the h/t ratio by the Canadian Standard were shown to give overestimate of the strength. The prisms tested with fiber-board capping gave slightly lower results (0.99 and 0.92) compared to the plaster capped prisms. The results showed that the ratios of failure stress, based on mortar bedded area, were 0.99 and 1.10 (face-shell bedding to full bedding).

The author concluded that care must be taken that prism construction is representative of practice on the building site, including the use of face-shell bedding instead of full bedding with hollow concrete blocks (unless stresses are based on mortar bedded area) and furrowing of the mortar joints in masonry using solid units.

CHEEMA and KLINGER[32] in 1986, used experimental results from tests on concrete blockwork prisms and constituent materials to calibrate linearly elastic finite element models for hollow and grouted concrete masonry prisms. The prisms were constructed from one type of nominal 400 x 200 x 200 mm, 2-core, hollow concrete block of 25.86 N/mm^2 compressive strength. Three types of mortar were used with compressive strengths of 12.07, 12.41 and 14.89 N/mm^2 respectively. Some of the prisms were left ungrouted and some were grouted with grout strengths of 24.55 or 30.00 N/mm^2. All the grouted prisms were face-shell bedded. Some of the ungrouted prisms were face-shell bedded and some were fully bedded. The prisms were capped with gypsum plaster.

The observed modes of failure for hollow prisms with

9.5 mm joints were either by disintegration of the face shells or splitting of the webs parallel to the direction of load. Grouted prisms, on the other hand, failed by vertical splitting through the block shell, starting at the bed joint. Neither grout nor mortar suffered much damage. Axial capacity depended on the splitting resistance of the shell and the crushing resistance of the grout.

The results showed that hollow prisms (based on net area) with 12.7 mm mortar joints were about 72% as strong as those with 9.5 mm joints. Hollow prisms (based on net area) were stronger than grouted prisms (based on gross area), and blocks alone were stronger than hollow prisms.

The results for the stress vs strain curves showed that the modulus of elasticity of hollow prisms (based on net area) were higher than the grouted ones (based on gross area), with hollow prisms reaching maximum stress at strains near 0.0011 compared to about 0.002 for grouted prisms. The hollow blocks behaved linearly, failing suddenly by splitting of the shell near the mortar joint. Grouted prisms were very non-linear and failed more gradually.

In the analytical model for concrete masonry prisms, both hollow and grouted prisms were modelled as being linear elastic. Material non-linearity was accounted for by using secant moduli for all materials. The strengths of the constituent materials was computed considering the effects of multiaxial stresses.

The idealised elastic material characteristics for block, mortar and grout were derived as follows:

Block: Secant modulus E_{bs} and splitting tensile strength f_{tb} of the block were computed using the expression as shown

in the following equations:

$$E_{bs} = E_b = 0.028 \ (w_b^{1.5}) \ f_b^{1/2} \qquad \ldots(2.6)$$

and

$$f_{tb} = 0.42 \ (f_b)^{1/2} \qquad \ldots(2.7)$$

Where

E_b Initial tangent modulus of concrete block, N/mm^2

E_{bs} Secant modulus of concrete block at prism failure, N/mm^2

f_b Compressive strength of the concrete block, N/mm^2

f_{tb} Tensile strength of the concrete block, N/mm^2

w_b Unit weight of the concrete block, Kg/m^3

The assumed Poisson's ratio used in the analysis for hollow prism was 0.28 corresponding to an axial strain at failure of 0.0015.

Mortar: An idealised stress vs strain curve for unconfined mortar is based on an initial tangent modulus of $E_m = 1000 \ f_m$. The strain at maximum stress was taken as 0.002. The confined mortar behaviour can be described by an idealised stress vs strain curve lying between the initial tangent and estimated lower bound curve. A secant modulus $E_{ms} = 500 \ f_m$, at a mortar strain of 0.002, was assumed to be a reasonable value for the confined mortar (Fig. 2.3). A Poisson's ratio of 0.28 for confined mortar was adopted.

$$E_{ms} = 500 \ f_m \qquad \ldots(2.8)$$

Where

E_{ms} Secant modulus of the mortar at prism failure, N/mm^2

f_m Uniaxial compressive strength of the mortar, N/mm^2

Grout: The selected secant modulus of grout E_{gs} corresponded to an axial strain of 0.002, the observed failure strain of a grouted prism. The formula suggested for the secant modulus of elasticity was as follows:

$$E_{gs} = 0.021 \ (w_g^{1.5}) \ (f_g)^{1/2} \qquad \ldots(2.9)$$

Where

E_{gs} Secant modulus of the grout at prism failure, N/mm^2

w_g Unit weight of the grout, Kg/m^3

f_g Compressive strength of the grout, N/mm^2

The Poisson's ratio of grout was taken as 0.37, corresponding to an axial strain of about 0.002. For analysing hollow prisms, all grout properties were set to zero.

The following observations were made from the analytical results for hollow prisms with a wide range of material characteristics:

1. Near the mortar interface, transverse tensile stresses act in the shell in both directions. Stresses perpendicular to the shell are three to four times larger than those parallel to the shell.

2. Transverse tensile stresses are highest in the middle of the outside web, halfway between the two face shells, and decrease rapidly to zero within 25.4 mm from the mortar-block interface.

3. In the bed joint, compressive stresses act in both transverse directions.

From these observations the authors predicted three modes of failure for hollow prisms: (1) block splitting, where the maximum principal transverse tensile stress in the block reaches the tensile strength of the block; (2) block crushing, where the maximum axial compressive stress in the block reaches the compressive strength of the block; and (3) mortar crushing, where the maximum axial compressive stress in the mortar reaches the confined crushing strength of the mortar.

Block splitting: This failure occurs when the principal transverse tensile stress in the block reaches the tensile strength of the block.

$$f_{tb} = (1/f)\ f_{hb1} \qquad \ldots(2.10)$$

Or

$$f_{hb1} = f\ f_{tb} \qquad \ldots(2.11)$$

Where

f_{hb1} Compressive strength of a hollow prism as governed by tensile failure of the block, N/mm^2

f_{tb} Tensile strength of the concrete block, N/mm^2

f An influence coefficient equal to the ratio of hollow prism strength as governed by splitting of the block to the tensile strength of the block, Fig. 2.4

Block crushing: Blocks also fail when the nominal compressive stress in the block, f_{hb2}, reaches the block's uniaxial compressive strength, f_b. The applied compressive stress at block failure, f_{hb}, is therefore given by

$$f_{hb} = f\ f_{tb}, \text{ but not more than } f_b \qquad \ldots(2.12)$$

Where

f_{hb} Compressive strength of a hollow prism as governed by block failure, N/mm^2

f_{hb2} Compressive strength of a hollow prism as governed by crushing failure of the block, N/mm^2

f_b Compressive strength of the concrete block, N/mm^2

Mortar crushing: Since the mortar joint in unfilled prism is as thick transversely as the block shells, the nominal compressive stress in the block and the mortar joint are equal, and at joint crushing is equal to the compressive strength of the confined mortar.

$$\text{i.e.} \quad f_{hm} = \Gamma f_m \qquad \ldots(2.13)$$

Where

f_{hm} Compressive strength of a hollow prism as governed by mortar failure, N/mm^2

f_m Uniaxial compressive strength of the mortar, N/mm^2

Γ Ratio of confined to unconfined crushing strength of the mortar in a hollow prism, Fig. 2.4

Based on the above three predictions for the various modes of failure, the authors summarised the capacity prediction procedure for the failure of hollow prisms as follows:

1. Find the modular ratio of mortar to block, using either the known secant moduli of the mortar and block (corresponding to maximum stresses) or values estimated using Eqns 2.6 and 2.8.

2. Find the compressive strength of a hollow prism, f_{hb}, as governed by principal tensile stress in the block, using Eqn. 2.12 and Fig. 2.4. If unknown, the tensile

strength of the block may be estimated using Eqn. 2.7.

3. Find the strength, f_{hm}, as governed by mortar crushing, using Eqn. 2.13 and Fig. 2.4.

4. The strength of hollow prisms, f_h, is the smaller of f_{hb} and f_{hm}.

The following observations were made from the analytical results for grouted prisms with a wide range of material characteristics:

1. The vertical compressive stresses in the block and grout varies from the applied compression by less than 15% away from the level of the bed joint, but by as much as 70% at the joint.

2. Transverse tensile stresses on the block are about equal in both directions at the mortar-block interface due to lateral expansion of the grout and the mortar.

3. Transverse stresses perpendicular to the shell decrease to zero within about 25.4 mm from the mortar-block interface. Transverse stresses parallel to the shell are also highest near the interface, decreasing gradually to uniform non-zero values away from the interface.

4. Approximately equal transverse compressive stresses act on the mortar joint in both directions and are largest near the mortar-block interface.

5. Transverse compressive stresses on the grout are largest at the level of the bed joint.

From these observations the authors predicted

five modes of failure for grouted prisms: (1) block splitting, where the maximum principal transverse tensile stress in the block reaches the tensile strength of the block; (2) block crushing, where the maximum axial compressive stress in the block reaches the compressive strength of the block; and (3) mortar crushing, where the maximum axial compressive stress in the mortar reaches the confined crushing strength of the mortar. (4) mortar splitting, where the maximum principal tensile stress in the mortar reaches the tensile strength of the mortar; and (5) grout crushing, where the maximum axial compressive stress in the grout reaches the confined crushing strength of the grout.

Block splitting: The prism fails by block splitting when the maximum principal tensile stress in the block reaches f_{tb}, the tensile strength of the block.

$$f_{pb1} = f_{tb}/\sigma_{1bi} \qquad \ldots(2.14)$$

Where

f_{pb1} Compressive strength of a grouted prism as governed by tensile failure of the block, N/mm^2

f_{tb} Tensile strength of the block, N/mm^2

σ_{1bi} Maximum principal tensile stress in the block due to unit applied axial compressive in a grouted prism, Fig. 2.5

Block crushing: Compressive failure occurs when

$$f_{pb2} = f_b\,[k + m\,(1 - k)] \qquad \ldots(2.15)$$

$$k = A_{bk}/(A_{bk} + A_g) \qquad \ldots(2.16)$$

$$m = E_{gs}/E_{bs} \qquad \ldots(2.17)$$

Where

A_{bk} Net cross-sectional area of concrete block, mm^2

A_g Area of grout, mm^2

E_{bs} Secant modulus of the concrete block at prism failure, N/mm^2

E_{gs} Secant modulus of the grout at prism failure, N/mm^2

f_b Compressive strength of the concrete block, N/mm^2

f_{pb2} Compressive strength of a grouted prism as governed by block crushing, N/mm^2

Mortar crushing: The prism fails when the mortar strength reaches the compressive strength of the confined mortar.

$$f_{pm1} = \delta\ f_m \qquad \ldots(2.18)$$

Where

f_{pm1} Compressive strength of a grouted prism as governed by mortar crushing, N/mm^2

f_m Uniaxial compressive strength of the mortar, N/mm^2

δ The ratio of the strength of a grouted prism, as governed by crushing of the mortar, to the uniaxial crushing strength of the mortar, Fig. 2.6

Mortar splitting: The prism strength is governed by the mortar splitting, f_{pm2}, where

$$f_{pm2} = f_{tm}/\sigma_{1mi} \qquad \ldots(2.19)$$

Where

f_{pm2} Compressive strength of a grouted prism, as governed by mortar splitting, N/mm^2

f_{tm} Tensile strength of the mortar, N/mm^2

σ_{1mi} Maximum principal stress in the mortar for unit applied axial compressive stress on the grouted prism, Fig. 2.7

Grout crushing: At prism failure, the axial compressive stress on the grout equals the compressive strength of confined grout.

$$f_{pg} = \Phi\ f_g \qquad \ldots(2.20)$$

Where

f_g Compressive strength of the grout, N/mm^2

f_{pg} Compressive strength of a grouted prism, as governed by grout failure, N/mm^2

Φ Ratio of the confined to unconfined crushing strength of the grout, Fig. 2.8

Based on the above five predictions for the various modes of failure, the authors summarised the capacity prediction procedure for the failure of grouted prisms as follows:

1. Find the modular ratios, E_{ms}/E_{bs} and E_{gs}/E_{bs}, using either known secant moduli for the block and mortar corresponding to maximum stress, or values estimated using Eqns 2.6 and 2.8. The secant modulus of the grout may be estimated using Eqn. 2.9.

2. Use Eqn. 2.14 and Fig. 2.5 to find f_{pb1}, the strength of a grouted prism, as governed by block splitting. If unknown, the tensile strength of the block may be estimated by Eqn. 2.7.

3. Use Eqn. 2.15 to find f_{pb2}, the strength of a grouted prism, as governed by block crushing.

4. Use Eqn. 2.18 and Fig. 2.6 to find f_{pm1}, the strength of a grouted prism, as governed by mortar crushing.

5. Use Eqn. 2.19 and Fig. 2.7 to find f_{pm2}, the strength

of a grouted prism, as governed by mortar splitting. If unknown, the tensile strength of the mortar may be estimated by:

$$f_{tm} = 0.58 \ (f_m)^{1/2} \qquad \ldots(2.21)$$

6. Use Eqn. 2.20 and Fig. 2.8 to find f_{pg}, the strength of a grouted prism, as governed by grout crushing.

7. The strength of the grouted prism, f_p, is the smallest of the five prism strengths computed in Steps 2 through 6 above. For normal materials, block splitting usually governs.

HAMID and CHUKWUNENYE[33] in 1986, studied the behaviour of concrete masonry prisms axially loaded normal to the bed face using three-dimensional finite element elastic analysis. The characteristics investigated were the effects of mortar bedding, mortar deformational properties, block size, prism height-to-thickness ratio (h/t), number of mortar joints and stiffness of the bearing plates. The analysis was developed using ANSYS, a general purpose finite element program. A three-dimensional plate element with surface loading capability was used to model the bearing plates. Due to the restrictions on ANSYS, it was impossible to use the compressive strength of the constituent materials directly. Instead, the elastic moduli (calculated at a stress level of 6.9 N/mm^2) of the different materials were used. A block-mortar modular ratio of 2.8 was determined for normal strength blocks and type S mortar. A Poisson's ratio of 0.2 was used for concrete blocks and 0.18 for mortar.

Two types of mortar bedding were analysed: face-shell bedding (the blocks were laid with the bed joint separated into two parallel strips) and full area bedding (all shells

were bedded including the cross-webs). The results of the analysis for the face-shell bedding prism showed that large lateral stresses were created in the block webs, resulting from the beam action caused by the gap existing between the webs. The results indicate that web cracking in face-shell bedded prisms will occur at a relatively low load level compared to that for full-bedded prisms. Face-shell bedded prisms also showed a non-uniform axial stress distribution at the prism end shells along the height of the prism. The distribution for fully-bedded prisms was fairly uniform, indicating a significant difference in behaviour between the two types of prisms.

The effect of the mortar properties on the behaviour of hollow block masonry prisms was investigated by changing the block-to-mortar modular ratio, E_b/E_m. The results of the analysis showed that an increase in the block-to-mortar modular ratio increases the lateral tensile stresses in the blocks due to an increase in the degree of deformational incompatibility between the stronger blocks and the weaker mortar.

The results also showed that for prisms built with block sizes thicker than 200 mm there is no appreciable difference in either the shape or the magnitude of the stresses. This indicates that block size has no effect on the behaviour of axially loaded prisms.

The effect of the prism height-to-thickness ratio, (h/t), on the behaviour of concrete masonry prisms was also investigated. The results of the analysis indicated two different modes of behaviour for prisms with h/t = 3.0 and h/t = 2.0. The middle portion of the prism is in compression for prisms with h/t = 3.0 and in tension for prisms with h/t = 2.0. Based on this result, the authors recommended the testing of 3-course high prisms to

determine the prism compressive strength (f'_m).

However, the authors believed that such a recommendation could not be easily implemented due to height limitations imposed by commercially available testing machines. To solve this problem, the authors proposed the testing of a 3-course prism with half blocks at the top and bottom. The results, for this type of prism, showed a definite similarity to those for the full 3-course high prism.

The results for prisms using different bearing plate thicknesses showed that the ASTM E 447 recommendation (i.e. using a bearing plate thickness equal at least one half of the distance from the edge of the bearing block to the most remote corner of the prism's cross-section) was too flexible and produced large lateral tensile stresses in the top block which could cause premature failure. The authors recommended using twice the bearing plate thickness specified by the ASTM E 447 Standard.

To the author's knowledge, the only study to date on specimens tested axially in a direction parallel to the unit bed face is that carried by the author himself in 1981[34] and presented in two papers in 1987 and 1988. In 1987[35], the author presented results from a two-dimensional finite element analysis for unfilled, partially and completely filled single-block specimens and two-block prisms axially loaded parallel to the unit bed face. This study simulated the compression zone of a reinforced masonry beam or part of a wall in a seismic zone where excessive horizontal forces can be expected.

The material properties (compressive strength, stress vs strain relationship, modulus of elasticity and Poisson's ratio) were obtained by testing the individual materials.

The block used in the analysis was a hollow block, with two legs to permit face-shell bedding and with nominal dimensions of 400 x 200 x 200 mm.

The results from an analysis of unfilled single-block specimens showed a non-uniformity in the elastic vertical stress distributions, with very high localized stresses at the outer and inner faces of the block legs and hollow cores respectively. On the other hand, the analysis, assuming **PIN/FIX** and **PIN/PIN** end conditions, of unfilled two-block prisms showed a very sharp increase in the elastic vertical compressive stresses at the outer face of the mortar joints with stresses in tension at the inner face. This non-uniformity was due to the shape of the block and the way it was loaded, with a tendency for the shell to deflect laterally (Fig. 2.9). The analysis also showed high tensile stresses (3.5 - 8.3 N/mm^2) and high shear stresses (1.2 - 4.3 N/mm^2) for the **PIN/FIX** and **PIN/PIN** two-block prisms respectively near the block legs and web connections, compared to the ultimate tensile and shear stresses given by ACI 318M-83.

From the results of this analysis the author was able to relate the mode of failure for the **PIN/FIX** and **PIN/PIN** unfilled two-block prisms to the unit compressive strength and the type of mortar.

The results for the partially filled single-block specimens and two-block prisms showed a more uniform elastic vertical stress distribution than the unfilled ones. The largest localized elastic vertical stresses occur at the inner face of the block legs for all the single-block specimens and at the inner face of the block legs and the mortar joints for all the two-block prisms. The uniformity of the vertical stresses was attributed to the presence of the concrete infill.

A definite similarity in the distribution of the elastic tensile and shear stresses was also observed between the partially filled single-block specimens and two-block prisms. These stresses tended to concentrate near the block legs. These high stresses were mainly due to the beam action caused by the presence of unfilled voids between the block legs. Appreciable differences were observed between the elastic tension stresses for the **PIN/FIX** and the ideal **PIN/PIN** single-block specimens with the ideal **PIN/PIN** specimens showing a very sharp increase in these stresses at the top and bottom block webs. This increase in tensile stress was also observed at the centre of the webs for both the **PIN/FIX** and **PIN/PIN** end conditions, for partially filled two-block prisms. As a result, the author suggested that the only way to determine the ultimate compressive strength, f'_m, for a partially filled prism is by testing a two-block prism.

Based on the results of this analysis the author was also able to predict the mode of failure for the **PIN/FIX**, partially filled prism. This mode of failure is quite complicated and depends on the compressive and tensile strength of the block and mortar type. For mortars of low strength, the failure first occurred by localized crushing of the inner face of the mortar joint followed by shearing near the block legs and lateral deflection of the block shells. For mortars with higher compressive strengths, the predicted mode of failure was due either to the block reaching its compressive strength or the block splitting at the centre of the webs, whichever occurred first.

The results for an analysis of the completely filled single-block specimen and the two-block prism showed almost uniformly distributed elastic vertical stresses. The elastic tensile and shear stresses were lower than those for all the other types of models analysed. Also these

stresses usually tended to concentrate near the block legs. Thus the author concluded that the completely filled specimen was the best case.

The predicted mode of failure for the completely filled single and two-block specimens was by crushing in the block legs followed by lateral deflection of the block shells. Based on the results of an analysis of completely filled specimens the author concluded that testing completely filled single-block specimens is sufficient to determine f'_m. Also, there is no relation between the block strength and the mortar type for this case.

Finally, the author concluded that for the type of block described in the analysis:

1. For the design of an unfilled masonry wall in accidental zones, where horizontal axial forces are expected, the ultimate compressive strength of blockwork masonry, f'_m, is determined from the unit block strength, loaded in a direction parallel to the bed face, and the mortar type.

2. For the analysis and design of reinforced concrete masonry beams or partially filled masonry walls in seismic zones, partially filled two-block prisms should be tested to determine f'_m.

3. For beams, or walls in seismic zones, blocks that permit full-bedded vertical mortar joints to be made are preferable. To determine f'_m for this type of construction, testing completely filled single-block specimens is sufficient.

The author[36] in 1988, presented experimental results in support of the above analytical investigation. Using the

same type of block and the three different fill conditions (unfilled, partially filled and completely filled), the author tested single-block specimens and two-block prisms in a direction parallel to the unit bed face.

The observed modes of failure and the load vs strain curves for all the specimens tested tended to confirm the modes of failure and stress distribution predicted using a two-dimensional finite element analysis.

The results showed that the strength of almost all the two-block prisms, with specimen height-to-thickness ratio, h/t = 4.0, was higher than that for single-blocks with h/t = 2.0. This is contrary to the well established reduction in strength with height factor for masonry prisms laid in stack-bond and loaded in a direction normal to the bed face.

The results also showed that the compressive strength of unfilled blocks tested parallel to the bed face was 29% lower than for units tested normal to the bed face. High, localized vertical and shear stresses tend to occur at the outer face of the block legs and near the connection points of the legs to the top and bottom webs respectively, leading to this reduction in strength. Partially filled single-block specimens showed a 34% reduction in compressive strength compared to unfilled single-blocks. The reason for this reduction was differences in the deformational characteristics of the concrete infill and block.

The results showed that the compressive strength of the partially filled two-block prisms is dependent on the type of mortar. Prisms with low mortar strength (17.80 N/mm^2), failed at a compressive strength which was 2% higher than the strength of the mortar, but 41% lower than the

strength of the block material, and 10% lower than the strength of the partially filled single-block specimens. The reduction in strength compared to the single-block specimen was due to the lower compressive strength of the mortar.

On the other hand, prisms with mortars of higher strength (average 23.6 N/mm^2), failed at a compressive strength which was 29% lower than the block material, and 8% lower than the compressive strength of mortar. This failure strength was 8% higher than the strength of the partially filled single-block specimens.

The load vs strain relationships showed that an extensive stress redistribution occurs at the higher stress levels, due to the non-linear behaviour of the mortar. Also a clear difference in the vertical strain levels between the inner face and the outer face of the mortar joints, and a high tensile strains at the centre of the webs near the unfilled void between the blocks was also evident. There was also an indication of increasing stiffness beyond the elastic region. This was due to lateral deflection of the block shell after crushing of the inner face of the mortar joints. All the partially filled prisms tested showed very high strain readings. The highest strain recorded was 0.015.

The results showed that the compressive strength of the mortar has an important effect on the strength of the partially filled two-block prisms. But for mortars of higher strength than the one used in the study, it can be expected that the splitting strength of the block will dominate the type of failure, and that the compressive strength of the prism, will stabilize at a constant value.

On the other hand, the results showed that using two

concrete infills with a 45% difference in compressive strength has little effect on the compressive strength of the prism.

The results showed that the compressive strength of the completely filled prisms is 4% higher than that of the completely filled single-block specimens, but 29% less than the compressive strength of the block material. The results also showed that the ideal case was the completely filled prism.

Finally, the author concluded that for the design of unfilled masonry walls in seismic zones, where high horizontal forces are expected, the ultimate compressive strength of blockwork masonry f'_m must be determined by either:

(i) Using tables or graphs relating the compressive strength of unfilled single-block compressed parallel to the unit bed face and the type of mortar.

Or

(ii) Masonry prisms laid in running bond, tested parallel to the unit bed face, and made from the same materials as those used in the actual construction.

For the design of partially filled blockwork beams and walls in seismic zones, the ultimate compressive strength of blockwork, f'_m, must be determined by either:

(i) Where the mortar used has a lower compressive strength than the partially filled single-block units tested parallel to the bed face, then f'_m is determined using tables or graphs relating the compressive strength of the partially filled single-block compressed parallel

to the unit bed face and the mortar type.

Or

(ii) Where the mortar used is of higher strength, then f'_m is determined by testing partially filled two-block prisms laid in running bond, and loaded parallel to the unit bed face.

Completely filled blockwork masonry beams and walls are the ideal form of construction. To determine f'_m for this case, testing completely filled single-block specimens is sufficient.

The National Concrete Masonry Association of America (NCMA)[37] in 1988, presented a report on a research investigation of the properties of masonry grout in concrete masonry.

The objectives of this research programme can be summarized as follows:

1. To establish the relationship between grout strengths determined by the standard method of sampling and testing grout (ASTM C 1019) and the strength of grout in grouted concrete masonry.

2. To develop recommendations for grout strength requirements as an alternative to proportion requirements.

3. To study the effect of the cement to aggregate ratio on grout properties.

4. To study the effect different concrete masonry units have on the properties of grout in grouted concrete

masonry.

5. To study the relationship between both the modulus of elasticity of concrete masonry, E_m, and the modulus of elasticity of grout, E_g vs the grout cement to aggregate ratio.

6. To study the relationship between the strength of grout and the modulus of elasticity of grout, E_g.

7. To study the relationship between the strength of concrete masonry units and modulus of elasticity of concrete masonry, E_m.

The research includes compressive strength tests on concrete masonry prisms, moulded grout specimens, grout specimens cut from grouted units and tests of component materials such as units, mortar and ingredients of mortar and grout.

Two types of concrete block units, with nominal dimensions of 400 x 200 x 200 mm, were used in the programme (normal and high strength concrete block units). Two types of mortar were used in accordance with the requirements of ASTM C 270-86b Standard, proportioned by volume (N = 1:1.25:6.75 and S = 1:0.50:4.50 cement: lime: sand proportions). Six types of grout were used, divided into fine mixes (1:3, 1:4 and 1:5 cement: sand proportions) and coarse mixes (1:2.4:1.6, 1:3:2 and 1:4.8:3.2 cement: sand: aggregate proportions). The prism was constructed with two full concrete blocks laid in stack-bond. The authors believed that 2-block prism is the most commonly used configuration for quality control and could be expected to produce consistent and predictable results for the purposes of comparison. Prisms made with normal strength units were laid up with Type N mortar; prisms made

with high strength units were laid up with type S mortar. For the ungrouted prism specimens, both the face-shell mortar bedding and the full mortar bedding were used. For filled prisms, the fine and coarse grouts were mixed to a 254 mm slump. Concrete blocks units were used to form grout mould in accordance with ASTM C 1019. The units forming the grout mould were lined with absorbent paper which prevented bond of the grout to the concrete blocks. Cut grout specimens were also prepared by filling one core of a block unit with grout and after curing, prisms measuring 194 x 89 x 89 mm high were sawn cut from the grouted core.

The results for the grout specimens showed that the compressive strength of block moulded specimens averaged 9.7% higher than that for the cut specimens. The reason for this difference in strength was attributed to the greater volume of masonry unit surrounding the moulded specimen than surrounding the cut specimen. This greater volume of masonry unit could have absorbed more water prior to the grout setting than in the case of block moulded specimens. Based on the grout results, the authors concluded that the standard ASTM C 1019 method for testing grout reflects strengths representative of the strength of grout in grouted concrete masonry. On the effect of the aggregate to cement ratio (A/C) on the grout compressive strength, for fine and coarse aggregates, the results showed that the relation between strength and A/C ratio was different for fine and coarse aggregate grout and that the grout compressive strength reduces as the A/C ratio increases.

The filled prism results showed that increasing the grout strength resulted in increasing the prism strength. The results show also that the increase in prism strength has a greater effect for grout strengths up to the strength of the units. Increasing the grout strength beyond that point has less effect on the masonry prism strength.

The results for the stress vs strain relationship for the grout appears linear over most of the loading range of the specimens tested. Elastic modulus was determined at data points between 5% and 33% of the grout strength. The modulus of elasticity of the grout vs compressive strength of the grout relationship was expressed as follows:

$$E_g = 500 \times \text{Grout strength, } N/mm^2 \quad \ldots(2.22)$$

Unfortunately, the authors based their work on 2-course high prisms and this does not truly reflect the actual strength of the prisms due to the effect of machine platen confinement.

Work was carried out on masonry prisms compressed normal to the unit bed face by AFSHARI and KALDJIAN[38] in 1989, to predict the behaviour and ultimate strength of concrete block masonry prisms, using the physical and geometric properties of mortar and block elements. Failure envelopes were established for the mortar using MOHR's theory of failure and for the block using the results of a numerical analysis of solid masonry prisms. A finite element analysis of solid, hollow and grouted masonry prisms was curried out using linear three-dimensional 8-node solid elements. A linear analysis was assumed to be adequate for brittle cementitious material such as concrete blocks, grout and mortar. A finite element model consisting of one-eighth of the concrete masonry prism under axial compressive stress was used to determine the general state of the internal stresses.

The results showed that the mortar was under a triaxial compressive stress while the block was under lateral bi-axial tension near the interface between the mortar and the block. Since the mortar used in the analysis was weaker than the block material, the stress vs strain

relation for the mortar falls below the one for the masonry unit. Therefore, for the same axial stress, the resulting longitudinal (axial) and lateral strains will be larger for the mortar than the block. However, since both materials were bonded together, the lateral stresses cause confining stresses in the mortar joint and tensile stresses in the masonry unit.

In determining the cause of failure of a masonry prism the authors assumed the failure envelope for hollow units of $A_n/A_g = 0.5$ to be close to the line. Although admitting that this assumption could not be verified experimentally, they gave the following explanation for their assumption: "Assume a solid unit is made of a hollow shell and grouted with the same material as the shell. The extra material in the block will expand laterally when axial stress is applied on the unit. The expansion of the extra material will result in additional lateral stresses pushing the shell portion outward, and thus will cause a solid unit to fail at a lower level of axial stress than an equivalent hollow unit". This assumption was supported by the results of the analysis which showed that for the same applied axial stress, f_a, and lateral tensile stress, f_{bt}, the solid unit had a larger lateral deflection and internal stress than the corresponding 50% hollow unit. An attempt was made to determine the level of axial compressive stress and lateral tensile stress at which the internal stresses and deformations of a solid unit are roughly equal to the equivalent hollow unit. Several finite element models with varying values of f_a and f_{bt} were run. The final result has been plotted in Fig. 2.10. In this figure, the line drawn through Point 2 and parallel to the heavy line drawn through Point 1 is proposed as the failure envelope for a solid block unit ($A_n/A_g = 1.0$). At the extreme ends of this failure envelope, the dashed lines represent the actual shape of the solid unit failure envelope. However, since

the combination of lateral and axial loading in a prism is seldom close to the extreme limits, the authors believed that it was safe to assume this to be a straight line. To accommodate the failure envelopes for values of A_n/A_g between 1.0 and 0.5, the authors suggested the following empirical expression for the lateral tensile stress f_{bt} on the masonry unit for $0.5 < A_n/A_g < 1.0$ was (Fig. 2.11):

$$f_{bt} = (D - f_a/f'_{bl})\ f'_{bt} \qquad \ldots(2.23)$$

and

$$D = 2/3\ (2 - A_n/A_g) \qquad \ldots(2.24)$$

Where

A_g Gross cross-sectional area of the masonry unit, mm^2

A_n Net cross-sectional area of the masonry unit, mm^2

f_a Axial compressive stress applied to a prism, N/mm^2

f'_{bl} Ultimate uniaxial flat-wise compressive strength of a masonry unit, N/mm^2

f_{bt} Lateral tensile stress applied to a masonry unit, N/mm^2

f'_{bt} Ultimate uni-axial or bi-axial lateral tensile strength of a masonry unit, N/mm^2

An attempt was also made to draw the loading curve for a mortar and masonry unit to represent the variation of the lateral tensile stress, f_{bt}, and the confining stress ,f_c, as the applied axial stress, f_a, on the prism increases. By considering the equilibrium of forces on a typical cross-section through the unit and mortar joints on top and bottom, regardless of the shape of the cross-section, the authors derived an expression for the average value of f_{bt} and f_c as follows:

$$f_{bt} = (t_j/h_u)\ f_c \qquad \ldots(2.25)$$

Where

f_c Confining stress in the mortar joint, N/mm^2

h_u Height of masonry unit, mm

t_j Thickness of the mortar joint, mm

To complete the analytical process, the authors required an expression describing the variation of the confining stress, f_c, in the mortar as a function of the axial stress, f_a, on the prism. They suggested one method of calculating this variation from experimentally measured strains in the mortar and the masonry unit. Using the fore-mentioned f_a versus f_c relationship, and Eqn. 2.25, it was possible to produce an expression for f_a in terms of f_{bt} alone. This expression was designated as the loading curve for the masonry unit.

The general failure criteria for a masonry prism proposed by the authors is shown in Fig. 2.12. The loading curve for the mortar must be calculated from experimentally measured stress vs strain curves for the mortar with different compressive strengths. The loading curve for the block may be obtained using the latter together with Eqn. 2.25. The failure envelope for the masonry unit was derived on the basis of the net to gross cross-sectional area of the masonry unit expressed by Eqns 2.23 and 2.24. The point at which the loading curve of the masonry unit and its corresponding failure envelope intersect gives the value of the ultimate compressive strength, f'_m, of the prism. The values of f_{bt} and f_c, corresponding to the value of $f_a = f'_m$, represent the average tensile stress in the masonry unit and the confining stress in the mortar joint, respectively.

2.3 MASONRY COLUMNS

2.3.1 Brickwork Masonry Columns

Tests on unreinforced brickwork masonry columns was reported as early as 1882. In 1886, it was considered that column strength was inversely proportional to height to thickness ratio. The first research on the effect of lateral reinforcement in brickwork piers was conducted at the University of Cornell[39] in 1900. This study showed that the placing of wire netting or mesh in every joint, increased considerably the compressive strength of the piers.

In 1923 the first tests on reinforced brickwork masonry columns were reported. BREBNER[40] tested square and circular cross-section, 6-course high brickwork prisms with a small percentages of vertical reinforcement and large amounts of horizontal reinforcement. BREBNER's results indicate that, for square cross-section prisms, the use of 5 mm diameter circular stirrups in each joint, which represent 5% of the prism's cross-section area, increased the prism's strength by 62%. Due to the high percentage of horizontal reinforcement, the influence of the 0.2% and 0.8% vertical reinforcement on the axial capacity of the square prism was not clear. The results showed that the strength of the prism with both horizontal and vertical reinforcement, is on average 16% lower than the those with horizontal reinforcement only and 36% higher than those with no reinforcement. The reason for the reduction in strength was not clearly explained, but it would seem that the vertical reinforcement was unable to reach its yield strength due to the failure of the links anchorage of the horizontal reinforcement. In the circular prisms, the presence of the horizontal reinforcement increased the prism compressive strength by an average of 36%. The

introduction of vertical reinforcement in the circular prisms increased the axial capacity by 19% compared to those with horizontal reinforcement and 62% to those with no reinforcement.

LYSE[39] in 1933, carried out tests on reinforced brickwork columns of similar format, each 3 m high with a slenderness ratio of 9.6. The results showed that the strength of reinforced brickwork masonry columns with vertical reinforcement can be predicted by combining the ultimate strength of the masonry with the yield strength of the vertical steel. The brickwork ultimate strength is therefore:

$$S = [A\ (K\ f'_b + \phi\ f'_s)]/1000 \qquad \ldots(2.26)$$

where

A	Cross-sectional area of column, mm^2
f'_b	Ultimate compressive strength of brick, N/mm^2
f'_s	Yield point of vertical reinforcement, N/mm^2
k	Ratio of masonry strength to brick strength
S	Column strength, KN
ϕ	Ratio of area of longitudinal steel to cross-sectional area of column

LYSE recommended that k be determined experimentally by testing small brickwork prisms constructed from the same material as the columns and cured under the same conditions.

WITHEY[41] in 1934, tested thirty-two brickwork columns under concentric load. The columns were 318 mm square and 1.8 m high with a slenderness ratio of 5.8. WITHEY found that the strength of brickwork columns increased as the

strength of the masonry and the percentage of vertical reinforcement increased. WITHEY indicated that 10 mm horizontal reinforcement in each course increased the strength of the columns and prevented complete collapse. WITHEY suggested the following equation to calculate the maximum capacity of brickwork columns:

$$P/A = f_b\ (1 - \phi) + \phi\ f_s + K\ \phi'\ f'_s \quad \ldots(2.27)$$

where

A	Column cross-sectional area, mm^2
f_b	Unit stress for plain brick column, N/mm^2
f_s	Yield point of longitudinal steel, N/mm^2
f'_s	Yield point of lateral hoop reinforcement, N/mm^2
P	Maximum load, Newton
K	Constant assumed to depend on the ratio of gross area to core area, and possibly on brick type
ϕ	Longitudinal steel ratio in terms of gross area
ϕ'	Lateral steel ratio in term of gross area

LYSE indicated that 6 mm horizontal reinforcement in every fourth joint was sufficient to ensure that the vertical reinforcement reached its yield strength. Also increasing the diameter of the horizontal reinforcement produces no appreciable increase in the column's capacity. The overall conclusion that can be drawn from the results of both studies is that placing horizontal reinforcement at every third and fourth course was economical and interfered little with the building of brickwork columns; placing horizontal reinforcement at closer spacing makes the bricklaying more difficult. Whereas, placing the horizontal reinforcement at every third or fourth course, unable the bricklayer to adjust any differences in the mortar joint thickness in the other unreinforced courses.

DAVEY and THOMAS[42] in 1950, tested a number of concentric and eccentric plain brick piers and reinforced brickwork columns. The variables considered in the plain piers were brick type, mortar type, cross-sectional area and pier height; the latter ranging from 0.27 to 3.2 m in order to study slenderness effects. With eccentricities ranging from t/12 to t/3, the results of the plain piers showed that the effects of slenderness are not independent of the eccentricity of loading. Concentric and eccentric reinforced brickwork columns were also tested each 2.74 m high and variable cross-sectional area. The largest slenderness ratio used was 6.0. The eccentricity of loading in these tests was high, never less than one quarter of the column depth and the percentage of vertical reinforcement used was low (0.11% to 0.25%).

However, the ultimate resisting moments were high compared to similar unreinforced columns. Failure of these columns occurred either due to spalling of the compression face or due to the yielding of vertical reinforcement.

The authors did not propose a failure theory or design method for either the plain or reinforced brickwork columns.

Another ultimate strength design method for reinforced brickwork columns was proposed by ANDERSON and HOFFMAN[43] in 1967, based on the American Concrete Institute (ACI 318-63) method for reinforced concrete columns. The authors concluded that the ACI ultimate design method for concrete columns could be used to design brickwork masonry columns provided that more reliable data could be obtained concerning the shape of the stress vs strain for brickwork masonry, the ultimate strain of the masonry and the effect of different percentages of vertical reinforcement on the behaviour of brickwork masonry.

BRETTLE[44] in 1970, proposed a computer aided ultimate strength design procedure for reinforced brickwork columns subjected to concentric and bi-axial bending. The program was used to analyse the brick columns tested by DAVEY and THOMAS. The results indicated that the experimental failure loads for plain columns were, on average, 30% higher than those computed using the theory, but 3% lower for reinforced ones. BRETTLE observed also that, provided the placing of lateral reinforcement did not substantially reduce the rate of brickwork laying, the lateral reinforcing of columns was the most important method of increasing their ultimate strength.

ARMSTRONG and HENDRY[45] in 1973, tested full-scale and model stack-bonded prisms, 6-course high, reinforced with a wide variety of lateral steel in each mortar joint. The authors reported an increase in strength of 30% to 40% in reinforced full-scale brickwork prisms compared to plain ones. They also pointed out that the effect of the surface area and number of wires had a more important influence on the compressive strength of the prisms than the cross-sectional area of the steel. The explanation given by the authors was that the most important parameter is the total force that can be transferred to the steel through its bond with the mortar.

OHLER and GOPFERT[46] in 1982, tested a number of reinforced prisms, of both sand lime and concrete masonry, constructed with two types of mortar. The prisms were 1.75 m in height and had a slenderness ratio of 7.3. Horizontal reinforcement was placed in every bed joint and consisted of either 6 mm diameter, rectangular stirrups, 6 mm diameter hooped stirrups or 3 mm diameter mesh. The results showed that mesh reinforcement in sand lime brickwork had the greatest effect on the strength enhancement of the prisms, and was some 24% higher than when unreinforced. The

reinforcement was found to be less effective in increasing the strength of prisms made of concrete blocks. One of the advantages of reinforcing the mortar joint was the change in the mode of failure of the prisms to be more ductile and for the tendency of the failure to be more localized.

ELTRAIFY[47] in 1983, presented an experimental study of columns constructed with half scale brickwork subjected to an axial load and bi-axial bending moments and a theoretical study which discusses the mathematical formulation leading to a computer program which enables a comparison to be made between a more exact theory with approximate methods developed originally for reinforced concrete. The theoretical study also includes the case of uniaxial bending.

To limit the number of factors affecting the capacity and behaviour of brickwork columns the author decided to use one type of brick, mortar and grout. The bricks used were half-scale bricks of 110.2 x 53.4 x 32.2 mm average dimensions with 43.2 N/mm^2 average compressive strength. The mortar mix 1:0.25:3 (cement: lime: sand) was used throughout the experimental investigation. The grout mix 1:0.1:3:2 (cement: lime: sand: gravel) was used with high W/C ratio to allow the grout to be poured down the small core of the column. The average cube compressive strength of the grout was 17.6 N/mm^2. Two type of reinforcement with different characteristic strengths of 250 and 460 N/mm^2 was used.

The columns tested were of 283 x 168 mm cross-sectional area with slenderness ratio ranging from 18.0 to 20.0. The steel rig used to test the specimens is shown in Fig. 2.13. The axial force was applied to the columns by hydraulic jack fixed to the steel frame at the top end. Whereas the flexural force was applied using two hydraulic

tension jacks. The axial force was applied in small increments up to a certain level of thrust and was then kept constant. The flexural force was then applied in increments until failure occurred.

The experimental results showed that the mid height moments were larger than the end moments. The reason for this finding, as denoted by the author, was the lateral deformation of the specimens after the bending moments were applied. Ratios of the mid height moments to the end moments of up to 2.6 were observed for the bending about the weak axis and up to 1.2 for bending about the major axis.

The theoretical part of the investigation was commenced to determine the strength of slender columns subjected to both axial compression and bi-axial bending. In this theoretical study two types of non-linearities were considered:

1. Material non-linearity; caused by the non-linear behaviour of the materials used.

2. Geometrical non-linearity; caused by the lateral deformation of the slender column.

These two types of non-linearities were used to determine the ultimate strength, strain and curvature distribution in a cross-section subjected to axial compressive force and bi-axial bending moments.

The theoretical procedure described by the author was very tedious, if not impossible, to be performed by hand calculations. So the author presented a computer program to carry out the iterative processes needed to solve the problem.

Using the computer program the author presented the M_x - M_y interaction diagrams for a typical rectangular section (Fig. 2.14). For these interaction diagrams the author assumed that the grout and brickwork have identical stress vs strain characteristics. The factors of safety used in the derivation were 2.5 and 1.15 for the brickwork and steel respectively.

On the effect of dividing half the column length into number of sections ranging between 4, 6 and 8. The theoretical results showed that varying the number of sections from 4, 6 and 8, has little effect on the ultimate moments. So the author decided to use four sections for deriving the bi-axial charts.

On the effect of slenderness the theoretical results showed that the ratio of the mid height moments to the end moments was greater about the minor axis, which coincided favorably with the experimental results, therefore the author suggested that the ultimate failure is expected to occur about this axis.

A parametric survey was carried out to study the effect of using different stress vs strain relationship on assessing the strength of sections subjected to bi-axial bending. Three types of stress vs strain relationships were used in the survey (i) linear, (ii) parabolic without a falling branch and (iii) parabolic with a falling branch. The ultimate compressive strain was assumed to take three values of 0.002, 0.003 and 0.004, giving the total of nine different stress vs strain curves used in the survey.

The results obtained showed that the ultimate axial force increased from type (i) to (ii) by an amount ranging from 12% to 20% as the eccentricity increased from 0.05t to 0.2t. Also between type (ii) and (iii), there was an

increase of 4% to 10% as the eccentricity increases. The main reason for the difference in the axial force was the increase in the area under the stress-block as the stress vs strain relationship changed from type (i) to (iii). The difference decreases with an increase in the ratio of reinforcement. This was caused by the increase in the neutral axis depth as the stress vs strain relationship changed from type (i) to (iii), which resulted in changing the lever arm for the three curves. So the bending moments were increased whilst the curvatures were decreased from type (i) to (iii).

As the ultimate strain increased from 0.002 to 0.004, the axial load increase from 1% to 8%. This percentage was increased with increase in eccentricity and amount of reinforcement. The main reason for the increase in axial load as the ultimate strain increase from 0.002 to 0.004 was the ratio of vertical reinforcement.

Based on the results the author suggested a modified CP110 approach which allows the derivation of bi-axial charts for different axial forces. Knowing the values of N_u, M_x and M_y, the area of the reinforcement needed can easily be found by selecting the appropriate design chart and is given by the intersection of M_x and M_y without going into any trial areas as adopted by CP110.

The author presented a comparison between the different methods used to determine the ultimate strength and deflection of brickwork columns subjected to axial compression and bi-axial moments. The results of the comparison showed that the 0.002 value for the ultimate strain predicts the ultimate moments very closely giving an average observed moments-to-theoretical moments of 1.03. The same results was found when the 0.002 value used to predict the deflection.

The overall conclusion made from the comparison analysis was that the modified CP110 approach can be used as alternative to the iterative approach and will give results which are conservative. With the modified approach either the parabolic or the rectangular stress-block could be used but the results showed that the maximum stress of the rectangle should be $0.3f_k$.

More recently EDGELL and TEMPLETON[48] in 1985, reported on the results of storey-height axially loaded brickwork masonry columns, 327 mm square, (i.e one and a half bricks); with the central hole, half a brick square, left unfilled. Rectangular stirrups, 6 mm diameter, were chosen, with the ends lapped 100 mm. Other types of reinforcement were considered as the programme developed, e.g expanded metal or circular stirrups. Two types of brick, of low and high strength were used with a 1:0.25:3 mortar. In the initial analysis, to determine the strength enhancement available with different distributions of reinforcement, a standard stirrup, 300 mm square, fabricated from 6 mm diameter steel, was incorporated in every 1st, 2nd or 4th course of both low and high strength brickwork columns. Two additional columns with welded rectangular stirrups every fourth course were also constructed. The results showed that useful strength enhancements of 31.2% and 20% for the low and high strength bricks respectively, compared to unreinforced columns were obtained when rectangular stirrup reinforcement was incorporated in every fourth course. Placing the stirrups in every fourth course was also considered to be more economical and interfered little with the building sequence. Noticeable differences were obtained in the modes of failure of columns reinforced with rectangular stirrups compared to those of unreinforced columns. Unreinforced columns failed by splitting at the perpendicular joints over the full height of the column to form four distinct "walls", the column completely

disintegrating at ultimate load. Reinforced columns, on the other hand, failed by the spalling of the brickwork outside the stirrups. In general a degree of structural integrity remained at failure. The results of tests using different types of bed joint reinforcement showed that a strength enhancement of almost 35% was achieved with columns containing hopped stirrup reinforcement. Those columns containing expanded metal (31.2%) and 50 mm square mesh (18.7%) reinforcement also had much higher strengths compared to the unreinforced column.

The authors observed a marked difference in the mode of failure of the columns containing mesh and expanded metal from those of unreinforced columns and those columns containing stirrup reinforcement. Numerous vertical cracks appeared across the width of the columns containing expanded metal and 25 mm mesh reinforcement. The column containing hopped stirrup reinforcement failed by spalling of the brickwork outside the stirrups leaving a clearly defined circular "core" of brickwork.

2.3.2 Blockwork Masonry Columns

SHANK and FOSTER[49] in 1931, tested unreinforced concrete blockwork pilasters subjected to eccentric loads. The variables studied included concrete block type, cross-section area and pilaster height. The results showed that the pilaster strength was half the unit strength. Furthermore, the pilaster strength was inversely proportional to block absorption and directly proportional to the modulus of elasticity.

FEEG et al[50] in 1979, at the University of Alberta, tested thirty-seven reinforced blockwork masonry columns under concentric load. The research programme was to

determine the effects of reinforcement detailing on the strength and behaviour of the columns. Short columns were tested to eliminate the effect of slenderness ratio. All columns were of 400 mm nominal cross-section and 1.44 m high. Thirty-four columns were constructed using 400 x 200 x 200 mm lightweight plain corner blocks with average strength on the unit net area of 17.03 N/mm^2. The column cross-section was composed of two blocks laid in running bond. Another three columns were built using 400 x 400 x 200 mm single core lightweight autoclaved pilaster concrete block units, with an average unit net area strength of 16.89 N/mm^2. Face-shell bedding was used and a mortar joint thickness of 10 mm was maintained throughout. A mortar mix having volume proportions of 1:0.5:4 (cement: lime: sand) was used with an average compressive strength of 12.82 N/mm^2 when cured under wet burlap, and 4.48 N/mm^2 when cured under laboratory conditions. Columns were filled with grout having volume mix proportions of 1:3:2 (cement: sand: aggregate), and an average cylinder compressive strength of 18.48 N/mm^2. The range of percentage of vertical reinforcement used in the study was 0.7% to 1.3%. Percentages larger than 1.3% were not feasible for this cross-section due to placement difficulties. All vertical reinforcement was placed coincident with a core centroid. The block unit thickness restricted the placement of horizontal reinforcement to a spacing of 200 mm. On the other hand, the mortar joint thickness restricted the size of tie reinforcement to be placed in the mortar joint. Tie diameters used in this investigation were 3.77, 4.76 and 6.35 mm.

The variables investigated were as follows:

1. Tie diameter and tie location within the mortar joint: Either in contact with the vertical reinforcement or in the mortar joint between the block outer shells.

2. The percentage of vertical reinforcement: Reinforcement areas varied between 0.7% to 1.3% of the column cross-sectional area.

3. Vertical reinforcement distribution: Columns with identical percentages of vertical reinforcement, but with different bar sizes were compared.

4. Yield strength of vertical reinforcement: 275 and 415 N/mm^2.

The test results showed that the behaviour of all the columns was essentially elastic for loads up to approximately 75% of the ultimate load. Strain measurement in the vertical reinforcement exhibited load vs strain relationships similar to the load vs deformation relationships of columns. Three modes of failure were observed:

1. Overall vertical splitting of the column.

2. Simultaneous crushing of the masonry and the buckling of the vertical reinforcement within the tie spacing.

3. As (2) but buckling was not confined to within the tie spacing.

The average modulus of elasticity was found to be approximately 800 times the masonry prism strength. The vertical deformation of the column doubled with the addition of grout and was increased further in the presence of tie reinforcement. The vertical deformation of the column increased with the addition of vertical reinforcement, but showed no definite trends for variations in the percentage of vertical reinforcement. Increasing the tie diameter increased the strength of the column compared

to columns with no ties. This was also accompanied by a decrease in the amount of vertical cracking at failure. No significant difference in strength was observed between columns having ties in contact with the vertical reinforcement and those which did not, although tie strains were larger for ties located in the mortar joint. The results also showed that the vertical reinforcement contributed its full yield strength to the strength of the column, and that column strength decreased as bar diameter increased.

It was further observed that the grout penetrated and fully filled the horizontal space between courses as a result of face-shell bedding, but was unable to fill the vertical space between masonry units. These planes of inherent weakness contributed to the vertical splitting of the columns when loaded. Failure to remove mortar dropping from the interior base of a column resulted in decreasing the column strength. Rust was noted on ungalvanized ties after failures of columns where they had been placed in the mortar joint. Small amounts of shrinkage cracking occurred in wall unit blocks, while in the columns made of pilaster units, larger amounts of shrinkage cracks were noted.

Unfortunately, FEEG in his study did not present any equations to predict ultimate load or deformation for the blockwork masonry columns.

SALIM[51] in 1980, tested under axial load blockwork masonry prism with helical confinement reinforcement at the core. The test specimens were constructed from concrete block units, 200 mm square and 200 mm high, with a net average strength of 36.0 N/mm^2. The average compressive strength for the mortar and the grout used were 23.7 N/mm^2 and 21.1 N/mm^2 respectively. The units were horizontally laid and the masonry prisms were built to have flush mortar

joints of nominal thickness, 9.5 mm. After construction, helical reinforcement, consisting of mild steel wire of 5.2 mm diameter with a core diameter of 108 mm centre to centre, was placed inside the prism and the core was grouted.

The observed mode of failure for the ungrouted prisms was tensile splitting which was initiated in the centre concrete block. The mode of failure for the grouted prisms (splitting of the units and compressive failure of the core) was similar to that of the ungrouted, but not as explosive. Cracking started at 70% to 75% of the ultimate capacity. Cracking of the prism reinforced with confinement wire started from the top or the bottom blocks at about 45% to 55% of ultimate load. The sudden failure was replaced by a more ductile failure. An increase in the compressive strength of the prism of between 30% and 38% was achieved by introduction of helical confinement reinforcement compared to unreinforced prisms.

The author concluded that the failure mechanism of blockwork masonry prisms was dependent on the elastic and inelastic properties of the jointing, grouting materials and the unit masonry.

More work was carried out on blockwork masonry columns at the University of Alberta by STURGEON et al[30] in 1980. Nine block high, short columns were constructed using 400 x 400 x 200 mm single core pilaster units and tested to failure. Some of the columns were tested under concentric load and some with eccentricity varying from 0 to 1/3 times the lateral dimension of the column. Full mortar bedding was used and a joint thickness of 10 mm was maintained. Nominal column dimensions were thus 1.8 m by 400 mm square. Variables considered in the materials or method of construction were:

1. Percent and grade of vertical reinforcement.

2. Grout compressive strength and slump.

3. Lateral tie details.

Three percentages of longitudinal steel, 0.76, 1.3 and 2.6 based on gross cross-sectional area of the column, were used. Where longitudinal steel was required, ties were wired directly to the steel, and all reinforcement was then placed in the column as a unit. Several columns were constructed without vertical reinforcement, but with grout and lateral ties. In these cases, the horizontal reinforcement was placed within the mortar joint of the cross-section. All lateral ties were fabricated from 6 mm diameter plain steel. Five types of lateral tie were used in the programme depending on the diameter of the longitudinal reinforcement. Two longitudinal reinforcement steel grades, 400 N/mm^2 and 600 N/mm^2 yield, were employed. five low slump (100 - 150 mm) concrete mixes with 28 day moist cured cylinder compressive strengths of 38.6, 35.2, 29.0, 17.7 and 10.3 N/mm^2 were selected for this study.

Failure of the ungrouted columns was sudden, complete and explosive. Vertical cracking was initiated at the block face centres at the top of the specimen and propagated down several courses just prior to failure. Grouted columns containing no lateral reinforcement showed a similar mode of failure to ungrouted columns. In this mode, vertical splitting of the shell originated at block face centres in the upper courses well in advance of column collapse. Subsequent loading elongated and widened these cracks until overall splitting of the shell and crushing of the concrete core occurred. Grouted columns containing lateral reinforcement in the mortar joints displayed a slightly different behaviour. Vertical cracking prior to failure

originated in the upper courses at the column corners rather than at block centres. In addition, the lateral ties tended to confine the block shell and prevent explosive spalling of the shell at failure. In general, for all the grouted, unreinforced columns tested, the shell-core interface bonding in the failure zone was completely broken, and the masonry shell could be easily removed in order to view the concrete core. Reinforced columns constructed with lateral ties having 90 deg. hooks and 65 mm extensions was peculiar only to those columns with 0.76% vertical reinforcement. Failure of these columns was characterized by simultaneous splitting of the shell, crushing of the core, and buckling of the vertical reinforcement between tie spacing. The ties provided adequate support for the vertical reinforcement and prevented buckling from occurring over more than one course.

In contrast, these ties did not adequately restrain buckling for higher percentages of vertical reinforcement. In these columns the tie hooks were pulled to form an angle of about 120 deg. and in extreme cases a number of tie hooks pulled out completely allowing bars to buckle over as many as five courses. This resulted in rather explosive failures for these columns regardless of concrete core strengths. Columns constructed with lateral ties using 135 deg. hooks and 100 mm extensions showed that these ties did not pull out even for the higher percentage of longitudinal reinforcement, and restricted buckling to the lateral tie spacing. Because of this confinement, failure was not as sudden and distress to the core and shell was not as extensive in the failure zones. In the case of all reinforced columns, cracking originated at the column corners in the upper courses in advance of column failure and extended down vertically as loading continued. As a result of these observations, the authors suggested the

following tie details for masonry columns:

1. For concrete block masonry columns constructed with 400 x 400 x 200 mm pilaster units, the use of 6 mm diameter plain steel for fabrication of lateral ties should be avoided when possible. These ties do not adequately contain core expansion. It is recommended that at least 10 mm diameter deformed lateral ties should be used for 32 mm diameter or smaller longitudinal bars as stated by the ACI 318-77 for reinforced concrete.

2. If it is necessary to use 6 mm diameter plain bars, it is recommended that 135 deg. bends plus a minimum of 100 mm extensions be employed. Alternatively, if 90 deg. bends plus 65 mm extensions are used, the overlapping extensions should be tack welded to prevent pulling.

3. A vertical spacing of 200 mm, is not sufficient to prevent buckling of the vertical reinforcement before yield is attained and it is recommended that this spacing be decreased for masonry columns constructed with units which permit a reduced spacing.

4. It is suggested that the lateral tie hooks should be positioned at different corner bar, on a rotational basis during construction.

The test results for the concentrically loaded columns showed that the increase in ultimate strength of the column is directly proportional to increase in the concrete strength. This was formulated by the authors by the following expression:

$$P_{uc} = [0.85\ f'_c\ A_c + 0.70\ f'_{mpn}\ A_{sh}]/1000 \qquad ...(2.28)$$

Where

A_c Core area of block unit, mm^2

A_{sh} Masonry shell area, mm^2

f'_c Standard concrete cylinder compressive strength, N/mm^2

f'_{mpn} Plain prism net area compressive strength, N/mm^2

P_{uc} Column ultimate load, KN

The introduction of lateral reinforcement resulted in an increase in the ultimate strength of the column by 8% to 28%. This additional strength increment was not considered in the above formula. Vertical reinforcement, on the other hand, resulted in a reduction in the load contribution of the block masonry shell. However, the load contribution of the vertical steel exceeds this decrease, and the net effect is to increase the ultimate load of the column. The yield strain in the longitudinal reinforcement was reached in only one column and the ultimate strain appears to be a constant which is independent of the concrete control cylinder strength and the percentage of vertical reinforcement, with a mean value of about 0.00142. The contribution of vertical reinforcement to the ultimate strength of masonry columns was expressed as:

$$P_s = E_s A_s/700 \qquad \ldots(2.29)$$

Where

A_s Cross-sectional area of longitudinal reinforcing steel, mm^2

E_s Elastic modulus of steel reinforcement, KN/mm^2

P_s Load carried by vertical reinforcement, KN

The empirical formula suggested by the authors to predict the ultimate strength of a concentrically loaded

short reinforced concrete block masonry column fabricated with materials and dimensions similar to those used in his study is as follows:

$$P_{uc} = [0.85\ f'_c(A_c - A_s)]/1000 + E_s\ A_s/700 \quad \ldots(2.30)$$

Eqn. 2.30 was considered by the authors to provide a conservative strength estimate for laterally reinforced columns fabricated with stiff well developed lateral ties and for columns reinforced with both lateral ties and Grade 40 longitudinal steel bars.

Alternatively, the authors suggested that the ultimate strength of the column may be conservatively predicted by the addition of the steel term in Eqn. 2.30 to the failure load of experimental prisms constructed with the same materials used in the column. This method was thought to give a more accurate value than that given by Eqn. 2.30.

Eccentrically loaded columns showed two different modes of failure. The first mode was peculiar to columns with load eccentricities of t/12 and t/6, regardless of concrete strength, grade or percentage of vertical reinforcement. This mode was characterized by the explosive removal of the column block shell on the compression face, with subsequent crushing of the concrete core and buckling of the vertical compression longitudinal steel. The second mode of failure was encountered with columns loaded with a eccentricity of t/3. These columns failed by local crushing either in the bottom or the top course. The reason given by the authors for this type of failure was that the loading plates for the larger eccentricities did not provide an adequate transfer of the load to the tension face of the column.

The ultimate strength design procedure suggested by

the authors for eccentrically loaded masonry columns was similar to the one suggested by the ACI 318-77 for eccentrically reinforced concrete columns. However, it is necessary to neglect any contribution of the block shell and the masonry column was analysed as though it were a reinforced concrete column with strength and dimensions equal to those of the masonry core.

Although high slump concretes produced extensive shrinkage cracking in the upper region of the core, tests showed that they do not have a detrimental effect on the structural performance of masonry subjected to concentric compression. Failures occur in the upper regions of both concentrically and eccentrically loaded masonry columns since bleeding and segregation during pouring and vibration produce a weaker concrete in the upper core.

AL-SARRAF, FAIYADH and KHALAF[52] in 1986, tested short blockwork columns under axial load to failure. The columns were divided into two series, one-block and two-block cross-sections. The percentage of vertical reinforcement varied from 0.6% to 4.26%. Two different lateral reinforcements, 6 mm diameter plain and 10 mm diameter deformed bars were used. All columns were 1.27 m high, constructed of 400 x 200 x 200 mm low strength (9.90 N/mm^2) 2-core concrete hollow blocks. An average mortar strength of 13.65 N/mm^2 and concrete infill strength of 17.25 N/mm^2 respectively was used to construct and fill the columns.

The results showed that at 40% to 50% of the ultimate failure load, cracks started at different locations in the columns. As the applied load was increased, the cracks continued to propagate in both the mortar and the blocks. Failure was attained by crushing and outward deformation of the masonry shell accompanied by outward buckling of the vertical reinforcement between the lateral ties. The core

of the column however remained in position with high internal disruption. The results also showed an approximate reduction in the $P_{(Tested)}/ P_{(Calculated)}$ ratio of 40% as between columns constructed with 6 mm diameter plain and 10 mm diameter deformed tie bars respectively. It was also shown that columns with three bars in a bundle give much lower $P_{(Tested)}/P_{(Calculated)}$ ratios than the two bar-bundled columns. The authors concluded that a design method similar to the American Standard (ACI 318M-83) for reinforced concrete can be used to predict the capacity of an axially loaded reinforced blockwork masonry column by substituting f'_m (ultimate compressive strength of blockwork masonry) in place of 0.85 f'_c (ultimate compressive strength of concrete) in the design formula. The value of f'_m was derived from the American Code for Masonry Structures (ACI 531R-79) using both methods A (relating the masonry strength to the unit strength and type of mortar) and B (relating masonry strength to prism strength). Using either value in the design formula leads to the evaluation of the anticipated failure load with a high margin of safety, on average, 16% to 19% respectively higher than that predicted theoretically.

The minimum size of lateral steel ties used for reinforced masonry columns should not be less than 10 mm in diameter which is exactly the same value recommended by the ACI Standard for reinforced concrete. It was also proposed that the range of minimum to maximum percentage of vertical reinforcement as recommended by the ACI for ordinary reinforced concrete be used for reinforced blockwork masonry columns. However, due to difficulties in the compaction process for the 2-core concrete block, it is practical to lower the 4% maximum steel ratio for concrete to 3% for blockwork masonry.

2.4 SUMMING UP OF PREVIOUSLY PUBLISHED WORK

As in some situations the blockwork masonry is subjected to horizontal forces in its own plane e.g. the compression zone in a reinforced blockwork masonry beam, or masonry wall accidentally or during an earthquake. It seems that some codes and standards have no clear indications to the difference in strength of the unit or the prism when compressed in a direction parallel, instead of normal, to the unit bed face.

The present study provides a comprehensive experimental and theoretical investigations to the difference in compressive strength and behaviour between blockwork masonry elements subjected to axial forces normal and parallel to the unit bed face and suggest methods to determine the ultimate compressive strength of blockwork masonry, f'_m in these different directions.

In the previously published work on blockwork masonry prisms some researchers suggest the testing of 3-course high half-block prisms instead of full-block prisms to determine f'_m.

In the present study the reasons for the difference in the compressive strength and behaviour between full and half-block prisms were discussed and the effects of the aspect ratio (l/t) and the difference in the mortar bedded area between the full and half-block prisms were investigated experimentally and theoretically.

In the previously published work it seems that there is some doubt about the reasons for the reduction in the compressive strength of blockwork masonry prisms with height. Some researchers related the reduction to the effect of core shape (i.e. the tapering of the block

shells) and to the texture of the interior face of the block cores. These excessive cross-sectional changes restrict the shrinkage settlement which occurs over the full height of the grouted column and results in plastic cracking as shrinkage proceeds. The severity of the plastic cracking increases with prism height.

In the present study different tests were set up to investigate the nature of the shrinkage cracks in blockwork masonry prisms using mixes of different slumps. Also investigated is the effect of the cohesion bond between block and concrete infill on the compressive strength of blockwork masonry prisms.

Most of the previous theoretical works carried out on blockwork masonry advocate the use of linear analysis. The present investigation pointed out the importance of using the material non-linear properties in the analysis of blockwork masonry assemblage.

In the present study an attempt was made to determine a new formula for shot term static modulus of elasticity of unfilled and filled blockwork masonry assemblage.

Due to the limited number of work carried out on axially loaded blockwork masonry columns using the 2-core hollow blocks. The present study investigate the effects of the presence of lateral ties and vertical bars on the compressive strength and behaviour of blockwork masonry columns and suggest new methods of estimating their ultimate strength.

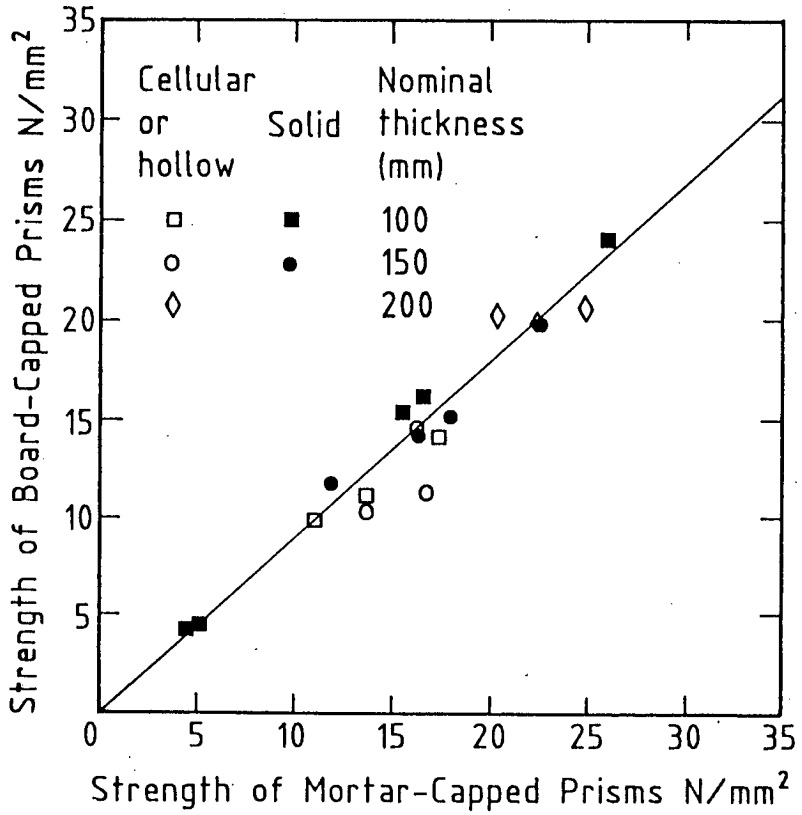

Fig. 2.1 - Relationship between indicated strength for mortar and board-capped prisms tested dry.

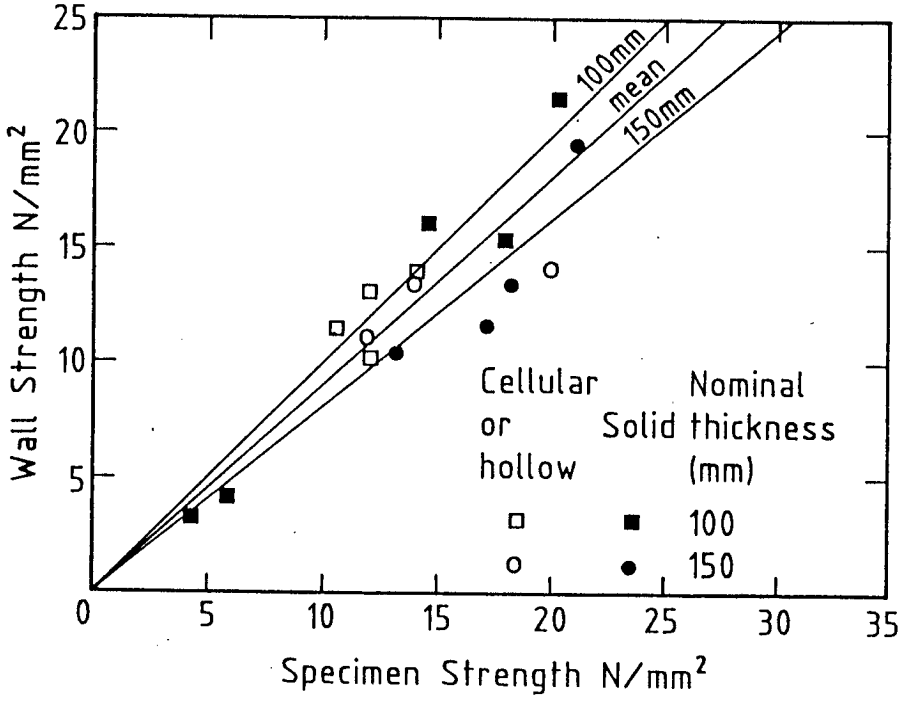

Fig. 2.2 - Wall strength against specimen strength for mortar-capped single blocks tested wet.

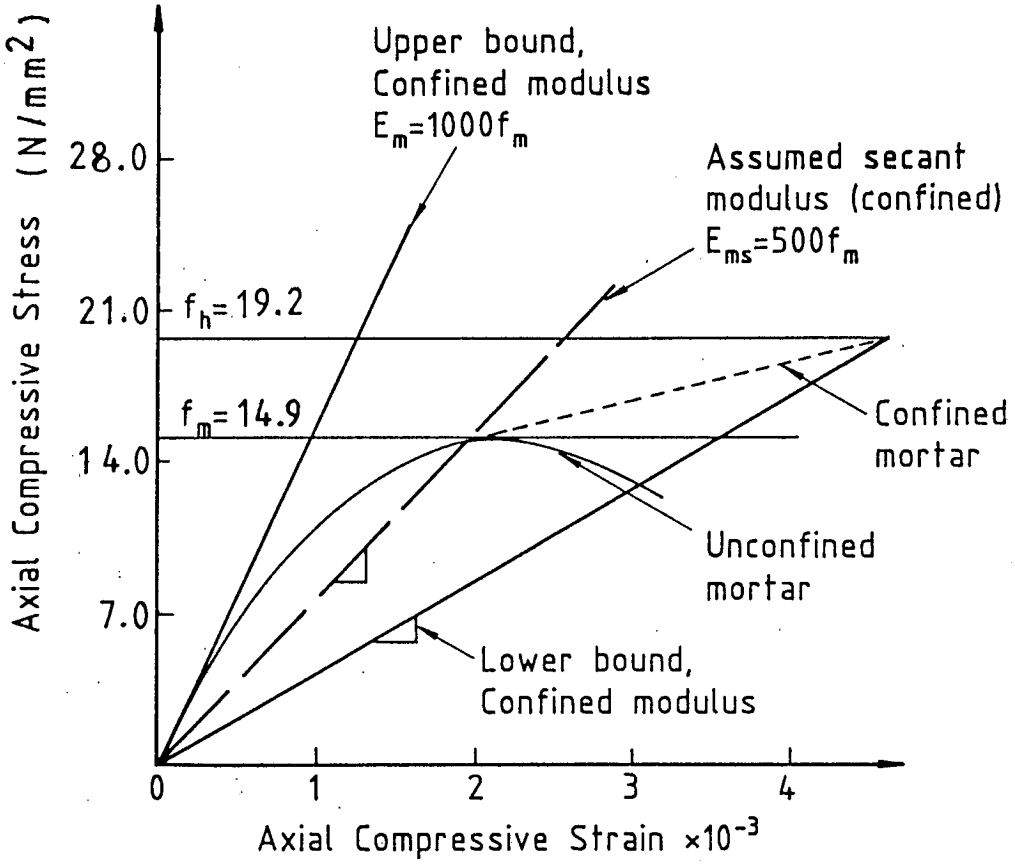

Fig. 2.3 - Idealised stress vs strain curve for mortar.

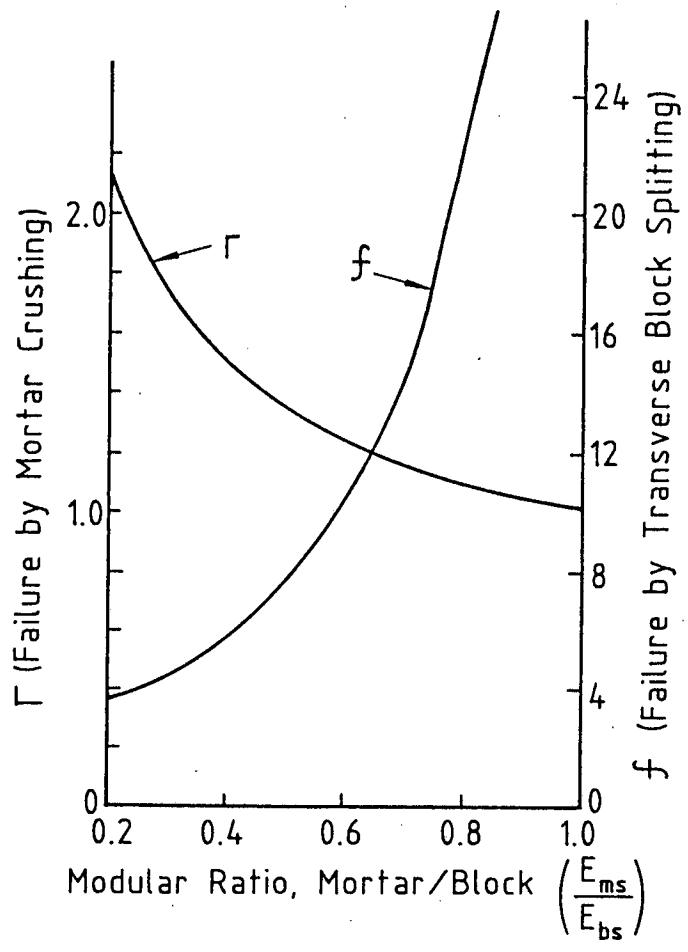

Fig. 2.4 - Failure curve for hollow prisms.

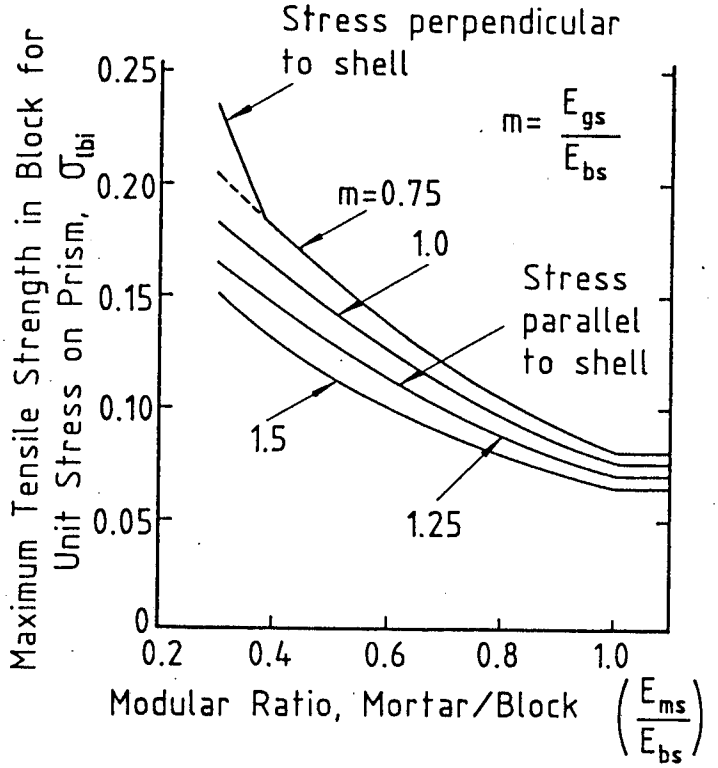

Fig. 2.5 - Failure curve for grouted prisms as governed by block splitting.

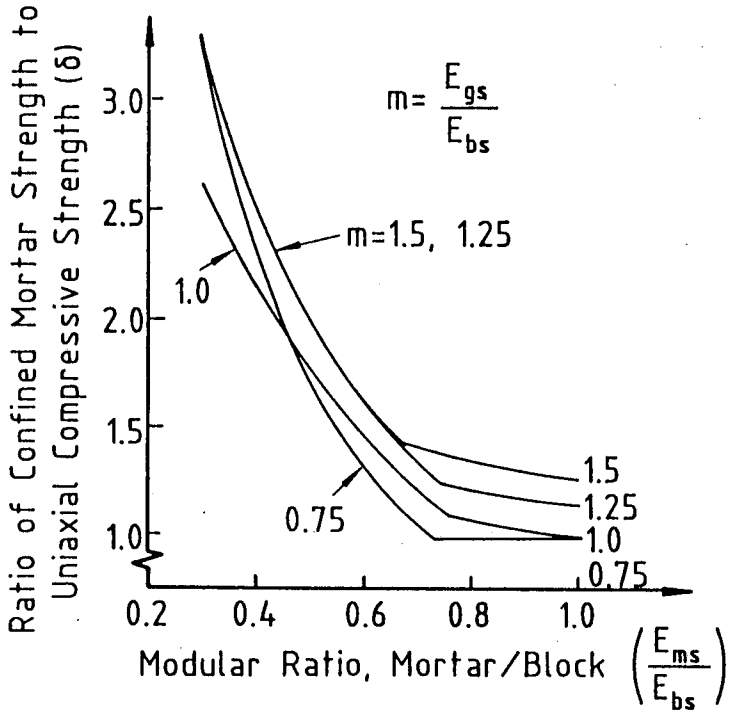

Fig. 2.6 - Failure curve for grouted prisms as governed by mortar crushing.

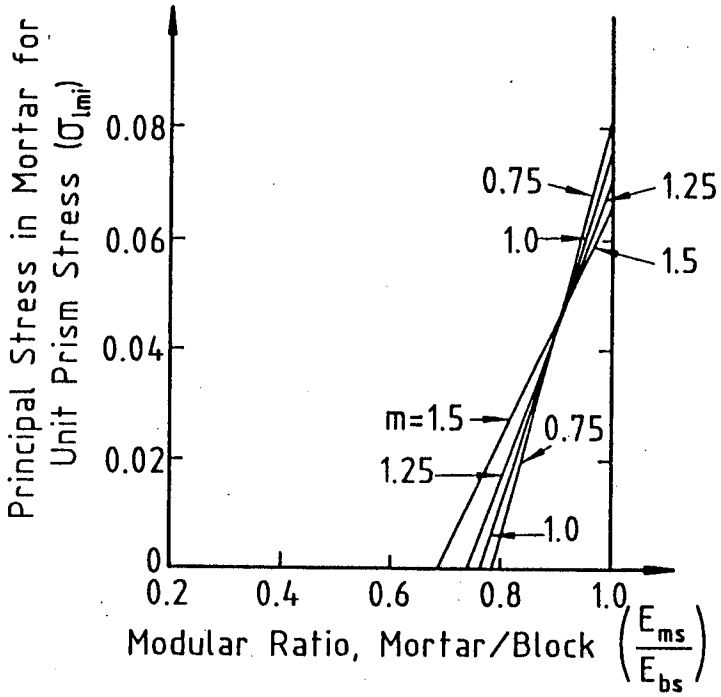

Fig. 2.7 - Failure curve for grouted prisms as governed by mortar splitting.

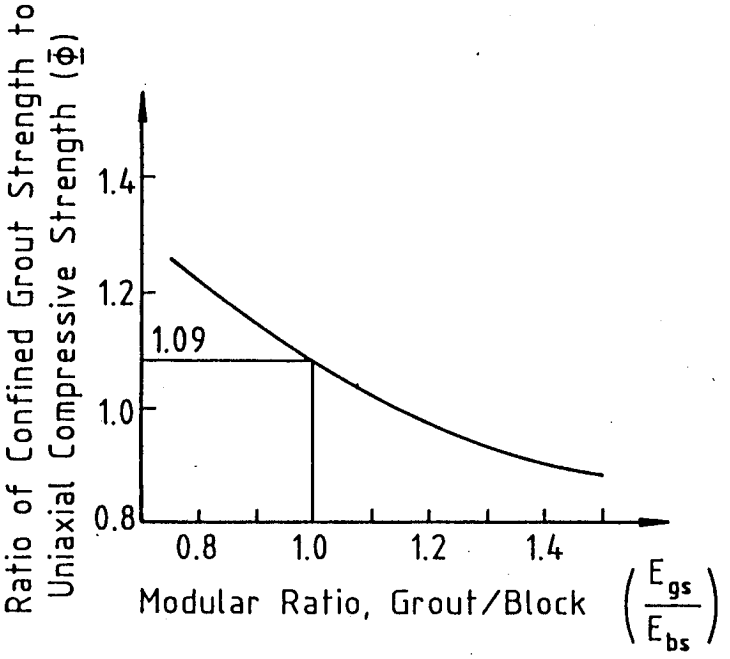

Fig. 2.8 - Failure curve for grouted prisms as governed by grout crushing.

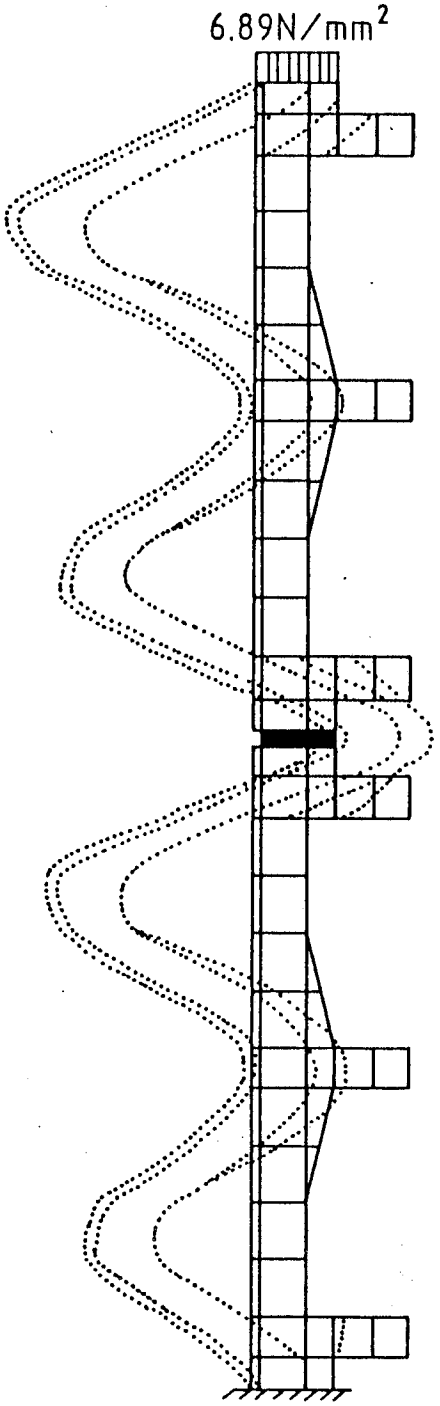

Fig. 2.9 - Magnified deflected shape.

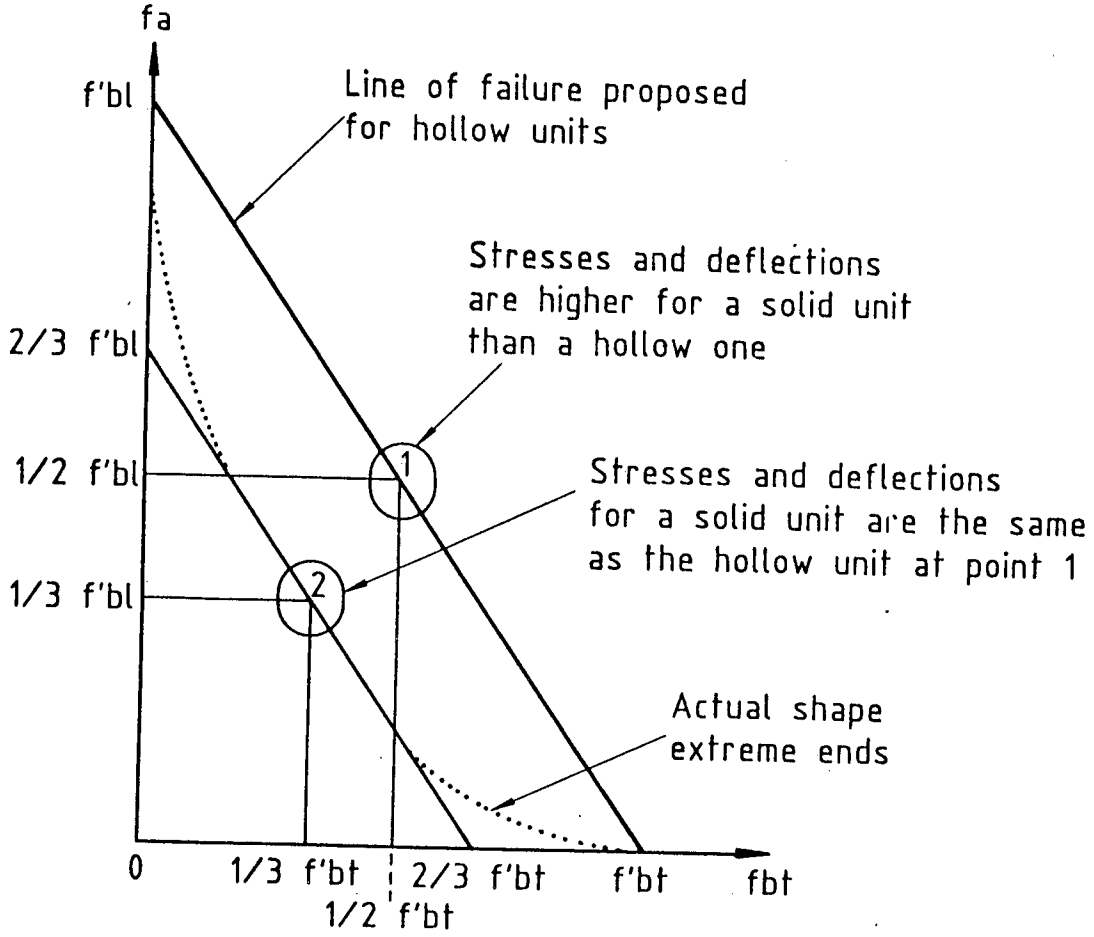

Fig. 2.10 - f_a vs f_{bt} for solid and hollow units with exactly the same properties.

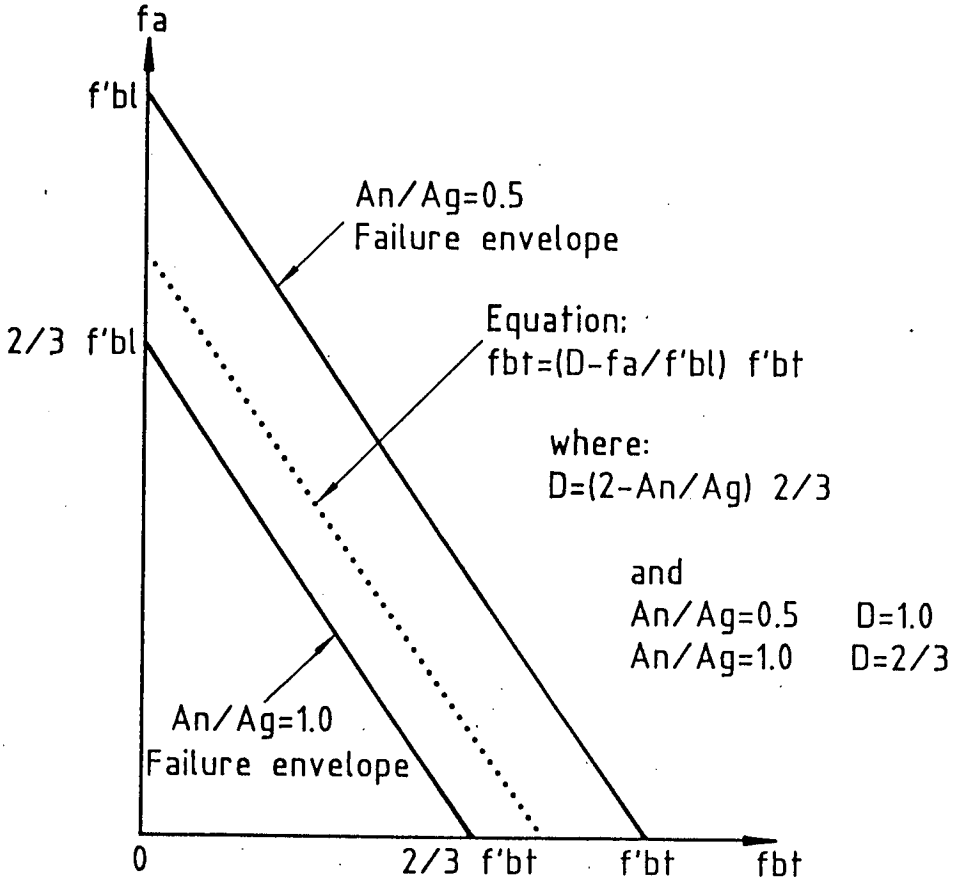

Fig. 2.11 - Proposed failure envelope for masonry units with varying A_n/A_g.

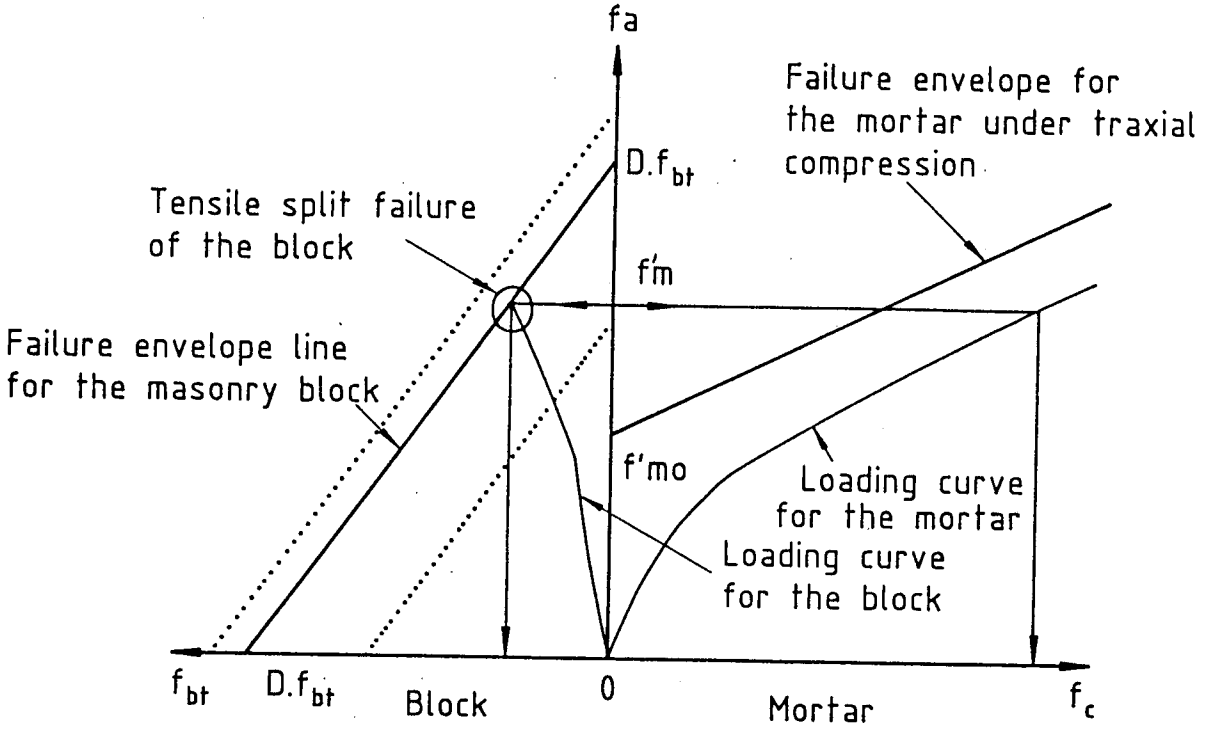

Fig. 2.12 - General behaviour of masonry prisms under uniform compressive loading.

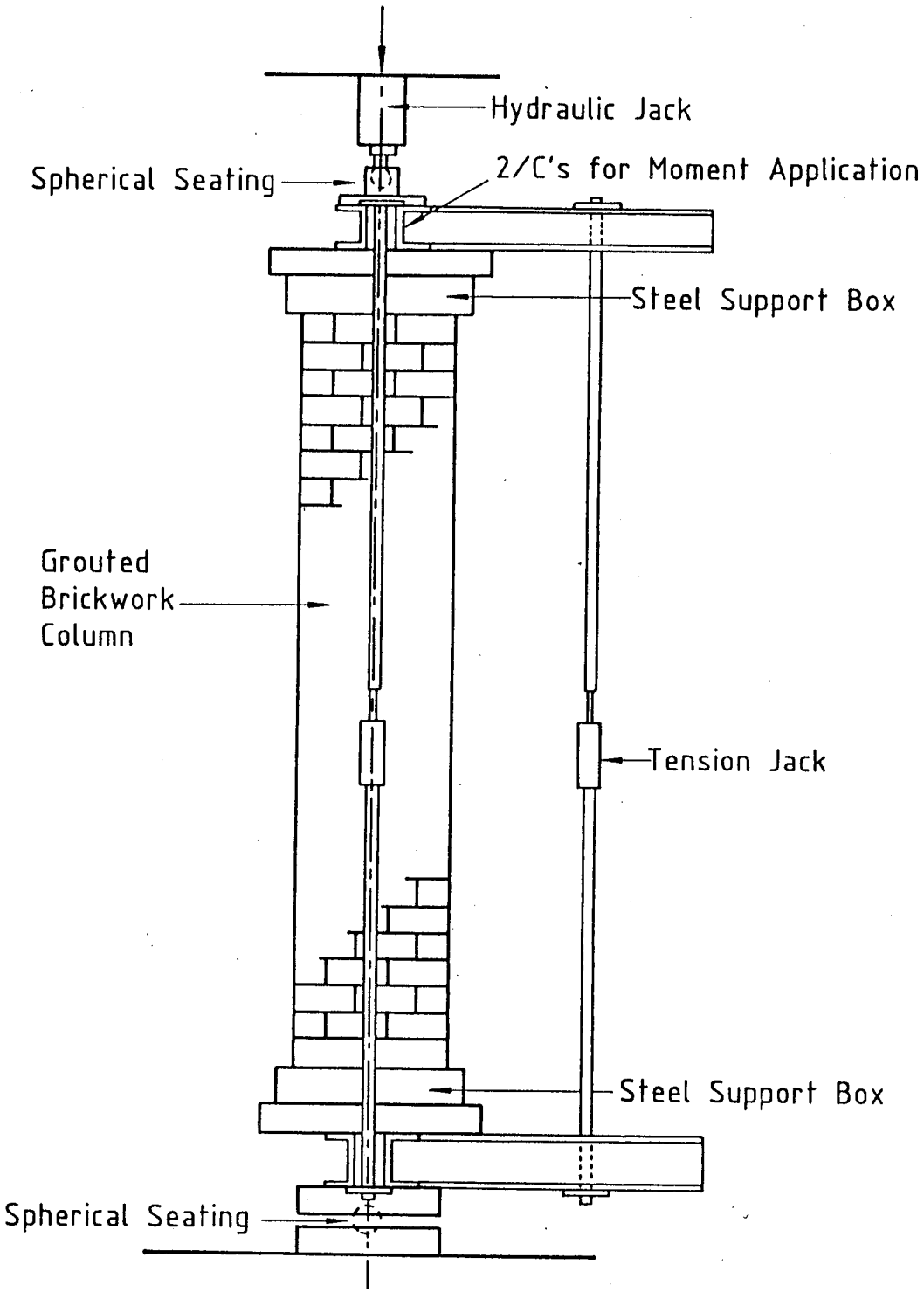

Fig. 2.13 - Steel test rig.

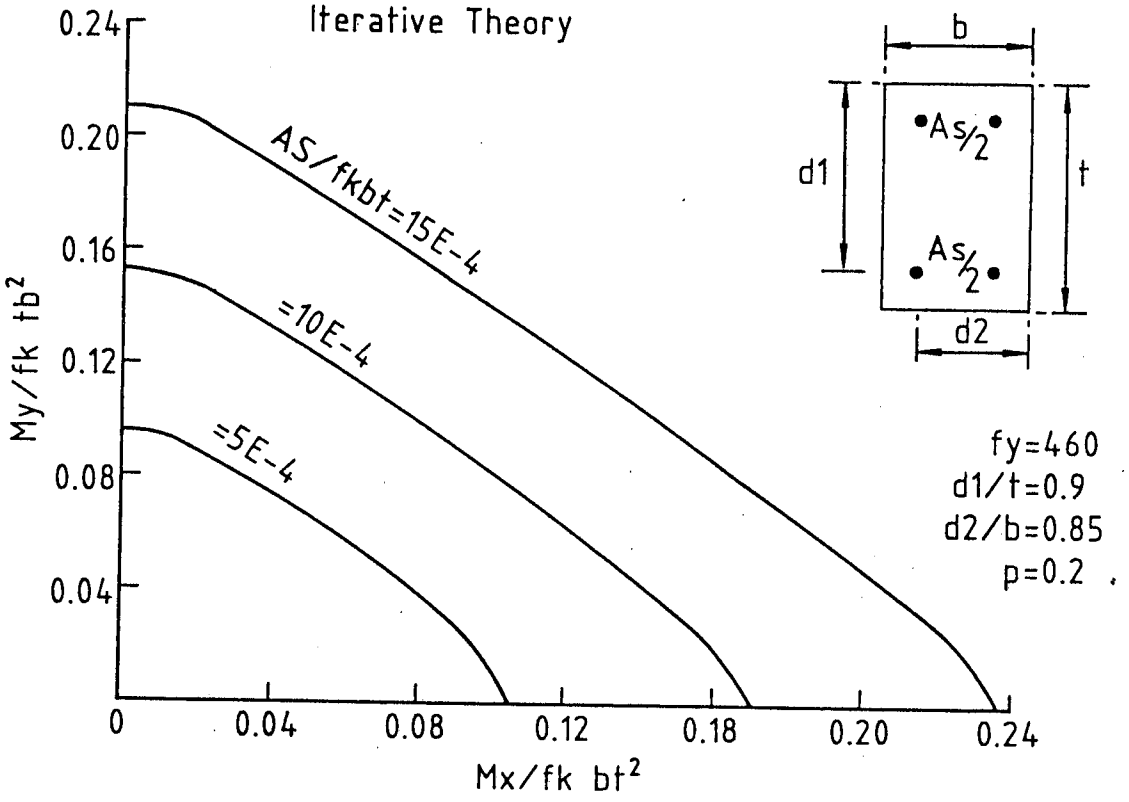

Fig. 2.14 - Interaction diagrams for a typical rectangular section.

CHAPTER 3

MECHANICAL PROPERTIES OF MATERIALS USED IN BLOCKWORK CONSTRUCTION

3.1 INTRODUCTION

This chapter is concerned with the determination of the mechanical properties of all the materials used in the construction and theoretical analysis of the blockwork masonry prisms and columns investigated in this study. The materials involved were concrete blocks, concrete infill, mortar and reinforcement. One type of concrete block, three mixes of concrete infill, three types of mortar and different diameters of plain and deformed bars were used. The chapter also deals with the difference in the compressive strength of unfilled and filled blockwork masonry specimens compressed normal and parallel to the unit bed face.

Reinforced blockwork masonry consists of four component materials, namely the concrete block, concrete infill, mortar and reinforcement. These four materials added to differences in the block shape in the three orthogonal directions gives the masonry non-homogeneous properties compared to those of concrete.

Previous tests[34,36] showed a reduction of at least 29% in unit block compressive strength compressed parallel to the bed face as compared to that compressed normal to the bed face. Some codes and standards[19,20,22] use tables or graphs, relating the ultimate compressive strength of blockwork masonry f'_m, to the unit block strength and the type of mortar.

This raises the question of the direction in which the

unit block should be tested in order to determine f'_m. The direction in which the specimens should be tested is particularly important in areas or zones where the masonry element is under large horizontal forces applied in a direction parallel to the unit bed face. Examples of such situations are the compression zone in a reinforced masonry beam[34,53,54] or part of a masonry wall subjected to horizontal forces in its own plane accidentally or during an earthquake.

In all of the above codes and standards[19,20,22] there is no clear answer or indication as to the differences in strength if the block is tested in a direction parallel to the unit bed face instead of normal.

The British Code of Practice, BS 5628: Part 2: 1985[21], however, recognizes that there maybe a difference in strength as between masonry built with the units compressed normal to the bed face and that in which units are compressed parallel to the bed face. Provision for various types of units is given in paragraph 19.1.1.4 of the code. BS 5628 determines the values of f_k for blockwork masonry from tables (Table 3.1) and graphs, relating the compressive strength of the unit to the mortar type.

In deciding the strength of concrete to be used in filling hollow blockwork masonry, British Standard BS 5628: Part 2: 1985[21] states that when masonry is built with hollow concrete blocks and the vertical cavities are filled completely with in situ concrete, the value of f_k should be obtained as if the blocks were solid provided that the characteristic concrete cube strength of the infill is not less than the compressive strength of the unit blocks, assessed on their net area. The American and Canadian Codes[19,20] both give the same specific condition about grout strength as the British Standard, in that the grout must be

at least as strong as the block.

Previous studies[27,28,29,30,31,32,33,34,35,36,38,71] on blockwork masonry have shown that the deformational characteristics of the concrete infill rather than its strength had a major effect on reducing the compressive strength of filled blockwork masonry prism, compressed either parallel or normal to the bed face, as compared to unfilled prisms.

In the present chapter, the stress vs strain curves, moduli of elasticity and Poisson's ratios for the block, concrete infill, mortar and reinforcement were determined. The difference in compressive strength of unfilled and filled, half and full-block specimens compressed normal and parallel to the bed face was studied. The effect of using different concrete infill mixes on the compressive strength and splitting strength of unfilled and filled blockwork specimens were investigated. The cohesive bond and shear strength between the concrete infill and the block material was also studied.

3.2 EXPERIMENTAL PROGRAMME

This section is divided into two parts. The first part deals with the experimental procedure for preparing and testing all the individual materials used in the construction and theoretical analysis of the blockwork masonry elements investigated in this study. The second part presents the experimental programme followed in preparing and testing the unfilled and filled unit concrete block specimens.

3.2.1 Material Mechanical Properties

3.2.1.1 Concrete block

Fig. 3.1 shows cross-sections of the typical concrete block which has been used throughout the investigation; Table 3.2 summarizes the dimensions of the blocks.

The mechanical properties for hollow blocks were determined by testing three blockwork masonry prisms (Fig. 3.2). Each consisted of three half-block units separated by a 1 - 2 mm dental plaster joint inserted between the half-blocks and also between the machine platens and prisms. This thickness was achieved by mixing the dental plaster with water in a plastic bag to the desired workability. The bags were then placed between the half-blocks and also between the specimen and the machine heads. A spirit level was used to adjust the specimen. Where the testing machine had a spherical head, this was prevented from rotating by using four pieces of wood at the corners of the head. The soft dental plaster was then pressed by the machine to accomplish the desired thickness[55].

Two axis (vertical and horizontal) electrical strain gauges were mounted at mid prism height and on two opposite sides. A computer strain logger was used to record the strain continuously throughout testing and until prism failure.

Unit half-blocks were tested in compression to determine their mechanical properties. Solid full-blocks cast at the same time as the hollow blocks were also compressed parallel to the bed face to compare their mechanical properties with the hollow units. Solid blocks, sawn to the dimensions of a 190 x 190 x 190 mm cube, were tested in compression. The average compressive strength was

then adjusted for specimen size[56] to determine the block material cube strength f_b.

3.2.1.2 Concrete infill

Three concrete infill strengths were used: low strengths (1:7:2) and (1:5:2), medium strength (1:3:2) and high strength (1:1:2) (cement: sand: aggregate proportions). Rapid hardening cement was used for the infill for the specimens compressed parallel to bed face and ordinary Portland cement for all other specimens. Both types conformed to BS 12: 1978[57]. The concrete infill was batched by volume and mixed to a high slump of 150 mm.

The sieve analyses were performed in accordance with BS 812: Part 1: 1975[58] for the concrete sand and for the 10 mm single size crushed aggregate. The results for the sieve analyses are given in Tables 3.3 and 3.4 respectively, and conform to the requirements of BS 882: 1983[59].

From each concrete batch, three 100 x 100 x 100 mm cubes, and three 200 x 100 mm cylinders were cast with every four to six prisms or columns in accordance with BS 1881: Part 108: 1983[60] and BS 1881: Part 110: 1983[61] respectively. Concrete units were used to form mould for the 184 x 122 x 122 mm block moulded concrete prisms (Fig. 3.3), in accordance with ASTM C 1019 Standard[62], but without using the lining absorbent papers on the face of unit. The mould were stripped 5 - 6 hours after casting which was sufficient time for any water absorption and also to prevent the development of bond between the concrete infill and the blocks. The ratio of volume to surface area of the block moulded prisms was similar to that for the hollow block cores so that the effect of water suction by

the blocks on the concrete infill compressive strength could be assessed. All the control specimens were cured under similar conditions to their companion prisms and columns.

To determine the mechanical properties for the three different concrete infill strengths, specimens consisting of three 100 x 100 x 100 mm steel moulded cubes, separated and capped with a thin layer, 1 - 2 mm, of dental plaster joints, were prepared by the same method as that used to determine the mechanical properties of the hollow blocks, and tested in compression (Fig. 3.4).

Vertical and horizontal strains were recorded continuously, using a data logger, on two opposite sides. Single steel moulded cubes, cylinders and block moulded concrete prisms were also tested in compression and splitting to compare results and to determine material strengths.

3.2.1.3 Mortar

Three types of mortar were used for the prisms : low strength (1:1:6), medium strength (1:0.5:4.5) and high strength (1:0.25:3) (cement: lime: sand proportions) and only high strength (1:0.25:3) mortar was used for columns. Rapid hardening cement was used to construct specimens compressed parallel to the bed face and ordinary Portland cement for all other specimens. The mortar was batched by volume and mixed to a suitable workability for block laying.

The sieve analysis was performed in accordance with BS 812: Part 1: 1975. The sieve analysis results for the mortar sand are given in Table 3.5, and conform to the

requirements of BS 1200: 1976[63].

Three 100 x 100 x 100 mm cubes and three 200 x 100 mm cylinders from each type of mortar were cast with every four to six prisms or columns in accordance with BS 1881: Part 108: 1983 and BS 1881: Part 110: 1983 respectively. All the cubes and cylinders were cured under the same conditions as their companion prisms or columns.

To determine the mechanical properties of the three different types of mortar, as for the concrete infill, specimens consisting of three 100 x 100 x 100 mm steel moulded cubes separated and capped with a thin layer, 1 -2 mm, of dental plaster were tested in compression. These were, prepared by the same method used for determining the mechanical properties of hollow blocks. Single steel moulded cubes and cylinders were also tested in compression and splitting to compare results and to determine material strengths.

Two-block prisms were constructed with a 10 mm mortar joint between the blocks to determine and compare the confined vertical stress vs strain curve of a 10 mm joint with values obtained by testing three steel moulded cube specimens or by testing mortar cylinders. After construction, the prisms were cured under polythene sheeting for fourteen days. The polythene was then removed and the specimens left for a further fourteen days to cure under ambient conditions in the laboratory before testing.

Electrical strain gauges of 10 mm length were mounted on the mortar joint at two opposite sides of the prism to record the strain for the confined 10 mm mortar joint.

3.2.1.4 Reinforcement bars

The reinforcement used throughout was 6 mm diameter hot rolled plain low yield steel bar and 8, 10, 12, 20 and 25 mm diameter hot rolled deformed high yield steel bars conforming to BS 4449: 1978[64].

A total of three samples for each type of reinforcement were tested in uniaxial tension, in accordance with BS 18: 1971[65], to determine the vertical stress vs strain curves of the steel. The strain was measured using an electrical resistance strain gauges fixed to the bar. Values of the yield strength, yield strain, ultimate tensile strength and elastic modulus are given in Table 3.6.

3.2.2 Concrete Block Specimens

Unfilled and filled half and full-block specimens were tested to failure under axial load applied either, normal or parallel to the bed face. The specimens were filled with one or other of the three concrete infill strengths. Rapid hardening cement was used for filling the specimens compressed parallel to bed face and ordinary Portland cement for other specimens. The concrete infill was batched by volume and mixed to a high slump of 150 mm then placed in the block in two layers. Each layer was hand compacted, using the same steel rod commonly used for compacting and making concrete cubes.

The filled block specimens and all the associated cubes and cylinders were cured under polythene sheeting for seven days in the case of rapid hardening cement and fourteen days in the case of the ordinary Portland cement. The polythene was then removed and all the specimens left

for a further seven or fourteen days, depending on the type of cement used, to cure under ambient conditions in the laboratory before testing.

Prior to testing, all the specimens were capped with a thin layer, 1 - 2 mm, of dental plaster, prepared by the same method used for determining the mechanical properties of the hollow blocks. After the plaster had hardened, some of the specimens were tested to failure without taking any strain measurements. Others were tested to failure and the strain recorded on two opposite sides of the specimen and at different selected locations. The loading rates were in accordance with BS 6073: Part 1: 1981[66].

To study the effect of the concrete infill strength on the block splitting strength, a steel rig (Fig. 3.5) was used, consisting of two semi-circular pieces, and similar to the one used in determining the tensile strength of concrete by cube splitting[67]. The same device was also used to determine the cohesion bond strength between the block and concrete by splitting a two-material specimen (Fig. 3.6) at the interface area. Some of the two- material specimens were tested in compression with a fixed machine head to study the difference in the stress vs strain curves between the block and concrete materials under the same vertical strain.

The shear strength between the block and the concrete was also determined by shearing a two-material specimen at the interface area (Fig. 3.7).

The loading patterns in all the compression tests in sections 3.2.1 and 3.2.2 were in accordance with BS 1881: Part 121: 1983[68] to enable the determination of the static modulus of elasticity for all the specimens tested. Using the above load pattern, strain measurements were recorded

at two stress levels, viz. 0.5 N/mm^2 and one third of the estimated ultimate strength of the specimen. The measurements were then repeated two to three times in a process of loading and unloading. In all the stress vs strain plots reported in this investigation results from the process of loading and unloading were omitted for clarity and only the first cycle of strain measurements is shown.

3.3 DISCUSSION OF EXPERIMENTAL RESULTS

In this section the results of the experimental programme for the material mechanical properties and the concrete block specimens are discussed.

3.3.1 Material Mechanical Properties

Table 3.7 lists the mechanical properties for all the materials used in this investigation. Poisson's ratios were found at initial stress and also at strains where maximum compressive stress occurs.

The vertical stress vs strain curves for unfilled three half-block prisms with 1 - 2 mm dental plaster joints, unit half-blocks and for a solid full-block tested parallel to the bed face, are shown in Fig. 3.8. Two other curves were also plotted, one representing the expression proposed by BS 8110: Part 2[69] for rigorous analysis which is defined by the following equation:

$$f = 0.8\, f_{cu}\, [(K\, n - n^2)/(1 + (K - 2)n)] \quad \ldots(3.1)$$

Where

$$n = \epsilon/\epsilon_{c,1} = \epsilon/0.0022 \quad \ldots(3.2)$$

$$K = (1.4\ \epsilon_{c,1}\ E_o)/f_{cu} = 3\ E_o/f_{cu} \qquad \ldots(3.3)$$

Where

f Stress in the block/concrete, N/mm^2

f_{cu} Characteristic compressive cube strength of the block/concrete, N/mm^2

ϵ Strain in the block/concrete

$\epsilon_{c,1}$ Strain in the block/concrete at maximum stress

E_o Modulus of elasticity of the block/concrete, N/mm^2

The other stress vs strain curve, representing a formula suggested by SAENZ[70], is as follows:

$$\sigma = E\ \epsilon/(1 + (\epsilon/\epsilon_0)^2) \qquad \ldots(3.4)$$

Where

$$E = 2\ \sigma_{max}/\epsilon_0$$

Where

E Initial tangent modulus, N/mm^2

σ Stress, N/mm^2

ϵ Strain

ϵ_0 Strain at maximum stress

σ_{max} Maximum stress, N/mm^2

The curve for the unfilled prism showed that the hollow sections were more stiff than the solid ones although the material was the same. Two reasons were given by AFSHARI and KALDJIAN[38] for the reduction in stiffness of the solid block. The first reason given assumes that a "solid" unit, consists of a hollow shell grouted with the same material as the shell, the extra material in the block

expands laterally when axial stress is applied. The expansion of the extra material results in additional lateral stresses pushing the shell portion outward thus causing a filled unit to fail at a lower level of axial stress than the equivalent hollow unit. The second reason was that for a given axial stress, a solid unit carries a higher axial load than a hollow one.

The expansion of the extra materials will not only effect the level of axial stress, as suggested by the above authors, but also affect the mode of failure and consequently cause a reduction in block stiffness. The lateral expansion of the extra material can clearly be seen in Fig. 3.9, which relates the lateral to the vertical strain for hollow and solid blocks.

Figs 3.10, 3.11 and 3.12 show the vertical stress vs strain curves for the different types of specimen tested, i.e. the three concrete mixes used in the present investigation namely: low strength (1:5:2), medium strength (1:3:2) and high strength (1:1:2) respectively.

Fig. 3.13 shows the lateral strain vs vertical strain for all the concrete mixes.

Two conclusions can be drawn from Figs 3.10 to 3.13 and Table 3.7. First, there was no major difference in strength between the block moulded concrete prisms, prepared in accordance with ASTM C 1019 Standard[62], and the rest of the specimens tested (concrete cylinders and three concrete cube specimens) as a result of water suction by the block shells. The second conclusion relates to the possibility of using a new specimen where the vertical and horizontal strains can be measured simultaneously to be used in determining the modulus of elasticity and the Poisson's ratio of the material. This new specimen

consisted of three steel moulded cubes separated and capped with 1 - 2 mm dental plaster joint.

Figs 3.14 and 3.15 show the vertical stress vs strain curves and the lateral strain vs vertical strain for the three different types of mortar mixes used in this study namely: low strength (1:1:6), medium strength (1:0.5:4.5) and high strength (1:0.25:3) respectively. The curves were determined by testing the proposed three steel moulded mortar cubes specimen. Fig. 3.16 on the other hand shows a typical vertical stress vs strain curve for high strength (1:0.25:3) mortar. This curve however was for the confined 10 mm mortar joint determined by testing a two-block prism with mortar joint between.

Two other curves, representing confined high strength (1:0.25:3) mortar, were also plotted on the same graph for comparison. The first was from previous work by the author[71,72]. The second was a theoretical prediction for a confined vertical stress vs strain curve for mortar, based on the stress vs strain curves determined by testing mortar cylinders[32].

The confined vertical stress vs strain curve for a 10 mm mortar joint showed a high plasticity and no sign of failure, but a steady increase in strength, reaching values higher than the three-cube specimens and the mortar cylinders.

3.3.2 Concrete Block Specimens

Table 3.8 summarizes the results for all the full and half-block specimens compressed normal and parallel to the bed face. Table 3.9 gives the results for the block splitting and bond strengths. On the other hand, Table 3.10

gives the results of the two-material specimens shear strength. Also given in the above tables are the associated material properties.

The mode of failure for the unfilled single-block specimens compressed normal to the bed face was by crushing and shearing at mid height of the middle web, followed by lateral deformation of the side block shells. Some longitudinal cracks were observed at the end shells at early stages of the loading process (Fig. 3.17 (i)).

The mode of failure of the unfilled single-block specimens compressed parallel to the bed face was completely different from the ones compressed normal to the bed face. First failure of the block occurred due to local crushing at the outer face of the block shells near the machine platens, followed by shearing at the corners between the side and end block shells then by splitting and complete disintegration of the specimen (Fig. 3.18 (i)). There was no indication of any major cracks during the loading process until failure.

Filled single-block specimens compressed normal to the bed face exhibit an almost similar mode of failure for all different concrete infill mixes. The specimens first suffer crushing of the block shells near the testing machine platen followed by lateral deformation of the block side shells. Some signs of longitudinal cracking at the centre of the block end shells were also observed (Fig. 3.17 (ii)). The concrete infill suffered slight damage approaching failure. Some of the specimens with a high strength concrete mix (1:1:2) withstood reloading of up to 80% of the ultimate recorded failure load.

The filled single-block specimens compressed parallel to the bed face, on the other hand, showed three different

modes of failure. The first mode was typical of a low strength concrete infill (4.34 N/mm^2). The specimen failed first by crushing of the concrete infill, followed by lateral deformation of the block shells to the outside and then by complete disintegration. Specimens with high strength concrete infill (39.44 N/mm^2) showed no signs of any major cracks in the concrete infill during testing and after failure. The mode of failure was by crushing and shearing of the block shells near the loading machine steel platen, followed by lateral deformation of the block shells (Fig. 3.18 (ii)). The third mode of failure was intermediate to the two modes explained previously, which is typical for specimens with concrete infill approximately equal in strength to that of the unfilled single-block specimen.

Comparing the stress vs strain curves for unfilled (Fig. 3.19 (i)) and filled (Fig. 3.19 (ii)) full-block specimens, compressed normal to the bed face, shows a rapid increase in the horizontal tensile strain in the filled specimen compared to the unfilled ones at stresses above about half the ultimate specimen strength. This is due mainly to the high Poisson's ratio of the concrete infill. The tensile strain plots for the filled specimens also show some signs of increasing stiffness near failure. This resulted from the high confinement of the specimen by the testing machine platen which prevented premature failure of the concrete block and consequently resulted in an increase in stiffness near failure.

The stress vs strain curves for all the unfilled (Fig. 3.20 (i)) and filled (Fig. 3.20 (ii)) full-block specimens compressed parallel to the bed face, on the other hand, showed that there is a reduction in the block stiffness for the filled blocks compared to the unfilled ones. This is clearly shown by the descending gradient of the stress vs

strain curves measured on the block side shells. This decline is primarily produced by the presence of the concrete infill which applies some tensile stress resulting from the high Poisson's ratio of the low and medium strength concrete infills. These high tensile stresses led to the failure of the block before the unfilled unit block compressive strength was attained and before the apparent material strength of the block f_b was reached. This phenomenon was also observed in earlier tests[27,28,33,36,71] on concrete block masonry prisms.

Fig. 3.21 shows the relation between the block specimen strength and the concrete infill strength (unfilled blocks compressive strength based on gross area were considered as blocks with zero concrete infill strength). A statistical computer program (MINITAB)[73] was used to derive the best fitting relationships which represented by the following formulae:

1. Filled block compressed normal to the bed face:

$$f_{bnf} = -0.0063\ (f_c)^2 + 0.65\ f_c + 11.4 \qquad \ldots(3.5)$$
$$r = \text{Correlation coefficient} = 0.98$$

2. Filled half-block compressed normal to the bed face:

$$f_{hnf} = 0.43\ f_c + 14.5 \qquad \ldots(3.6)$$
$$r = 0.96$$
$$\text{for } f_c = 0.0 \text{ to } 45.31$$

3. Filled block compressed parallel to the bed face:

$$f_{bpf} = -0.0174\ (f_c)^2 + 0.92\ f_c + 8.0 \qquad \ldots(3.7)$$
$$r = 0.93$$

Fig. 3.21 also shows the respective reduction and increase in strength of the filled specimens compressed

normal and parallel to the bed face compared to the apparent block material strength, f_b. The figure also shows that the strength of the specimen compressed normal to the bed face increased as the concrete infill strength was increased by using a 1:1:2 mix. This increase results from the similarity in the deformational characteristics between the concrete and the block. Some of the filled specimens with high strength concrete withstood a reloading of 80% of the specimen failure load. This suggests that despite failure of the block shells, the concrete infill was still intact and able to withstand reloading.

This behaviour of the concrete infill was clearly shown by the stress vs strain curves (Fig. 3.22) for two-material specimens compressed normal to the bed face using a fixed machine head, where for the same level of vertical strain, the block material showed a higher strength than the concrete material. Fig. 3.22 also shows that at high level of vertical stress the lateral strain in the concrete infill is higher than that for the block material.

This leads to the conclusion that matching the deformational characteristics of the concrete infill with those of the block may be more effective than increasing the concrete infill strength[27,28,29,36,71].

On the other hand, using a 1:1:2 mix reduced the strength of specimens compressed parallel to the bed face. Therefore using a 1:1:2 mix has the same effect in reducing the specimen strength when compressed parallel to the bed face as a 1:7:2 mix. This suggests that stiff concrete infill works as a cleavage forcing the blocks to split before attaining their unfilled single-block compressive strength.

Half-block specimens compressed normal to the bed face

showed a steady linear increase in strength as the concrete strength increased. The compressive strength of full-block specimens must be modified by a reduction factor of 0.85 compared to that for half-block specimens. This reduction may be caused by differences in the aspect ratios (block length-to-thickness) between the full-block (l/t = 2.05) and the half-block (l/t = 1.0) specimens.

On the other hand, filled single-block specimens compressed parallel to the bed face failed at strengths modified by a reduction factor of 0.80, for concrete infill strengths ranging from 0 to 21.23 N/mm^2 (specimens with zero concrete infill strength are the unfilled blocks) compared to specimens tested normal to the bed face. The decrease was caused by differences in the direction in which the single-block specimens were tested.

The presence of the concrete infill had the same reduction effect on the block splitting strength compared to the unfilled ones (Fig. 3.23), as in the case of the block compressive strength. This relation is best represented as follows:

$$f_{bt} = 0.64 + 0.20\ (f_c)^{1/2} \qquad \text{...(3.8)}$$
$$r = 0.97$$

Fig. 3.24 gives the best fitting curve relating the full-block tensile splitting strength to the filled block compressive strength. This can be represented as follows:

$$f_{bt} = 0.30\ (f_{bnf})^{1/2} \qquad \text{...(3.9)}$$
$$r = 0.97$$

This relation gives values for the block tensile strength which are some 44.4% lower than the allowable tensile strength values for concrete predicted using the

formula suggested by the American Concrete Code[74]. This formula relates the concrete splitting strength to the cube compressive strength as follows:

$$f_{ct} = 0.54 \ (f_c)^{1/2} \qquad \ldots(3.10)$$

Half-block specimens show a 10% increase in splitting strength compared to the full-block specimens. This increase may be due to the size effect.

Half-block specimens can be used to determine the block tensile splitting strength provided the half-block compressive strength is corrected for the aspect ratio before being inserted in the above formula.

Fig. 3.25 gives the relation for the cohesion bond strength between the block and the concrete as a function of the concrete cube compressive strength for the full-block two-materials specimen. The following equation is the best representation of the relation:

$$f_{bb} = 0.24 \ (f_c)^{1/2} \qquad \ldots(3.11)$$
$$r = 0.94$$

The cohesion bond strength between the block and the concrete given by Eqn. 3.11 was 55.6% lower than the value of splitting strength for concrete derived by Eqn. 3.10. Two-material half-block specimens gave an almost similar relation for the cohesion bond strength as the two material full-block specimens.

The shear bond between the block and the concrete (Fig. 3.26) was related to concrete cube compressive strength as follow:

$$f_{bv} = 0.17 \ (f_c)^{0.67} \qquad \ldots(3.12)$$
$$r = 0.98$$

While the relation for concrete was as follow:

$$f_{cv} = 0.18 \ (f_c)^{1/2} \qquad \ldots(3.13)$$

3.4 CONCLUSIONS

1. The strength of filled half and full-block specimens compressed normal to the bed face increased as the concrete infill strength increased. Specimens compressed parallel to the bed face and filled with high strength concrete have almost the same strength as those filled with low strength concrete.

2. The reason for the reduction in strength of specimens filled with low strength concrete, as compared to unfilled ones, is the high lateral expansion of the concrete infill at high stresses due to differences in Poisson's ratios between the block and the concrete. Best results can be achieved by providing a concrete infill with the same deformational characteristics as the blocks.

3. Due to the need for high capacity machines to determine the compressive strength of full-blocks, half-block specimens can be tested instead. The compressive strength is then multiplied by 0.85 as an aspect ratio reduction factor.

4. The splitting strength of filled blocks is less than that of unfilled ones. This is due to the same effect which caused the reduction in block compressive strength. For ease of handling, half-block specimens

can be used for the splitting test, provided that the strength is multiplied by 0.90 as a size reduction factor.

5. The cohesion bond strength between the block and the concrete given by Eqn. 3.11 was 55.6% lower than the value of splitting strength for concrete derived by Eqn. 3.10. This is true for this investigation because the cohesion bond strength depends on the block surface texture.

7. Suction of water by the block had a negligible effect on the concrete infill strength.

8. A new specimen is suggested, for standardization purposes, to determine the concrete and mortar modulus of elasticity and Poisson's ratios from the same test. The specimen consists of three steel moulded cubes separated by 1 - 2 mm thick layers of dental plaster.

9. Vertical stress vs strain curves for the confined 10 mm mortar joint should be used for analysis or design in blockwork masonry, rather than those for the mortar cylinder or the suggested three steel moulded cubes specimen.

Table 3.1

Typical table used to determine characteristic compressive strength, f_k, of masonry BS 5628: Part 2: 1985.

Table 3. Characteristic compressive strength, f_k, of masonry

(A) Constructed with bricks or other units having a ratio of height to least horizontal dimension of 0.6

Mortar designation	Characteristic compressive strength of masonry, f_k (N/mm²)								
	Compressive strength of unit (N/mm²)								
	7	10	16	20	27.5	35	50	70	100
(i)	3.4	4.4	6.0	7.4	9.2	11.4	15.0	19.2	24.0
(ii)	3.2	4.2	5.3	6.4	7.9	9.4	12.2	15.1	18.2

(B) Constructed with solid concrete blocks having a ratio of height to least horizontal dimension of 1.0

	Compressive strength of unit (N/mm²)						
	7	10	15	20	35	60	70 or greater
(i)	4.4	5.7	7.7	9.5	14.7	19.3	24.7
(ii)	4.1	5.4	6.8	8.2	12.1	15.7	19.4

(C) Constructed with solid concrete blocks having a ratio of height to least horizontal dimension of between 2.0 and 4.0

	Compressive strength of unit (N/mm²)						
	7	10	15	20	35	50	70 or greater
(i)	6.8	8.8	12.0	14.8	22.8	30.0	38.4
(ii)	6.4	8.4	10.6	12.8	18.8	24.4	30.2

(D) Constructed with structural units other than solid concrete blocks having a ratio of height to least horizontal dimension of between 2.0 and 4.0

	Compressive strength of unit (N/mm²)						
	7	10	15	20	35	50	70 or greater
(i)	5.7	6.1	6.8	7.5	11.4	15.0	19.2
(ii)	5.5	5.7	6.1	6.5	9.4	12.2	15.1

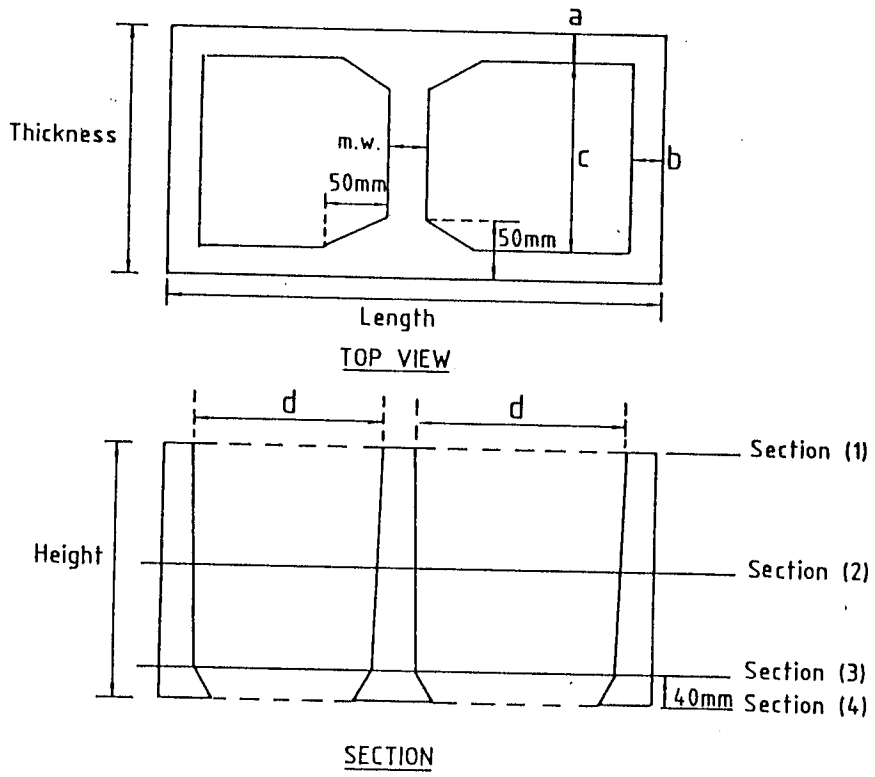

Fig. 3.1 - Cross-sections of a typical concrete block.

Table 3.2

Dimensions of a typical concrete block used in the investigation.

Section	Length * (l) Full/Half (mm)	Height h (mm)	Thickness t (mm)	a (mm)	b (mm)	m.w. Full/Half (mm)	c (mm)	d (mm)	A_n Full/Half (mm^2)
(1)	390/190	189	190	33	30	55/22.5	124	137.5	41700/19900
(2)	390/190	189	190	35	33	59/24.5	120	132.5	44000/21050
(3)	390/190	189	190	36	34	61/25.5	118	130.5	45002/21551
(4)	390/190	189	190	47	46	81/35.5	96	108.5	54828/26464

Volume of block cavities by calculation = 0.005522 m^3.
Volume of block cavities by sand method = 0.005506 m^3. (BS 6073: Part 2: 1981)[66].
Block percentage solid = 60 %
Block material constant mass (oven dry) density = 2127 kg/m^3.
* Half-block length = 390/2 - 5 = 190 mm. (Taking into consideration the thickness lost in cutting the block to half by the electrical saw, usually equal to 10 mm).

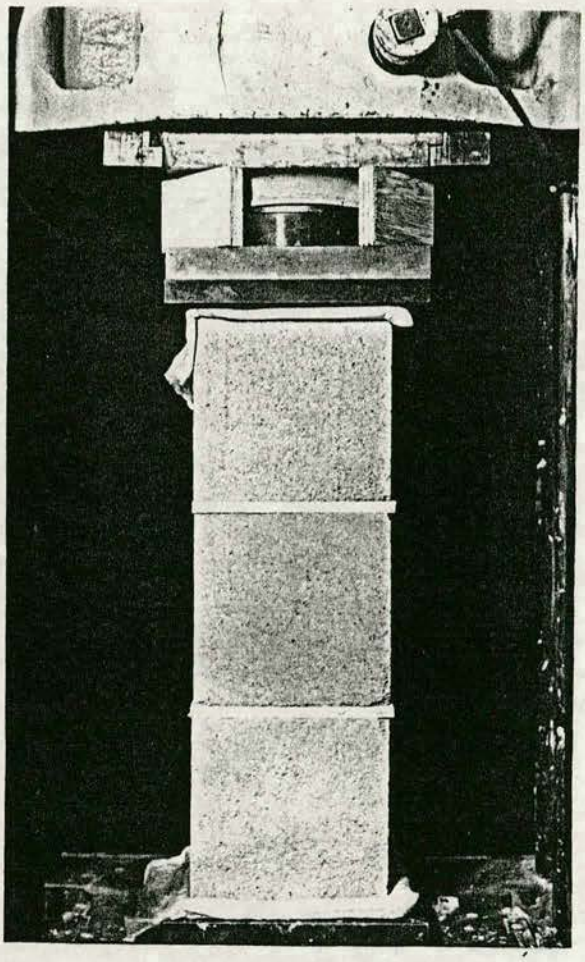

Fig. 3.2 - Unfilled half-block prism with 1 - 2 mm dental plaster joints.

Table 3.3

Sieve analysis of concrete sand.

Test sieve	% By weight passing through sieve	
	Test result	BS 882 limit (Table 5)
10.00 mm	100	100
5.00 mm	100	89 - 100
2.36 mm	88	60 - 100
1.18 mm	75	30 - 100
600 μm	64	15 - 100
300 μm	34	5 - 70
150 μm	5	0 - 15

Table 3.4

Sieve analysis of 10 mm single size crushed aggregate.

Test sieve	% By weight passing through sieve	
	Test result	BS 882 limit (Table 4)
14.00 mm	100	100
10.00 mm	98	85 - 100
5.00 mm	17	0 - 25
2.36 mm	1	0 - 5

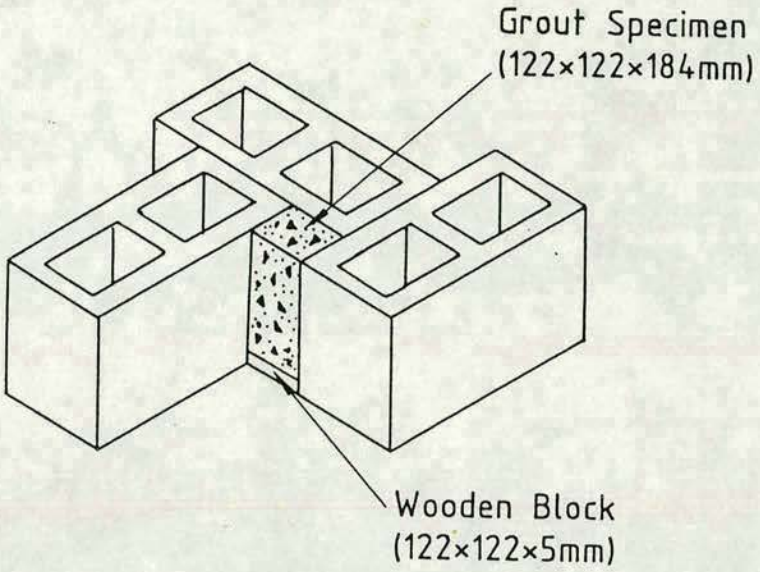

Fig. 3.3 - Illustration of block moulded concrete infill specimen fabrication.

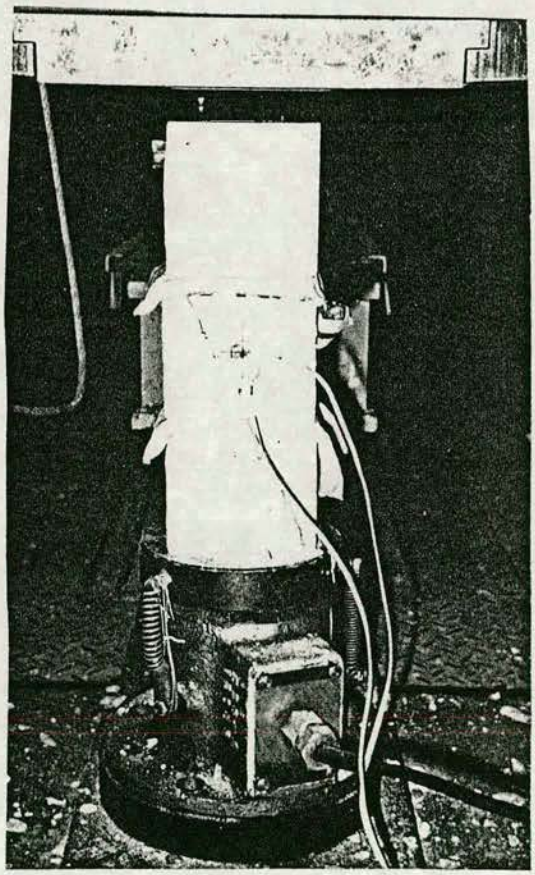

Fig. 3.4 - Three steel moulded concrete cubes separated and capped with 1 - 2 mm dental plaster joints.

Table 3.5

Sieve analysis of mortar sand.

Test sieve	% By weight passing through sieve	
	Test result	BS 1200 limit type S sand (Table 1)
6.30 mm	100	100
5.00 mm	100	98 - 100
2.36 mm	97	90 - 100
1.18 mm	93	70 - 100
600 μm	82	40 - 100
300 μm	40	5 - 70
150 μm	8	0 - 15
75 μm	4	0 - 5

Table 3.6

Properties of reinforcement.

Designation	Nominal diameter (mm)	Area (mm^2)	Yield strength (N/mm^2)	Yield strain (%)	Ultimate strength (N/mm^2)	Young's modulus (kN/mm^2)
Hot rolled plain low yield steel bars	6	28.27	441.51	0.21	516.66	200
Hot rolled deformed high yield steel bar	8	50.27	527.86	0.26	619.38	200
	10	78.54	519.06	0.26	635.77	190
	12	113.10	486.31	0.28	615.99	175
	20	314.16	536.88	0.28	649.35	178
	25	490.87	490.28	0.26	592.14	189

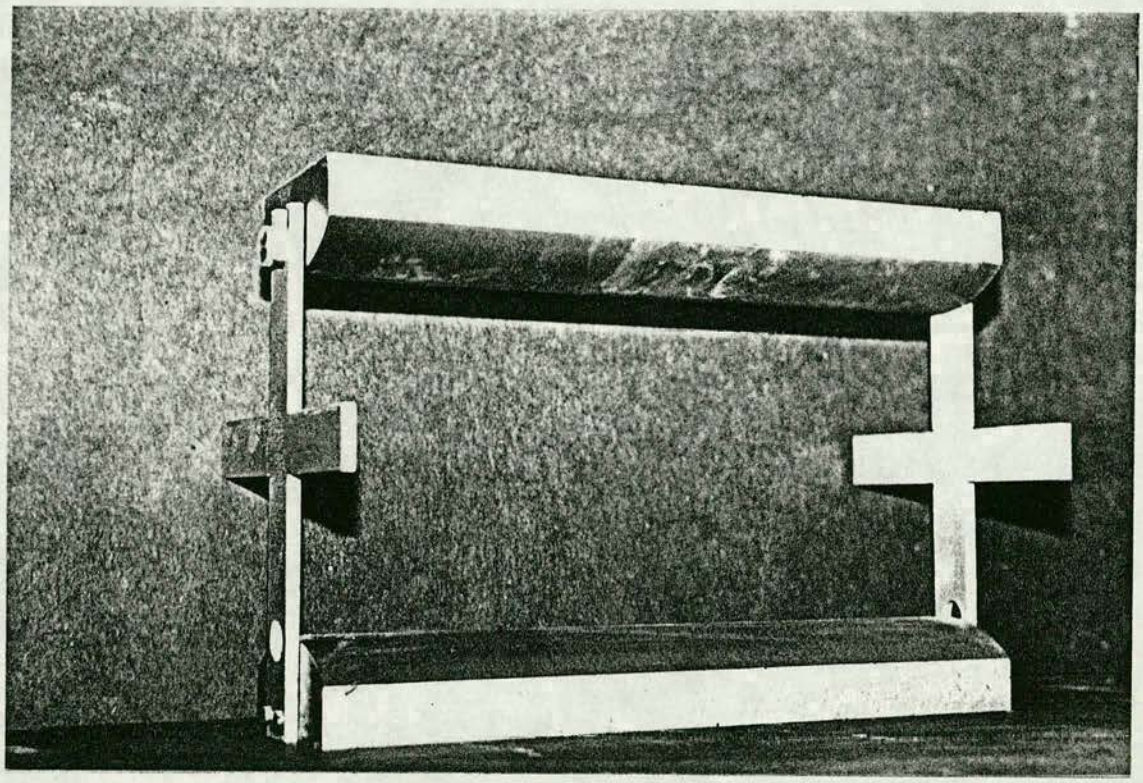

Fig. 3.5 - Steel rig for concrete block splitting test.

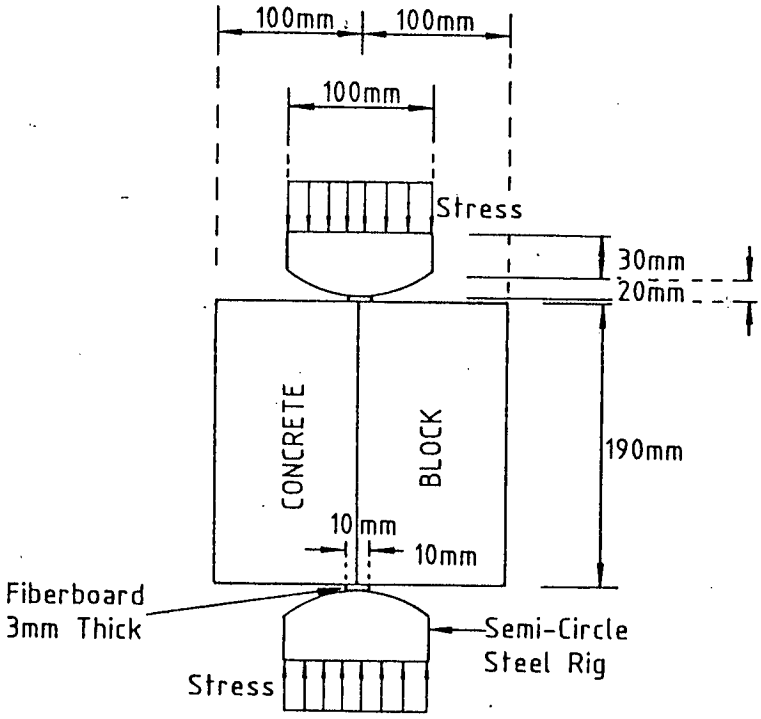

Fig. 3.6 - Two-materials splitting bond specimen.

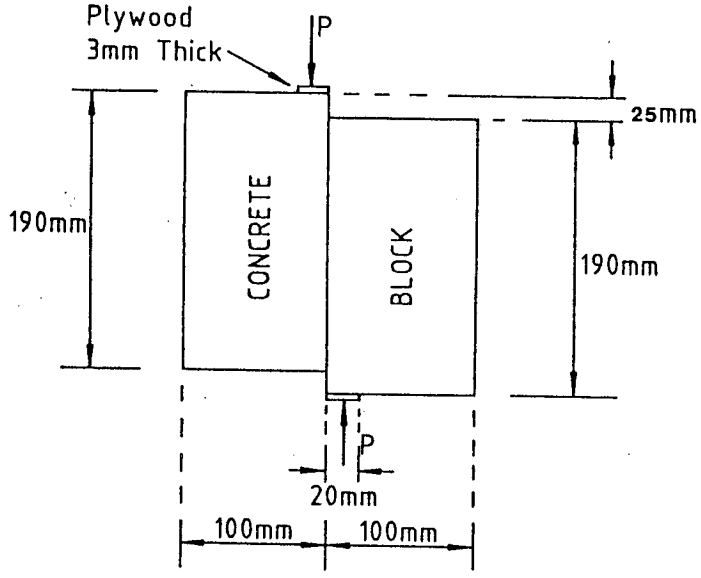

Fig. 3.7 - Two-materials shear bond specimen.

Table 3.7

Material mechanical properties.

Material	Specimens or single-cube strength (N/mm^2)	Cylinder strength (N/mm^2)	Three-cubes specimen strength (N/mm^2)	Block moulded prism (N/mm^2)	Density (Kg/m^3)	Tangent Modulus of elasticity (N/mm^2)	Secant * Modulus of elasticity (N/mm^2)	Poisson's ratio Initial stress	Poisson's ratio Maximum stress
Block									
Solid ✱	24.29	-	-	-	2113	19118	13014	0.20	0.25
Prism ✦	21.89	-	-	-	2127	33100	28977	0.15	0.20
Half-block	25.66	-	-	-	2127	38054	38054	0.13	0.18
Concrete									
1:7:2	5.50	4.85	4.74	4.65	1950	-	-	-	-
1:5:2	8.81	8.27	7.21	7.14	1978	6032	4674	0.24	0.33
1:3:2	22.52	17.20	16.53	18.24	2034	16033	11444	0.18	0.24
1:1:2	42.08	37.78	32.93	34.08	2286	28320	17180	0.14	0.22
Mortar									
1:1:6	8.14	8.02	6.90	-	1798	5603	3696	0.26	0.40
1:0.5:4.5	16.54	14.64	12.45	-	1875	10250	5000	0.22	0.35
1:0.25:3	26.57	25.03	21.71	-	1948	14119	8140	0.18	0.25
10 mm mortar joint									
1:1:6	-	-	-	-	-	2500	1232	-	-
1:0.5:4.5	-	-	-	-	-	4100	2652	-	-
1:0.25:3	-	-	-	-	-	5500	4037	-	-
steel	-	-	-	-	-	205000	-	0.30	-

* Secant modulus of elasticity at 2/3 the maximum compressive strength of specimens.

✱ Cube compressive strength of block material f_b = 24.29 N/mm^2.

✦ Unfilled three half-block prism with 1 - 2 mm dental plaster joints.

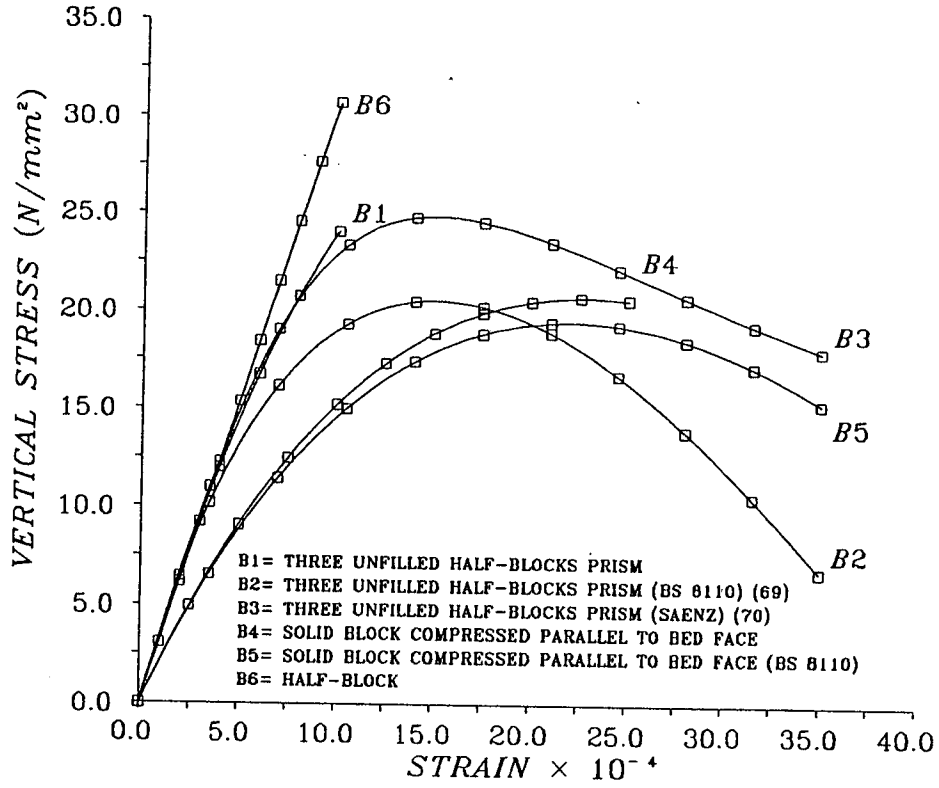

Fig. 3.8 - Vertical stress vs strain curves for block material.

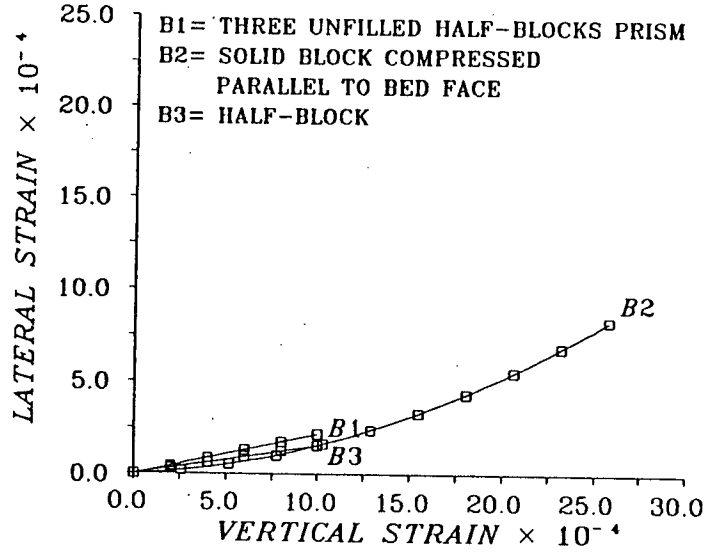

Fig. 3.9 - Lateral strain vs vertical strain curves for block material.

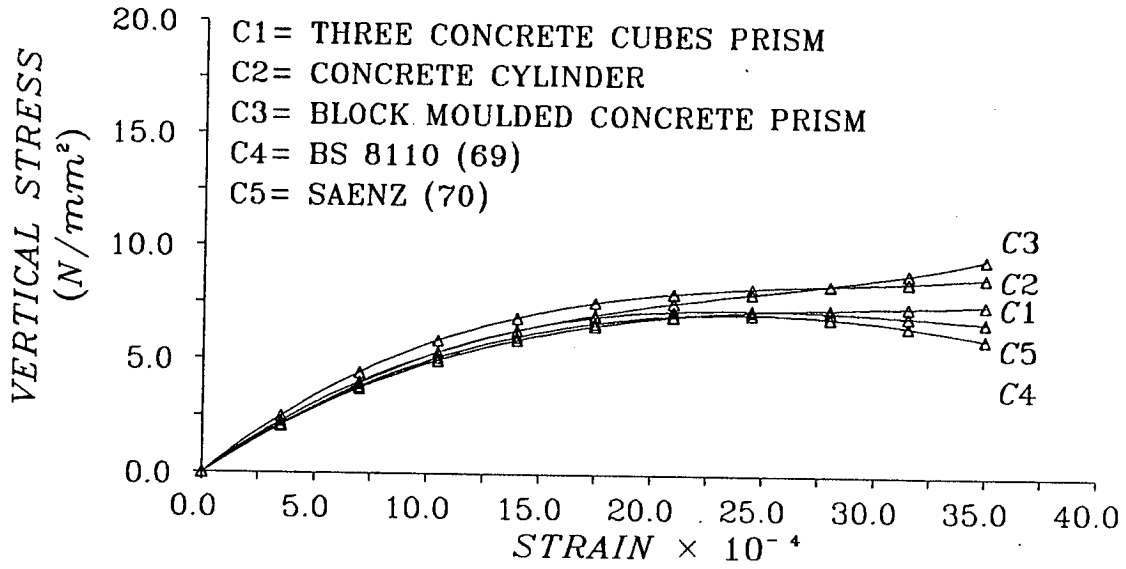

Fig. 3.10 - Vertical stress vs strain curves for low strength (1:5:2) concrete.

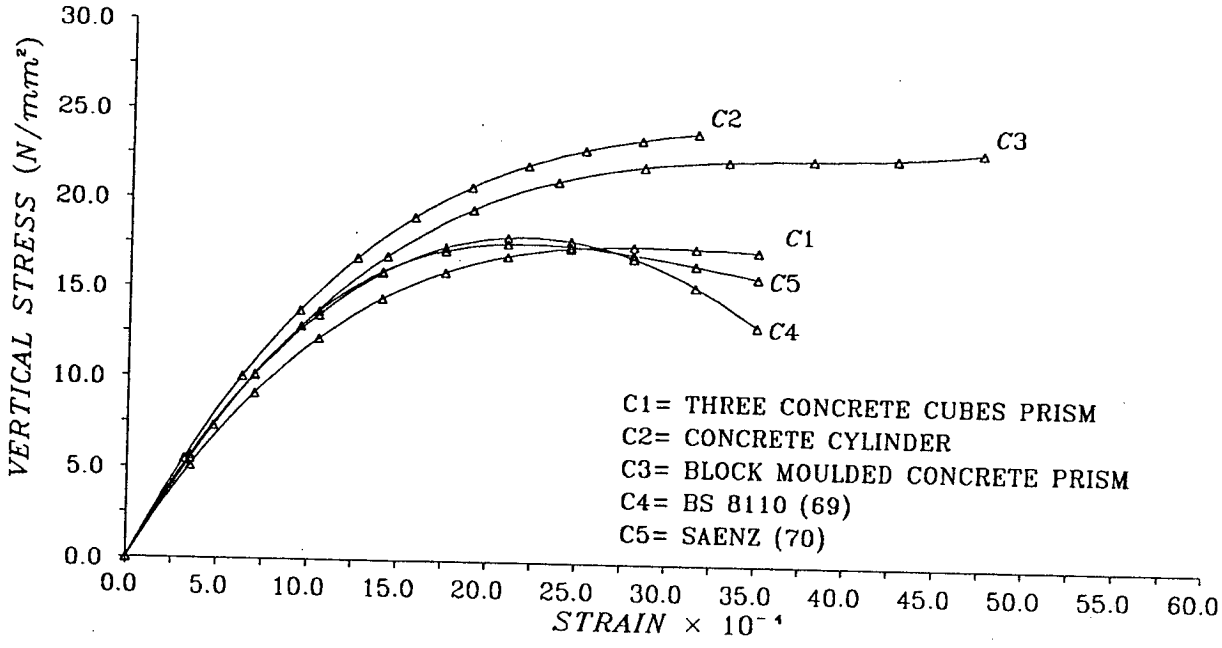

Fig. 3.11 - Vertical stress vs strain curves for medium strength (1:3:2) concrete.

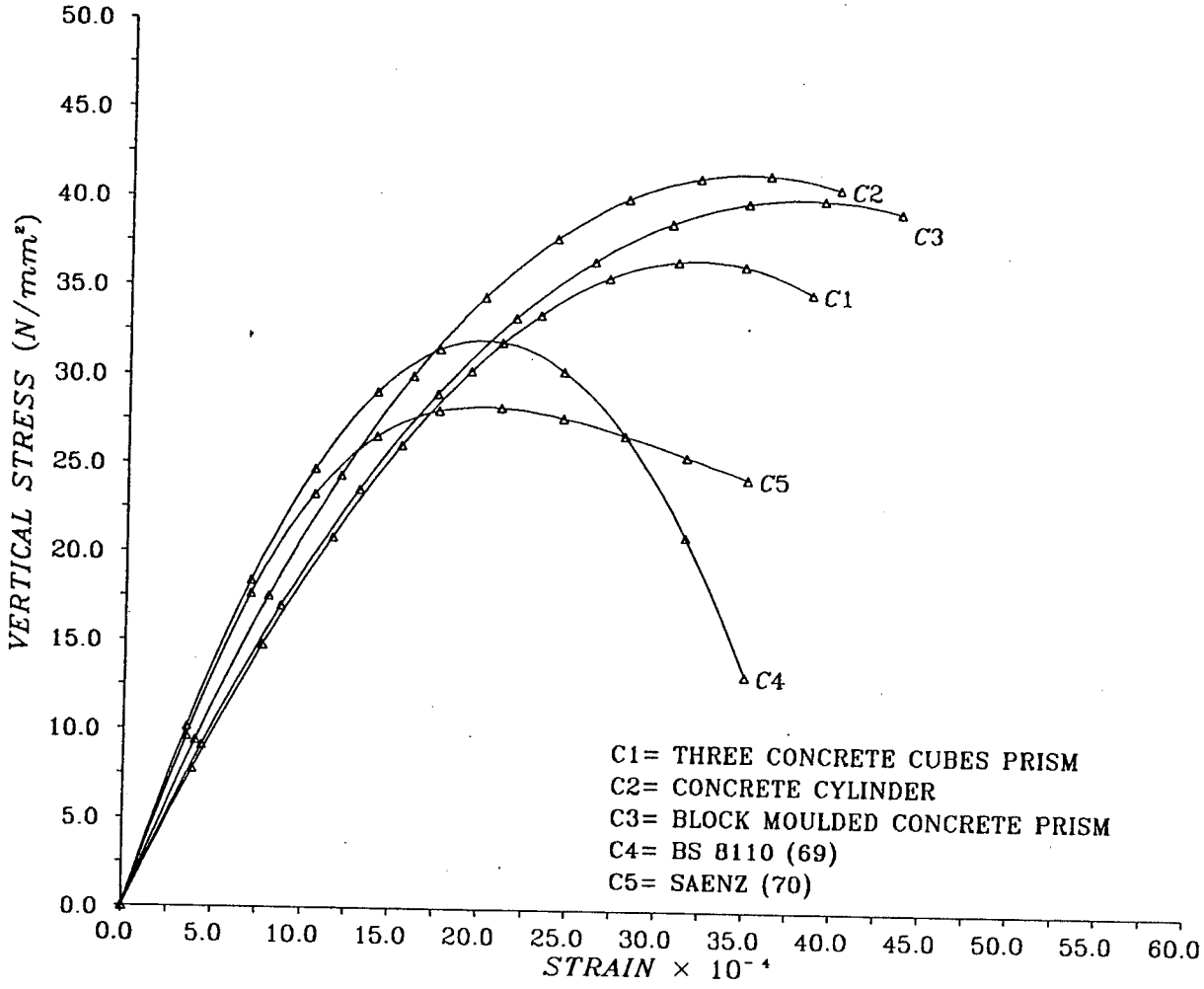

Fig. 3.12 - Vertical stress vs strain curves for high strength (1:1:2) concrete.

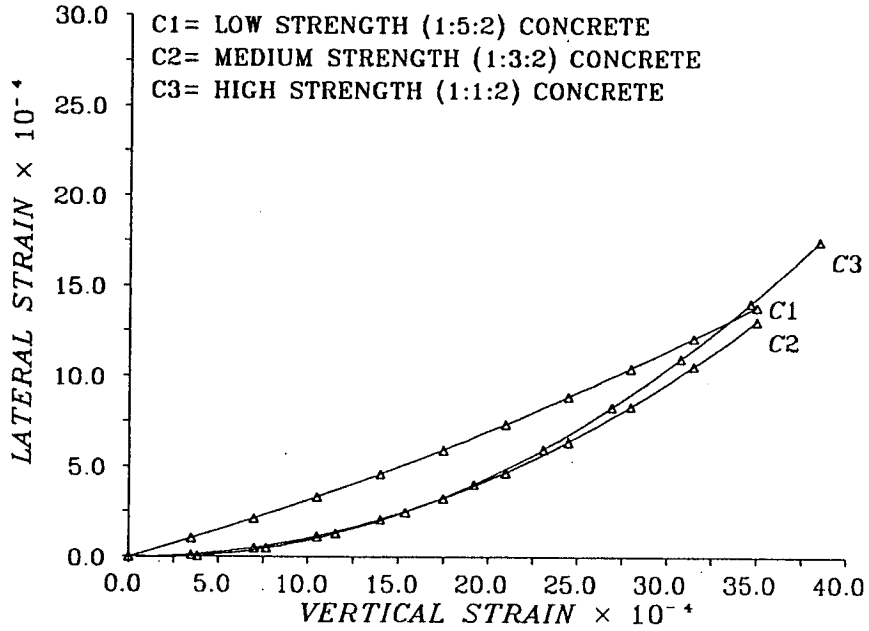

Fig. 3.13 - Lateral strain vs vertical strain curves for concrete.

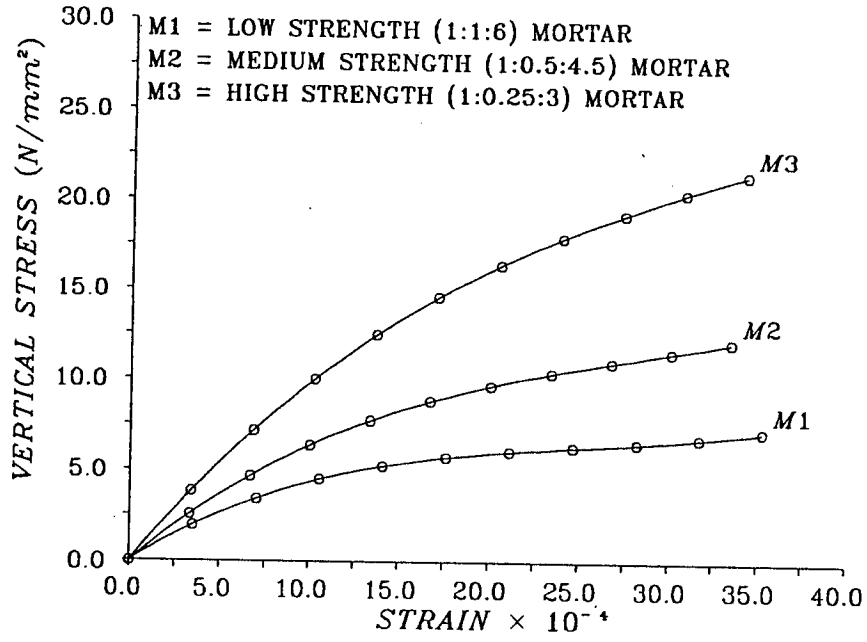

Fig. 3.14 - Vertical stress vs strain curves for mortar, based on suggested three steel moulded cubes specimen.

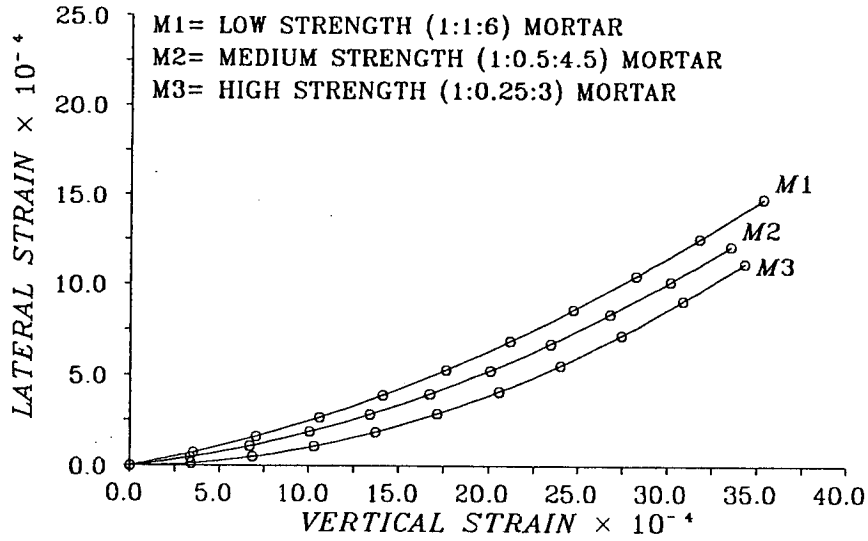

Fig. 3.15 - Lateral strain vs vertical strain curves for mortar, based on suggested three steel moulded cubes specimen.

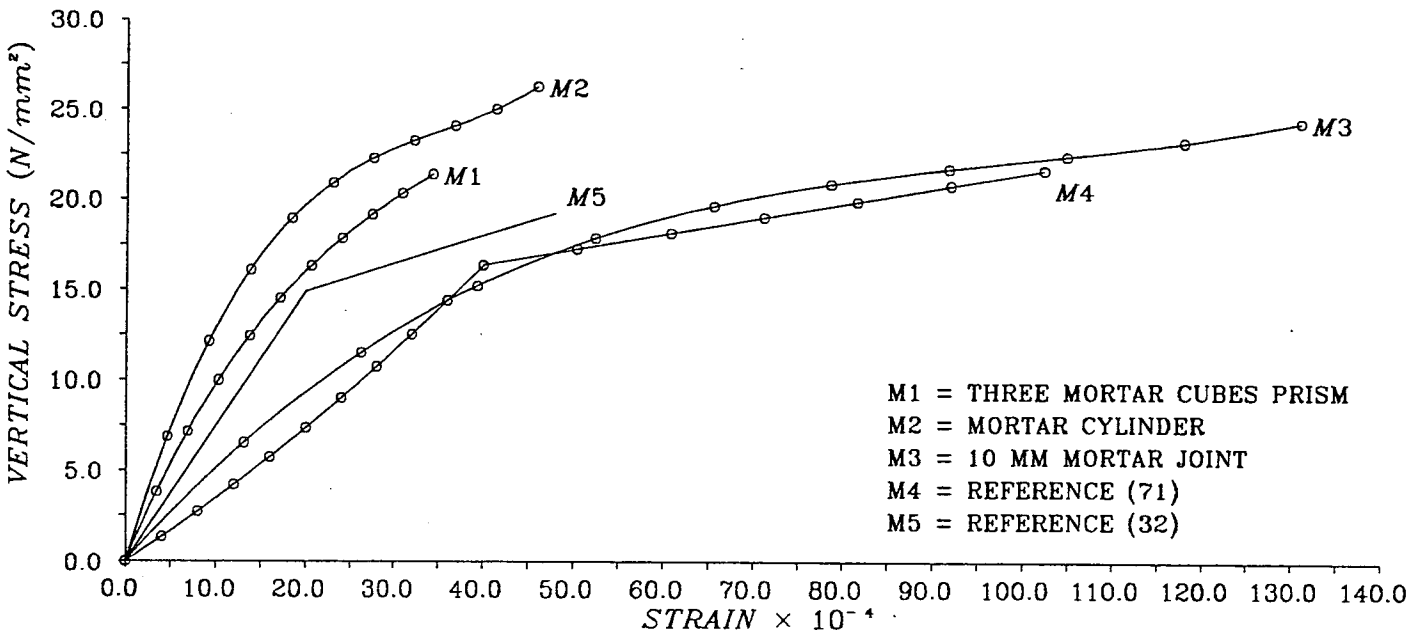

Fig. 3.16 - Typical vertical stress vs strain curves for confined 10 mm high strength (1:0.25:3) mortar joint.

Table 3.8

Compressive strength of single-block specimens.

Specimen	Number of tests	Average compressive strength (N/mm^2) Area used Net	Gross	S.D. (N/mm^2)	Mix proportions by volume	Infill compressive strength (N/mm^2)
			Full-block compressed normal to bed face *			
Unfilled	10	20.04	11.28	2.10/1.19	-	-
Filled	3	-	19.84	0.70	1:5:2	11.85
Filled	3	-	17.57	0.51	1:5:2	12.21
Filled	3	-	20.04	1.01	1:5:2	15.71
Filled	3	-	23.86	0.72	1:3:2	26.07
Filled	3	-	24.63	1.50	1:3:2	29.34
Filled	3	-	28.12	2.31	1:1:2	44.66
			Half-block compressed normal to bed-face ♦			
Unfilled	7	25.66	14.15	2.67/1.47	-	-
Filled	3	-	22.44	1.66	1:5:2	12.21
Filled	3	-	22.46	2.61	1:5:2	15.71
Filled	7	-	24.63	3.23	1:3:2	24.72
Filled	5	-	34.14	1.49	1:1:2	45.31
			Full-block compressed parallel to bed face ♣			
Unfilled	10	22.20	8.18	2.24/0.83	-	-
Filled	3	-	11.79	1.87	1:7:2	2.44
Filled	4	-	10.52	1.27	1:7:2	6.24
Filled	6	-	20.28	2.91	1:3:2	21.23
Filled	4	-	16.88	0.95	1:1:2	39.44

Cube compressive strength of block material f_b = 24.29 N/mm^2.

* Net area = Area at section (1) = 41700 mm^2. (See Table 3.2).

Gross area = 390 x 190 = 74100 mm^2.

♦ Net area = Area at section (1) = 19900 mm^2. (See Table 3.2).

Gross area = 190 x 190 = 36100 mm^2.

♣ Net area = 2(189 x 35) = 13230 mm^2. (Dimensions at section (2)). (See Table 3.2).

Gross area = 190 x 189 = 35910 mm^2.

Table 3.9

Splitting and bond strength of concrete blocks.

Specimen	Number of tests	Average splitting * strength (N/mm^2) Area used Net	Gross	S.D. (N/mm^2)	Mix proportions by volume	Infill comp./split. strength (N/mm^2)
			Full-block specimen ♣			
Unfilled	10	2.16	0.69	0.24/0.08	-	-
Filled	6	-	1.18	0.06	1:5:2	12.03/1.02
Filled	5	-	1.77	0.15	1:3:2	26.39/2.11
Filled	5	-	2.07	0.08	1:1:2	44.66/3.15
			Half-block specimen ♦			
Unfilled	5	2.23	0.66	0.27/0.08	-	-
Filled	6	-	1.21	0.12	1:5:2	12.21/1.02
Filled	8	-	1.68	0.14	1:3:2	26.39/2.11
Filled	6	-	2.01	0.08	1:1:2	45.31/3.21
			Solid block			
Full-block ♣	6	-	1.51	0.33	-	-
Half-block ♦	6	-	1.55	0.30	-	-
			Two-material specimen			
Full-block ♣	5	-	0.67	0.20	-	11.00/1.00
Full-block	5	-	1.19	0.12	-	26.39/2.11
Full-block	10	-	1.68	0.06	-	34.72/2.72
Half-block ♦	8	-	0.66	0.16	-	11.00/1.00
Half-block	8	-	1.10	0.29	-	27.39/2.27
Half-block	5	-	1.64	0.05	-	34.72/2.72

Cube compressive strength of block material fb = 24.29 N/mm^2.

* Formula used $f_{bt} = 2F/\pi lh$.

♣ Unfilled = l x h = (33+33+59) 189 = 23625 mm^2. (Dimensions at section (2)). (See Table 3.2).
Filled = l x h = 390 x 189 = 73710 mm^2.

♦ Unfilled = l x h = (24.5+33) 189 = 10867.5 mm^2. (Dimensions at section (2)). (See Table 3.2).
Filled = l x h = 190 x 189 = 35910 mm^2.

Table 3.10

Shear strength of two-material specimens.

Specimen	Number of tests	Average shear * strength (N/mm^2)	S.D. (N/mm^2)	Mix proportions by volume	Infill compressive strength (N/mm^2)
1	6	0.87	0.15	1:5:2	12.03
2	6	1.06	0.19	1:3:2	26.39
3	10	2.15	0.87	1:1:2	44.66

Cube compressive strength of block material f_b = 24.29 N/mm^2.

* Area used = 190 x 165 = 31350 mm^2. (See Fig. 3.7).

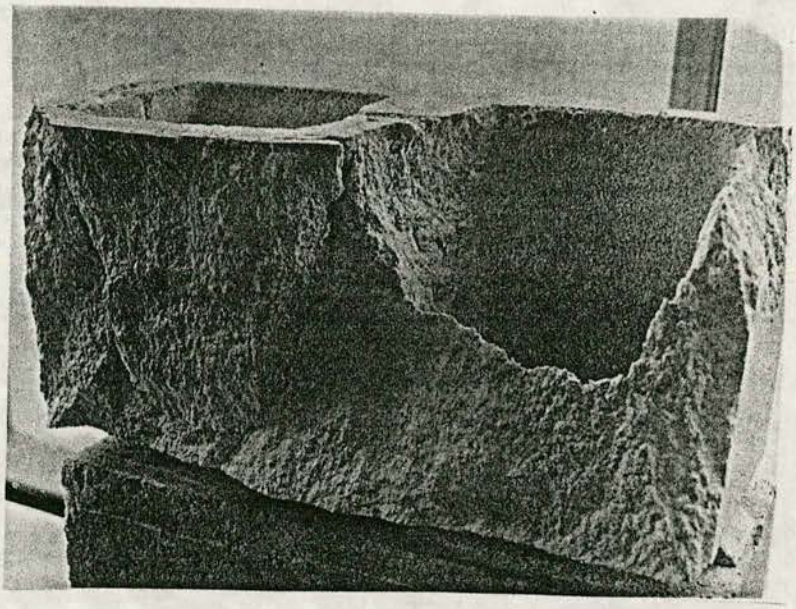

(i) Unfilled.

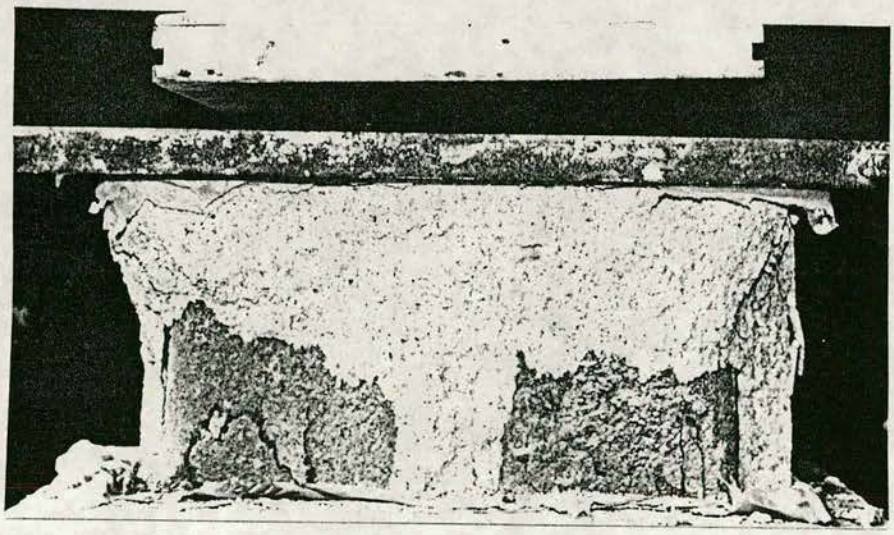

(ii) Filled.

Fig. 3.17 - Typical mode of failure for single-block specimens compressed normal to bed face. (i) Unfilled, (ii) Filled.

(i) Unfilled.

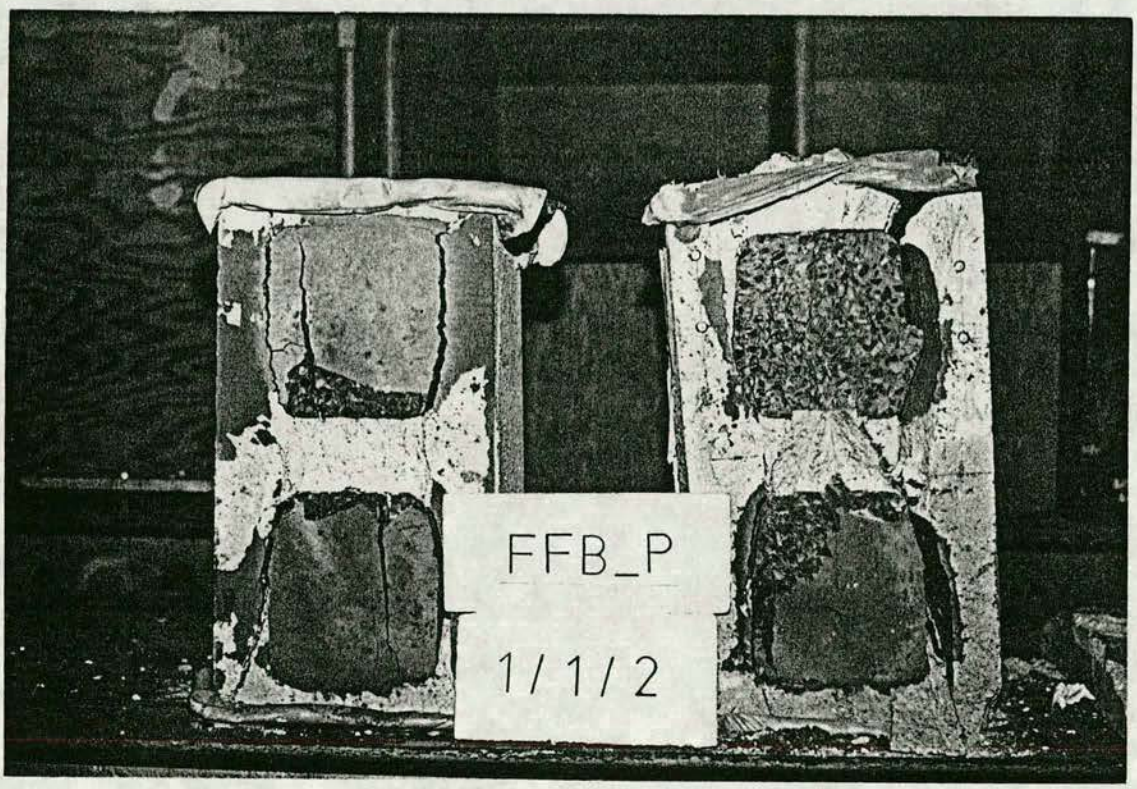

(ii) Filled.

Fig. 3.18 - Typical mode of failure for single-block specimens compressed parallel to bed face. (i) Unfilled, (ii) Filled.

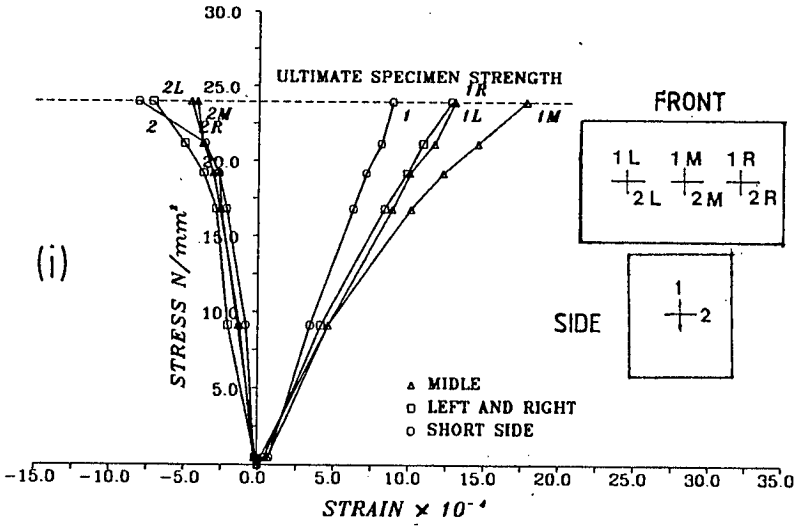

(i) Unfilled.

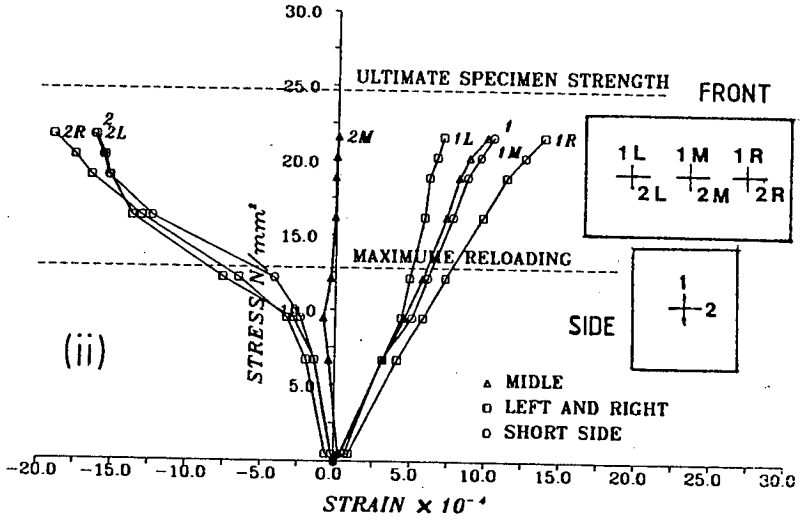

(ii) Filled.

Fig. 3.19 - Vertical stress vs strain curves for single-block specimen compressed normal to bed face. (i) Unfilled, (ii) Filled.

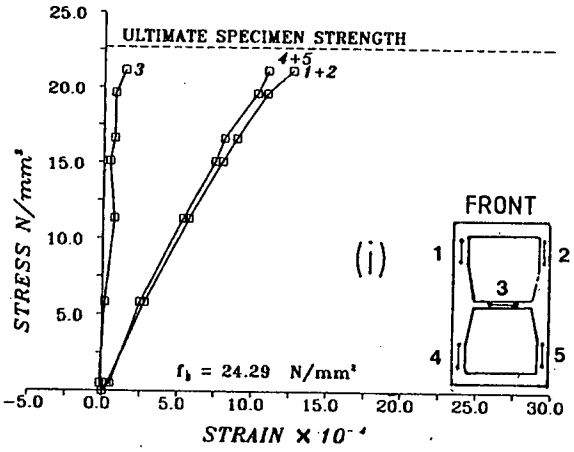

(i) Unfilled.

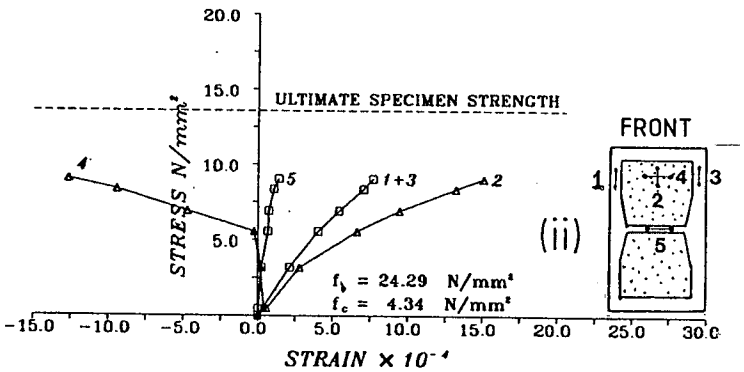

(ii) Filled.

Fig. 3.20 - Vertical stress vs strain curves for single-block specimen compressed parallel to bed face. (i) Unfilled, (ii) Filled.

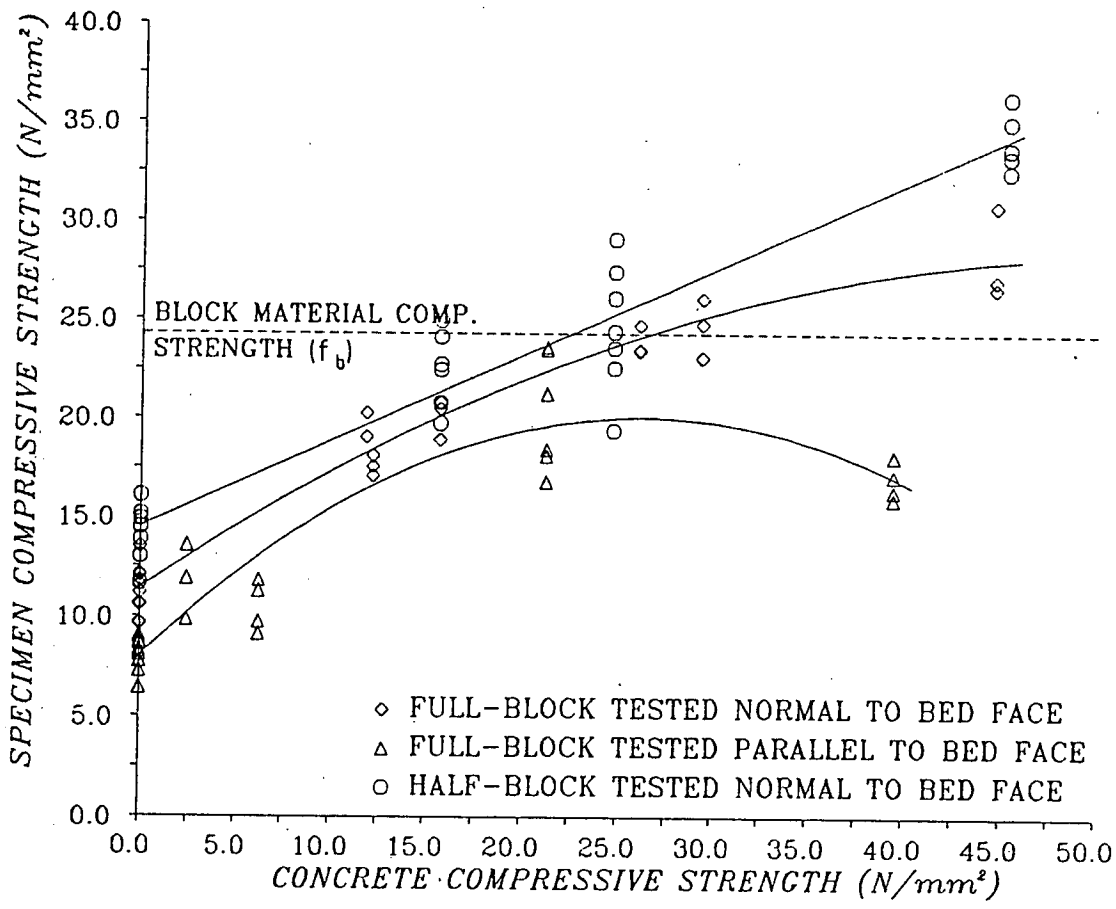

Fig. 3.21 - Effect of concrete infill strength on single-block specimens compressive strength.

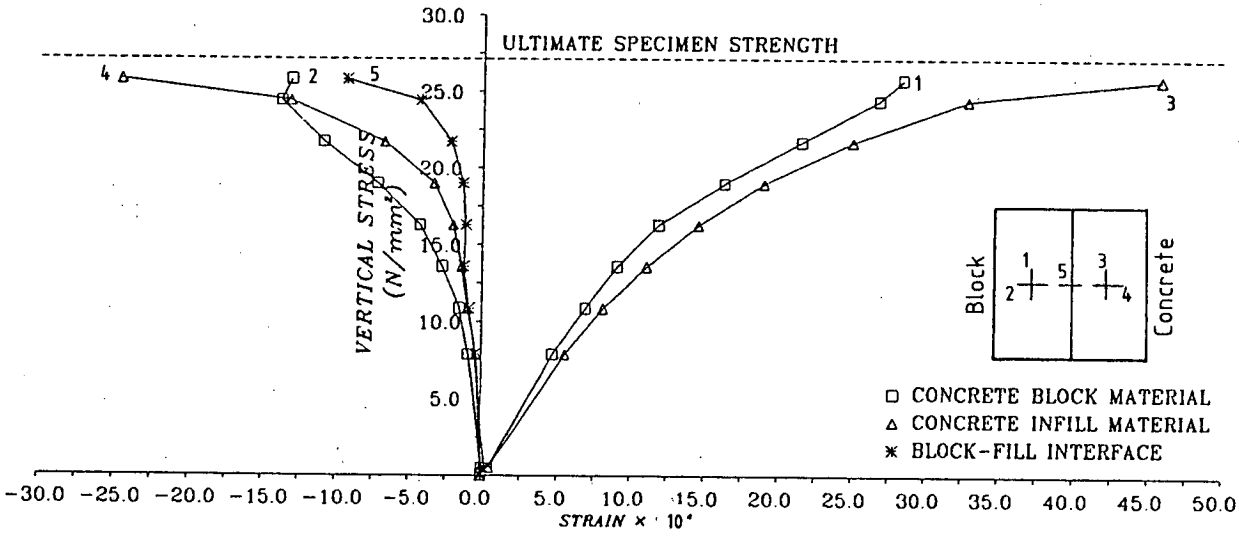

Fig. 3.22 - Typical vertical stress vs strain curves for two-materials specimen.

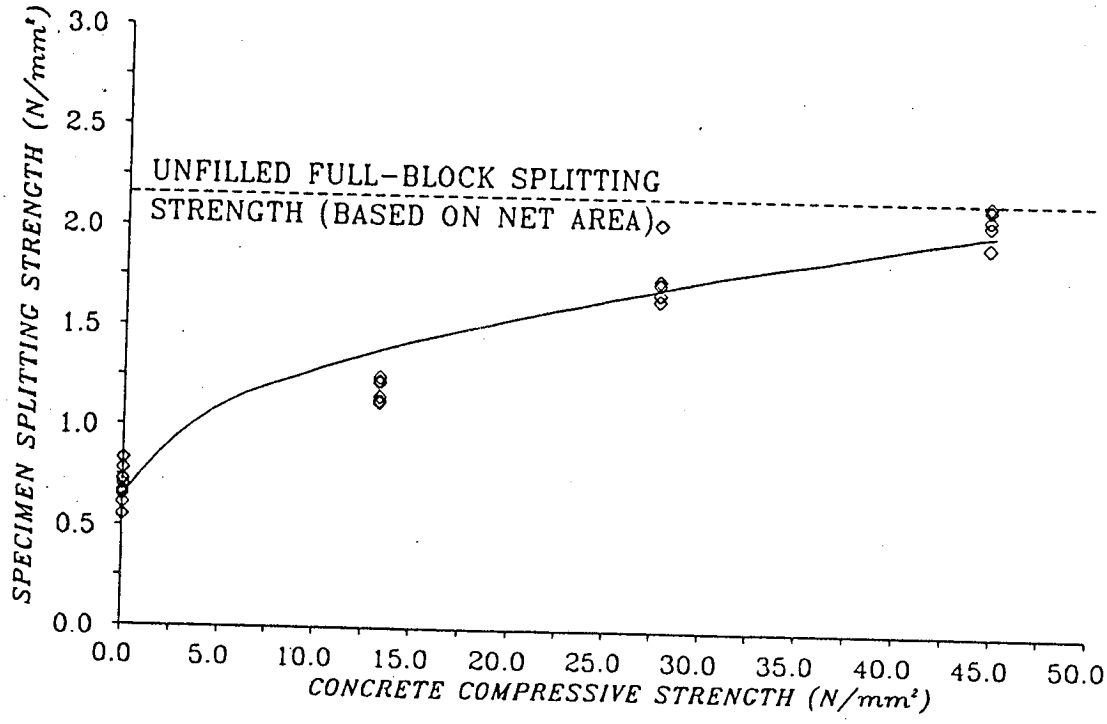

Fig. 3.23 - Effect of concrete infill strength on unit block splitting strength.

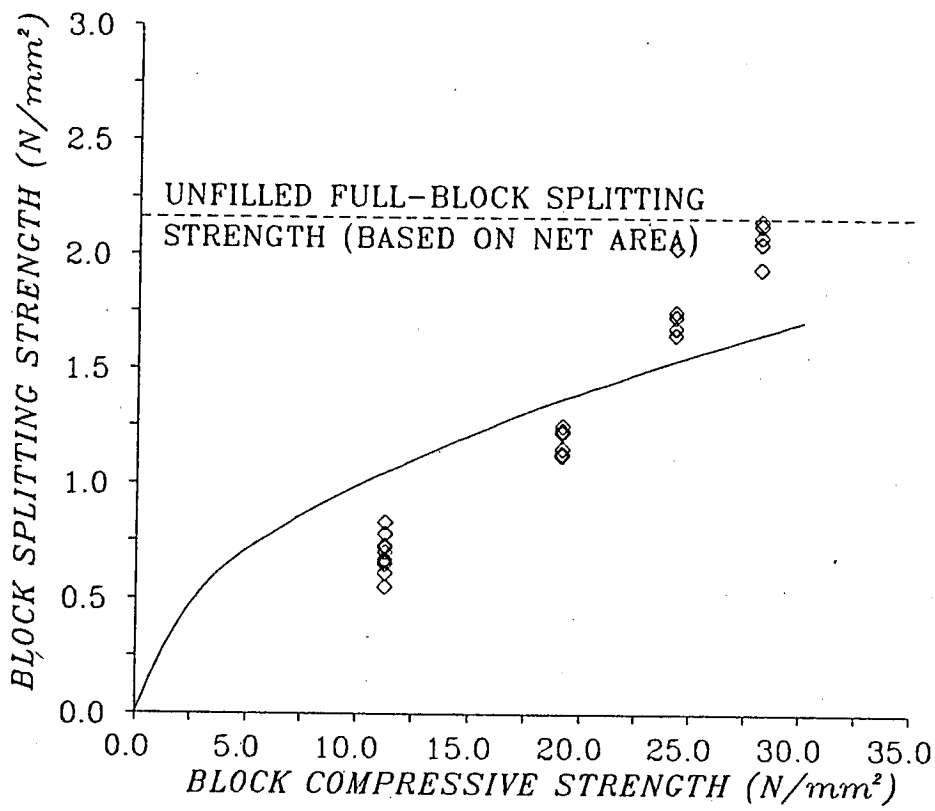

Fig. 3.24 - Block splitting strength vs block compressive strength.

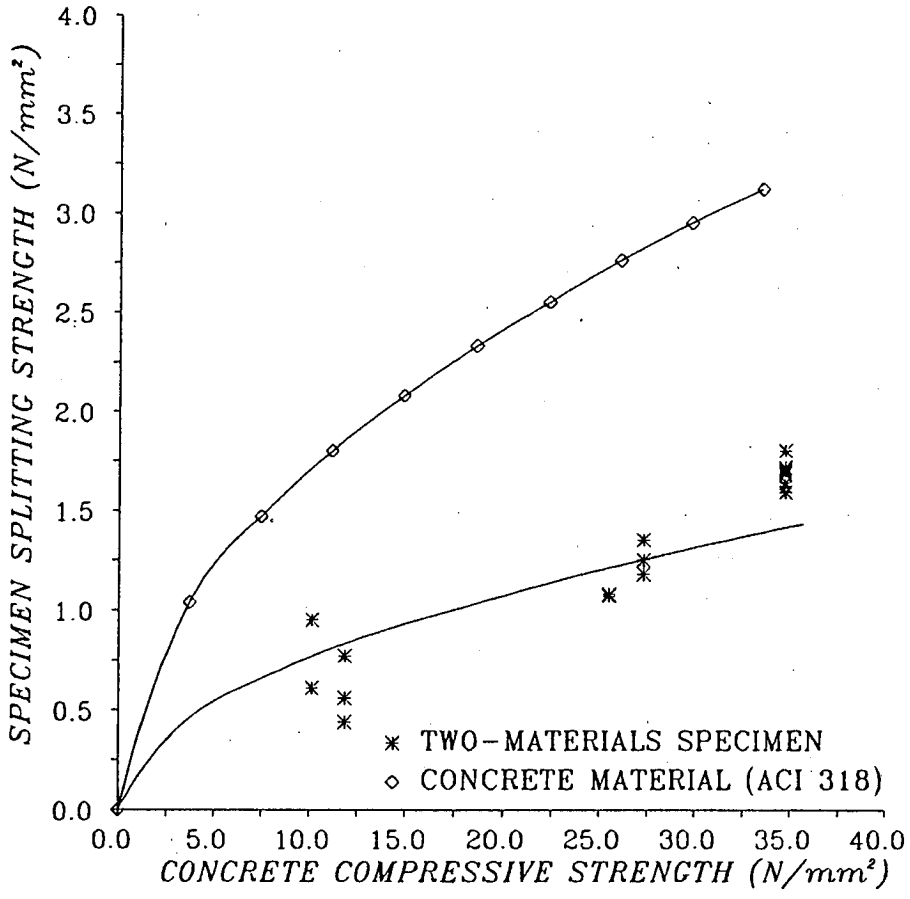

Fig. 3.25 - Effect of concrete strength on cohesion bond strength with block material.

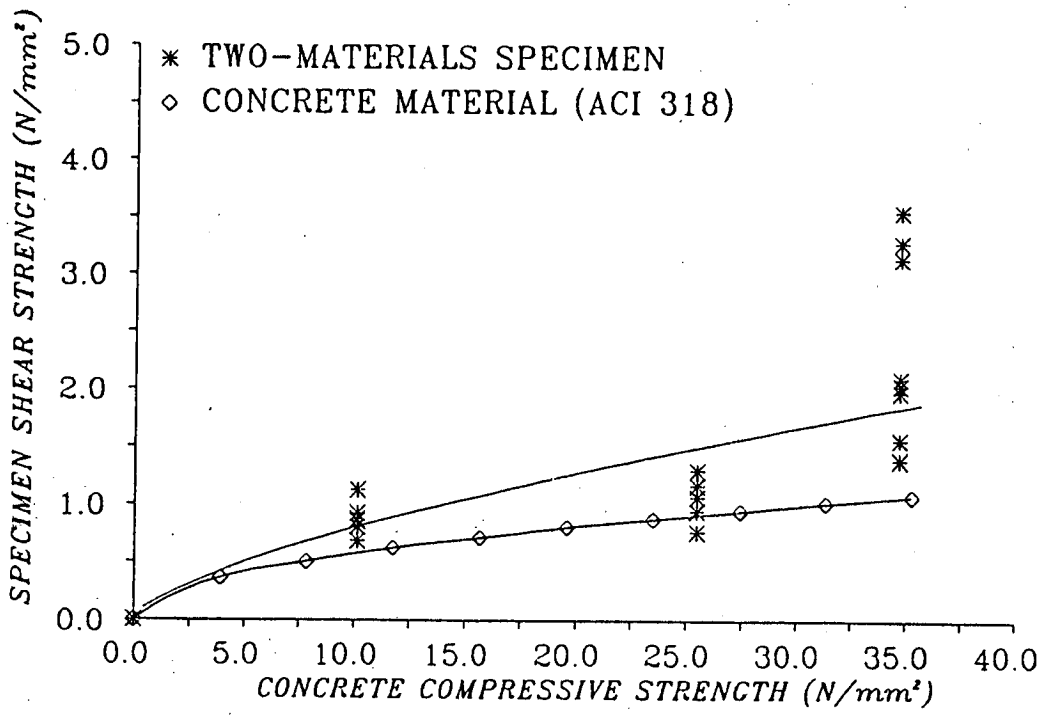

Fig. 3.26 - Effect of concrete strength on shear bond strength with block material.

CHAPTER 4

CONCRETE BLOCK MASONRY PRISMS COMPRESSED PARALLEL TO THE UNIT BED FACE

4.1 INTRODUCTION

This chapter is divided into two major sections. The first deals with the experimental investigation which is concerned with the determination of the compressive strength and a study of the behaviour of two-block prisms, compressed in a direction parallel to the unit bed face. The second presents the theoretical investigation of the two-block prisms using a two-dimensional linear and three-dimensional non-linear finite element analyses (FEA).

The specimens were built using three different mortar types and infilled with three different concrete mixes respectively. The specimens simulate the compression zone in a reinforced blockwork masonry beam (Fig. 4.1), or part of a masonry wall subjected to horizontal forces in its own plane accidentally or during an earthquake.

As mentioned in chapter 3 and in order to determining the ultimate compressive strength of a blockwork masonry prism, f'_m, some codes and standards[19,20,22] use either tables or graphs, relating the blockwork compressive strength to the unit block strength and the type of mortar. This method was originally derived from prism testing for codes and standards purposes. Alternatively tests on stack-bonded masonry prisms[24,25] (Fig. 4.2), with a height-to-thickness ratio (h/t) between 2.0 and 5.0, made of the same constituent materials as those used during construction, were subjected to axial compressive load applied in a direction normal to the unit bed face.

There are no clear indications in any of the references quoted as to the difference in strength of the prism when compressed in a direction parallel (Fig. 4.3), instead of normal, to the unit bed face.

As referred to in chapter 3 the British Code of Practice, BS 5628: Part 2: 1985[21], recognizes that there maybe a difference in strength as between masonry built with the units compressed normal to the bed face and that in which units are compressed parallel to the bed face.

BS 5628 determines the values of f_k for blockwork masonry from tables and graphs, relating the compressive strength of filled concrete block masonry to the solid unit block strength and the type of mortar, provided that the compressive strength of the infill is not less than that of the blocks assessed on their net area. If the infill strength is less than that of the block material, the strength of the filled blockwork is to be taken as that of the infill, as if the block were solid.

Previous studies[35,36,71] on blockwork masonry prisms, compressed parallel to the unit bed face, indicated that since blockwork masonry prisms have three component materials, namely concrete block, mortar and concrete infill, these three materials give the blockwork masonry non-homogeneous properties compared with concrete.

Several studies[27,28,29,30,31,32,33,34,35,36,38,71] on blockwork masonry have shown that the deformational characteristics of the concrete infill rather than its strength had a major effect on reducing the compressive strength of filled blockwork masonry prism, compressed either parallel or normal to the bed face, as compared to unfilled prisms.

Mortar plasticity had also been shown[71,72,75,76,77,78,79] to

cause a reduction in the compressive strength of both filled and unfilled prisms by applying additional tensile stresses to the blocks resulting from differences in the mechanical properties of the stiff coarse aggregate blocks and soft fine aggregate mortar.

A study of the effects of this non-homogeneity on the prism strength and behaviour, taking into consideration the wide range of concrete blocks, mortar types and concrete infill strengths, using classical principles of mechanics is very difficult, if not impossible. Therefore, standard finite element software, LUSAS[80], which is a general purpose package was used to explain and understand the behaviour of the block, concrete infill and mortar as they interact with each other as an entity.

The objective of the present investigation is to produce a method of obtaining f'_m, for use in the strength design theory of masonry structural elements, in situations where high in-plane horizontal forces are expected. The effects of using different types of mortar and concrete infill mixes on f'_m and on the prisms' behaviour and mode of failure were also studied.

4.2 EXPERIMENTAL PROGRAMME

Thirty-six prisms were constructed vertically by placing one block on top of the other with a 10 mm mortar joint in between. This method of construction differs from the conventional method of construction where the blocks are laid horizontally with a vertical mortar joint in between. The reason for adopting this method of construction was to ensure that the mortar joint between the two blocks would be completely filled with no air voids.

The main objective however of the present investigation is to study the effects of using different types of mortar and concrete infill on determining f'_m, and not to examine the effects of the method of construction on site and in the laboratory.

The prisms were constructed using three different mortar types: low strength (1:1:6), medium strength (1:0.5:4.5) and high strength (1:0.25:3) (cement: lime: sand) proportions. The prisms are designated in Fig. 4.4 (i), Table A.1 (Appendix A) and in the text as **2BP-MJ (2-Block Prisms with Mortar Joint)**.

Some of the two-block prisms were constructed without a mortar joint. Instead, a thin layer, 1 - 2 mm, of dental plaster was placed between the two blocks prior to test. The prisms are designated in Fig. 4.4 (ii), Table A.1 (Appendix A) and in the text as **2BP-DPJ (2-Block Prisms with Dental Plaster Joint)**. The 1 - 2 mm thickness was achieved by compressing the soft dental plaster in the same way as used in chapter 3[55].

Three different concrete infill mixes: low strength (1:5:2), medium strength (1:3:2) and high strength (1:1:2) (cement: sand: aggregate) proportions, were used for filling some of the prisms. Rapid hardening cement was used in all types of mortar and mixes of concrete.

The prisms were first built, then left under polythene sheeting for three days to allow the mortar joints to gain in strength. After three days the prisms were filled with concrete, batched by volume, mixed to a high slump of 150 mm then cast in two layers. Each layer was hand compacted, using the same steel rod commonly used for compacting and making concrete cubes. After compaction the top of the concrete infill was trowelled level.

After casting the prisms were left to cure under polythene sheeting for seven days. The polythene was then removed and the specimens left for a further seven days to cure under ambient conditions in the laboratory prior to testing. Steel moulded cubes and cylinders, cast and cured with the specimens, were tested in compression to determine the strength of the mortar and concrete infill mixes.

Demec points and electrical strain gauges were placed on the specimens at selected locations 24 hours before testing. Prior to testing, all the specimens were capped with a thin layer, 1 - 2 mm, of dental plaster[55] prepared by the same method explained in chapter 3.

The loading rates were in accordance with BS 6073: Part 1: 1981[66] and the loading pattern was in accordance with BS 1881: Part 121: 1983[68] to enable the determination of the static modulus of elasticity for all the specimens tested. By using this loading pattern, the strain measurements were recorded at two stress levels, viz. 0.5 N/mm^2 and one third of the ultimate specimen strength. The measurements were then repeated two to three times in a process of loading and unloading. In all the stress vs strain curves reported in this investigation, values from the results of loading and unloading were omitted for clarity, only values from the first cycle of strain measurements are shown.

4.3 THEORETICAL PROGRAMME

The theoretical programme is divided into five major sections. The first section gives a summary of some of the features of the FEA program used. The second section deals with the reasons for choosing the two-dimensional elastic linear FEA to study the effect of using the steel bearing

plate in applying the external stress. The third section gives the advantages of using the three-dimensional plastic non-linear FEA in the analysis for unfilled and filled **2BP-MJ** prisms. The fourth section presents the mechanical properties for the materials used in the FEA. The fifth section demonstrates the finite element meshes used in the two and three-dimensional analyses and the assumption used in reducing the size of these meshes.

4.3.1 General

The mathematical analysis of concrete masonry prisms with different materials, many degrees of freedom and complex geometry by the method of classical principles of mechanics is very difficult, if not impossible. Therefore approximate numerical methods are used to solve this problem. A standard finite element software, LUSAS[80], which is a general purpose package was selected for this investigation. This package permits the use of two and three-dimensional linear and non-linear material properties and was used to determine deformations, direct, shear and principal stresses at different locations in the prisms.

The linear two-dimensional analysis was used only to study the importance of using a steel bearing plate in applying the load on the prism. This analysis is not sufficient to perform an accurate analysis on unfilled and filled prisms because of the materials' non-linearity, mainly the mortar material[36,71,75,76,77,78,79], and the triaxial state of stress anticipated in masonry prisms[29,32,33,38]. Therefore a non-linear three-dimensional analysis was conducted for unfilled and filled **2BP-MJ** prisms, to get a better impression of the prism deformations and stresses and to study the effect of using different types of mortar and concrete infill on the prism behaviour and strength.

The FEA program LUSAS has a special facility of separating each prism material individually. This facility has the advantage of studying the distribution of stress in each material separately; also of explaining the complex behaviour of the block, concrete and mortar as they interact with each other as an entity in blockwork masonry prisms.

4.3.2 Two-Dimensional Elastic Linear FEA

A two-dimensional elastic linear FEA was utilized to study the effect of using a steel bearing plate in applying vertical stress on the prisms. Two linear analyses were conducted using the unfilled **2BP-MJ** prism with a high strength (1:0.25:3) mortar joint. The only difference between the two analyses is the presence of a steel bearing plate. In these analyses a specific level of vertical stress was applied on the prism, which is similar to the value derived experimentally for the unfilled **2BP-MJ** prisms with a high strength (1:0.25:3) mortar joint (Table 4.1). In the first analysis the external level of vertical stress was applied directly to the top of the prism. In the second analysis the external level of vertical stress was applied by using an 88 mm thick steel bearing plate.

The two-dimensional linear analysis was chosen to study the effect of using the steel bearing plate, because it is easier, faster and does not need a large computer memory space as is the case with a non-linear analysis. Also, the results obtained give sufficient information on the effect of using a steel bearing plate to apply the vertical stress.

4.3.3 Three-Dimensional Plastic Non-Linear FEA

Two non-linear thee-dimensional analyses were employed. In the first analysis a specific level of vertical stress was applied on the prisms, which is similar to the value derived experimentally (Table 4.1). This specific analysis was conducted for an unfilled prism, constructed with a high strength (1:0.25:3) mortar, and for a filled prism, constructed using the same type of mortar but filled with medium strength (1:3:2) concrete. The second analysis was a parametric study in which the level of the vertical stress applied to the unfilled **2BP-MJ** prisms is the average experimental value of the compressive strength for an unfilled prisms constructed with low strength (1:1:6) mortar. In the case of the filled **2BP-MJ** prisms, the level of the vertical stress applied is the average experimental value of the compressive strength for prisms built with medium strength (1:0.25:3) mortar and filled with low strength (1:5:2) concrete (Table 4.1).

The parametric study was carried out by fixing the level of vertical stress applied to the analysed prisms and changing the materials for the three types of mortar (1:1:6, 1:0.5:4.5 and 1:0.25:3) and three mixes of concrete (1:5:2, 1:3:2 and 1:1:2) as used in the experimental investigation.

The reasons for the specific analysis are to compare the experimental and theoretical results for unfilled and filled **2BP-MJ** prisms and to get a more accurate impression of the prism's deformed shape, stress distribution, crack formation and mode of failure. The reasons for the parametric study analysis are to examine the effects of using different types of mortar and concrete infills on the behaviour and strength of the unfilled and filled prisms.

4.3.4 Material Mechanical Properties Used in the FEA

The material mechanical properties (compressive strength, modulus of elasticity and Poisson's ratio) used in the analyses were obtained from the experimental part of this investigation (see Table 3.7).

The material's initial tangent modulus of elasticity and Poisson's ratio were used in the elastic linear analysis. Where the plastic non-linear analysis provided by LUSAS[80] required the input of the entire vertical stress vs strain curve for the materials, the relationship was approximated by a series of straight lines.

The vertical stress vs strain curves used for the block material (see Fig. 3.8) and three different concrete mixes (see Figs 3.10, 3.11 and 3.12) were found using the stress vs strain curves for rigorous analysis of non-critical concrete sections given in BS 8110: Part 2: 1985[69]. The curves were derived by substituting the magnitudes of the material strengths and the moduli of elasticity given in Table 3.7 into Eqns 3.1 to 3.3 (see chapter 3).

The confined vertical stress vs strain curves for the 10 mm joint using three different types of mortar were obtained by testing unfilled two-block prisms, constructed with a 10 mm mortar joint, in a direction normal to the bed face. The vertical stress vs strain curve for the mortar joint (see Fig. 3.16) takes into account the effects of mortar thickness compared to block; also the confinement exerted on the joint by the stiff concrete blocks.

The vertical stress vs strain curves for all the above materials were idealised in a series of straight lines as required by the FEA. Figs 4.5, 4.6 and 4.7 show typical

idealised vertical stress vs strain curves for the block, (1:3:2) concrete and (1:0.25:3) mortar materials respectively.

The values of Poisson's ratio for all the materials used in the non-linear FEA were derived experimentally by plotting the lateral strain vs vertical strain (see Figs 3.9, 3.13 and 3.15) and taking the values of Poisson's ratio at a strain corresponding to the material's maximum compressive strength (see Table 3.7).

CHEEMA and KLINGNER[32], in determining the material properties to be used in a linearly elastic finite element analysis, suggested using an idealised vertical stress vs strain curve for confined mortar based on the unconfined vertical stress vs strain curve for a mortar cylinder (see Fig. 3.16). They also found values for the Poisson's ratio through experimentation similar to those given in Table 3.7 and used in the non-linear FEA presented herein.

In the case of the steel bearing plate, linear material properties was assumed. This is acceptable for the steel since, for the levels of vertical stress applied, it would remain elastic.

4.3.5 Finite Element Model

4.3.5.1 Two-dimensional model

The two-dimensional finite element model was developed by using plane strain membrane elements, one with four nodes (QPN4) and the other with three nodes (TPN3). The FEA model was developed by considering only 1/2 of the prism (Fig. 4.8) in the analysis.

In generating the mesh (Fig. 4.9), certain assumptions were made to simplify and reduce the size of the mesh:

1. Full advantage was taken of symmetry.

2. The tapering of face shells and webs was ignored; instead the average shell thickness was used (see Table 3.2, block section (2)).

3. The interfaces between the blocks and the mortar were assumed to be rigid because frictional forces created by compression prevent slipping[33,35,38,71].

The prisms were restrained at the bottom in two directions and the axial load was applied by means of uniform pressure with and without using the 88 mm thick steel bearing plate. The top surface of the prism or the bearing plate was restrained in the horizontal direction and free in the vertical direction, which is the direction of loading. The plane of symmetry was restrained in a direction normal to the plane and free in the other direction.

4.3.5.2 Three-dimensional model

The three-dimensional finite element computer model was developed by using solid elements, one with eight nodes (HX8) and the other with six nodes (PN6). The FEA model was developed by considering 1/4 of the prism (Fig. 4.10) in the analysis.

In generating the mesh (Fig. 4.11) certain assumptions were made to simplify and reduce the size of the mesh. The first three assumptions are similar to the ones made in the two-dimensional analysis. The other assumptions are:

1. perfect bond was assumed between the blocks and concrete infill (no concrete infill shrinkage).

2. In the case of unfilled prisms the material properties for the concrete infill was assumed to be linearly elastic with very low modulus of elasticity (0.000001) and Poisson's ratio (0.000001).

The prisms were restrained at the bottom in three directions and the axial load was applied by means of uniform pressure using an 88 mm thick steel bearing plate. The top surface of the plate was restrained in the two horizontal directions and free in the vertical direction, which is the direction of loading. All the planes of symmetry were restrained in a direction normal to the plane and free in the other two directions.

4.4 DISCUSSION OF EXPERIMENTAL RESULTS

Discussion of the experimental results is considered in two sections. The first deals with the observed modes of failure for the unfilled and filled prisms. The second deals with the experimental results.

4.4.1 Modes of Failure

The observed mode of failure for all the unfilled **2BP-MJ** prisms was first by local crushing at the outer faces of the mortar joint, followed by shearing and splitting of the block shells sideways. There was some sign of cracking at the outer face of the mortar joint prior to failure (Fig. 4.12).

The unfilled **2BP-DPJ** prisms first failed by crushing

of the block side shells, followed by complete disintegration of the prism (Fig. 4.13). Both types of unfilled prism showed an abrupt mode of failure.

The common feature in the mode of failure of all the filled **2BP-MJ** prisms, was first the occurrence of crushing at the mortar joint followed by shearing and sideways splitting of the block shells.

The prisms with high strength (1:1:2) concrete, showed no signs of any major cracks in the concrete either during testing or after failure. On the other hand, the prisms with low strength (1:5:2) concrete, showed a crushing type of cracking in the concrete at failure. The prisms with medium strength (1:3:2) concrete showed some signs of crushing of the concrete, but not as severe as those filled with low strength concrete (Fig. 4.14).

Filled **2BP-DPJ** prisms showed the same three dissimilar modes of failure, with regard to the strength of the concrete infill mix used, observed for the single-block specimens. The only difference was that the initiation of first crushing and shearing in the block was near the dental plaster joint and not near the machine platens (Fig. 4.15).

4.4.2 Experimental Results

Table 4.1 lists the results for all the unfilled and filled two-block prisms tested. Also listed are all the associated material properties.

The stress vs strain curves, for the unfilled **2BP-MJ** prisms (Fig. 4.16), show the mortar joint yielding at high stress compared with the block[36,71,72]. The stiffness of the

block material was also seen to be much higher than that of the mortar, as would be expected. The curves also denoted some confinement at the mortar joint (curves 2,4) and showed some evidence of increasing stiffness at the outer face of the mortar joint prior to failure (curve 3). This was basically caused by splitting of the block shells to the outside prior to failure[35,36,71]. The stress vs strain curves show that the mortar joint absorbs most of the energy applied to the prisms; this was illustrated by the area under the vertical stress vs strain curve for the mortar. The high ductility of the mortar resulted primarily from the insignificant ratio of the mortar thickness to the other two dimensions[1,26,28,33,71], and the confinement stress afforded by the blocks[1,28,29,32,33,34,35,36,38].

Unfilled **2BP-DPJ** prisms failed by crushing of the block shells which was clearly shown by the high strain readings at the block shells (Fig. 4.17). On the other hand, the unfilled **2BP-MJ** prisms failed by crushing at the mortar joint. This explained why the average strength value of the unfilled **2BP-DPJ** specimens, was slightly higher than that of the unfilled **2BP-MJ** ones.

The effect of the cube compressive strength of mortar on the unfilled prism strength is clearly shown in Fig. 4.18. The figure shows that the presence of the mortar joint in unfilled prisms caused a small reduction in the prism compressive strength compared to unfilled prisms with dental plaster joint. The figure also shows that increasing the mortar cube strength by at least 166.9% produces an increase of only 6.2% on the compressive strength of unfilled prisms[26,28,33,36,71]. This was mainly due to the insignificant ratio of the mortar joint thickness to the block height (1/39), and also due to confinement of the mortar by the stiff blocks.

A statistical computer program (MINITAB)[73] was used to derive the following best fit equation relating the compressive strength of an unfilled prism with mortar joint to the strength of the mortar as follows:

$$f'_m = 21.9 + 0.11\, f_{mr} \qquad \text{...(4.1)}$$
$$r = 0.96$$

Table 4.1 shows that most of the unfilled prisms with a mortar joint failed at a compressive strength higher than the mortar cube strength. This suggests that the mortar strength in a joint is apparently higher than the mortar cube strength. This is due to the relatively small mortar thickness compared to the unit height, and the confinement of the mortar by the stiff concrete blocks.

The stress vs strain curves for the filled **2BP-MJ** prisms (Fig. 4.19) show a reduction in the block stiffness compared to the corresponding one for unfilled prisms. This reduction was also observed in the single-block specimens and was ascribed to the presence of the concrete infill, and its high Poisson's ratio[35,36,71], which caused premature failure of the specimen prior to reaching the unfilled block compressive strength or the block material strength.

The curves also showed the phenomenon of mortar yielding at the outer face of the mortar joint (curve 3), and almost zero strain at the centre of the mortar joint (curve 1). This confirmed the observed mode of failure where the first indication of prism failure was crushing at the outer face of the mortar joint. The curves indicate an increase in stiffness before failure, caused by the tendency of the block shells to split to the outside prior to failure. This was even more critical for prisms filled with a high strength (1:1:2) concrete mix. This suggested that the stiff concrete infill works as a cleavage forcing

the blocks to split before attaining their unfilled block compressive strength.

The stress vs strain curves for the filled **2BP-DPJ** prisms, (Fig. 4.20), show a reduction in the block stiffness compared to the corresponding unfilled prisms. This reduction was caused by the high Poisson's ratio of the concrete, as explained previously for the filled **2BP-MJ** prisms.

Fig. 4.21 summarizes the relation between the prism strength and the cube compressive strength of the concrete for prisms with equal mortar strength, also for prisms with dental plaster joints.

A noticeable dissimilarity was the reduction by a factor of 0.75 in the curve for prisms with a mortar joint compared to those with a dental plaster joint. This fall was primarily caused by the presence of the mortar joint, which caused a reduction in the prism strength by introducing tensile stresses which were in addition to those already in existence as a result of the presence of concrete infill. These extra tensile stresses result from the difference in Poisson's ratio between the concrete block and the mortar and was responsible for the confinement stresses in the mortar as observed earlier in the stress vs strain curves.

HILSDORF[76] reported a Poisson's ratio for mortar of about 0.20 near zero axial strain and 0.50 or more near crushing. MAHER and DAVID[75] reported values of 0.20 at 0.001 axial strain, about 0.30 at 0.002, and greater than 1.0 near crushing. Such large apparent values of Poisson's ratio were probably due to the presence of longitudinal cracks in the material rather than a true material property.

The effect of changing the mortar strength on the compressive strength of the filled prism with concrete infill of almost equal strength is clearly shown in Fig. 4.22. It can be seen that increasing the mortar strength by at least 166.9% produces an increase of only 23.9% and 3.8% on the compressive strength[26,28,33,36,71] of prisms with low and high strength concretes respectively. The reasons for the insignificant effect on the prism strength of increasing the mortar strength are the same as the ones for unfilled **2BP-MJ** prism.

This leads to the conclusion that f'_m was not actually related to a change in mortar strength but to the presence of the mortar joint by itself as a plane of weakness. f'_m can thus be determined by first testing a filled single-block specimen in a direction parallel to unit bed face then, multiplying the compressive strength so found by a factor of (0.75). This represents the reduction in prism strength resulting from the presence of the mortar joint as a plane of weakness. Thus the compressive strength of filled **2BP-MJ** prisms is govern by:

$$f'_m = 0.75\ f_{bpf} \qquad \ldots(4.2)$$

Fig. 4.23 shows the effect of the h/t (prism height-to-thickness) ratio on the strength of unfilled and filled single-block specimen and **2BP-DPJ** prisms with the same concrete infill strengths, all tested parallel to the bed face. It can be seen that the strength of almost all two-block prisms, with h/t = 4.0, was either equal or greater than the corresponding single-block specimens with h/t = 2.0[36,71]. This is contrary to the well known reduction in strength with height for masonry prisms laid in stack-bond and compressed normal to the bed face. No clear explanation was found to this behaviour.

4.5 DISCUSSION OF THEORETICAL RESULTS

The discussion is divided into four major sections. The first section is a general discussion of the common features of the results of the specific analysis and parametric study analysis. The second section deals with the results of the two-dimensional linear FEA and the effect of using the steel bearing plate. The third and fourth sections present the results of the non-linear three-dimensional FEA for unfilled and filled **2BP-MJ** prisms respectively.

4.5.1 General

The contour plots for the linear two-dimensional FEA presented in this investigation are for 1/2 prism model. While the colour contour plots for the non-linear three-dimensional FEA of deformation and stress are for 1/4 prism model. By symmetry the other 1/2 or 3/4 of the prism should have similar distribution of deformation and stress as the one for the 1/2 or 1/4 prism model respectively. In the three-dimensional colour contour plots the lines of contact between the different colours represents the value of the contour and each individual colour represents a range of values. These are explained by boxes of the fill colour, the associated contour value being annotated at the colour interface.

In general, it was found that an understanding of the contour plots of the prisms deformation in the Y-, X- and Z-directions is important in obtaining a clear picture of how the stresses are distributed throughout the prisms.

The contour plots of the direct horizontal stresses in the X- and Z-directions show confinement stresses located

near the steel platens of the machine. These stresses have a limited effect on the rest of the prism and mainly result from differences in material properties of the blocks and the stiff steel platens. These in turn produced confinement stresses on the blocks[26,55,81,82,83,84]. This suggests that the unfilled and filled two-block masonry prisms can be used as standard test specimens to determine f'_m, in situations where high in-plane horizontal forces are expected.

4.5.2 Elastic Linear FEA for Unfilled 2BP-MJ Prism

The specific level of vertical stress applied to the unfilled **2BP-MJ** prism in the two linear FEA was 8.86 N/mm^2. This value was derived experimentally as the average strength of three unfilled **2BP-MJ** prisms constructed with high strength (1:0.25:3) mortar (Table 4.1).

Applying the vertical stress directly to the top of the **2BP-MJ** prism was found to give unrealistic results. This was clearly shown by the magnified deformed shape (Fig. 4.24 (i)). The figure shows a simply supported beam action[33,35] created at the top side of prism, with an excessively high vertical deformation and unacceptably high elastic tensile and shear stresses (35.03 N/mm^2 and 21.17 N/mm^2 respectively) (Figs 4.25 (i) and (ii)), compared to the allowable ultimate tensile and shear stresses given by the ACI 318M-83[74] which are:

$$f_{ct} = 0.58 \quad (f_b)^{1/2} \qquad \ldots(4.3)$$

$$f_{cv} = 0.18 \quad (f_b)^{1/2} \qquad \ldots(4.4)$$

On the other hand, applying the vertical stress using an 88 mm thick steel bearing plate gave a more realistic result, with no indication of high deformation (Fig. 4.24 (ii)) or high tensile and shear stresses (5.92 N/mm^2 and

14.42 N/mm^2 respectively) (Figs 4.26 (i) and (ii)) .

All other prisms analysed were loaded with a steel bearing plate and non-linear material properties were used throughout.

4.5.3 Plastic Non-Linear FEA for Unfilled 2BP-MJ Prism

4.5.3.1 Analysis of prism with specific level of vertical stress

The specific level of stress applied to the unfilled **2BP-MJ** prism in this non-linear analysis was 8.86 N/mm^2. This value is similar to the value derived experimentally for prisms built with high strength (1:0.25:3) mortar (Table 4.1).

Prism Deformation

The contour plot of the prism deformation in the Y-direction (Fig. 4.27) shows that the prism top surface shortens with a maximum cumulative vertical deformation of 0.817 mm with respect to the fixed prism bottom surface. The contour plot of the prism horizontal deformation in the X-direction (Fig. 4.28) shows that there is a greater tendency for the block side shells near the mortar joint to deform outward, with a maximum deformation of 0.050 mm, than near the machine platens. Also shown is the tendency of the mortar joint to deform inward with a maximum deformation of 0.020 mm. The way in which the prism deformed in the X-direction suggests that using a weaker mortar joint results in a higher outward deformation in the X-direction and consequently higher compressive and tensile stresses to the inside and outside faces of the block side

shells respectively. On the other hand, the contour plot of the prism deformation in the Z-direction (Fig. 4.29) shows a greater tendency for the prism side shells to deform outward between the prism webs, with a maximum deformation of 0.036 mm, near the mortar joint. The way in which the prism deformed horizontally is affected by the high plasticity of the mortar joint.

Comparing the maximum vertical deformation obtained from the non-linear analysis with that obtained from the linear analysis with steel bearing plate, it was found that the former is 59.7% higher than the latter. This large difference reflects the importance of using non-linear material properties in the analysis of blockwork masonry assemblages.

Stresses in the Block Material

The contour plots of the direct stresses in the block material in the Y-, X- and Z-directions are shown in Figs 4.30, 4.31, and 4.32 respectively. The contour plots of the major and two minor principal stresses are given in Figs B.1, B.2 and B.3 (Appendix B) respectively.

The contour plot of the direct vertical stress in the Y-direction shows that the maximum compressive vertical stress, 30.90 N/mm^2, is located at the inner faces of the block side shells as would be expected from the way the prism deformed in the X-direction. The figure also shows some tensile vertical stresses, with a maximum value of 2.17 N/mm^2, at the inner faces of the block end shells near the mortar joint. These tensile vertical stresses are the result of the plasticity of the mortar joint, where by the block end shells near the mortar joint lift up as the mortar under the prism side shells squeezes.

The contour plot of the direct horizontal stress in the X-direction shows that the maximum tensile stress, 7.80 N/mm^2, is located at the inner faces of the block end shells near to the mortar joint. The reason for this is similar to the reason for the tensile vertical stresses. The contour plot of the direct horizontal stress in the Z-direction shows that the maximum tensile stress, 4.28 N/mm^2, covers most of the prism webs and a small area on the prism side shells. The tensile stresses in the Z-direction at the block end shells near to the mortar joint, result from differences in the mechanical properties between the fine sand mortar joint and the coarse aggregate concrete blocks. No tensile stresses were observed near the mortar joint in the X-direction.

The contour plots of the principal stresses (Appendix B) show a higher tensile stress, 4.27 N/mm^2 (MST1), on the prism mid-webs and some of the prism side shells (Fig. B.2) and 8.91 N/mm^2 (MST2), on the inner faces of the block end shells near the mortar joint (Fig. B.3).

The distribution of the horizontal and principal stresses suggests that the prism has a greater tendency to split vertically along the prism side shells rather than the mid-webs.

Fig. 4.33 shows the contour plot of the maximum shear stress in the block material. The figure shows high shear stresses at the prism side shells with a maximum value of 12.54 N/mm^2. This value is quite high compared to that suggested by the ACI code for concrete given by Eqn. 4.4. The distribution of the maximum shear stress suggests that the prism side shells tend to shear from the prism webs.

Although the stress results are quite high as compared to the allowable stresses, the results are sufficient to

give a clear idea of the way the stresses are distributed in unfilled **2BP-MJ** prisms, subjected to axial load in a direction parallel to the unit bed face.

Despite the 59.7% increase in the vertical deformation of the prism from the non-linear analysis, compared to the linear analysis, the increase of 11.2% in the maximum tensile stress in the X-direction and the decrease of 13.5% in shear stress is small compared to the high increase in deformation. This result emphasizes again the importance of material non-linearity in the analysis of blockwork masonry assemblages.

Stresses in the Mortar Material

The contour plots of the direct stresses in the mortar joint in the Y-, X- and Z-directions are shown in Figs 4.34, 4.35, and 4.36 respectively. The contour plots of the major and two minor principal stresses are given in Figs B.4, B.5 and B.6 (Appendix B) respectively.

The contour plot of the direct vertical stress in the Y-direction shows that the highest vertical stress is located at the outer faces of the mortar joint, with a maximum value of 24.02 N/mm^2. This value tends to decrease towards the centre of the mortar joint where it changes to a tensile stress of 2.19 N/mm^2. The vertical stresses at the mortar joint are distributed as expected, since the vertical stresses transfer to the mortar joint through the prism side shells. The high vertical stresses at the outer faces of the mortar joint are consistent with the observed mode of failure for all the unfilled **2BP-MJ** prisms, in the experimental investigation, where by the first sign of local crushing occurred at the outer faces of the mortar joint.

A clear similarity was observed in the distribution of the direct horizontal stresses in the X- and Z-directions. Both horizontal stresses show that the mortar joint is subjected to confinement stresses in the X- and Z-directions with maximum values of 7.54 N/mm^2 in the X-direction and 7.13 N/mm^2 in the Z-direction. These maximum stresses are located at the outer faces of the mortar joint and tend to reduce towards the centre of the mortar joint. There the stresses become tensile, with maximum values of 0.074 N/mm^2 in the X-direction and 0.63 N/mm^2 in the Z-direction. The confinement stresses are caused by differences in the deformational characteristics of the soft mortar joint and the stiff concrete blocks. The tensile stresses result from a tendency for the mortar to deform inward due to uplift of the block end shells near the mortar joint.

Fig. 4.37 shows the contour plot of the maximum shear stress at the mortar joint. The figure shows that the maximum value, 8.75 N/mm^2, is located at the outer faces of the mortar joint. This value of shear stress tends to decrease towards the centre of the mortar joint. The location of the highest shear stresses at the mortar joint is in good agreement with the location of these stresses in the block material. This means that the outer faces of the mortar joint work as part of the prism side shells. Also, both sheared to the outside at failure.

All the contour plots of stresses at the mortar joint discussed so far, show a non-uniformity in their distribution, with high stresses at the outer faces of the mortar joint and almost zero stress at the inner face. This non-uniformity is attributed to the shape of the block and the way in which it is loaded[35,71].

4.5.3.2 Parametric study analysis

The level of vertical stress applied to the unfilled **2BP-MJ** prisms for the parametric study was 8.34 N/mm^2 which is the average experimental value of compressive strength for prisms built with low strength (1:1:6) mortar.

In order to examine the effect of changing the mortar type on the prism deformations and stresses, the parametric study was conducted by fixing the applied level of vertical stress and changing the types of mortar joint for the unfilled **2BP-MJ** prisms to low (1:1:6), medium (1:0.5:4.5) and high (1:0.25:3) strength.

The effect of changing the type of mortar on the prism deformation is clearly shown by the contour plots for the horizontal deformation in the X-direction (Figs 4.38, 4.39 and 4.40) and in the Z-direction (Figs 4.41, 4.42 and 4.43) for prisms built with low, medium and high strength mortar joints respectively. The figures show that the horizontal deformations, in prisms built with a low strength mortar joint, are mainly located at the joint as inward and outward squeezing of the joint. On the other hand, prisms built with medium or high strength mortar joints show that the horizontal deformations exist over most of the prism side shells and webs.

Tables 4.2 and 4.3 give the results of the maximum values of deformations and stresses respectively for the unfilled **2BP-MJ** prisms, as derived from the parametric study analysis. Table 4.2 provides the results of the maximum values of the deformations in the Y-, X- and Z-directions; the level of vertical stress applied during the parametric study analysis; the average experimental compressive strength of the prisms and the cube compressive strength of the different types of mortar. Table 4.3, on

the other hand, gives the maximum values of direct, shear and principal stresses in each individual material.

To assess the effect of changing the cube compressive strength of mortar on the maximum values of deformation and stress in the prisms, the results of the parametric study were plotted in an X-Y plotter. The X-axis represent the cube compressive strength of the mortar and the Y-axis represent the prism maximum values of deformation or stress.

The effect of increasing the cube compressive strength of mortar on the prism deformation in the Y-, X- and Z-directions is shown in Fig. 4.44. The figure shows that the prism vertical deformation decreases by 5.4% as a result of changing the mortar strength from 7.27 to 19.40 N/mm^2. The reason for the small effect on deformation as the mortar strength increases is the insignificant thickness of the mortar joint compared to the block (1/39)[1,26].

For the same range of mortar strength, the prism deformations in the X- and Z-directions show that the prism's outward horizontal deformation decreases by 20.59% in the X-direction and by 71.1% in the Z-direction, as the mortar strength increases. On the other hand, the prism's inward horizontal deformation decreases by 58.8% in the X-direction and is almost constant, (0.005 mm), in the Z-direction. Table 4.2 shows that, for a prism built with low strength mortar joint, the outward horizontal deformation in the Z-direction is higher by 92.8% than that in the X-direction. For prism built with a high strength mortar joint, the outward horizontal deformation in the X-direction is 28.2% greater than that in the Z-direction. For a prism built with a medium strength mortar, little difference exist. The outward deformation in a prism built with low strength mortar is mainly located at the mortar

joint. In prisms built with medium or high strength mortars, most of the outward deformation is in the prism side shells.

Although the values of stress differ, the stress distributions for all the prisms analysed in this parametric study are similar to the contour plots of stresses for prisms analysed using the specific analysis. Information on how these stresses are distributed is given in the relevant contour plots of stresses from the specific analysis.

Figs 4.45, 4.46 and 4.47 show the effect of changing the cube compressive strength of the mortar on the maximum values of direct stress in the Y-, X- and Z-directions respectively. Fig. 4.45 shows that the vertical stress in the Y-direction, in the block material and mortar joint, increases by 0.6% and decreases by 7% respectively as a result of changing the mortar strength from 7.27 to 19.04 N/mm^2. A prism analysed with medium strength (1:0.5:4.5) mortar joint shows similar percentages of increase and decrease in the vertical stresses as for a prism built with high strength (1:0.25:3) mortar joint. These small percentage changes in stresses support the conclusion, derived previously, that the mortar joint has no significant effect on the prism strength. This is due to the small ratio of mortar thickness to block (1/39)[1,26,28,33], also to the high confinement of the mortar joint by the stiff blocks.

Fig. 4.46 shows that the confinement stress in the X-direction, at the mortar joint, decreases by 64.8% as a result of changing the mortar strength from 7.27 to 19.04 N/mm^2. For the same range of mortar strengths, the tensile stress at the block material decreases by 35.7%. As shown in Fig. 4.31, the maximum tensile stress at the block

material in the X-direction is not caused by mortar confinement but the result of uplifting of the blocks end shells near the mortar joint.

Similarly, the confinement stress in the Z-direction, (Fig. 4.47), at the mortar joint decreases by 66.6% and the tensile stress in the block material decreases by 15.9%, as the mortar strength increases. As shown in Fig. 4.32, some of the high tensile stresses at the block material, in the Z-direction, are caused by mortar confinement.

The decrease in the horizontal stresses as the mortar compressive strength increases is expected since increasing the mortar compressive strength decreases the plasticity of the mortar joint.

The results also show that the horizontal tensile stresses in the X-direction, at the block material, are higher by 136.3%, 93.3% and 80.8% than in the Z-direction, for prisms built with low, medium and high strength mortar joint respectively. Similarly, the results of the maximum values of minor principal stresses show an increases of 149.1%, 106.5% and 107.4% between the tensile stresses caused by uplifting of the blocks end shells and mortar confinement.

The results of the horizontal stresses suggest that changing the mortar compressive strength has little influence on the compressive strength of unfilled **2BP-MJ** prisms. They also suggest that the prism has more tendency to split along the prism side shells rather than the prism webs.

Fig. 4.48 shows the effect of changing the cube compressive strength of the mortar on the maximum values of shear stress. The figure shows that the shear stress at

the block material and the mortar joint decreases by 1.5% and increases by 99.3% respectively, as a result of changing the mortar strength from 7.27 to 19.04 N/mm^2. The high increases in shear stresses at the mortar joint suggest that the mortar attempts to behave in a similar manner to the block material. The shear stress results show again that changing the mortar compressive strength has little effect on the unfilled prism strength.

To sum up the effect of changing the cube compressive strength of mortar from 7.27 to 19.04 N/mm^2 on the compressive strength of unfilled prisms. It seems that the effect is not so great, since increasing the mortar strength has little effect on the major principal stresses and has only resulted in decreasing the tensile stresses.

Due to the complex nature of the deformations and stress distributions in unfilled prisms the general conclusion derived from the results of the specific and the parametric study analyses is that the failure of unfilled **2BP-MJ** prisms is dominated by localized crushing, splitting and shear failures. It is expected that the unfilled prisms will fail due to a combination of compression, tension and shear in an abrupt mode of failure.

The predicted mode of failure for the unfilled prism with low strength (1:1:6) mortar joint is as follows: First, by localized crushing at the outer faces of mortar joint followed by the combination of block crushing and shearing near the joint. As the mortar strength increases, the possibility of localized crushing increases, either at the mortar joint or at the block shells, followed by complete disintegration of the prism.

From the stress values and distributions, the strength of unfilled **2BP-MJ** prisms will depend on the block unit

compressive strength and the mortar type.

4.5.4 Plastic Non-Linear FEA for Filled 2BP-MJ Prism

4.5.4.1 Analysis of prism with specific level of vertical stress

The specific level of vertical stress applied to the filled **2BP-MJ** prisms in this analysis was 15.26 N/mm^2, which is the average experimental compressive strength of the prisms built with high strength (1:0.25:3) mortar and filled with medium strength (1:3:2) concrete (Table 4.1).

Prism Deformation

The contour plot of deformation in the Y-direction (Fig. 4.49) shows that the prism shortens vertically, with a maximum deformation of 0.747 mm at the prism top surface with respect to the prism fixed bottom surface. The contour plot of the prism horizontal deformation in the X-direction, (Fig. 4.50), shows a clear tendency for the prism side shells to deform outward, with a maximum deformation of 0.029 mm between the prism webs. The figure shows similar horizontal deformations of the block side shells in the vicinity of the mortar joint and the machine platens, which is not the case for the unfilled prism. The contour plot of the prism horizontal deformation in the Z-direction (Fig. 4.51) shows that the prism side shells and concrete infill tend to deform outward in a manner similar to the deformation in the X-direction, with a maximum value of 0.030 mm. This is similar to the value in the X-direction.

The value for the maximum outward horizontal deformation of the filled **2BP-MJ** prisms, in the X- and Z-directions are 41.6% and 17.2% less respectively than that for the unfilled **2BP-MJ** prisms. This suggests that the filled prisms are stiffer than the unfilled ones due to the presence of the concrete infill.

Stresses in the Block Material

The contour plots of the direct stresses in the block material in the Y-, X- and Z-directions are shown in Figs 4.52, 4.53, and 4.54 respectively. The contour plots of the major and two minor principal stresses are given in Figs B.7, B.8 and B.9 (Appendix B) respectively.

The contour plot of the direct vertical stress in the Y-direction shows that a maximum vertical stress value of 26.51 N/mm^2 is located at the prism bottom corner, near to the machine platen. The rest of the block shells are under a uniform stress ranging from 15.28 to 19.09 N/mm^2, with the exception of the inner faces of the blocks shells, where the compressive stress reaches a value of 22.91 N/mm^2. The high compressive stress at the inner faces of the block shells, is due to the way the prism deformed in the X-direction.

The distribution of vertical stress suggests that the prism side shells take a higher vertical stress than the prism mid-webs. This means that the concrete infill is not stiff enough as compared to block shells to transfer the vertical stresses to the prism mid-webs.

The contour plots of the direct horizontal stresses in the X- and Z-directions show that the prism end shells are under confinement stresses near the steel platens, with a

maximum value of 10.37 N/mm^2 in the X- and Z-directions. The maximum tensile stress value of 2.49 N/mm^2, in the X-direction, is located at the prism mid-webs and the outer faces of the prism shells, between the prism webs. The tensile stresses at the prism mid-webs result from the confinement of the concrete infill by the blocks. The tensile stresses at the prism side shells result from the outward deformation of the concrete. Both tensile stresses are caused by the high value of Poisson's ratio of the concrete. The direct stress in the Z-direction shows that the maximum tensile stress of 2.66 N/mm^2 is located at the prism mid-webs and side shells. The reason for these tensile stresses is similar to that which caused tensile stresses in the X-direction. Some of the horizontal tensile stresses in the X- and Z-directions, at the block end shells near the mortar joint, result from mortar confinement by the stiff blocks.

In considering the equilibrium of horizontal stresses in any cross-section, at the mortar joint, for filled **2BP-MJ** prisms, the assumption that the horizontal tensile stresses are uniformly distributed[29,32,33,38] is justified.

The contour plots of the minor principal stresses (Appendix B) show higher tensile stresses of 2.48 N/mm^2 (MST1), on the prism mid-webs (Fig. B.8) and 2.66 N/mm^2 (MST2), on the prism side shells (Fig. B.9). These values of tensile stresses are coincidentally similar to the tensile stresses in the X- and Z-directions. Both values of maximum tensile stress are higher than the experimental value of ultimate tensile strength for block material (2.16 N/mm^2) (see Table 3.9). This suggests that the filled prism has a similar tendency to split along the prism mid-webs and side shells.

Fig. 4.55 shows the contour plot of the maximum shear

stresses in the block material. The figure shows high shear stresses at the prism side shells, with a maximum value of 9.68 N/mm^2. This value is quite high compared to the value suggested by the ACI code for concrete as given by Eqn. 4.4. The distribution of the shear stresses suggests that the prism side shells tend to shear from the prism webs.

Stresses in the Concrete Material

The contour plots of the direct stresses in the concrete material in the Y-, X- and Z-directions are shown in Figs 4.56, 4.57, and 4.58 respectively. The contour plots of the two minor and one major principal stresses are given in Figs B.10, B.11 and B.12 (Appendix B) respectively.

The contour plot of the direct vertical stress in the Y-direction shows that most of the higher values of vertical stress are located at the contact areas between the block webs and concrete infill. The vertical stresses are almost uniformly distributed, ranging from 11.58 to 14.94 N/mm^2.

The contour plots of the direct horizontal stresses in the X- and Z-directions, are affected by the high localized vertical stresses at the contact areas between the block webs and concrete infill. Both horizontal stresses show high confinement stresses at the contact areas, with almost similar maximum values in the X-direction (3.23 N/mm^2) and the Z-direction (3.27 N/mm^2). These confinement stresses tend to reduce away from the contact areas, changing to tensile stresses with a maximum value of 0.93 N/mm^2 in the X-direction, and 0.57 N/mm^2 in the Z-direction.

The explanation for the way the horizontal stresses

are distributed is as follows:

Since the concrete infill under compression tries to deform outward, due to its high Poisson's ratio, the blocks try to restrict this movement. This restriction sets up confinement stresses in the concrete and tensile stresses in the blocks.

The contour plots of the minor principal stresses (Figs B.11 and B.12) show similar values of maximum stresses and of stress distribution to the horizontal stresses in the X- and Z-directions.

The contour plot of maximum shear stress (Fig. 4.59) shows that the highest value of shear stress, 6.81 N/mm^2, is located at the centre core of the concrete infill. This stress tends to reduce towards the outer faces of the concrete infill. The distribution of maximum shear stresses suggests that the concrete tries to shear to the outside leaving an undisturbed central core in the middle.

Stresses in the Mortar Material

The contour plots of the direct stresses in the mortar joint in the Y-, X- and Z-directions are shown in Figs 4.60, 4.61, and 4.62 respectively. The contour plots of the major and two minor principal stresses are given in Figs B.13, B.14 and B.15 (Appendix B) respectively.

The contour plot of the direct vertical stress in the Y-direction shows that the maximum value, 18.68 N/mm^2, is located at the outer faces of the mortar joint. This value tends to decrease towards the centre of the mortar joint, reaching a value of 13.21 N/mm^2. The difference in the values of vertical stress between the outer faces and the

centre of the mortar joint suggests that the concrete infill is not sufficiently stiff to transfer the applied vertical stress to the mortar joint, when compared to the stiffness of the block material.

The distribution of vertical stresses in the mortar joint shows more uniformity in the filled **2BP-MJ** prisms than in the unfilled prism. It is also noted that the value of the maximum vertical stress in filled prisms is 22.2% lower than in the unfilled prisms. The reason for these differences is the presence of the concrete which affects the distribution of the vertical stresses by carrying some of the applied vertical stress from the block shells and mortar joint.

The contour plots of the direct horizontal stresses in the X- and Z-directions show higher confinement stresses at the outer faces of the mortar joint in areas of high vertical stresses. The maximum confinement stress value of 4.75 N/mm^2 is obtained in the Z-direction. This value is 33.3% lower than the value obtained in the unfilled prism. A greater uniformity in the distribution of the horizontal stresses is observed in the filled prisms compared to the unfilled ones. These confinement stresses again result from differences in deformational characteristics between the soft mortar joint and the stiff concrete blocks.

Based on the way the horizontal stresses at the mortar joint are distributed and also their maximum values, it seems that the mortar joint has little effect on the compressive strength of filled prisms[1,26,28,33,35,36,71].

Fig. 4.63 shows the contour plot of the maximum shear stress in the mortar joint. The figure shows that the maximum shear stress, 7.18 N/mm^2, is located at the outer faces of the mortar joint in areas of higher vertical

stress. This stress tends to reduce towards the centre of the mortar joint.

4.5.4.2 Parametric study analysis

The level of vertical stress applied to the filled **2BP-MJ** prisms for the parametric study was 11.26 N/mm^2, which is the average experimental compressive strength of prisms built with high strength (1:0.25:3) mortar and filled with low strength (1:5:2) concrete. This level of vertical stress was kept constant on the prism, while the concrete material was changed to low (1:5:2), medium (1:3:2) and high (1:1:2) strength to study the effect of changing the concrete strength on the maximum values of deformation and stress in the prism.

The effect of increasing the cube compressive strength of concrete on the prism deformations is shown by the contour plots for the horizontal deformations in the X-direction (Figs 4.64, 4.65 and 4.66) and in the Z-direction (Figs 4.67, 4.68 and 4.69), for prism filled with low (1:5:2), medium (1:3:2) and high (1:1:2) strength concrete respectively.

The figures show that the horizontal deformations in the X- and Z-directions for prisms filled with low or medium strength concrete is an outward deformation limited to areas between the prism webs. For prisms filled with high strength concrete, it is an outward deformation all over the prism height and between the machine platens. This type of deformation is usually featured in solid prisms made of one type of concrete material.

Tables 4.4 and 4.5 give results of the maximum values of deformations and stresses respectively for the filled

2BP-MJ prisms, as derived from the parametric study analysis. Table 4.4 provides the results of the maximum values of deformations in the Y-, X- and Z-directions; the level of vertical stress applied during the parametric study; the average experimental compressive strength of the prisms and the cube compressive strength of the different concrete infill mixes. Table 4.5, on the other hand, gives the maximum values of direct, shear and principal stresses in each individual material.

The effect of increasing the cube compressive strength of concrete on the prism deformations is shown in Fig. 4.70. The figure shows that the prism vertical deformation decreases by 53.2%, as a result of changing the concrete strength from 4.97 to 39.44 N/mm^2. Similarly, the prism outward horizontal deformation decreases by 70%, in both the X- and Z-directions, as the concrete strength increases. The only prism which shows a small inward deformation of 0.006 mm at the mortar joint is the filled prism with low strength concrete.

The decreases in the vertical and horizontal deformations as the concrete strength increases, are due to the increase in prism stiffness as a result of using a stronger concrete.

Although the values of stress differ, the stress distributions for all the prisms analysed in this parametric study are similar to the contour plots of stresses for prisms analysed using the specific analysis. Information on how these stresses are distributed is given in the relevant contour plots of stresses from the specific analysis.

Figs 4.71, 4.72 and 4.73 show the effect of changing the cube compressive strength of the concrete on the

maximum values of direct stress in the Y-, X- and Z-directions respectively. Fig. 4.71 shows that the vertical stress in the block material and mortar joint decreases by 49.5% and 45.5% respectively as a result of changing the concrete strength from 4.97 to 39.44 N/mm^2. On the other hand, the vertical stresses in the concrete infill increase by 45.5% as the concrete strength increases.

This suggests that as the concrete strength increases, the applied vertical stress starts shifting from the block material to the concrete. The figure also shows that when the cube compressive strength of concrete is approximately equal to 39.44 N/mm^2 (this strength is 62.4% higher than the cube compressive strength of the block material), the vertical stresses in all the prism materials are almost uniform ranging from 10.10 to 14.90 N/mm^2. This suggests that the deformational characteristics of both materials are almost the same.

Fig. 4.72 shows that the confinement stress in the X-direction in the mortar joint decreases by 44% and in the concrete, by 47.5%, as result of changing the concrete strength from 4.97 to 39.44 N/mm^2. On the other hand, the tensile stresses in the block material decrease by 83% as the concrete strength increases. The decrease in the confinement stress, in the mortar joint, was due to the shifting of the high vertical stresses from the prism shells to the concrete infill as the compressive strength of the concrete increases. Decrease in the confinement and tensile stresses in the concrete infill and block material respectively as the concrete strength increases are the result of the reduction in the concrete infill Poisson's ratio.

Similarly, the maximum values of confinement stress in the Z-direction (Fig. 4.73), decreases by 42.1% in the

mortar joint and by 44.2% in the concrete infill, whilst the tensile stress in the block material decreases by 78.3%, as the concrete strength increases. The reasons for all these reductions are similar to those discussed for the stresses in the X-direction.

The results of the horizontal stresses in all the materials show small differences between the stresses in the X- and Z-directions. Similarly, no difference is observed between the minor principal stresses.

Fig. 4.74 shows the effect of changing the cube compressive strength of concrete on the maximum values of shear stress. The figure shows that the shear stress in the block material and the mortar joint, decreases by 43.4% and 47.4% respectively as a result of changing the concrete strength from 4.97 to 39.44 N/mm^2. On the other hand, the shear stress in the concrete infill, increases by 87.6% as the compressive strength of the concrete increases.

To sum up the effect of changing the cube compressive strength of concrete from 4.97 to 39.44 N/mm^2 on prism strength. It seems that the prism strength increases as the concrete infill strength increases. This is a result of shifting the applied vertical stress from the block material to the concrete infill, and consequently a greater contribution from the concrete infill to the strength of the prism. An optimum prism strength will be achieved when the deformational characteristics of all materials are the same.

Due to the complex nature of the deformations and the stress distributions in the filled **2BP-MJ** prisms. The general conclusion derived from the results of the specific and the parametric study analyses, is that the failure of filled **2BP-MJ** prisms is dominated by localized crushing,

splitting and shear failures. It is concluded that the filled prisms fail due to a combination of compression, tension and shear modes of failure.

The predicted mode of failure for the filled **2BP-MJ** prisms with low or medium strength concrete is dominated by block shell-concrete infill separation and lateral deformation with some block shells, mortar and concrete infill crushing near the mortar joint. Prisms filled with high strength concrete fail by crushing of the block shells and concrete infill simultaneously. But as shown in the experimental investigation, high strength concrete infill works as a cleavage by forcing the blocks to split before attaining their unfilled block compressive strength.

Based on the stress values and distributions, it would appear that the strength of filled **2BP-MJ** prisms, does not depend on the block unit compressive strength and the mortar type. In order to determine f'_m, filled **2BP-MJ** prisms must be tested.

In general, a clear similarity exists between the predicted modes of failure and the values of stress for the unfilled and filled **2BP-MJ** prisms obtained from both the FEA and the experimental investigation. The FEA, however, provides a clear picture of the deformations and stress distributions for unfilled and filled prisms in the Y-, X- and Z-directions. The FEA also answers several questions regarding how the different materials interact with each other in axially loaded prisms. These matters are difficult to observe experimentally.

4.6 CONCLUSIONS

1. The ultimate compressive strength for unfilled blockwork masonry, f'_m, in areas where high in-plane horizontal forces are expected, should be determined by one of the following two methods:

   (i) On the basis of the compressive strength of a unit block compressed parallel to the bed face and the type of mortar, or by using Eqn. 4.1 for the type of blocks used in this investigation.

   (ii) Tests on two-block masonry prisms made from the same materials as those to be used in the actual construction and compressed parallel to the unit bed face.

2. The ultimate compressive strength for filled blockwork masonry, f'_m, in areas where high in-plane horizontal forces are expected, should be determined by one of the following methods:

   (i) Testing a single-block specimen filled with the same concrete as that used in actual construction, in a direction parallel to the unit bed face, then multiplying the specimen's compressive strength by a reduction factor of 0.75 (Eqn. 4.2), which represents the reduction caused by the presence of the mortar joint.

   (ii) Testing two-block masonry prisms built from the same materials as those to be used in the actual construction and compressed parallel to the unit bed face.

3. The presence of the mortar joint in unfilled prisms

caused a small reduction in the prism compressive strength compared to unfilled prisms with dental plaster joint. Increasing the mortar strength by at least 166.9% produces an increase of only 6.2% on the compressive strength of unfilled prisms. This was mainly due to the insignificant ratio of the mortar joint thickness to the block height (1/39), and also due to confinement of the mortar by the stiff blocks.

4. Most of the unfilled prisms with a mortar joint failed at a compressive strength higher than the mortar cube strength. This suggests that the mortar strength in a joint is apparently higher than the mortar cube strength. This is due to the relatively small mortar thickness compared to the unit height, and the confinement of the mortar by the stiff concrete blocks.

5. The presence of concrete infill significantly reduced the compressive strength of all the two-block prisms with mortar or with dental plaster joint as compared to unfilled prisms. The best compressive strength result was achieved when the deformational characteristics of the concrete infill matched those of the concrete block.

   A stiff concrete infill works as a cleavage forcing the blocks to split before attaining their unfilled block compressive strength. The extent of reduction in strength of all prisms filled with stiff concrete infill is similar to the ones filled with soft concrete infill.

6. The presence of the mortar joint in the filled prisms caused a reduction by a factor of 0.75 in the prism strength as compared to the ones with dental plaster

joint. This reduction resulted from the high Poisson's ratio of the mortar near ultimate load, compared to that of the concrete blocks. This was responsible for introducing confinement stresses in the mortar and producing splitting stresses in the blocks.

Increasing the mortar strength by at least 166.9% produces an increase of only 23.9% and 3.8% on the compressive strength of prisms with low and high strength concretes respectively. This was due to the insignificant ratio of mortar joint thickness to height of the block (1/39) and mortar confinement by the stiff blocks.

7. The strength of two-block prisms, with a value of h/t = 4.0, are surprisingly, higher than the corresponding single-block specimens with a value of h/t = 2.0.

8. In the finite element analysis of any masonry element subjected to compressive stress, steel bearing plates should be used to apply the stress to the element. Otherwise excessive high deformation and unacceptable high tensile and shear stresses will results at the location of the applied stress.

9. The finite element analysis shows that the effect of the machine platens is limited to areas near these platens. Thus, using unfilled and filled two-block prisms as a standard specimen to determine f'_m in areas where high in-plane forces are expected is acceptable.

10. Despite the 59.7% increase in the vertical deformation of the unfilled prism from the non-linear analysis, compared to the linear analysis, the increase of 11.2% in the maximum tensile stress in the X-direction and the decrease of 13.5% in shear stress is small

compared to the high increase in deformation. This reflects the importance of the materials' non-linearity in the analysis of blockwork masonry assemblage.

11. The results of the finite element analysis show that changing the mortar compressive strength has little influence on the compressive strength of an unfilled prism. Also, the prism has a greater tendency to split along the prism side shells than through the prism mid-webs.

12. In considering the equilibrium of horizontal stresses in any cross-section, at the mortar joint, for filled **2BP-MJ** prisms, the assumption that the horizontal tensile stresses are uniformly distributed is justified.

13. As a result of the specific analysis of filled **2BP-MJ** prism, an explanation of how the concrete blocks and infill interact with each other in filled prisms is presented on page 172.

14. The distribution of vertical and horizontal stresses in the mortar joints of filled **2BP-MJ** prisms are more uniform than for unfilled ones.

15. The parametric study analysis for filled **2BP-MJ** prisms shows that as the concrete infill strength increases, the applied vertical stress starts shifting from the block material to the concrete infill. The study also shows that when the cube compressive strength of concrete infill is 62.4% higher than the cube compressive strength of concrete block the stresses in all the prism materials are almost uniform. This suggests that the deformational characteristics of

both materials are almost the same.

16. The parametric study analysis for filled **2BP-MJ** prisms shows a large reduction (83% and 78.3% in the X- and Z-directions respectively) in the tensile stresses in the block material as a result of changing the concrete infill strength from 4.97 to 39.44 N/mm^2.

17. The predicted modes of failure and stresses for unfilled and filled **2BP-MJ** prisms provided by the FEA are similar to the ones observed and determined from the experimental investigation. The FEA, however, provides a clear picture of the deformations and stress distributions for unfilled and filled prisms in the Y-, X- and Z-directions. The FEA also provides information on how the different materials interact with each other and how the prisms behave under axial compression. This information is difficult if not impossible to obtain experimentally.

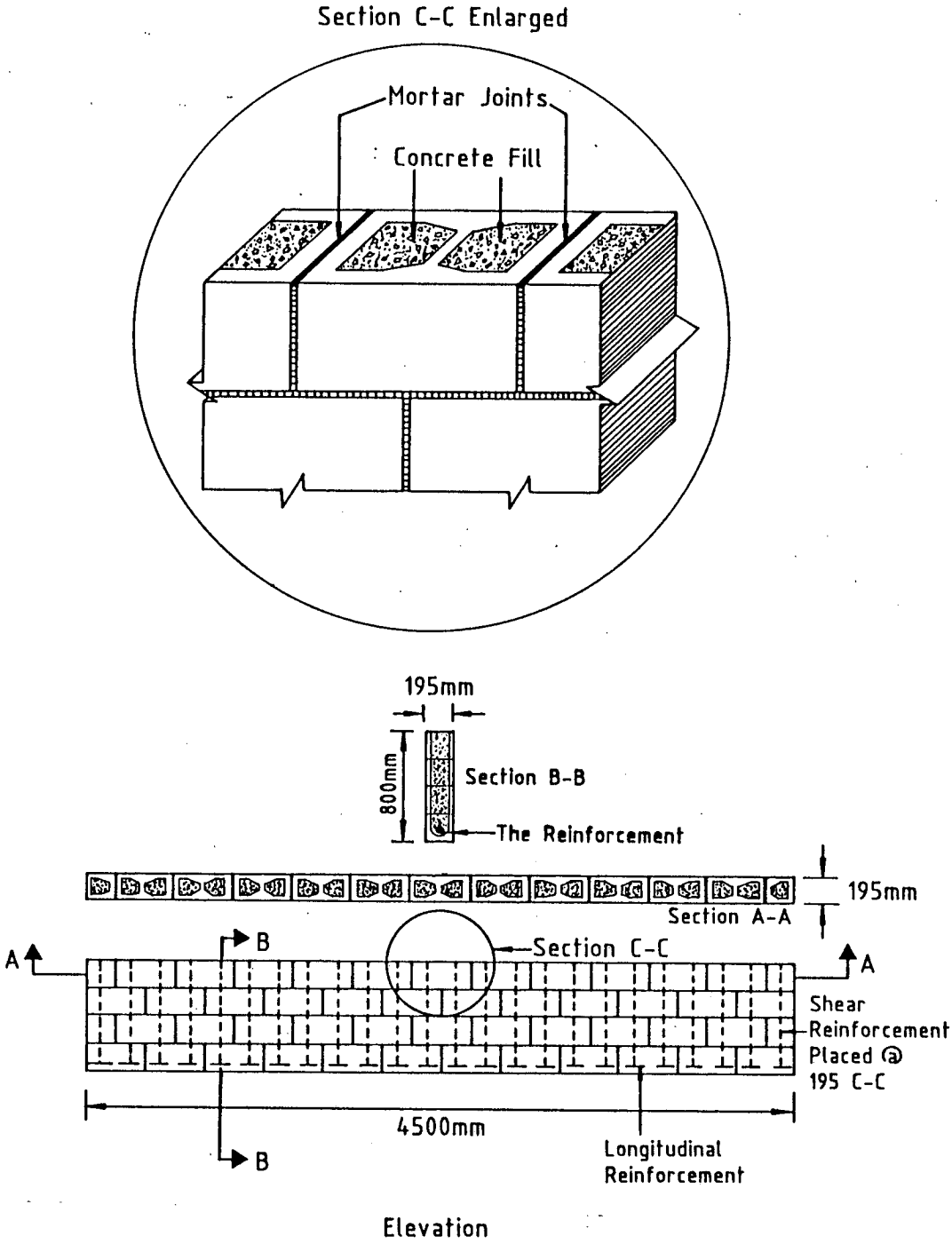

Fig. 4.1 - Typical compression zone in reinforced blockwork masonry beam.

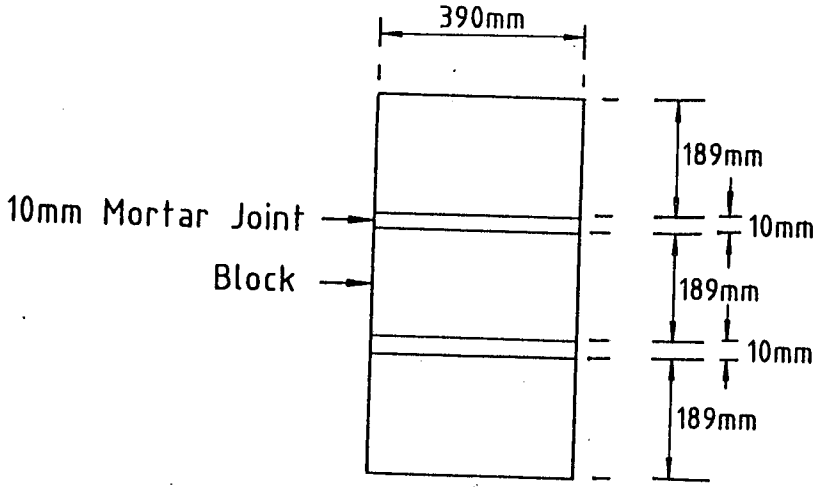

Fig. 4.2 - Typical stack-bonded blockwork masonry prism compressed in a direction normal to unit bed face.

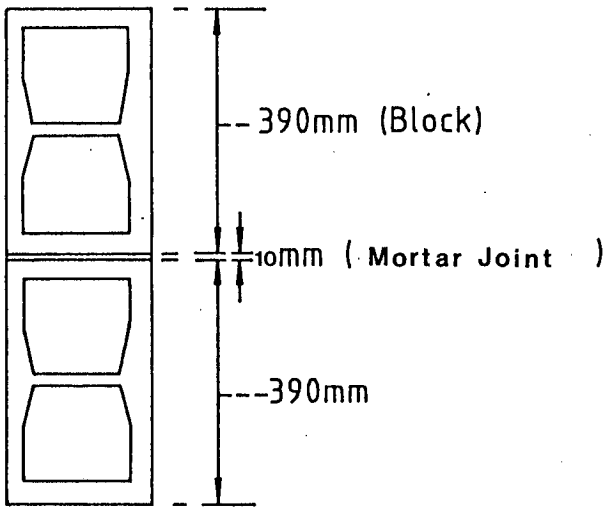

Fig. 4.3 - Typical two-block masonry prism compressed in a direction parallel to unit bed face.

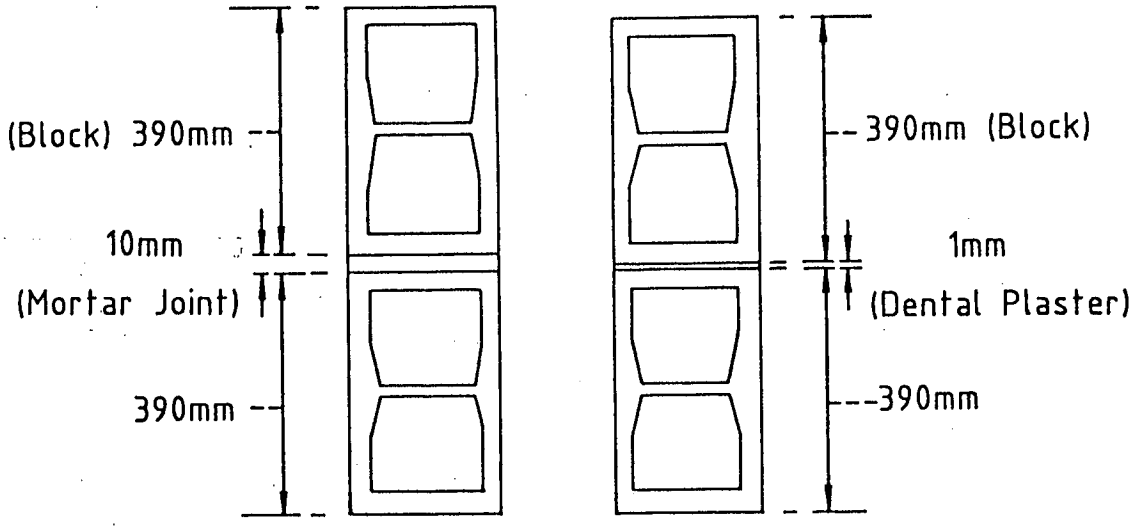

(i) 2BP-MJ prism

(ii) 2BP-DPJ prism

2-block prism with mortar joint.

2-block prism with dental plaster joint.

Fig 4.4 - Types of two-block masonry prism tested. (i) 2BP-MJ prism, (ii) 2BP-DPJ prism.

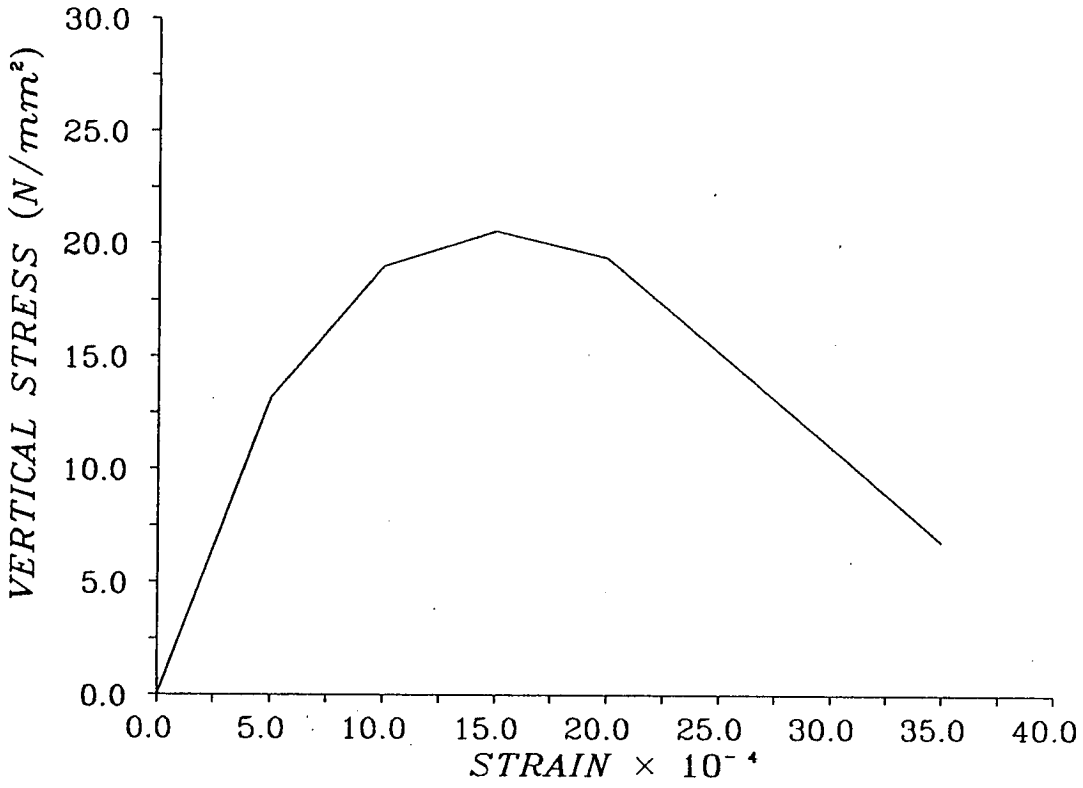

Fig. 4.5 - Idealised stress vs strain curve for block material used in FEA.

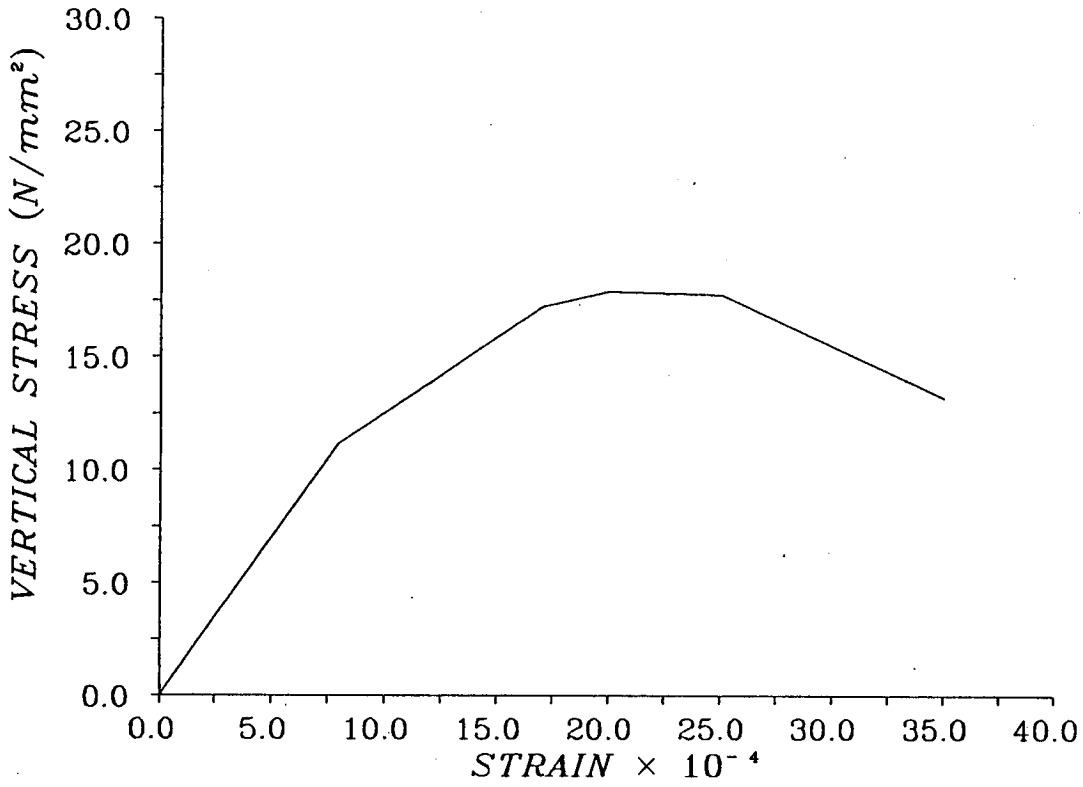

Fig. 4.6 - Idealised stress vs strain curve for medium strength (1:3:2) concrete used in the FEA.

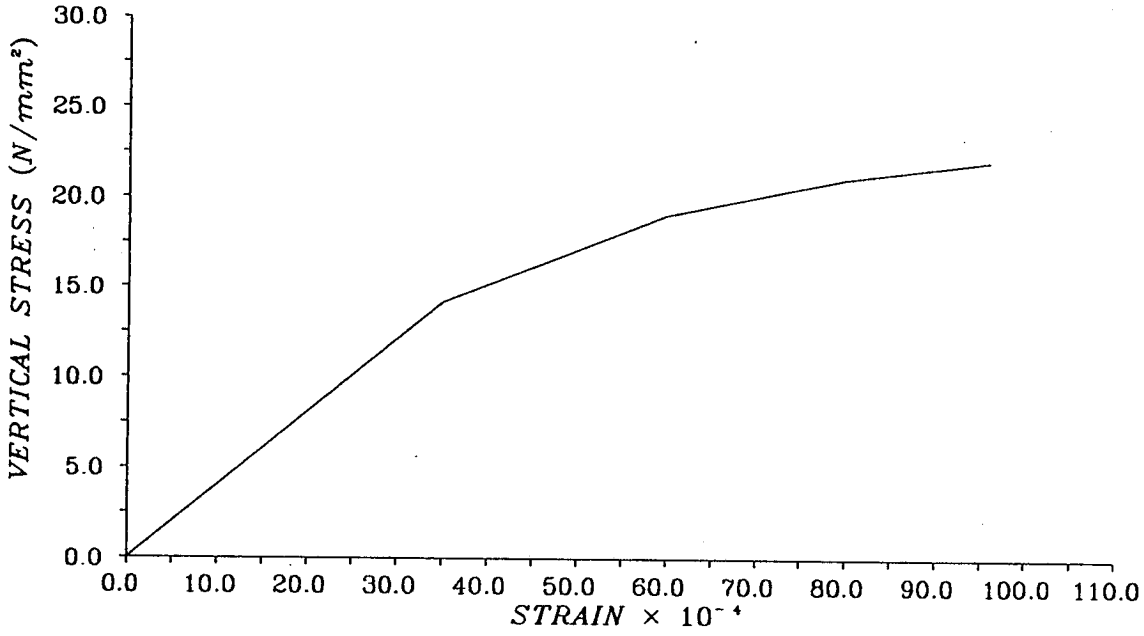

Fig. 4.7 - Idealised stress vs strain curve for confined 10 mm high strength (1:0.25:3) mortar used in the FEA.

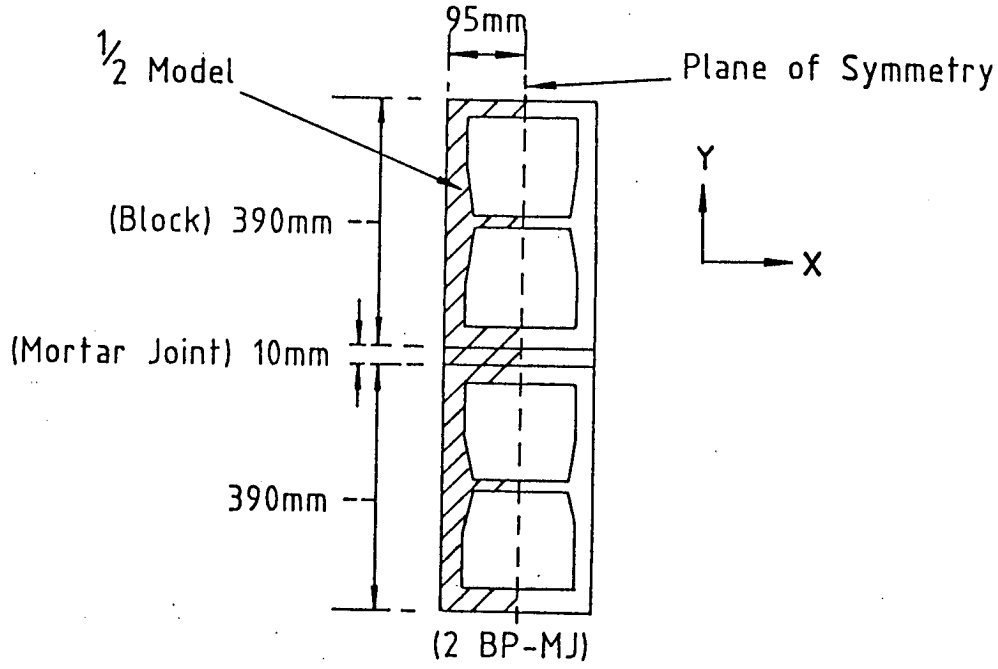

Fig. 4.8 - 1/2 prism model used in linear FEA.

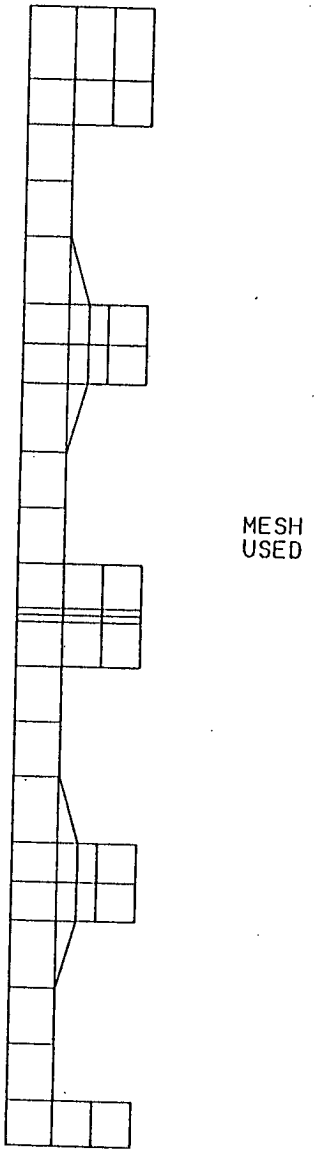

Fig. 4.9 - Two-dimensional mesh used in linear FEA.

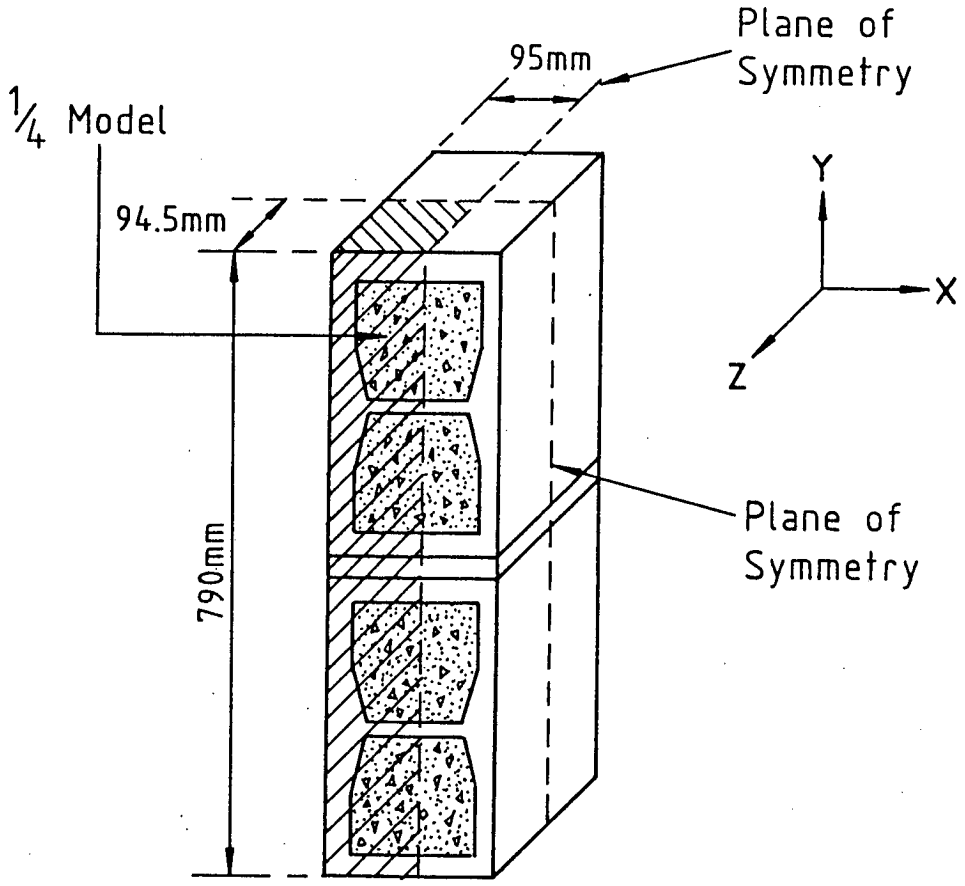

Fig. 4.10 - 1/4 prism model used in non-linear FEA.

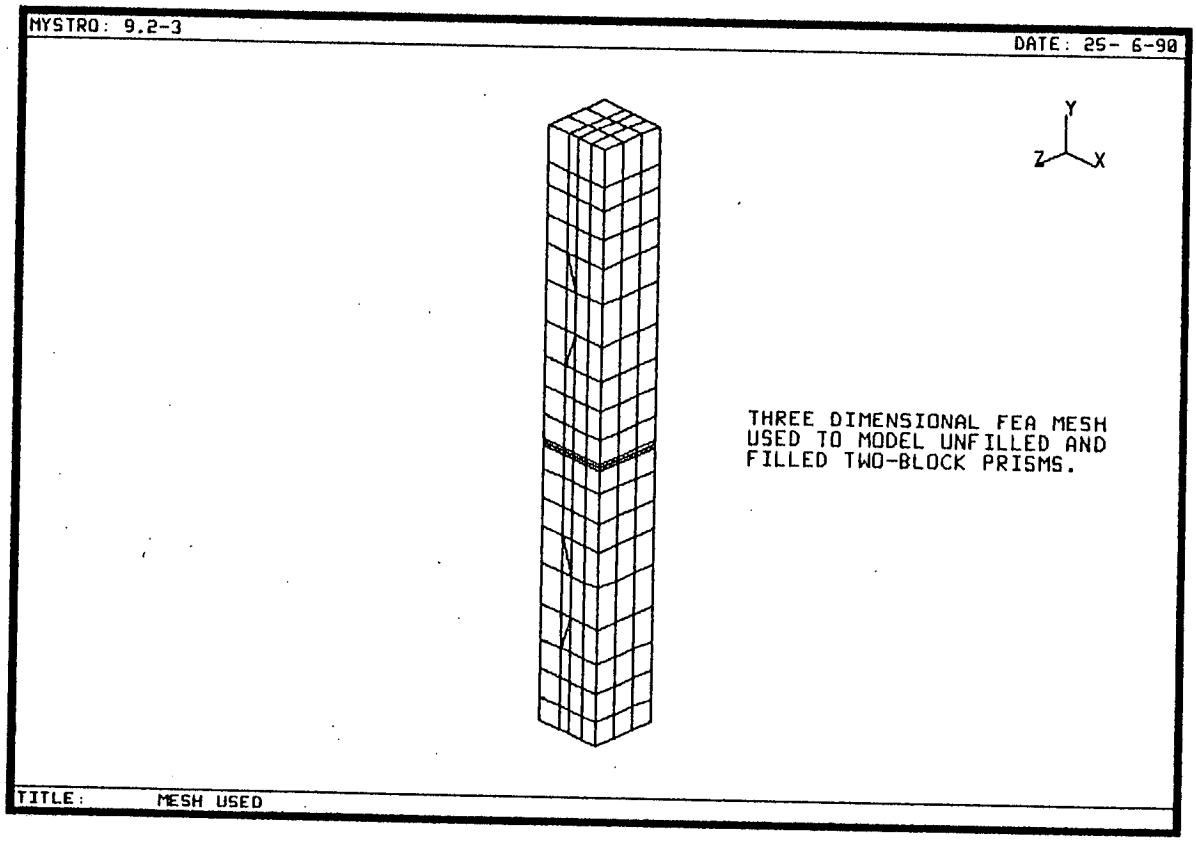

Fig. 4.11 - Three-dimensional mesh used in non-linear FEA.

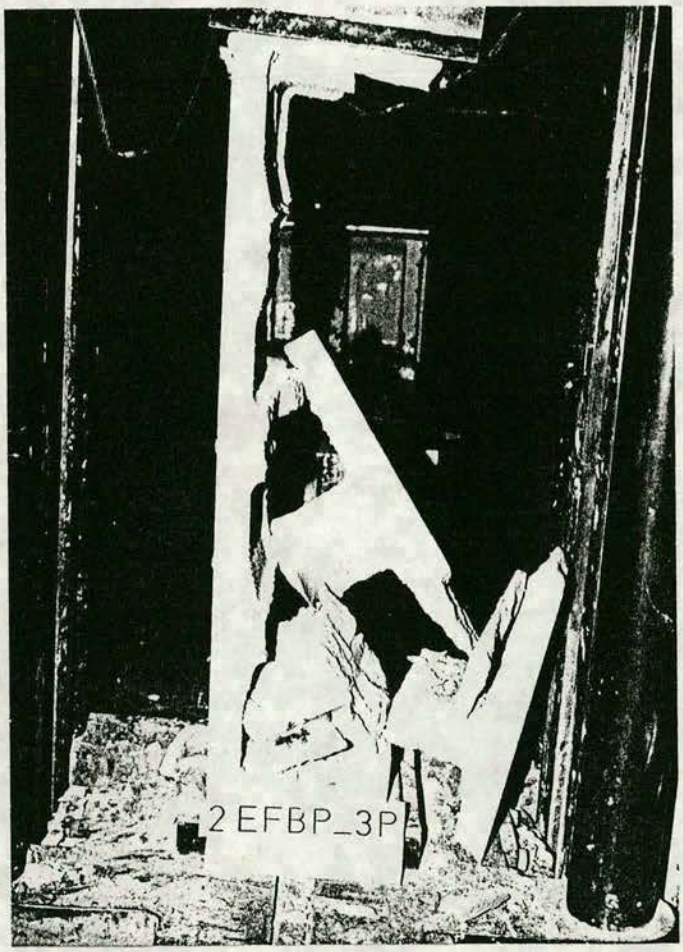

Fig. 4.12 - Unfilled 2BP-MJ prism after failure, mortar strength 19.40 N/mm^2.

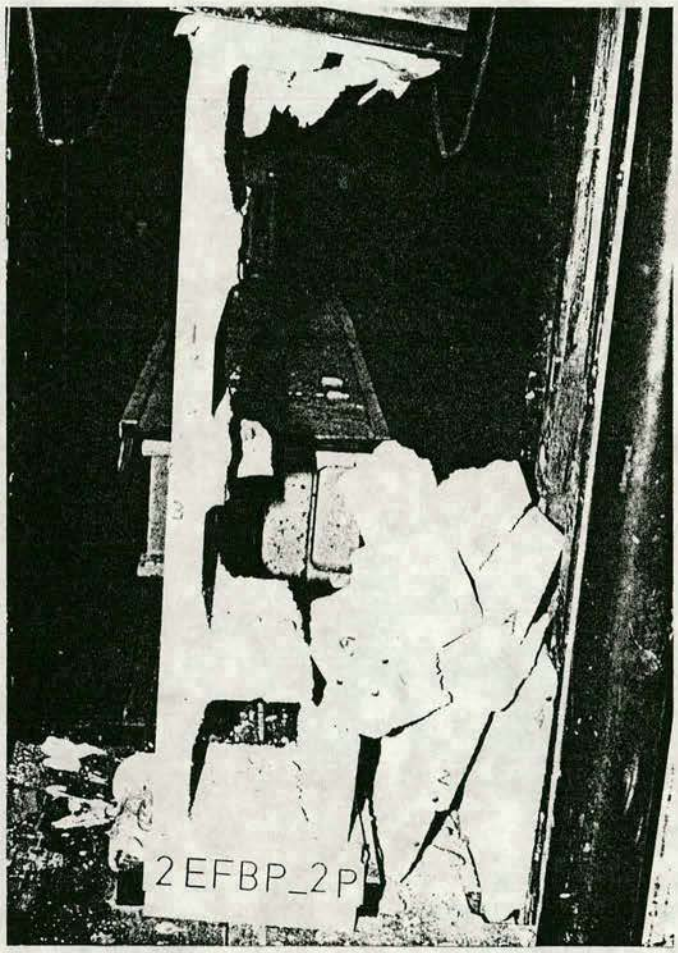

Fig. 4.13 - Unfilled 2BP-DPJ prism after failure.

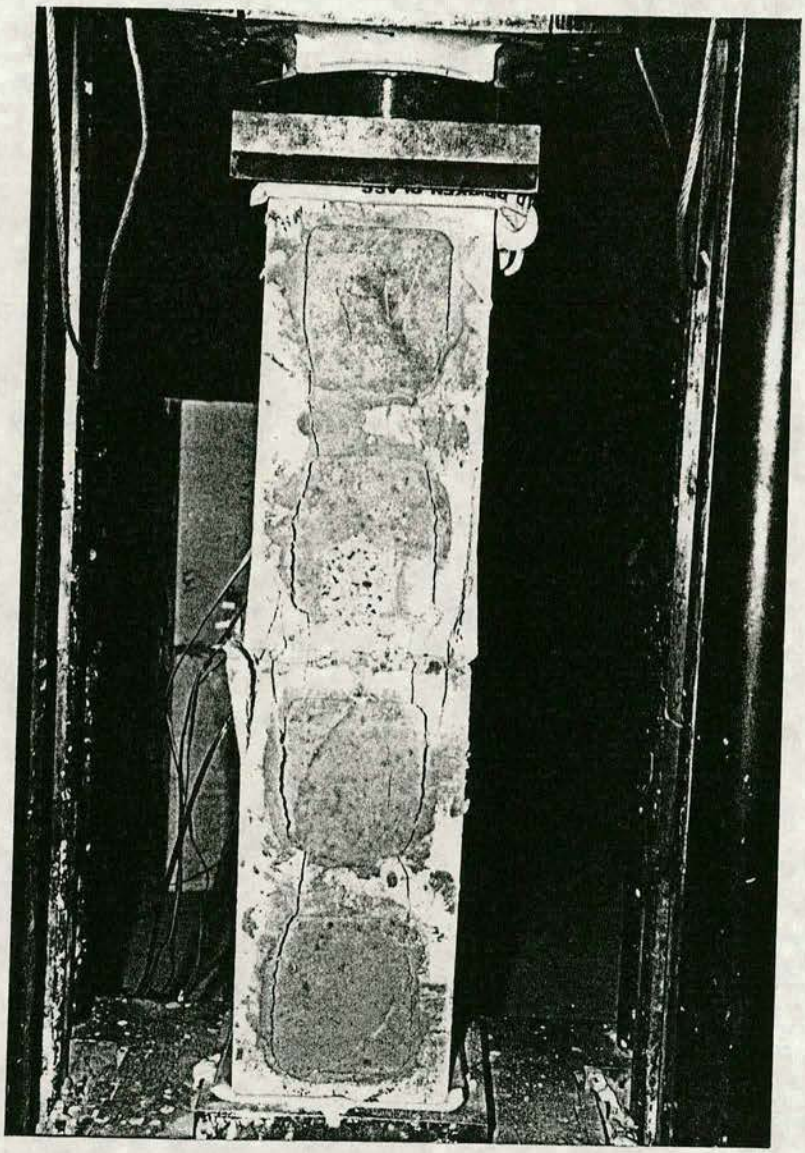

Fig. 4.14 - Filled 2BP-MJ prism after failure, mortar strength 19.40 N/mm^2, concrete strength 22.31 N/mm^2.

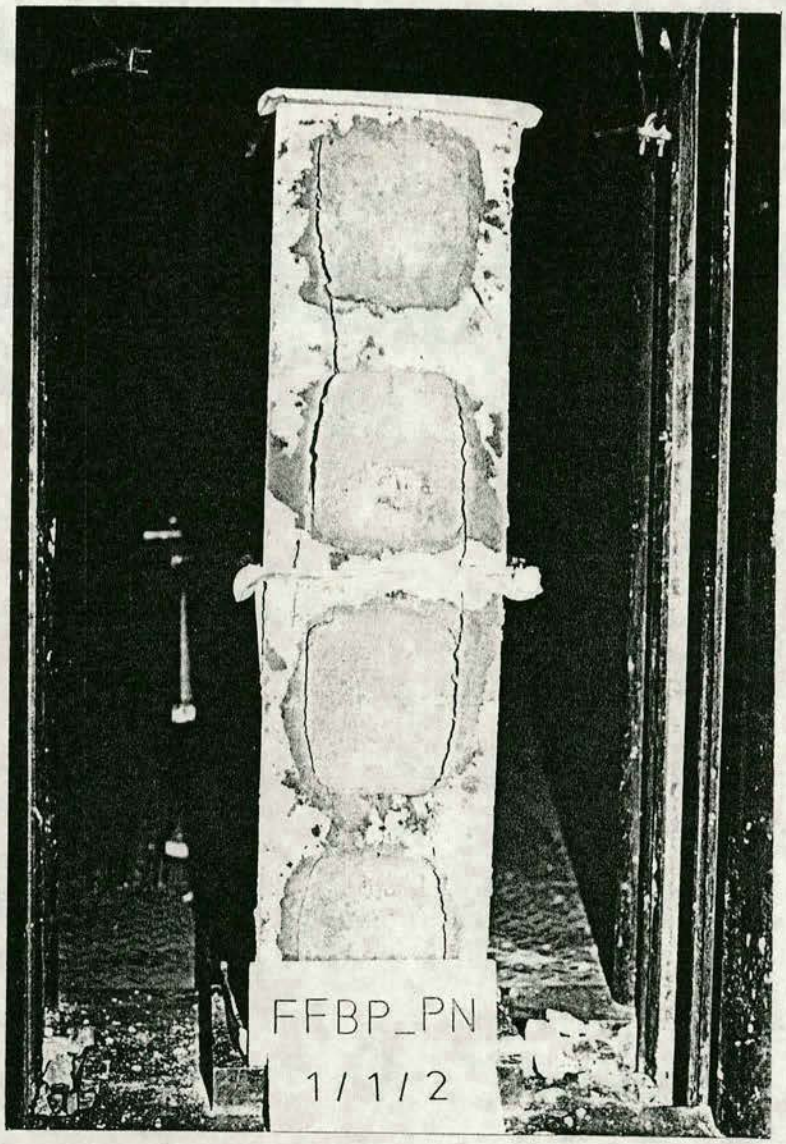

Fig. 4.15 - Filled 2BP-DPJ prism after failure, concrete strength 39.44 N/mm^2.

Table 4.1

Compressive strength of two-block prisms and component materials.

Prism type	Average compressive * strength (N/mm^2) Area used Net	Gross	S.D. (N/mm^2)	Material cube compressive ♦ strength (N/mm^2) Mortar (f_{mr})	Infill (f_c)
		Prism with a mortar joint (2BP-MJ) ♦			
Unfilled	22.64	8.34	0.80/0.30	7.27	-
Unfilled	23.26	8.57	1.01/0.37	10.64	-
Unfilled	24.04	8.86	1.98/0.73	19.40	-
Filled	-	9.09	0.35	7.27	4.97
Filled	-	11.05	1.97	7.27	39.44
Filled	-	11.26	0.34	19.40	4.97
Filled	-	15.26	0.39	19.40	22.31
Filled	-	11.47	2.12	19.40	39.44
		Prism with dental plaster joint (2BP-DPJ) ♦			
Unfilled	24.09	8.86	2.44/0.90	-	-
Filled	-	13.09	0.53	-	4.97
Filled	-	21.26	1.71	-	22.31
Filled	-	14.89	0.84	-	39.44

* Average and S.D. are calculated for three prisms.

♣ Cube compressive strength of block material f_b = 24.29 N/mm^2.

♦ Net area = 2(189 x 35) = 13230 mm^2. (Dimensions at section (2)). (See Table 3.2).
Gross area = 190 x 189 = 35910 mm^2.

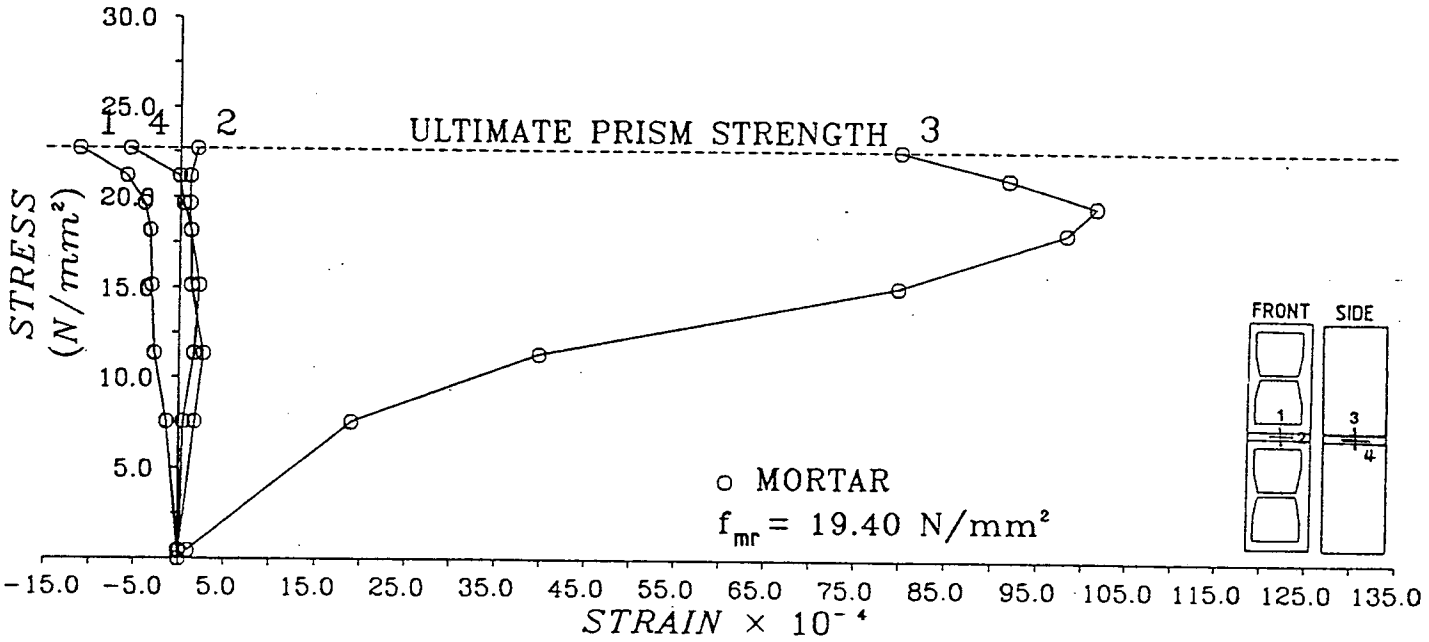

Fig. 4.16 - Stress vs strain curves for unfilled 2BP-MJ prism, mortar strength 19.40 N/mm^2.

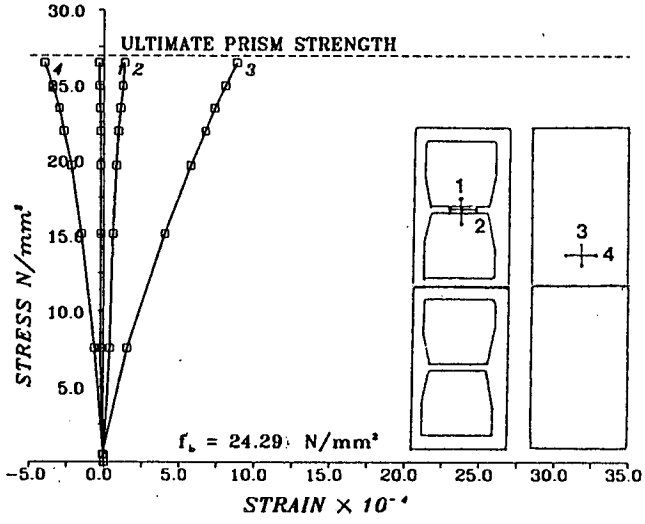

Fig. 4.17 - Stress vs strain curves for unfilled 2BP-DPJ prism.

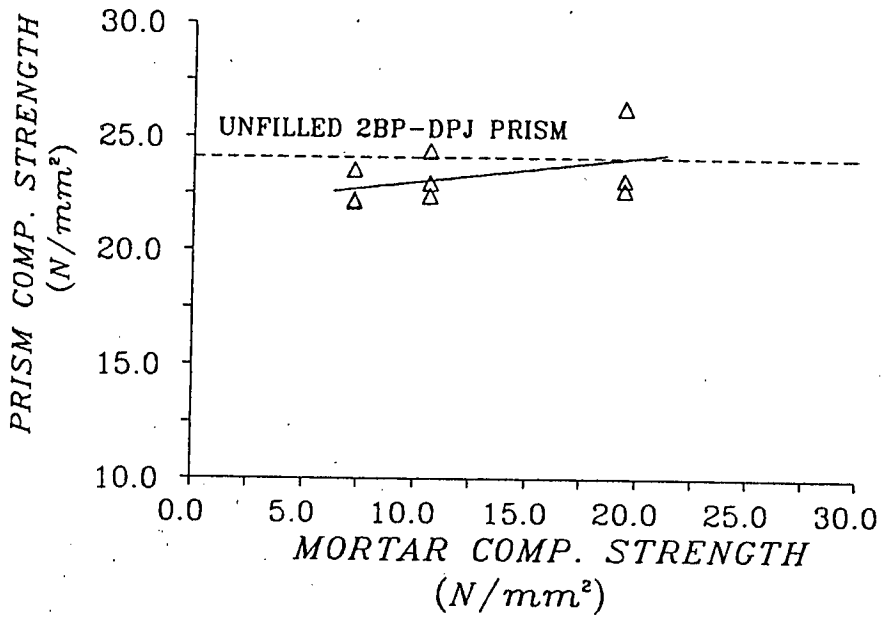

Fig. 4.18 - Effect of mortar strength on unfilled 2BP-MJ prism strength.

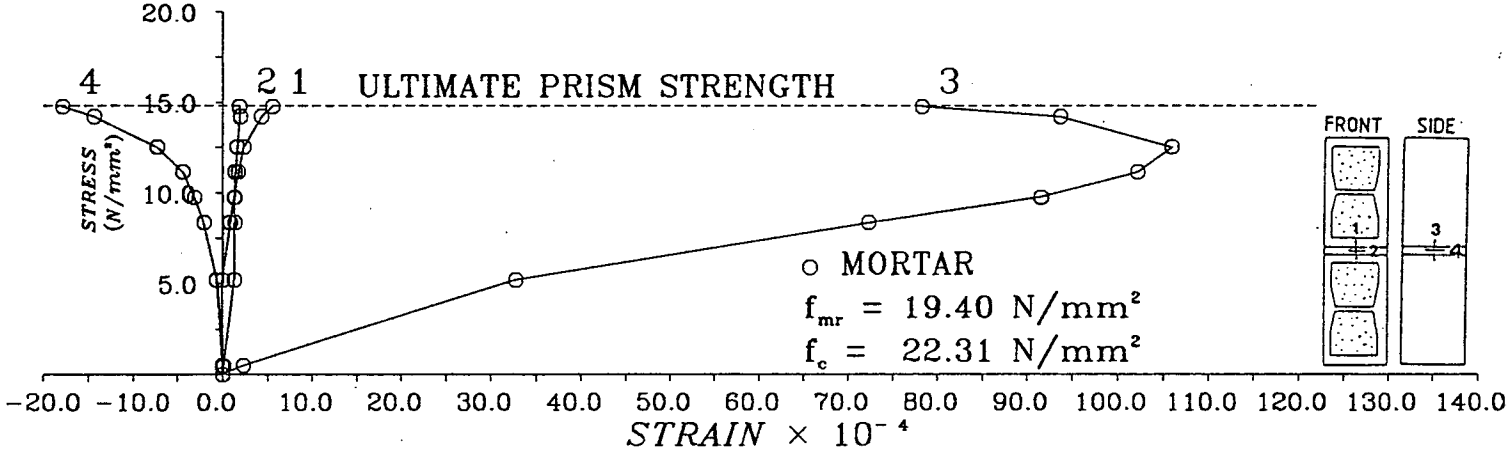

Fig. 4.19 - Stress vs strain curves for filled 2BP-MJ prism, mortar strength 19.40 N/mm^2, concrete strength 22.31 N/mm^2.

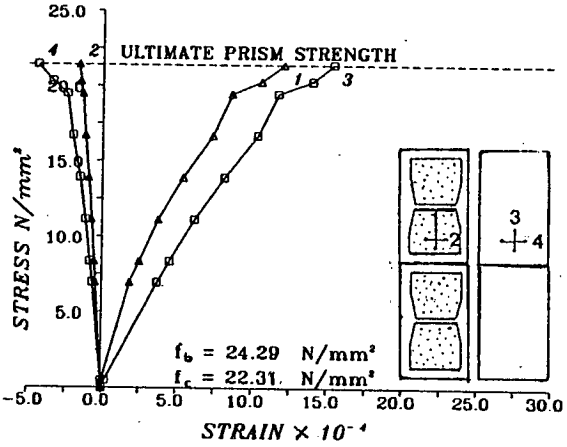

Fig. 4.20 - Stress vs strain curves for filled 2BP-DPJ prism, concrete strength 22.31 N/mm^2.

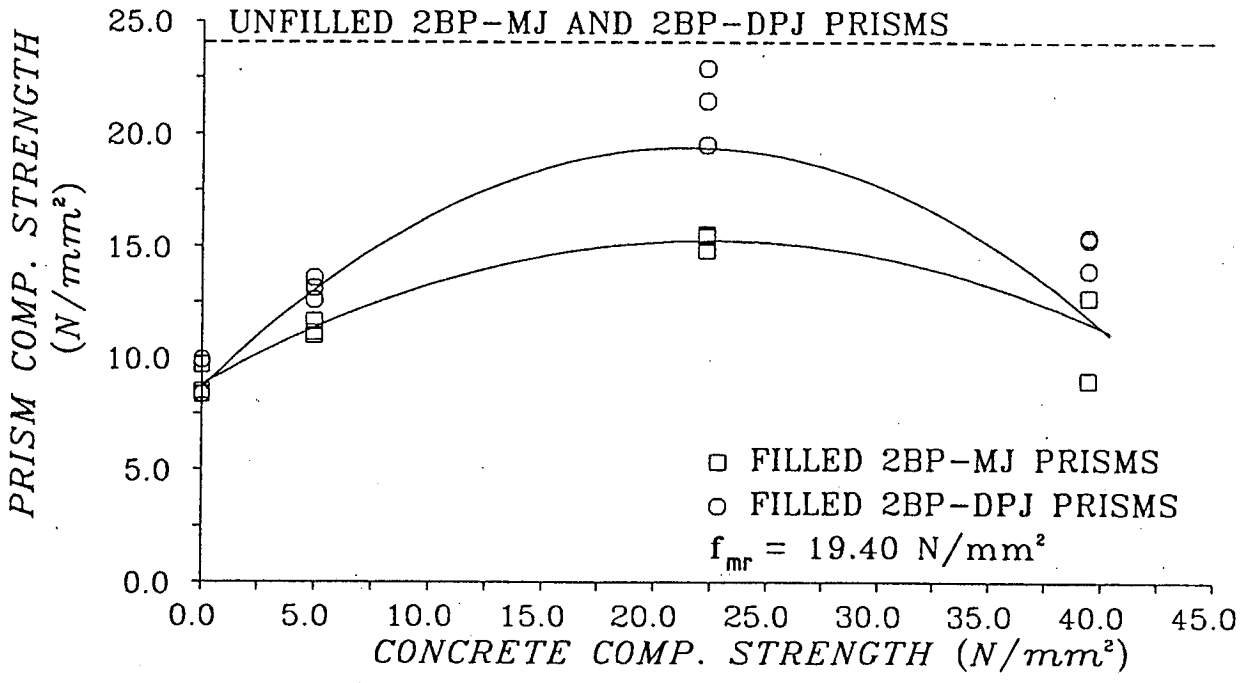

Fig. 4.21 - Effect of concrete infill strength on filled 2BP-MJ prisms strength, with almost similar mortar strength, and on 2BP-DPJ prisms strength.

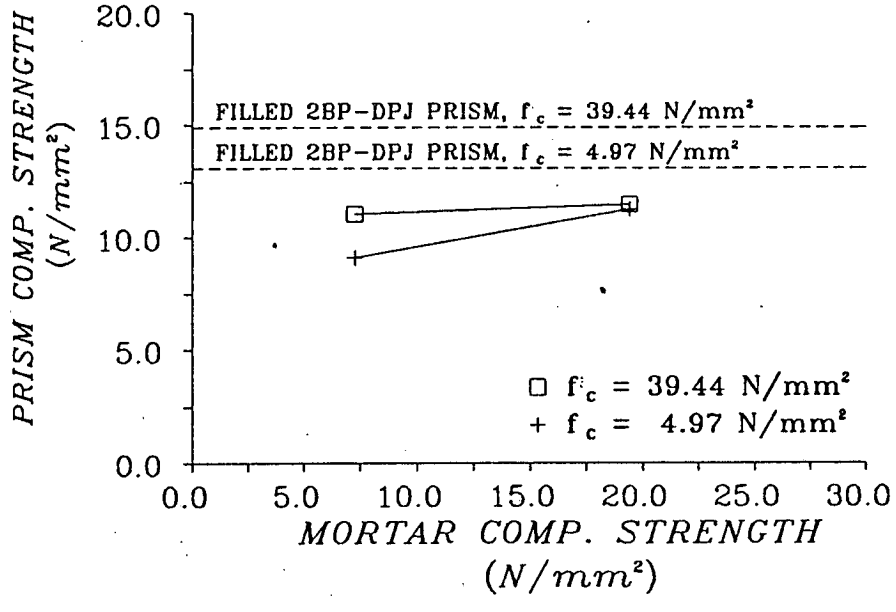

Fig. 4.22 - Effect of mortar strength on filled 2BP-MJ prisms strength, with almost similar concrete strength.

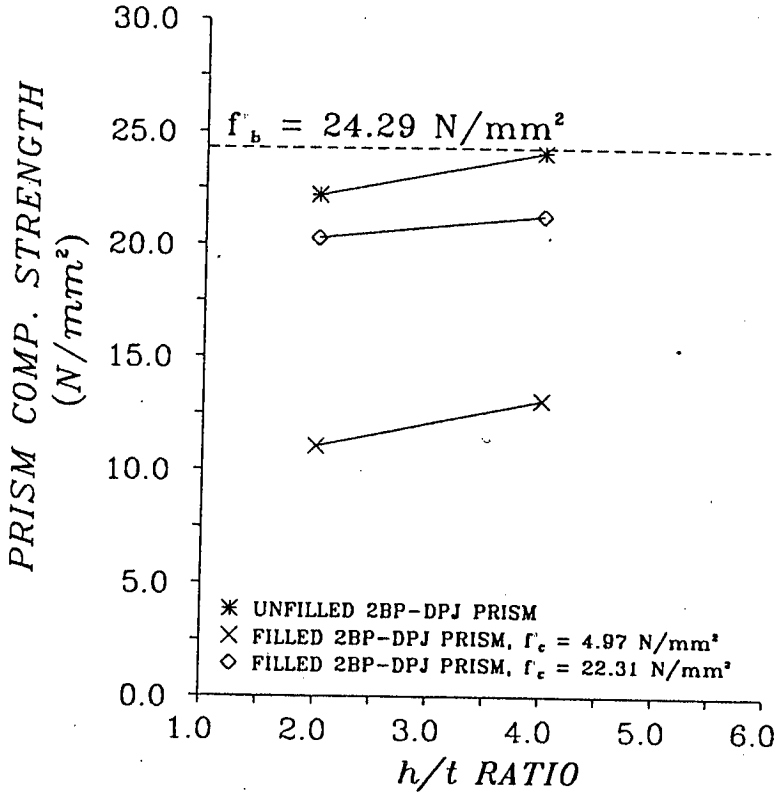

Fig. 4.23 - Effect of h/t ratio on specimens strength.

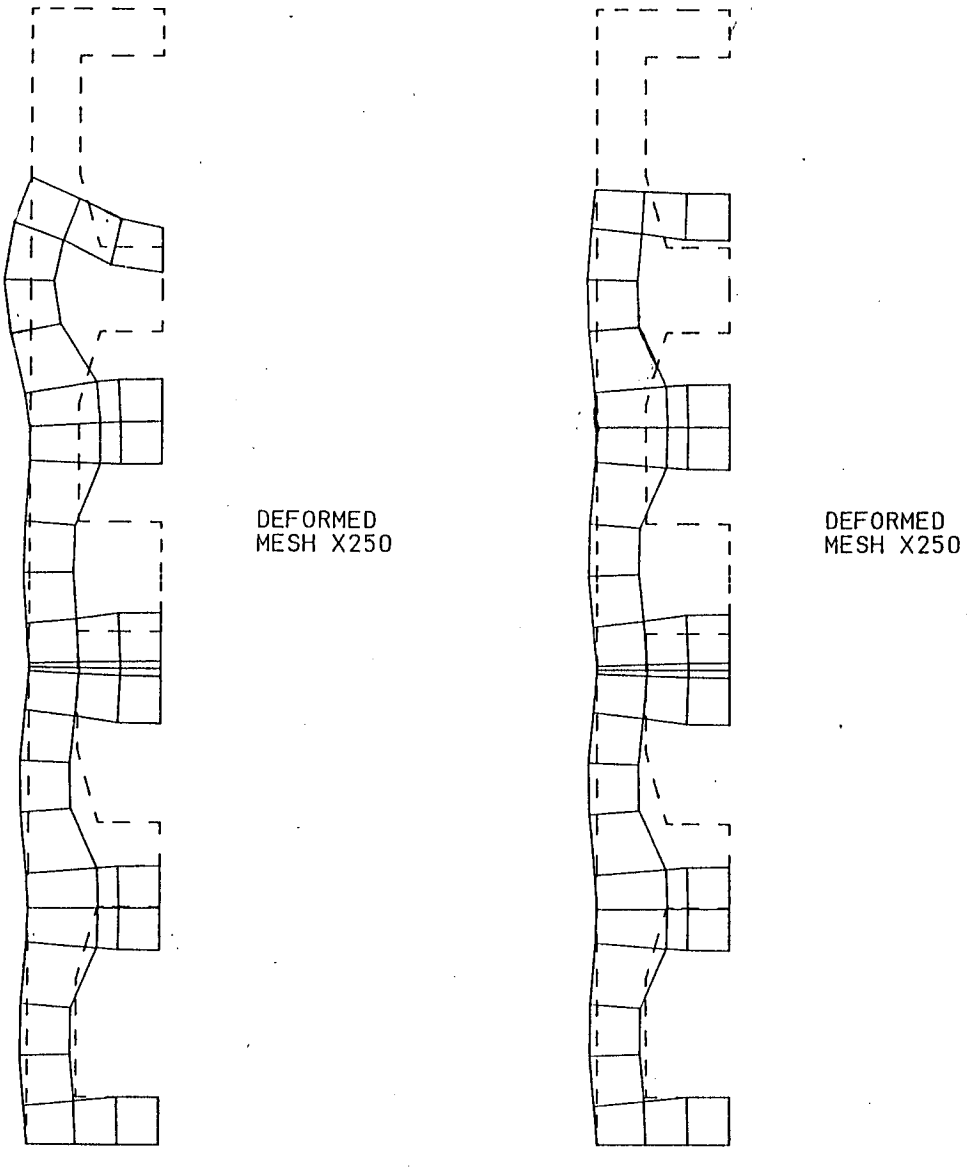

(i) Without steel bearing plate.

(ii) With steel bearing plate.

Fig. 4.24 - Prism deformed shape using two-dimensional linear FEA. (i) Without steel bearing plate, (ii) With steel bearing plate.

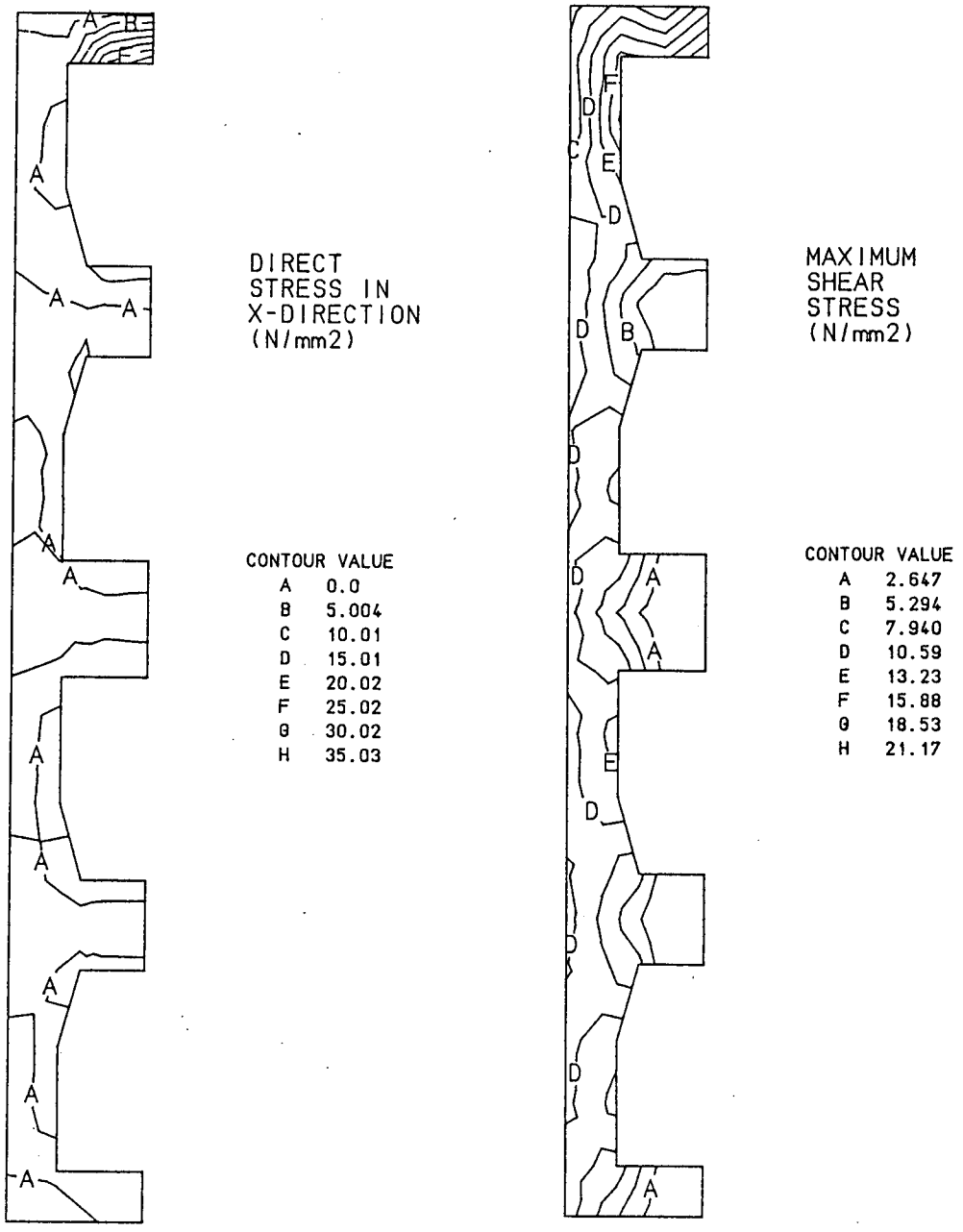

(i) Horizontal stress in X-direction.

(ii) Shear stress.

Fig. 4.25 - Stress results of two-dimensional linear FEA, without steel bearing plate. (i) Horizontal stress in X-direction, (ii) Shear stress.

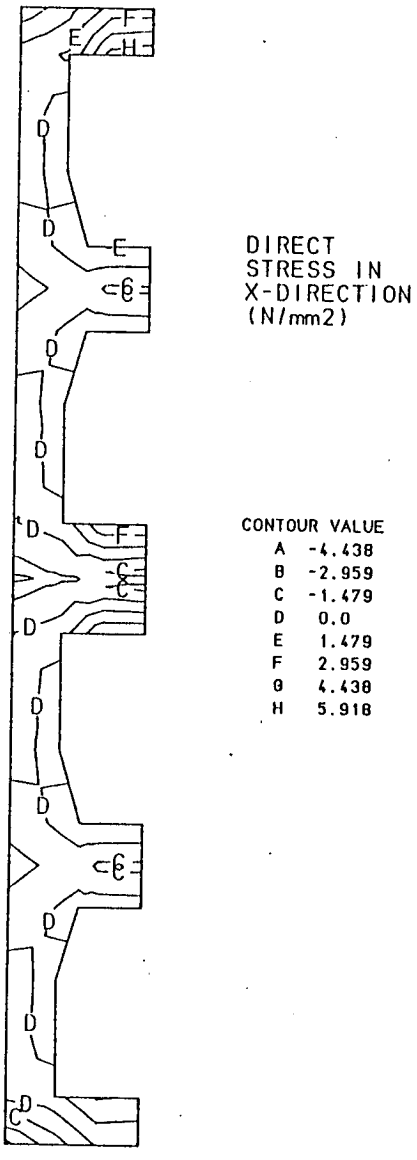

(i) Horizontal stress in X-direction.

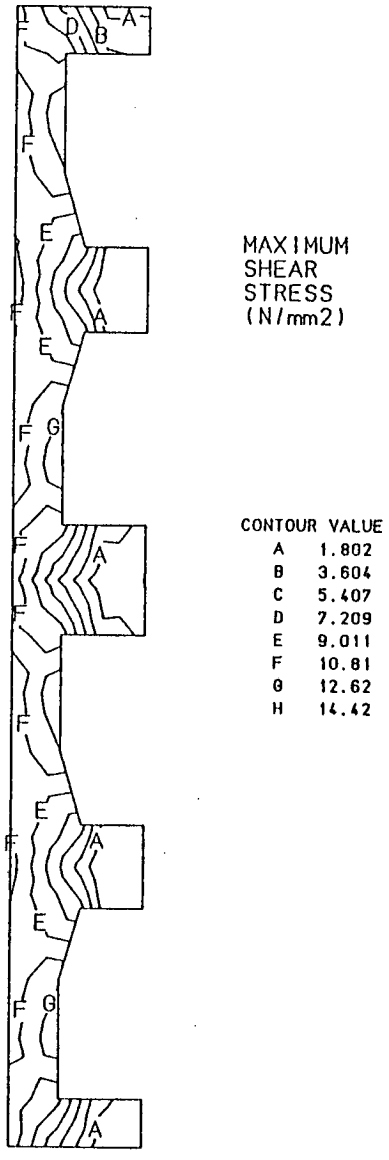

(ii) Shear stress.

Fig. 4.26 - Stress results of two-dimensional linear FEA, with steel bearing plate. (i) Horizontal stress in X-direction, (ii) Shear stress.

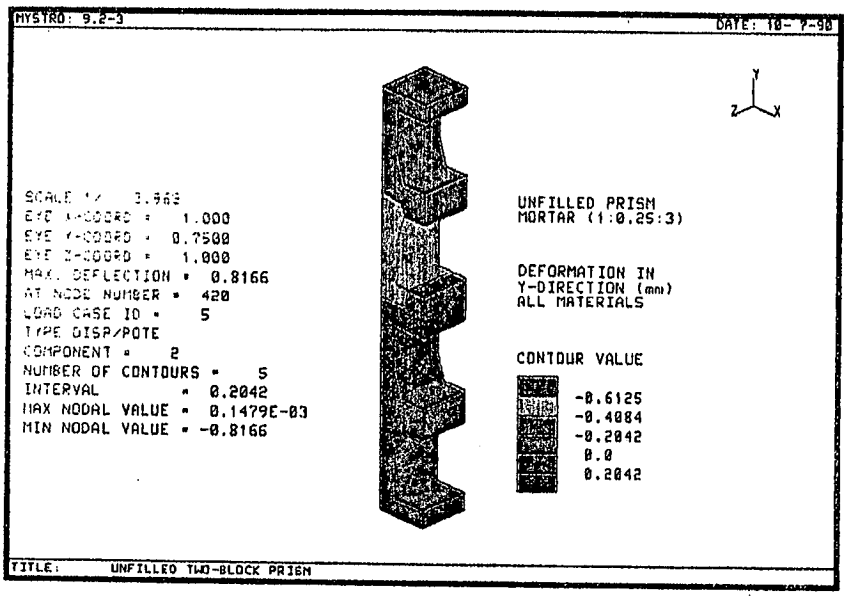

Fig. 4.27 - Deformation of unfilled 2BP-MJ prism in Y-direction, specific non-linear FEA.

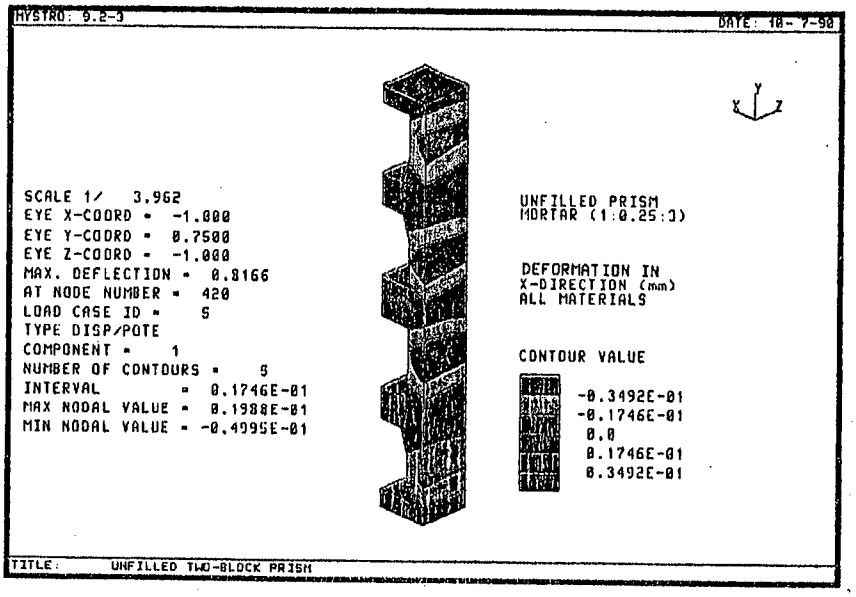

Fig. 4.28 - Deformation of unfilled 2BP-MJ prism in X-direction, specific non-linear FEA.

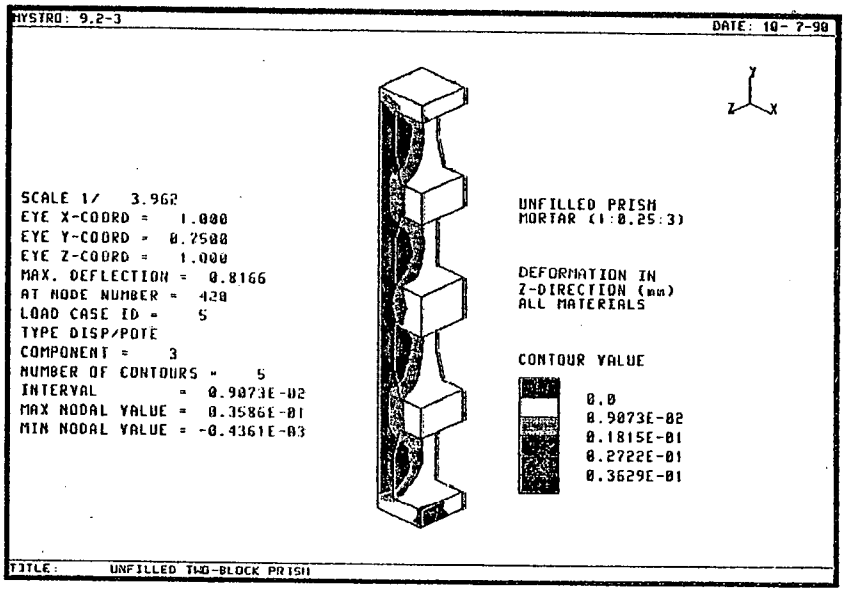

Fig. 4.29 - Deformation of unfilled 2BP-MJ prism in Z-direction, specific non-linear FEA.

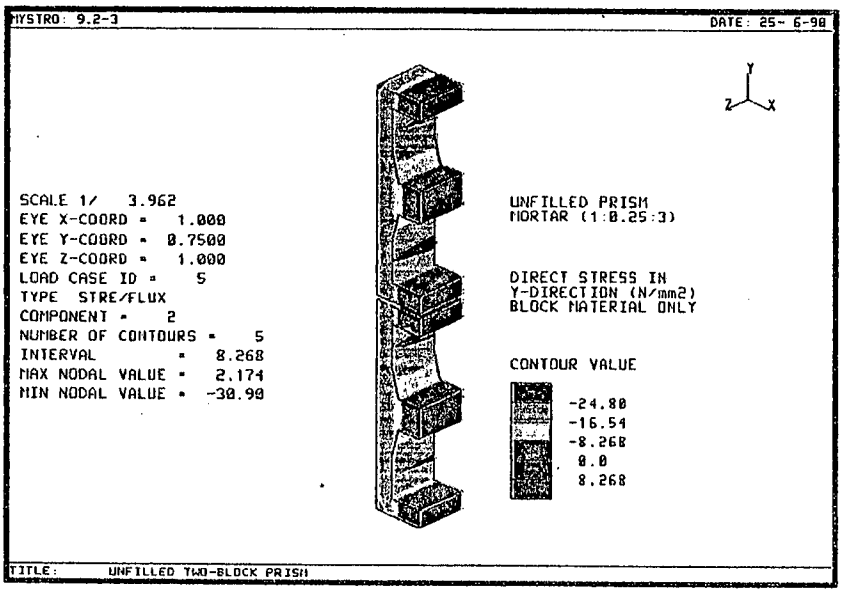

Fig. 4.30 - Direct stress in Y-direction, block material of unfilled 2BP-MJ prism, specific non-linear FEA.

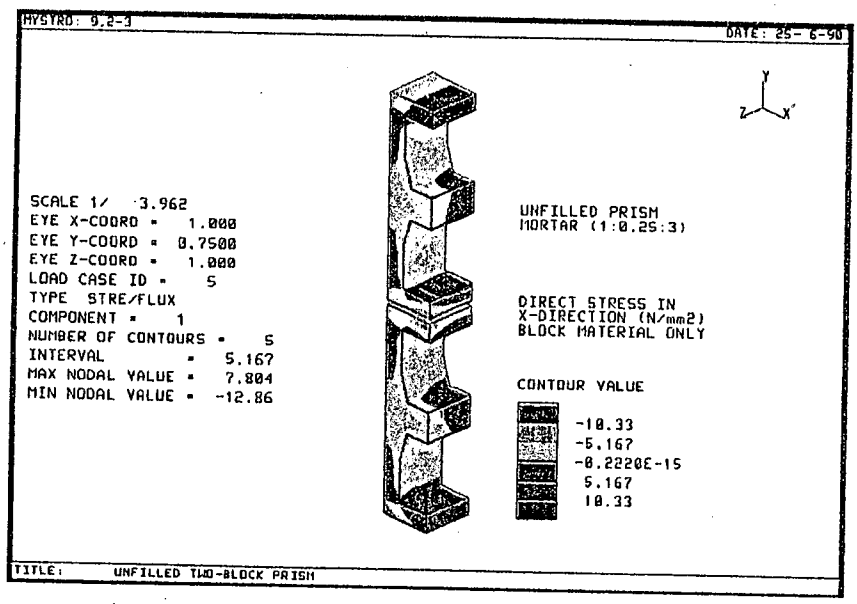

Fig. 4.31 - Direct stress in X-direction, block material of unfilled 2BP-MJ prism, specific non-linear FEA.

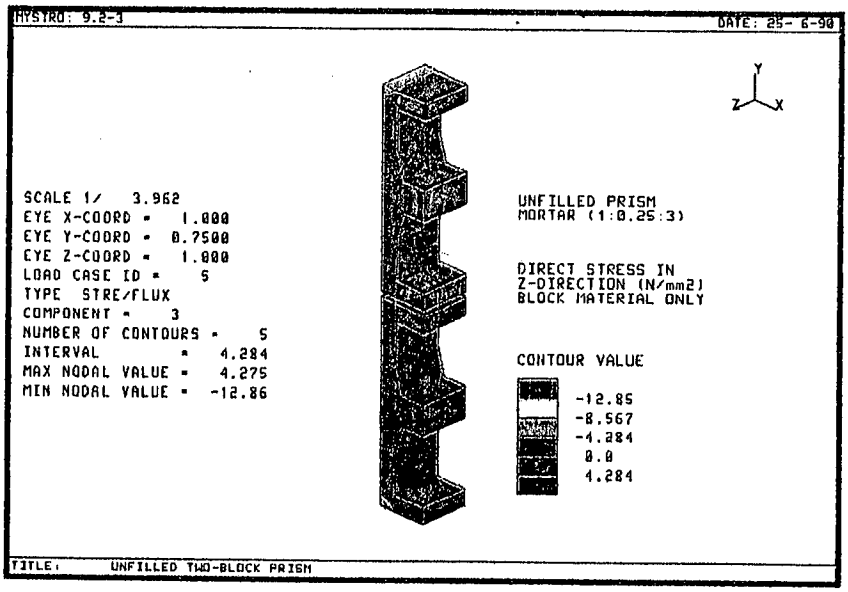

Fig. 4.32 - Direct stress in Z-direction, block material of unfilled 2BP-MJ prism, specific non-linear FEA.

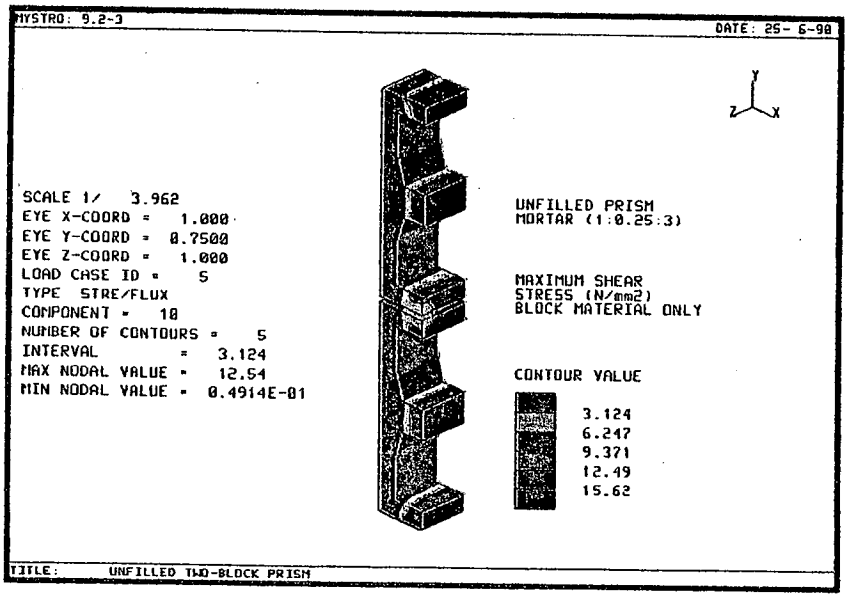

Fig. 4.33 - Maximum shear stress, block material of unfilled 2BP-MJ prism, specific non-linear FEA.

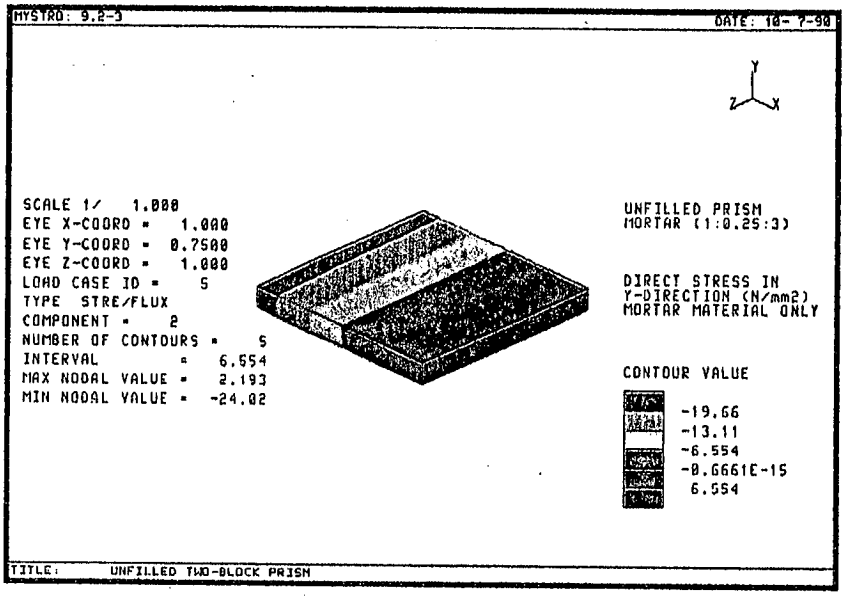

Fig. 4.34 - Direct stress in Y-direction, mortar material of unfilled 2BP-MJ prism, specific non-linear FEA.

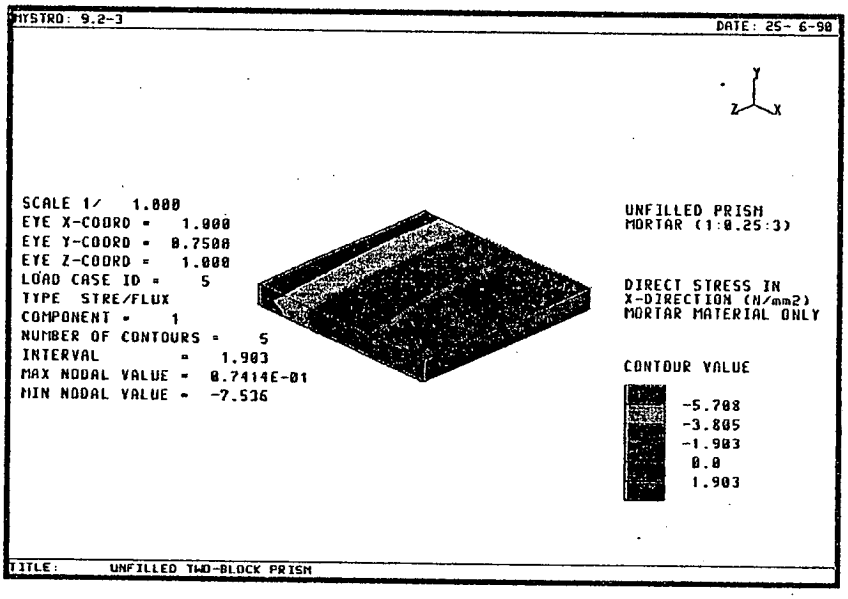

Fig. 4.35 - Direct stress in X-direction, mortar material of unfilled 2BP-MJ prism, specific non-linear FEA.

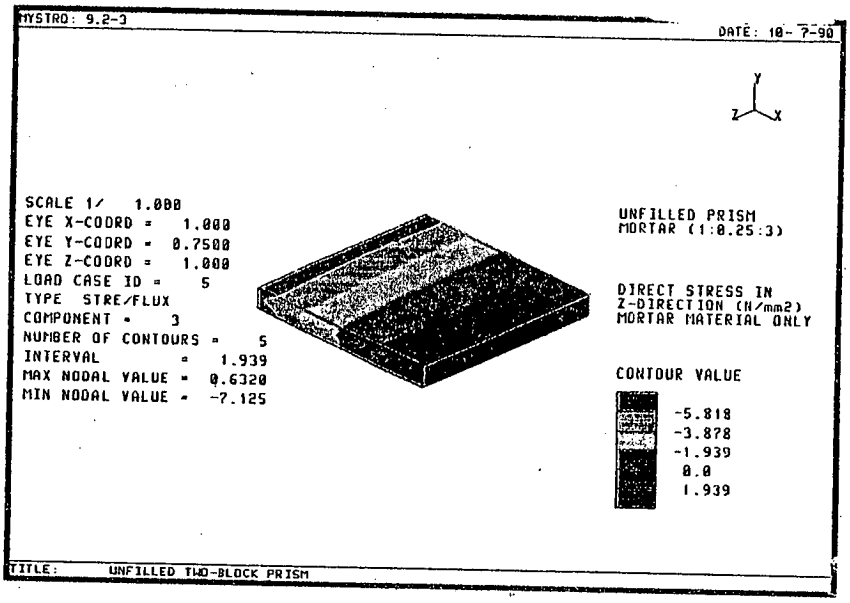

Fig. 4.36 - Direct stress in Z-direction, mortar material of unfilled 2BP-MJ prism, specific non-linear FEA.

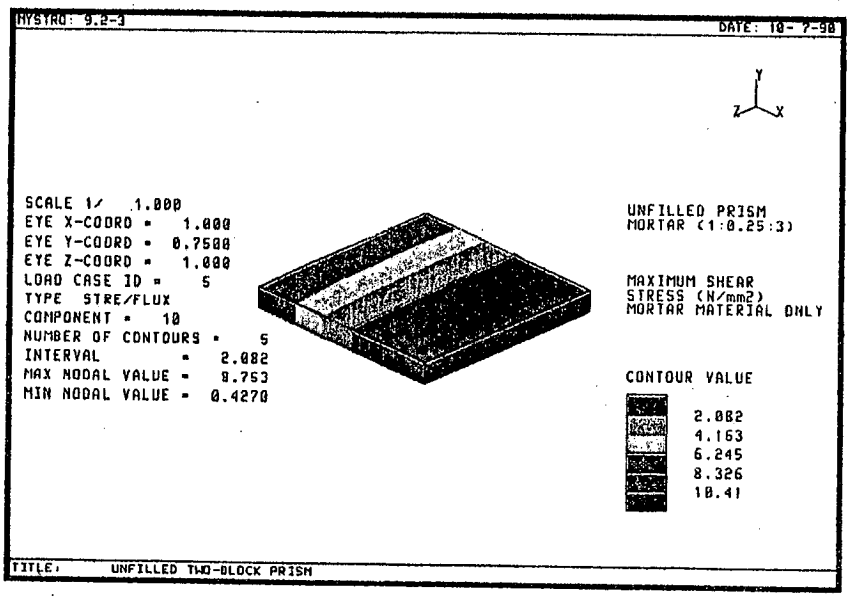

Fig. 4.37 - Maximum shear stress, mortar material of unfilled 2BP-MJ prism, specific non-linear FEA.

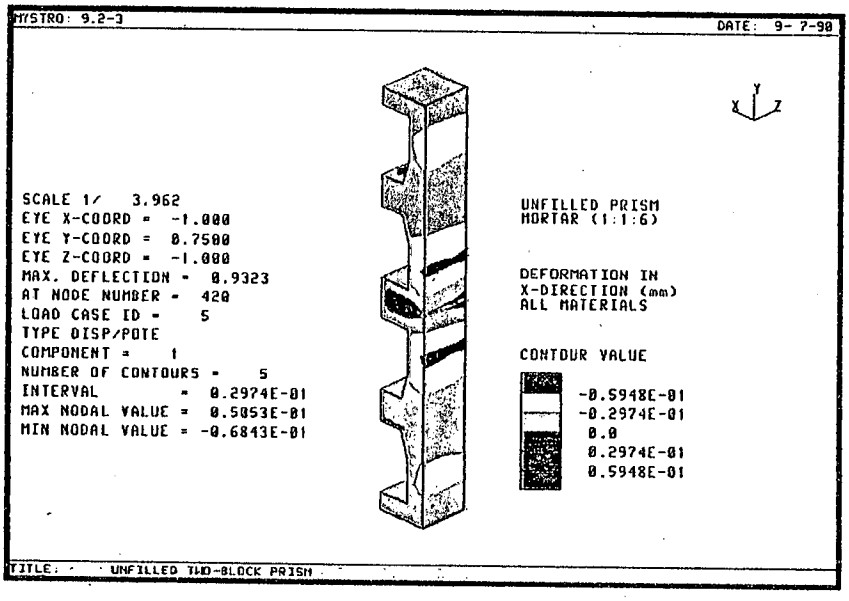

Fig. 4.38 - Deformation of unfilled 2BP-MJ prism in X-direction, parametric study non-linear FEA, 1:1:6 mortar.

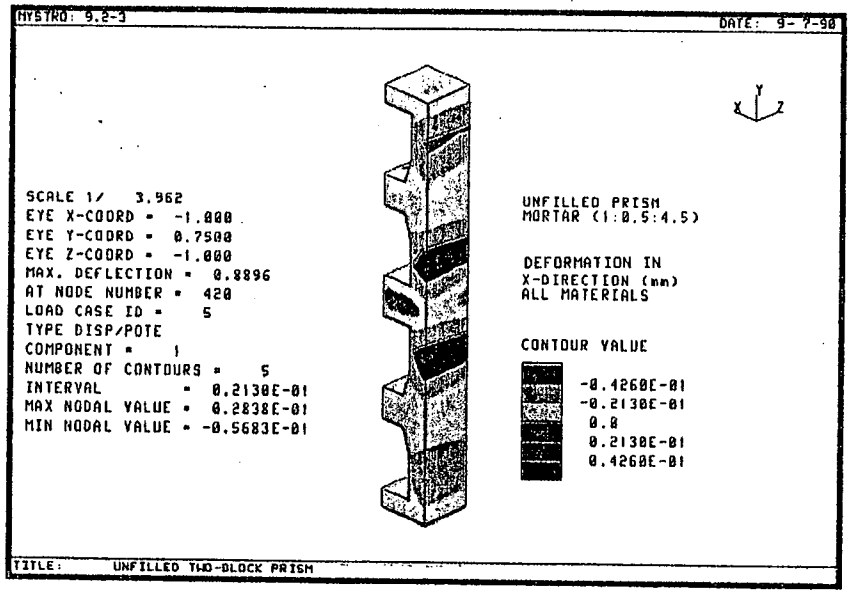

Fig. 4.39 - Deformation of unfilled 2BP-MJ prism in X-direction, parametric study non-linear FEA, 1:0.5:4.5 mortar.

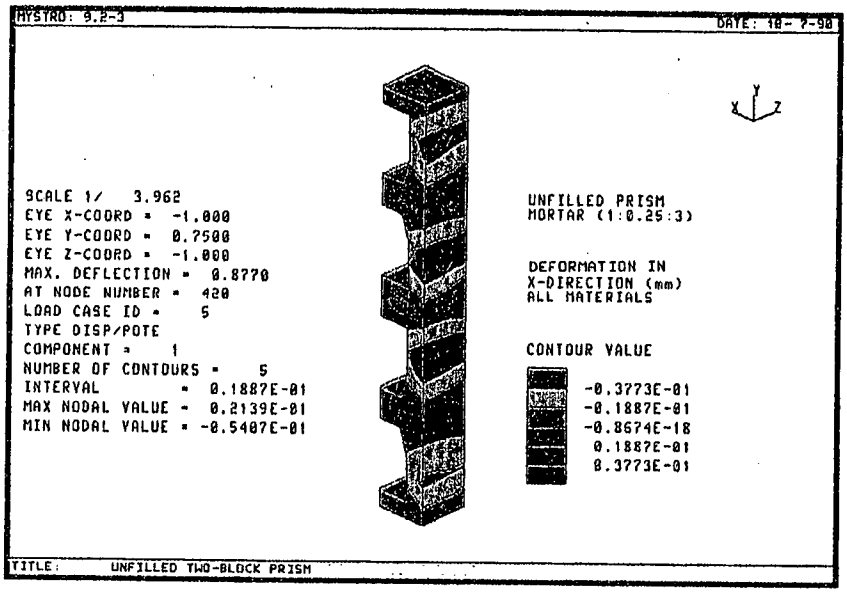

Fig. 4.40 - Deformation of unfilled 2BP-MJ prism in X-direction, parametric study non-linear FEA, 1:0.25:3 mortar.

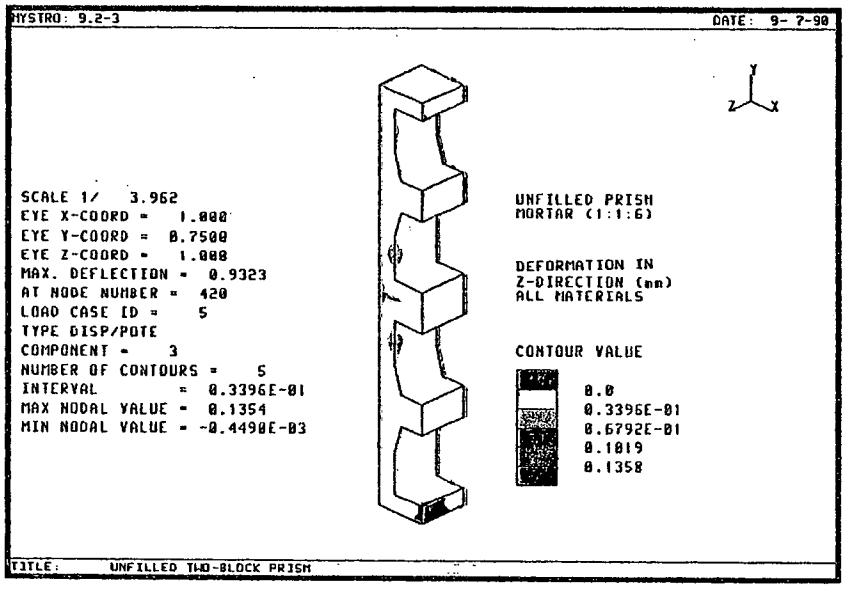

Fig. 4.41 - Deformation of unfilled 2BP-MJ prism in Z-direction, parametric study non-linear FEA, 1:1:6 mortar

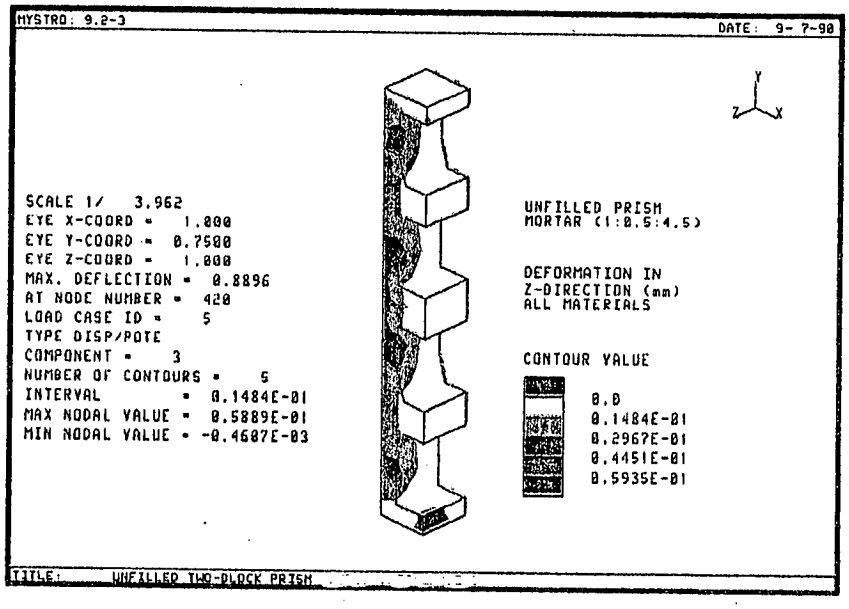

Fig. 4.42 - Deformation of unfilled 2BP-MJ prism in Z-direction, parametric study non-linear FEA, 1:0.5:4.5 mortar.

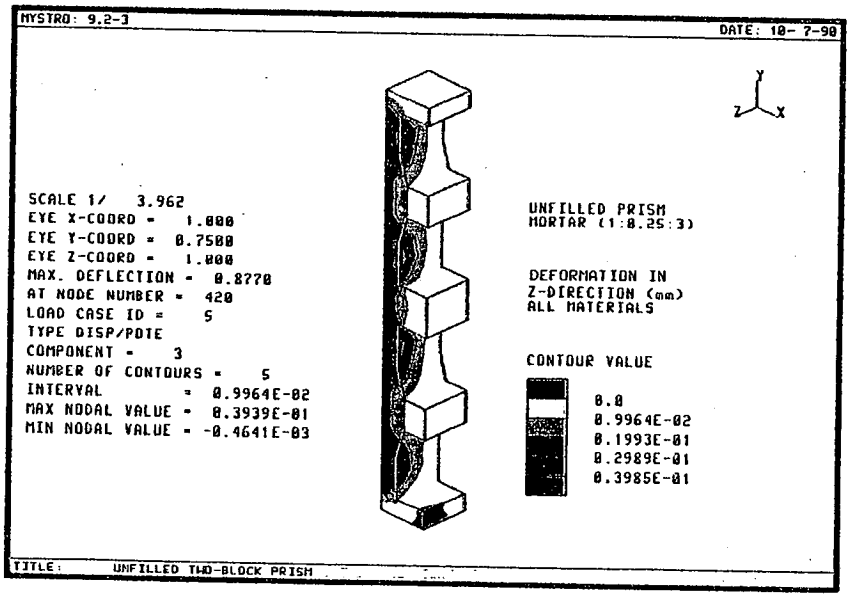

Fig. 4.43 - Deformation of unfilled 2BP-MJ prism in Z-direction, parametric study non-linear FEA, 1:0.25:3 mortar.

Table 4.2

Deformation results of the parametric study non-linear FEA for unfilled 2BP-MJ prism.

Prism type	Deformation results * (mm) YD	XD	ZD	Applied stress (N/mm^2)	Prism strength (N/mm^2)	Mortar strength (N/mm^2)
Unfilled (1:1:6)	0.002 -0.930	0.051 -0.068	0.135 -0.005	8.34	8.34	7.27
Unfilled (1:0.5:4.5)	0.002 -0.890	0.028 -0.057	0.059 -0.005	8.34	8.57	10.64
Unfilled (1:0.25:3)	0.002 -0.880	0.021 -0.054	0.039 -0.005	8.34	8.86	19.40

* Figures quoted in the table are the upper and lower maximum values of deformation.
YD, XD and ZD = Deformation in the Y-, X- and Z-directions.
+ve values = In the +ve direction of the axes.
-ve values = In the -ve direction of the axes.

Table 4.3

Stress results of the Parametric study non-linear FEA for unfilled 2BP-MJ prism.

Prism type	Stress results * (N/mm^2) YST	XST	ZST	SST	MJST	MST1	MST2
			Block material				
Unfilled (1:1:6)	3.61 -32.50	12.90 -16.50	5.46 -13.80	13.30 0.05	2.81 -34.40	5.46 -13.90	13.60 -12.00
Unfilled (1:0.5:4.5)	2.69 -32.70	9.47 -13.80	4.90 -13.90	13.10 0.05	2.28 -34.50	4.89 -13.90	10.10 -12.10
Unfilled (1:0.25:3)	2.30 -32.70	8.30 -14.00	4.59 -14.00	13.10 0.05	1.99 -34.60	4.58 -14.00	9.50 -12.10
			Mortar material				
Unfilled (1:1:6)	2.88 -27.00	1.08 -23.30	1.67 -23.20	4.51 0.32	1.07 -29.60	1.63 -23.40	2.93 -20.60
Unfilled (1:0.5:4.5)	2.67 -25.30	0.67 -15.40	1.14 -15.10	6.34 0.40	0.67 -26.50	1.14 -15.50	2.70 -14.50
Unfilled (1:0.25:3)	2.32 -25.10	0.09 -8.20	0.68 -7.75	8.99 0.45	0.08 -25.30	0.68 -8.31	2.34 -7.53

* Figures quoted in the table are the upper and lower values of stress.

YST, XST and ZST = Direct stress in the Y-, X- and Z-directions.

SST = Maximum shear stress.

MJST, MST1 and MST2 = Major, minor 1 and 2 principal stresses.

+ve values = Tension.

-ve values = Compression.

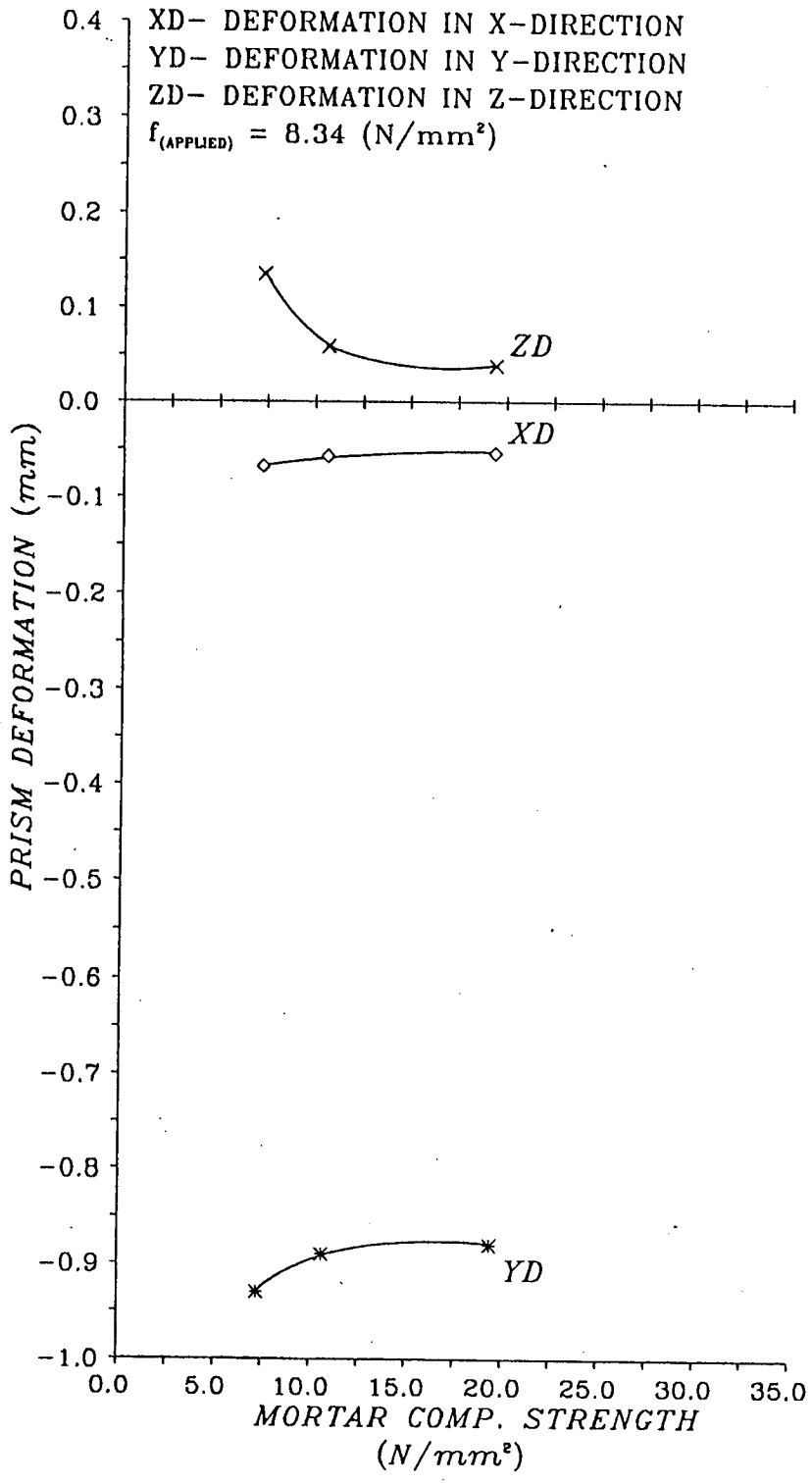

Fig. 4.44 - Effect of mortar strength on unfilled 2BP-MJ prism deformation, parametric study non-linear FEA.

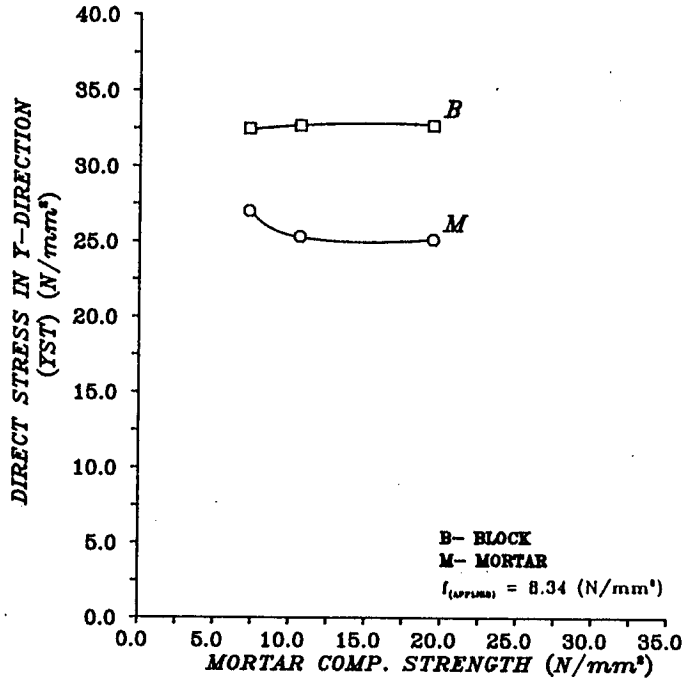

Fig. 4.45 - Effect of mortar strength on unfilled 2BP-MJ prism direct stress in Y-direction, parametric study non-linear FEA.

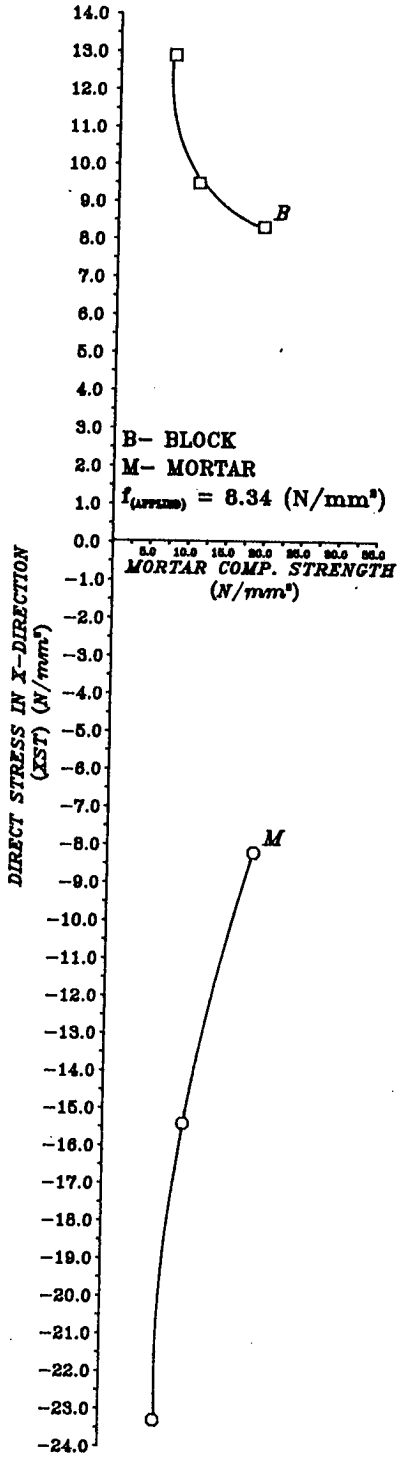

Fig. 4.46 - Effect of mortar strength on unfilled 2BP-MJ prism direct stress in X-direction, parametric study non-linear FEA.

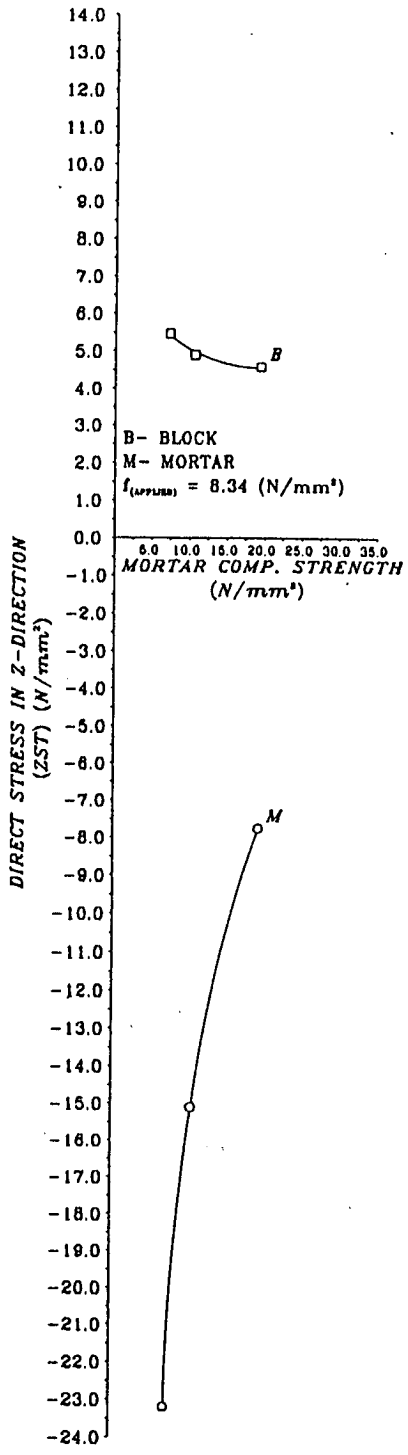

Fig. 4.47 - Effect of mortar strength on unfilled 2BP-MJ prism direct stress in Z-direction, parametric study non-linear FEA.

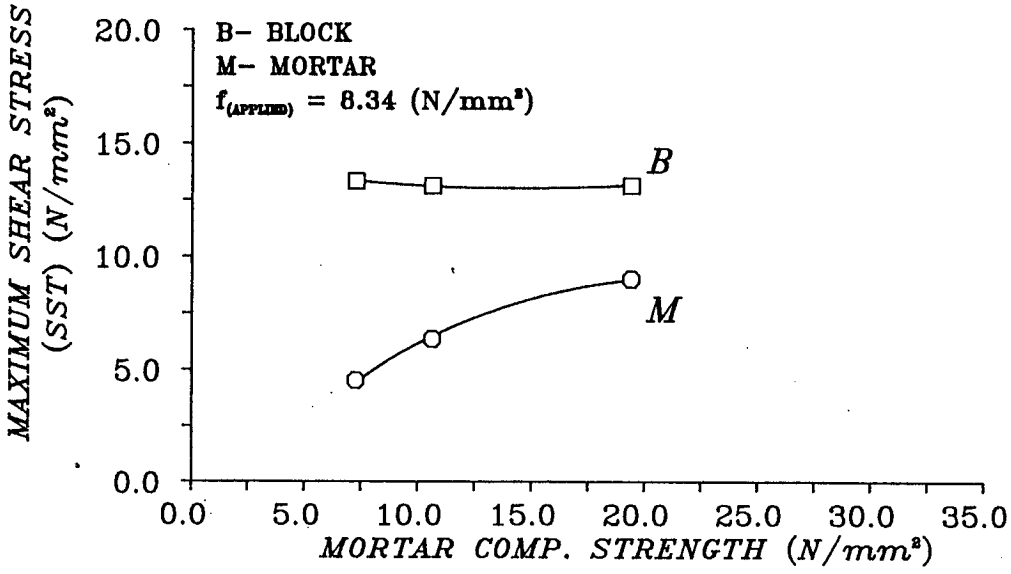

Fig. 4.48 - Effect of mortar strength on unfilled 2BP-MJ prism maximum shear stress, parametric study non-linear FEA.

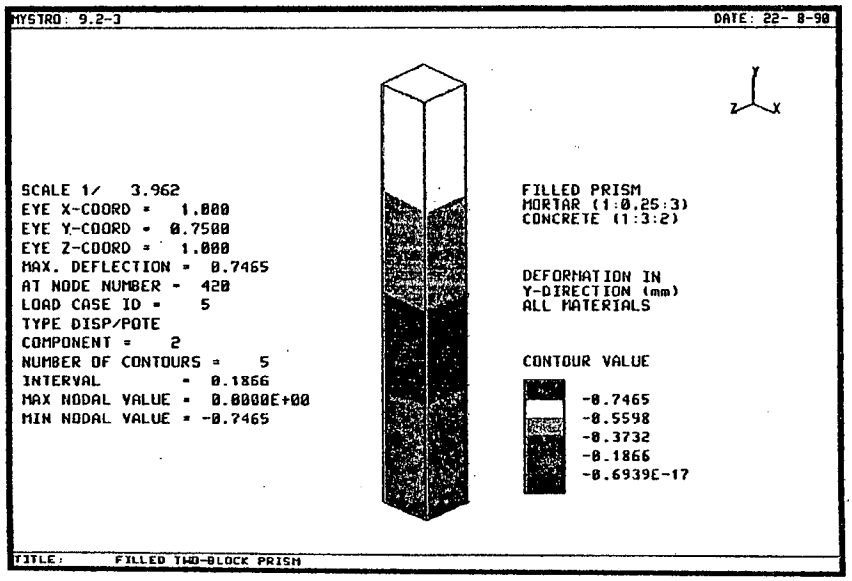

Fig. 4.49 - Deformation of filled 2BP-MJ prism in Y-direction, specific non-linear FEA.

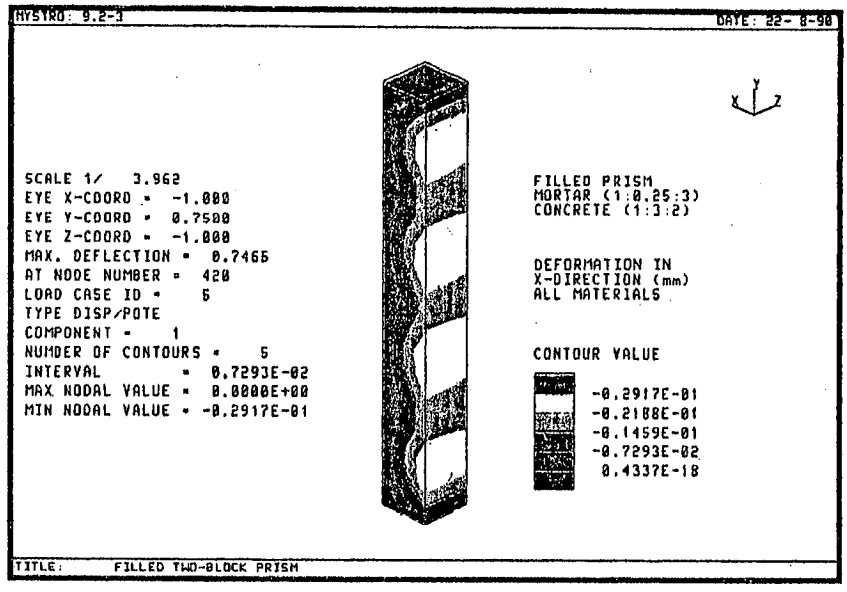

Fig. 4.50 - Deformation of filled 2BP-MJ prism in X-direction, specific non-linear FEA.

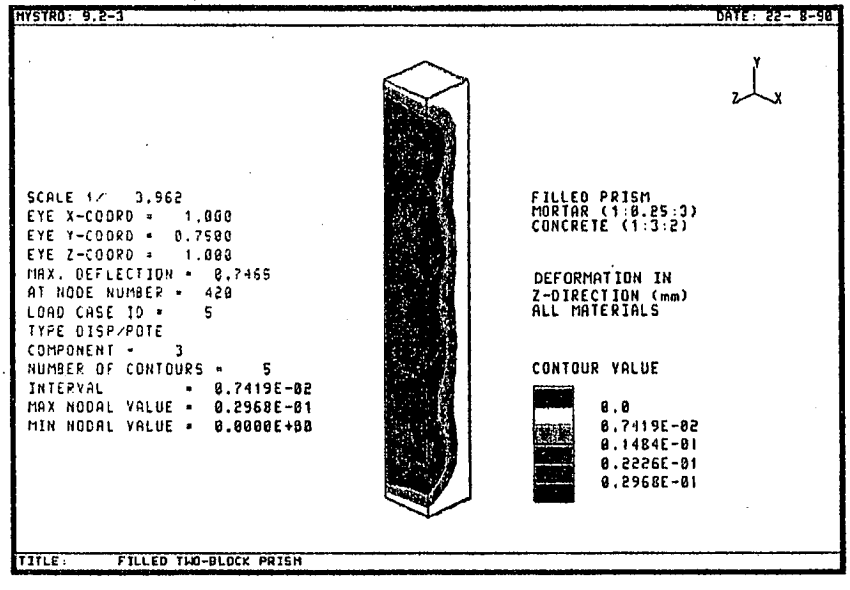

Fig. 4.51 - Deformation of filled 2BP-MJ prism in Z-direction, specific non-linear FEA.

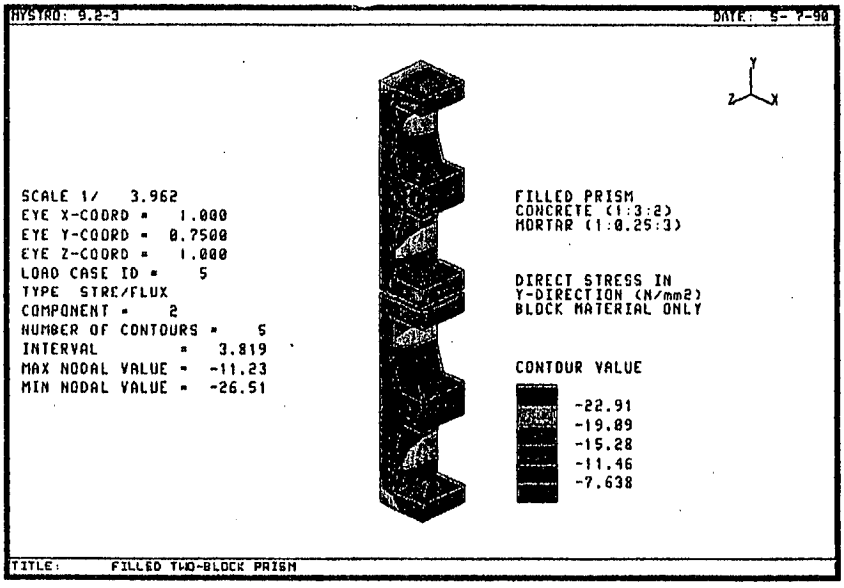

Fig. 4.52 - Direct stress in Y-direction, block material of filled 2BP-MJ prism, specific non-linear FEA.

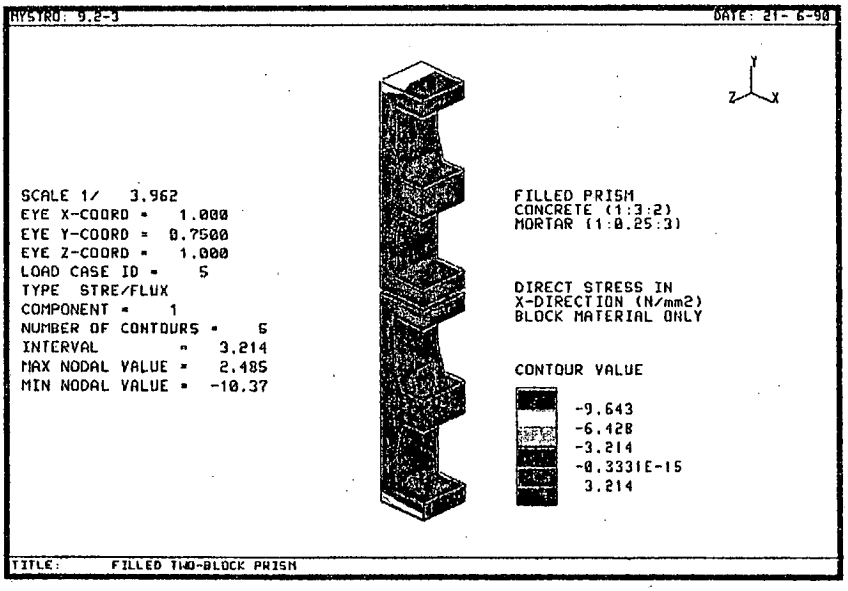

Fig. 4.53 - Direct stress in X-direction, block material of filled 2BP-MJ prism, specific non-linear FEA.

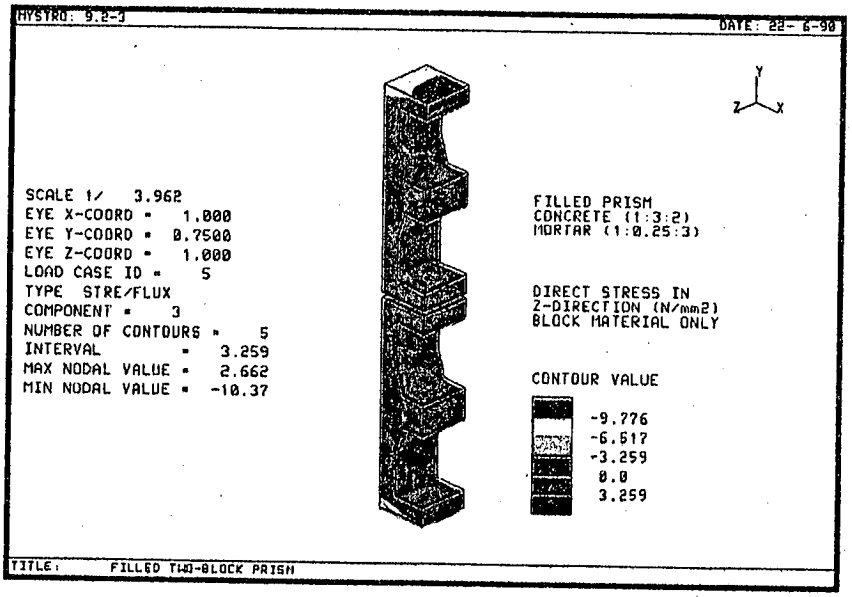

Fig. 4.54 - Direct stress in Z-direction, block material of filled 2BP-MJ prism, specific non-linear FEA.

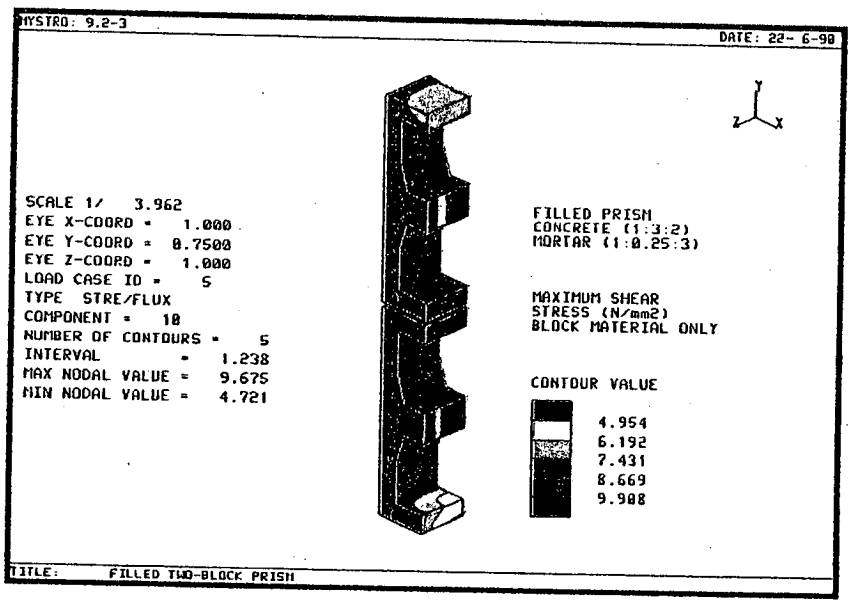

Fig. 4.55 - Maximum shear stress, block material of filled 2BP-MJ prism, specific non-linear FEA.

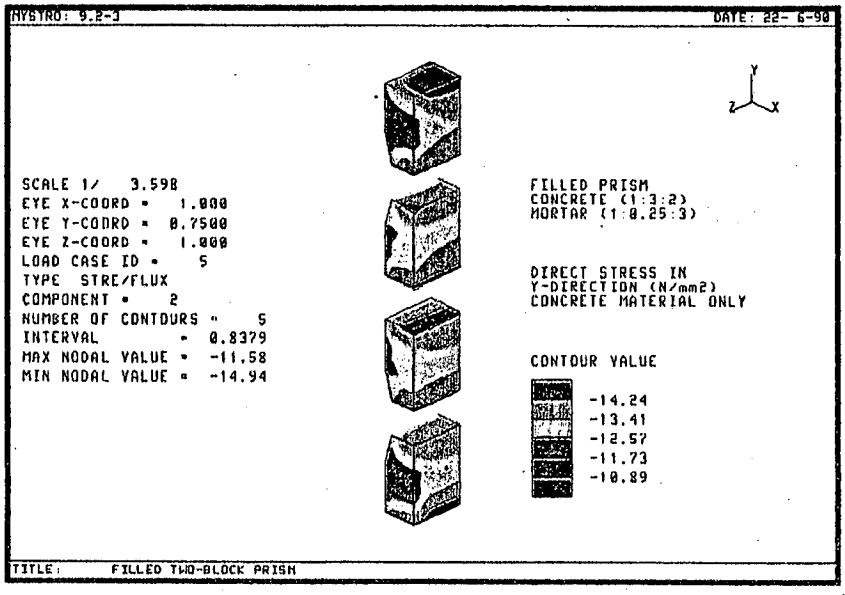

Fig. 4.56 - Direct stress in Y-direction, concrete material of filled 2BP-MJ prism, specific non-linear FEA.

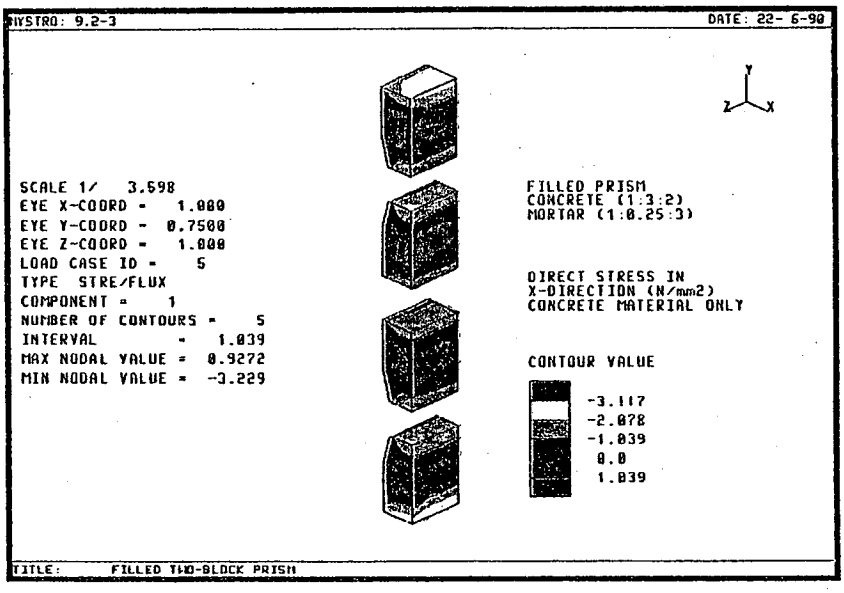

Fig. 4.57 - Direct stress in X-direction, concrete material of filled 2BP-MJ prism, specific non-linear FEA.

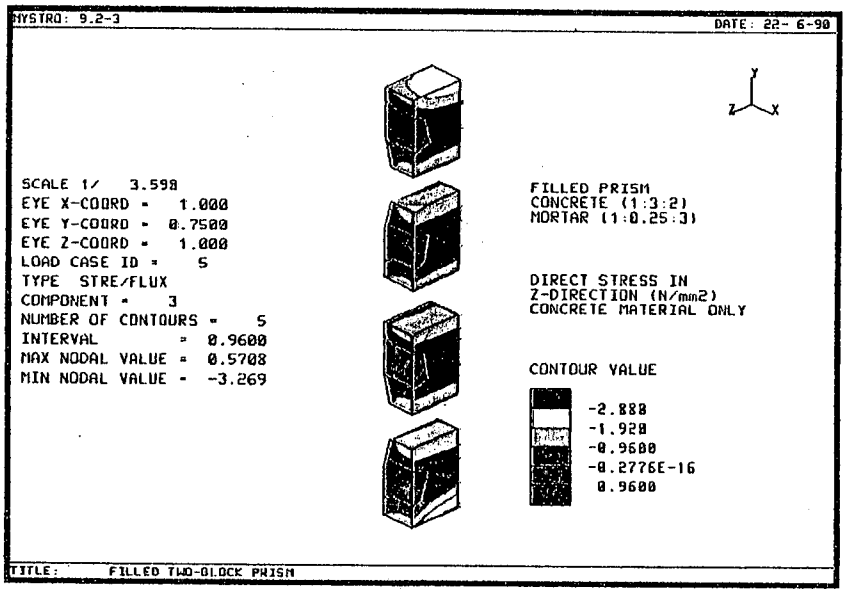

Fig. 4.58 - Direct stress in Z-direction, concrete material of filled 2BP-MJ prism, specific non-linear FEA.

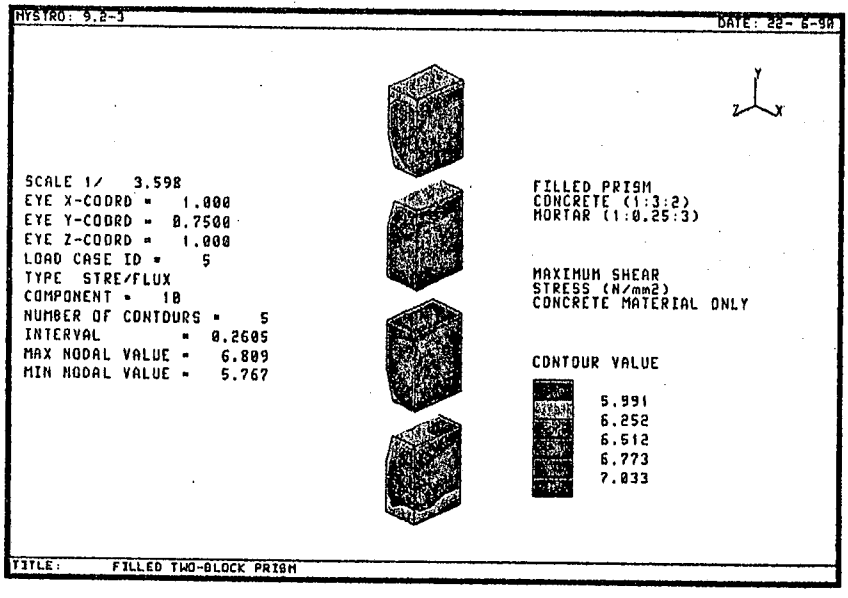

Fig. 4.59 - Maximum shear stress, concrete material of filled 2BP-MJ prism, specific non-linear FEA.

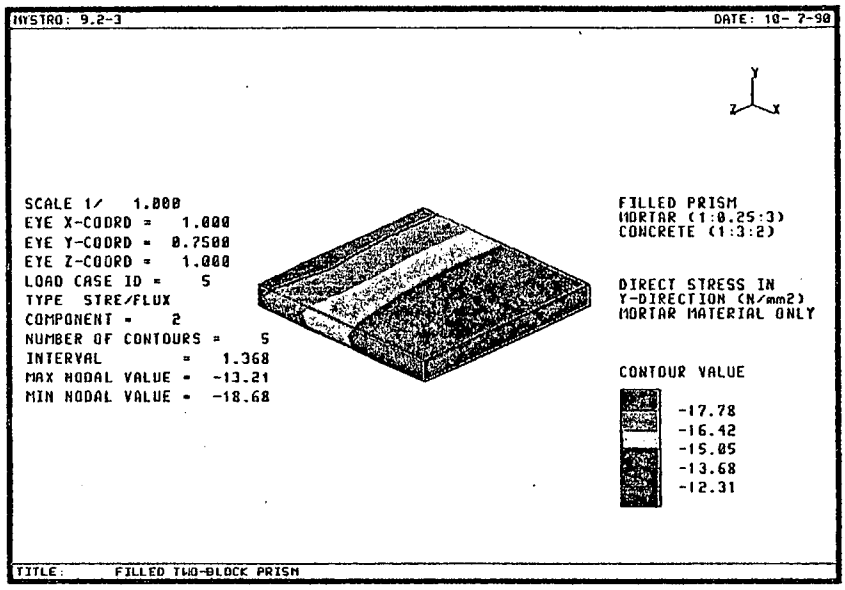

Fig. 4.60 - Direct stress in Y-direction, mortar material of filled 2BP-MJ prism, specific non-linear FEA.

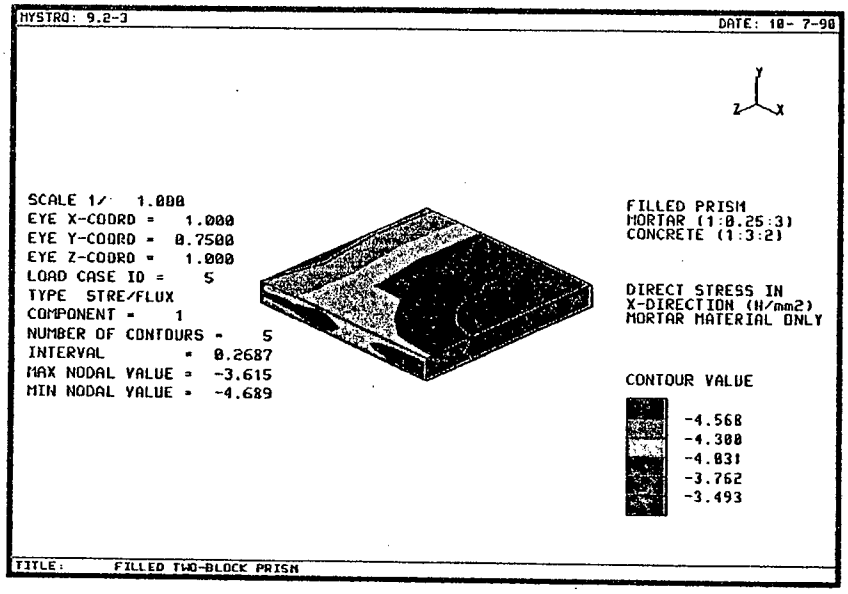

Fig. 4.61 - Direct stress in X-direction, mortar material of filled 2BP-MJ prism, specific non-linear FEA.

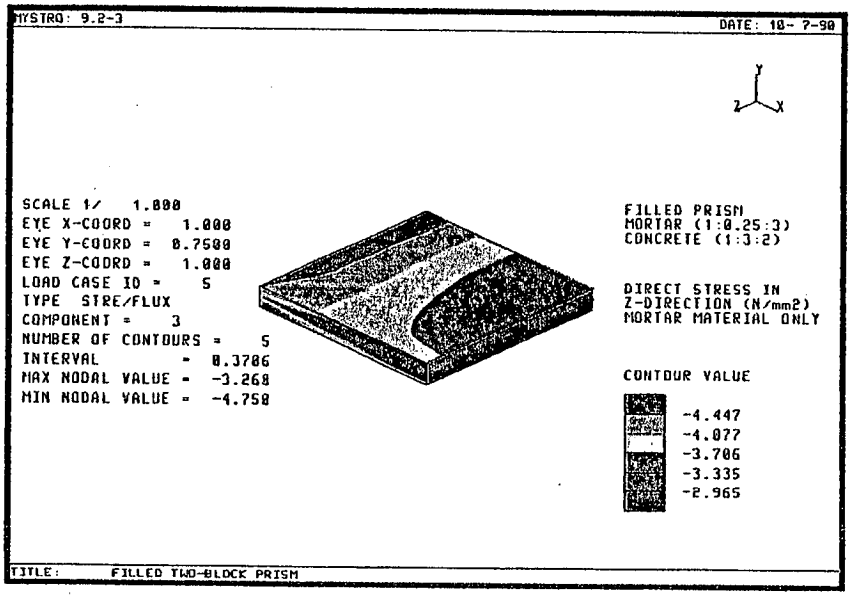

Fig. 4.62 - Direct stress in Z-direction, mortar material of filled 2BP-MJ prism, specific non-linear FEA.

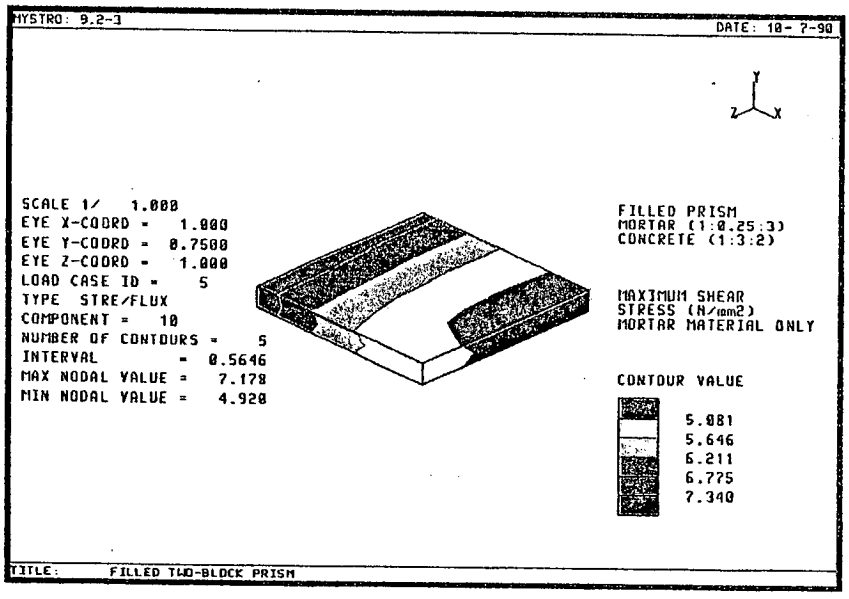

Fig. 4.63 - Maximum shear stress, mortar material of filled 2BP-MJ prism, specific non-linear FEA.

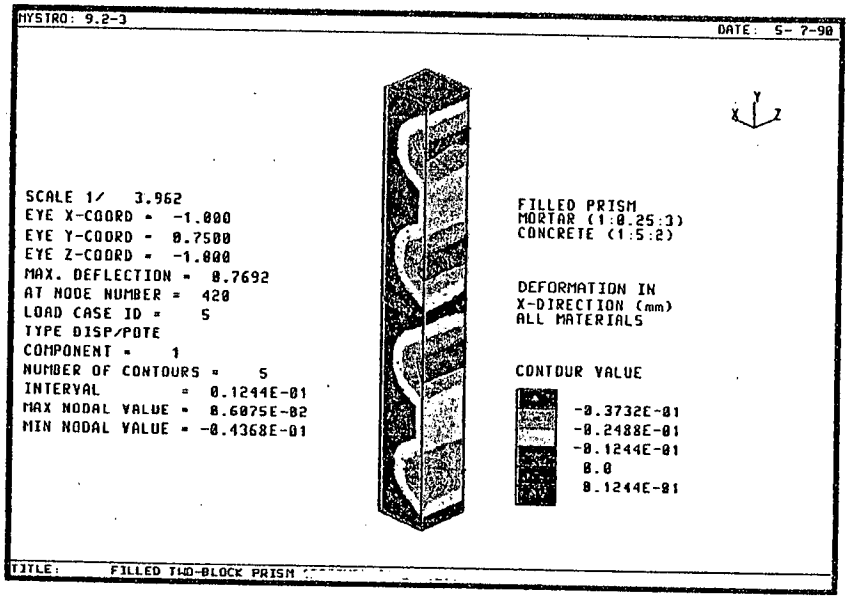

Fig. 4.64 - Deformation of filled 2BP-MJ prism in X-direction, parametric study non-linear FEA, 1:5:2 concrete.

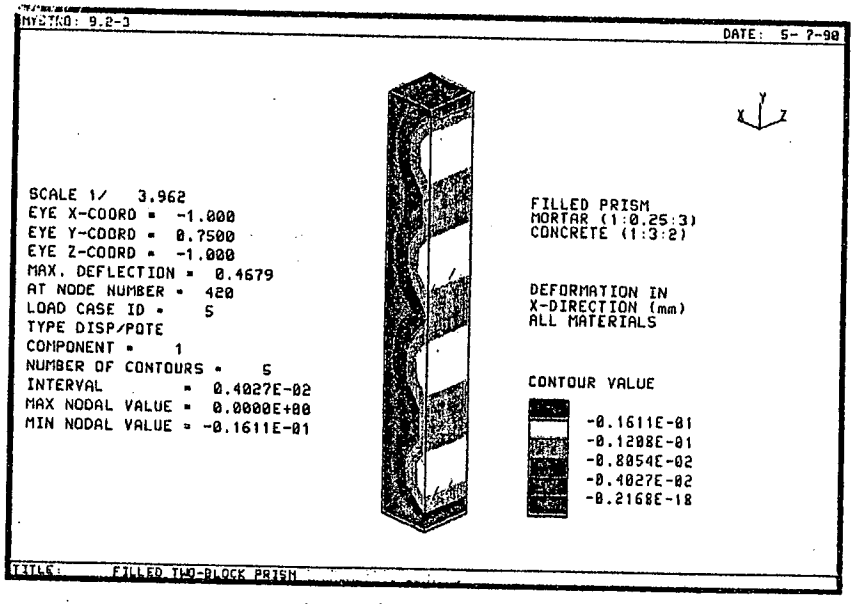

Fig. 4.65 - Deformation of filled 2BP-MJ prism in X-direction, parametric study non-linear FEA, 1:3:2 concrete.

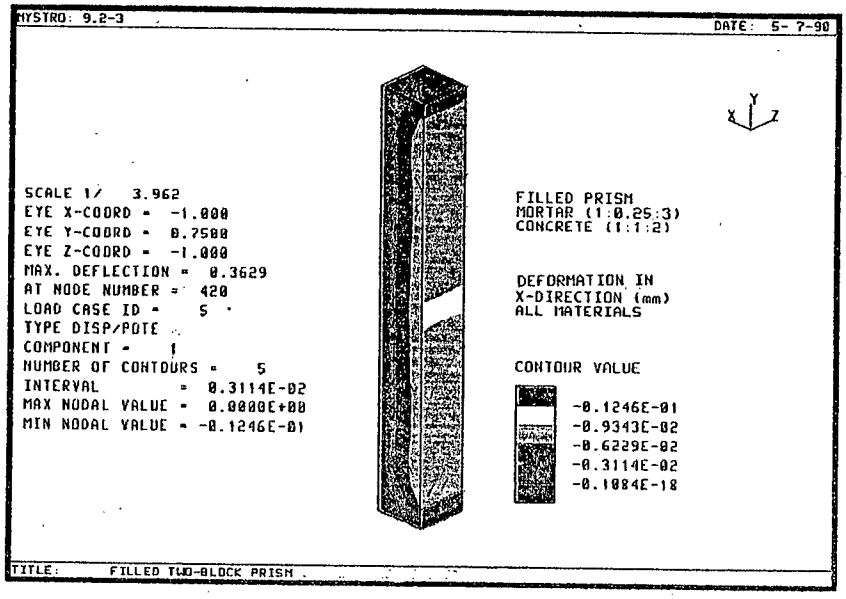

Fig. 4.66 - Deformation of filled 2BP-MJ prism in X-direction, parametric study non-linear FEA, 1:1:2 concrete.

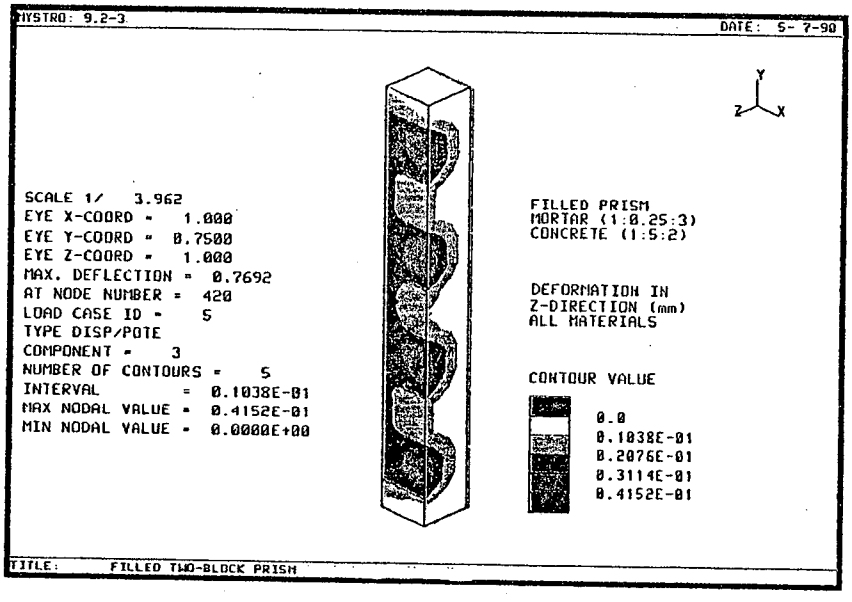

Fig. 4.67 - Deformation of filled 2BP-MJ prism in Z-direction, parametric study non-linear FEA, 1:5:2 concrete.

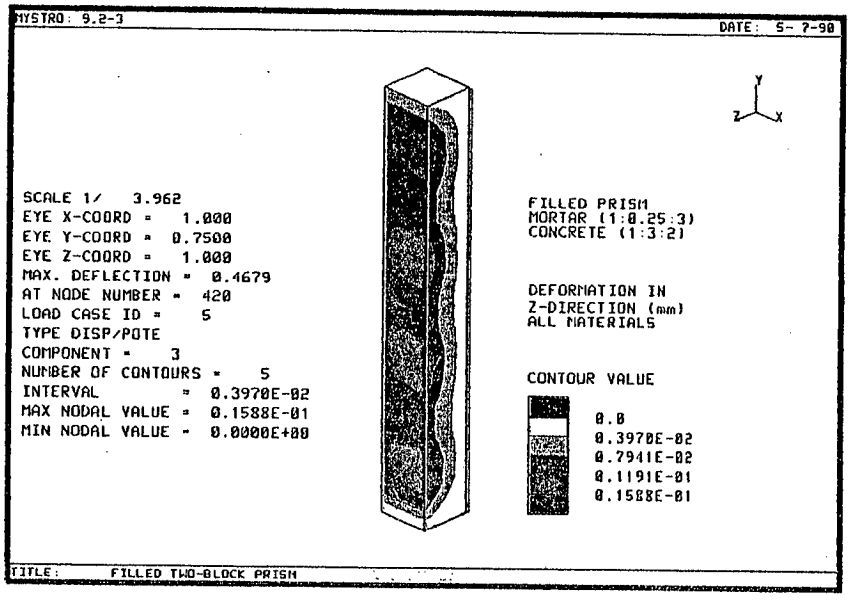

Fig. 4.68 - Deformation of filled 2BP-MJ prism in Z-direction, parametric study non-linear FEA, 1:3:2 concrete.

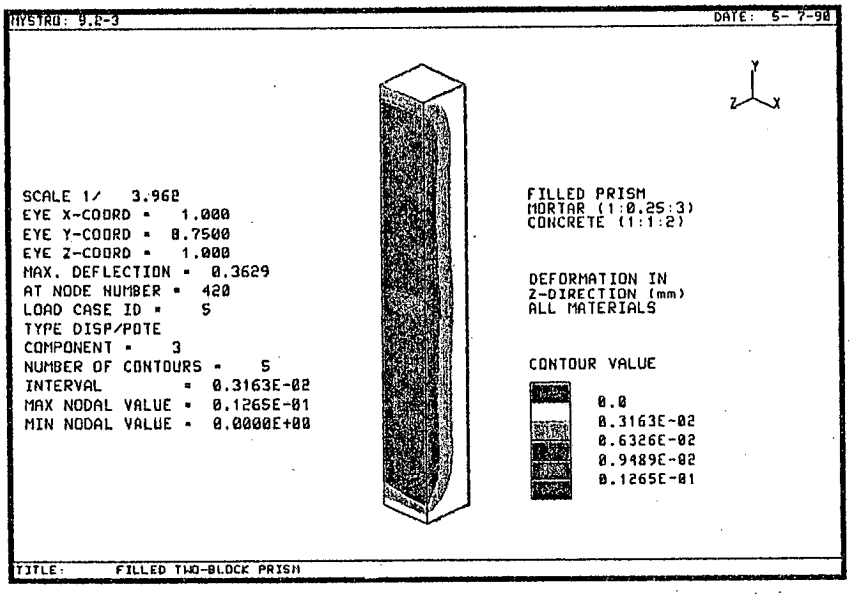

Fig. 4.69 - Deformation of filled 2BP-MJ prism in Z-direction, parametric study non-linear FEA, 1:1:2 concrete.

Table 4.4

Deformation results of the parametric study non-linear FEA for filled 2BP-MJ prism.

Prism type	Deformation results * (mm) YD	XD	ZD	Applied stress (N/mm^2)	Prism strength (N/mm^2)	Infill strength (N/mm^2)
Filled (1:5:2)	0.000 -0.770	0.006 -0.044	0.042 0.000	11.26	11.26	4.97
Filled (1:3:2)	0.000 -0.470	0.000 -0.016	0.016 0.000	11.26	15.26	22.31
Filled (1:1:2)	0.000 -0.360	0.000 -0.013	0.013 0.000	11.26	11.47	39.44

* Figures quoted in the table are the upper and lower maximum values of deformation.
YD, XD and ZD = Deformation in the Y-, X- and Z-directions.
+ve values = In the +ve direction of the axes.
-ve values = In the -ve direction of the axes.

Table 4.5

Stress results of the Parametric study non-linear FEA for filled 2BP-MJ prism.

Prism type	Stress results * (N/mm^2) YST	XST	ZST	SST	MJST	MST1	MST2
			Block material				
Filled (1:5:2)	-3.96 -29.50	5.94 -12.10	4.66 -12.10	11.00 2.15	-4.03 -31.20	4.66 -12.10	6.30 -10.30
Filled (1:3:2)	-8.06 -18.90	1.60 -5.67	1.69 -5.67	7.48 3.37	-8.11 -19.80	1.60 -5.67	1.69 -4.82
Filled (1:1:2)	-10.10 -14.90	1.01 -3.71	1.01 -3.71	6.23 4.05	-10.10 -15.50	0.97 -3.71	1.02 -3.06
			Concrete material				
Filled (1:5:2)	-4.78 -8.18	0.94 -3.39	0.70 -3.21	3.06 2.18	-4.78 -8.35	0.66 -3.39	1.06 -3.03
Filled (1:3:2)	-8.22 -10.30	0.67 -2.09	0.28 -2.15	4.93 3.93	-8.22 -10.30	0.27 -2.15	0.70 -2.09
Filled (1:1:2)	-10.60 -11.90	0.27 -1.78	0.12 -1.79	5.74 4.91	-10.60 -11.90	0.11 -1.78	0.27 -1.75
			Mortar material				
Filled (1:5:2)	-5.09 -21.30	-1.64 -5.97	-1.13 -5.70	8.02 1.94	-5.09 -21.40	-1.64 -6.08	-1.13 -5.61
Filled (1:3:2)	-9.48 -14.10	-2.81 -3.95	-2.42 -3.96	5.25 3.42	-9.48 -14.20	-2.81 -3.96	-2.42 -3.87
Filled (1:1:2)	-10.60 -11.60	-2.49 -3.34	-2.46 -3.30	4.22 4.03	-10.60 -11.60	-2.50 -3.34	-2.45 -3.30

* Figures quoted in the table are the upper and lower values of stress.

YST, XST and ZST = Direct stress in the Y-, X- and Z-directions.

SST = Maximum shear stress.

MJST, MST1 and MST2 = Major, minor 1 and 2 principal stresses.

+ve values = Tension.

-ve values = Compression.

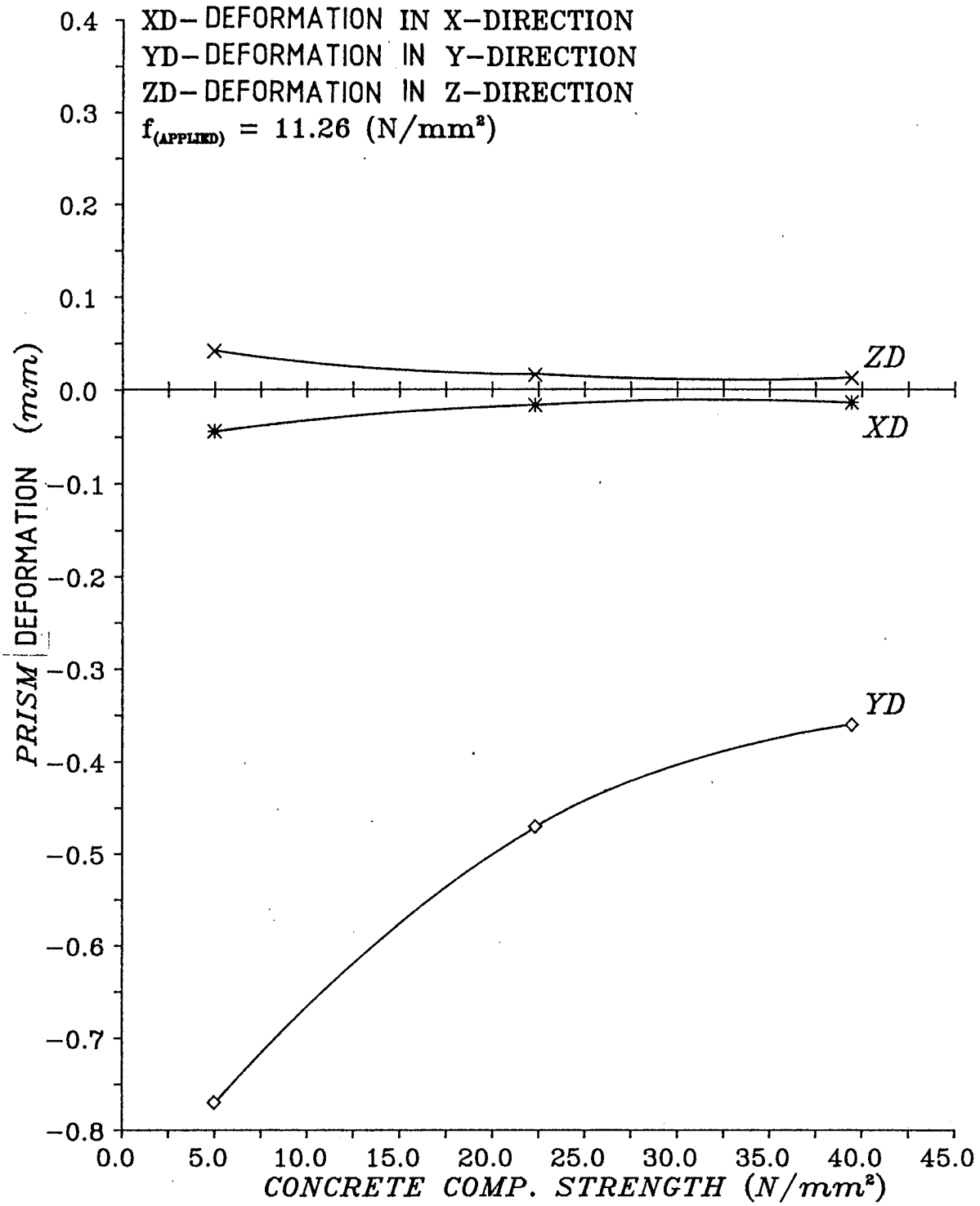

Fig. 4.70 - Effect of concrete infill strength on filled 2BP-MJ prism deformation, parametric study non-linear FEA.

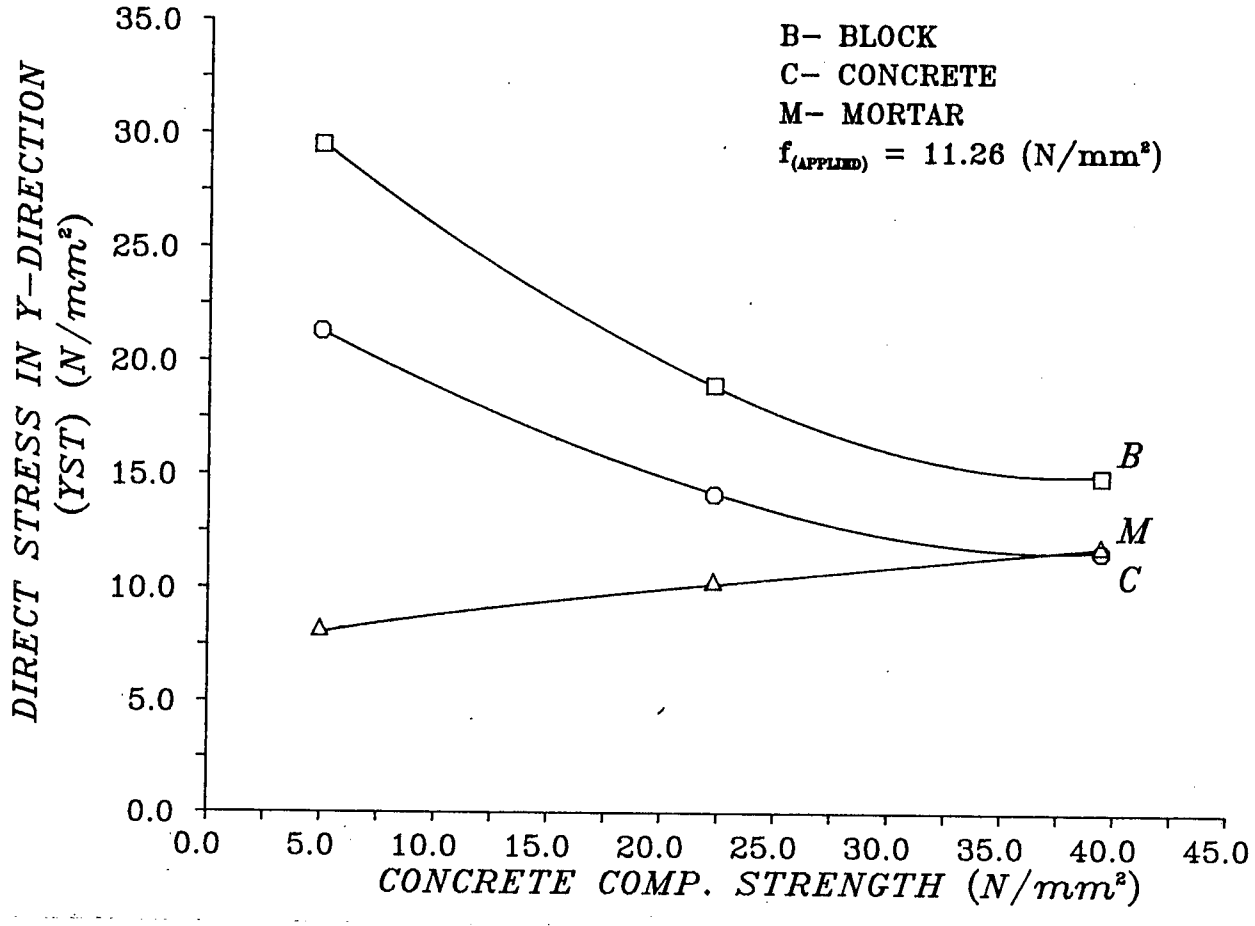

Fig. 4.71 - Effect of concrete infill strength on filled 2BP-MJ prism direct stress in Y-direction, parametric study non-linear FEA.

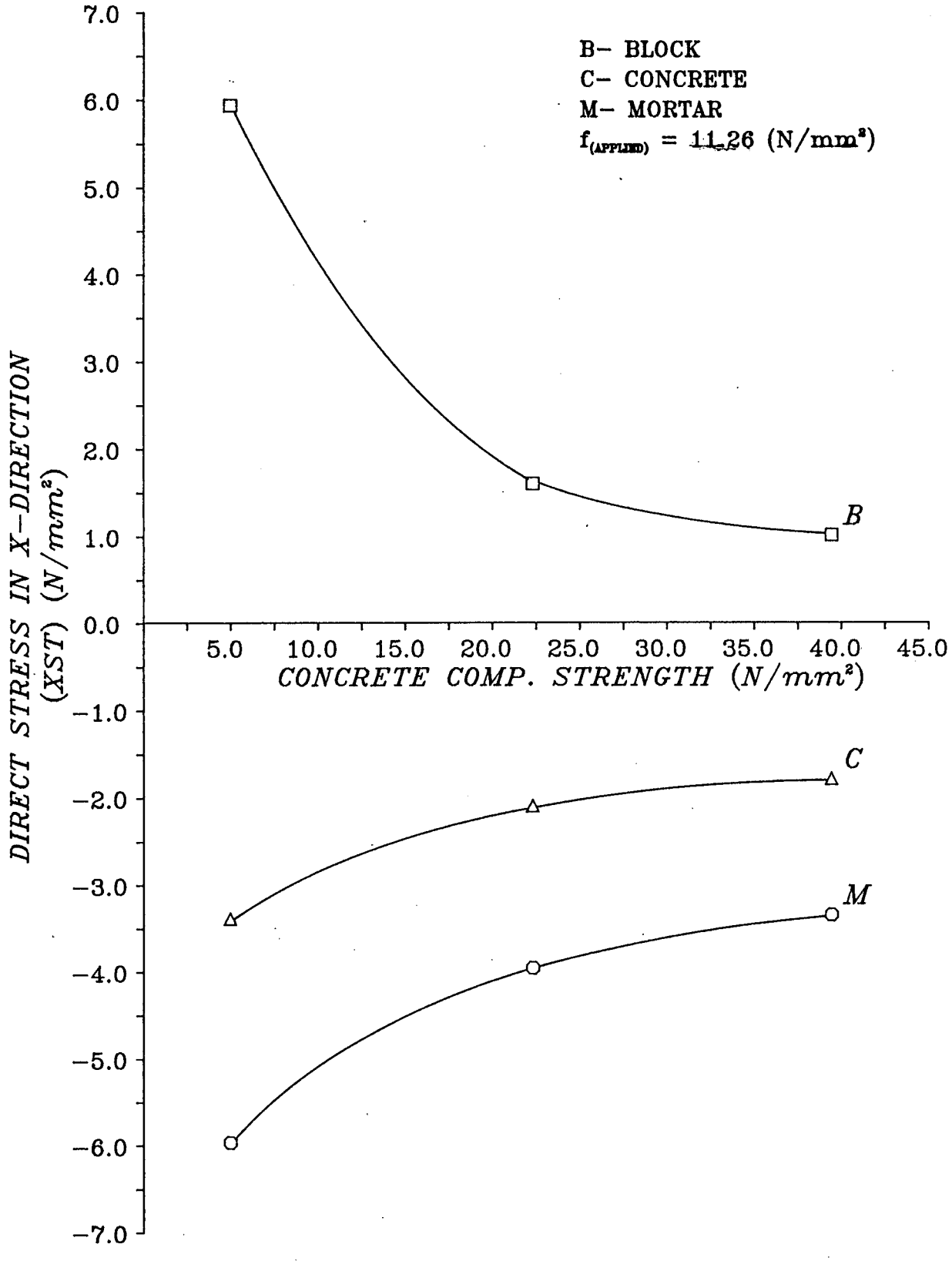

Fig. 4.72 - Effect of concrete infill strength on filled 2BP-MJ prism direct stress in X-direction, parametric study non-linear FEA.

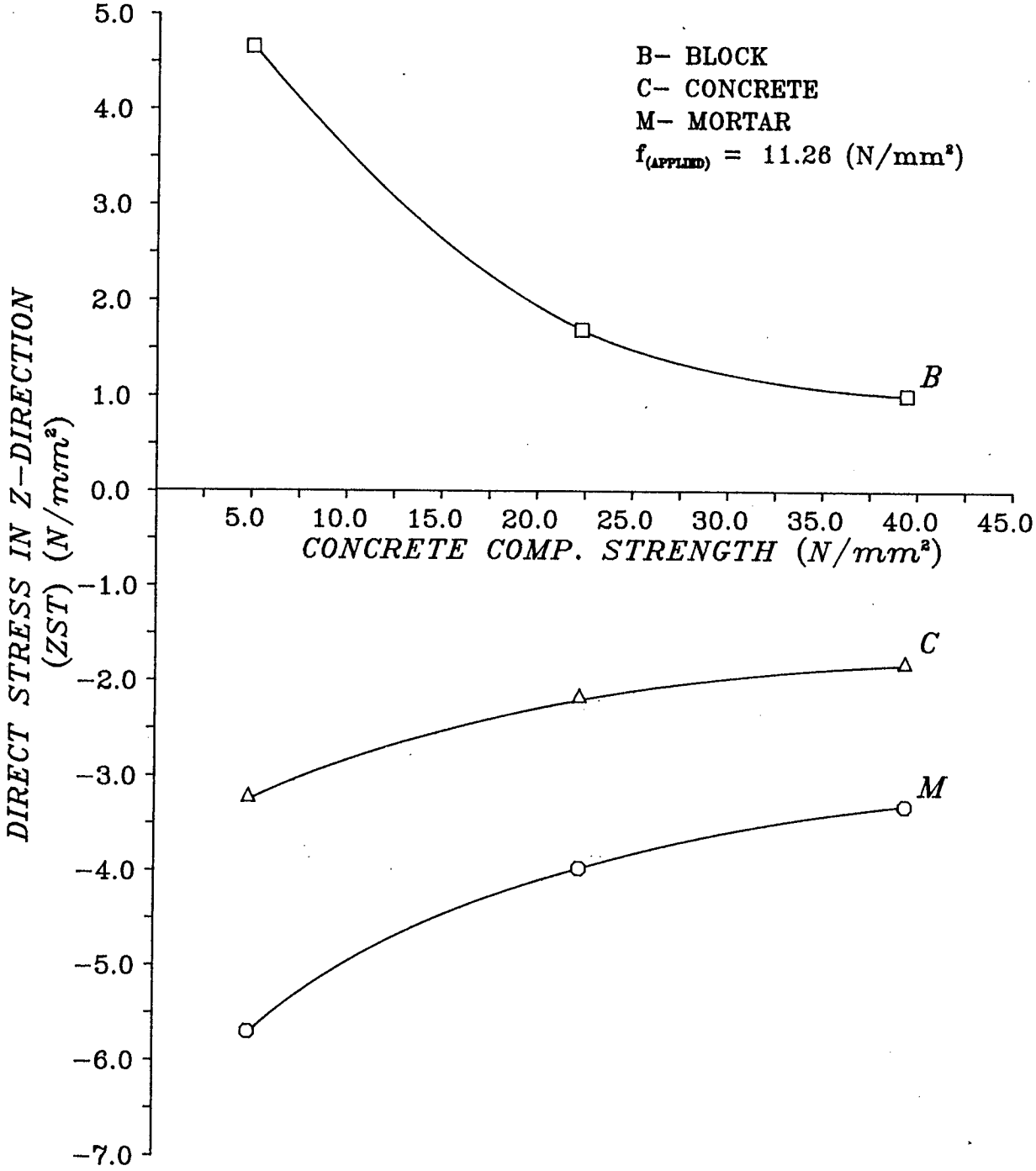

Fig. 4.73 - Effect of concrete infill strength on filled 2BP-MJ prism direct stress in Z-direction, parametric study non-linear FEA.

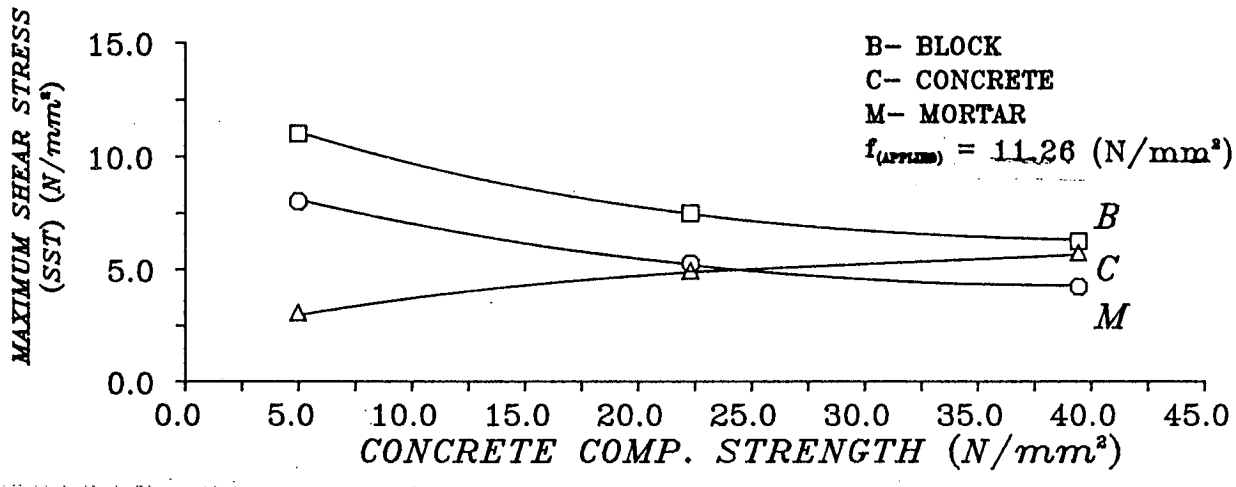

Fig. 4.74 - Effect of concrete infill strength on filled 2BP-MJ prism maximum shear stress, parametric study non-linear FEA.

CHAPTER 5

CONCRETE BLOCK MASONRY PRISMS COMPRESSED NORMAL TO THE UNIT BED FACE

5.1 INTRODUCTION

This chapter presents the results of an experimental and theoretical investigations carried out to study the effects of using different concrete infill mixes and mortar joint types on the compressive strength and behaviour of unfilled and filled, full and half, 3-course high blockwork masonry prisms compressed normal to the unit bed face. Methods are recommended to determine values of the ultimate compressive strength of blockwork masonry, f'_m, to be used in the strength design theory for masonry structures.

As mentioned in chapter 4, stack-bonded blockwork masonry prism testing is one of the commonly used methods adopted by several governing codes and standards[24,25] to determine the ultimate compressive strength of blockwork masonry prisms, f'_m.

Previous work by DRYSDALE and HAMID[28,29] on concrete block masonry prisms showed that using values for the masonry compressive strength, f'_m, based on block strength and mortar type, was not appropriate for grouted concrete block masonry. This is due to the mortar joint having a negligible effect on the compressive strength. They suggested that matching the deformational characteristics of the grout and the block may be more efficient in increasing the masonry strength than increasing the grout strength.

They also concluded that testing 3-course high half-block prisms represents more accurately the strength of concrete block masonry because it exhibits a failure mode similar to that for walls. It was therefore concluded that the half-block prism be used as a standard specimen to determine f'_m due to ease of handling. The failure mechanisms for the 3-course high half-block concrete masonry prism were described and corresponding failure criteria were developed.

However, using the results of tests on half-block prisms is not acceptable due to differences in the aspect ratio, (l/t) (prism length-to-thickness), and differences in the mortar bedded area, caused by the presence of the mid-web, between the full and half-block prisms. This will be demonstrated later in this chapter, and also investigated in more details in chapter 6.

The objective of the present investigation is to produce a method of obtaining f'_m, for use in the strength design theory of masonry structural elements in situations where in-plane horizontal forces are not expected to occur. The effects of using different types of mortar and concrete infill mixes on f'_m and on the prisms' behaviour and mode of failure were also studied experimentally and theoretically using a three-dimensional finite element analysis (FEA).

5.2 EXPERIMENTAL PROGRAMME

A total of fifty-seven full-block prisms and thirty-nine half-block prisms were tested axially normal to the bed face. The prisms were constructed by an experienced mason to ensure that the 10 mm horizontal mortar joints between the concrete blocks were completely filled. The

prisms were built using three different mortar types: low strength (1:1:6), medium strength (1:0.5:4.5) and high strength (1:0.25:3) (cement: lime: sand) proportions. The prisms are designated in Fig. 5.1 (i), in Table A.1 (Appendix A) and in the text as **3FBP-MJ** (**3**-course high **F**ull-**B**lock **P**risms with **M**ortar **J**oints).

Some of the prisms were constructed without a mortar joints. Instead, a thin layer, 1 - 2 mm, of dental plaster was placed between the blocks. The prisms are designated in Fig. 5.1 (ii), in Table A.1 (Appendix A) and in the text as **3FBP-DPJ** (**3**-course high **F**ull-**B**lock **P**risms with **D**ental **P**laster **J**oints). The 1 - 2 mm thickness was achieved using the method described for capping[55] in chapters 3 and 4. Other prisms were constructed using a 10 mm thick polystyrene sheet to simulate a zero strength mortar joint. These prisms are designated in Fig. 5.1 (iii), in Table A.1 (Appendix A) and in the text as **3FBP-PJ** (**3**-course high **F**ull-**B**lock **P**risms with **P**olystyrene **J**oints).

Some prisms were left unfilled. Others were cast with three different types of concrete infill: low strength (1:5:2), medium strength (1:3:2), and high strength (1:1:2) (cement: sand: aggregate) proportions.

Similarly, three different types of unfilled and filled 3-course high half-block prisms (**3HBP-MJ**, **3HBP-DPJ** and **3HBP-PJ**) were constructed to compare their compressive strength and behaviour with full-block prisms.

After construction the prisms were left for four days under polythene sheeting to allow the mortar joints to gain in strength. The prisms were then filled with concrete which was batched by volume, mixed to a high slump of 150 mm then cast in two layers. Each layer was compacted using a 25 mm poker vibrator until full compaction was attained.

The surface of the concrete infill was then trowelled level.

After casting, the prisms were left to cure under polythene sheeting for fourteen days. The polythene was then removed and the specimens left for a further fourteen days to cure under ambient conditions in the laboratory prior to testing. Steel moulded cubes and cylinders were cast and cured along with the specimens. These were tested in compression to determine the strength of the mortar and concrete infill mixes.

Demec points and electrical strain gauges were placed on the specimens at selected locations 24 hours prior to testing. The specimens were then capped with a thin layer, 1 - 2 mm, of dental plaster[55] prepared by the method explained in chapters 3 and 4.

The loading rates and patterns used for testing are similar to those adopted in chapters 3 and 4 to determine the static modulus of elasticity for all the specimens tested. In all the stress vs strain curves reported in this investigation, values obtained from the results of loading and unloading were omitted for clarity, only values from the first cycle of strain measurements are shown.

5.3 THEORETICAL PROGRAMME

The theoretical programme is divided into three major sections. The first section presents the features of the specific and parametric study analyses using a non-linear three-dimensional FEA conducted for the unfilled and filled **3FBP-MJ** prisms. The second section gives the mechanical properties of the materials used in the FEA. The third section demonstrates the finite element mesh used in the

three-dimensional analysis and the assumptions used in reducing the size of the mesh.

5.3.1 Three-Dimensional Plastic Non-Linear FEA

Specific and parametric study non-linear three-dimensional finite element analyses, were conducted using the general purpose package LUSAS[80] for unfilled and filled **3FBP-MJ** prisms. In the specific analysis, the levels of vertical stress applied to the unfilled and filled **3FBP-MJ** prisms are the average compressive strengths derived experimentally (Table 5.1). The specific analysis was conducted for unfilled **3FBP-MJ** prisms constructed with high strength (1:0.25:3) mortar and for filled **3FBP-MJ** prisms constructed using the same type of mortar but filled with medium strength (1:3:2) concrete.

In the parametric study, the level of vertical stress applied to the unfilled **3FBP-MJ** prisms is the average experimental value of the compressive strength for an unfilled prism constructed with low strength (1:1:6) mortar joints. In the case of filled **3FBP-MJ** prisms, the applied level of vertical stress is the average experimental compressive strength for prisms built with medium strength (1:0.25:3) mortar and filled with low strength (1:5:2) concrete (Table 5.1).

As for the parametric studies conducted for the two-block prisms presented in chapter 4, the parametric studies presented herein were carried out by fixing the level of vertical stress on the analysed prism and changing the materials for the three types of mortar and three mixes of concrete infill as used in the experimental investigation.

5.3.2 Material Mechanical Properties Used in the FEA

The mechanical properties and vertical stress vs strain curves for the materials used in the non-linear FEA for unfilled and filled **3FBP-MJ** prisms are similar to those used in the FEA for **2BP-MJ** prisms given in chapter 4.

5.3.3 Finite Element Model

The three-dimensional finite element computer model was developed using the solid elements used in chapter 4. The FEA model was developed by considering 1/4 of the prism (Fig. 5.2) in the analysis. In generating the mesh, (Fig. 5.3), the assumptions adopted herein are similar to those used in chapter 4 for generating the unfilled and filled **2BP-MJ** three-dimensional models.

5.4 DISCUSSION OF EXPERIMENTAL RESULTS

The discussion of the experimental results is divided into three sections. The first and second sections deal with the observed modes of failure for full and half 3-course high prisms. The third section deals with the experimental results.

5.4.1 Modes of Failure for Full-Block Prisms

The mode of failure for all the unfilled **3FBP-MJ** prisms was not affected by the type of mortar used. The common mode of failure was longitudinal splitting along the block end and side shells with crushing and shearing of the block mid-web (Fig. 5.4). Checking the mortar joints at different locations after failure indicated that the mortar

had been reduced to a powder at certain stage of the loading process.

The mode of failure, for the unfilled **3FBP-DPJ** prisms, showed a crushing type of failure at the mid height of the block middle web followed by shearing and splitting of the block shells (Fig. 5.5).

Similar to the unfilled **3FBP-MJ** prisms, the mode of failure for the filled **3FBP-MJ** prisms was not affected by the type of mortar used. However, the concrete infill has a major influence on the mode of failure of the prism.

Two modes of failure were observed for the filled **3FBP-MJ** prisms. Mode I was typical for a low to medium strength concrete infill. The failure was dominated by block shell-concrete infill separation and lateral deformation, with some signs of block shell, mortar and concrete infill crushing near a mortar joint. In some of the prisms, crushing of the concrete infill occurred after failure at the horizontal level of the mortar joints (Fig. 5.6 (i)). Some prisms showed little damage to the concrete after failure (Fig. 5.6 (ii)). This mode of failure indicates that the block shells store most of the energy applied to the prism then release it to the concrete at failure. Mode II was typical of a high strength concrete infill. The prism failed by crushing of the block shell and the concrete near one of the mortar joints simultaneously. Less sign of block shell-concrete infill separation was observed after failure (Fig. 5.7). As for unfilled prisms with mortar joints, checking the mortar joints at different locations after failure indicated that the mortar had been reduced to a powder at a certain stage of the loading process.

The mode of failure for all the filled **3FBP-DPJ** prisms

was by longitudinal splitting along the block end shells and block shell-concrete infill separation, but showed clear signs of concrete crushing after failure near one of the dental plaster joints (Fig. 5.8).

On the other hand, all the filled **3FBP-PJ** prisms showed major longitudinal splitting along the block ends, side shells and block shell-concrete infill separation at early stage of the loading process caused by horizontal expansion of the concrete (Fig. 5.9).

5.4.2 Modes of Failure for Half-Block Prisms

As for the unfilled **3FBP-MJ** prisms, the mode of failure for half-block prisms was not affected by the type of mortar used. All unfilled **3HBP-MJ** prisms displayed a longitudinal block shell splitting type of failure, with some sign of crushing near one of the mortar joints (Fig. 5.10).

The unfilled **3HBP-DPJ** prisms failed due to crushing of the block shells near one of the dental plaster joints (Fig. 5.11).

As for unfilled **3HBP-MJ** prisms, the mode of failure of the filled **3HBP-MJ** prisms did not vary as a result of using different types of mortar. However, differences were observed as a result of using different concrete strengths.

Two major modes of failure were observed for the filled **3HBP-MJ** prisms. Mode I was typical of prisms filled with low to medium strength concrete infill. The failure was dominated by longitudinal splitting and block shell-concrete infill separation. There were clear signs of crushing of the concrete infill, mortar and block shells

near to the mortar joints. Removal of the block shells after failure showed a pyramid crushing type of concrete failure at the horizontal level of one of the mortar joints (Fig. 5.12). Mode II was typical of prisms filled with high strength concrete infill. The prisms failed as one solid unit with the block and concrete infill crushed simultaneously near to one of the mortar joints. Less evidence of block shell-concrete separation was observed after failure (Fig. 5.13). For both modes of failure, checking the mortar at different locations after failure indicated that the mortar had been reduced to a powder at certain stage of the loading process.

The mode of failure for all the filled **3HBP-DPJ** prisms was by longitudinal splitting and block shell-concrete infill separation. Removal of the block shells after failure, showed a pyramid crushing type of failure of the concrete at the horizontal level of one of the dental plaster joints (Fig. 5.14). Prisms filled with high strength concrete showed better cohesion between block shell and concrete after failure than prisms filled with low to medium strength concrete.

On the other hand, all the filled **3HBP-PJ** prisms showed major longitudinal splitting of the block shells together with block shell-concrete infill separation during early stages of the loading process. This occurred mostly at mid height and resulted from horizontal expansion of the concrete followed by a pyramid type of crushing of the concrete at the horizontal level of one of the polystyrene joints (Fig. 5.15).

5.4.3 Experimental Results

Tables 5.1 and 5.2 summarize the experimental results

for the full and half, 3-course high prisms respectively. The associated material properties are also given.

Typical stress vs strain curves for the unfilled **3FBP-MJ** prisms (Fig. 5.16) show almost identical vertical stress vs strain curves for the mortar as for the block. The curves also show a tensile horizontal strain at the end and side shells of the middle block.

Similarly, typical stress vs strain curves for the unfilled **3HBP-MJ** prisms (Fig. 5.17) show similar vertical stress vs strain curves for the mortar and the block. The curves also show a tensile horizontal strain in the mortar and the block.

The effect of the mortar compressive strength on the strength of unfilled, full and half-block prisms with mortar joints is shown in Fig. 5.18. The presence of a mortar joint of strength 9.19 N/mm^2 in unfilled, full-block prism and 15.39 N/mm^2 in unfilled half-block prism produces a reduction in prisms strength of 10.2% and 5.9% respectively compared to the strength of the unfilled prism with dental plaster joints (**3FBP-DPJ**). This was caused by tensile stresses exerted on the stiff blocks by the soft mortar joints as a result of the high Poisson's ratio of the mortar material[71,72,75,76,77,78,79]. The results showed also that increasing the mortar strength for the unfilled full and half-block prisms by 188.8% and 72.5% resulted in increasing the prisms strength by 20.1% and 23.7% respectively. Fig. 5.18 also shows that the curve for the full-block prisms was a concave upwards parabola, whereas the curve for the half-block prisms was a concave downwards parabola. The difference in the shape of the strength curves resulted from the difference in the values of aspect ratio, as between the full-block prism, ($l/t = 2.05$), and half-block prism, ($l/t = 1.0$), (the effect of the aspect

ratio (l/t) will be discussed in more detail in chapter 6). Another reason was the difference in the mortar bedded area, caused by the presence of the mid-web, between the full and half-block prisms, and its effect on the prism strength and mode of failure. For the above reasons, the unfilled full-block prisms failed at a reduction factor of 0.80 compared to the unfilled half-block prisms.

Testing unfilled half-block prisms instead of full-block prisms, for the sake of ease of handling[28,29], to determine the ultimate compressive strength for unfilled blockwork masonry, f'_m, does not seem to be good practice[85]. Higher strengths are obtained by testing half-block prisms instead of full-block ones, thus producing an overestimate of the actual value of f'_m.

The stress vs strain curves for the filled **3FBP-MJ** prisms, (Fig. 5.19), show a reduction in the prism stiffness compared to unfilled ones. This reduction is mainly due to the presence of the concrete infill which applies some tensile stress resulting from the high value of Poisson's ratio for the concrete[27,28,29,30,31,32,33,38]. These high tensile stresses produce failure of the prism prior to attaining the apparent material strength of the block, f_b. Mortar joints, on the other hand, gave more plasticity than in the case of unfilled prisms.

The stress vs strain curves for the filled **3HBP-MJ** prisms, (Fig. 5.20), show a similar behaviour pattern to the filled **3FBP-MJ** prisms except for the presence of high tensile splitting strain at the block shell near to ultimate stress.

Fig. 5.21 shows the effect of concrete compressive strength on the strength of filled, full and half 3-course high prisms with similar mortar strengths. Filling the full

and half-block prisms with concrete has a large influence on their compressive strength[27,28,29,32,33,35,36,71]. Both types of prism show a significant decrease in strength (based on gross area) compared to that of unfilled prisms (based on net area).

The strength of the half-block prisms increased uniformly with increase in strength of the concrete. At a concrete strength of approximately 45 N/mm^2 (this strength is 85.3% higher than the cube compressive strength of the block material) the strength of a filled half-block prism approached the strength of an unfilled half-block prism.

The filled full-block prisms, on the other hand, showed virtually no change in strength for a wide range of concrete strengths (0 - 30 N/mm^2) (prisms with zero concrete strength are the unfilled prisms). At a concrete strength of approximately 35 N/mm^2 (this strength is 44.1% higher than the cube compressive strength of the block material) the strength of a filled, full-block prism was approximately equal to the strength of a similar unfilled prism. The gain in strength is due to a similarity in the deformational characteristics, also the value of Poisson's ratio of the concrete (μ_c = 0.22 at an axial strain of 0.002) compared to that of the block (μ_b = 0.20 at an axial strain of 0.0015). For the range of concrete strengths used, the contribution of the concrete to the strength of the filled prism was small[28,29,35,36,71,85].

Fig. 5.22 shows the effect of the compressive strength of mortar on the strength of filled **3FBP-MJ** prisms with similar concrete infill strength. The presence of a mortar joints, of strength 13.52 N/mm^2 in a filled, full-block prism with high strength (1:1:2) concrete infill produces an increase in prism strength of 88.9%, compared to prisms with polystyrene joints. On the other hand, changing the

mortar strength from 13.52 to 26.80 N/mm^2 (an increase of 98.2%) produces an increase of only 7.6% in the prism strength[1,26,28,33,36,71].

The same result was obtained for prisms filled with low strength (1:5:2) concrete (average, 10.09 N/mm^2). The presence of a mortar joints, of strength 15.39 N/mm^2, produced an increase in prism strength of 262.1% compared to prisms with polystyrene joints. On the other hand, changing the mortar strength from 15.39 to 26.44 N/mm^2 (an average increase of 71.8%) produced an increase in prism strength of 0.7%.

The overall conclusion based on these results, was that the presence of mortar joints, even though of low strength (1:1:6), contributed greatly to the strength of the filled prisms. Increasing the mortar strength above this value increased the prism strength by a negligible amount.

The first explanation for this phenomenon is that the presence of the mortar in the joints, even though of low strength, transfers the vertical stresses to the adjacent stiff blocks. The second explanation is the influence of the horizontal confinement stresses exerted on the mortar joint by the stiff concrete blocks which increases the apparent mortar strength[1,28,29,32,33,34,35,36,38,71]. These confinement stresses increase proportionally as the mortar strength decreases, due to the high Poisson's ratio of the mortar[71,72,75,76,77,78,79]. The third explanation is the relatively small thickness of the mortar joint to block height[26,28,33,36,71]. For all the above reasons, the contribution of the presence of the mortar joints to the prism strength will be a function of the block and mortar strengths.

By considering the equilibrium of the deformation and stresses at the mortar joint in a filled blockwork masonry prism (Fig. 5.23 (i)), the inward lateral deformation of the mortar will be offset by the concrete infill which will have lateral outward deformation. This effect forces the mortar to deform outward (Fig. 5.23 (ia)) (as also shown by the bold arrows in Fig. 5.23 (ib)). This restriction on the mortar joint movement will increase their confinement and consequently their strength. Fig. 5.23 (ia) shows that the concrete blocks in a filled prism are not subjected to splitting tensile stresses caused by the mortar, in the X-direction (the block is actually under tensile splitting stresses in a Y-direction). But the tensile stresses in the outward direction add to the tensile stresses exerted on the block by the concrete infill. On the other hand, the block in unfilled prism (Fig. 5.23 (iia, b)) is under tensile splitting stresses in the X- and Y-directions, exerted by the mortar joints.

This explains why the strength of the mortar joints does not play an important role in the strength of a filled blockwork masonry prism. Finally, due to the small ratio of mortar thickness to block height (1/18.9), the influence of mortar joints on the strength of a filled prism is insignificant[1,26,28,33,36,71].

The aspect ratio, (l/t), and difference in mortar bedded area were again the main reasons for the decrease in strength of the filled full-block prisms, by an average factor of 0.80 compared to the filled half-block prisms. Also, testing filled half-block prisms to obtain the strength of a filled full-block prism, is not recommended.

Fig. 5.24 shows the relationship between the strength of filled, full and half, 3-course high prisms with dental plaster joints and the concrete infill strength. The figure

shows that the presence of concrete had the same effect of reducing the prism strength compared to that of the unfilled prism. Filled **3FBP-DPJ** prisms show a steady increase in strength with concrete strength. This relationship differs from that for filled, **3FBP-MJ** prisms. On average, the gain in strength of the **3FBP-DPJ** prisms was 24% compared to that for filled **3FBP-MJ** prisms (this percentage is calculated without including prisms with low strength concrete as these results exhibit large deviations compared to the other two). The reason for the difference in strength is the presence of the mortar joints as planes of high plasticity. This reduces the contribution of the block units to the strength of the prism. Instead, the mortar behaves as a plane of weakness due to its high Poisson's ratio.

The strength of **3FBP-DPJ** prisms was on average 21.6% higher than the companion **3HBP-DPJ** prisms due to the greater contribution of the block units to the strength of the prisms.

To study the effect of the presence of the mortar joints in filled full and half-block prisms farther, a comparison between Figs 5.21 and 5.24 shows that the half-block prism compressive strength increased by 28.8% due to the presence of high strength mortar joints (26.54 N/mm^2). On the other hand, the presence of the mortar joints in filled, full-block prisms caused irregular reductions depending on the concrete infill strength.

Fig. 5.25 relates the strength of filled, full and half-block prisms with polystyrene joints to concrete strength. Two relations are shown in Fig. 5.25. The first relation was based on a concrete infill net area (A_c = 19272 mm^2 for full-block prisms and A_c = 9636 mm^2 for half-block prisms). The second relation was based on a prism gross

area (A_g = 74100 mm^2 for full-block prisms and A_g = 36100 mm^2 for half-block prisms).

Based on the prism gross area, Fig. 5.25 shows that the absence of the mortar joint caused an average reduction of 54.4% and 64.2% in the strength of full and half-block prisms respectively (the result for the full-block prisms with low strength concrete infill was not considered due to large deviations between this result and the other two). This reduction was expected since there was no medium to transfer the stresses through the blocks. It can also be seen that for the wide range of concrete infill strengths (8.57 - 35.22 N/mm^2) the increase in full and half-block prisms strengths of 179.1% and 123.3% respectively is less than the 297% and 173.7% increase in the strength of the concrete infill.

Based on the net area of the concrete infill for half-block prisms, Fig. 5.25 shows that the strength of concrete infill increased by 44.6%, 28.2% and 18.1% corresponding to concrete cube strengths of 12.87, 20.15 and 35.22 N/mm^2 respectively. This resulted from the confinement of the concrete by the block units. The same trend was also observed in full-block prisms. The difference in the percentage increases in concrete strength suggests that the concrete block provides more confinement to the soft concrete infill than to the stiff concrete infill. Also, soft concrete deforms more laterally than stiff concrete, due its high Poisson's ratio.

The formula for the broken line passing through the results of both full and half-block prisms with polystyrene joints (Fig. 5.25), based on the prism gross area, is as follows:

$$f'_m = 1.3 + 0.25\ f_c \qquad \ldots(5.1)$$

The gradient of this line is 0.25, which represents the contribution of the concrete infill to the strength of the **3FBP-PJ** prism; also the contribution of the concrete to the strength of any filled prism of differing mortar joint strength.

The constant value of 1.3 N/mm^2, which is the intersection of the broken line with the Y-axis, indicates that the unfilled blockwork masonry prism had some strength even when the mortar joint strength was almost zero. This constant is a function of the block material strength and can be determined for different block types and strengths by testing prisms with very soft joint material such as the ones used in this investigation (10 mm thick polystyrene).

Using this constant value and the results for unfilled, full and half-block prisms together with the block strength and their corresponding mortar strengths, the contribution of the presence of the mortar joint to the prism strength can be determined. Since as shown earlier the presence of the mortar joints in the prism, even though of low strength, works as a media to transfer the applied vertical stress to the adjacent stiff concrete blocks. Also it was shown that changing the mortar strength had little effect on the prisms' compressive strength. Therefore, the contribution of the presence of the mortar joints to the prism strength will be a function of the block and mortar strengths. This contribution was found to be equal to $0.30\ f_b + 0.10\ f_{mr}$ for full-block prism and $0.30\ f_b + 0.20\ f_{mr}$ for half-block prism.

Thus, to determine the compressive strength of a unfilled or filled blockwork masonry prism, f'_m, based on prism gross area, the following formulae were suggested:

Full 3-course high prism (3FBP-MJ)

$$f'_m = 0.30\ f_b + 0.10\ f_{mr} + 0.25\ f_c + 1.3 \qquad ...(5.2)$$

Half 3-course high prism (3HBP-MJ)

$$f'_m = 0.30\ f_b + 0.20\ f_{mr} + 0.25\ f_c + 1.3 \qquad ...(5.3)$$

The above formulae have been derived for one type of concrete block. A better understanding of the complex behaviour of blockwork masonry prisms will be achieved if more prism tests are carried out using different block types and strengths to justify the above formulae. Meanwhile, the small constant value of 1.3 N/mm^2, which is a function of the block material strength, can be ignored in the above formulae until further tests are completed.

Therefore, to determine the ultimate compressive strength of a blockwork masonry prism, f'_m, based on prism gross area, the above formulae reduced to the following:

Full 3-course high prism (3FBP-MJ)

$$f'_m = 0.30\ f_b + 0.10\ f_{mr} + 0.25\ f_c \qquad ...(5.4)$$

Half 3-course high prism (3HBP-MJ)

$$f'_m = 0.30\ f_b + 0.20\ f_{mr} + 0.25\ f_c \qquad ...(5.5)$$

A comparison between the predicted, using Eqns 5.4 and 5.5, and the experimental values of f'_m, based on prism gross area, is given in Table 5.3. Fig. 5.26 shows the above two formulae plotted against the results of filled full and half-block prisms with almost similar mortar strength.

The interesting feature of the above formulae is the indication of the extent of the contribution of the concrete material[28,29,36,71,85] to the strength of filled prisms.

5.5 DISCUSSION OF THEORETICAL RESULTS

The discussion is divided into three major sections. The first section is a general discussion of common features in the results of the specific and parametric study analyses. The second section discusses the results of the specific and parametric study analyses conducted for the unfilled **3FBP-MJ** prisms. The third section addresses the results of the specific and parametric study analyses carried out for filled **3FBP-MJ** prisms.

5.5.1 General

In general, it was found that an understanding of the prism's deformation in the Y-, X- and Z-directions is important in obtaining a clear picture of how the stresses are distributed throughout the prisms.

The contour plots of the direct horizontal stresses in the X- and Z-directions show confinement stresses located near the steel platens of the machine. These stresses have a limited effect on the rest of the prism and mainly result from differences in the material properties of the blocks and the stiff steel platens. These in turn produced confinement stresses on the blocks[55,81,82,83,84]. This suggests that the unfilled and filled 3-course high blockwork masonry prisms can be used as standard test specimens to determine f'_m in situations where in-plane horizontal forces are not expected.

5.5.2 Plastic Non-Linear FEA for Unfilled 3FBP-MJ Prism

5.5.2.1 Analysis of prism with specific level of vertical stress

The specific level of stress applied to the unfilled **3FBP-MJ** prisms in this non-linear analysis was 12.01 N/mm^2, which is the average experimental value of compressive strength for unfilled prisms built with high strength (1:0.25:3) mortar (Table 5.1).

Prism Deformation

The contour plot of the prism deformation in the Y-direction (Fig. 5.27) shows that the prism top surface shortens with a maximum cumulative vertical deformation of 0.71 mm with respect to the prism bottom surface. The contour plot of the prism horizontal deformation in the X-direction (Fig. 5.28) shows a greater tendency for the prism end shells to deform outward, with a maximum deformation of 0.077 mm at the prism mid height. On the other hand, the contour plot of the prism horizontal deformation in the Z-direction (Fig. 5.29) shows an extraordinary mode of deformation compared to the deformation in the X-direction. The figure shows that the maximum outward deformation of 0.045 mm of the prism side shells is located mainly near the mortar joints. This type of deformation results from the high plasticity of the mortar joints and the prism aspect ratio (l/t = 2.05) (prism length-to-thickness).

Due to the incompatibility of deformations caused by differences in the values of a horizontal deformation of 0.032 mm between the X- and Z-directions, the prism end shells will be separated from the rest of the prism and

longitudinal cracks will be developed at the line of contact between the end and side prism shells.

Stresses in the Block Material

The contour plots of the direct stresses in the Y-, X- and Z-directions in the block material are shown in Figs 5.30, 5.31, and 5.32 respectively. The contour plots of the major and two minor principal stresses are given in Figs C.1, C.2 and C.3 (Appendix C) respectively.

The contour plot of the direct vertical stress in the Y-direction shows that the block at prism mid height is under a constant compressive stress, ranging from 19.65 to 22.11 N/mm^2. The maximum vertical stress of 27.73 N/mm^2 is located at bottom corner of the prism near the steel platen.

The contour plots of the direct horizontal stresses in the X- and Z-directions show that the maximum tensile stress of 2.50 N/mm^2 in the X-direction and 2.13 N/mm^2 in the Z-direction are located at the vicinity of the mortar joints. These stresses tend to reduce to zero at a distance of 1/3 the block height from the mortar joints. The tensile stresses in both horizontal directions converted to confinement stresses near the top and bottom steel platens.

In considering the equilibrium of the horizontal stresses at any cross-section of the middle block of the unfilled **3FBP-MJ** prism, the assumption that the tensile stresses is uniformly distributed[32,33,38] is not justifiable. The middle 1/3 of the block height is under zero stress and the stress distribution can be assumed to be triangular with maximum stress at the mortar joints and zero at a distance of 1/3 block height from the mortar joints.

The tensile horizontal stresses are the result of differences in the material mechanical properties between the fine sand mortar joints and the coarse aggregate concrete blocks.

The contour plots of the minor principal stresses (Appendix C) show higher tensile stresses of 1.60 N/mm^2 (MST1), on the prism side shells (Fig. C.2) and 2.87 N/mm^2 (MST2), on the prism end shells (Fig. C.3). The maximum value of tensile stress on the prism end shells is higher than the experimental ultimate tensile strength for hollow unit block (2.16 N/mm^2) (see Table 3.9). This suggests that the unfilled prism has more tendency to split along the end shells than through the side shells[1,26].

Fig. 5.33 shows the contour plot of the maximum shear stress in the block material. The figure shows that the maximum shear stress of 10.96 N/mm^2 is located in the block mid-web, at the bottom side of the prism. This value is quite high compared to that suggested by the ACI code for concrete given by Eqn. 4.4. The distribution of the maximum shear stress suggests that the initiation of shear failure is likely to occur at the bottom side of the prism, with shearing of the prism side shells to the outside and vertical splitting of the prism end shells.

Due to the high tensile principal stresses on the prism end shells and the manner of distribution of the shear stresses, the unfilled prism has more tendency to split along the end shells than through the side shells. This tendency for splitting along the prism end shells was observed in the modes of failure of the unfilled **3FBP-MJ** prisms during the experimental part of this investigation and was attributed to the prism aspect ratio (l/t = 2.05).

Stresses in the Mortar Material

The contour plots of the direct stresses in the Y-, X- and Z-directions in the mortar joints are shown in Figs 5.34, 5.35, and 5.36 respectively. The contour plots of the major and two minor principal stresses are given in Figs C.4, C.5 and C.6 (Appendix C) respectively.

The contour plot of the direct vertical stress in the Y-direction shows that the higher vertical stress is located at the inner faces of the mortar joints, with a maximum value of 22.40 N/mm^2. This value tends to decrease towards the outer corners of the mortar joints. The distribution of vertical stresses at the mortar joints suggests that the applied vertical stress is higher at the inner faces of the prism hollow cores than at the outer faces. This results from the way the prism deformed in the horizontal direction.

A clear similarity was observed between the contour plots of the direct horizontal stresses in the X- and Z-directions. Both horizontal stresses show that the mortar joints are under confinement stresses in the X- and Z-directions with maximum values of 6.84 N/mm^2 in the X-direction and 6.63 N/mm^2 in the Z-direction. These maximum stresses are located at the inner faces of the mortar joints and tend to reduce towards the outer corners of the mortar joints.

Fig. 5.37 shows the contour plot of the maximum shear stress at the mortar joints. The figure shows an almost uniform distribution of shear stresses at the mortar joints.

5.5.2.2 Parametric study analysis

The level of vertical stress applied to the unfilled **3FBP-MJ** prisms for the parametric study was 10.00 N/mm^2, which is the average experimental value of compressive strength for prisms built with low strength (1:1:6) mortar.

To examine the effect of changing the mortar type on the prism deformations and stresses, a parametric study was carried out by fixing the applied level of vertical stress and changing the types of mortar joints, for the unfilled **3FBP-MJ** prisms, to low (1:1:6), medium (1:0.5:4.5) and high (1:0.25:3) strength.

The effect of changing the mortar strength on prism deformation is clearly shown by the contour plots for the horizontal deformation in the X-direction (Figs 5.38, 5.39 and 5.40) and in the Z-direction (Figs 5.41, 5.42 and 5.43) for prisms built with low, medium and high strength mortar joints respectively. The figures show that the horizontal deformations in prisms built with low strength mortar joints are mainly located at the joints as a local inward and outward squeezing of the joints. On the other hand, prisms built with medium to high strength mortar joints show that the deformation exists over most of the prism side and end shells.

Tables 5.4 and 5.5 give the maximum values of deformations and stresses respectively for the unfilled **3FBP-MJ** prisms, as derived from the parametric study analysis. Table 5.4 gives the maximum values of deformation in the Y-, X- and Z-directions; the level of vertical stress applied during the parametric study analysis; the average experimental compressive strength of the prisms and the cube compressive strength of the different types of mortar. Table 5.5, on the other hand, gives the maximum

values of direct, shear and principal stresses in each individual material.

As in the analysis of the unfilled **2BP-MJ** prism, and to assess the effect of changing the mortar strength on the maximum values of deformations and stresses in the prisms, the results of the parametric study are plotted in an X-Y plot.

The effect of increasing the cube compressive strength of the mortar on the prism maximum values of deformation is shown in Fig. 5.44. This figure shows that the prism maximum value of vertical deformation increases by 23.3% as a result of changing the mortar strength from 9.19 to 26.54 N/mm^2. The explanation of this phenomenon is that in prisms with low strength mortar joints, most of the vertical deformation is in the soft mortar joints, whereas in prisms with high strength mortar joints both the joints and the blocks contribute more equally to the vertical deformation. So the overall cumulative vertical deformation of prisms with high strength mortar joints is more than prisms with low strength mortar joints.

The results also show that the maximum value of vertical deformation of prism built with medium strength (1:0.5:4.5) mortar is almost similar to that for prism built with high strength mortar.

On the contrary, for the same range of mortar strengths, the prism outward horizontal deformation decreases by 32.5% in the X-direction and by 55.2% in the Z-direction, as the mortar strength increases. Table 5.4 also reveals that prisms with low and medium strength mortar joints tend to deform respectively inward and outward in the -ve and +ve X- and Z-directions at the mortar joints, whereas prisms with high strength mortar

joints tend to deform outward only. This will have an effect on the prism strength.

Although the values of stress differ, the stress distributions for all the prisms analysed in this parametric study are similar to the contour plots of stresses for prisms analysed using the specific analysis. Information on how these stresses are distributed is given in the relevant contour plots of stresses from the specific analysis.

Figs 5.45, 5.46 and 5.47 show the effect of changing the cube compressive strength of the mortar on the maximum values of the direct stresses in the Y-, X- and Z-directions respectively. Fig. 5.45 shows that the maximum values of vertical stress at the block material and mortar joints increases by 33.5% and 6.3% respectively, as a result of changing the mortar strength from 9.19 to 26.54 N/mm^2. Prisms built with medium strength (1:0.5:4.5) mortar joints show a similar increase in the vertical stresses to prisms built with high strength (1:0.25:3) mortar joints. This supports the conclusion, derived previously, that the presence of mortar joints, even though of low strength, is enough to develop the block strength. Further increase in the mortar joint strength has no great influence on the unfilled **3FBP-MJ** prism strength. This was mainly due to the insignificant ratio of the mortar joint thickness to the block height (1/18.9), and also due to confinement of the mortar by the stiff blocks[1,26,28,33,36,71].

Fig. 5.46 shows that the maximum values of confinement stress in the X-direction in the mortar joints decreases by 63.8% as a result of changing the mortar strength from 9.19 to 26.54 N/mm^2. For the same range of mortar strength, the maximum values of tensile stress in the block material decreases by 29.4%.

Similarly, the maximum values of confinement stress in the Z-direction in the mortar joints (Fig. 5.47), decreases by 64.5% and the maximum values of tensile stress in the block material decreases by 32.4% as the mortar strength increases.

The decrease in the maximum values of horizontal stresses as the mortar compressive strength increases is expected since increasing the mortar compressive strength decreases the outward deformation of the mortar joints, as a result of the increase in the mortar Poisson's ratio.

The results also show small differences between the maximum values of direct horizontal tensile stresses in the X- and Z-directions for all types of prism analysed. But the results of the maximum values of the minor principal stresses show that the tensile stresses on the prism end shells (MST2) are 53.3%, 17.6% and 75.9% higher than those on the prism side shells (MST1).

The differences in the tensile stresses between the prism end and side shells are the result of the prism aspect ratio (l/t = 2.05), whereby the prism has more tendency to split on the end shells than the side shells. This result supports the observed mode of failure for unfilled prisms during the experimental part of this investigation.

Fig. 5.48 shows the relationship between the maximum values of shear stress in the block and the mortar materials as affected by a change in the mortar strength. The figure shows that the shear stresses in the block material and the mortar joints increase by 18.7% and 69.9% respectively as a result of changing the mortar strength from 9.19 to 26.54 N/mm^2. This can be explained by a rise in the vertical stresses in both materials as the mortar

compressive strength increases.

To sum up the effect of increasing the mortar compressive strength from 9.19 to 26.54 N/mm^2 on the strength of unfilled prisms. It seems that the effect is not so great, since increasing the mortar strength resulted in decreasing the tensile stresses and increasing the compressive stresses. So prisms built with low strength (1:1:6) mortar show higher tensile stresses rather than compressive stresses, while prisms built with high strength (1:0.25:3) mortar show the opposite.

Due to the complex nature of the deformations and stress distributions in unfilled prisms, the general conclusion derived from the results of the specific analysis and the parametric study analysis is that the failure of unfilled **3FBP-MJ** prisms is dominated by incompatible deformation, localized crushing, splitting and shear failures. It is expected that the unfilled prisms will fail due to a combination of compression, tension and shear stresses in an abrupt mode of failure.

The predicted mode of failure for an unfilled prism with low strength (1:1:6) mortar joints is first, by localized crushing at one of the mortar joints, followed by the combination of block crushing, splitting and shearing. As the mortar strength increases, the possibility of localized crushing increases at either the mortar joints or at the blocks, followed by complete disintegration of the prism in an abrupt mode of failure.

For all types of unfilled prisms discussed in this study, there is a high possibility of an abrupt and unstable mode of failure occurring when the prism approaches its ultimate load. The prism tends to split vertically along the prism shells and at the line of

intersection of the end and side prism shells, due to the high tensile stresses in the block material near the mortar joints, and due to deformation incompatibility. From the stress values and distribution of stress, the strength of unfilled **3FBP-MJ** prisms will depend on the block unit compressive strength and the mortar type.

5.5.3 Plastic Non-Linear FEA for Filled 3FBP-MJ Prism

5.5.3.1 Analysis of prism with specific level of vertical stress

The specific level of vertical stress applied to the filled **3FBP-MJ** prism in this non-linear analysis was 14.53 N/mm^2, which is the average experimental value of compressive strength for prisms built with high strength (1:0.25:3) mortar and filled with medium strength (1:3:2) concrete (Table 5.1).

Prism Deformation

The contour plot of the prism deformation in the Y-direction (Fig. 5.49) shows that the prism top surface shortens vertically with a maximum deformation of 0.50 mm with reference to the prism bottom surface. The contour plot of prism horizontal deformation in the X-direction (Fig. 5.50), shows that the prism end shells tend to deform outward with a maximum deformation of 0.048 mm at the prism mid height. The contour plot of the prism horizontal deformation in the Z-direction (Fig. 5.51), shows that the prism side shells tend to deform outward in a similar manner to the end shells in the X-direction, but the maximum value at mid height is almost half (0.025 mm) the value in the X-direction. The reason for the difference in

the horizontal deformation is attributed to the prism aspect ratio (l/t = 2.05).

Due to the incompatibility of deformation, caused by a difference in the values of horizontal deformation between the X- and Z-directions of 0.023 mm, the end shells will be separated from the rest of the prism and longitudinal cracks will be developed at the line of contact between the end and side prism shells.

The figure also shows that the deformation of the filled prism in the Z-direction is completely different from the deformation of an unfilled prism with the same mortar type. The reason for this is the presence of the concrete infill and its high Poisson's ratio, which caused the infill to push the prism side shells outward at failure.

The values of deformation for the filled **3FBP-MJ** prism in the Y-, X- and Z-directions are 29.6%, 37.7% and 44.4% less than those for the unfilled **3FBP-MJ** prism. This suggests that filled prisms are stiffer than unfilled **3FBP-MJ** prisms due to the presence of the concrete infill.

Stresses in the Block Material

The contour plots of the direct stresses in the Y-, X- and Z-directions in the block material is shown in Figs 5.52, 5.53, and 5.54 respectively. The contour plots of the major and two minor principal stresses are given in Figs C.7, C.8 and C.9 (Appendix C) respectively.

The contour plot of the direct vertical stress in the Y-direction shows that a maximum vertical stress of 22.18 N/mm^2 is located at the bottom corner of the prism, near to

the machine platen. The rest of the block shells are under a uniform stress ranging from 14.60 to 16.43 N/mm^2.

The contour plots of the direct horizontal stresses in the X- and Z-directions show that the prism shells are subjected to confinement stresses near the steel platens with a maximum value of 7.62 N/mm^2 in the Z-direction. The rest of the prism shells are under uniform tensile stresses with a maximum value of 1.51 N/mm^2 in the X-direction and 1.46 N/mm^2 in the Z-direction. No large localized tensile stresses were observed near to the mortar joints, as was the case with the unfilled prisms. This supports the conclusion, derived previously, that in filled **3FBP-MJ** prisms, the concrete infill offsets the inward lateral deformation of the mortar joints and forces them to deform outward. The tensile stresses thus developed were directed outward onto the block shells and had no influence on their strength (see Fig. 5.23).

The main explanation for the existence of horizontal tensile stresses in the prism shells is the tendency for the concrete infill to deform outward as a result of its high Poisson's ratio. This observation was also reached during the experimental part of the investigation.

In considering the equilibrium of the horizontal stresses at any cross-section in the middle block of the filled **3FBP-MJ** prisms, the assumption that the horizontal tensile stresses are uniformly distributed[32,33,38] over the full height of the middle block is justified.

The contour plots of the minor principal stresses (Appendix C) show higher tensile stresses of 1.23 N/mm^2 (MST1), on the prism side shells (Fig. C.8) and 1.68 N/mm^2 (MST2), on the prism end shells (Fig. C.9). These values of maximum tensile stress are less than the ultimate tensile

strength of a unit block filled with (1:3:2) concrete (1.77 N/mm^2) (see Table 3.9). This suggests that the filled prism has less tendency to split due to high tensile stresses.

Fig. 5.55 shows the contour plot of the maximum shear stress in the block material. As for the unfilled **3FBP-MJ** prism, the maximum value of shear stress is quite high compared to the value suggested by the ACI code for concrete, as given by Eqn. 4.4. The figure shows that the distribution of shear stresses is irregular with most of the prism side shells subjected to high shear stresses. This irregularity is caused by the presence of the concrete which influences the behaviour of the prism at failure. This is supported even more by the location of the maximum value of shear stress (9.34 N/mm^2) at the prism mid height. The distribution of the maximum shear stress suggests that the initiation of shear failure will occur at the prism mid height, with shearing of the prism side shells to the outside and vertical splitting of the prism end shells. This will also be accompanied by shearing on the faces of the prism side shells.

Due to the higher tensile principal stresses acting on the prism end shells and also to the way the shear stresses are distributed, the filled prism has a greater tendency to split along the end shells than along the side shells[1,26]. This tendency to split along the prism end shells was observed in the modes of failure for filled **3FBP-MJ** prisms during the experimental part of the investigation and was attributed to the prism aspect ratio (l/t = 2.05).

Stresses in the Concrete Material

The contour plots of the direct stresses in the Y-, X- and Z-directions in the concrete infill are shown in Figs

5.56, 5.57, and 5.58 respectively. The contour plots of the major and two minor principal stresses are given in Figs C.10, C.11 and C.12 (Appendix C) respectively.

The contour plot of the direct vertical stress in the Y-direction shows that most of the higher values of the vertical stress are located in small areas at the levels of the mortar joints, with a maximum value of 31.55 N/mm^2. This maximum value suggests that the concrete in these areas has already failed in compression. The rest of the concrete column is under a small level of vertical stress, ranging from 9.45 to 11.05 N/mm^2. The explanation for the high vertical stresses at the levels of the mortar joints is the high plasticity of the mortar.

The contour plots of the direct horizontal stresses in the X- and Z-directions is affected by the high localized vertical stresses at the levels of the mortar joints. Both horizontal stresses showed high confinement stresses at the levels of the mortar joints with almost similar maximum values in the X-direction (11.96 N/mm^2) and in the Z-directions (11.50 N/mm^2). These stresses tend to decrease away from the levels of the mortar joints, changing to tensile stresses, with a maximum value of 0.96 N/mm^2 in the X-direction, at mid height levels of the three blocks.

The confinement stresses are exerted on the concrete by the blocks in two ways. First, due to the tendency of concrete to deform outward as a result of its high Poisson's ratio. Second, as a result of failure of the concrete at the levels of the mortar joints, due to the high vertical and shear stresses at these locations.

The contour plot of the maximum shear stress, Fig. 5.59, shows that the highest value of shear stress, 10.09 N/mm^2, is located at the levels of the mortar joints. This

stress tends to reduce away from the these locations.

The distribution of vertical, horizontal, shear and principal stresses in the concrete infill suggests a new hypothesis for the failure of filled prisms. The hypothesis is presented as follows:

Since all prism materials are under the same level of applied vertical stress, the vertical shortening of the stiff blocks and the concrete is less than the soft mortar joints. This means that most of the vertical shortening is in the mortar joints and consequently the concrete, at the levels of the mortar joints, tries to match this shortening. Internally high, localized vertical and shear stresses will develop at the concrete in these areas and failure of the concrete by compression and shear will be imminent. This will force the concrete to deform outward, confined by the block shells near the mortar joints. This means that the initiation of block shell-concrete infill separation and deformation will occur first at the levels of the mortar joints. Added to the high Poisson's ratio of the concrete this will cause the failure of filled prisms even before developing the apparent compressive strength of block material, f_b.

Stresses in the Mortar Material

The contour plots of the direct stresses in the Y-, X- and Z-directions in the mortar joints are shown in Figs 5.60, 5.61, and 5.62 respectively. The contour plots of the major and two minor principal stresses are given in Figs C.13, C.14 and C.15 (Appendix C) respectively.

The contour plot of the direct vertical stress in the Y-direction shows that the maximum value of 16.94 N/mm^2 is

located at the outer faces of the mortar joints. This value tends to decrease towards the inner faces of the mortar joints, reaching a value of 6.85 N/mm^2.

The distribution of vertical stresses in the mortar joints, in the filled **3FBP-MJ** prism is completely different from that in the unfilled **3FBP-MJ** prism. In the filled prism, the vertical stresses are higher in the outer faces of the mortar joints than in the inner faces, whereas in the unfilled prisms the opposite is true. This is also the case with the value of maximum vertical stress, which in the filled, is 24.4% lower than for the unfilled prism. These differences can be explained by the presence of the stiff concrete, which affects the distribution of the vertical stresses by carrying some of the applied vertical stress from the block shells and the mortar joints.

The contour plots of the direct horizontal stresses in the X- and Z-directions show higher confinement stresses at the outer faces of the mortar joints in areas of high vertical stress. A maximum confinement stress value of 4.52 N/mm^2 is reported in the Z-direction. Greater uniformity in the distribution of the confinement stresses is observed in the unfilled prisms compared to the filled prisms.

Fig. 5.63 shows the contour plot of the maximum shear stress at the mortar joints. The figure shows that the maximum shear stress of 6.43 N/mm^2 is located at the outer face of the mortar joints in areas of higher vertical stress.

5.5.3.2 Parametric study analysis

The level of vertical stress applied to the filled **3FBP-MJ** prism in the parametric study was 13.85 N/mm^2, which

is the average experimental value of compressive strength for prisms built with high strength (1:0.25:3) mortar and filled with low strength (1:5:2) concrete. This level of vertical stress was kept constant on the prism, while the concrete infill varied from low (1:5:2) to medium (1:3:2) and high (1:1:2) strength to study the effect of changing the concrete strength on the maximum values of deformation and stress in the prism.

The effect of increasing the concrete strength on the prism deformations is shown by the contour plots for the horizontal deformations in the X-direction (Figs 5.64, 5.65, 5.66) and in the Z-direction (Figs 5.67, 5.68, 5.69), for prism filled with low (1:5:2), medium (1:3:2) and high (1:1:2) strength concrete respectively. The figures show no great difference in the distribution of the horizontal deformations for the different type of concrete mixes used in the analysis. All the prisms deformed as if the prisms were made of one type of material.

Tables 5.6 and 5.7 give the results of the maximum values of deformations and stresses respectively for the filled **3FBP-MJ** prisms, as derived from the parametric study analysis. Table 5.6 provides the maximum values of deformation in the Y-, X- and Z-directions; the level of vertical stress applied during the parametric study analysis; the average experimental compressive strength of the prisms and the cube compressive strength of the different concrete infill mixes. Table 5.7, on the other hand, gives the maximum values of direct, shear and principal stresses in each individual material.

The effect of increasing the cube compressive strength of the concrete on the prism maximum values of deformation is shown in Fig. 5.70. The figure shows that the vertical deformation of the prism decreases by 40.4% as a result of

changing the concrete strength from 9.98 to 34.02 N/mm^2. Similarly, the prism outward horizontal deformation decreased by 63.5% and 63.2% in the X- and Z-directions respectively, as the concrete strength increased. Decreases in the maximum values of vertical and horizontal deformations as the concrete strength increases can be explained by the increase in prism stiffness caused by using a stronger concrete.

Although the values of stress differ, the stress distributions for all the prisms analysed in this parametric study are similar to the contour plots of stresses for prisms analysed using the specific analysis. Information on how these stresses are distributed is given in the relevant contour plots of stresses from the specific analysis.

Figs 5.71, 5.72 and 5.73 show the effect of changing the concrete strength on the maximum values of direct stress in the Y-, X- and Z-directions. Fig. 5.71 shows that the vertical stress in the block material and mortar joints decrease by 30.3% and 28.4% respectively as a result of changing the concrete strength from 9.98 to 34.02 N/mm^2. On the other hand, the maximum values of vertical stress in the concrete infill increase by 137.1% as the concrete strength increases.

This suggests that as the concrete strength increases, the applied vertical stress starts shifting from the block shells to the concrete. The figure also shows that when the cube compressive strength of the concrete is approximately 25 N/mm^2, the vertical stresses in the block shells and the concrete infill are the same.

Fig. 5.72 shows that the maximum values of confinement stress in the X-direction decreases by 19.6% in the mortar

joints and increases by 39.4% in the concrete infill as a result of changing the concrete strength from 9.98 to 34.02 N/mm^2. This was due to the decrease in the applied vertical stress in the block shells and mortar joints and the increase in these stresses in the concrete.

As shown previously, the block shells are responsible for the confinement stresses on the concrete infill. Although the confinement stresses on the concrete in the X-direction increases by 39.4% as a result of increasing the concrete compressive strength, the tensile stresses in the block shells decrease by 24%. This supports the conclusion derived previously that the high Poisson's ratio of the concrete is responsible for failure of the filled prisms.

Similarly, the maximum values of the confinement stress in the Z-direction in the mortar joints (Fig. 5.73), decrease by 19.6% and the tensile stress in the block shells decreases by 26.3% as the concrete strength increases. On the other hand, the maximum values of confinement stresses in the concrete infill increase by 34.9% as the concrete strength increased.

The results for the maximum values of tensile stresses in the block shells for prism filled with low strength concrete (1:5:2), revealed also that the tensile stress in the Z-direction are some 21.2% higher than in the X-direction. This means that the tensile stresses on the prism end shells are higher than on the side shells. This difference is even greater (72.4%) comparing the maximum values of the minor principal stresses on the prism end (MST2) and side (MST1) shells.

Similarly, the maximum values of minor principal tensile stresses on the prism end shells (MST2), for prisms filled with medium (1:3:2) and high strength (1:1:2)

concrete, are higher by 57.5% and 77.4% respectively than on the prism side shells (MST1).

The differences in the maximum values of tensile stresses between the prism end and side shells is the result of the prism aspect ratio (l/t = 2.05), whereby the prism has a greater tendency to split on the prism end shells than through the side shells[1,26]. This result supports the observed mode of failure for filled prisms during the experimental part of this investigation.

Fig. 5.74 shows the effect of changing the cube compressive strength of the concrete on the maximum values of the shear stress. The figure shows an increase of 250.1% in the values of maximum shear stress in the concrete infill as a result of changing the concrete strength from 9.98 to 34.02 N/mm^2. For the same range of concrete strength, the maximum shear stresses in the block shells and mortar joints decrease by 25.5% and 30.7% respectively.

To sum up the effect of changing the cube compressive strength of concrete from 9.98 to 34.02 N/mm^2 on prisms strength. It seems that the prisms strength increases as the concrete infill increases. This was due to the shifting of the applied vertical stress from the block material to the concrete infill, which means a greater contribution of the concrete infill to the strength of the prism. An optimum prism strength will be achieved when the deformational characteristics of all materials are the same.

Due to the complex nature of the deformations and the stress distributions in the filled **3FBP-MJ** prisms, the general conclusion derived from the results of the specific analysis and the parametric study analysis is that failure of filled **3FBP-MJ** prisms is dominated by incompatible

deformation, localized crushing, splitting and shear failures. It is anticipated that the filled prisms will fail due to a combination of compression, tension and shear modes of failure.

The predicted mode of failure for the filled **3FBP-MJ** prisms with low to medium strength concrete infill is dominated by block shell-concrete infill separation and lateral deformation with some block shells, mortar and concrete infill crushing near the mortar joints. The first initiation of block shell outward deformation is near the levels of the mortar joints. Prisms filled with high strength concrete fail by simultaneous crushing of the block shells and concrete infill near one of the mortar joints.

From the stress values and distribution, the strength of filled **3FBP-MJ** prisms do not depend directly on the block unit compressive strength and the mortar type[1,26,28,33,36,71]. To determine f'_m, filled **3FBP-MJ** prisms should be tested.

In general, a clear similarity was noticed between the predicted modes of failure and the values of stress for the unfilled and filled **3FBP-MJ** prisms from the FEA as compared to the observed modes of failure and the values of stress determined from the experimental investigation. Using the FEA, however, provided a clear picture to the deformations and stress distributions for unfilled and filled prisms in the Y-, X- and Z-directions. The FEA also provides answers to questions on how different materials interact with each other in axially loaded blockwork masonry prisms which are difficult if not impossible to observe experimentally.

5.6 CONCLUSIONS

1. The ultimate compressive strength for unfilled blockwork masonry, f'_m, in situations where in-plane horizontal forces are not expected to occur, can be determined by one of the following two methods:

   (i) On the basis of the compressive strength of a unit block compressed normal to the bed face and the type of mortar, or by using Eqn. 5.4 for the type of blocks used in this investigation.

   (ii) Tests on 3-course high full-block stack-bonded masonry prisms made from the same materials as those to be used in the actual construction and compressed normal to the unit bed face.

2. The ultimate compressive strength for filled blockwork masonry, f'_m, in situations where in-plane horizontal forces are not expected to occur, can be determined by testing 3-course high full-block stack-bonded masonry prisms, built from the same materials as those used in the actual construction and compressed normal to the unit bed face, or by using Eqn. 5.4 for the type of blocks used in this investigation.

3. Testing unfilled and filled half-block prisms to determine f'_m, over estimates the actual compressive strength of the blockwork masonry assemblage by 25%. This is due to the difference in values of aspect ratio, as between the full-block prism, ($l/t = 2.05$), and half-block prism, ($l/t = 1.0$), and also due to the difference in the mortar bedded area caused by the presence of the mid-web in full-block prism.

4. The presence of a low strength (1:1:6) mortar in the

joints of unfilled full-block prisms compressed normal to the unit bed face caused a reduction of 10.2% in the prism strength compared to unfilled prisms with a dental plaster joint. Changing the mortar strength by 188.8% increases the prism strength by 20.1%.

5. The presence of concrete infill significantly reduced the compressive strength of 3-course high prisms with mortar joints or with dental plaster joints. With only one exception, the best compressive strength results were achieved when the deformational characteristics of the concrete infill matched those of the concrete block. This was achieved by using concrete infill with a cube compressive strength of 45% to 50% higher than that of the concrete block.

6. In filled prisms compressed normal to the unit bed face, the presence of the mortar joints, even though of low strength, are essential to develop the block strength. Their presence, however, caused a further reduction in the prism strength in addition to that caused by the presence of the concrete infill. This reduction resulted from the high plasticity and Poisson's ratio of the mortar, compared to that of the concrete blocks. This was responsible for introducing confinement stresses in the mortar and splitting stresses in the blocks.

7. In filled 3-course high full-block prisms of similar concrete strength, the presence of a low strength (1:1:6) mortar joint, contributed greatly to the strength of the filled prisms. Increasing the mortar strength by 98.2% above this value increased the prism strength by a negligible amount.

8. Empirical formulae (Eqns 5.4 and 5.5) were suggested

to determine f'_m, for unfilled and filled, full and half-block prisms taking into account the block, mortar and concrete infill strength. The formulae showed that the strength of the concrete infill is not fully reflected in the strength of prisms compressed normal to the bed face.

9. The results of the horizontal deformations from the specific and parametric study FEA, for unfilled and filled **3FBP-MJ** prisms shows incompatibility in the horizontal deformation in the X- and Z-directions. Due to this incompatibility, the prism end shells will be separated from the rest of the prism and longitudinal cracks will be developed at the line of contact between the end and side prism shells.

10. The distribution of vertical, horizontal, shear and principal stresses resulting from the specific and parametric study non-linear FEA for unfilled and filled **3FBP-MJ** prisms showed that the effect of the steel platens was limited to areas near the platens only. Thus, using the 3-course high prism as a standard specimen to determine f'_m is acceptable.

11. The specific non-linear FEA for unfilled prisms showed that, although the vertical and major principal stresses increase as the mortar strength increases, the confinement stresses on the mortar joints decrease considerably. This consequently resulted in decreasing the tensile stresses in the block shells near the mortar joints. This explains why changing the mortar joints strength has no great influence on the unfilled prism strength.

12. In considering the equilibrium of horizontal stresses at the middle block of the unfilled 3-course high

prisms, constructed with high strength (1:0.25:3) mortar, it is better to assume a triangular stress distribution with maximum at the mortar joints and zero at 1/3 of the block height. In the case of the filled prisms, assume the horizontal stresses to be uniformly distributed at the middle block, irrespective of what type of mortar or concrete is used in their construction.

13. A new hypothesis is presented on page 278 for the failure of filled 3-course high prisms as a result of the specific non-linear FEA.

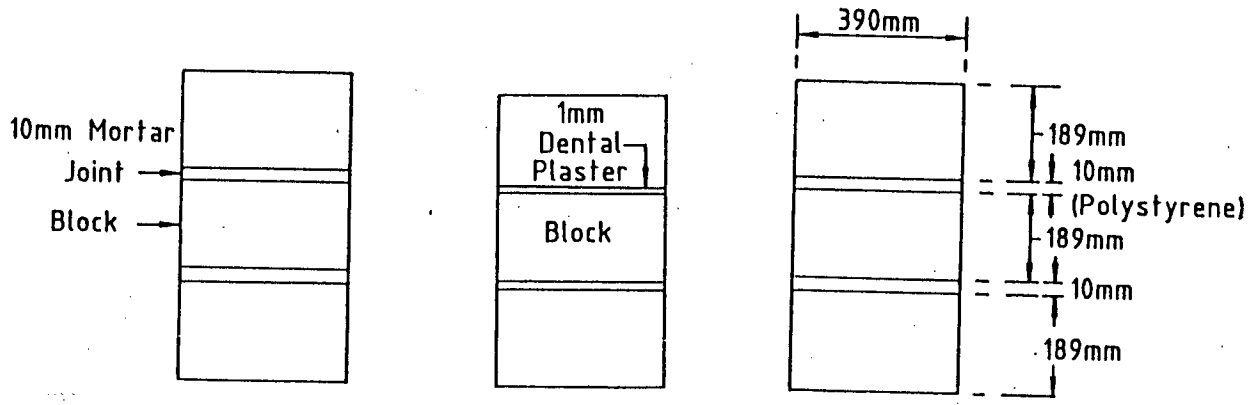

(i) 3FBP-MJ prism.

(ii) 3FBP-DPJ prism.

(iii) 3FBP-PJ prism.

3-course high full-block prism with mortar joints.

3-course high full-block prism with dental plaster joints.

3-course high full-block prism with polystyrene joints.

Fig. 5.1 - Types of 3-course high blockwork masonry prism tested. (i) 3FBP-MJ prism, (ii) 3FBP-DPJ prism, (iii) 3FBP-PJ prism.

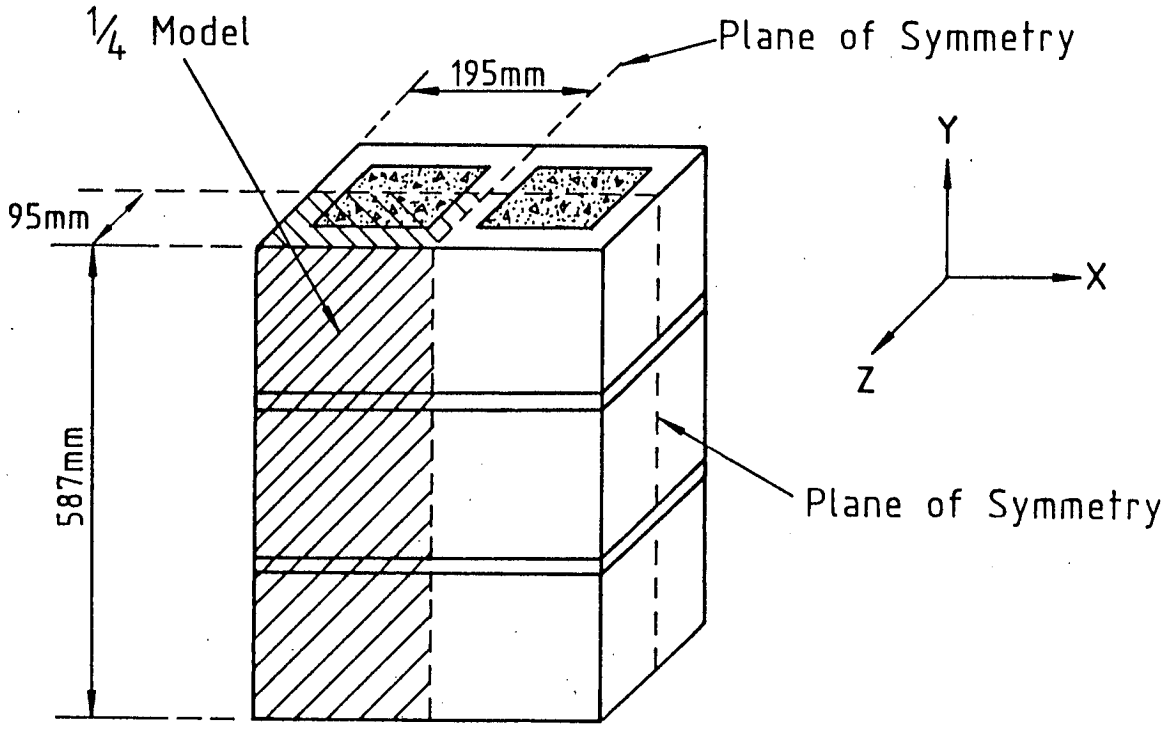

Fig. 5.2 - 1/4 prism model used in non-linear FEA.

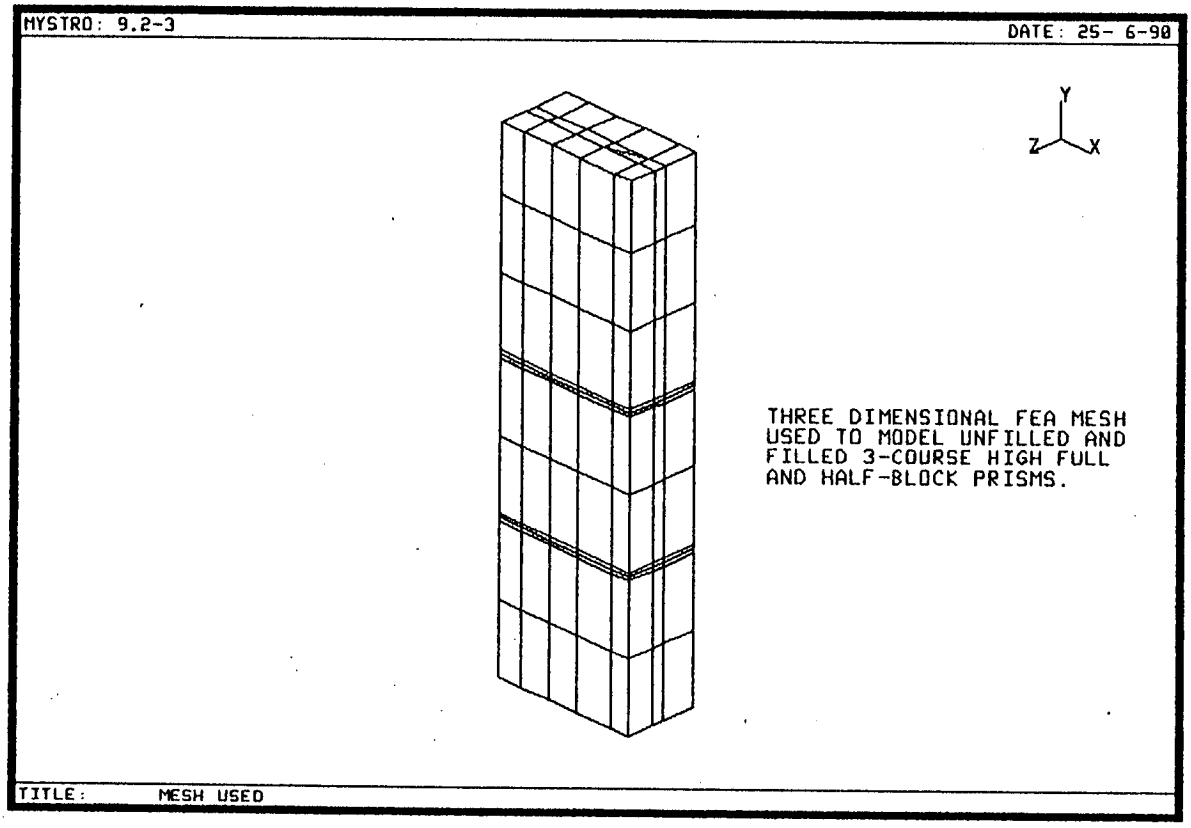

Fig. 5.3 - Three-dimensional mesh used in non-linear FEA.

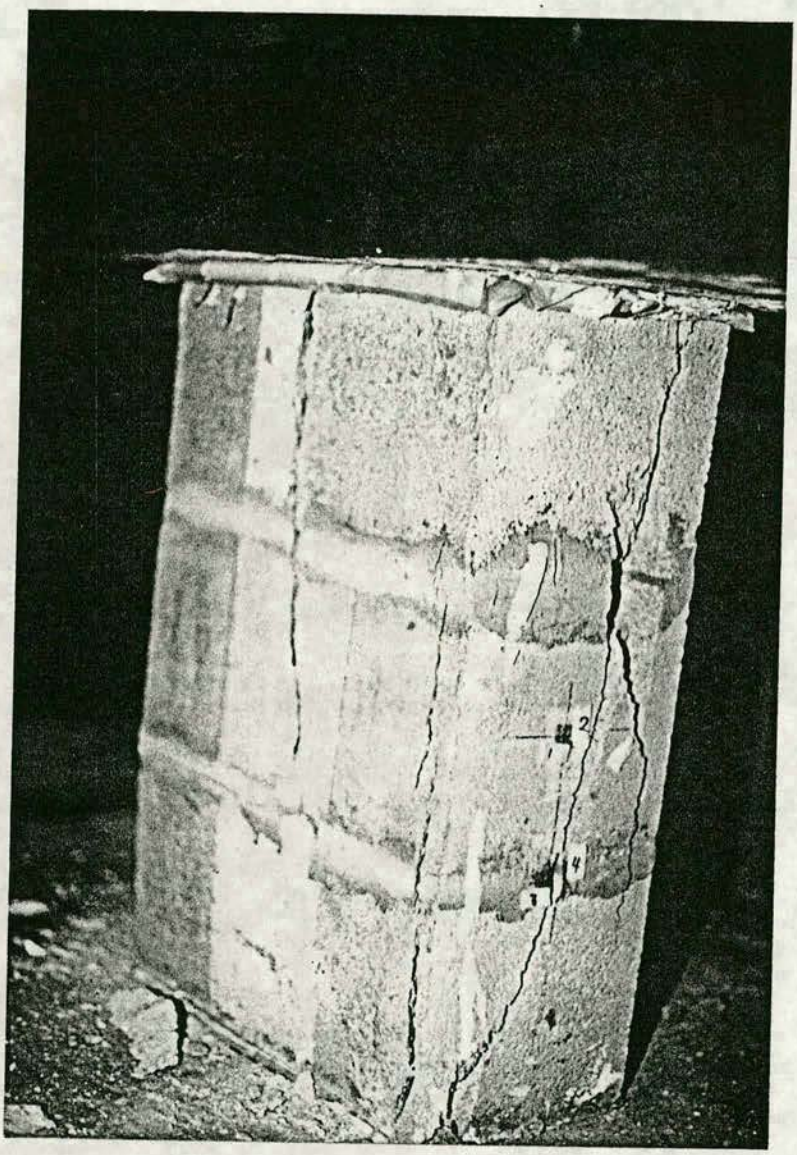

Fig. 5.4 - Unfilled 3FBP-MJ prism after failure, mortar strength 26.54 N/mm^2.

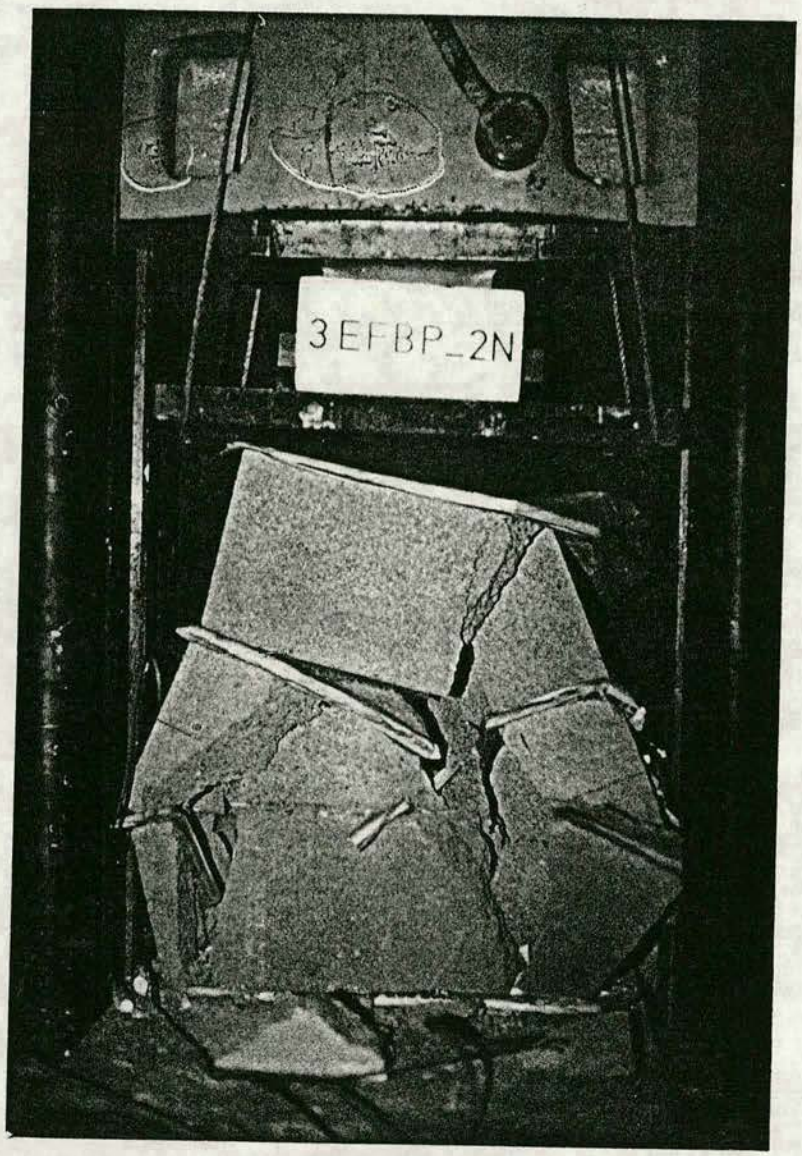

Fig. 5.5 - Unfilled 3FBP-DPJ prism after failure.

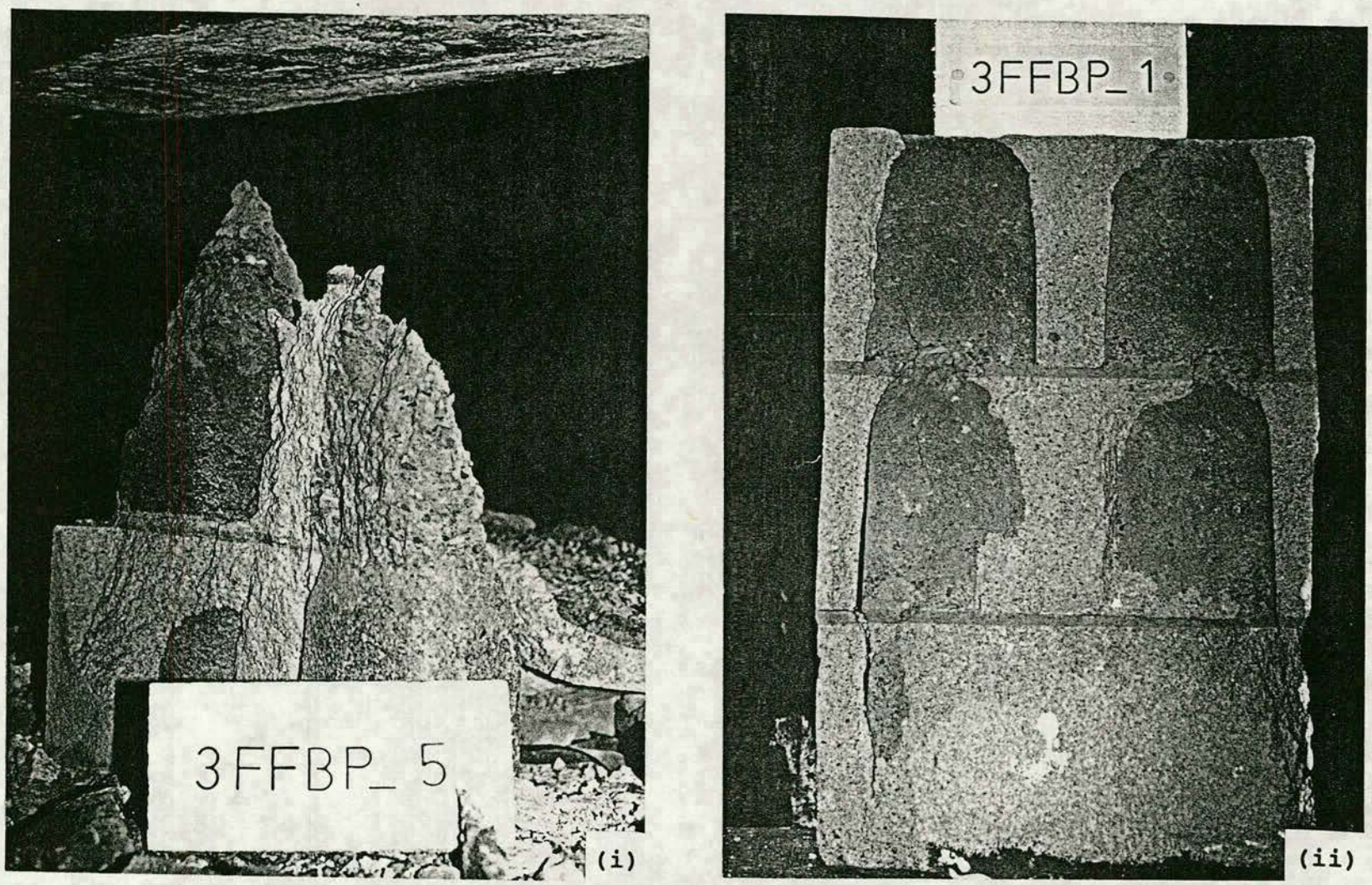

Fig. 5.6 - Filled 3FBP-MJ prism Mode I failure, mortar strength 26.54 N/mm^2, concrete strength 28.75 N/mm^2.

Fig. 5.7 - Filled 3FBP-MJ prism Mode II failure, mortar strength 26.80 N/mm^2, concrete strength 34.02 N/mm^2.

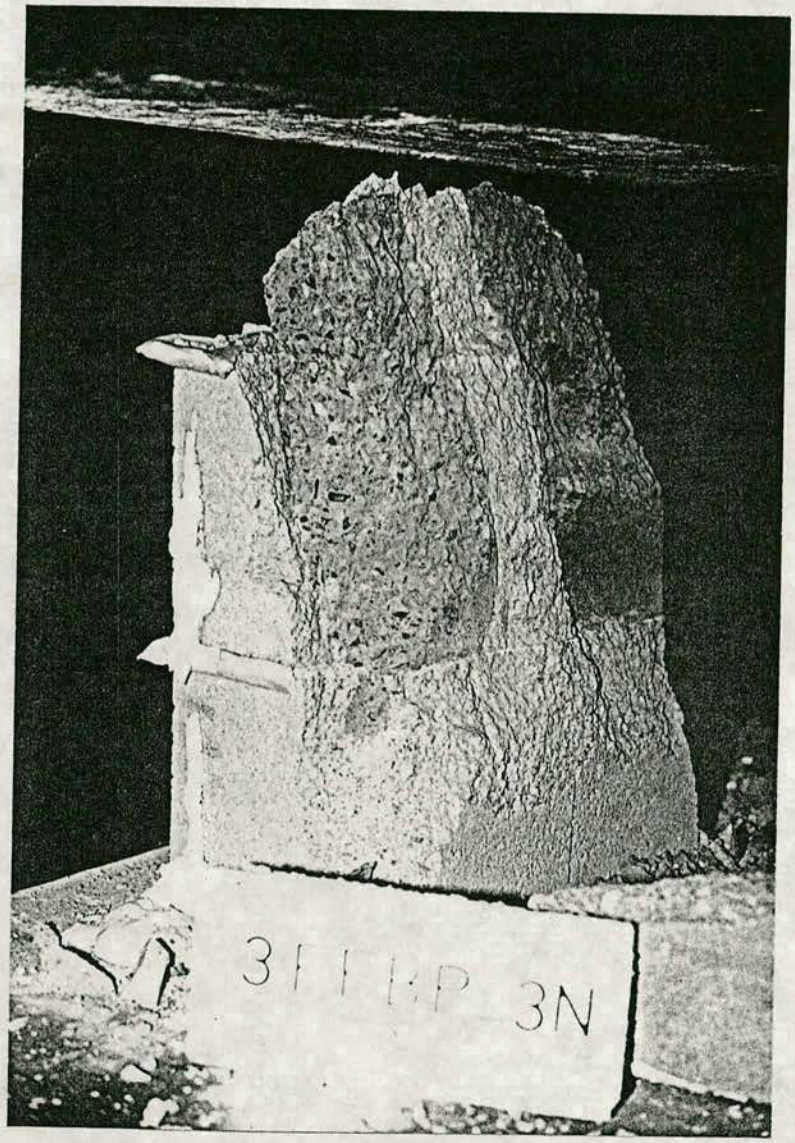

Fig. 5.8 - Filled 3FBP-DPJ prism after failure, concrete strength 19.00 N/mm^2.

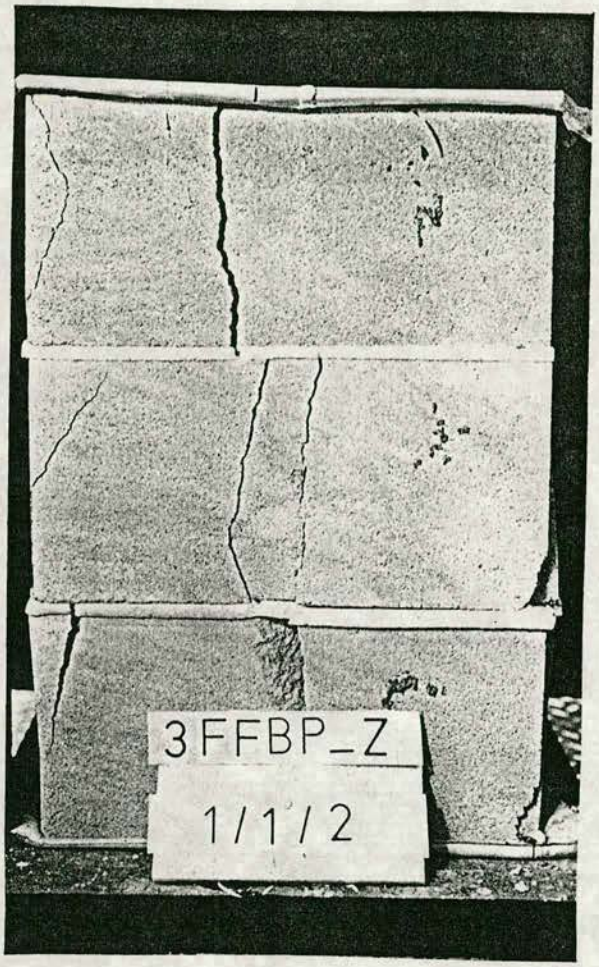

Fig. 5.9 - Filled 3FBP-PJ prism after failure, concrete strength 34.02 N/mm^2.

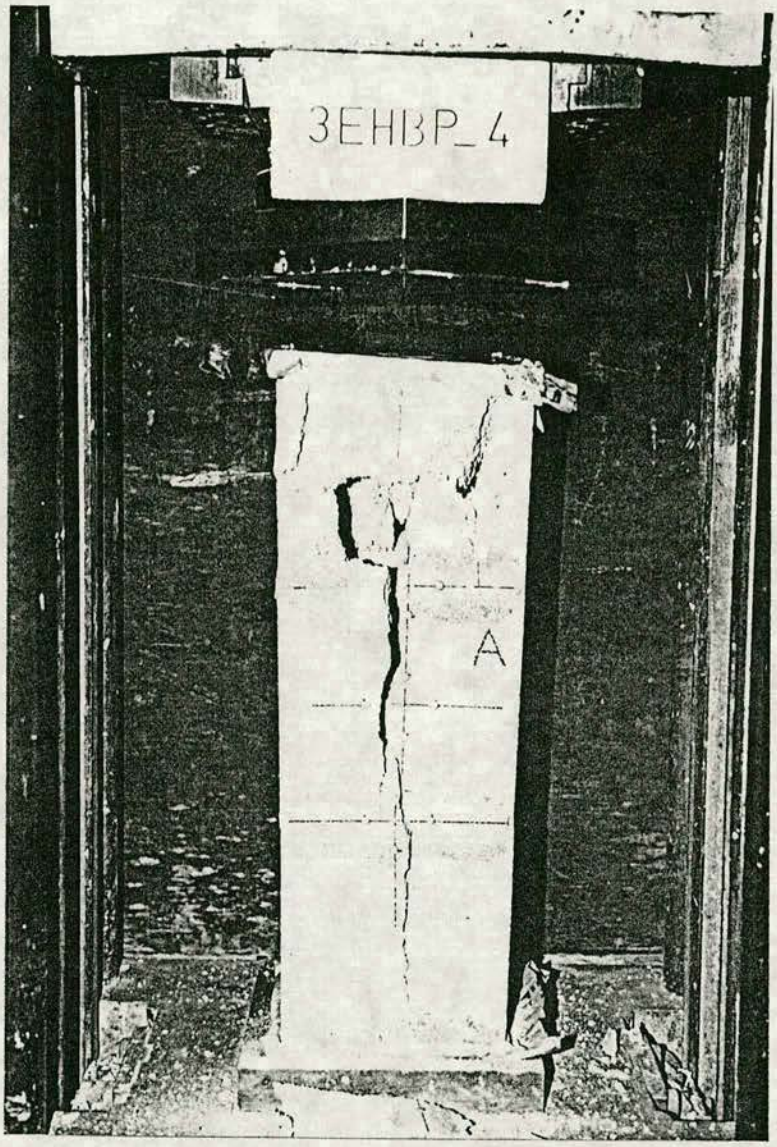

Fig. 5.10 - Unfilled 3HBP-MJ prism after failure, mortar strength 26.54 N/mm^2.

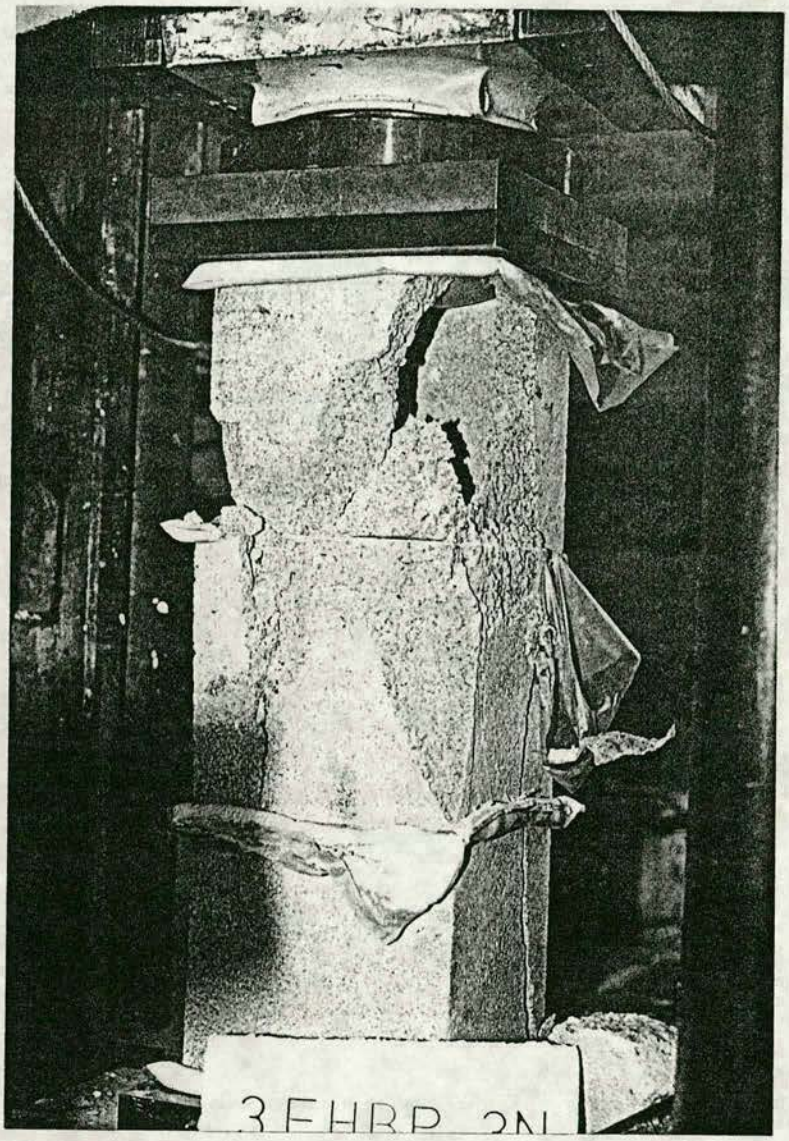

Fig. 5.11 - Unfilled 3HBP-DPJ prism after failure.

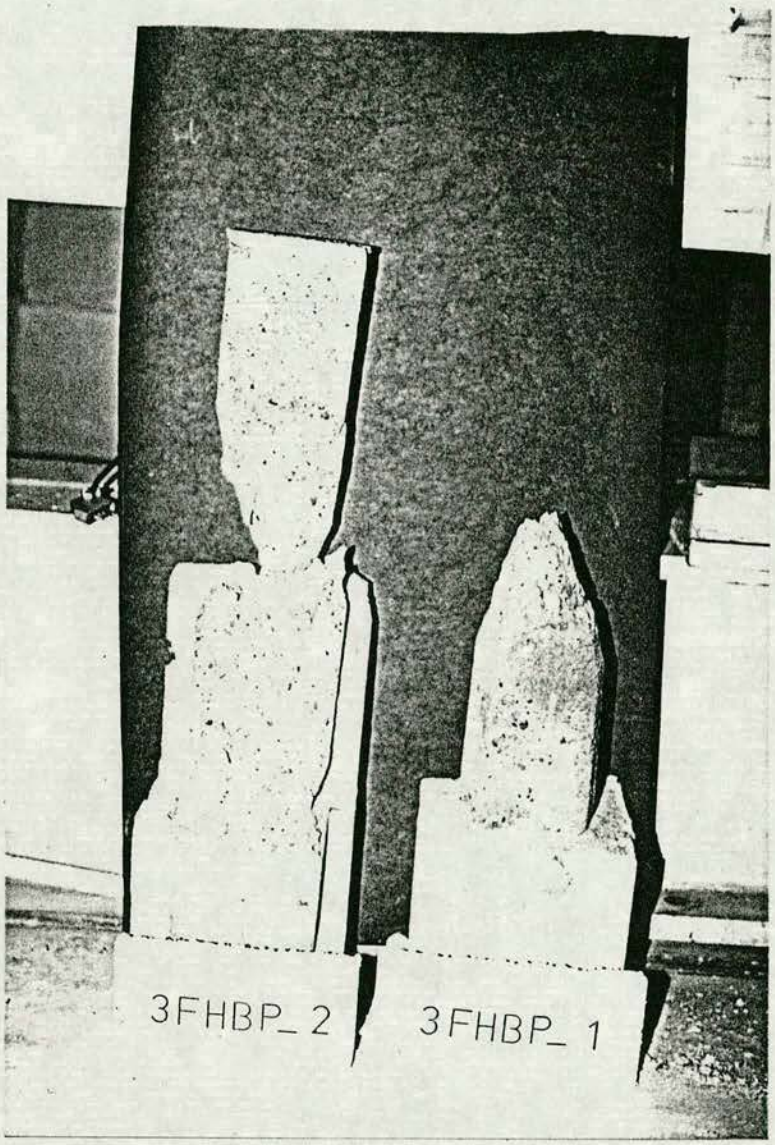

Fig. 5.12 - Filled 3HBP-MJ prism Mode I failure, mortar strength 26.54 N/mm^2, concrete strength 28.75 N/mm^2.

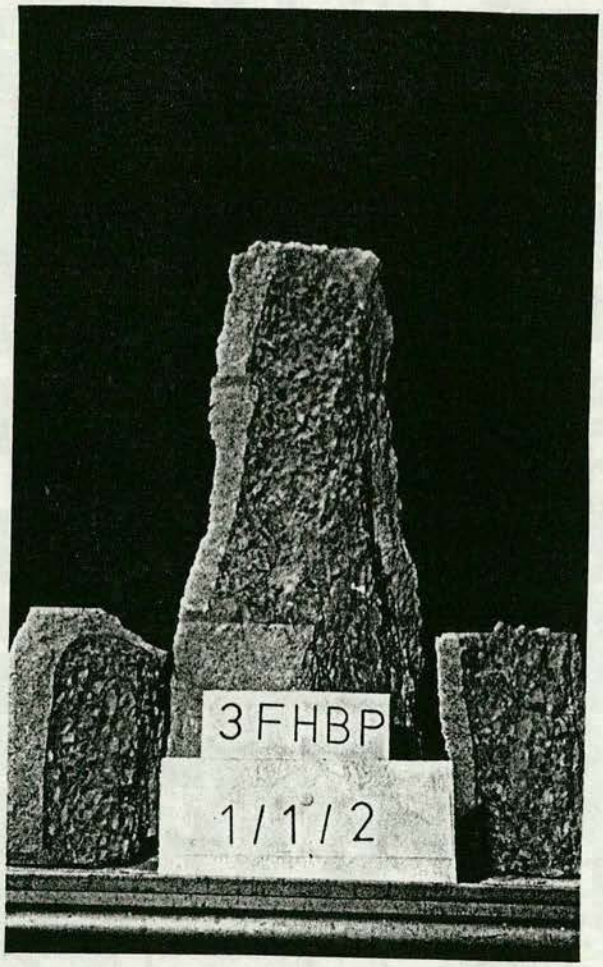

Fig. 5.13 - Filled 3HBP-MJ prism Mode II failure, mortar strength 26.54 N/mm^2, concrete strength 45.31 N/mm^2.

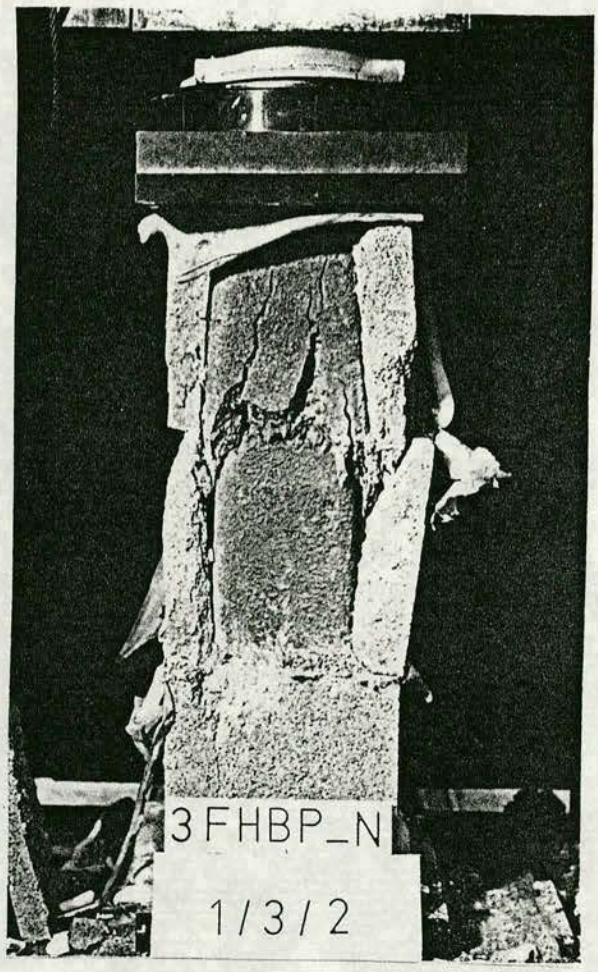

Fig. 5.14 - Filled 3HBP-DPJ prism after failure, concrete strength 14.85 N/mm^2.

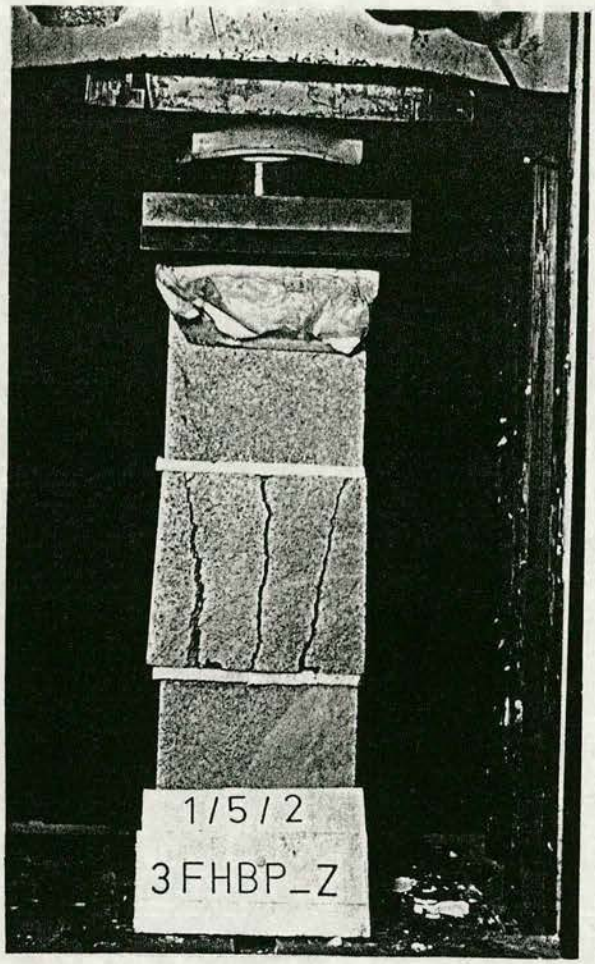

Fig. 5.15 - Filled 3HBP-PJ prism after failure, concrete strength 12.87 N/mm^2.

Table 5.1

Compressive strength of 3-course high full-block prisms and component materials.

Prism type	Average compressive * strength (N/mm^2) Area used: Net	Gross	S.D. (N/mm^2)	Material cube compressive ♦ strength (N/mm^2): Mortar (f_{mr})	Infill (f_c)
		Prism with mortar joints (3FBP-MJ) ♦			
Unfilled	17.78	10.00	1.07/0.60	9.19	-
Unfilled	17.39	9.63	0.85/0.43	15.39	-
Unfilled	21.35	12.01	0.41/0.23	26.54	-
Filled	-	15.76	2.03	9.19	19.40
Filled	-	17.93	0.59	13.52	32.03
Filled	-	13.76	1.27	15.39	8.57
Filled	-	11.36	0.15	15.39	15.71
Filled	-	13.42	1.05	20.15	23.52
Filled	-	13.85	1.31	26.44	9.98
Filled	-	14.53	0.23	26.54	28.75
Filled	-	19.29	1.55	26.80	34.02
		Prism with dental plaster joints (3FBP-DPJ) ♦			
Unfilled	19.80	11.15	2.89/1.63	-	-
Filled	-	14.24	1.06	-	9.27
Filled	-	17.34	1.44	-	19.00
Filled	-	24.82	1.76	-	34.02
		Prism with polystyrene joints (3FBP-PJ) ♣			
Filled	13.09	3.40	0.62/0.16	-	8.57
Filled	16.14	4.20	0.50/0.13	-	11.73
Filled	24.47	6.37	4.44/1.16	-	24.60
Filled	36.50	9.49	3.22/0.84	-	34.02

* Average and S.D. are calculated for three prisms.

♦ Cube compressive strength of block material f_b = 24.29 N/mm^2.

♦ Net area = Area at section (1) = 41700 mm^2. (See Table 3.2).
Gross area = 390 x 190 = 74100 mm^2.

♣ Net area = 74100 - Area at section (4) = 19272 mm^2. (See Table 3.2).
Gross area = 390 x 190 = 74100 mm^2.

Table 5.2

Compressive strength of 3-course high half-block prisms and component materials.

Prism type	Average compressive * strength (N/mm^2) Area used: Net	Gross	S.D. (N/mm^2)	Material cube compressive ♦ strength (N/mm^2): Mortar (f_{mr})	Infill (f_c)
			Prism with mortar joints (3HBP-MJ) ♦		
Unfilled	20.60	11.36	2.68/1.47	15.39	-
Unfilled	24.18	13.33	0.66/0.36	20.15	-
Unfilled	25.49	14.06	0.38/0.21	26.54	-
Filled	-	15.64	1.13	26.54	8.27
Filled	-	20.46	1.08	26.54	28.75
Filled	-	26.44	0.78	26.54	45.31
			Prism with dental plaster joints (3HBP-DPJ) ♦		
Unfilled	21.89	12.07	2.02/1.11	-	-
Filled	-	13.77	0.56	-	12.87
Filled	-	14.47	0.84	-	14.85
Filled	-	20.13	1.05	-	35.22
			Prism with polystyrene joints (3HBP-PJ) ♣		
Filled	18.61	4.97	1.37/0.37	-	12.87
Filled	25.84	6.90	1.71/0.46	-	20.15
Filled	41.58	11.10	0.73/0.19	-	35.22

* Average and S.D. are calculated for three prisms.

♯ Cube compressive strength of block material fb = 24.29 N/mm^2.

♦ Net area = Area at section (1) = 19900 mm^2. (See Table 3.2).
Gross area = 190 x 190 = 36100 mm^2.

♣ Net area = 36100 - Area at section (4) = 9636 mm^2. (See Table 3.2).
Gross area = 190 x 190 = 36100 mm^2.

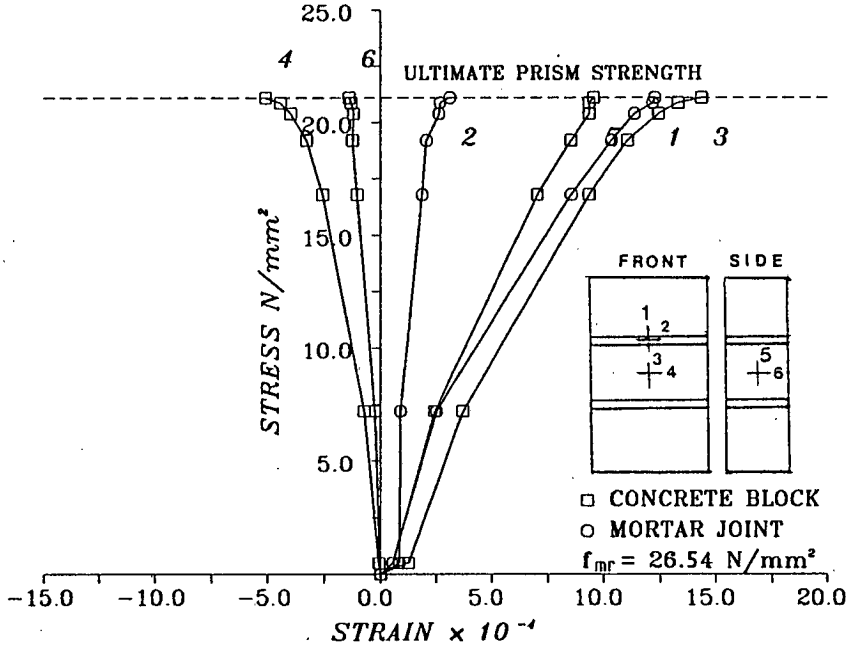

Fig. 5.16 - Stress vs strain curves for unfilled 3FBP-MJ prism, mortar strength 26.54 N/mm^2.

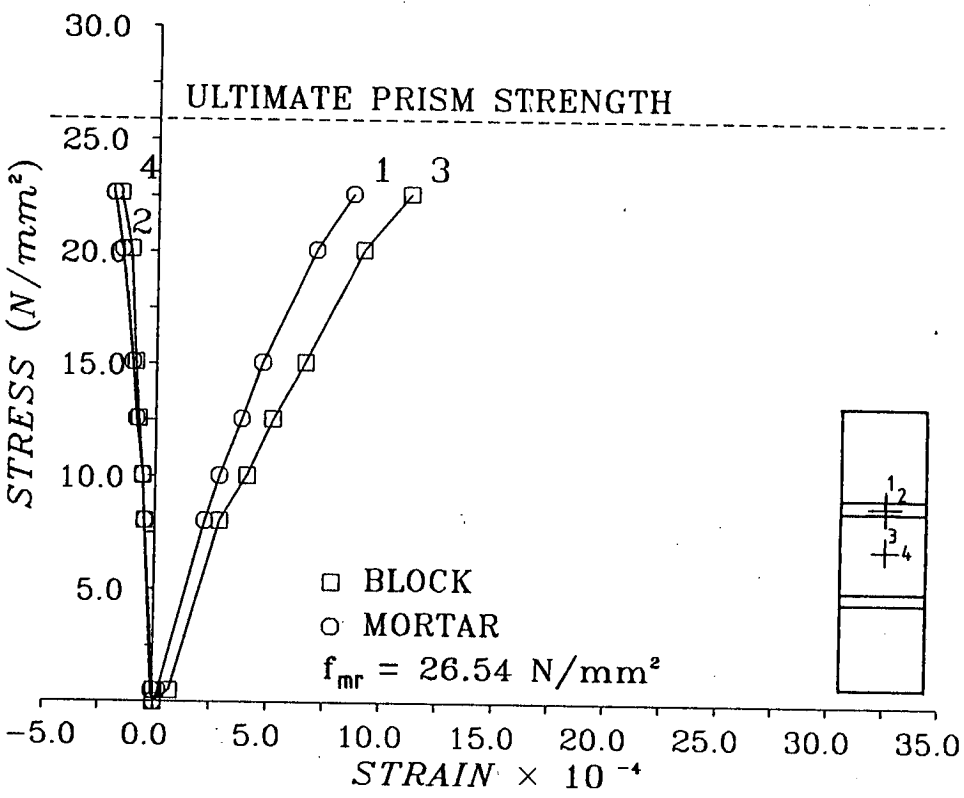

Fig. 5.17 - Stress vs strain curves for unfilled 3HBP-MJ prism, mortar strength 26.54 N/mm^2.

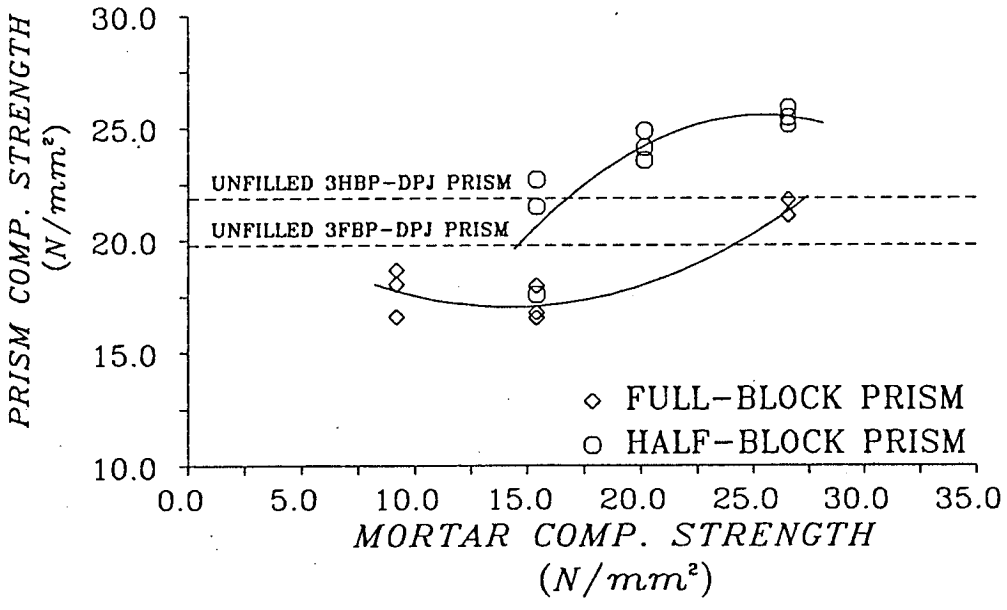

Fig. 5.18 - Effect of mortar strength on unfilled 3FBP-MJ and 3HBP-MJ prisms strength.

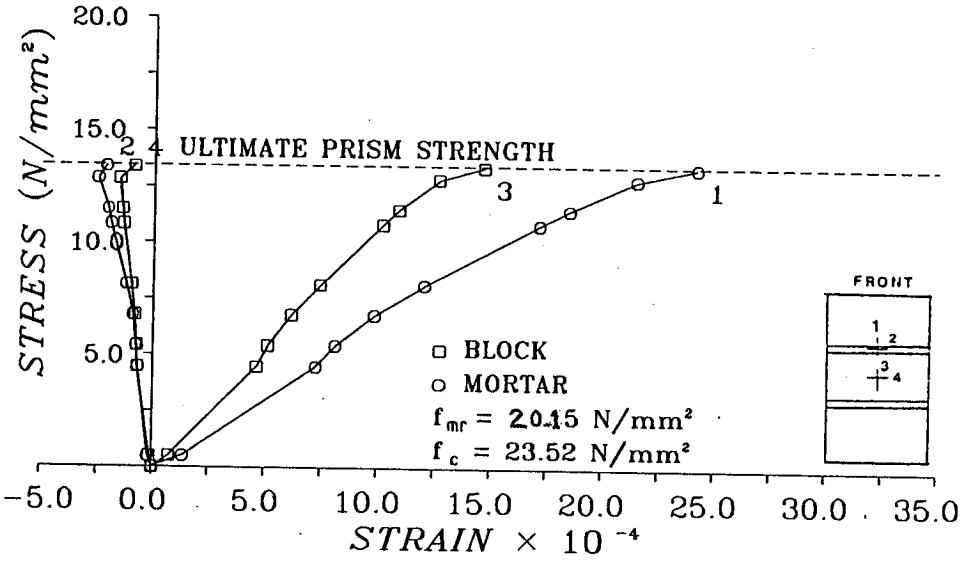

Fig. 5.19 - Stress vs strain curves for filled 3FBP-MJ prism, mortar strength 20.15 N/mm^2, concrete strength 23.52 N/mm^2.

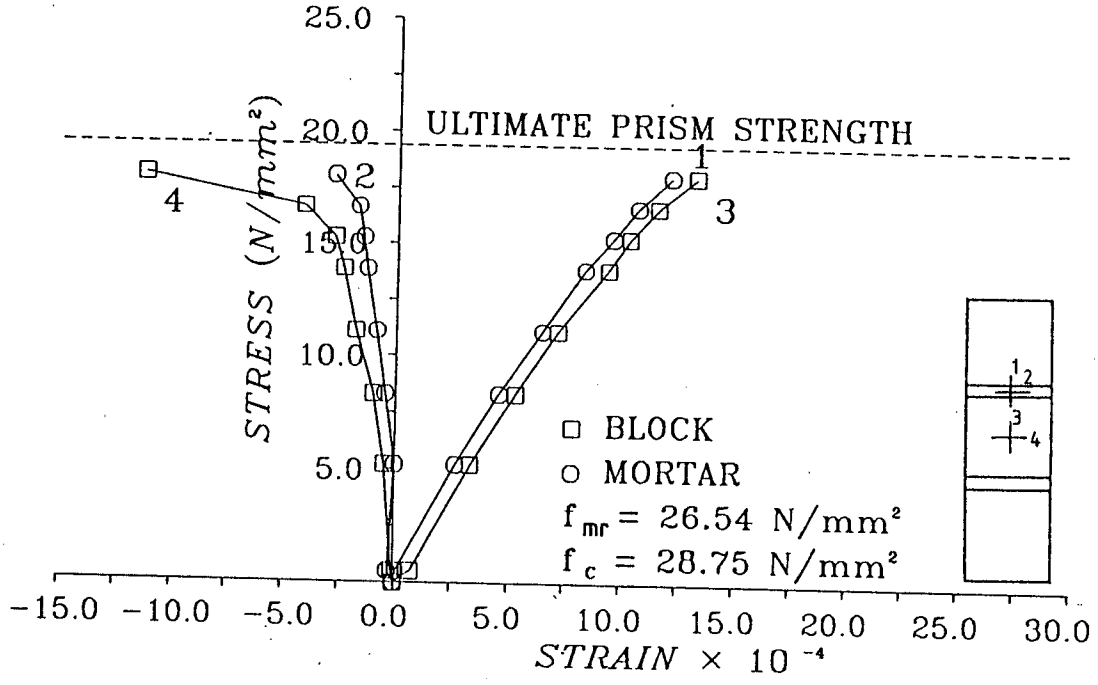

Fig. 5.20 - Stress vs strain curves for filled 3HBP-MJ prism, mortar strength 26.54 N/mm^2, concrete strength 28.75 N/mm^2.

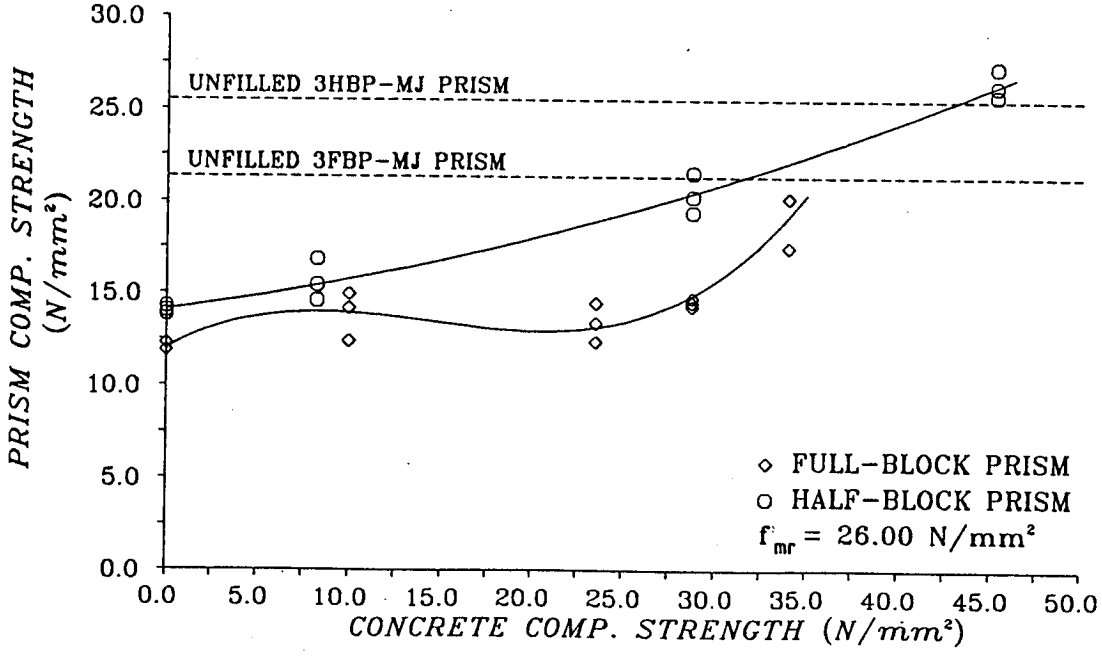

Fig. 5.21 - Effect of concrete infill strength on filled 3FBP-MJ and 3HBP-MJ prisms strength, with similar mortar strength.

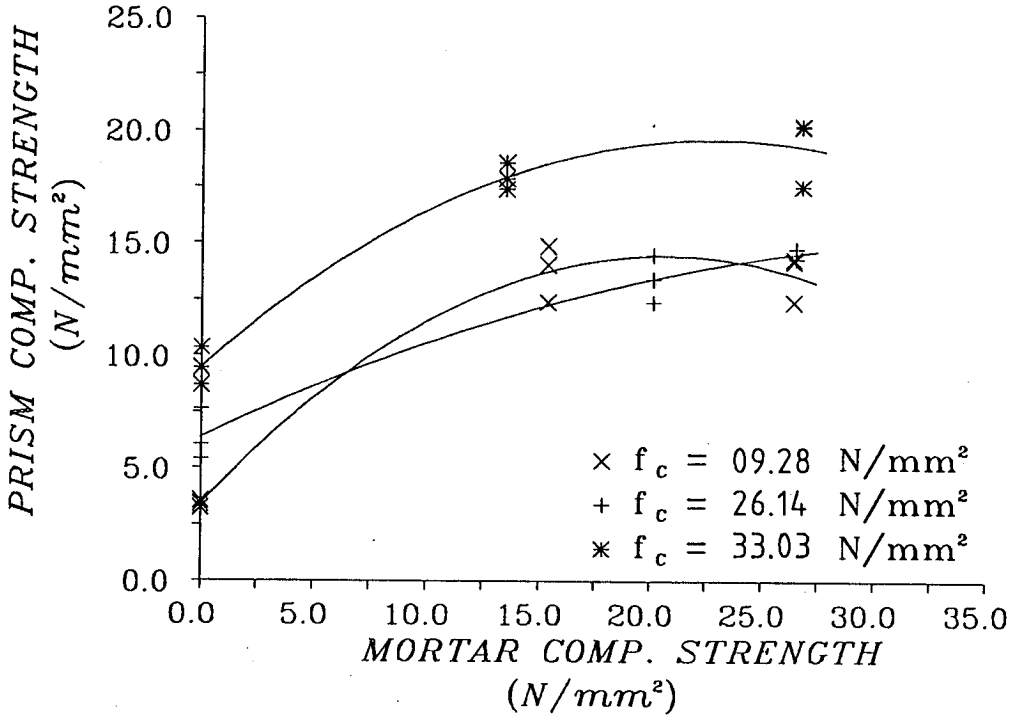

Fig. 5.22 - Effect of mortar strength on filled 3FBP-MJ prisms strength, with similar concrete strength.

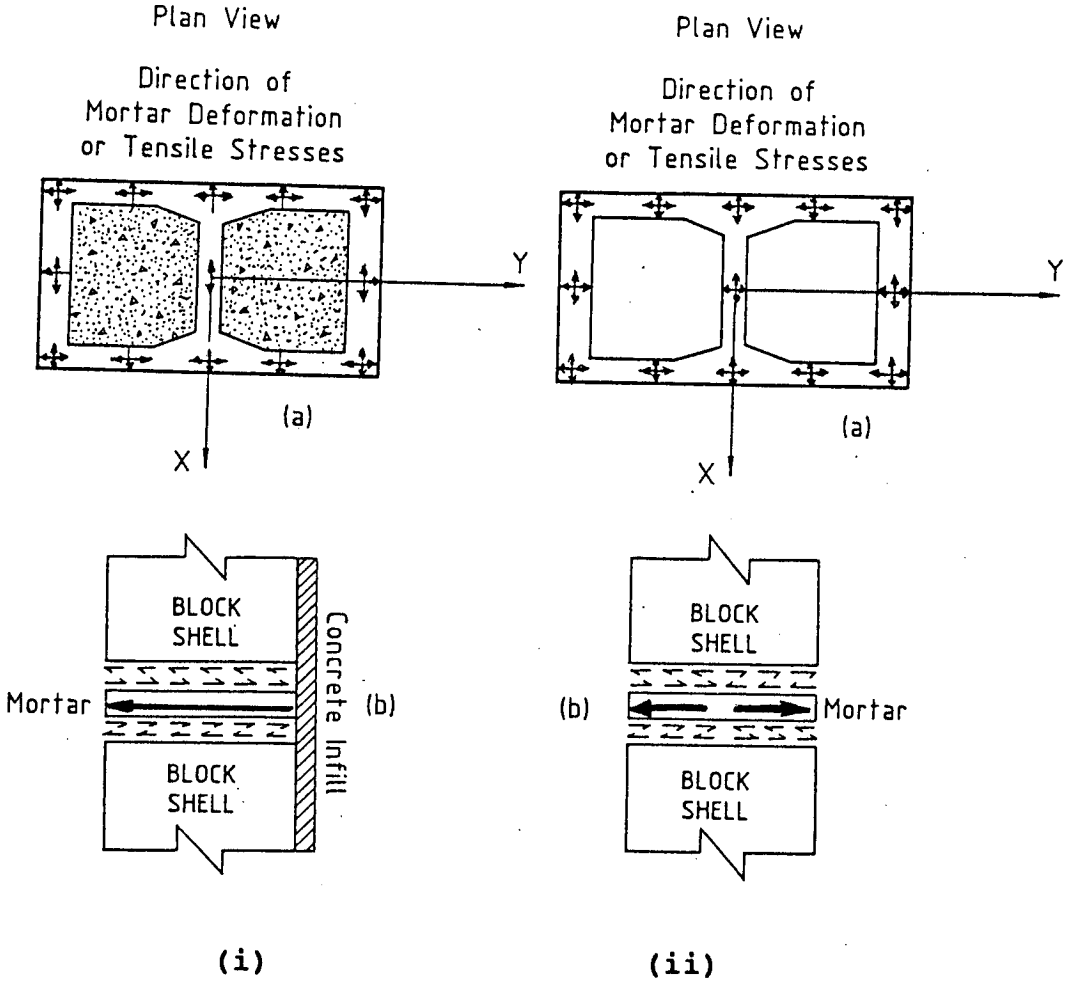

Fig. 5.23 - Displacement and stresses at block-mortar interface. (i) Filled prism, (ii) Unfilled prism.

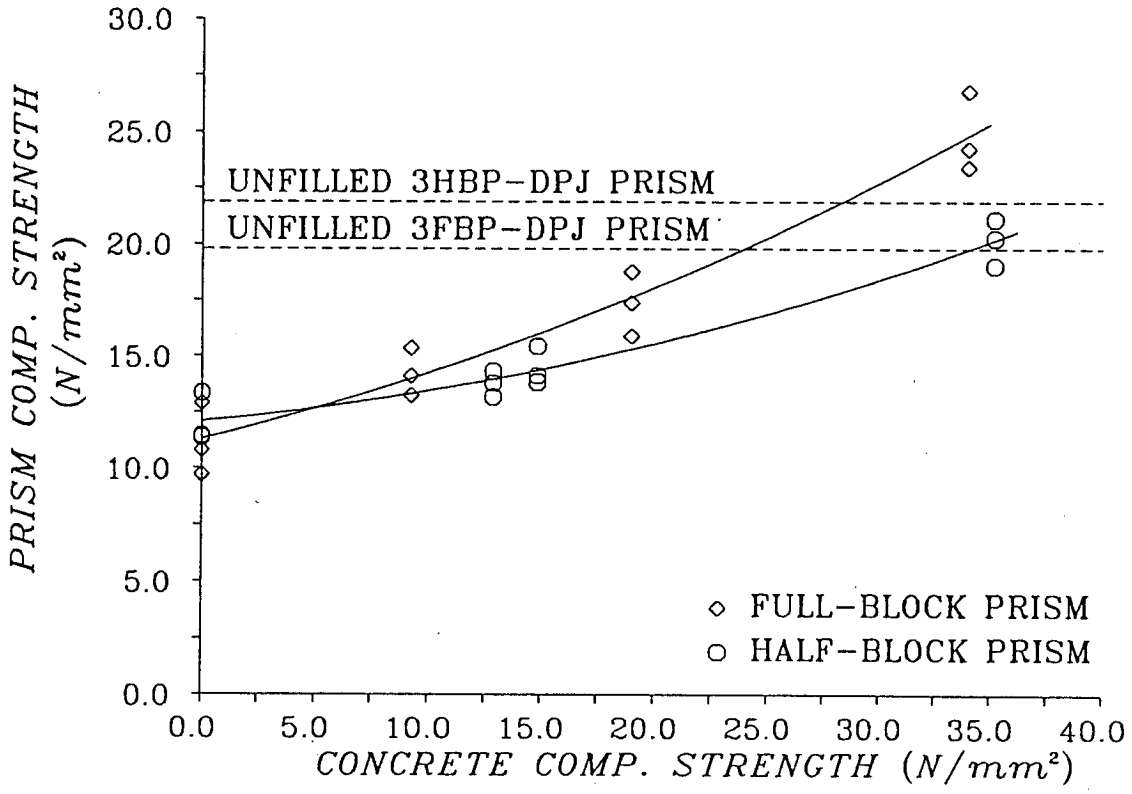

Fig. 5.24 - Effect of concrete infill strength on filled 3FBP-DPJ and 3HBP-DPJ prisms strength.

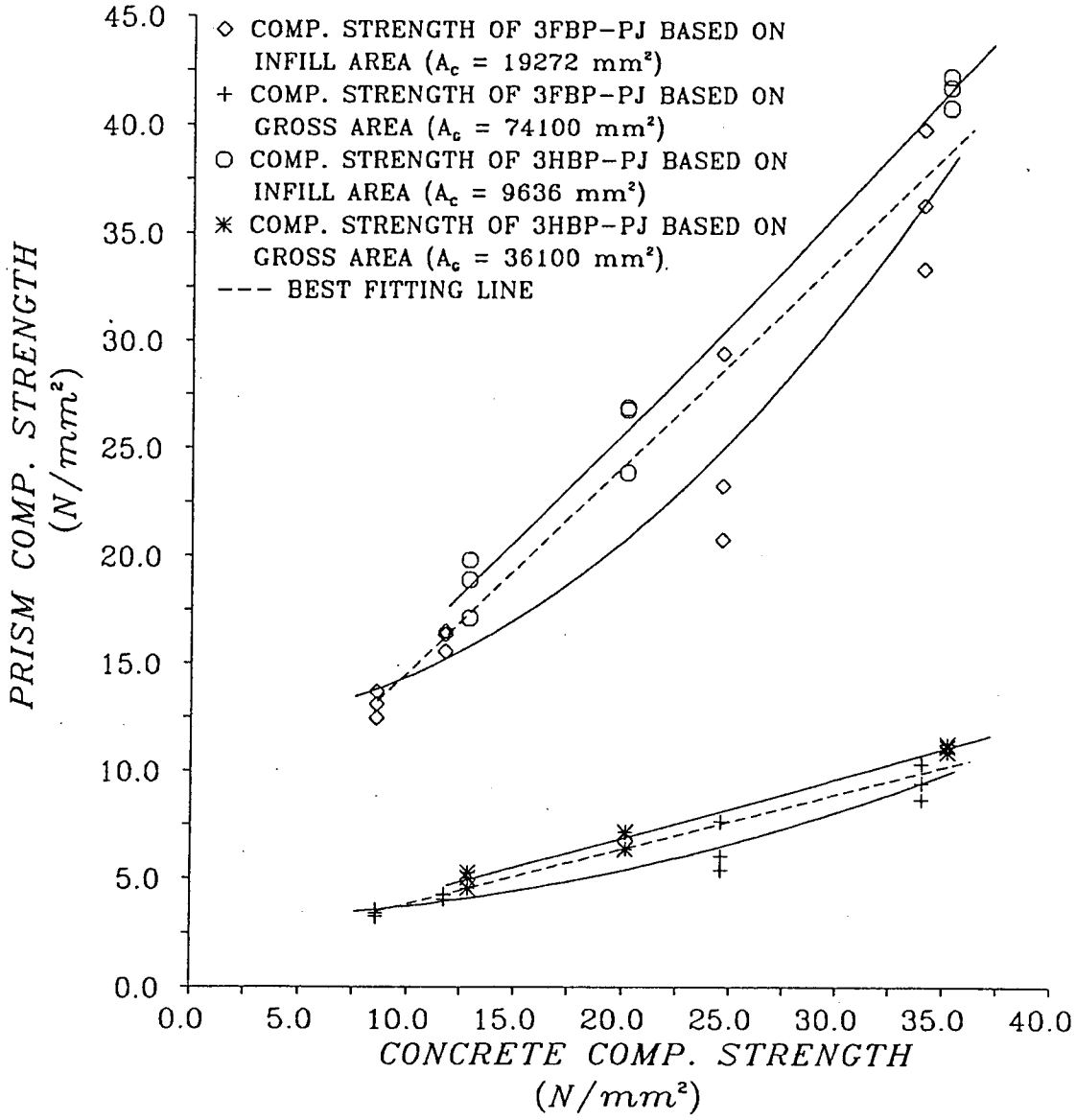

Fig. 5.25 - Effect of concrete infill strength on filled 3FBP-PJ and 3HBP-PJ prisms strength.

Table 5.3

Comparison between experimental and theoretical values of f'_m, for unfilled and filled 3FBP-MJ and 3HBP-MJ prisms.

Prism type	Average experimental f'_m (N/mm^2) Gross area	Average theoretical f'_m (N/mm^2) Gross area	Ratio * f'_m (Exp.)/ f'_m (Theo.)
	Full-block prism with mortar joints (3FBP-MJ)		
Unfilled	10.00	8.21	1.22
Unfilled	9.63	8.83	1.09
Unfilled	12.01	9.94	1.21
Filled	15.76	13.06	1.21
Filled	17.93	16.65	1.08
Filled	13.76	10.97	1.25
Filled	11.36	12.76	0.89
Filled	13.42	15.18	0.89
Filled	13.85	12.43	1.11
Filled	14.53	17.13	0.85
Filled	19.29	18.48	1.04
		Average =	1.08
	Half-block prism with mortar joints (3HBP-MJ)		
Unfilled	11.36	10.37	1.10
Unfilled	13.33	11.32	1.18
Unfilled	14.06	12.60	1.12
Filled	15.64	14.66	1.07
Filled	20.46	19.78	1.03
Filled	26.44	23.92	1.11
		Average =	1.10

* Ratio of f'_m (Experimental)/ f'_m (Theoretical).

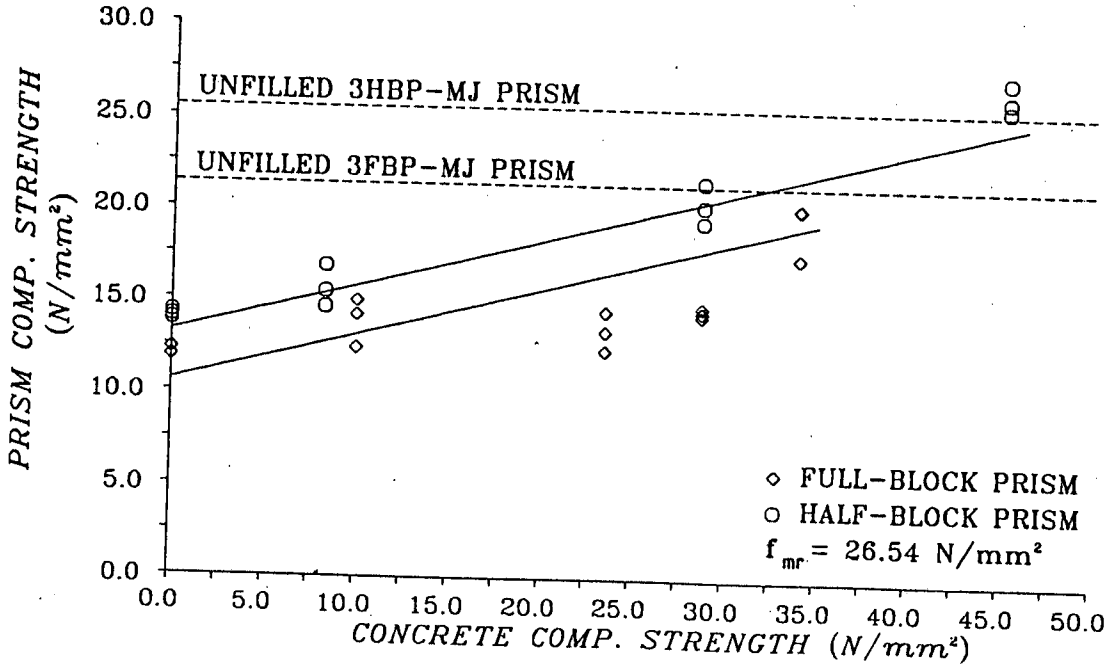

Fig. 5.26 - Comparison between experimental and theoretical values of f'_m, for unfilled and filled 3FBP-MJ and 3HBP-MJ prisms, with similar mortar strength.

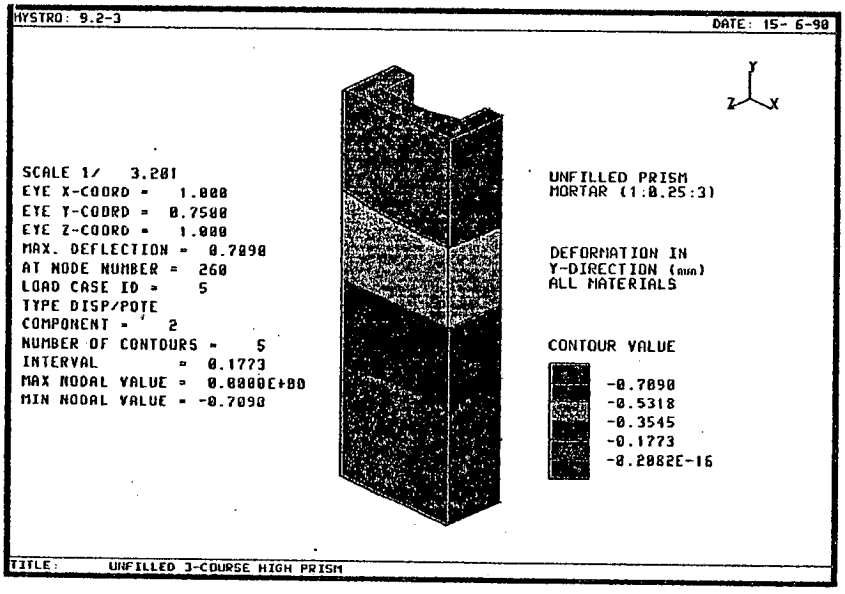

Fig. 5.27 - Deformation of unfilled 3FBP-MJ prism in Y-direction, specific non-linear FEA.

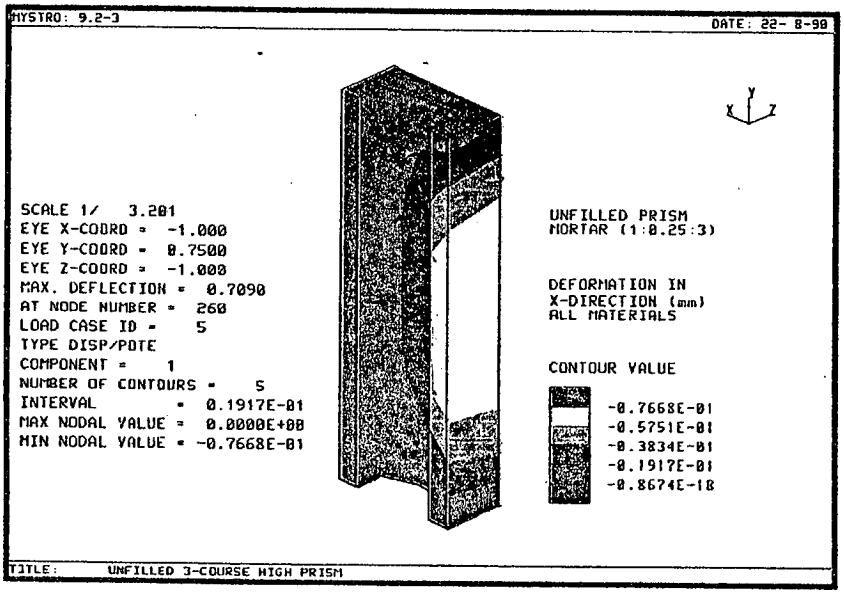

Fig. 5.28 - Deformation of unfilled 3FBP-MJ prism in X-direction, specific non-linear FEA.

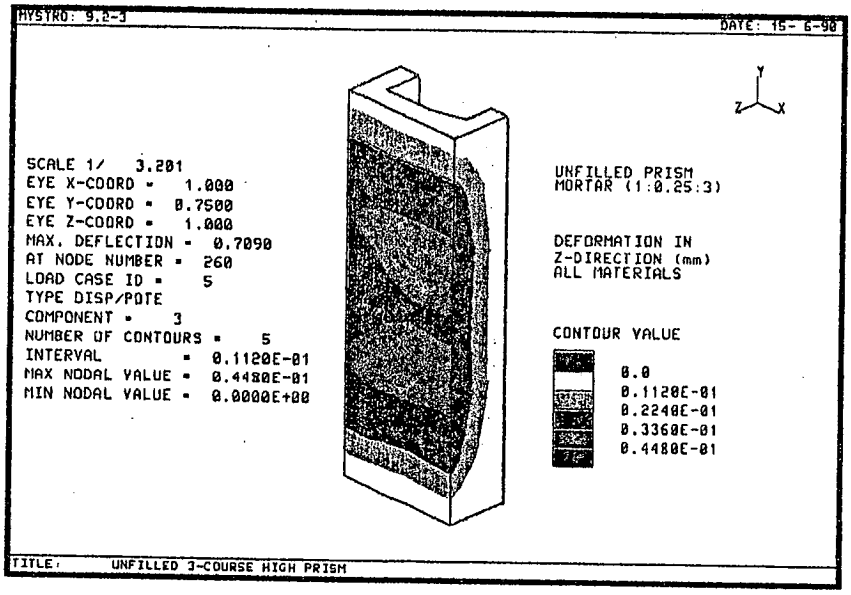

Fig. 5.29 - Deformation of unfilled 3FBP-MJ prism in Z-direction, specific non-linear FEA.

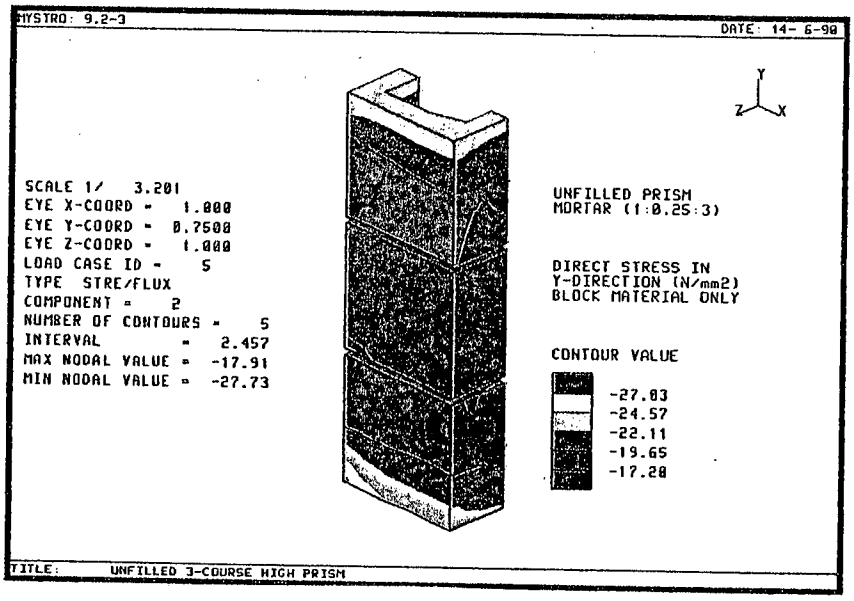

Fig. 5.30 - Direct stress in Y-direction, block material of unfilled 3FBP-MJ prism, specific non-linear FEA.

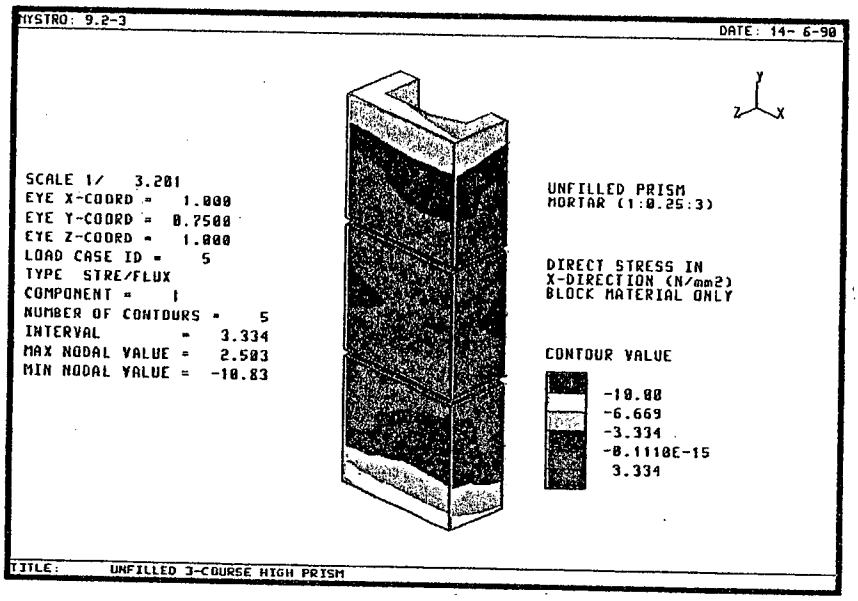

Fig. 5.31 - Direct stress in X-direction, block material of unfilled 3FBP-MJ prism, specific non-linear FEA.

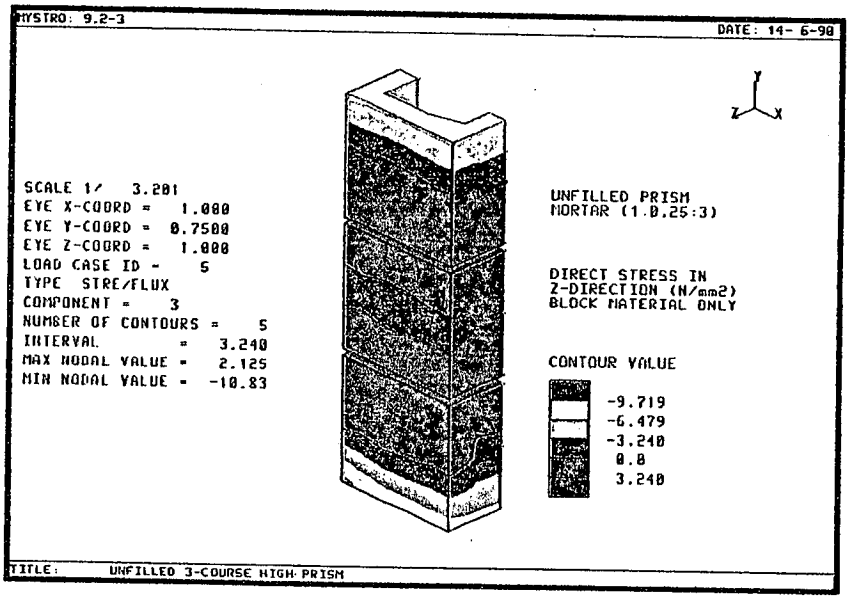

Fig. 5.32 - Direct stress in Z-direction, block material of unfilled 3FBP-MJ prism, specific non-linear FEA.

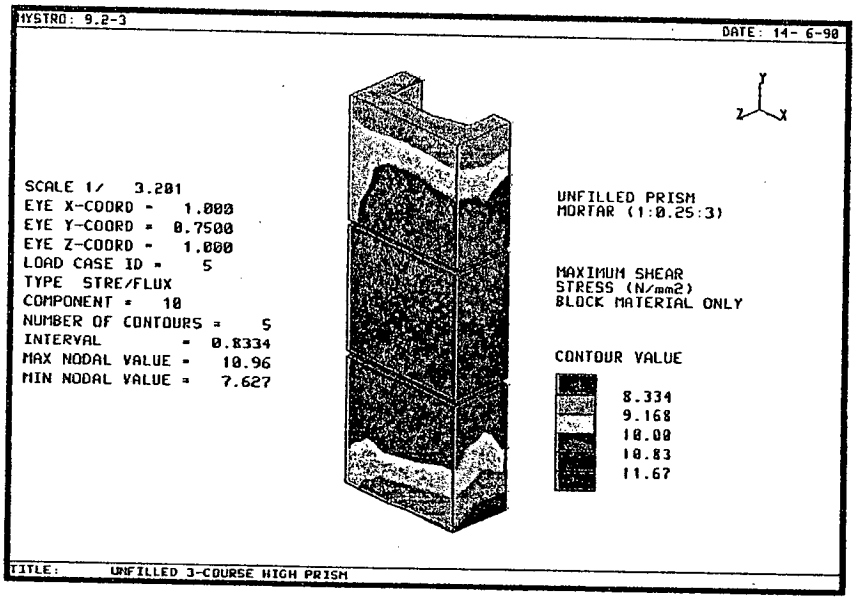

Fig. 5.33 - Maximum shear stress, block material of unfilled 3FBP-MJ prism, specific non-linear FEA.

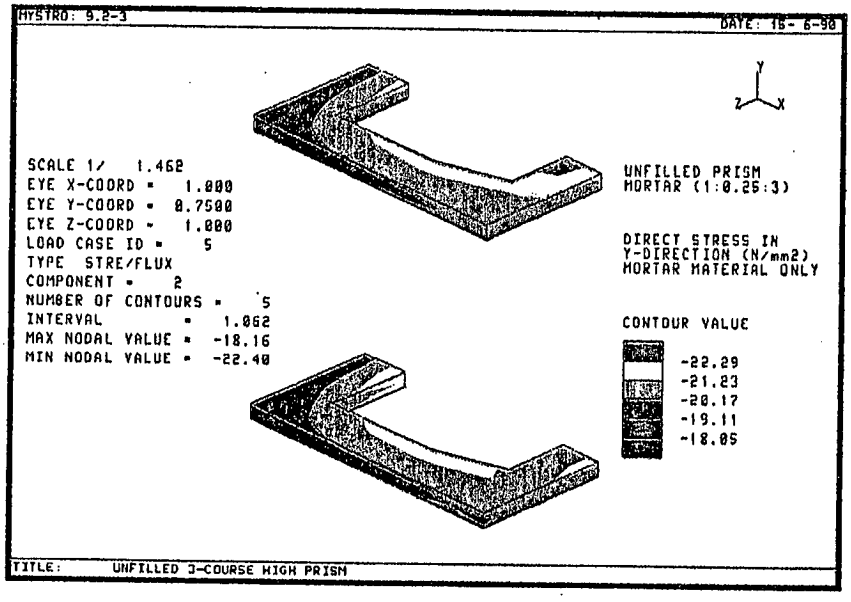

Fig. 5.34 - Direct stress in Y-direction, mortar material of unfilled 3FBP-MJ prism, specific non-linear FEA.

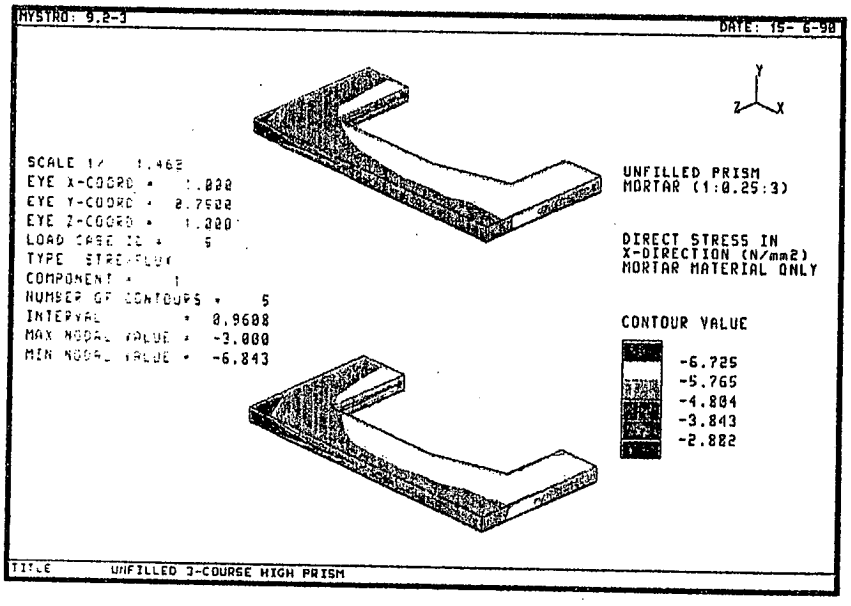

Fig. 5.35 - Direct stress in X-direction, mortar material of unfilled 3FBP-MJ prism, specific non-linear FEA.

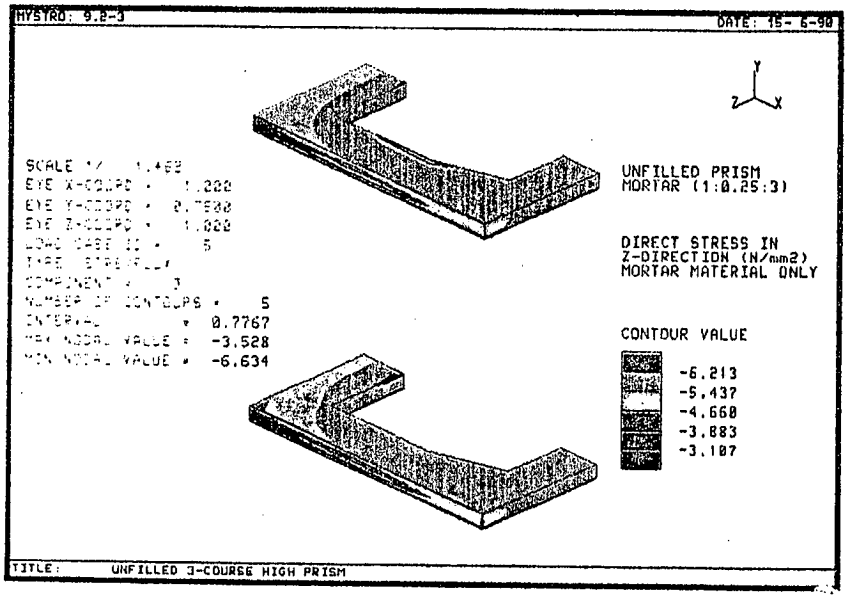

Fig. 5.36 - Direct stress in Z-direction, mortar material of unfilled 3FBP-MJ prism, specific non-linear FEA.

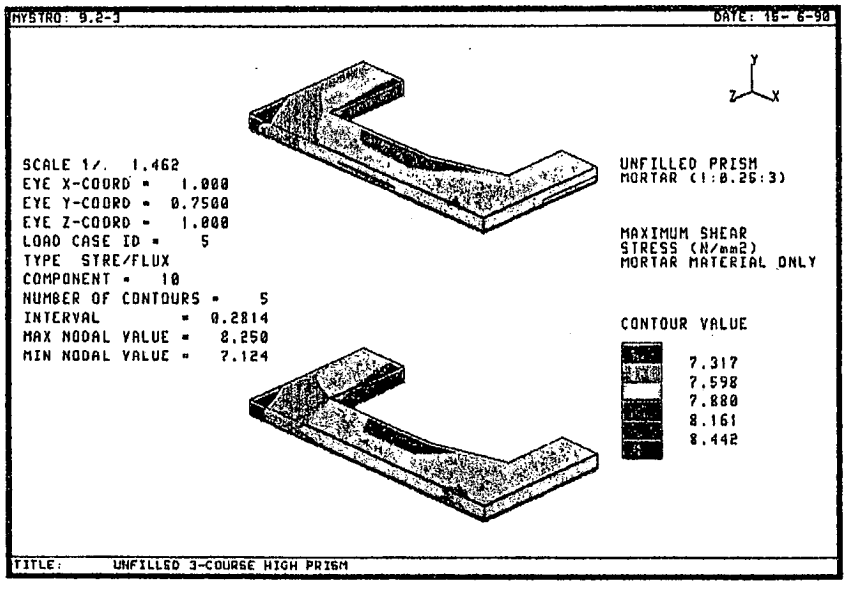

Fig. 5.37 - Maximum shear stress, mortar material of unfilled 3FBP-MJ prism, specific non-linear FEA.

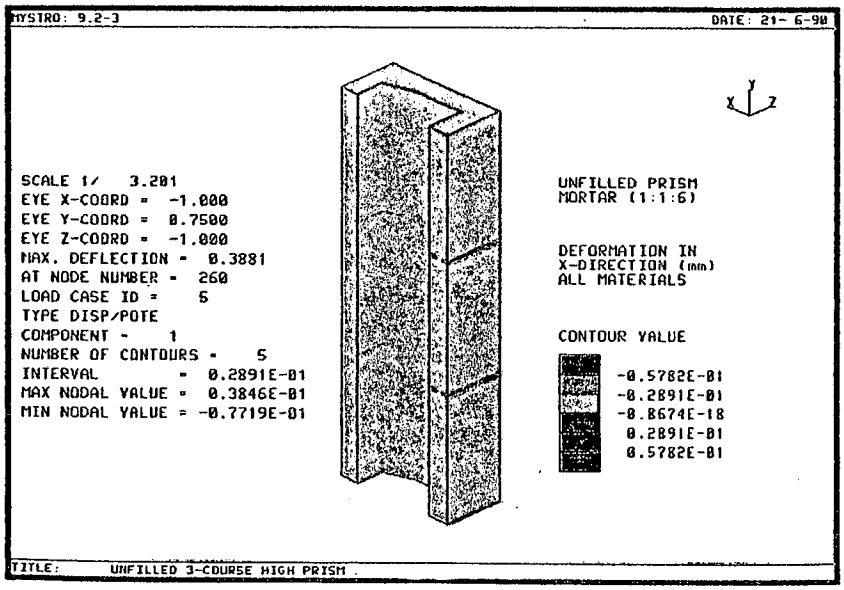

Fig. 5.38 - Deformation of unfilled 3FBP-MJ prism in X-direction, parametric study non-linear FEA, 1:1:6 mortar.

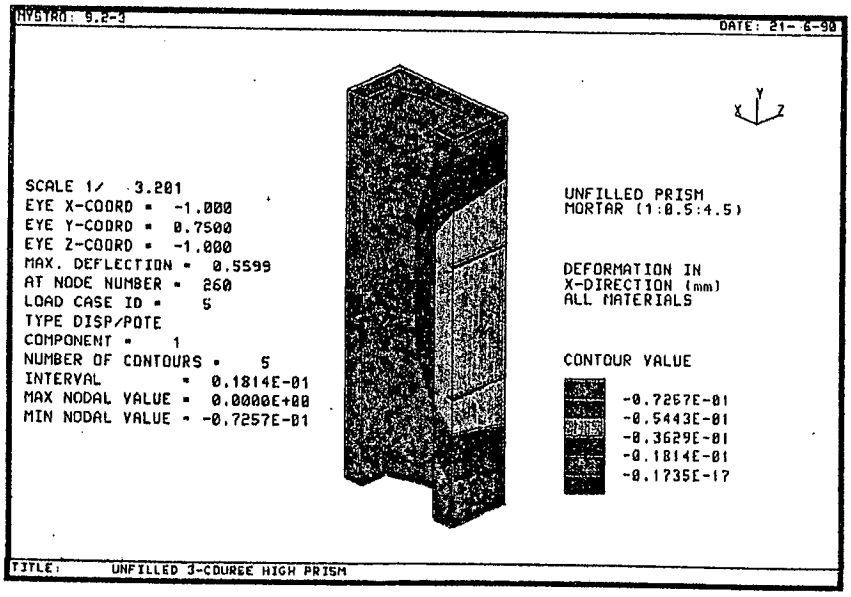

Fig. 5.39 - Deformation of unfilled 3FBP-MJ prism in X-direction, parametric study non-linear FEA, 1:0.5:4.5 mortar.

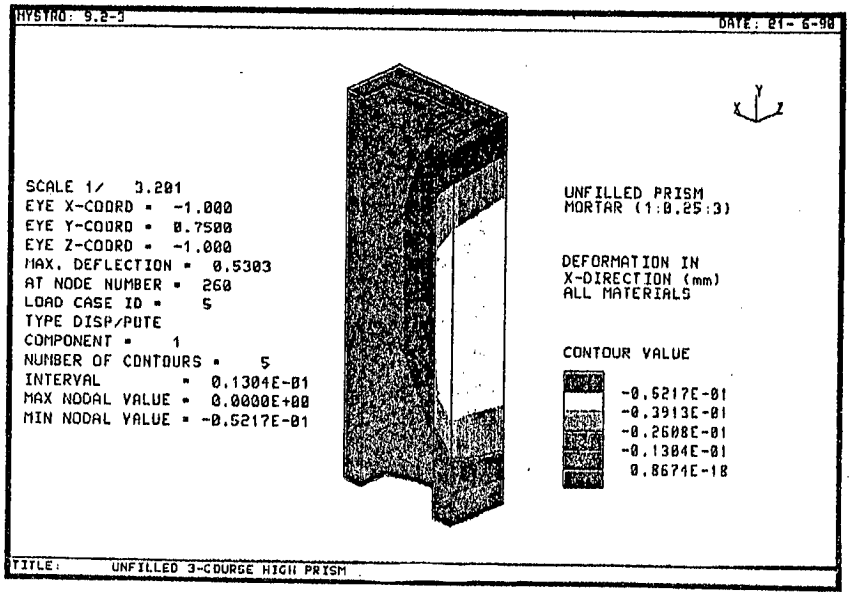

Fig. 5.40 - Deformation of unfilled 3FBP-MJ prism in X-direction, parametric study non-linear FEA, 1:0.25:3 mortar.

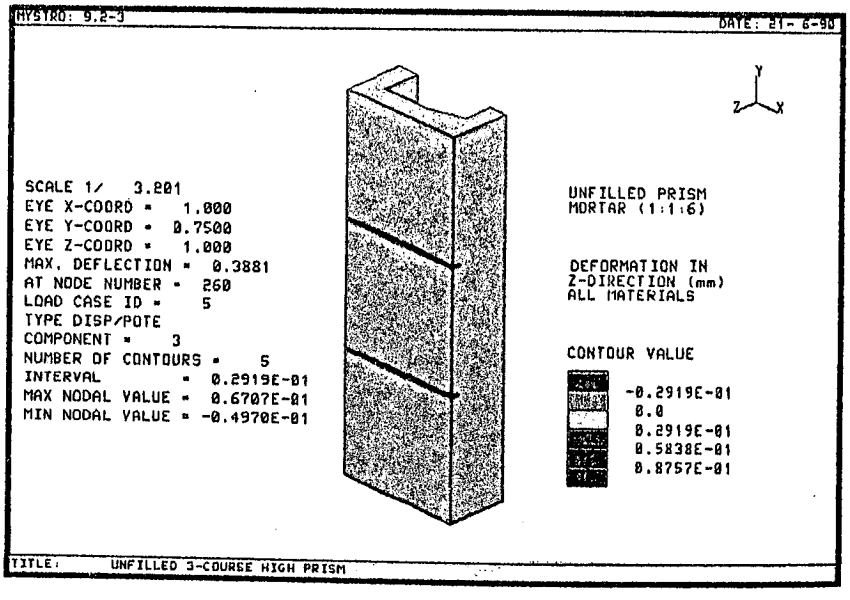

Fig. 5.41 - Deformation of unfilled 3FBP-MJ prism in Z-direction, parametric study non-linear FEA, 1:1:6 mortar.

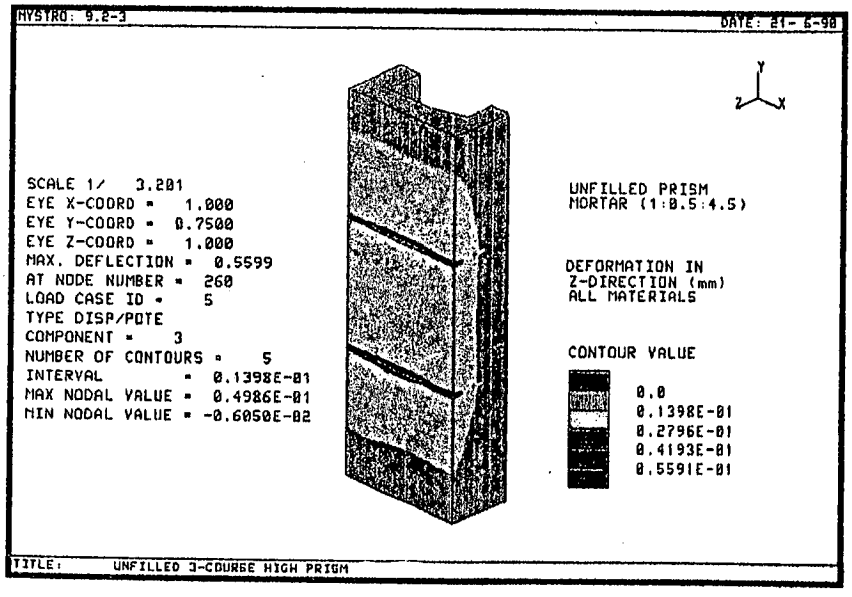

Fig. 5.42 - Deformation of unfilled 3FBP-MJ prism in Z-direction, parametric study non-linear FEA, 1:0.5:4.5 mortar.

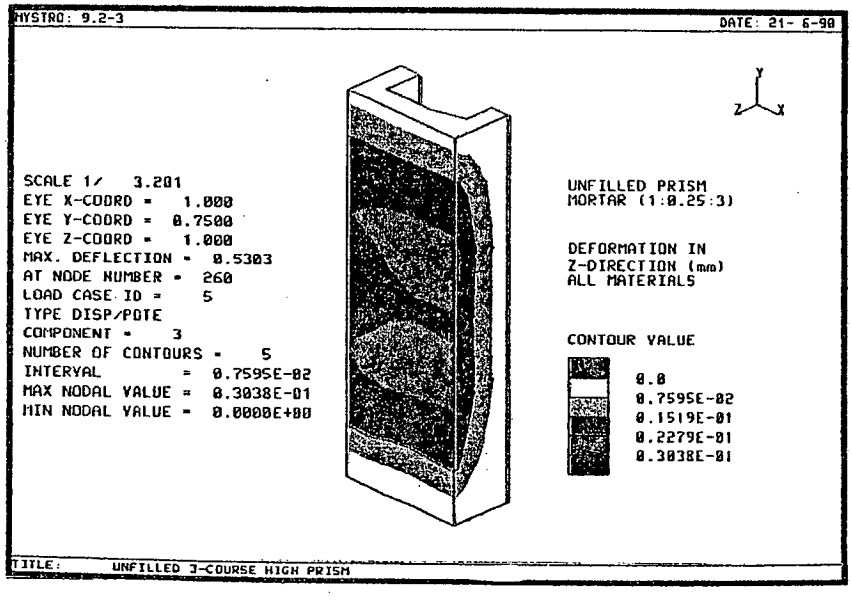

Fig. 5.43 - Deformation of unfilled 3FBP-MJ prism in Z-direction, parametric study non-linear FEA, 1:0.25:3 mortar.

Table 5.4

Deformation results of the parametric study non-linear FEA for unfilled 3FBP-MJ prism.

Prism type	Deformation results * (mm) YD	XD	ZD	Applied stress (N/mm^2)	Prism strength (N/mm^2)	Mortar strength (N/mm^2)
Unfilled (1:1:6)	0.000 -0.430	0.039 -0.077	0.067 -0.050	10.00	10.00	9.19
Unfilled (1:0.5:4.5)	0.000 -0.540	0.000 -0.073	0.050 -0.006	10.00	9.63	15.39
Unfilled (1:0.25:3)	0.000 -0.530	0.000 -0.052	0.030 0.000	10.00	12.01	26.54

* Figures quoted in the table are the upper and lower maximum values of deformation.
YD, XD and ZD = Deformation in the Y-, X- and Z-directions.
+ve values = In the +ve direction of the axes.
-ve values = In the -ve direction of the axes.

Table 5.5

Stress results of the parametric study non-linear FEA for unfilled 3FBP-MJ prism.

Prism type	Stress results * (N/mm^2) YST	XST	ZST	SST	MJST	MST1	MST2
			Block material				
Unfilled (1:1:6)	-11.90 -16.40	2.31 -3.96	2.04 -3.96	7.59 4.96	-11.90 -16.80	1.52 -3.96	2.33 -3.58
Unfilled (1:0.5:4.5)	-15.40 -22.10	2.11 -7.42	2.18 -7.42	9.35 6.72	-15.40 -22.90	1.88 -7.42	2.21 -6.63
Unfilled (1:0.25:3)	-15.40 -21.90	1.63 -7.30	1.38 -7.30	9.01 6.73	-15.40 -22.60	1.08 -7.32	1.90 -6.53
			Mortar material				
Unfilled (1:1:6)	-7.62 -17.40	-2.48 -13.50	-3.35 -13.50	4.28 1.90	-7.62 -19.40	-4.52 -13.50	-2.46 -11.50
Unfilled (1:0.5:4.5)	-13.50 -19.90	-4.14 -11.50	-4.90 -11.40	5.64 3.91	-13.50 -21.10	-6.19 -11.40	-4.12 -10.30
Unfilled (1:0.25:3)	-15.10 -18.50	-2.55 -4.89	-2.81 -4.79	7.27 5.78	-15.10 -18.80	-3.49 -4.80	-2.53 -4.68

* Figures quoted in the table are the upper and lower values of stress.

YST, XST and ZST = Direct stress in the Y-, X- and Z-directions.

SST = Maximum shear stress.

MJST, MST1 and MST2 = Major, minor 1 and 2 principal stresses.

+ve values = Tension.

-ve values = Compression.

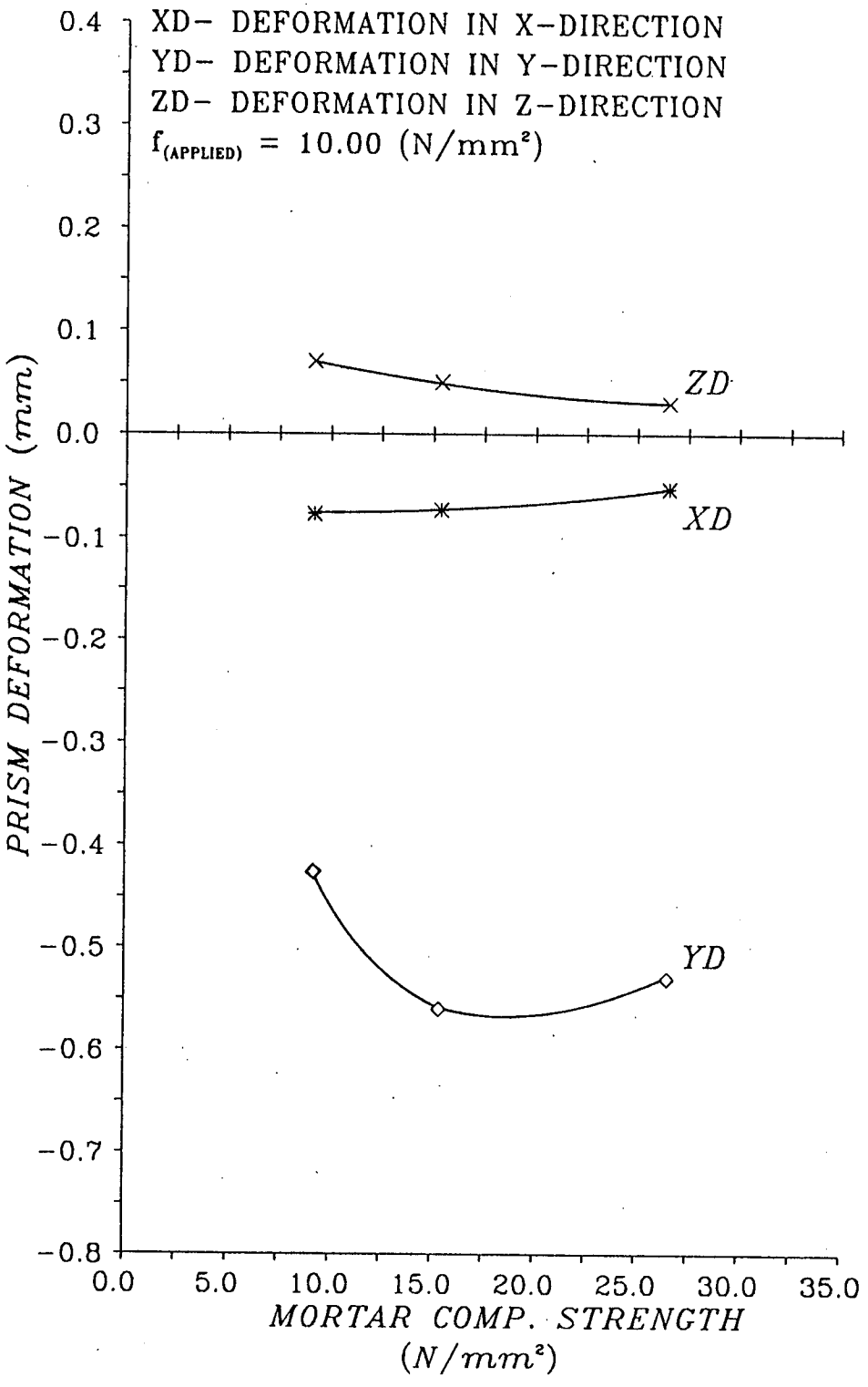

Fig. 5.44 - Effect of mortar strength on unfilled 3FBP-MJ prism Deformation, parametric study non-linear FEA.

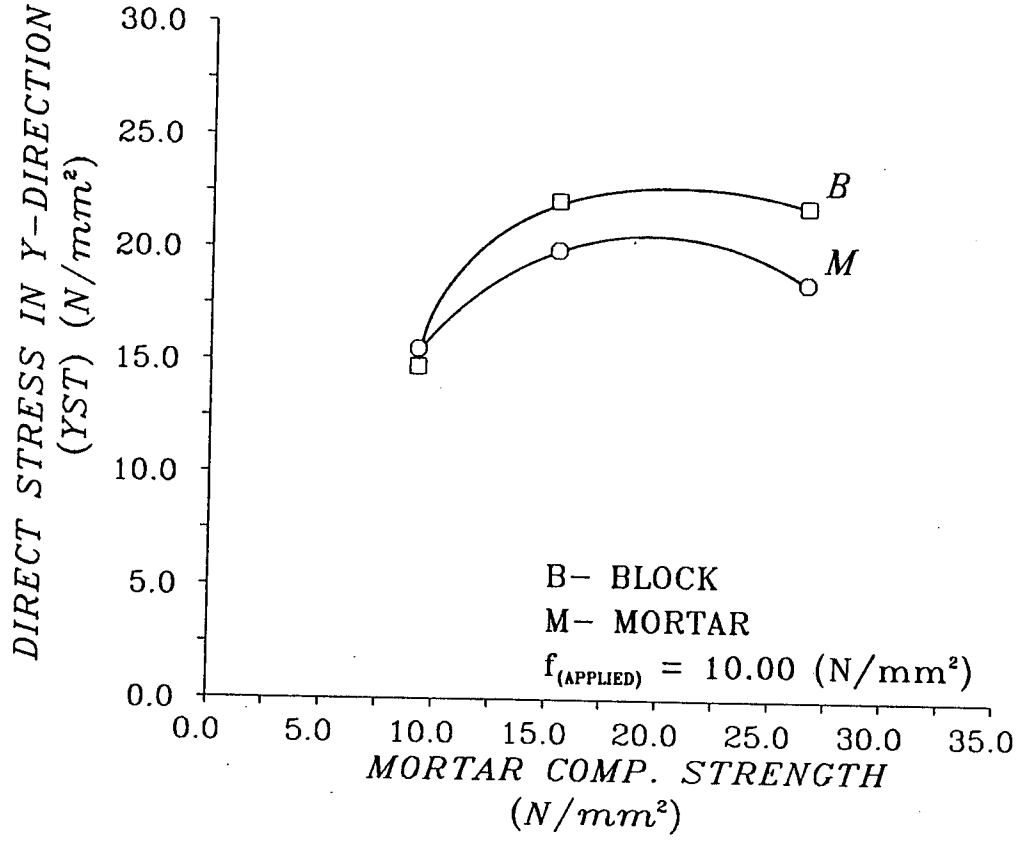

Fig. 5.45 - Effect of mortar strength on unfilled 3FBP-MJ prism direct stress in Y-direction, parametric study non-linear FEA.

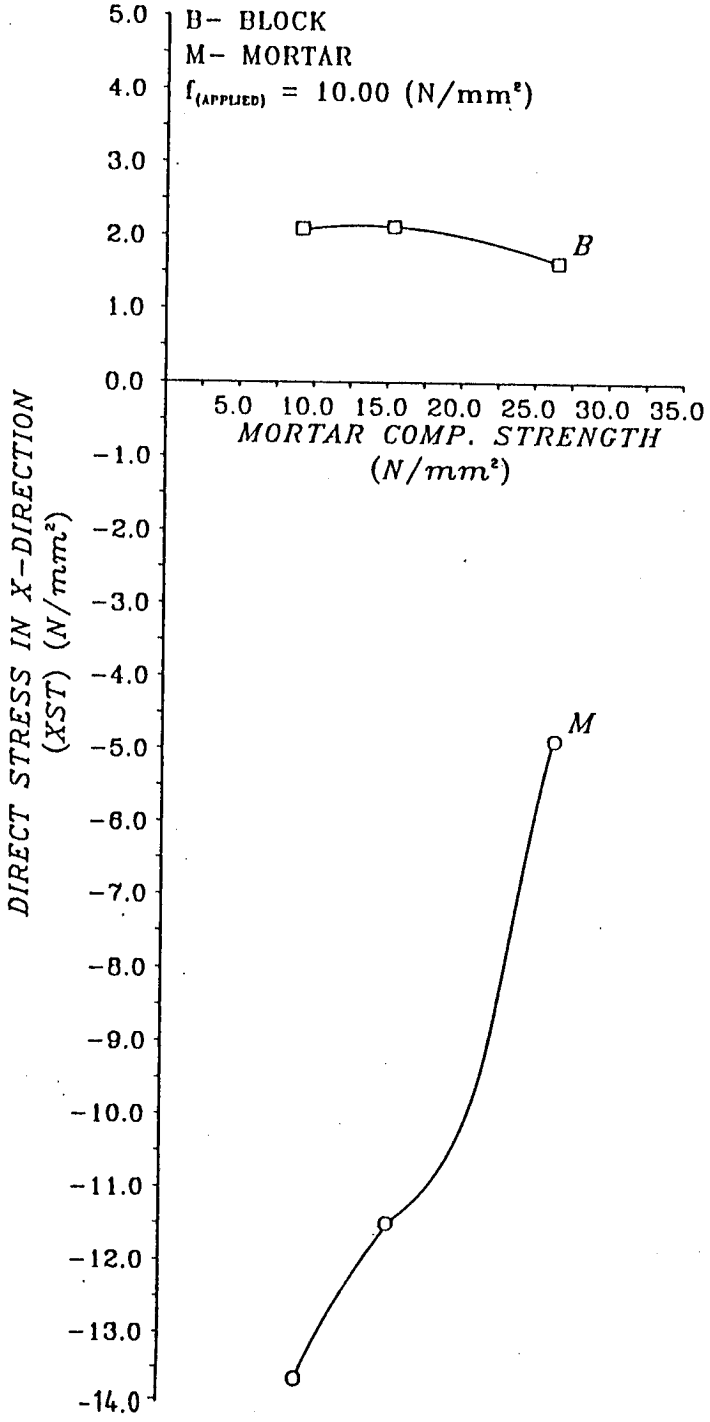

Fig. 5.46 - Effect of mortar strength on unfilled 3FBP-MJ prism direct stress in X-direction, parametric study non-linear FEA.

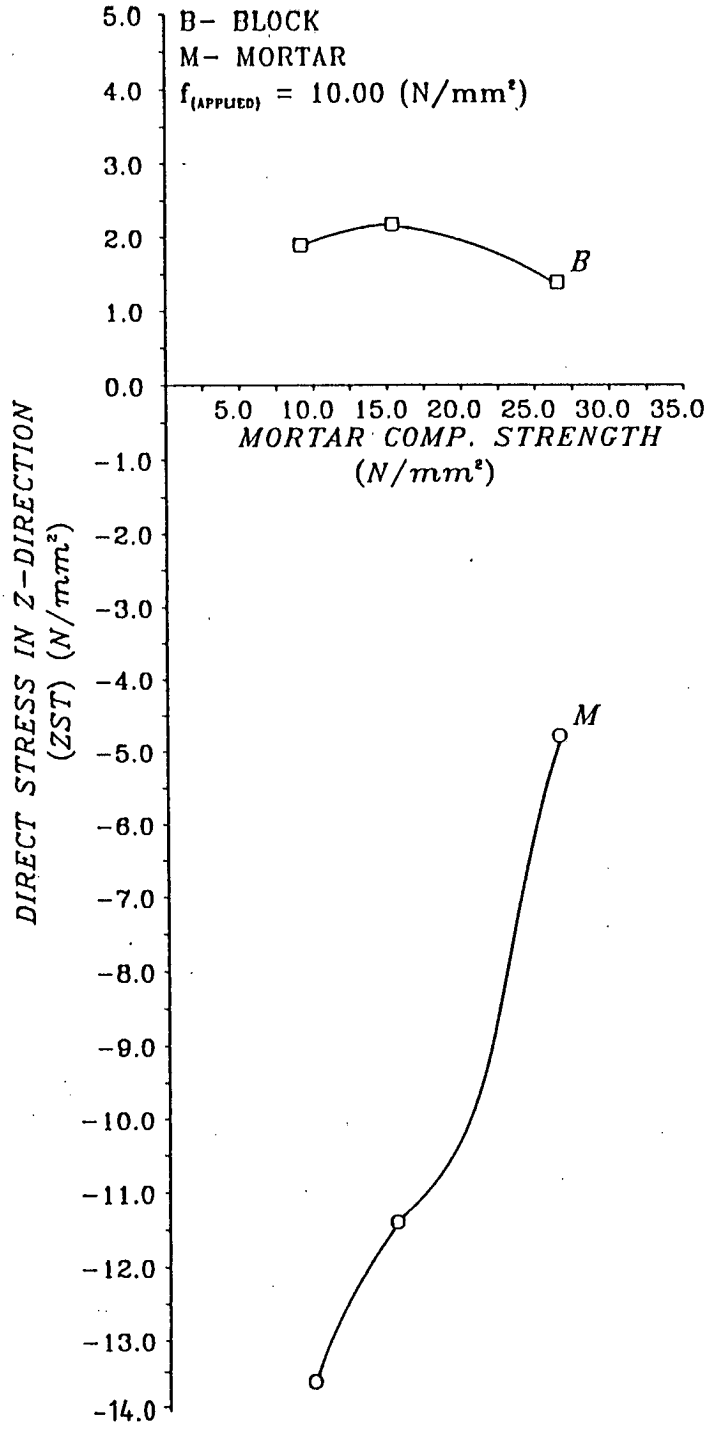

Fig. 5.47 - Effect of mortar strength on unfilled 3FBP-MJ prism direct stress in Z-direction, parametric study non-linear FEA.

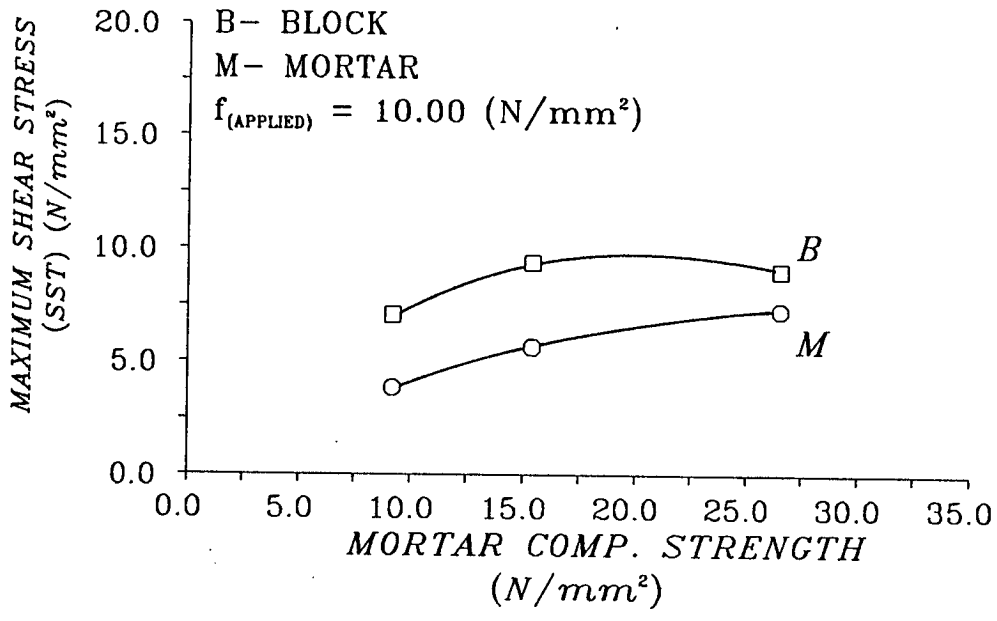

Fig. 5.48 - Effect of mortar strength on unfilled 3FBP-MJ prism maximum shear stress, parametric study non-linear FEA.

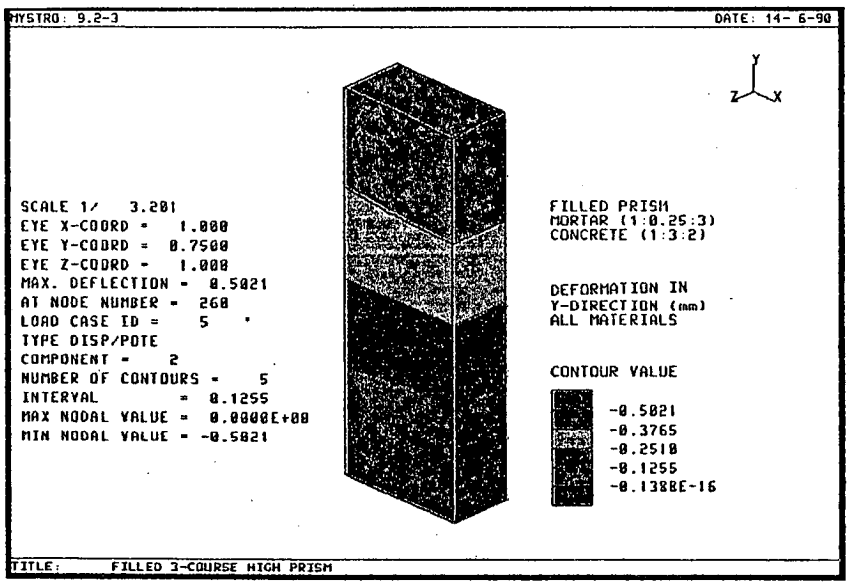

Fig. 5.49 - Deformation of filled 3FBP-MJ prism in Y-direction, specific non-linear FEA.

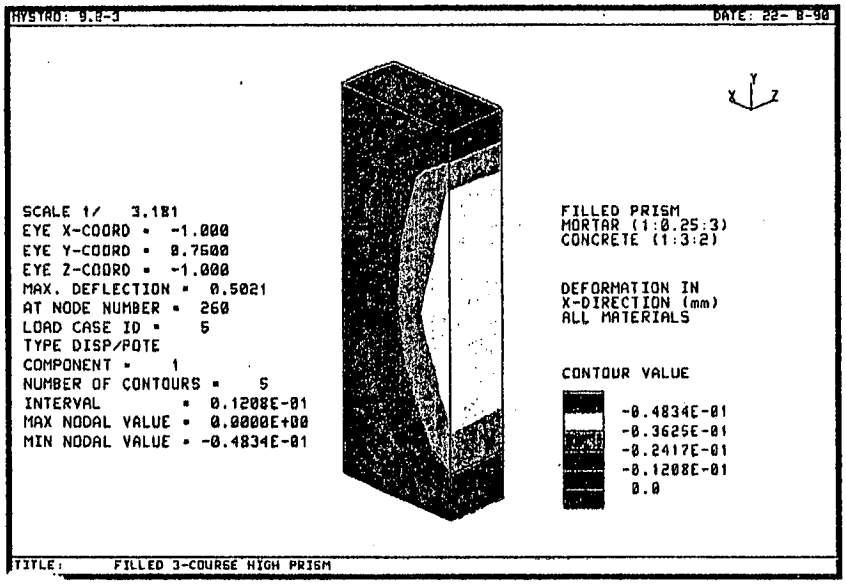

Fig. 5.50 - Deformation of filled 3FBP-MJ prism in X-direction, specific non-linear FEA.

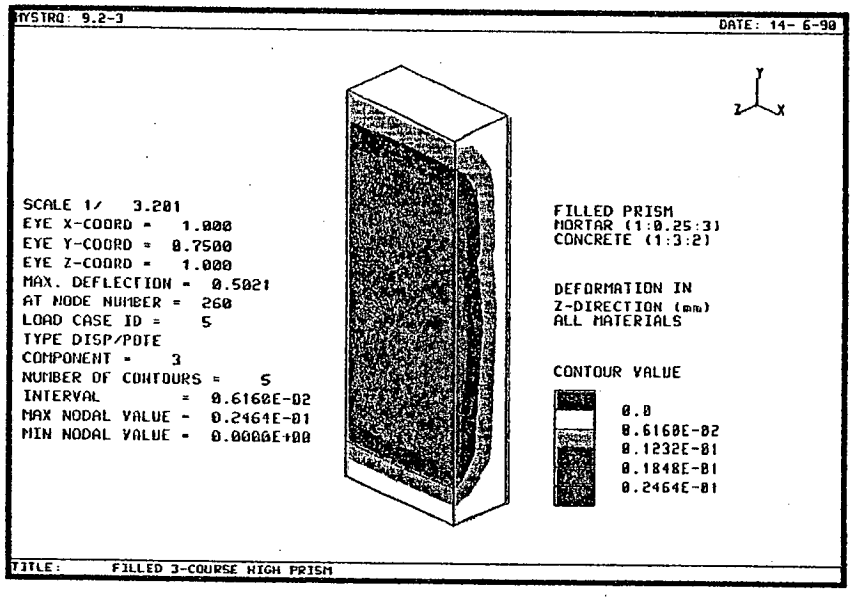

Fig. 5.51 - Deformation of filled 3FBP-MJ prism in Z-direction, specific non-linear FEA.

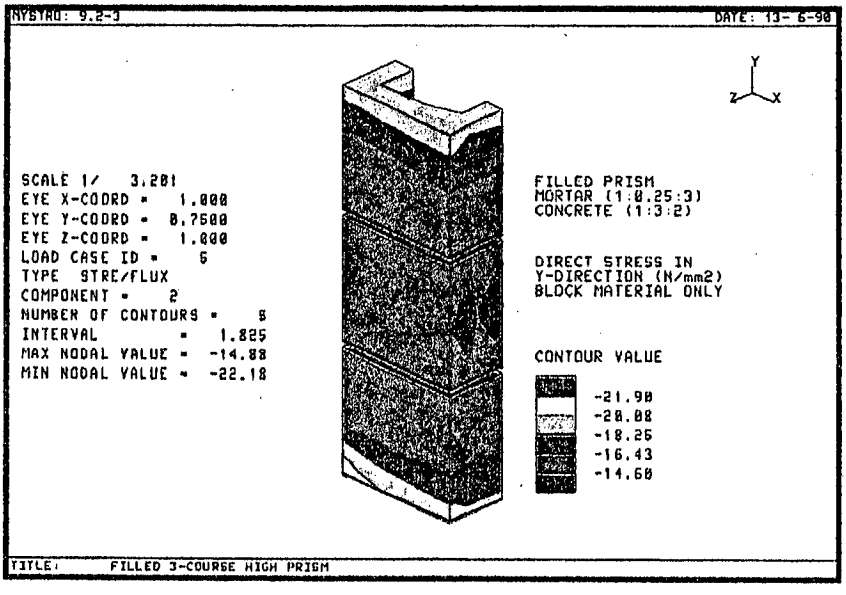

Fig. 5.52 - Direct stress in Y-direction, block material of filled 3FBP-MJ prism, specific non-linear FEA.

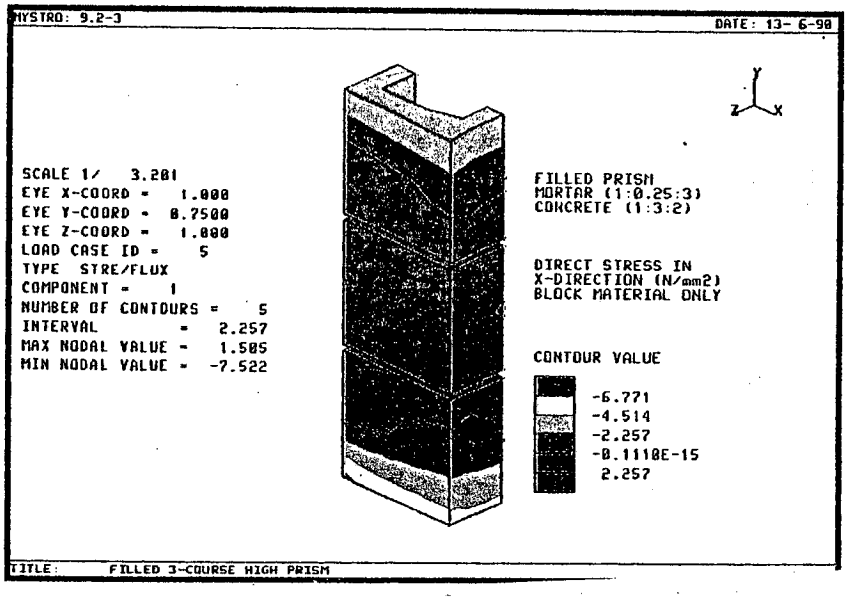

Fig. 5.53 - Direct stress in X-direction, block material of filled 3FBP-MJ prism, specific non-linear FEA.

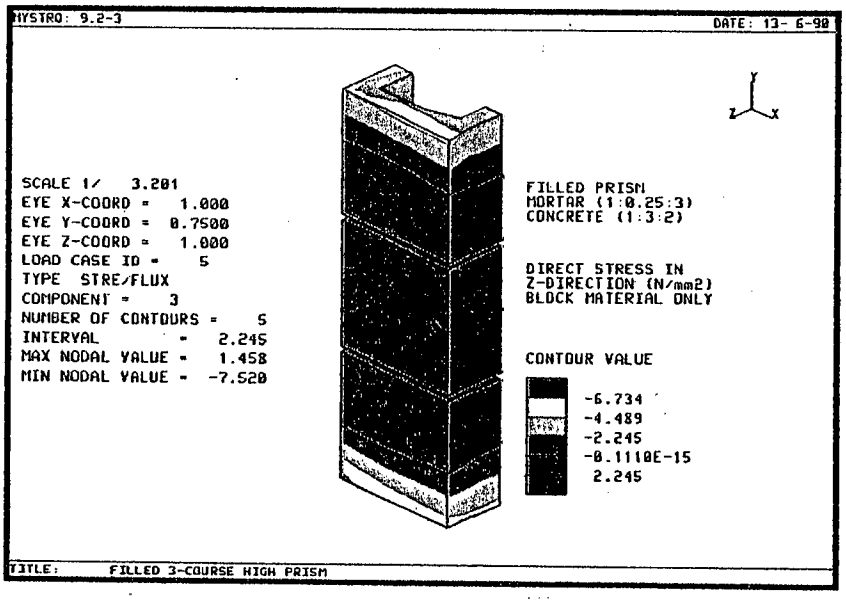

Fig. 5.54 - Direct stress in Z-direction, block material of filled 3FBP-MJ prism, specific non-linear FEA.

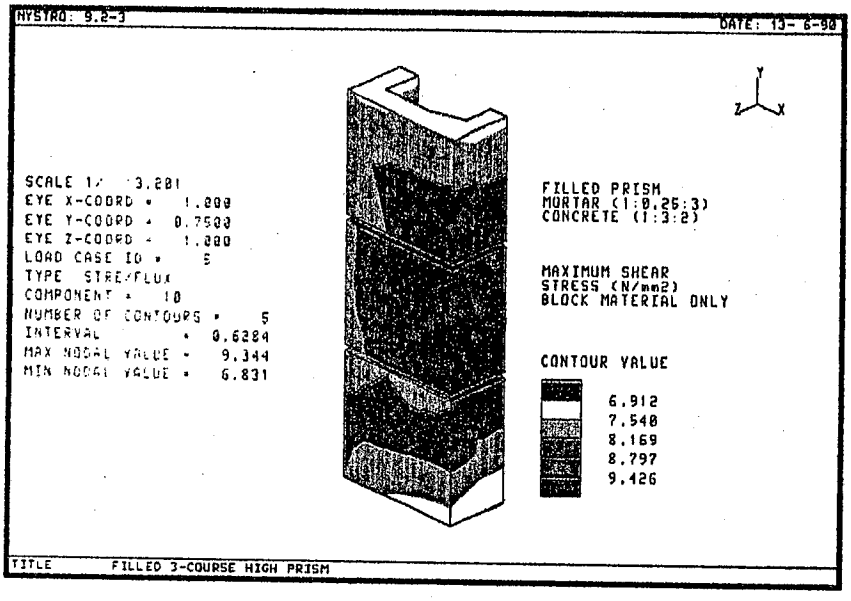

Fig. 5.55 - Maximum shear stress, block material of filled 3FBP-MJ prism, specific non-linear FEA.

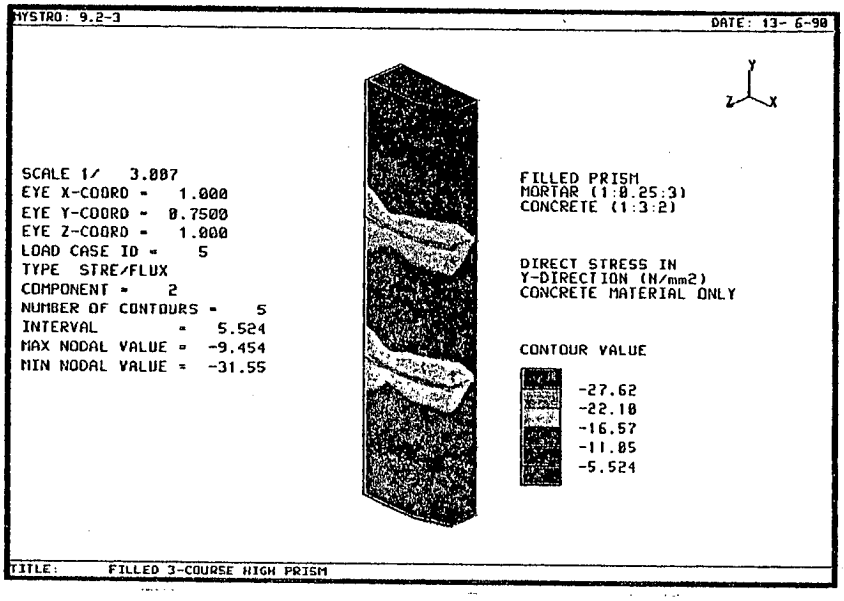

Fig. 5.56 - Direct stress in Y-direction, concrete material of filled 3FBP-MJ prism, specific non-linear FEA.

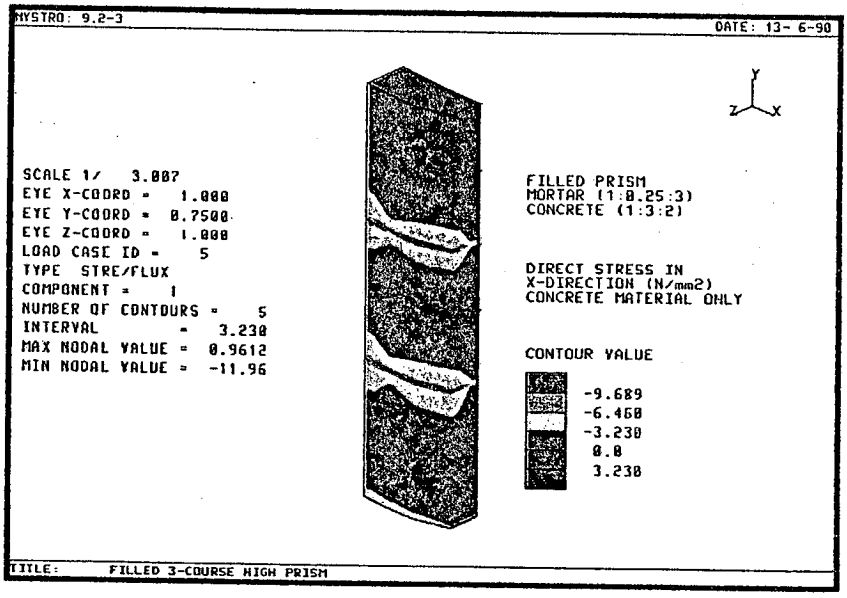

Fig. 5.57 - Direct stress in X-direction, concrete material of filled 3FBP-MJ prism, specific non-linear FEA.

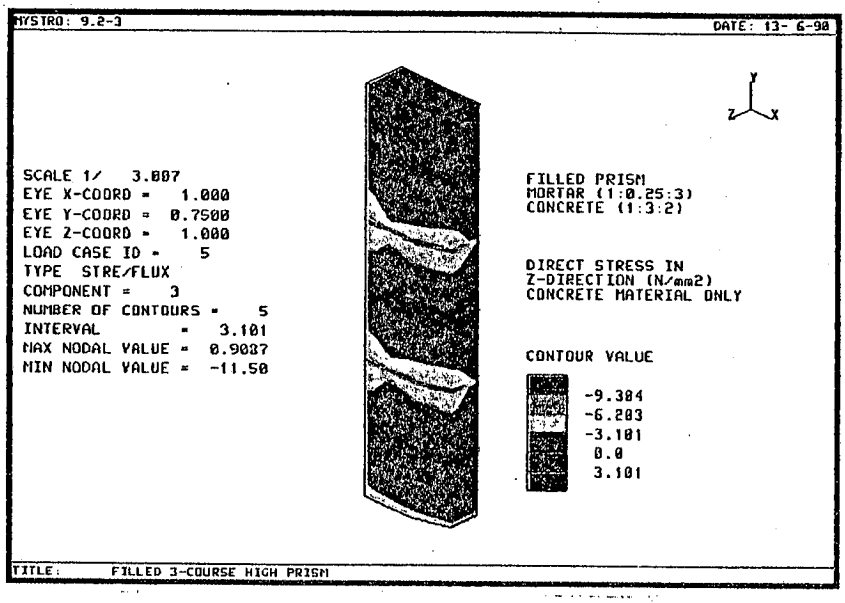

Fig. 5.58 - Direct stress in Z-direction, concrete material of filled 3FBP-MJ prism, specific non-linear FEA.

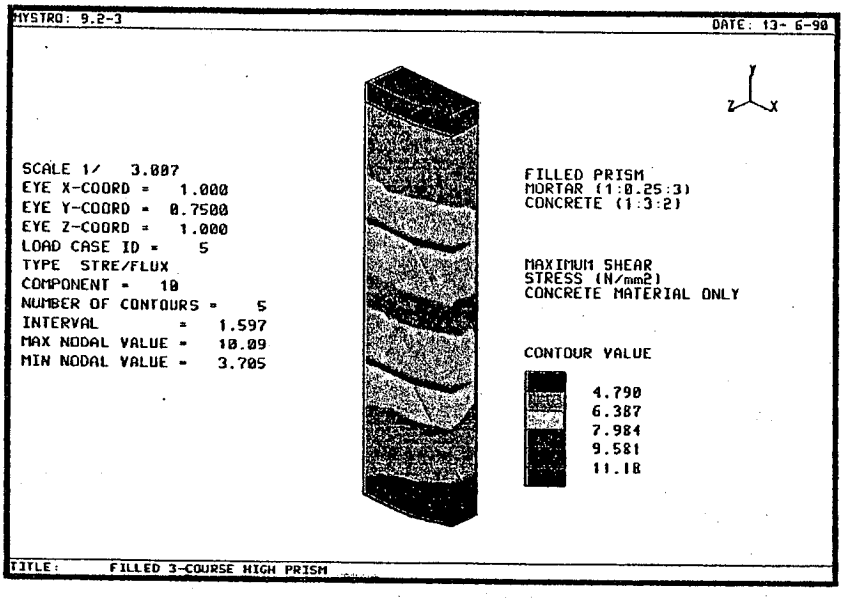

Fig. 5.59 - Maximum shear stress, concrete material of filled 3FBP-MJ prism, specific non-linear FEA.

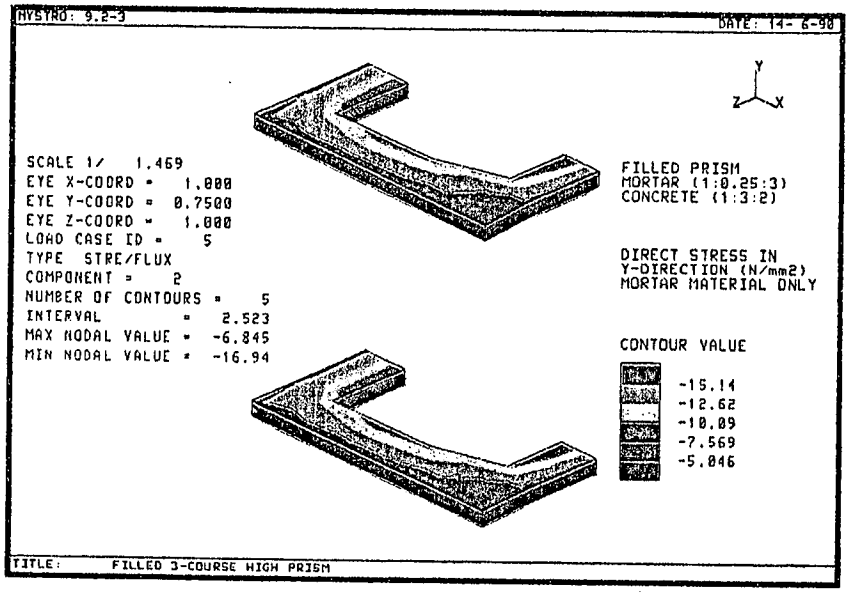

Fig. 5.60 - Direct stress in Y-direction, mortar material of filled 3FBP-MJ prism, specific non-linear FEA.

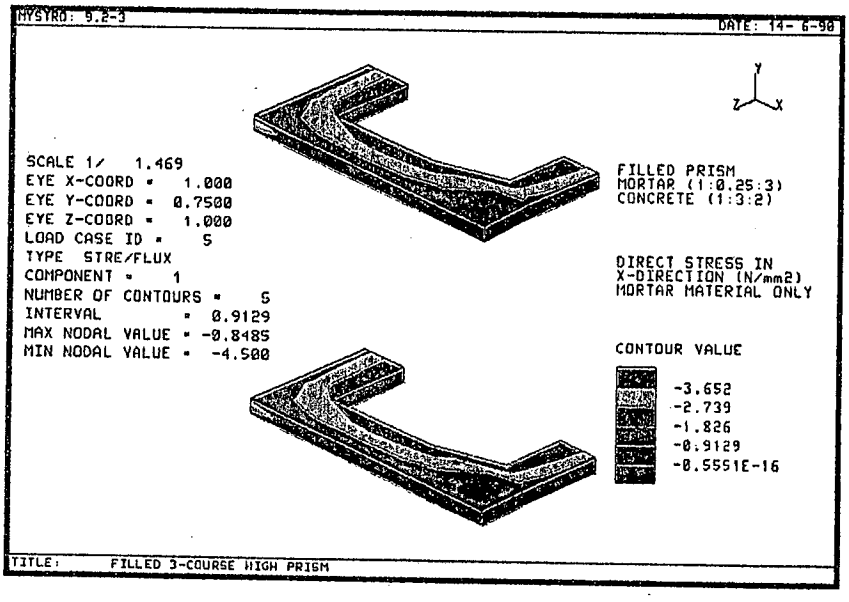

Fig. 5.61 - Direct stress in X-direction, mortar material of filled 3FBP-MJ prism, specific non-linear FEA.

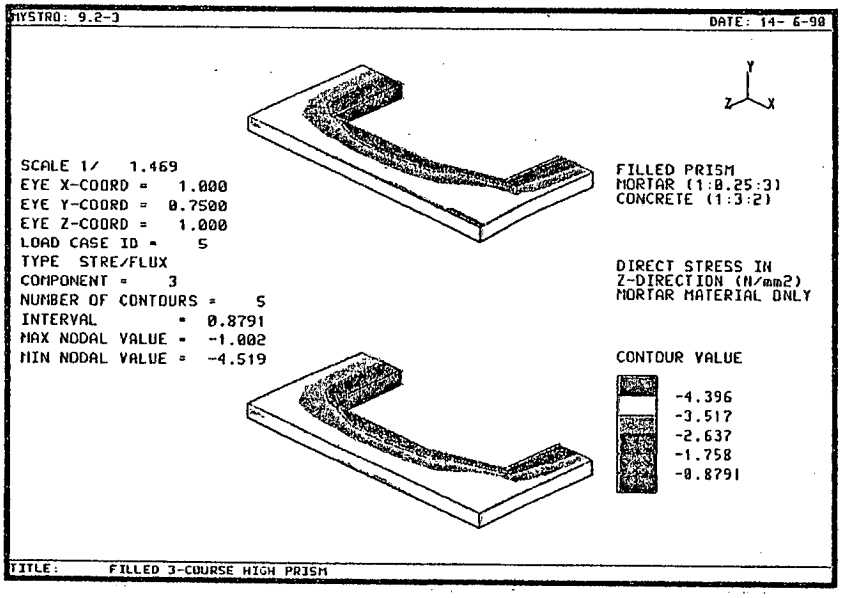

Fig. 5.62 - Direct stress in Z-direction, mortar material of filled 3FBP-MJ prism, specific non-linear FEA.

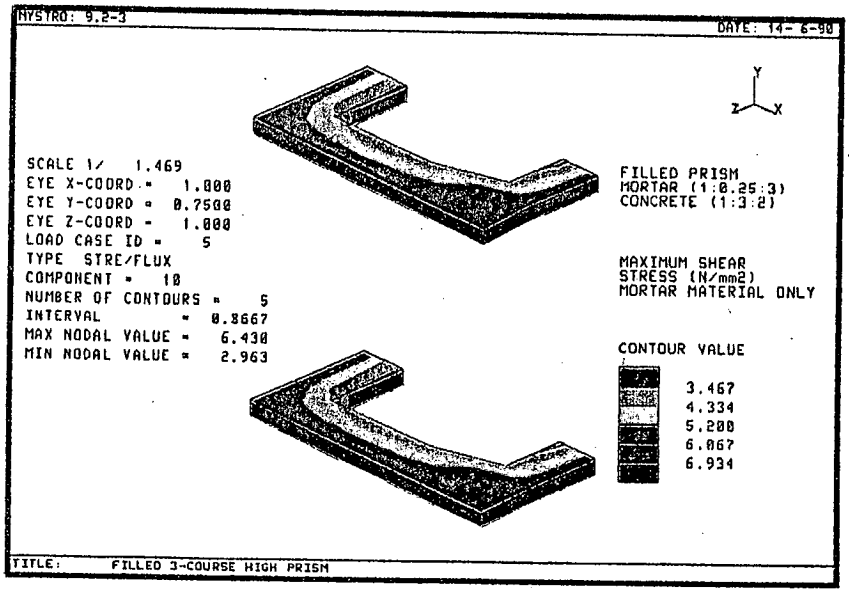

Fig. 5.63 - Maximum shear stress, mortar material of filled 3FBP-MJ prism, specific non-linear FEA.

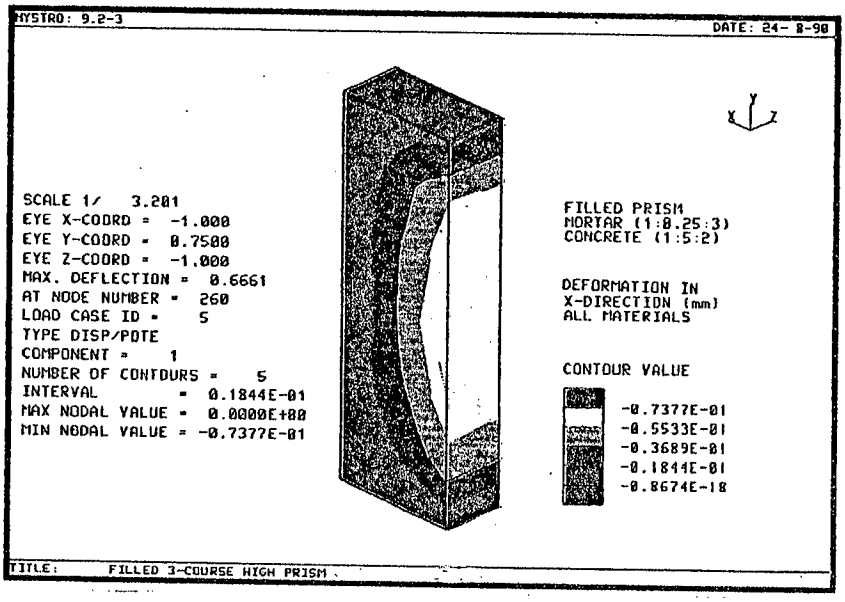

Fig. 5.64 - Deformation of filled 3FBP-MJ prism in X-direction, parametric study non-linear FEA, 1:5:2 concrete.

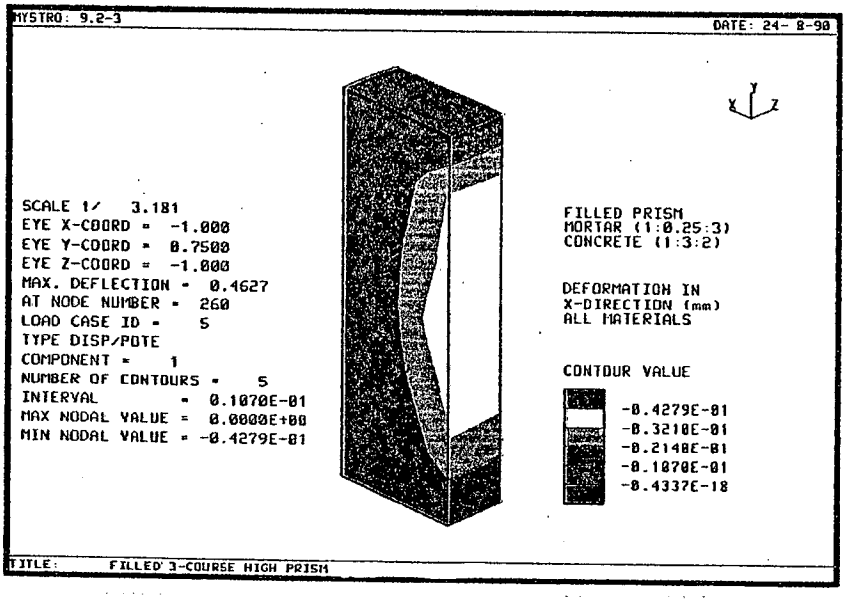

Fig. 5.65 - Deformation of filled 3FBP-MJ prism in X-direction, parametric study non-linear FEA, 1:3:2 concrete.

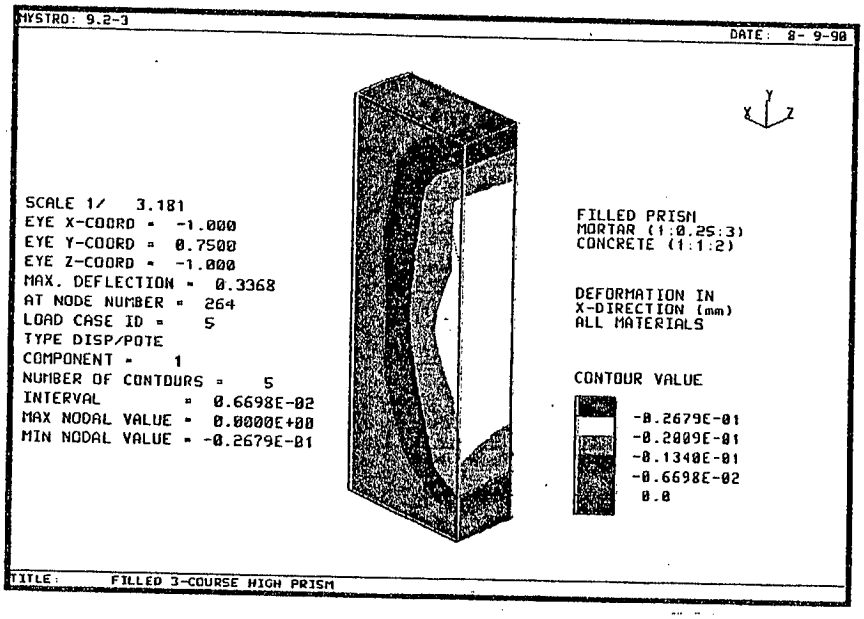

Fig. 5.66 - Deformation of filled 3FBP-MJ prism in X-direction, parametric study non-linear FEA, 1:1:2 concrete.

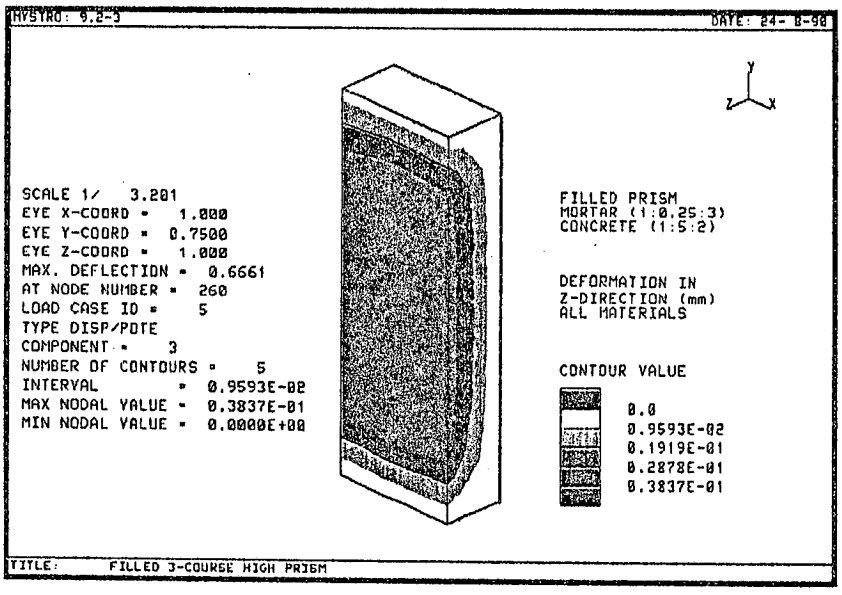

Fig. 5.67 - Deformation of filled 3FBP-MJ prism in Z-direction, parametric study non-linear FEA, 1:5:2 concrete.

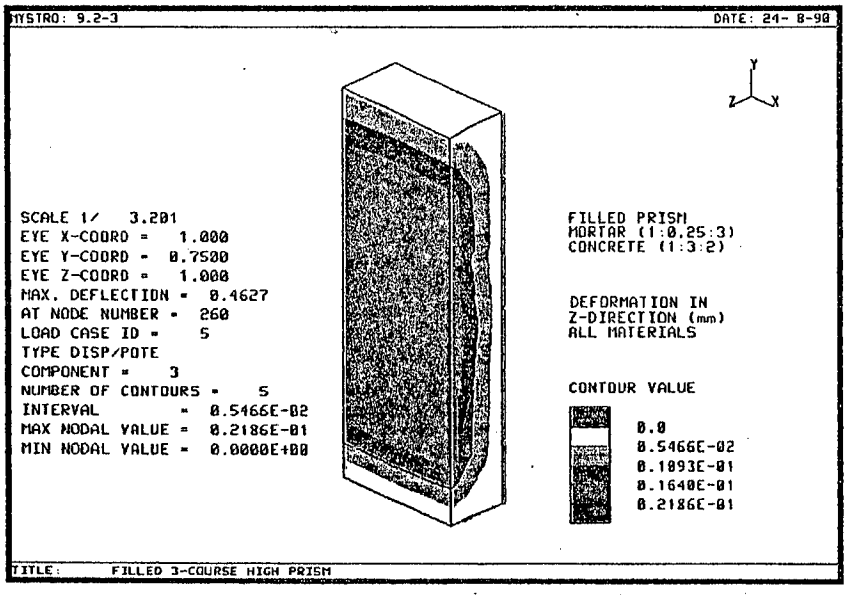

Fig. 5.68 - Deformation of filled 3FBP-MJ prism in Z-direction, parametric study non-linear FEA, 1:3:2 concrete.

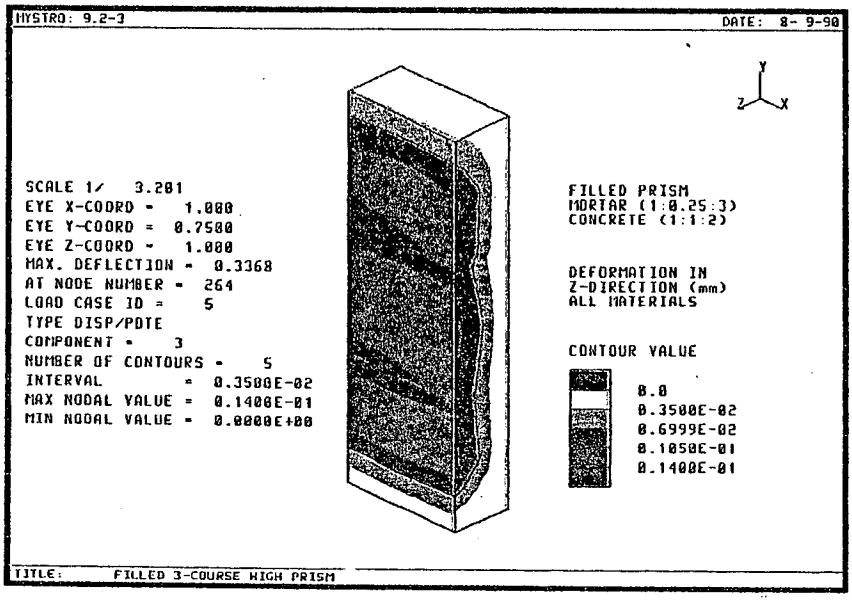

Fig. 5.69 - Deformation of filled 3FBP-MJ prism in Z-direction, parametric study non-linear FEA, 1:1:2 concrete.

Table 5.6

Deformation results of the parametric study non-linear FEA for filled 3FBP-MJ prism.

Prism type	Deformation results * (mm) YD	XD	ZD	Applied stress (N/mm^2)	Prism strength (N/mm^2)	Infill strength (N/mm^2)
Filled (1:5:2)	0.000 -0.570	0.000 -0.074	0.038 0.000	13.85	13.85	9.89
Filled (1:3:2)	0.000 -0.460	0.000 -0.043	0.022 0.000	13.85	14.53	28.75
Filled (1:1:2)	0.000 -0.340	0.000 -0.027	0.014 0.000	13.85	19.29	34.02

* Figures quoted in the table are the upper and lower maximum values of deformation.
YD, XD and ZD = Deformation in the Y-, X- and Z-directions.
+ve values = In the +ve direction of the axes.
-ve values = In the -ve direction of the axes.

Table 5.7

Stress results of the Parametric study non-linear FEA for filled 3FBP-MJ prism.

Prism type	Stress results * (N/mm^2) YST	XST	ZST	SST	MJST	MST1	MST2
			Block material				
Filled	-15.90	1.79	2.17	10.10	-15.90	1.27	2.19
(1:5:2)	-24.10	-8.72	-8.72	7.05	-25.20	-8.71	-7.67
Filled	-14.20	1.36	1.38	8.91	-14.20	1.06	1.67
(1:3:2)	-20.90	-6.72	-6.72	6.65	-21.60	-6.72	-5.98
Filled	-11.50	1.36	1.60	7.52	-11.51	0.93	1.65
(1:1:2)	-16.80	-4.28	-4.28	5.25	-17.30	-4.28	-3.80
			Concrete material				
Filled	-3.19	0.42	0.51	3.97	-3.19	0.41	0.55
(1:5:2)	-16.70	-8.97	-8.82	1.23	-16.70	-8.97	-8.81
Filled	-8.97	0.95	0.89	9.68	-8.97	0.79	1.26
(1:3:2)	-30.30	-11.50	-11.00	3.46	-30.30	-11.60	-10.90
Filled	-12.30	1.14	1.24	13.90	-12.30	0.97	1.40
(1:1:2)	-39.60	-12.50	-11.90	5.01	-39.70	-12.60	-11.80
			Mortar material				
Filled	-10.00	-1.66	-1.61	6.98	-10.00	-1.67	-1.60
(1:5:2)	-18.30	-4.59	-4.69	4.20	-18.40	-4.62	-4.52
Filled	-6.41	-0.85	-1.02	6.02	-6.41	-1.02	-0.85
(1:3:2)	-16.00	-4.34	-4.28	2.75	-16.10	-4.34	-4.28
Filled	-3.68	-0.47	-0.60	4.84	-3.68	-0.60	-0.46
(1:1:2)	-13.10	-3.69	-3.77	1.59	-13.10	-3.70	-3.68

* Figures quoted in the table are the upper and lower values of stress.

YST, XST and ZST = Direct stress in the Y-, X- and Z-directions.

SST = Maximum shear stress.

MJST, MST1 and MST2 = Major, minor 1 and 2 principal stresses.

+ve values = Tension.

-ve values = Compression.

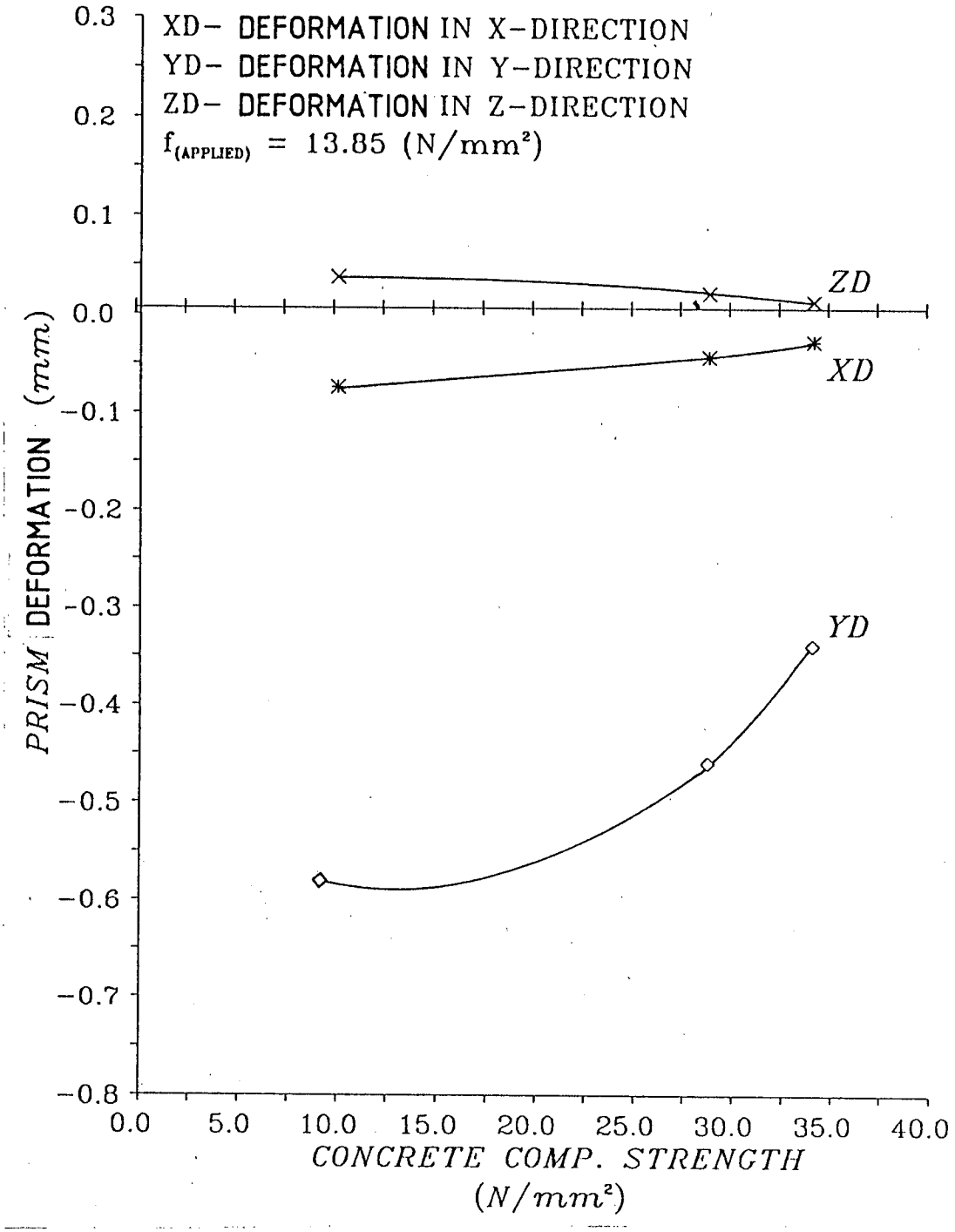

Fig. 5.70 - Effect of concrete infill strength on filled 3FBP-MJ prism deformation, parametric study non-linear FEA.

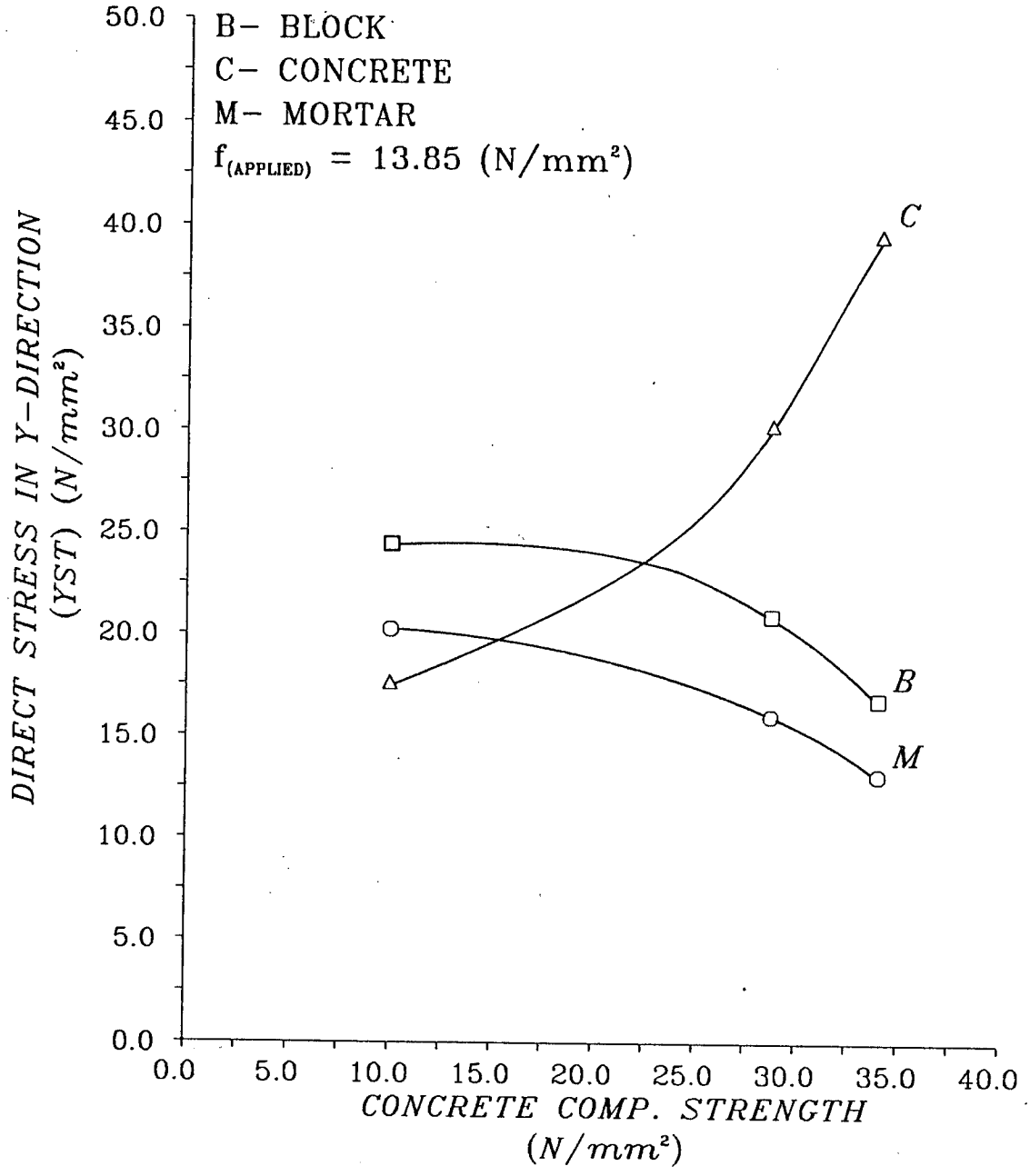

Fig. 5.71 - Effect of concrete infill strength on filled 3FBP-MJ prism direct stress in Y-direction, parametric study non-linear FEA.

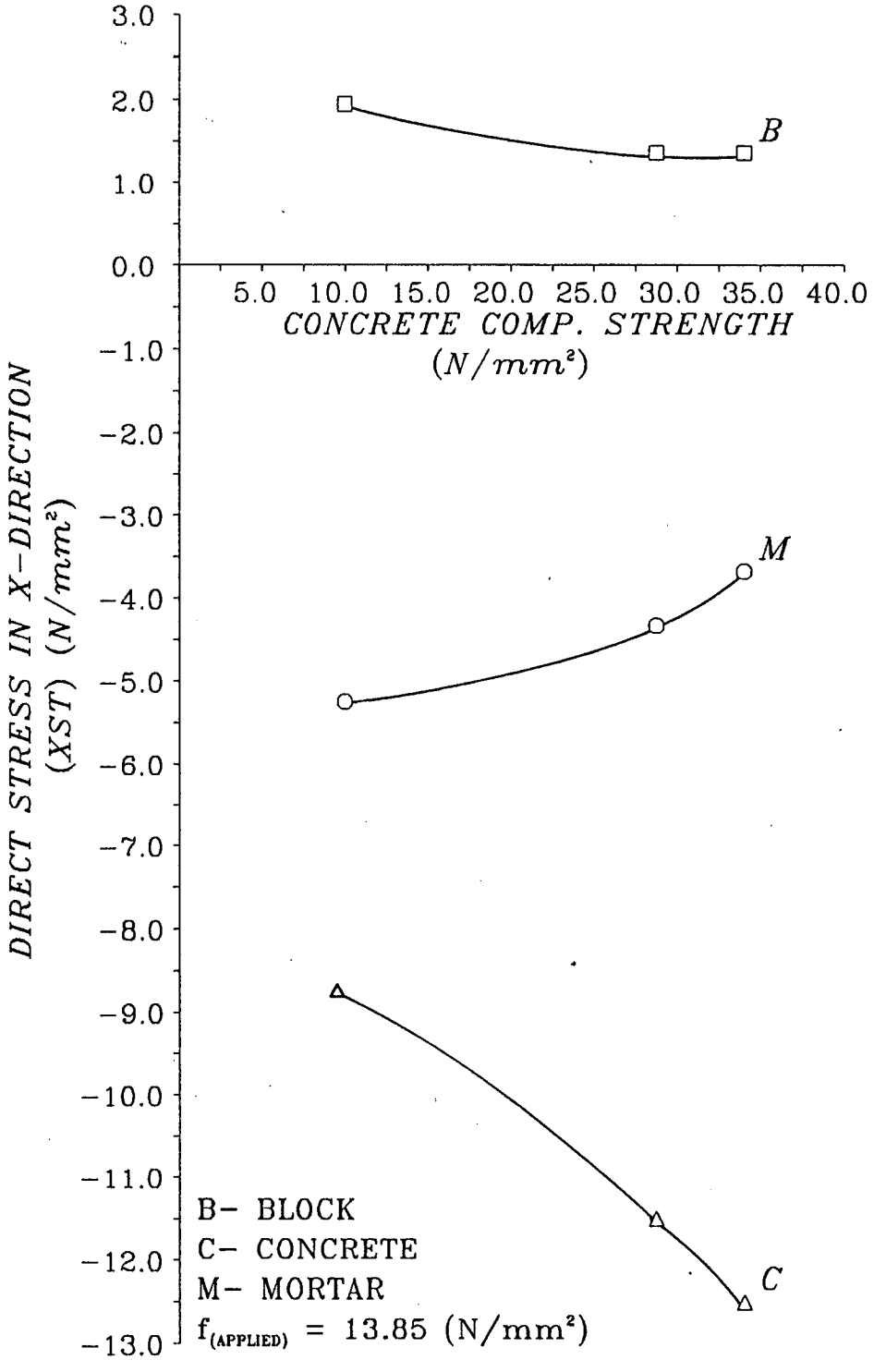

Fig. 5.72 - Effect of concrete infill strength on filled 3FBP-MJ prism direct stress in X-direction, parametric study non-linear FEA.

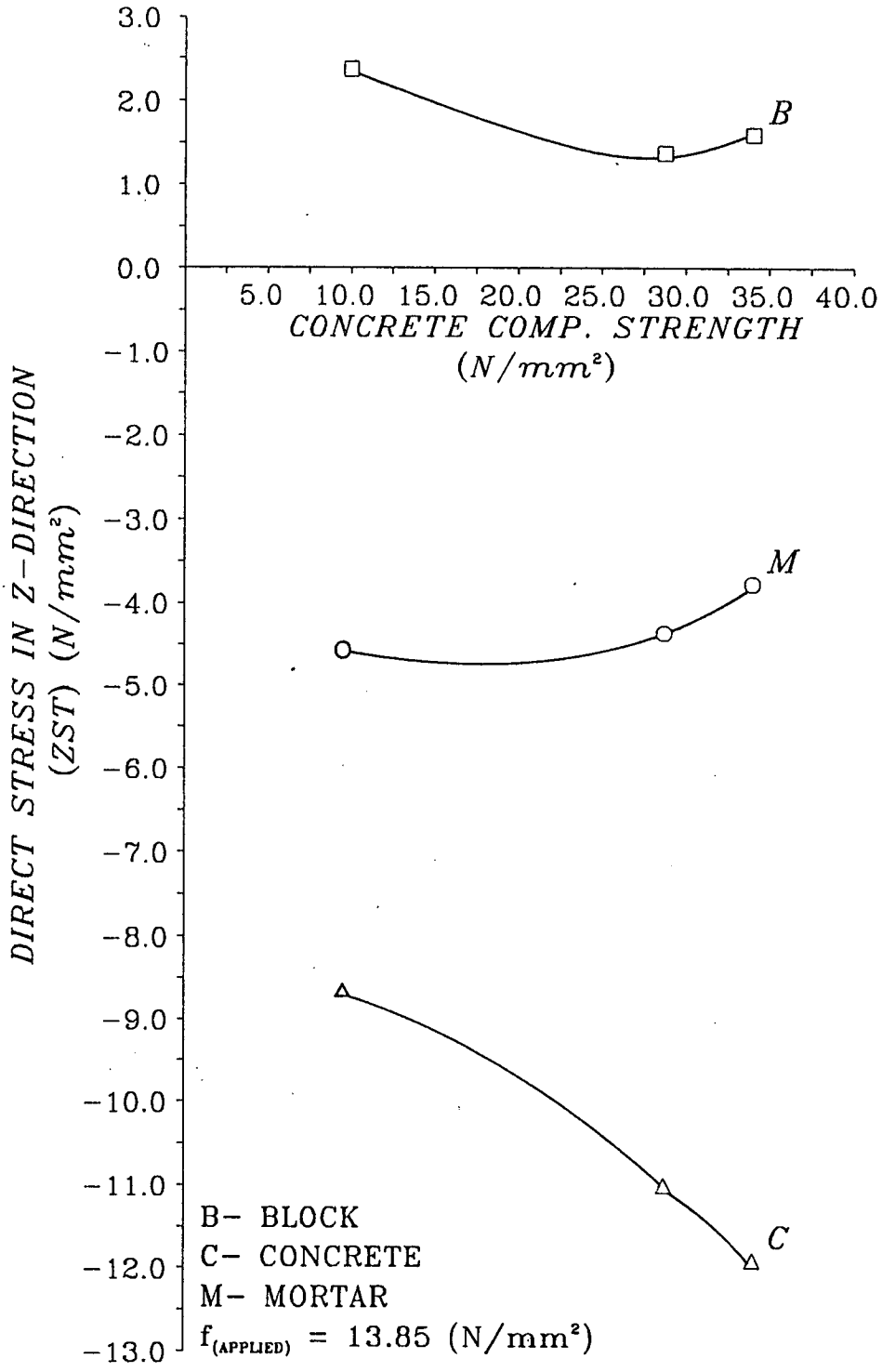

Fig. 5.73 - Effect of concrete infill strength on filled 3FBP-MJ prism direct stress in Z-direction, parametric study non-linear FEA.

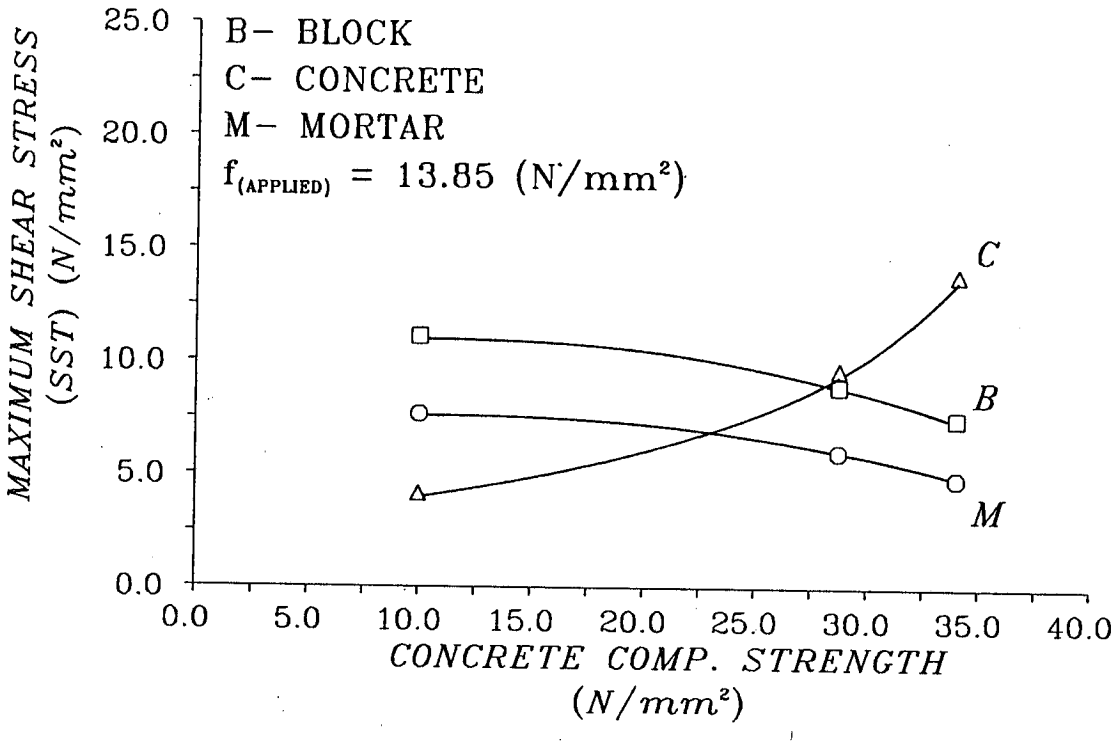

Fig. 5.74 - Effect of concrete infill strength on filled 3FBP-MJ prism maximum shear stress, parametric study non-linear FEA.

CHAPTER 6

FACTORS AFFECTING COMPRESSIVE STRENGTH OF BLOCKWORK MASONRY

6.1 INTRODUCTION

This chapter presents the results of an experimental and theoretical investigations of the factors, other than concrete infill strengths and mortar types, which affect the compressive strength and behaviour of unfilled, filled and solid blockwork masonry prisms compressed normal to the unit bed face. The following factors were studied: (a) prism height-to-thickness ratio (h/t), (b) aspect ratio (prism length-to-thickness) (l/t), (c) mortar thickness, (d) shrinkage in 28 days and (e) bond between block and concrete infill.

As shown earlier, testing blockwork masonry prisms is a common method[24,25] of determining the ultimate compressive strength of blockwork masonry, f'_m. This method involves the testing of stack-bonded masonry prisms, with a prism height-to-thickness ratio (h/t) of between 2.0 and 5.0, made of the same materials as used in actual construction, and compressed normal to the unit bed face.

BOULT[27] in his work on filled, full-block masonry prisms compressed normal to the bed face, gave an explanation for the reduction in prism strength with height as it relates to the shrinkage of the grout and the degree of restraint offered by the core shape which resulted in plastic cracking as shrinkage proceeds. Relating the reduction in strength with height to the plastic cracks, however is not well founded. It has been established[55,81,82,83,84] that the artificial confining effect at the top and bottom ends of the prism due to the machine

platens is the main reason for the increase in the apparent compressive strength of concrete block prisms with h/t values ≤ 2.0.

As mentioned in chapter 5, DRYSDALE and HAMID[28,29] in their work on concrete block masonry prisms proposed, for ease of handling, the testing of 3-course high, half-block prisms. This test was claimed to accurately assess the strength of concrete block masonry in that it exhibits a failure mode similar to that for walls.

As shown in chapter 5, using the results based on half-block prisms in order to ease handling is not acceptable due to the difference in value of the aspect ratio (l/t) (prism length-to-thickness) of full-block (l/t = 2.05) and half-block (l/t = 1.0) prisms; also due to the difference in the mortar bedded area between the two prisms. The effect of these two variables on the compressive strength of blockwork prisms were investigated experimentally and theoretically in more detail in this chapter.

In their work on half-block concrete masonry prisms, the above authors also showed that increasing the joint thickness from 9.5 to 19.0 mm produced a decrease in the compressive strength of the prism of 16% for ungrouted masonry, whereas for grouted masonry the decrease was only 3%.

The aim of this investigation is to study the effects of h/t ratio, aspect ratio (l/t), mortar thickness, shrinkage in 28 days and bond between the block and concrete infill on the compressive strength and behaviour of unfilled and filled blockwork masonry prisms compressed normal to the bed face. Methods of determining the ultimate blockwork compressive strength f'_m are also suggested.

6.2 EXPERIMENTAL PROGRAMME

A total of thirty-three full-block and twenty-one half-block stack-bonded prisms of varying h/t and l/t ratios, were constructed by an experienced mason. This ensured that the horizontal mortar joints between the concrete blocks were completely filled. High strength (1:0.25:3) mortar was used throughout. Some of the prisms were left unfilled and some were cast with medium strength (1:3:2) concrete.

The prisms are designated in Table A.1 (Appendix A) and in the text as **2FBP-MJ** (2-course high **F**ull-**B**lock **P**risms with **M**ortar **J**oint), **3FBP-MJ** (3-course high **F**ull-**B**lock **P**risms with **M**ortar **J**oints) and **6FBP-MJ** (6-course high **F**ull-**B**lock **P**risms with **M**ortar **J**oints). Similarly, three different types of unfilled and filled half-block prisms **2HBP-MJ**, **3HBP-MJ** and **6HBP-MJ**, were constructed and tested to compare their compressive strength and behaviour with the full-block prisms.

The methods adopted herein for the construction and curing of specimens are similar to those ones used in chapter 5.

Two experiments were devised to investigate the extent of shrinkage on the plastic cracks between the block and the concrete infill and the effect of that on the compressive strength of the prism. In the first experiment, three prisms, each consisting of three half-blocks, were built using the method explained above. The first prism was filled with a low slump (75 mm), 1:3:2 concrete mix. The second prism filled from the same mix but with the W/C ratio adjusted to give a medium slump (175 mm). Finally, a mix with a high slump, 220 mm, was used to fill the third prism.

In the second experiment, three prisms, each consisting of three full-blocks in height, were built. The inner surfaces of the hollow blocks were coated with oil prior to construction. The prisms were then left under polythene sheeting for four days to allow the mortar joints to gain in strength. Thereafter, the prisms were filled with a medium strength (1:3:2) concrete and as before cast in two layers, compacting each layer with a 25 mm poker vibrator. After casting, the prisms were left to cure using the method described previously.

The hardened half-block prisms from the first shrinkage experiment were cut, using an electrical diamond saw, into four equal sections to observe the plastic cracks between the block and the concrete, also to study the effect of using different concrete mixes with different slumps on the appearance of the hardened concrete. The full-block prisms from the second shrinkage experiment were capped and tested in compression until failure.

Results for the unfilled and filled, 3-course high full and half-block prisms with mortar joints referred to in chapter 5 were used in this chapter to compare their compressive strength and behaviour with the specimens tested and analysed herein.

Steel moulded cubes and cylinders were tested in compression to determine the strength of the mortar and concrete infill mixes. Demec points and electrical strain gauges were placed on the specimens at selected locations 24 hours before testing.

Prior to testing, all the specimens were capped with a thin layer, 1 - 2 mm, of dental plaster[55] as explained in chapters 3, 4 and 5.

Loading rates were in accordance with BS 6073: Part 1: 1981[66] and the loading pattern was in accordance with BS 1881: Part 121: 1983[68]. The static modulus of elasticity was determined for all the specimens tested, as described in chapters 3,4 and 5.

6.3 THEORETICAL PROGRAMME

A number of non-linear, three-dimensional parametric FEA studies were conducted using a standard package, LUSAS[80]. The first analysis studied the effects of differences in the aspect ratio (l/t) and the mortar bedded area on the compressive strength and behaviour of unfilled and filled, full (l/t = 2.05) and half (l/t = 1.0) block prisms. The second analysis compared the strength and behaviour of the filled **3FBP-MJ** prism with a solid **3SBP-MJ** prism (**3**-course high **S**olid-**B**lock **P**rism with **M**ortar **J**oints) (see Table A.1, Appendix A). The third analysis studied the effect of changing the aspect ratio, (l/t) (prism length-to-thickness), on the deformations and internal stresses in a solid **3SBP-MJ** prism compressed normal to the unit bed face. The aspect ratios considered were l/t = 1.0, 1.5, 2.05, 2.5, 3.0 and 4.0.

To the author's knowledge, no previous work has been reported on the effect of aspect ratio (l/t) on the compressive strength of [illegible] block masonry prisms. Most of the work reported is concerned with the effect of h/t ratios (block height-to-thickness).

BS 5628[21] suggests decreasing the characteristic compressive strength, f_k, for the brickwork masonry prisms having a ratio of prism height to least horizontal dimension (h/t) of between 2.0 and 4.0 compared to prisms with h/t = 5.0 or more. The Australian Standard 3700[22]

gives a correction factor for the characteristic compressive strength of the unit to take into account the h/t ratio.

The levels of vertical stress applied to the unfilled and filled, full and half-block prisms for the first parametric study are the lowest average value of compressive strength for unfilled, (12.01 N/mm^2), and filled, (14.53 N/mm^2), full or half-block prisms. These levels of vertical stress were derived experimentally for unfilled prisms constructed with high strength (1:0.25:3) mortar and for filled prisms constructed with the same type of mortar and filled with medium strength (1:3:2) concrete (see Tables 5.1 and 5.2). On the other hand, the level of vertical stress applied to the **3SBP-MJ** prisms for the second and third parametric studies was similar to the level of vertical stress applied to the filled prisms (14.53 N/mm^2) in the first analysis.

The non-linear analysis was carried out to obtain a more accurate assessment of the effect of aspect ratio and the mortar bedded area on the stress values and distributions in blockwork masonry prisms. The results obtained from the analyses were deformations, direct, shear and principal stresses.

6.3.1 Material Mechanical Properties Used in the FEA

One type of mortar (1:0.25:3), and concrete infill (1:3:2) were used in the analyses to limit the number of variables. The material's mechanical properties and vertical stress vs strain curves for the hollow blocks, mortar and concrete used in the non-linear FEA for the unfilled and filled, full and half-block prisms are similar to those used in the FEA for the **2BP-MJ** and **3FBP-MJ** prisms

described in chapters 4 and 5.

The complete vertical stress vs strain curve for the solid concrete blocks used in the FEA were found using the stress vs strain curves for rigorous analysis of non-critical concrete sections given in BS 8110: Part 2: 1985[69]. The curves were derived by substituting the magnitudes of the material strengths and the moduli of elasticity given in Table 3.7. The curve was then idealised in a series of straight lines, as required by the FEA (Fig. 6.1). The value of Poisson's ratio for solid concrete blocks was derived experimentally by plotting the lateral strain vs vertical strain and taking the values of Poisson's ratio at a strain corresponding to the material's maximum compressive strength (see Table 3.7).

6.3.2 Finite Element Model

The FEA mesh used in the analysis of the unfilled and filled **3FBP-MJ** and **3HBP-MJ** prisms was similar to the one used in chapter 5 (see Fig. 5.3). The FEA model was developed by considering 1/4 of the prism in the case of full-block prisms and 1/2 in the case of half-block prisms.

The mesh used for the **3SBP-MJ** prisms (Fig. 6.2) was different from the one used for the unfilled and filled, full and half-block prisms. The reason for this is to enable the prism dimension to be changed to satisfy the l/t ratios considered in the analysis. The three-dimensional finite element computer model was developed using a solid three-dimensional element with eight nodes (HX8) for all materials. The FEA model was developed by considering 1/4 of the prism in the analysis (Fig. 6.3).

The assumptions used to simplify and reduce the size

of the mesh were similar to those adopted in chapters 4 and 5.

All prisms were restrained at the bottom in three directions and the axial load was applied by means of uniform pressure using an 88 mm thick steel bearing plate. The top surface of the plate was restrained in the two horizontal directions and free in the vertical direction, which is the direction of loading. All the planes of symmetry were restrained in a direction normal to the plane and free in the other two directions.

6.4 DISCUSSION OF EXPERIMENTAL RESULTS

The discussion of the experimental results is divided into three sections. The first and second deal with the observed modes of failure for full and half-block prisms. The third deals with the experimental results.

6.4.1 Modes of Failure for Full-Block Prisms

The modes of failure for all the unfilled and filled **3FBP-MJ** prisms compressed normal to the bed face were discussed in chapter 5. A common feature was observed in the modes of failure for all the unfilled and filled full-block prisms tested in this investigation, whereby checking the mortar at different locations after failure gave the indication that the mortar had changed to a powder substance at some stage of the loading process.

The unfilled and filled **2FBP-MJ** prisms constructed with high strength (1:0.25:3) mortar and filled with medium strength (1:3:2) concrete showed different modes of failure to the unfilled and filled, **3FBP-MJ** prisms.

The unfilled **2FBP-MJ** prisms failed by clear crushing of the block side shells and mid-webs at the level of the mortar joint, followed by separation of the side shells from the mid-webs (Fig. 6.4).

The mode of failure of the filled **2FBP-MJ** prisms showed several longitudinal cracks in the prism side and end shells during the loading process. This was followed by block side shell separation and outward deformation with some signs of block shell, mortar and concrete crushing near the mortar joint (Fig. 6.5).

As in the filled **3FBP-MJ** prisms, some of the **2FBP-MJ** prisms showed crushing of the concrete at the level of the mortar joint and some showed little damage to the concrete after failure (Mode I). The reason for differences in the modes of failure was explained in chapter 5.

Unfilled and filled **6FBP-MJ** prisms, constructed with high strength (1:0.25:3) mortar and filled with medium strength (1:3:2) concrete, showed similar modes of failure to the unfilled and filled **3FBP-MJ** prisms.

The unfilled **6FBP-MJ** prisms showed a greater tendency to split longitudinally along the block end shells than the unfilled **3FBP-MJ** prisms (Fig. 6.6). The prisms showed an abrupt mode of failure, with no signs of major cracks during the loading process until failure.

Most of the filled **6FBP-MJ** prisms showed crushing of the concrete at one of the mortar joints after failure (Fig. 6.7). The mode of failure was less abrupt than the unfilled **6FBP-MJ** prisms. Some signs of cracking were observed at the block end and side shells at 80% to 90% of the ultimate load.

6.4.2 Modes of Failure for Half-Block Prisms

The modes of failure for all the unfilled and filled **3HBP-MJ** prisms compressed normal to the bed face were discussed in chapter 5. As in full-block prisms a common feature was observed in the modes of failure for all the unfilled and filled half-block prisms tested in this investigation, whereby checking the mortar at different locations after failure gave the indication that the mortar had changed to a powder substance at some stage of the loading process.

The unfilled and filled **2HBP-MJ** prisms constructed with high strength (1:0.25:3) mortar and filled with medium strength (1:3:2) concrete showed different modes of failure to the unfilled and filled **3HBP-MJ** prisms.

The unfilled **2HBP-MJ** prisms showed a V-shape crushing type of failure in the block shells at the level of the mortar joint (Fig. 6.8).

The filled **2HBP-MJ** prisms showed similar longitudinal cracks during the loading process to the filled **3HBP-MJ** prisms, followed by a pyramid crushing type of concrete failure at mid height, with block shell-concrete infill separation (Fig. 6.9).

Unfilled and filled **6HBP-MJ** prisms constructed with high strength (1:0.25:3) mortar and filled with medium strength (1:3:2) concrete, showed similar modes of failure to the unfilled and filled **3HBP-MJ** prisms.

The unfilled **6HBP-MJ** prisms (Fig. 6.10) showed an abrupt mode of failure, with no sign of major cracks during the loading process until failure.

The filled **6HBP-MJ** prisms showed crushing of the concrete at one of the mortar joints after failure (Fig. 6.11). The mode of failure was less abrupt than the unfilled **6HBP-MJ** prisms, with some sign of cracking at the block end and side shells at 80% to 90% of the ultimate load.

6.4.3 Experimental Results

Tables 6.1 and 6.2 summarize the experimental results for all the specimens tested in this chapter.

The effect of the h/t ratio on the compressive strength of unfilled and filled, full and half-block prisms is shown in Fig. 6.12. The result indicates a clear reduction in strength as the h/t ratio increased from 2.0 to 6.0. The strength of the unfilled full-block prisms reduced by 29.7% as the h/t ratio increased from 2.0 to 6.0, whereas the strength of the unfilled half-block prisms reduced by 9.9%. The reduction for filled full-block prisms was 9.5%, compared with 33.1% for half-block prisms. The main reason for the reduction in strength with height was the reduction in the influence of the artificial confinement stresses at the top and bottom of the prisms resulting from the difference in stiffness between the blockwork and steel platen materials[55,81,82,83,84].

In deciding the height of the prism to be used as a standard specimen to determine the compressive strength of blockwork masonry f'_m, a comparison between the strength values for unfilled **3FBP-MJ** prisms (21.35 N/mm^2) and filled **3FBP-MJ** prisms (14.53 N/mm^2) with unfilled **6FBP-MJ** prisms (17.48 N/mm^2) and filled **6FBP-MJ** prisms (15.23 N/mm^2), suggested that testing 3-course high, full-block prisms as the standard specimen gave values which were representative

of the value of f'_m.

In comparing the strength of unfilled **2FBP-MJ**, **3FBP-MJ** and **6FBP-MJ** prisms with the companion half-block prisms another significant result was observed. The percentage reductions in strength of unfilled full-block prisms for the three different heights was 4.1%, 16.2% and 25.2% as compared to half-block prisms respectively, based on differences in the aspect ratio (l/t) and the mortar bedded area. This suggested that the percentage reduction in strength caused by the aspect ratio (l/t) increased as the prism height increased. These differences were maybe due to the reduced influence of the artificial confinement of the machine platen with prism height. This was noticed in the mode of failure of unfilled **6FBP-MJ** prisms, where the prism shows more tendency to split longitudinally along the block end shells. Filled full-block prisms, on the other hand, failed with a percentage reduction of 27.6%, 29% and 2.1% compared to filled **2HBP-MJ**, **3HBP-MJ** and **6HBP-MJ** prisms respectively. It seems that the degree of influence of artificial confinement caused by the machine platen is influenced by the l/t ratio and also by whether the prism is unfilled or filled. This in turn influenced the mode of failure of the prism and its strength.

Increasing the mortar thickness from 5 to 20 mm, had the effect of reducing the strength of both the unfilled and filled full-block prisms (Fig. 6.13). The reduction effect on strength was less in the case of filled full-block prisms (11.6%) than unfilled (17.6%) ones.

Figs 6.14 (i), (ii) and (iii) are photographs of three different cross-sections through the midle of the **3HBP-MJ** prisms filled with concrete mixes of 75 , 175 and 220 mm slumps respectively. These show that the location of the plastic cracks caused by shrinkage was similar for the

three different types of slump used and that they were usually located near the top surface of the specimens. This suggests that water evaporation from the top surface of the specimen was the main reason for these plastic cracks. The crack penetration depth (50 - 105 mm) and width (1 - 3 mm) increased as the slump increased. Some unfilled voids were observed in specimen filled with the highest slump concrete mix. These voids were caused by the presence of air bubbles and also by the evaporation of the excess water left over after the concrete hardened. Prisms filled with a low slump mix also showed some unfilled voids resulting from insufficient compaction.

Table 6.1 gives the compressive strength result for the no-bond (coated with oil) **3FBP-MJ** prisms. Although good adhesion bond exist between block and infill for prisms without oil (Eqn. 3.11), the result of compressive strength for prisms coated with oil showed little difference compared with a similar prism without oil. This suggests that plastic cracks caused by shrinkage have no great effect on the ultimate compressive strength of blockwork masonry prisms, $f'_m{}^{(30)}$.

6.5 DISCUSSION OF THEORETICAL RESULTS

The discussion is divided into four major sections. The first and second sections discuss the results of the parametric study analyses conducted for the unfilled and filled **3FBP-MJ** and **3HBP-MJ** prisms. The third section addresses differences in the theoretical results between the **3FBP-MJ** and **3SBP-MJ** prisms. The forth section considers the effect of the aspect ratio (l/t) on the values and distributions of the deformation and internal stress for the **3SBP-MJ** prisms.

6.5.1 Parametric Study Analysis for Unfilled 3FBP-MJ and 3HBP-MJ Prisms

The level of vertical stress applied to the unfilled **3FBP-MJ** and **3HBP-MJ** prisms in the parametric study was 12.01 N/mm^2, which is the average experimental value of compressive strength for unfilled **3FBP-MJ** prisms built with high strength (1:0.25:3) mortar.

In order to examine the effect of varying the aspect ratio (l/t) and the mortar bedded area between the full and half-block prisms on the results of deformations and stresses, the parametric study was based upon fixing the applied level of vertical stress and changing the model from a full to a half-block prism (this was achieved by changing the computer model's horizontal restraint at the planes of symmetry).

The effect of differences in the aspect ratio (l/t) and the mortar bedded area between the full and half-block prisms on the prism's deformation is clearly shown by the contour plots for the horizontal deformation in the X-and Z-directions. The horizontal deformation in the X- and Z-directions for a 3-course high full-block prism is given in chapter 5 (see Figs 5.28 and 5.29 respectively) and for a half-block prism in Figs 6.15 and 6.16 respectively.

The figures show a clear similarity, for horizontal deformation in the Z-direction, between the full and half-block prisms, but show a clear difference in the distributions and values in the X-direction. The deformation in the X-direction for the half-block prism shows a great tendency to local outward squeezing of the mortar joints. On the other hand, in the full-block prism the deformation exists over most of the prism's end shells.

Table 6.3 gives results for the maximum values of deformation in the Y-, X- and Z-directions for the unfilled **3FBP-MJ** and **3HBP-MJ** prisms, as derived from the parametric study analysis; the level of vertical stress applied during the parametric study analysis and the compressive strength of the experimental prisms.

Table 6.3 shows that the vertical deformation of a half-block prism is 3.4% higher than a full-block prism. On the other hand, the horizontal deformation of full-block prisms in the X-direction is 40% higher than that of the half-block prism. Both prisms show similar values (0.045 mm) for the horizontal deformation in the Z-direction. The table also shows that the values of horizontal deformation for half-block prisms are equal in the X- and Z-directions. This suggests that the horizontal deformation of the half-block prism resulting from the differences in the aspect ratio (l/t) is more compatible in the X- and Z-directions than for full-block prisms. This means that, for half-block prisms, there is less possibility of end shell separation from the rest of the prism and no chance of splitting along the line of contact between the prism end and the side shells due to incompatibility of deformation in the horizontal directions as is the case with full-block prisms. The separation of the prism end shells from the rest of the prism will definitely have a weakening effect on the compressive strength of the full-block prisms.

Table 6.4 provides the maximum values of direct, shear and principal stresses in each individual material, as derived from the parametric study analysis. The table shows that the maximum values of the direct vertical stress in the block material for full-block prisms are slightly higher (2.3%) than that for half-block prisms. On the other hand, the maximum value of direct horizontal tensile stress in the block material in the X-direction for the full-block

prism is 9.7% higher than that for the half-block prism. The tensile stress in the full-block prism is even higher (23.7%) if the maximum values of the minor principal stress (MST2) are considered. Although the values of maximum tensile stress (MST2) in full-block prism (2.87 N/mm^2) and half-block prism (2.32 N/mm^2) are higher than the experimental ultimate tensile strength for unit hollow block (2.16 N/mm^2) (see Table 3.9), a full-block prism has a greater possibility for splitting than a half-block prism.

Table 6.4 also shows a small difference between the maximum values of direct horizontal tensile stress in the X- and Z-directions for both prisms. The results for the maximum values of the minor principal stress show differences of 79.4% and 42.3% between the maximum value of the minor tensile principal stresses on the prism's end (MST2) and side (MST1) shells for full and half-block prisms respectively.

The above results explain why the average experimental value of compressive strength (based on net area) for the unfilled 3-course high half-block prism is 16.2% higher than that for the full-block prism. They also show how differences in the aspect ratio (l/t) and the mortar bedded area between the full and half-block prisms affect their compressive strength.

6.5.2 Parametric Study Analysis for Filled 3FBP-MJ and 3HBP-MJ Prisms

The level of vertical stress applied to the filled **3FBP-MJ** and **3HBP-MJ** prisms for the parametric study was 14.53 N/mm^2, which is the average experimental value of compressive strength for filled **3FBP-MJ** prisms built with

high strength (1:0.25:3) mortar and filled with medium strength (1:3:2) concrete.

The effects of the difference in the aspect ratio (l/t) and the mortar bedded area between the full and half-block prisms on the prism's deformation are clearly shown by the contour plots for the horizontal deformations in the X- and Z-directions. The horizontal deformation in the X- and Z-directions for a full-block prism are given in chapter 5 (see Figs 5.50 and 5.51 respectively) and for a half-block prism in Figs 6.17 and 6.18 respectively.

The figures show a clear similarity for the horizontal deformation in the Z-direction between the full and half-block prisms, but show a clear difference in the distributions and values in the X-direction. The horizontal deformation of the full-block prism in the X-direction shows that the prism end shells tend to deform outward with a maximum deformation of 0.048 mm at the prism mid height. On the other hand, the prism end shells in the half-block prism tend to deform outward with a maximum value of 0.025 mm at the prism mid height.

Table 6.5 gives the results for the maximum values of deformation in the Y-, X- and Z-directions; the level of vertical stress applied during the parametric study analysis and the average experimental compressive strength of the filled **3FBP-MJ** and **3HBP-MJ** prisms.

Table 6.5 shows that the maximum value of vertical deformation for the half-block prism is the same as that for the full-block prism. On the other hand, the maximum value of horizontal deformation for the full-block prism in the X-direction is 92% higher than that for the half-block prism. Both prisms show the same values of horizontal deformation in the Z-direction (0.025 mm). Table 6.5 also

shows that the values of horizontal deformation for half-block prisms are almost equal in both directions, where in full-block prisms the deformation in the X-direction is 92% higher than that in the Z-direction. This suggests that the horizontal deformations of the half-block prisms are more compatible in both horizontal directions than those in full-block prisms. This results from differences in the aspect ratio (l/t) between the two prisms.

As in the case of unfilled, full-block prisms, the incompatibility of deformations between the X- and Z-directions for filled full-block prisms will result in the separation of the prism end shells from the rest of the prism and also in the development of longitudinal cracks at the line of contact between the prism end and side shells.

Table 6.6 provides the results of the maximum values of direct, shear and principal stresses in each individual material as derived from the parametric study analysis. The table shows that the maximum value of the direct vertical stress in the block material for a full-block prism is 3'.6% higher than that for a half-block prism. On the contrary, this stress in the concrete material for half-block prisms is 2.1% higher than that for full-block prisms. This suggests that the applied vertical stress is shifting from the block to the concrete in the case of the half-block prism. This phenomenon was also true for the maximum values of the major principal stresses. This phenomenon results from differences in the aspect ratio (l/t) and the mortar bedded area between the two types of prism.

The table also shows that although the maximum values of direct horizontal tensile stresses in the block material for the half-block prism are higher than that for a full-block prism, the maximum values of the minor tensile principal stresses are almost equal. Also, the maximum

values of the minor tensile principal stresses (MST2) in both types of prism are almost the same as the experimental ultimate tensile strength for a unit block filled with (1:3:2) concrete mix (1.77 N/mm^2) (see Table 3.9).

The results also show a small difference between the maximum values of the direct horizontal tensile stress in the X- and Z-directions for both prisms, but show differences of 36.6% and 38.3% between the maximum value of the minor tensile principal stresses on the prism's end (MST2) and side (MST1) shells for full and half-block prisms respectively.

Based on the results of deformations and stresses, the only reason for the reduction of 29% in the average experimental value of compressive strength for the filled **3FBP-MJ** prisms, compared to the **3HBP-MJ** prisms, is the incompatibility of deformation between the X- and Z-directions in full-block prisms. This incompatibility is caused by the difference in aspect ratio (l/t) and mortar bedded area between the full and half-block prisms.

6.5.3 Comparison Between Filled 3FBP-MJ and Solid 3SBP-MJ Prisms

The level of vertical stress applied to the solid **3SBP-MJ** prism was 14.53 N/mm^2, which is the average experimental value of compressive strength for filled **3FBP-MJ** prisms built with high strength (1:0.25:3) mortar and filled with medium strength (1:3:2) concrete (see Table 5.1).

Prisms Deformation

The deformation of the solid **3SBP-MJ** prism in the Y-direction (Fig. 6.19) shows that the prism top surface shortens vertically with a maximum deformation of 0.636 mm with respect to the prism bottom surface. Although the level of vertical stress applied to both prisms is the same, this deformation is 26.7% higher than that for a filled **3FBP-MJ** prism (see Fig. 5.49). The contour plots for the horizontal deformations in the X- and Z-directions (Figs 6.20 and 6.21 respectively) for the solid **3SBP-MJ** prism are similar to that for the filled **3FBP-MJ** prism (see Figs 5.50 and 5.51). On the other hand, the values of the horizontal deformations in the X- and Z-directions for the solid **3SBP-MJ** prism are 12.5% and 12% higher respectively than that for the filled **3FBP-MJ** prism.

As with the filled **3FBP-MJ** prism, the solid **3SBP-MJ** prism shows incompatibility of deformation caused by a difference in the values of horizontal deformation of 92.9% between the X- and Z-directions. The reason for this incompatibility in the horizontal deformation is the prism aspect ratio (l/t = 2.05).

Due to the incompatibility of deformation in the solid **3SBP-MJ** prism, the prism end faces will be separated from the rest of the prism and longitudinal cracks will develop at the line of contact between the prism end and side faces.

Stresses in Block Material

The contour plots of the direct stresses in the Y-, X- and Z-directions in the block material for the solid **3SBP-MJ** prism are shown in Figs 6.22, 6.23, and 6.24

respectively. The contour plots of the major and two minor principal stresses are given in Figs D.1, D.2 and D.3 (Appendix D) respectively.

The contour plots for the direct vertical stress in the Y-direction for the solid **3SBP-MJ** prism show that the maximum compressive vertical stress, 18.90 N/mm^2, is located at the prism bottom corner near the machine platen. The rest of the prism is under a uniform stress ranging from 12.80 to 15.64 N/mm^2. The maximum value of the direct vertical stress in the solid **3SBP-MJ** prism is 14.8% lower than that for the filled **3FBP-MJ** prism (see Fig. 5.52). This indicates that the solid **3SBP-MJ** prism is under stressed and that the ultimate compressive strength of the solid-block prisms, made from the same materials as hollow blocks, is higher than that for a filled **3FBP-MJ** prisms.

The contour plots for the direct horizontal stress in the X-direction for the solid **3SBP-MJ** prism show similar distributions to that for the filled **3FBP-MJ** prism (see Fig. 5.53). But the solid **3SBP-MJ** prism shows that the value of the maximum horizontal tensile stress in the X-direction decreases by 45% compared to that for a filled **3FBP-MJ** prism. On the other hand, the solid **3SBP-MJ** prism shows different distributions for the horizontal stress in the Z-direction compared to that for the filled **3FBP-MJ** prism (see Fig. 5.54). The solid **3SBP-MJ** prism shows that most of the horizontal tensile stresses in the Z-direction are located in the vicinity of the mortar joints[1,26]. This is not exactly the case with the filled **3FBP-MJ** prism, where the tensile stresses cover most of the prism height. Similarly, the value of the maximum tensile stress in the Z-direction for the solid **3SBP-MJ** prism is 32.2% lower than that for the filled **3FBP-MJ** prism.

The results also show that the maximum value of

tensile stress in solid **3SBP-MJ** prisms is 0.99 N/mm^2 (MST2). This value is less than the experimental ultimate tensile strength for a unit solid block (1.71 N/mm^2) (see Table 3.9). On the other hand, the maximum value of tensile strength in filled **3FBP-MJ** prisms is 1.68 N/mm^2 (MST2), which is almost equal to the experimental ultimate tensile strength for a unit block filled with (1:3:2) concrete mix (1.77 N/mm^2) (see Table 3.9).

The main reason for the differences in the distribution and values of the horizontal and minor principal stresses is the presence of the concrete infill in the case of the filled **3FBP-MJ** prism and its high Poisson's ratio.

The maximum values of the horizontal and minor principal tensile stresses in the solid **3SBP-MJ** prism again suggest that the compressive strength of a solid-block prism, made from the same material as the hollow blocks, is higher than that for a filled **3FBP-MJ** prism.

It was also observed that the maximum values of the tensile stress for the solid **3SBP-MJ** prism in the Z-direction is 19.3% higher than that in the X-direction. This difference is the result of the prism aspect ratio (l/t = 2.05). This difference suggests that the solid **3SBP-MJ** prism has a greater tendency to split along the prism end faces than the side faces[1,26].

A significant difference was observed in the distribution of maximum shear stress between the solid **3SBP-MJ** and filled **3FBP-MJ** prisms. In the solid **3SBP-MJ** prism (Fig. 6.25) most of the prism mid height is under uniform shear stress, ranging from 7.09 to 7.65 N/mm^2, which is the maximum value of shear stress. The prism is expected to shear at the bottom side near the machine platen. On the

other hand, the filled **3FBP-MJ** prism (sèe Fig. 5.55) shows a non-uniformity in the distribution of shear stress with a maximum value of 9.34 N/mm^2 located at the prism mid height. The prism is expected to shear at mid height.

Stresses in Mortar Material

The contour plots of the direct stresses in the Y-, X- and Z-directions in the mortar joints for the solid **3SBP-MJ** prism are shown in Figs 6.26, 6.27, and 6.28 respectively. The distributions of the major and two minor principal stresses are given in Figs D.4, D.5 and D.6 (Appendix D) respectively.

The contour plots of the direct vertical stress in the Y-direction show that the higher values of vertical stress are located at the centre core of the prism, with a maximum value of 15.05 N/mm^2. This value tends to decrease towards the outer faces of the mortar joints. The way the vertical stresses in the mortar joints are distributed suggests that the applied vertical stress is higher at the centre core of the prism than at the outer faces.

A clear similarity was observed in the distribution of the direct horizontal stress in the X- and Z-directions. Both horizontal stresses show that the mortar joints are under confinement stresses in the X- and Z-directions with maximum values of 3.59 N/mm^2 in the X-direction and 3.48 N/mm^2 in the Z-direction. These maximum values of stress are located at the centre core of the prism and tend to reduce toward the outer faces of the mortar joints. The reason for these confinement stresses is the difference in the deformational characteristics between the soft mortar joints and the stiff concrete blocks.

Fig. 6.29 shows the contour plots of the maximum shear stress in the mortar joints. The figure shows an almost uniform distribution of shear stress at the mortar joints. This uniformity is attributed to the small thickness of the mortar joints.

Based on the distribution and values of deformation and stress, the predicted mode of failure for the solid **3SBP-MJ** prisms is by separation of the prism end faces from the rest of the prism and the development of longitudinal cracks along the lines of contact between the prism end and side faces caused by the incompatibility of deformation. Longitudinal cracks will develop at the prism end shells, at a later stage of the loading process, initiated in the vicinity of the mortar joints, and then propagate through the solid-blocks. It is expected that the solid prisms will fail due to a combination of compression, tension and shear stresses. It is anticipated that the ultimate compressive strength of the solid **3SBP-MJ** prism, made of the same material as the hollow blocks, will be higher than that for a filled **3FBP-MJ** prisms.

6.5.4 Parametric Study Analysis on the Effect of the Aspect Ratio (l/t) on the Compressive Strength of Solid 3SBP-MJ Prism

The level of vertical stress applied to the solid **3SBP-MJ** prisms with different aspect ratios was 14.53 N/mm^2, which is the average experimental value of compressive strength for the filled **3FBP-MJ** prisms built with high strength (1:0.25:3) mortar and filled with medium strength (1:3:2) concrete (see Table 5.1).

This parametric study assumed constant values for the block height (h = 189 mm) and thickness (t = 190 mm) and varied the block length (l = 190, 285, 390, 475, 570 and

760 mm) in a solid **3SBP-MJ** prism. This gives a range of prisms with different aspect ratios of l/t = 1.0, 1.5, 2.05, 2.5, 3.0 and 4.0.

After several runs, maximum values for the prism's deformation, direct, shear and principal stresses were determined. Table 6.7 gives the maximum values of the deformation in the Y-, X- and Z-directions and the level of vertical stress applied during the parametric study analysis. Table 6.8 gives the maximum values of the direct, shear and principal stresses in each individual material.

Although the values of deformation and stress differ, the deformations and stress distributions for all the prisms analysed in this parametric study are similar to those for the solid **3SBP-MJ** prism analysed in section 6.5.3. Information about deformations or stress distributions is given in the relevant deformation and stress figures in section 6.5.3.

To assess the effect of the aspect ratio (l/t) on the prism deformations and stresses, the results of the parametric study were plotted on an X-Y plotter. The X-axis represents changes in the aspect ratio (l/t). The Y-axis represents the maximum values of deformation and stress in the prisms as derived from the parametric study.

Fig. 6.30 shows the effect of changing the aspect ratio on the prism's deformation in the Y-, X- and Z-directions. The figure shows small changes in the prism's deformation in the Y- and Z-directions, for the ranges of the aspect ratio considered in the study. On the other hand, significant changes were observed in the prism's deformation in the X-direction. Changing the aspect ratio from l/t = 1.0 to l/t = 4.0 increases the prism's deformation in the X-direction by 221.4%.

This means that prisms with aspect ratios more than 1.0 have greater incompatibility of deformation between the X- and Z-directions. This, in turn has a weakening effect on the prism compressive strength by causing separation of the prism end faces from the rest of the prism and the introduction of longitudinal cracks at the lines of contact between the prism end and side faces.

Fig. 6.31 shows the effect of changing the aspect ratio on the maximum value of direct stress in the Y-direction. The figure shows that changing the aspect ratio from 1.0 to 4.0 increased the direct vertical stress in the block material by 11.2%. No major changes in these stresses in the mortar joints were observed. Similarly, the maximum value of the major principal stress in the block material increased by 13.7% with an increase in aspect ratio from 1.0 to 4.0. These increases indicate that the compressive strength of the prism decreases as the aspect ratio increases.

Fig. 6.32 shows the effect of changing the aspect ratio on the maximum value of direct horizontal stress in the prism in the X-direction. The figure shows a considerable decrease in the maximum tensile stress in the prism in the X-direction as the aspect ratio increases. Changing the aspect ratio from 1.0 to 4.0 decreases the horizontal tensile stress in the X-direction by 50.5%. No significant changes were observed in the maximum values of the confinement stresses in the mortar joints in the X-direction.

Fig. 6.33 shows the effect of changing the aspect ratio on the maximum value of the direct horizontal stress in the Z-direction. The figure shows that changing the aspect ratio has a negligible effect on the maximum values of the horizontal tensile and confinement stresses in the

block material and the mortar joints respectively in the Z-direction.

Table 6.8 shows that the maximum values of the horizontal and minor principal tensile stresses in all the analysed solid prisms are less than the experimental ultimate tensile strength for solid unit block (1.71 N/mm^2) (see Table 3.9).

Table 6.8 also shows that the difference between the horizontal tensile stresses in the block material in the X- and Z-directions increased as the aspect ratio increased. The table shows that for prisms with an aspect ratio of 1.0 there is no difference in the horizontal tensile stresses in the X- and Z-directions, but for prisms with an aspect ratio of 4.0, the tensile stresses in the Z-direction are 100% higher than that in the X-direction. The difference in the tensile stresses is even greater (116.3%) for the maximum values of the minor principal stresses on the prism end faces (MST2) compared to the side faces (MST1).

These results suggest that prisms with aspect ratios greater than 1.0 have a greater tendency to split along the prism end faces than the side faces[1,26].

Fig. 6.34 shows that changing the aspect ratio has a negligible effect on the values of the maximum shear stress.

Based on the maximum values of the major principal stresses in the block material the decreases in prisms strength with increases in the aspect ratio (l/t) are calculated as a reduction factors to the strength of solid **3SBP-MJ** prism with aspect ratio of 1.0 (Table 6.9).

6.6 CONCLUSIONS

1. The strength of the full and half-block prisms, compressed normal to the unit bed face, decreased as the h/t ratio increased from 2.0 to 6.0. This is true for both unfilled and filled prisms. The compressive strength of unfilled and filled, full-block prisms decreased by 29.7% and 9.5% respectively as the h/t ratio increased from 2.0 to 6.0. The results show that f'_m for unfilled or filled blockwork masonry, can be satisfactorily represented by testing an unfilled or filled, 3-course high, full-block prism as a standard specimen.

2. The effects of the aspect ratio, (l/t), and the presence of the mid-web, which results in the dissimilarity of the mortar bedded area between full-block (l/t = 2.05) and half-block (l/t = 1.0) prisms, were the main reasons for the reduction in the compressive strength and the difference in the behaviour between unfilled and filled full-block prisms and the companion half-block prisms. Thus, testing unfilled and filled half-block prisms, instead of full-block prisms, for the sake of ease of handling, to determine the ultimate compressive strength, f'_m, is not recommended. Since a higher strength is obtained by testing half-block prisms and the value of f'_m will be overestimated.

3. Increasing the mortar thickness from 5 to 20 mm, reduced the strength of both unfilled and filled full-block prisms. This reduction was less for filled, full-block prisms (11.6%) than for unfilled full-block prisms (17.6%).

4. Plastic cracking caused by shrinkage are not a serious

problem in concrete filled blockwork masonry. The cracks were usually located near the surface of the prism. Water evaporation from the top surface of specimens was the main reason for these cracks. Fresh concrete surfaces should therefore be covered after casting to reduce shrinkage caused by water evaporation. The crack penetration depth and width increased as the concrete infill slump increased. Prisms filled with high slump concrete infill mixes resulted in unfilled voids caused by the presence of air bubbles and also by the evaporation of the excess water left over after the concrete hardened. Using low slump mixes was also found to be impractical due to the amount of work needed in the compaction process.

5. Breaking the bond completely between blocks and concrete infill in a 3-course high full-block prism, as if there were cracks between the two materials, was found to have no effect on the ultimate compressive strength of blockwork masonry, f'_m.

6. The finite element analysis provided an explanation as to how differences in aspect ratio (l/t) and mortar bedded area between the full and half-block prisms affects the compressive strength and behaviour of unfilled and filled prisms.

Unfilled and filled, full-block prisms, with an aspect ratio of $l/t = 2.05$ and fully bedded with mortar, suffer incompatibility of deformation between the X- and Z-directions. This will result in the separation of the prism end shells from the rest of the prism and the development of longitudinal cracks at the line of contact between the prism end and side shells.

7. Using FEA, it is possible to create a clear image of how the deformations and stresses in a solid 3-course high prism are distributed. It is also possible to predict the mode of failure and ultimate compressive strength of the prism compared to a filled 3-course high prism. The results show that most of the horizontal tensile stresses in the Z-direction in a solid-block prism are located in the vicinity of the mortar joints. This is not exactly the case for the filled **3FBP-MJ** prisms, where the tensile stresses cover most of the prism height. The predicted mode of failure for the solid **3SBP-MJ** prisms is by separation of the prism end faces from the rest of the prism and the development of tensile splitting cracks along the prism end faces caused by the incompatibility of deformation and high horizontal tensile stresses on this face. The longitudinal cracks, caused by the high horizontal tensile stresses on the prism end faces, will be initiated in the vicinity of the mortar joints, then progress through the solid blocks. The ultimate compressive strength of the solid **3SBP-MJ** prism, made of the same material as the hollow blocks, should be higher than that for the filled **3FBP-MJ** prisms.

8. Using FEA, it was possible to conduct a parametric study to investigate the effect of changing the aspect ratio (l/t) on the distributions and values of deformation and stress in a solid 3-course high prism.

Changing the aspect ratio from 1.0 to 4.0 resulted in increasing the prism's deformation in the X-direction by 221.4%. This means that prisms with aspect ratios more than 1.0 have a greater incompatibility of deformation between the X- and Z-directions. This in turn, has a weakening effect on

the prism compressive strength by causing the separation of the prism end faces from the rest of the prism and the development of longitudinal cracks at the lines of contact between the prisms end and side faces.

Increasing the aspect ratio from 1.0 to 4.0 resulted in an increase in the maximum values of the direct vertical stress and the major principal stress in the block material by 11.2% and 13.7% respectively. It also resulted in an increase in the difference between the horizontal tensile stresses in the block material in X- and Z-directions. The results show that, for prisms with an l/t = 1.0, there is no difference in the horizontal tensile stresses between the X- and Z-directions, but for prisms with an l/t = 4.0, the tensile stresses in the Z-direction are 100% higher than that in the X-direction. The difference in the tensile stresses is even higher, at 116.3%, when determined by comparing the maximum values of the minor principal stresses on the prism end faces (MST2) with the side faces (MST1).

9. Based on the results of the FEA, the decrease in prisms strength with increase in the aspect ratio (l/t) were calculated as a reduction factor to the strength of solid 3SBP-MJ prism with an aspect ratio of 1.0.

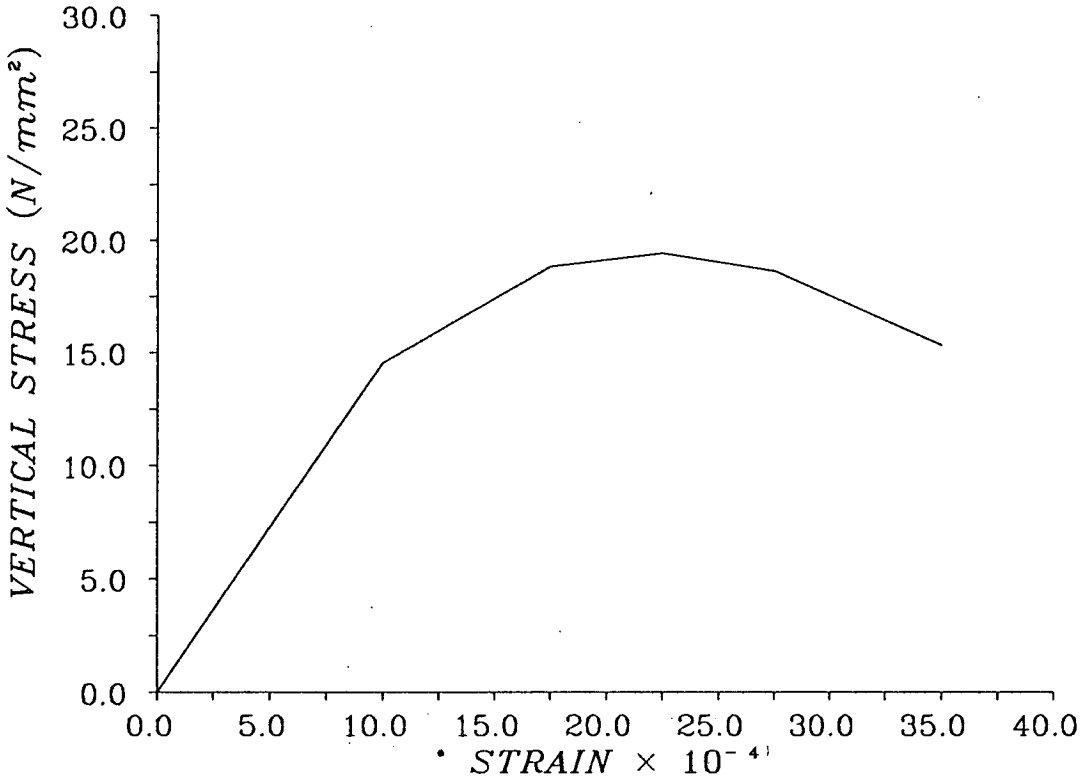

Fig. 6.1 - Idealised stress-strain curve for solid concrete block material used in FEA.

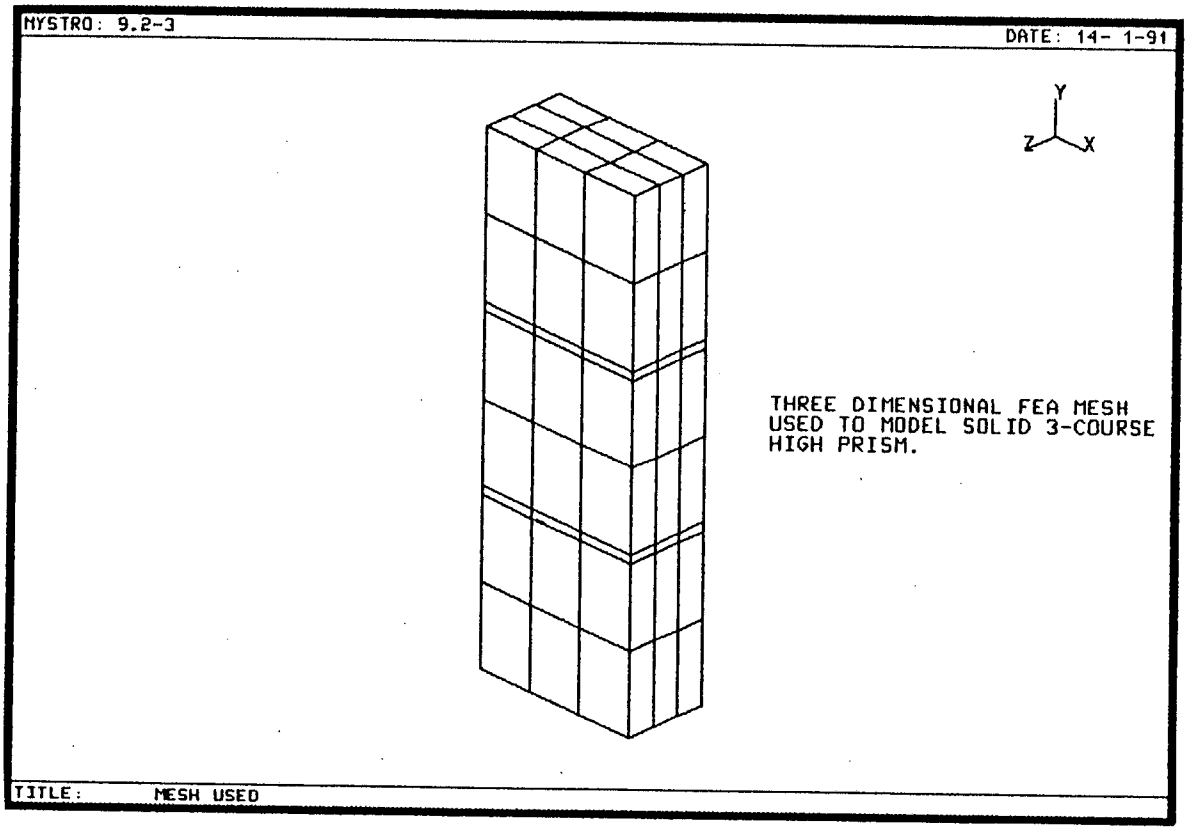

Fig. 6.2 - Three-dimensional mesh used in non-linear FEA of solid 3SBP-MJ prism.

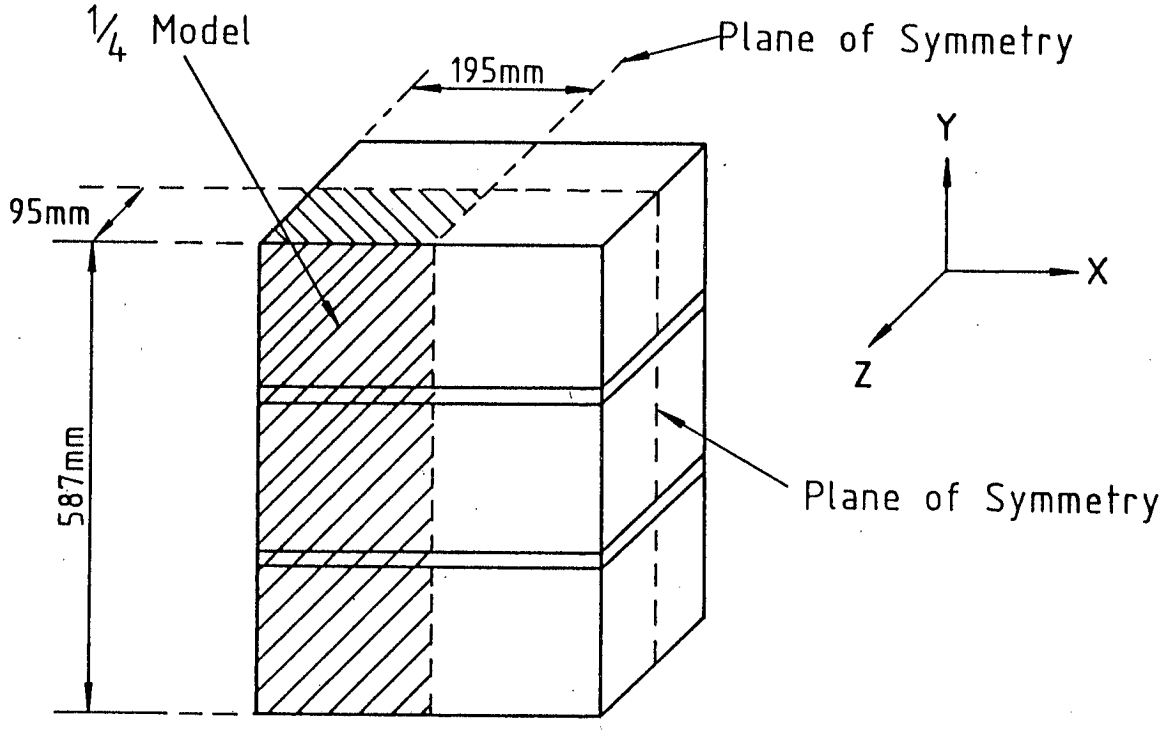

Fig. 6.3 - 1/4 prism model used in non-linear FEA of solid 3SBP-MJ prism.

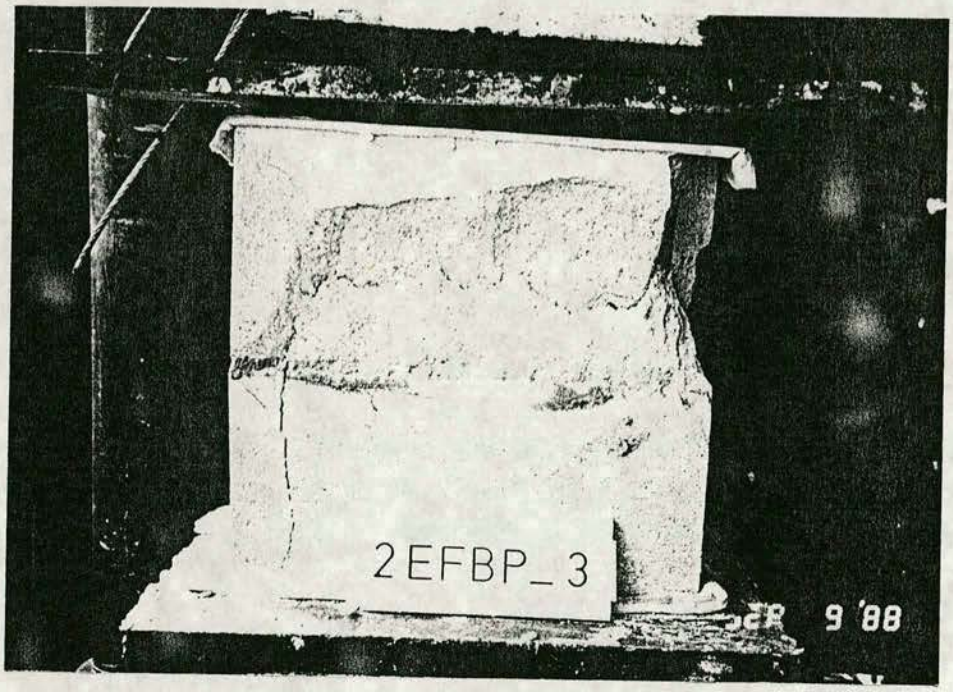

Fig. 6.4 - Unfilled 2FBP-MJ prism after failure, mortar strength 21.21 N/mm^2.

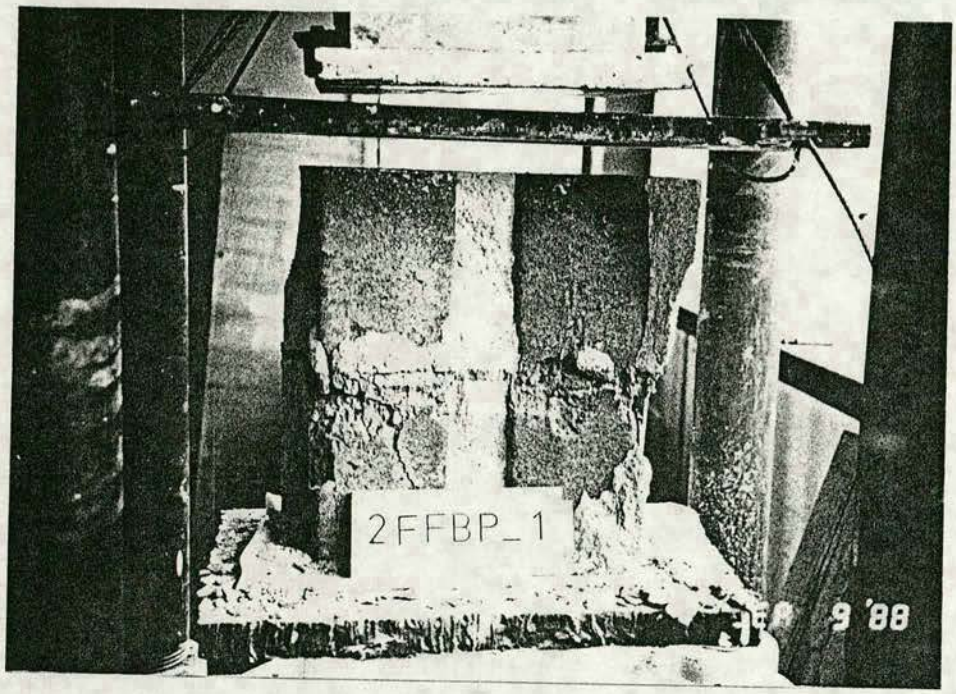

Fig. 6.5 - Filled 2FBP-MJ prism after failure, mortar strength 21.21 N/mm^2, concrete strength 17.11 N/mm^2.

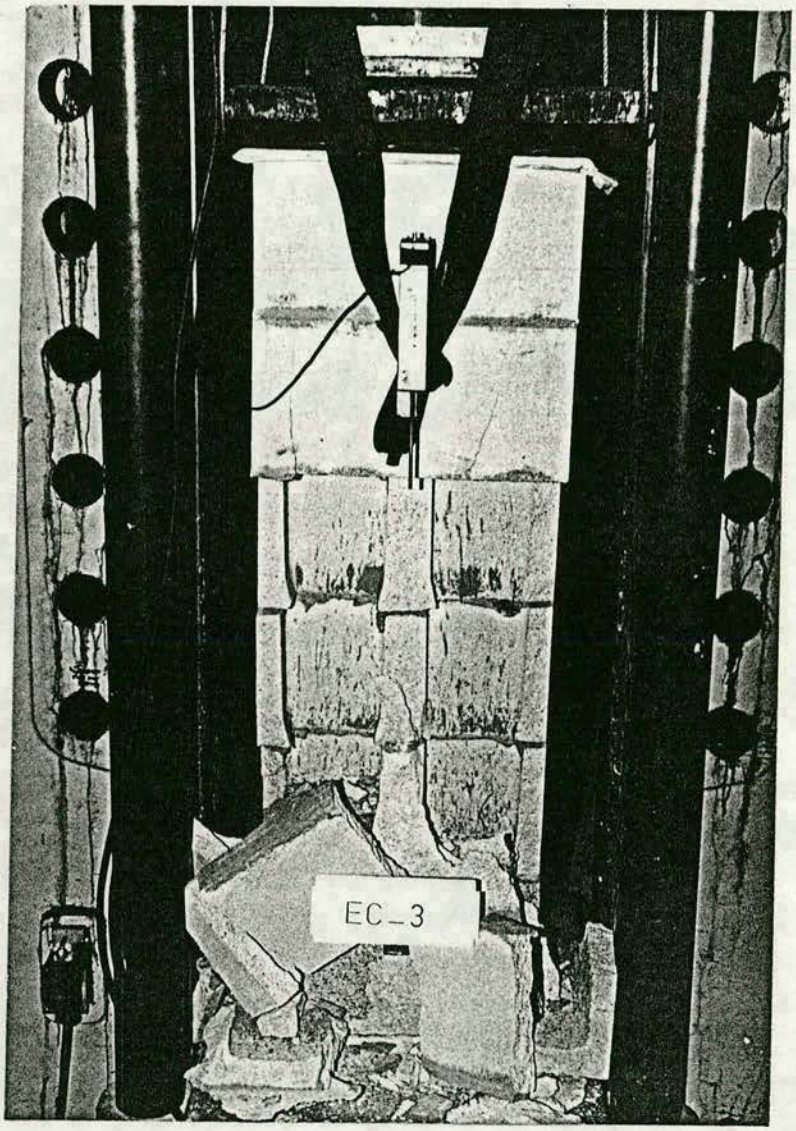

Fig. 6.6 - Unfilled 6FBP-MJ prism after failure, mortar strength 26.58 N/mm^2.

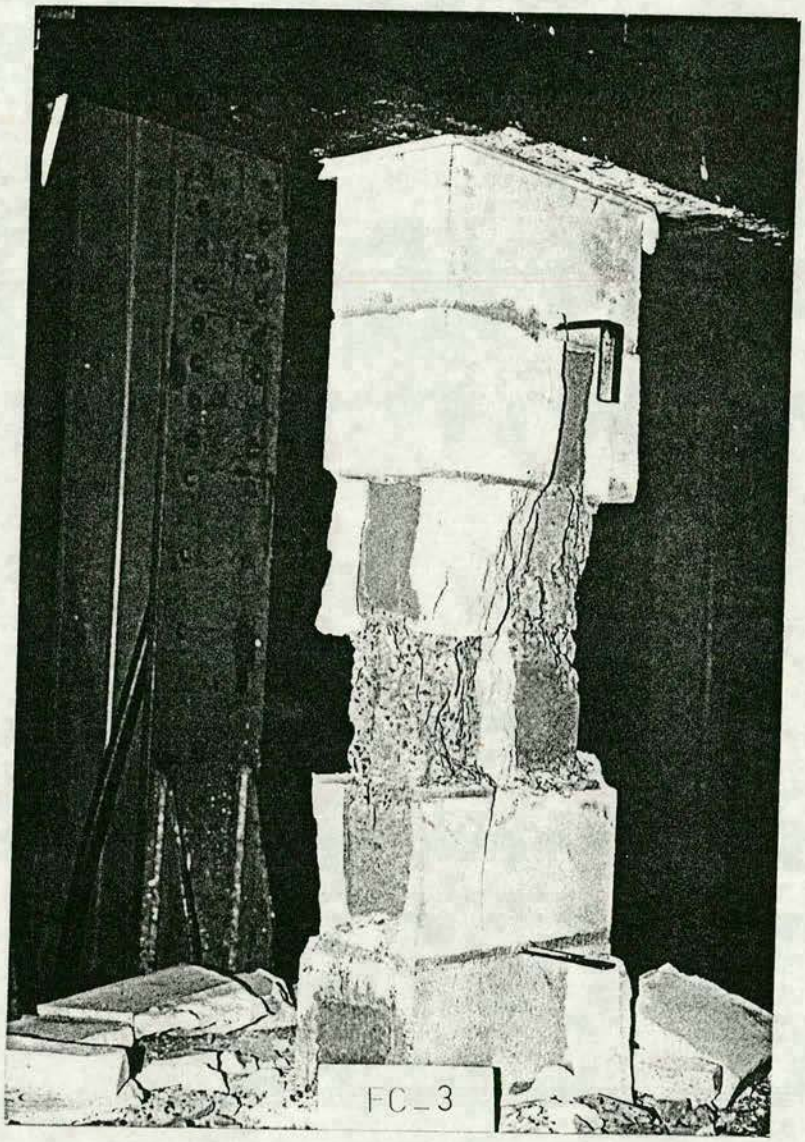

Fig. 6.7 - Filled 6FBP-MJ prism after failure, mortar strength 26.58 N/mm^2, concrete strength 20.81 N/mm^2.

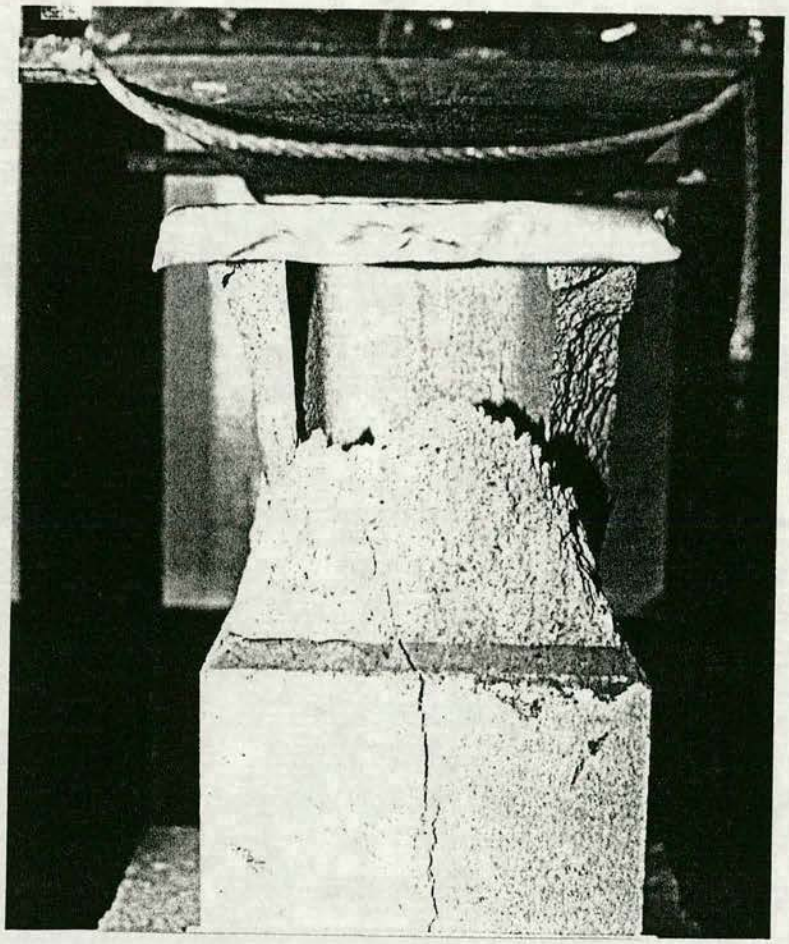

Fig. 6.8 - Unfilled 2HBP-MJ prism after failure, mortar strength 21.21 N/mm^2.

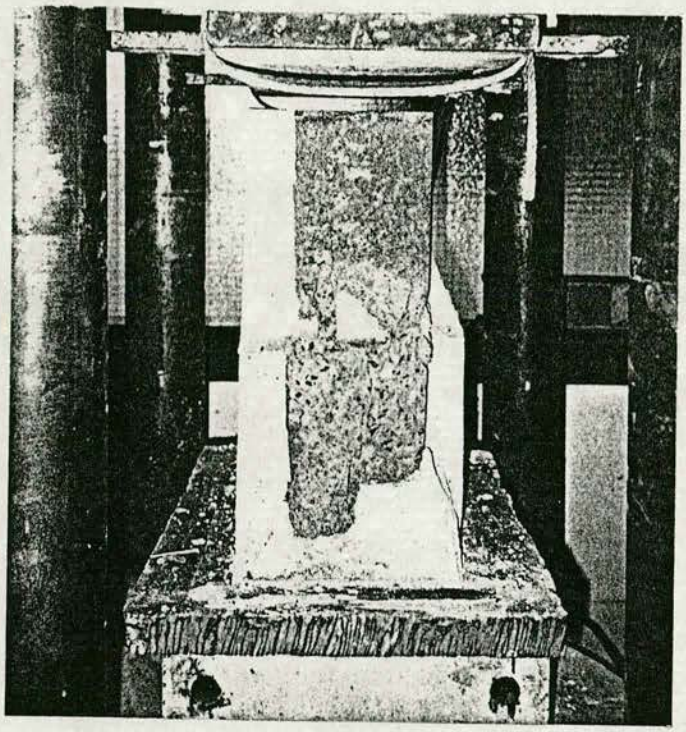

Fig. 6.9 - Filled 2HBP-MJ prism after failure, mortar strength 21.21 N/mm^2, concrete strength 17.11 N/mm^2.

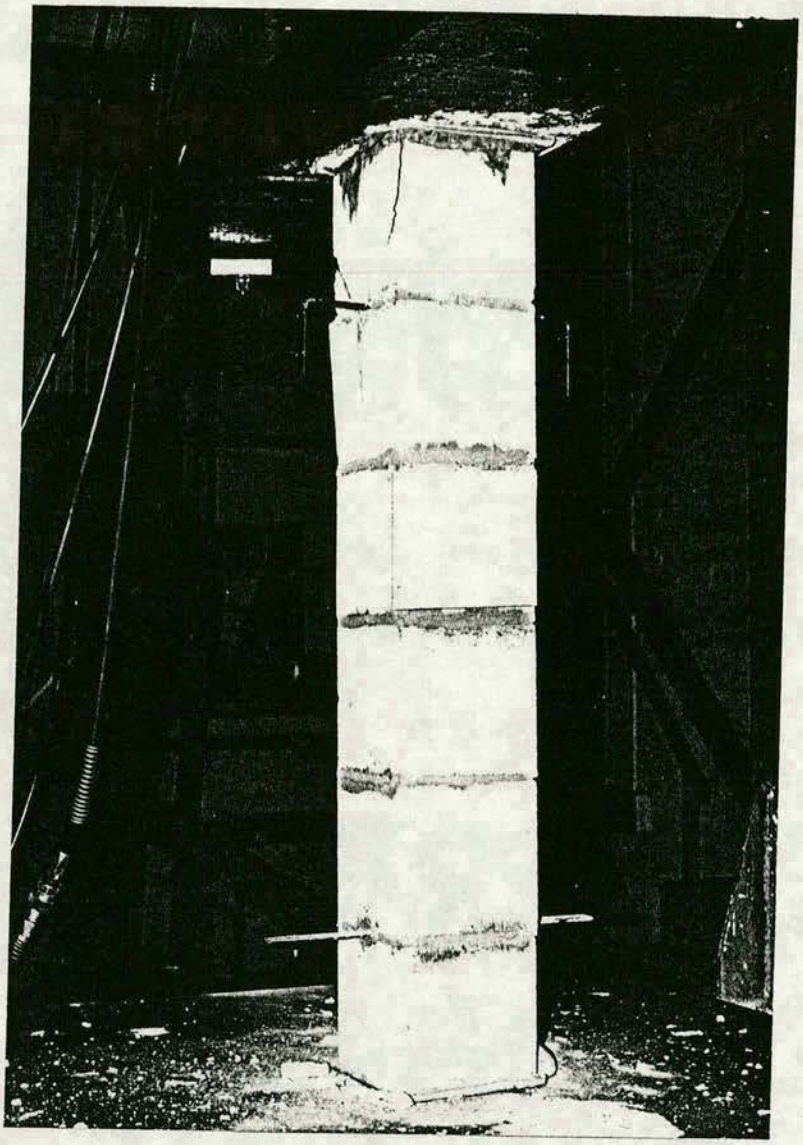

Fig. 6.10 - Unfilled 6HBP-MJ prism after failure, mortar strength 25.95 N/mm^2.

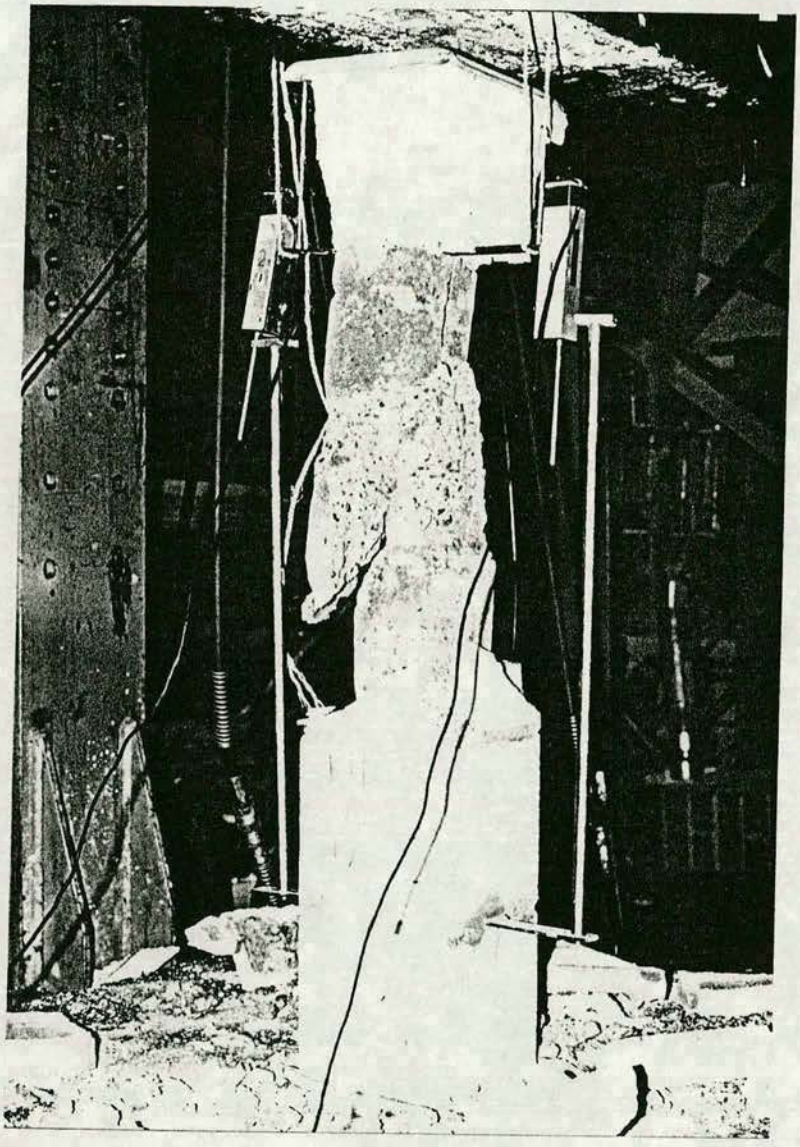

Fig. 6.11 - Filled 6HBP-MJ prism after failure, mortar strength 25.95 N/mm^2, concrete strength 19.66 N/mm^2.

Table 6.1

Compressive strength of full-block prisms compressed normal to bed face.

Prism type	Average compressive * strength (N/mm^2) Area used Net	Gross	S.D. (N/mm^2)	Material cube compressive ♦ strength (N/mm^2) Mortar f_{mr}	Infill f_c
		2FBP-MJ Prism ♦			
Unfilled	24.88	14.00	1.84/1.03	21.21	-
Filled	-	16.82	1.02	21.21	17.11
		3FBP-MJ prism ♦			
Unfilled	21.35	12.01	0.41/0.23	26.54	-
Filled	-	14.53	0.23	26.54	28.75
		6FBP-MJ prism ♦			
Unfilled	17.48	9.84	0.55/0.31	26.58	-
Filled	-	15.23	0.92	26.58	20.81
		Prism with 5 mm mortar joints ♦			
Unfilled	23.27	13.10	1.55/0.87	21.18	-
Filled	-	14.46	1.05	21.18	16.46
		Prism with 20 mm mortar joints ♦			
Unfilled	19.18	10.80	2.59/1.46	21.21	-
Filled	-	12.78	1.09	21.21	17.11
		Prism coated with oil ♦			
Filled	-	14.09	0.43	25.64	19.26

* Average and S.D. are calculated for three prisms.

♦ Cube compressive strength of block material f_b = 24.29 N/mm^2.

♦ Net area = Area at section (1) = 41700 mm^2. (See Table 3.2).

Gross area = 390 x 190 = 74100 mm^2.

Table 6.2

Compressive strength of half-block prisms compressed normal to bed face.

Prism type	Average compressive * strength (N/mm^2) Area used Net	Gross	S.D. (N/mm^2)	Material cube compressive ♦ strength (N/mm^2) Mortar f_{mr}	Infill f_c
		2HBP-MJ Prism ♦			
Unfilled	25.95	14.30	0.39/0.22	21.21	-
Filled	-	23.23	0.44	21.21	17.11
		3HBP-MJ prism ♦			
Unfilled	25.49	14.06	0.38/0.21	26.54	-
Filled	-	20.46	1.08	26.54	28.75
		6HBP-MJ Prism ♦			
Unfilled	23.37	12.88	0.78/0.43	25.95	-
Filled	-	15.55	0.96	25.95	19.66

* Average and S.D. are calculated for three prisms.

♯ Cube compressive strength of block material f_b = 24.29 N/mm^2.

♦ Net area = Area at section (1) = 19900 mm^2. (See Table 3.2).

Gross area = 190 x 190 = 36100 mm^2.

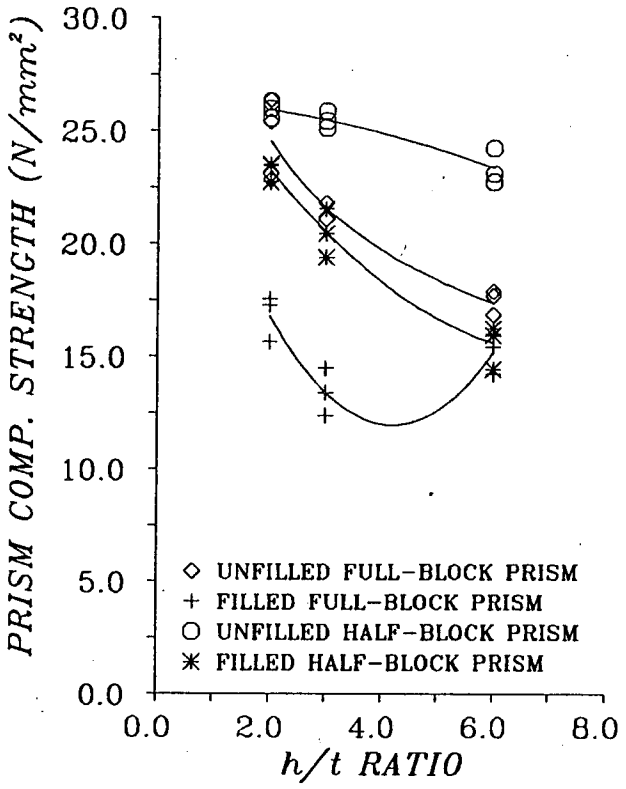

Fig. 6.12 - Effect of h/t ratio on compressive strength of unfilled and filled, full and half-block stack-bonded prisms.

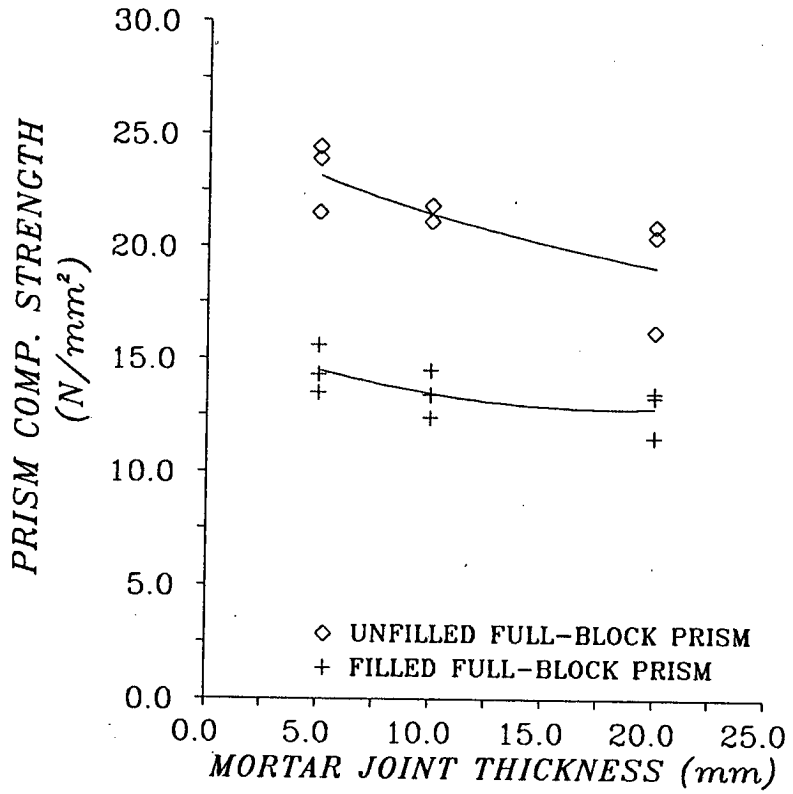

Fig. 6.13 - Effect of mortar joint thickness on compressive strength of unfilled and filled 3FBP-MJ prisms.

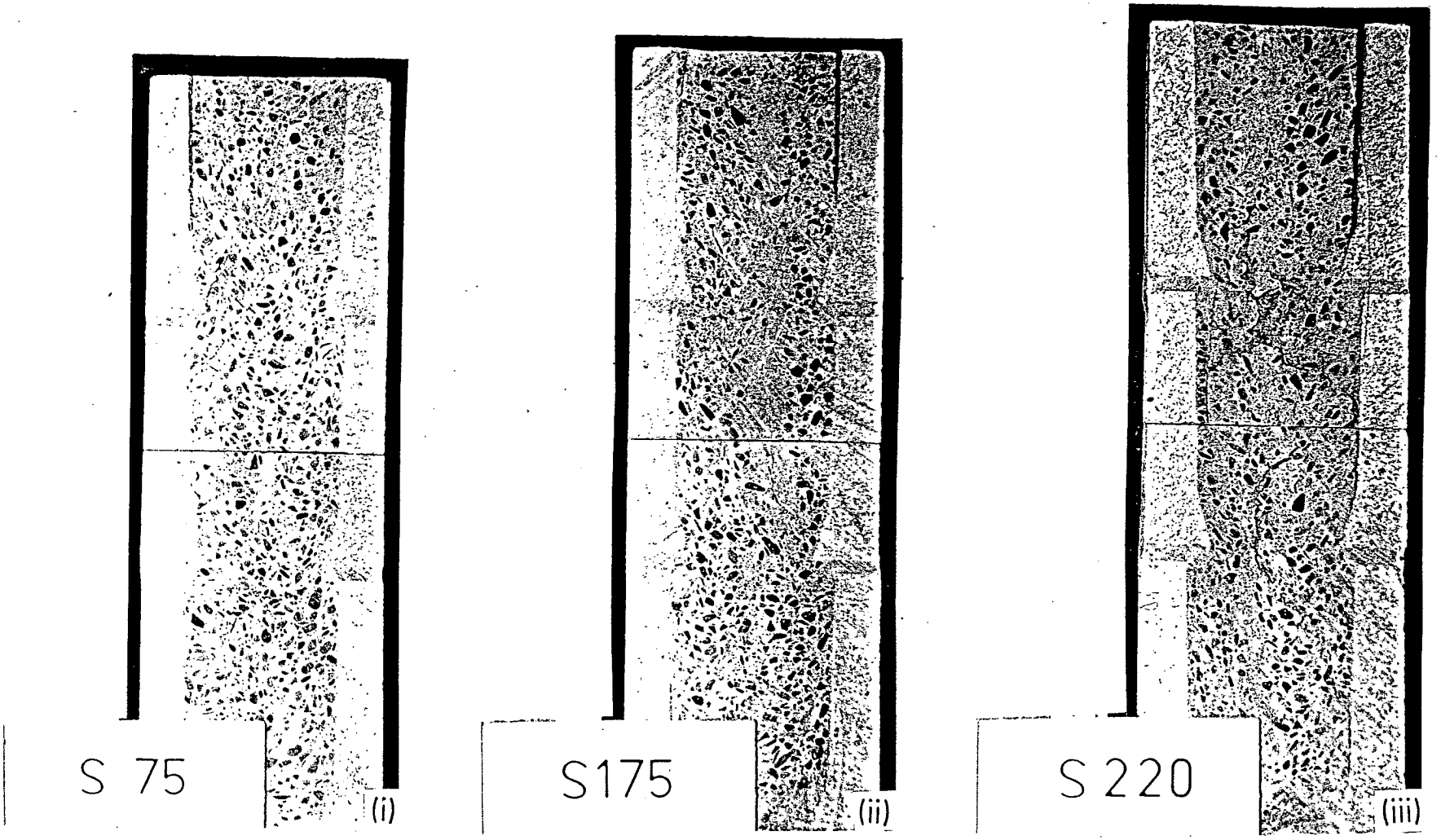

Fig. 6.14 - Photographs of cross-section in 3HBP-MJ prisms filled with concrete mix of different slumps. (i) 75 mm, (ii) 175 mm (iii) 220 mm.

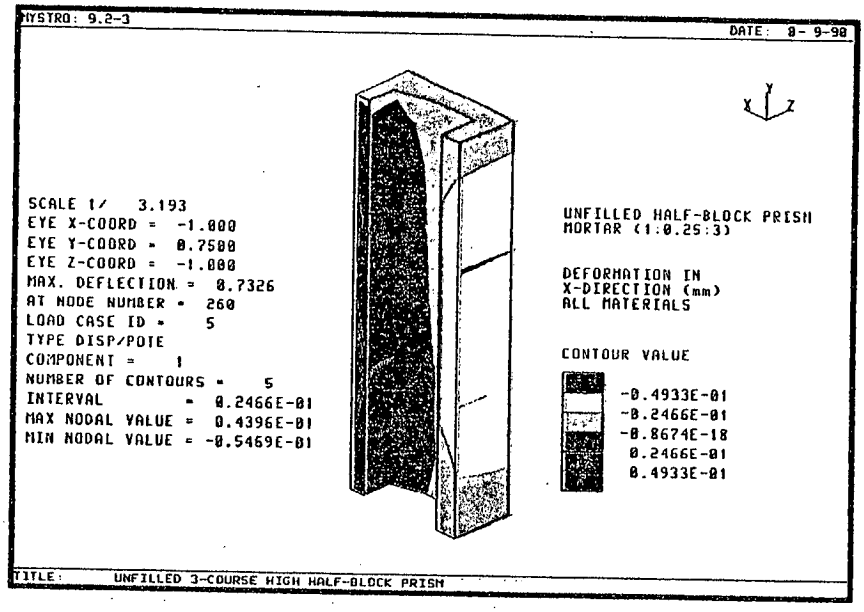

Fig. 6.15 - Deformation of unfilled 3HBP-MJ prism in X-direction, parametric study non-linear FEA.

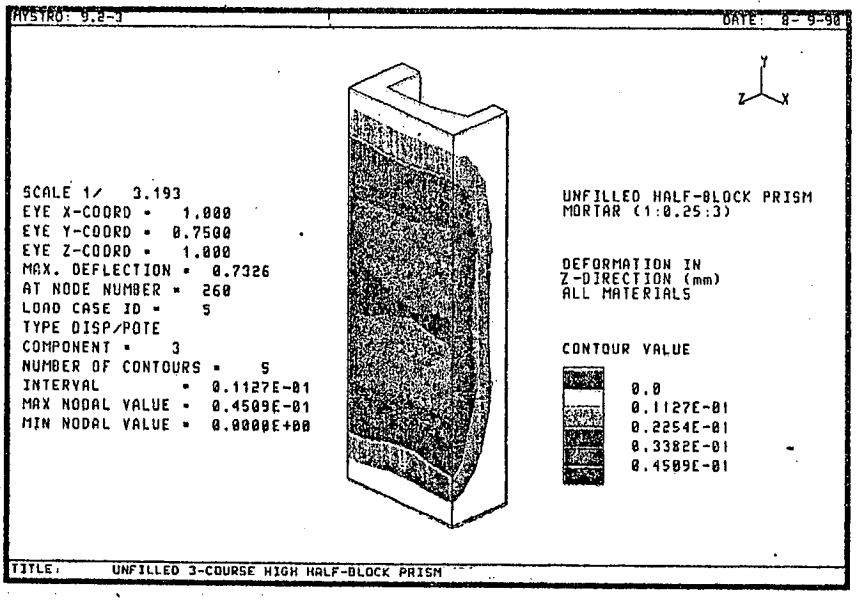

Fig. 6.16 - Deformation of unfilled 3HBP-MJ prism in Z-direction, parametric study non-linear FEA.

Table 6.3

Deformation results of the parametric study non-linear FEA for unfilled 3FBP-MJ and 3HBP-MJ prisms.

Prism type	Deformation results * (mm) YD	XD	ZD	Applied stress (N/mm^2)	Prism strength (N/mm^2)
Full-block	0.000 -0.709	0.000 -0.077	0.045 0.000	12.01	12.01
Half-block	0.000 -0.733	0.044 -0.055	0.045 0.000	12.01	14.06

* Figures quoted in the table are the lower and upper maximum values of deformation.
YD, XD and ZD = Deformation in the Y-, X- and Z-directions.
+ve values = In the +ve direction of the axes.
-ve values = In the -ve direction of the axes.

Table 6.4

Stress results of the parametric study non-linear FEA for unfilled 3FBP-MJ and 3HBP-MJ prisms.

Prism type	Stress results * (N/mm^2) YST	XST	ZST	SST	MJST	MST1	MST2
			Block material				
Full-block	-17.91	2.50	2.13	10.96	-17.96	1.60	2.87
	-27.73	-10.83	-10.83	7.63	-28.87	-10.84	-9.69
Half-block	-18.30	2.28	2.24	11.20	-18.30	1.63	2.32
	-27.10	-10.30	-10.30	7.88	-27.90	-10.30	-9.53
			Mortar material				
Full-block	-18.16	-3.00	-3.53	8.25	-18.16	-4.18	-2.98
	-22.40	-6.84	-6.63	7.12	-22.76	-6.64	-6.48
Half-block	-18.60	-2.71	-3.72	8.87	-18.60	-4.41	-2.70
	-23.00	-7.23	-7.04	7.24	-23.80	-7.04	-6.45

* Figures quoted in the table are the upper and lower maximum values of stress.

YST, XST and ZST = Direct stress in the Y-, X- and Z-directions.

SST = Maximum shear stress.

MJST, MST1 and MST2 = Major, minor 1 and 2 principal stresses.

+ve values = Tension.

-ve values = Compression.

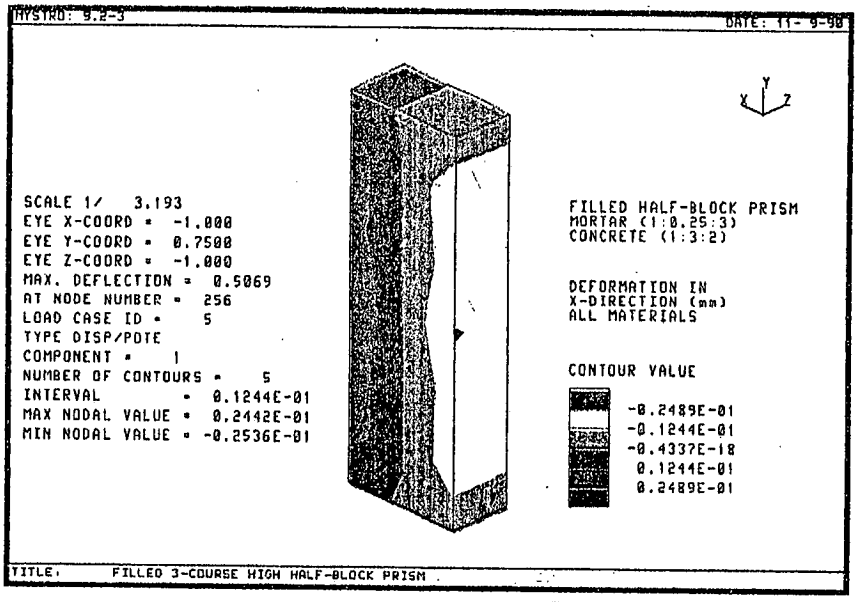

Fig. 6.17 - Deformation of filled 3HBP-MJ prism in X-direction, parametric study non-linear FEA.

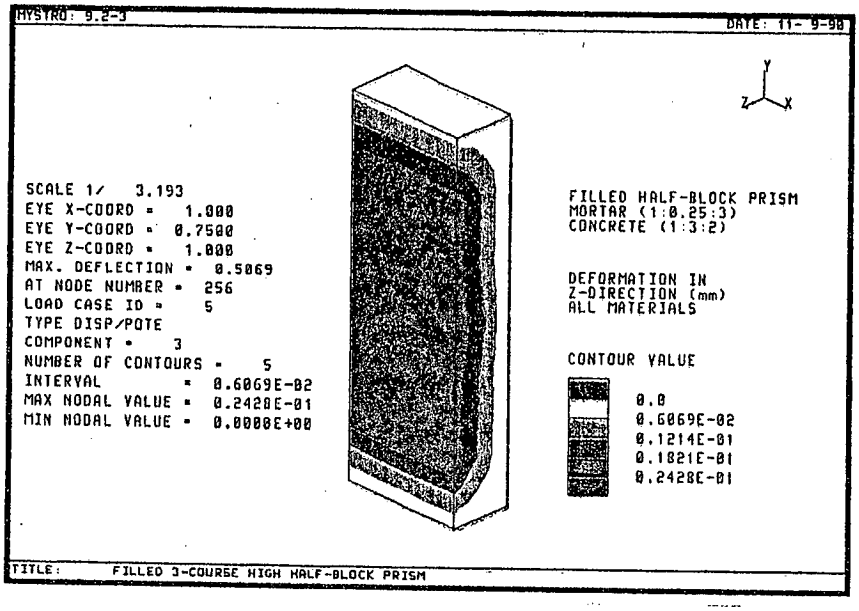

Fig. 6.18 - Deformation of filled 3HBP-MJ prism in Z-direction, parametric study non-linear FEA.

Table 6.5

Deformation results of the parametric study non-linear FEA for filled 3FBP-MJ and 3HBP-MJ prisms.

Prism type	Deformation results * (mm) YD	XD	ZD	Applied stress (N/mm^2)	Prism strength (N/mm^2)
Full-block	0.000 -0.502	0.000 -0.048	0.025 0.000	14.53	14.53
Half-block	0.000 -0.509	0.024 -0.025	0.024 0.000	14.53	20.46

* Figures quoted in the table are the upper and lower maximum values of deformation.
YD, XD and ZD = Deformation in the Y-, X- and Z-directions.
+ve values = In the +ve direction of the axes.
-ve values = In the -ve direction of the axes.

Table 6.6

Stress results of the parametric study non-linear FEA for filled 3FBP-MJ and 3HBP-MJ prisms.

Prism type	Stress results * (N/mm^2) YST	XST	ZST	SST	MJST	MST1	MST2
			Block material				
Full-block	-14.88	1.51	1.46	9.34	-14.88	1.23	1.68
	-22.18	-7.52	-7.52	6.83	-23.02	-7.52	-6.69
Half-block	-15.10	1.74	1.55	9.14	-15.10	1.28	1.77
	-21.40	-6.91	-6.91	7.08	-21.90	-6.91	-6.36
			Concrete material				
Full-block	-9.45	0.96	0.91	10.09	-9.46	0.80	1.44
	-31.55	-11.96	-11.50	3.71	-31.56	-12.08	-11.37
Half-block	-9.55	0.93	0.91	10.30	-9.55	0.78	1.34
	-32.20	-12.30	-11.80	3.98	-32.20	-12.40	-11.60
			Mortar material				
Full-block	-6.85	-0.85	-1.00	6.43	-6.85	-1.01	-0.84
	-16.94	-4.50	-4.52	2.96	-17.00	-4.50	-4.45
Half-block	-6.32	-0.67	-0.85	6.46	-6.32	-0.86	-0.66
	-16.90	-4.58	-4.54	2.77	-17.10	-4.40	-4.40

* Figures quoted in the table are the upper and lower maximum values of stress.

YST, XST and ZST = Direct stress in the Y-, X- and Z-directions.

SST = Maximum shear stress.

MJST, MST1 and MST2 = Major, minor 1 and 2 principal stresses.

+ve values = Tension.

-ve values = Compression.

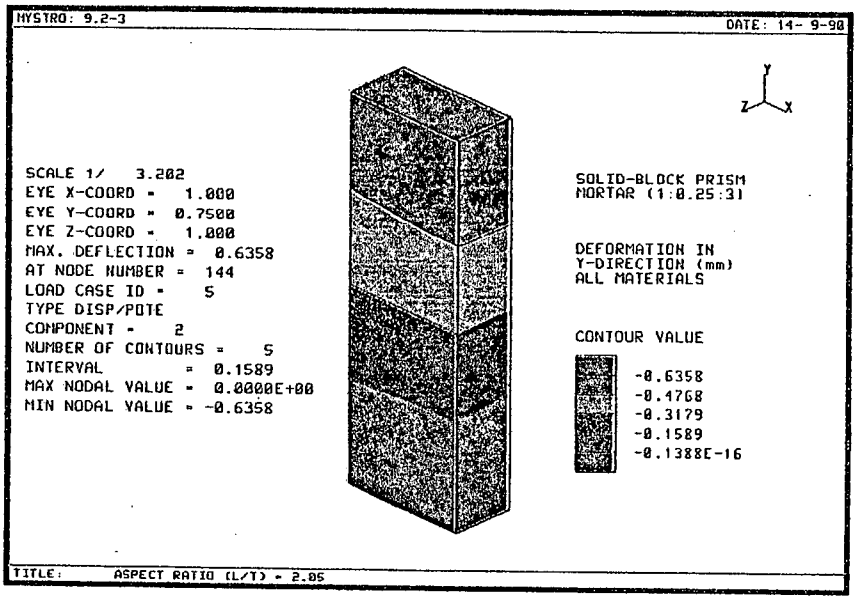

Fig. 6.19 - Deformation of solid 3SBP-MJ prism in Y-direction, parametric study non-linear FEA.

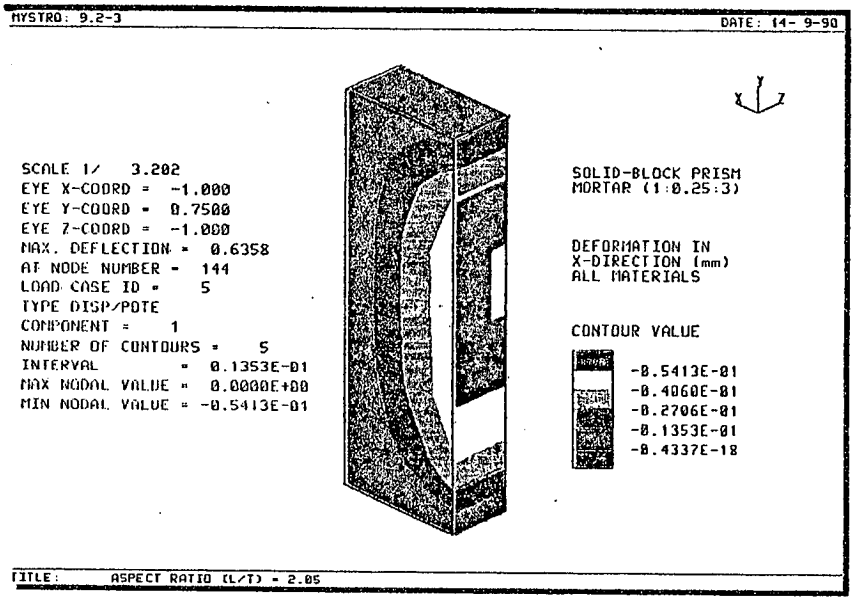

Fig. 6.20 - Deformation of solid 3SBP-MJ prism in X-direction, parametric study non-linear FEA.

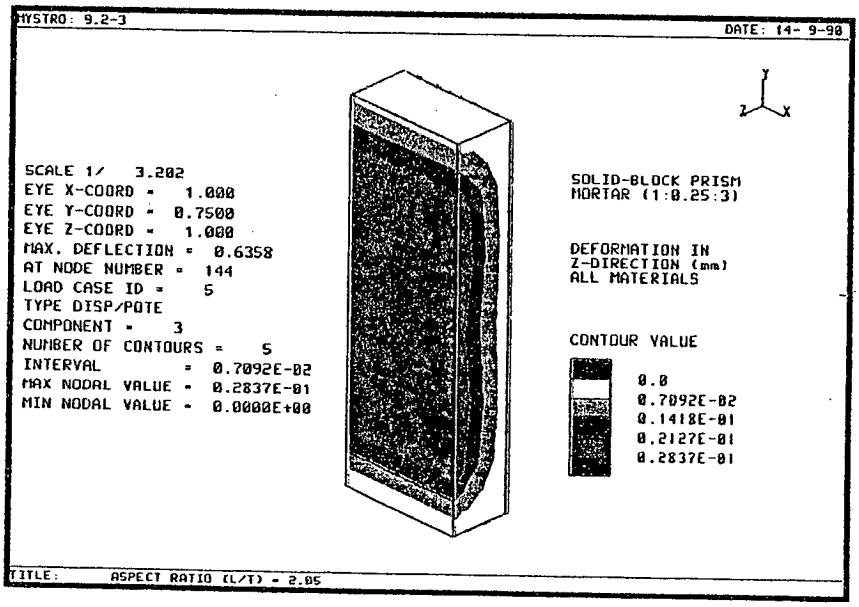

Fig. 6.21 - Deformation of solid 3SBP-MJ prism in Z-direction, parametric study non-linear FEA.

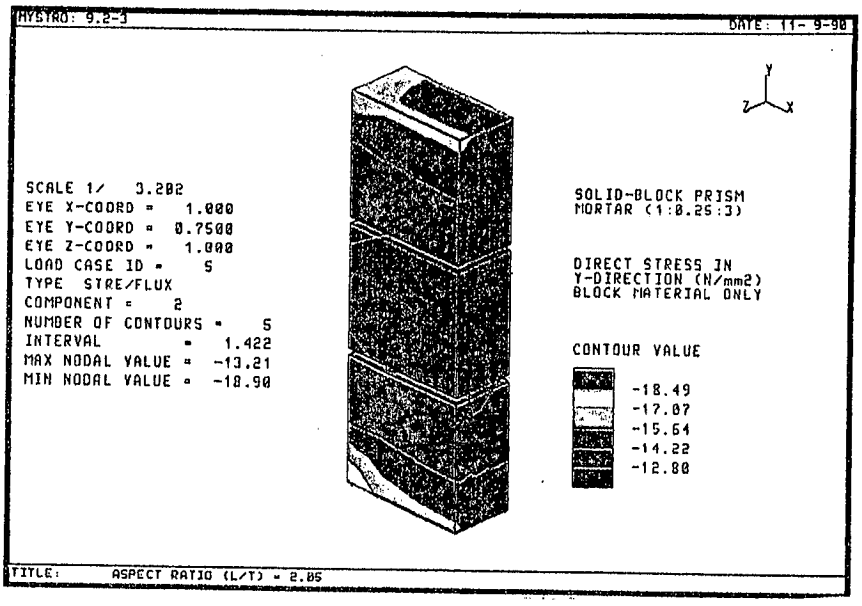

Fig. 6.22 - Direct stress in Y-direction, block material of solid 3SBP-MJ prism, parametric study non-linear FEA.

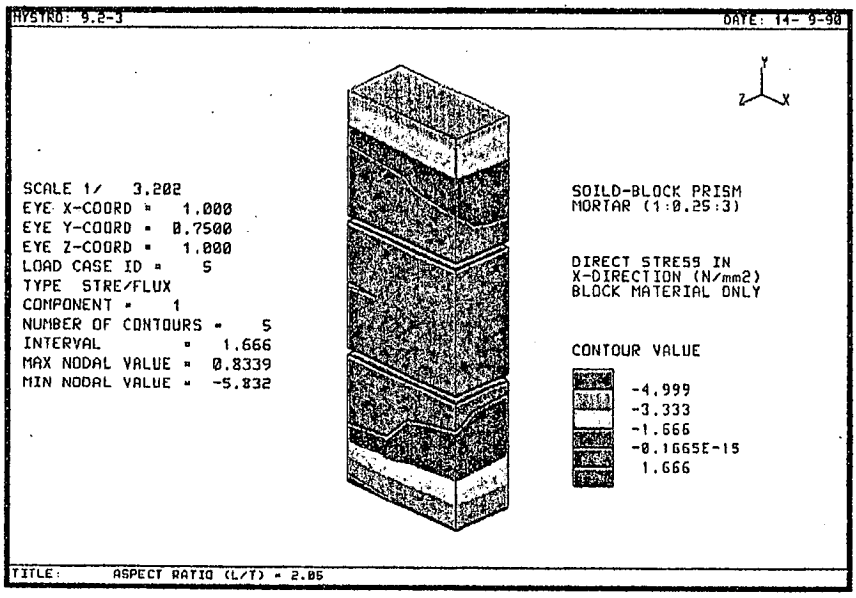

Fig. 6.23 - Direct stress in X-direction, block material of solid 3SBP-MJ prism, parametric study non-linear FEA.

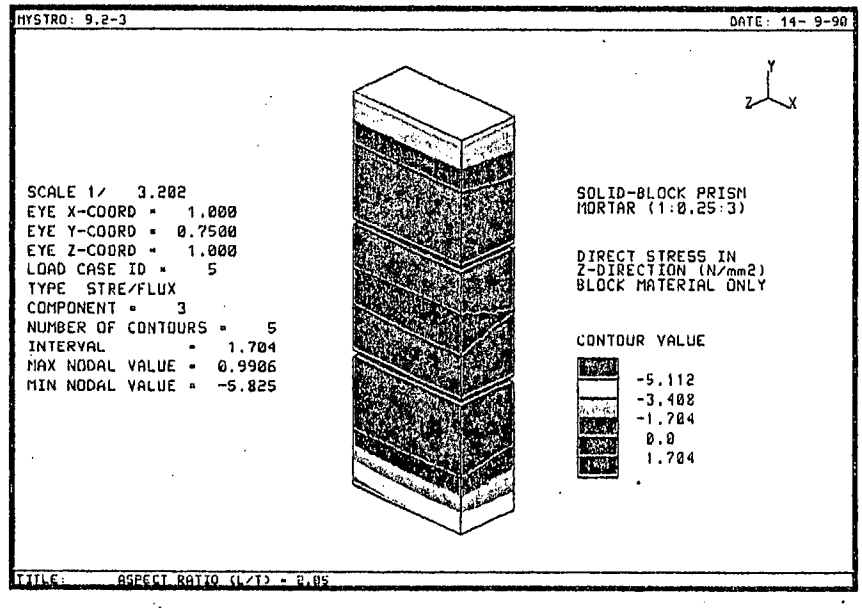

Fig. 6.24 - Direct stress in Z-direction, block material of solid 3SBP-MJ prism, parametric study non-linear FEA.

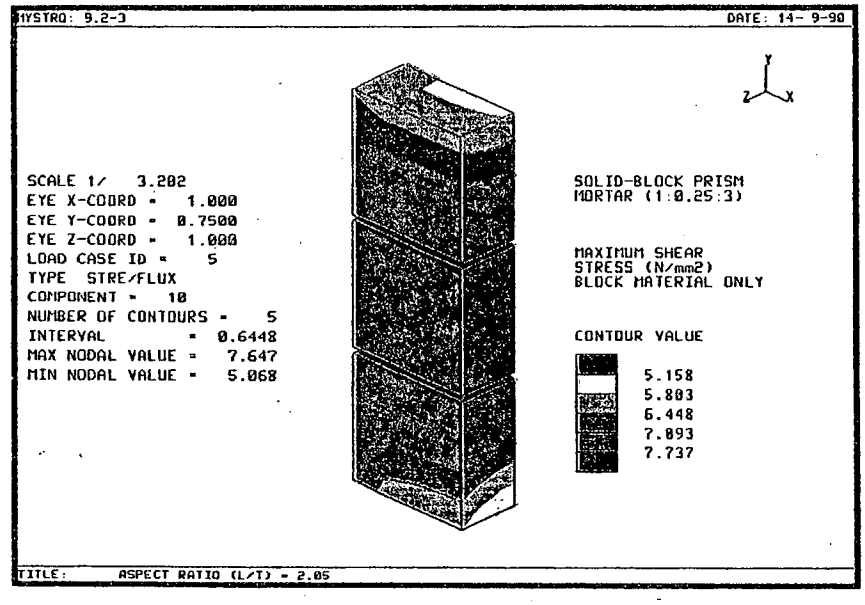

Fig. 6.25 - Maximum shear stress, block material of solid 3SBP-MJ prism, parametric study non-linear FEA.

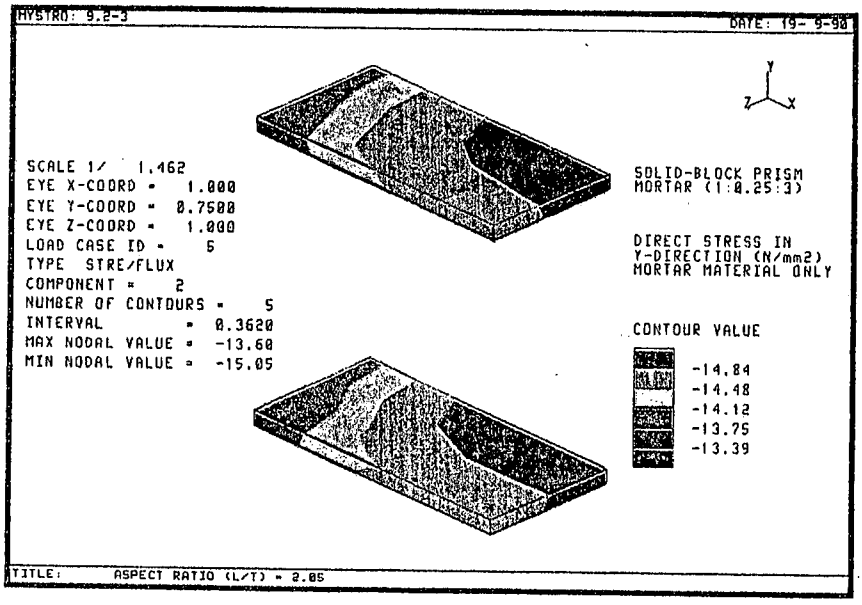

Fig. 6.26 - Direct stress in Y-direction, mortar material of solid 3SBP-MJ prism, parametric study non-linear FEA.

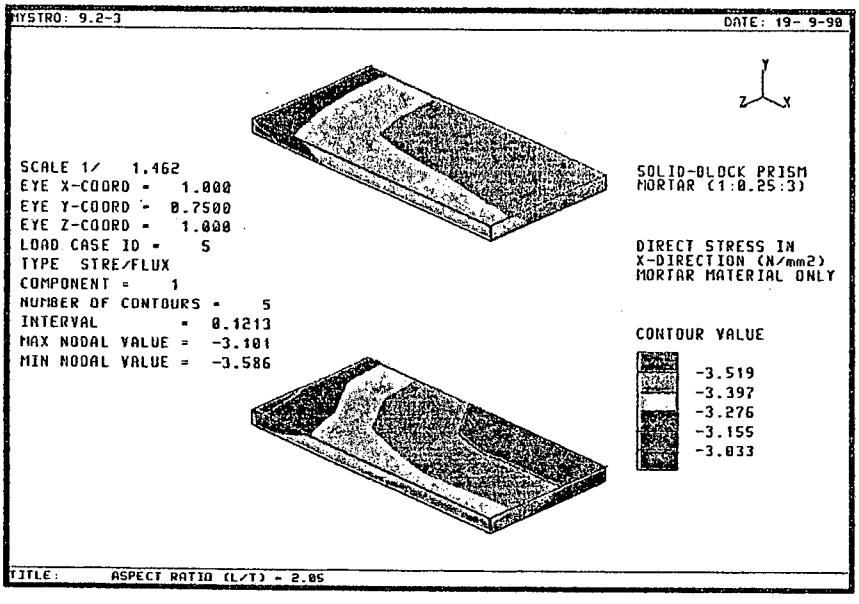

Fig. 6.27 - Direct stress in X-direction, mortar material of solid 3SBP-MJ prism, parametric study non-linear FEA.

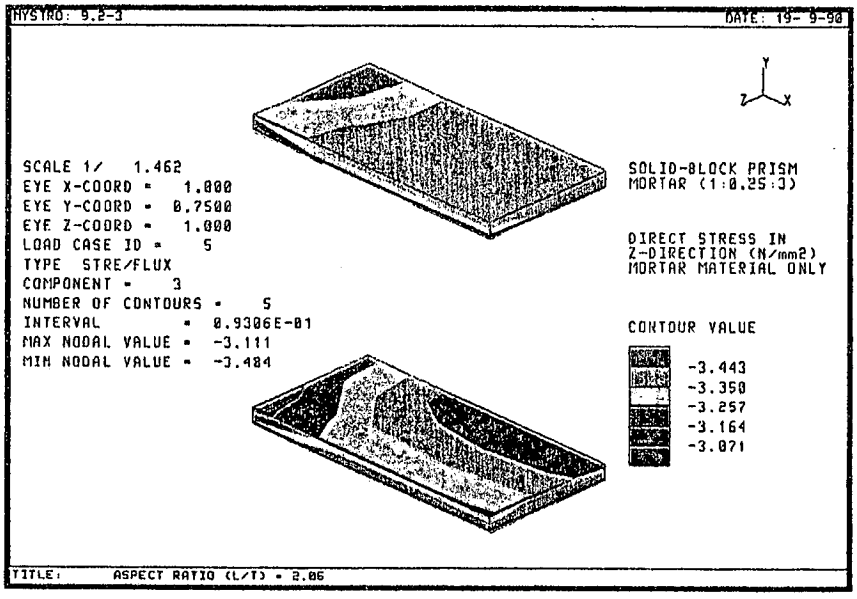

Fig. 6.28 - Direct stress in Z-direction, mortar material of solid 3SBP-MJ prism, parametric study non-linear FEA.

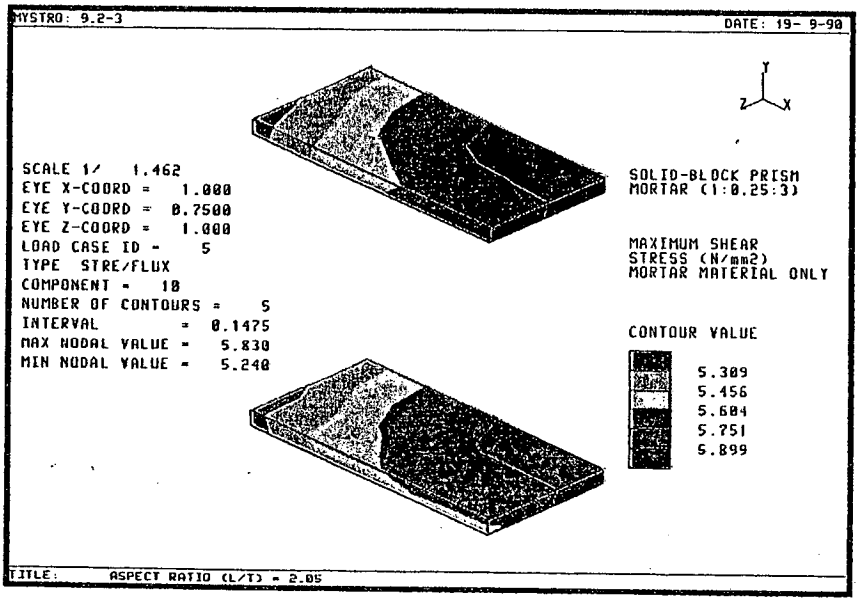

Fig. 6.29 - Maximum shear stress, mortar material of solid 3SBP-MJ prism, parametric study non-linear FEA.

Table 6.7

Deformation results of the parametric study non-linear FEA conducted to study the effect of l/t ratio on compressive strength of solid 3SBP-MJ prism.

Aspect ratio (l/t)	Deformation results * (mm) YD	XD	ZD	Applied stress (N/mm^2)
1.0	0.000 -0.637	0.000 -0.028	0.028 0.000	14.53
1.5	0.000 -0.636	0.000 -0.040	0.028 0.000	=
2.05	0.000 -0.636	0.000 --0.054	0.028 0.000	=
2.5	0.000 -0.637	0.000 -0.065	0.029 0.000	=
3.0	0.000 -0.638	0.000 -0.075	0.030 0.000	=
4.0	0.000 -0.640	0.000 -0.090	0.031 0.000	=

* Figures quoted in the table are the upper and lower maximum values of deformation.
YD, XD and ZD = Deformation in the Y-, X- and Z-directions.
+ve values = In the +ve direction of the axes.
-ve values = In the -ve direction of the axes.

Table 6.8

Stress results of the parametric study non-linear FEA conducted to study the effect of l/t ratio on compressive strength of solid 3SBP-MJ prism.

Aspect ratio (l/t)	Stress results * (N/mm^2) YST	XST	ZST	SST	MJST	MST1	MST2
			Block material				
1.0	-13.50	1.07	1.07	7.58	-13.60	1.03	1.10
	-17.80	-5.59	-5.59	5.21	-18.20	-5.59	-5.22
1.5	-13.30	0.956	1.02	7.59	-13.30	0.756	1.02
	-18.40	-5.71	-5.71	5.13	-18.90	-5.71	-5.21
2.05	-13.20	0.834	0.991	7.65	-13.20	0.647	0.991
	-18.90	-5.83	-5.83	5.07	-19.50	-5.83	-5.21
2.5	-13.00	0.722	1.02	7.68	-13.00	0.675	1.02
	-19.30	-5.92	-5.90	5.04	-20.00	-5.91	-5.21
3.0	-12.70	0.622	1.05	7.74	-12.70	0.624	1.05
	-19.60	-5.98	-5.97	5.02	-20.40	-5.97	-5.18
4.0	-12.20	0.530	1.06	7.87	-12.20	0.485	1.06
	-19.80	-6.03	-6.00	5.06	-20.70	-6.01	-5.07
			Mortar material				
1.0	-14.10	-3.17	-3.17	5.80	-14.10	-3.17	-3.17
	-15.00	-3.47	-3.47	5.43	-15.00	-3.48	-3.47
1.5	-13.80	-3.12	-3.12	5.82	-13.80	-3.12	-3.11
	-15.10	-3.51	-3.47	5.32	-15.10	-3.51	-3.47
2.05	-13.60	-3.10	-3.11	5.83	-13.60	-3.12	-3.10
	-15.10	-3.59	-3.48	5.24	-15.10	-3.59	-3.48
2.5	-13.30	-3.05	-3.07	5.88	-13.30	-3.07	-3.04
	-15.10	-3.68	-3.50	5.13	-15.10	-3.68	-3.50
3.0	-13.00	-2.98	-2.99	5.94	-13.00	-2.99	-2.97
	-15.30	-3.78	-3.51	4.99	-15.30	-3.78	-3.51
4.0	-12.30	-2.85	-2.85	6.30	-12.30	-2.86	-2.84
	-15.50	-3.98	-3.55	4.74	-15.50	-3.98	-3.55

* Figures quoted in the table are the upper and lower values of maximum stress.

YST, XST and ZST = Direct stress in the Y-, X- and Z-directions.

SST = Maximum shear stress.

MJST, MST1 and MST2 = Major, minor 1 and 2 principal stresses.

+ve values = Tension.

-ve values = Compression.

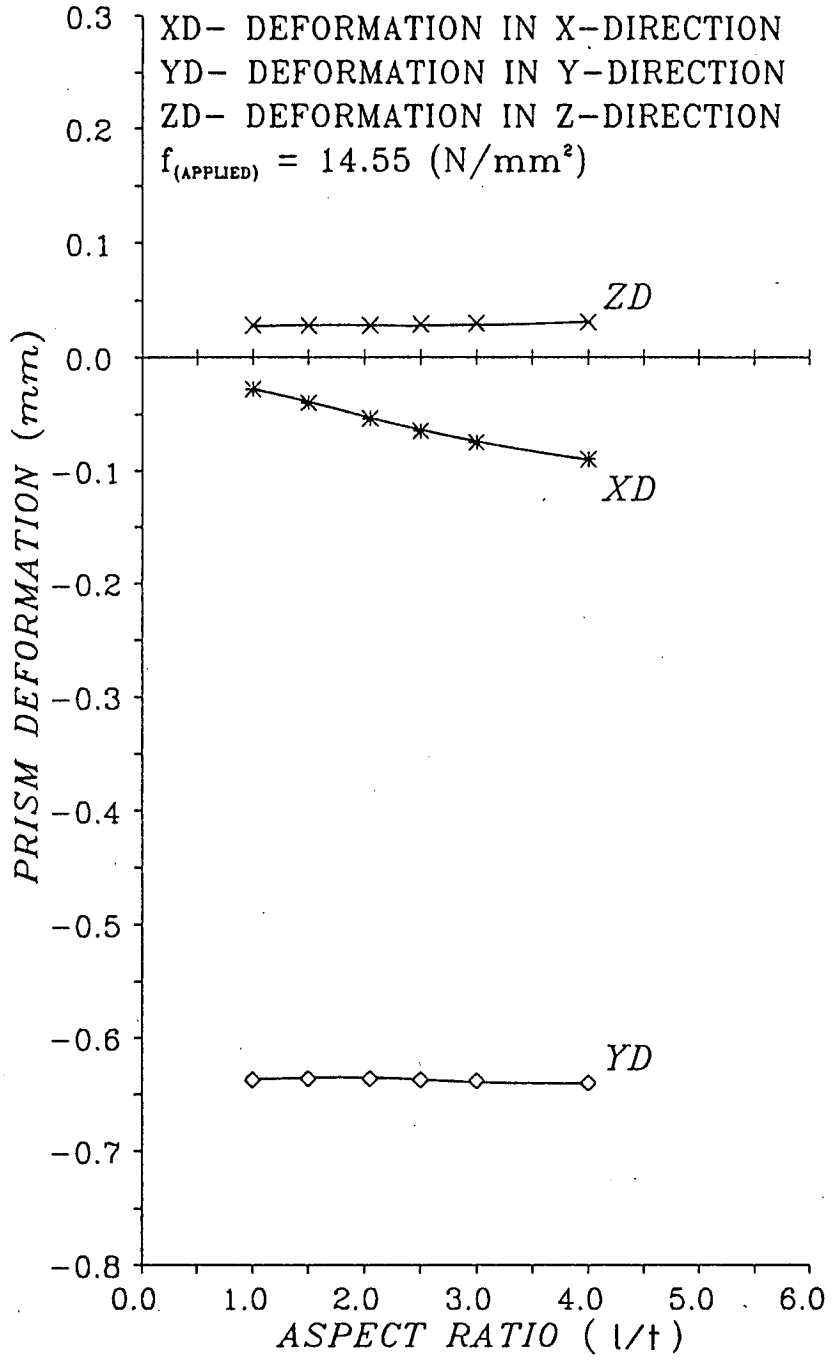

Fig. 6.30 - Effect of l/t ratio on solid 3SBP-MJ prism deformation, parametric study non-linear FEA.

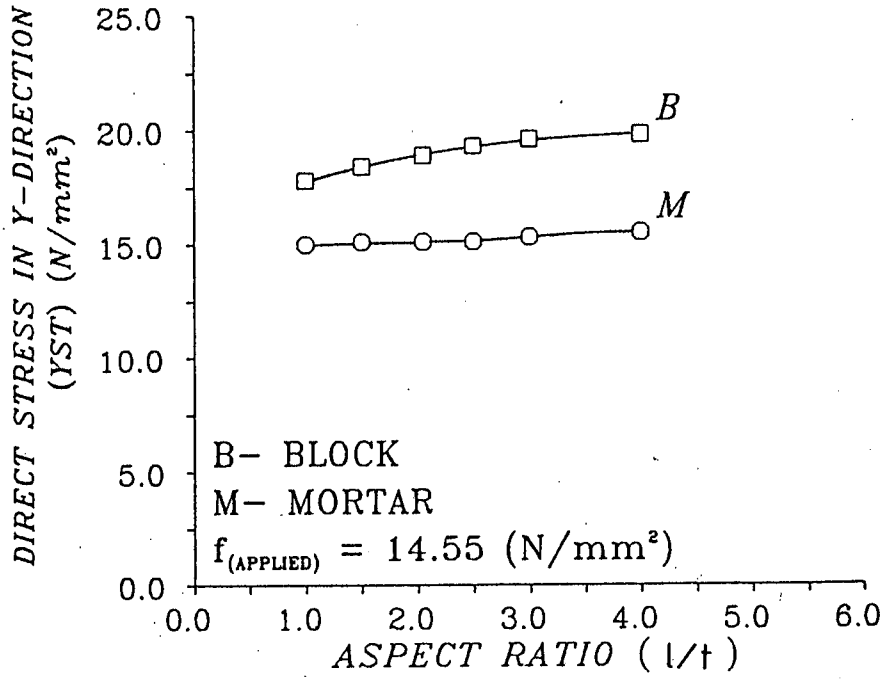

Fig. 6.31 - Effect of l/t ratio on solid 3SBP-MJ prism direct stress in Y-direction, parametric study non-linear FEA.

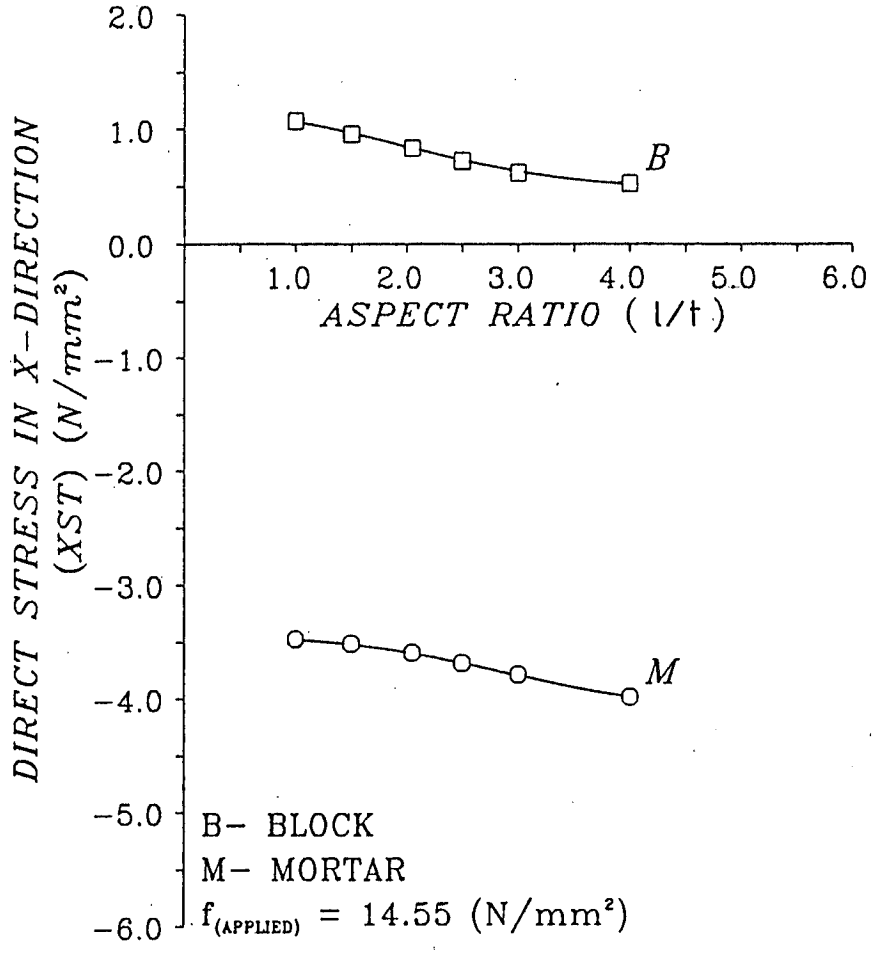

Fig. 6.32 - Effect of l/t ratio on solid 3SBP-MJ prism direct stress in X-direction, parametric study non-linear FEA.

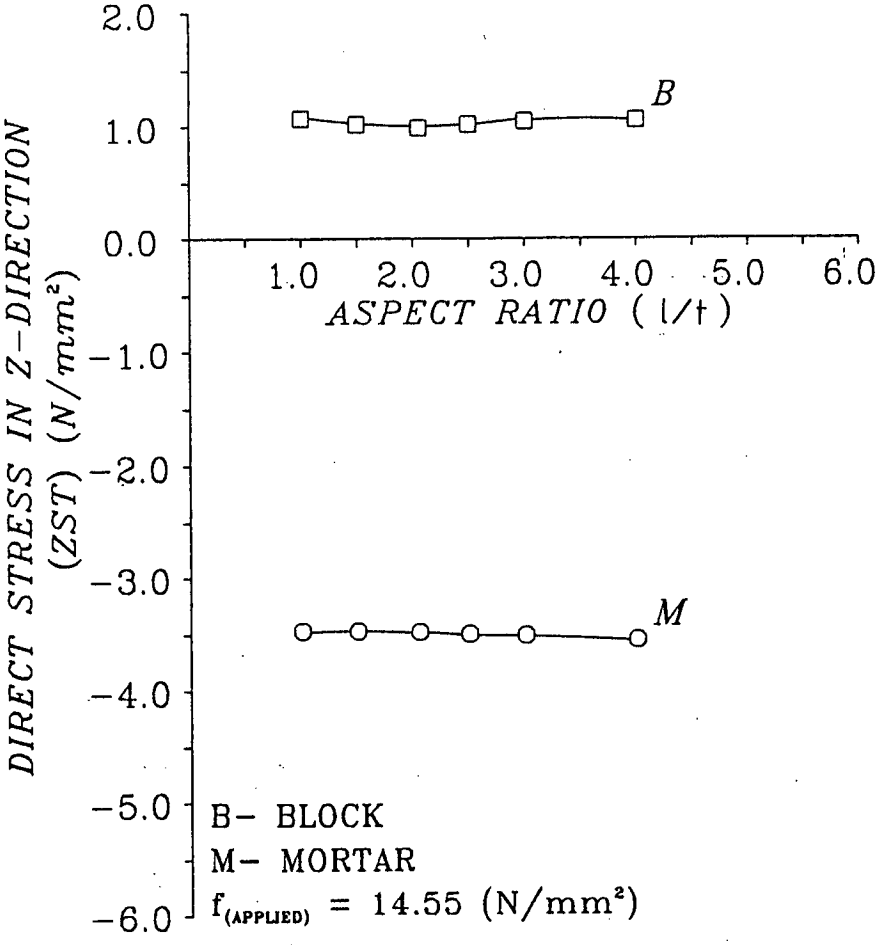

Fig. 6.33 - Effect of l/t ratio on solid 3SBP-MJ prism direct stress in Z-direction, parametric study non-linear FEA.

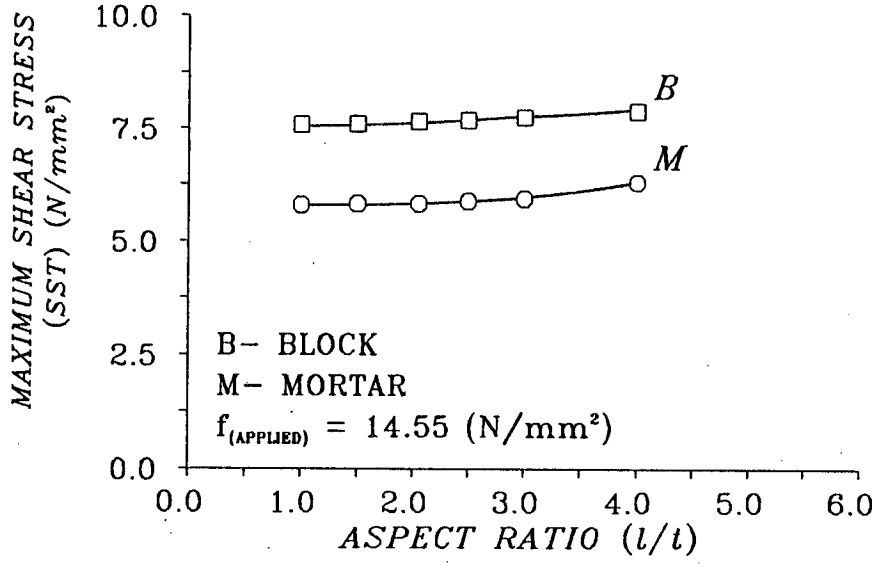

Fig. 6.34 - Effect of l/t ratio on solid 3SBP-MJ prism maximum shear stress, parametric study non-linear FEA.

Table 6.9

Reduction factors for the compressive strength of a solid 3SBP-MJ prism as a result of changing the aspect (l/t) ratio.

Prism length-to-thickness ratio (l/t)	Reduction factor
1.00	1.00
1.50	0.96
2.05	0.93
2.50	0.91
3.00	0.89
4.00	0.88

CHAPTER 7

REINFORCED BLOCKWORK MASONRY COLUMNS

7.1 INTRODUCTION

Blockwork masonry columns can be used as separate elements or in association with other load bearing elements such as masonry walls. Incorporating blockwork columns into walls can increase wall stiffness and from the architectural point of view, blockwork rendering or the use of cladding materials to overcome the differences between the blockwork masonry facing walls and the flat ordinary reinforced concrete columns can be unnecessary. Hollow blocks offer the advantage of using reinforced concrete filled masonry elements without the need for formwork. The reinforcement increases the axial and eccentric load bearing strength of the masonry elements and also enables the design of cross-sections which are smaller than equivalent unreinforced elements.

This chapter presents the results of an experimental investigation carried out to study the performance of reinforced blockwork masonry columns and suggests a method of design, which takes into account the properties of blockwork masonry construction. The results of tests on forty-one axially loaded blockwork columns, with varying lateral and vertical reinforcement, are reported. Results from chapter 6 for the unfilled and filled **6FBP-MJ** and **6HBP-MJ** prisms (in this chapter they are referred to as unfilled and filled unreinforced columns) are used to compare their compressive strength and behaviour with reinforced specimens.

7.2 EXPERIMENTAL PROGRAMME

In total, forty-one short stack-bonded blockwork masonry columns were constructed and tested under axial load, to determine their strength and study the mechanism of failure. The columns were divided into two main series, full-block (390 x 190 mm) and half-block (190 x 190 mm) cross-sections. The columns were all six-course high with a slenderness ratio of 6.26. Details of a typical blockwork masonry column and the different forms of reinforcement are shown in Fig. 7.1.

One type of mortar (1:0.25:3) and one type of concrete infill (1:3:2) were used throughout. The columns were constructed by an experienced mason ensuring the complete filling of the 10 mm horizontal mortar joints between the concrete blocks. The mason was also instructed to gauge the height of the columns in accordance with the length of the vertical reinforcement, which had been cut to lengths corresponding to the calculated column height. The cuts were smooth to ensure good contact with the machine platens during the loading process.

The block at the base of each column was a bond beam type (Fig. 7.2 (i)), in which the end shells and mid-web had been removed to make it possible to clean the column of mortar dropping after construction[30] and also to assist in the fixing of the vertical reinforcement to the first lateral tie under the column. This type of block was as provided by the block supplier. The rest of the column blocks were either full or half-blocks. The full-blocks were provided with 20 mm wide by 20 mm deep grooves, cut with a diamond saw, at the sides of the block mid-webs (Fig. 7.2 (ii)), to accommodate the lateral ties. These grooves were also necessary to ensure a positive contact between the lateral ties and vertical reinforcement and to

provide the allowable cover for the reinforcement[21]. It was not possible to obtain blocks with such grooves from the supplier, but blocks with a 20 mm or more dip in the mid-web (Fig. 7.2 (iii)), can easily be produced by using a steel mould with such dips, as is the case with various different shapes and types of concrete block available on the market.

The placement of lateral ties at the mortar joints was avoided because previous studies[86] had shown that placing lateral ties at the mortar joints causes a high concentration of tensile splitting stresses around the ties, resulting in a reduction of the compressive strength of the masonry assemblage. Also, placing the lateral ties at the mortar joints means that concrete blocks with thicker shells are required to comply with the required concrete cover to the reinforcement[21].

The lateral ties were placed in every course during the construction of the columns, including the top and bottom sides, to prevent any local failure. This gives a constant spacing of 189 mm. The lateral ties, for the full-block columns, were placed in the 20 mm wide by 20 mm deep grooves during construction. In the case of half-block columns, taking advantage of block tapering, the dimensions of the lateral ties were made slightly smaller than the half-block wide core. This enabled the ties to be held in the hollow cores by friction first and then by mortar after the construction.

Two steel brackets, 25 mm wide by 6 mm thick, were placed in prepared positions at the first and fifth mortar joints. These brackets were used later to mount two electrical displacement transducers (LVDT's) on both sides of the column to measure changes in length with the load increments. High yield electrical strain gauges, 10 mm

long, were mounted and protected by a water proof coating on two lateral ties and two vertical bars to measure the strain in the reinforcement at the mid height of the column.

After construction, the columns were left under polythene sheeting for four days to allow the mortar joints to gain in strength. After four days, the vertical reinforcement was placed in position by tying the vertical bars to the lateral ties at the column top and bottom sides. The columns were then filled with concrete, batched by volume, mixed to a high slump of 150 mm then cast in two layers. Each layer was compacted using a 25 mm poker vibrator until full compaction, after which the top of the concrete infill was trowelled level. The methods adopted herein for curing the columns are similar to those used in chapters 5 and 6.

Steel moulded cubes and cylinders, cast and cured with the specimens, were tested in compression to determine the strength of the mortar and concrete mixes.

Twelve of the forty-one, full and half-block columns built, were unreinforced columns, tested either unfilled or filled, under axial load to determine the short term static modulus of elasticity of the blockwork masonry (E_m). The rest of the columns were filled reinforced columns, divided into four series as follows (see Table A.1, Appendix A):

CS1FB, CS1HB * - Columns with three different diameters of lateral ties (6, 8, 10 mm ϕ), and without vertical reinforcement to study the effect of lateral tie confinement on the strength and behaviour of masonry columns.

CS2FB, CS2HB - Columns reinforced with different percentages of vertical reinforcement (full-block: 0.42%, 1.7%, 3.4% and half-block: 0.56%, 1.8%, 3.5%), and without lateral ties, to study the effect of the absence of lateral ties on the strength and behaviour of masonry columns.

CS3FB, CS3HB - Columns reinforced with the same percentage of vertical reinforcement (full-block: 1.7%, 5.3% and half-block: 1.8%, 5.4%), and with different diameters of lateral ties (6, 8, 10 mm ϕ) to choose the best lateral tie to be used in blockwork masonry columns.

CS4FB, CS4HB - Columns with 8 mm ϕ lateral ties and different percentage of vertical reinforcement (full-block: 0.42%, 1.7%, 3.4%, 5.3%, and half-block: 0.56%, 1.3%, 1.8%, 3.5%, 5.4%) to study the effect of changing the percentage of vertical reinforcement on the strength and behaviour of masonry columns.

* **CS1FB** - Column Series 1 Full-Block.
CS1HB - Column Series 1 Half-Block.

A summary of the major column details and variables for the full and half-block columns is given in Tables 7.1 and 7.2 respectively.

Prior to testing, all the specimens were capped with a thin layer, 1 - 2 mm, of dental plaster[55] prepared by the same method explained in chapters 3, 4, 5 and 6. The specimens were positioned in the testing machine before the dental plaster had hardened such that the centre of the upper platen coincided with the centre point of the specimen ensuring that the load would be applied axially.

The unfilled columns were tested in a 1MN capacity Avery Universal compression testing machine, which had a

ball seating to allow for the possibility of the loading plate being slightly off level. The other filled unreinforced and reinforced columns were tested in a steel rig, in which the load was applied by two 2MN capacity jacks through a 150 mm thick steel bearing plate to ensure uniformity.

After the specimens were positioned in the testing machine, all the strain measuring devices were connected to a data logger to record the strain continuously throughout testing up to failure.

The load was applied at a rate in accordance with BS 6073: Part 1: 1981[66] and the loading pattern was in accordance with BS 1881: Part 121: 1983[68] to enable the determination of the static modulus of elasticity for all the specimens tested, as has been explained in chapters 3, 4, 5 and 6.

7.3 DISCUSSION OF EXPERIMENTAL RESULTS

The discussion of the experimental results is divided into two major sections. The first and second deal with the observed modes of failure for the full and half-block columns. The second deals with the experimental results.

7.3.1 Modes of Failure for Full and Half-Block Columns

7.3.1.1 Unreinforced columns

The mode of failure for the unfilled and filled, unreinforced full and half-block columns was discussed in chapter 6. (For comparison refer to the mode of failure of unfilled and filled **6FBP-MJ** and **6HBP-MJ** prisms).

7.3.1.2 Reinforced columns

Columns, reinforced with 6 and 8 mm ϕ lateral ties only, (**CS1FB** and **CS1HB**) showed a different mode of failure to the filled unreinforced columns. The concrete cores remained intact even after all the block shells were crushed and had deformed outward (Fig. 7.3). The failure was more ductile with no complete collapse at ultimate load, as was the case with unreinforced columns. Some signs of block shell cracking was observed at 80% to 90% of the ultimate load. Full-block columns reinforced with 10 mm ϕ lateral ties showed premature splitting of the block side shells and crushing of the concrete cores (Fig. 7.4), which may have been caused by some stress concentration as a result of using ties of larger diameter.

Columns, reinforced with different percentages of vertical reinforcement only, (**CS2FB** and **CS2HB**) showed an abrupt mode of failure at ultimate load with the buckling of vertical bars. This caused an explosive failure of the block shells, followed by complete disintegration of the columns (Fig. 7.5).

Columns, reinforced with the same percentage of vertical reinforcement and different diameters of lateral ties (6, 8 and 10 mm ϕ), (**CS3FB** and **CS3HB**) showed similar modes of failure for the three diameters of lateral tie used. The failure was dominated by localized block shell crushing and outward deformation at one or two courses (Fig. 7.6) and not throughout the column height as was the case with the modes of failure for all the above columns. This was due to the constraint of the vertical bars buckling between the lateral ties. The concrete cores remained intact even with all the block shells crushed and deformed outward. The failure was more ductile with no complete collapse at ultimate load. The vertical bars

buckled to the outside between the lateral ties at the final stages of the loading process. Block shell cracking was observed at 80% to 90% of the ultimate load.

All other columns, reinforced with 8 mm ϕ lateral ties and different percentages of vertical reinforcement (**CS4FB** and **CS4HB**), showed a similar mode of failure to that of the **CS3FB** and **CS3HB** columns discussed above.

7.3.2 Experimental Results

7.3.2.1 Short term static modulus of elasticity of blockwork masonry

The changes in length over the 4-courses of the unfilled and filled blockwork masonry columns were measured using two electrical displacement transducers (LVDT's) mounted on steel brackets on the opposite sides of the columns. The readings from these transducers were recorded continuously until failure, using a data logger. The average changes in length were then divided by the gauge length to convert the readings to strain over the 4-courses of the column height.

Figs 7.7 and 7.8 show typical vertical stress vs strain curves for the unfilled and filled, full and half-block columns respectively.

From the process of loading and unloading, the average short term static modulus of elasticity for three of each unfilled and filled, full and half-block masonry columns was determined (see Figs 7.7 and 7.8 and Table 7.3).

Many previous attempts have been made to find a formula for the modulus of elasticity of brickwork and blockwork masonry. SAHLIN[2] related the modulus of

elasticity of brickwork masonry to the moduli of both the brick and the mortar by the following theoretical equation:

$$E_m = \frac{1}{(1 - \delta)/E_j + \delta/E_b} \quad \text{with} \quad E_j \leq E_b \qquad \ldots(7.1)$$

Where

E_m Modulus of elasticity of masonry, N/mm^2

E_j Modulus of elasticity of the mortar joint, N/mm^2

E_b Modulus of elasticity of brick unit, N/mm^2

and

$$\delta = \frac{h_b}{h_b + h_j} \qquad \ldots(7.2)$$

Where

h_b Brick height, mm

h_j Mortar joint thickness, mm

In order to determine the modulus of elasticity of the mortar joint, (E_j), SAHLIN quoted the expression suggested by HANSEN[87] for two-phase material (referring to concrete) as given by the following equation:

$$E_j = \frac{1}{(1 - g)/E_p + g/E_g} \qquad \ldots(7.3)$$

Where

g The volume of aggregate per unit volume of mix

E_g Modulus of elasticity of aggregate, N/mm^2

E_p Modulus of elasticity of cement paste, N/mm^2

Most of the other researchers and standards related the modulus of elasticity of masonry to the ultimate compressive strength of masonry, f'_m. Although relating the modulus of elasticity to the masonry strength is irrelevant from a theoretical standpoint, it has some practical value.

The British Code of Practice (BS 5628: Part 2)[21] related the short term modulus of elasticity for clay, calcium silicate and concrete masonry, including reinforced masonry with infill concrete to f_k as follows:

$$E_m = 900\ f_k \qquad \ldots(7.4)$$

The American Masonry Code (ACI 531R-79)[19] related the modulus of elasticity of masonry to f'_m as follows:

$$E_m = 1000\ f'_m \leq 17225\ N/mm^2 \qquad \ldots(7.4)$$

Unfortunately, The ACI Code does not refer to the type of masonry material (brickwork, solid blockwork, hollow blockwork or filled blockwork) which this formula represents.

The Canadian Standard (CSA-CAN3-S304)[20] recommends the modulus of elasticity of unfilled masonry to be as follows:

$$E_m = 1000\ f'_m \leq 20685\ N/mm^2 \qquad \ldots(7.7)$$

Based on experimental data, HATZINIKOLAS et al[86] recommended a conservative value for the modulus of elasticity of unfilled masonry as follows:

$$E_m = 750\ f'_m \qquad \ldots(7.5)$$

FEEG et al[50] suggested the modulus of elasticity of filled blockwork masonry to be as follows:

$$E_m = 800\ f'_m \qquad \ldots(7.6)$$

Based on the results of the present study and on the theoretical expression suggested by SAHLIN, the modulus of elasticity of unfilled blockwork masonry can be determined as follows:

$$E_m = \frac{1}{(1 - \delta)/\alpha\ E_{mrs} + \delta/E_{bs}} \qquad \ldots(7.8)$$

Where

$$\alpha = E_{js}/E_{mrs} = 0.45 \quad \text{(for 10 mm mortar joint)}$$

In this expression the value of α is the average of three types of mortar (1:1:6, 1:0.25:3 and 1:0.5:4.5) and was found to be equal to 0.45 for a 10 mm mortar joint. For mortar joints of different thicknesses, the value of α can be found by testing specimens similar to the ones used in chapter 3 to determine E_{mrs} and E_{js}. The value of α takes into consideration the thickness of the mortar joint and the effect of the concrete block confinement. It is expected that the value of α can be used in general for all unfilled blockwork masonry built with hollow concrete blocks.

The modulus of elasticity of filled blockwork masonry is not easy to determine due to the presence of the concrete infill. As shown in chapter 5, the contribution of the concrete infill to the strength of filled blockwork prisms was only 25%, so it can be expected that the

concrete infill will contribute the same percentage to the modulus of elasticity. On this basis, the short term static modulus of elasticity of filled blockwork masonry could be determined as follows:

$$E_m = \frac{1}{(1 - \delta)/\alpha\ E_{mrs} + \delta/E_{bs}} + \Gamma\ E_{cs} \qquad \ldots(7.9)$$

Where

$$\Gamma = 0.25$$

The above two formulae were found to give excellent results when compared to the average experimental values of modulus of elasticity for unfilled and filled blockwork masonry (Table 7.3).

7.3.2.2 Strain measurements

Table 7.4 gives the results of the average strain measurements recorded over 4-courses of the column height, the vertical bars and lateral ties during the testing of the unreinforced and reinforced columns.

All the average strains reported herein represent the values at ultimate load or at the limit of the ascending load vs strain curve. Although the strain has been monitored continuously during the loading process, it was found difficult to monitor the strain for the descending part of the load vs strain curve. This was due to the sudden failure of the specimens cased by the release of the energy stored in the machine on the specimens at failure.

The recorded strain over 4-courses for the unreinforced full and half-block columns shows that the

strain for filled columns is 43.8% and 44.1% respectively lower than that for unfilled columns. This means that the shortening over 4-courses of the filled column is lower than for the unfilled column. This was also observed in the specific non-linear FEA for unfilled and filled **3FBP-MJ** prisms, where the vertical deformation of the filled prisms is 29.6% lower than that for the unfilled prism. This was attributed to an increase in stiffness resulting from the presence of the concrete infill.

Full-block columns, reinforced with 6 and 8 mm ϕ lateral ties and without vertical bars, (**CS1FB**) show an increase in the recorded strains over 4-courses of 25.1% and 19.1% respectively compared to filled unreinforced columns. This means that the laterally reinforced columns are more ductile than the filled unreinforced columns. On the other hand, columns reinforced with 10 mm ϕ lateral ties show a decrease of 17.1%, compared to filled unreinforced columns. The decrease in strain may be due to failure of the column caused by the high concentration of tensile splitting stresses around the lateral ties near the block mid-webs. This resulted in premature splitting of the column side shells. These high splitting stresses are the result of the size of the lateral ties used.

Half-block columns, reinforced with 6, 8 and 10 mm ϕ lateral ties and without vertical bars (**CS1HB**), show increases in the recorded strains over 4-courses of 40.8%, 35.2% and 54% respectively compared to filled unreinforced columns. The increase in the strain of the half-block column reinforced with 10 mm ϕ lateral ties supports the explanation given previously for the decrease in strain of the full-block column reinforced with 10 mm ϕ lateral ties, namely premature splitting of the block side shells.

The strain measurements on the ties for the laterally

reinforced full and half-block columns (**CS1FB** and **CS1HB**) show that the strain values are all lower than the ties' yield strain (see Table 3.6). A maximum strain value of 5.09 x 10^{-4} was recorded on the 6 mm ϕ ties.

The full-block columns reinforced with 4T10 and 4T20 mm ϕ vertical bars and without lateral ties (**CS2FB**) show increases in the recorded strains over 4-courses of 26% and 8.5% respectively compared to the filled unreinforced column. On the other hand, full-block columns reinforced with 8T20 mm ϕ vertical bars showed a decrease of 12.2%. This suggests that as the percentage of vertical reinforcement increases, the possibility of the buckling of vertical bars increases. Similarly, the strain on the vertical bars decreases (12.75 x 10^{-4}, 10.59 x 10^{-4} and 8.42 x 10^{-4} respectively) as the percentage of vertical bars increases.

The half-block columns (**CS2HB**) show similar trends to the full-block columns, with decreases in the recorded strains over 4-courses and decreases in the vertical bar strain as the percentage of vertical reinforcement increases.

Full-block columns, reinforced with the same percentage of vertical reinforcement (1.7%) and with 6, 8 and 10 mm ϕ lateral ties, (**CS3FB**) show increases in the recorded strains over 4-courses of 74.8%, 50.1% and 70.4% respectively, compared to filled unreinforced columns. The strain recorded on the vertical bars for the three different columns (16.65 x 10^{-4}, 15.63 x 10^{-4} and 14.41 x 10^{-4} respectively) is almost half the bar's yield strain (28 x 10^{-4}) (see Table 3.6).

Half-block columns, reinforced with the same percentage of vertical reinforcement (1.8%) and with 6, 8

and 10 mm ϕ lateral ties, (**CS3HB**) show increases in the recorded strains over 4-courses of 42.2%, 52.4% and 33.9% respectively, compared to filled unreinforced columns. On the other hand, the strain recorded on the vertical bars (14.86×10^{-4}, 14.87×10^{-4} and 12.84×10^{-4} respectively) is almost half the bars' yield strain (average 27×10^{-4}) (see Table 3.6).

Full-block columns, reinforced with 8 mm ϕ lateral ties and different percentages of vertical reinforcement (0.42%, 1.7%, 3.4% and 5.3%) (**CS4FB**), show increases in the recorded strains over 4-courses of 64.1%, 50.1%, 8% and 1.1% respectively, compared to filled unreinforced columns. The descending order of the percentage increases suggests that the ductility of the columns decreases as the percentage of vertical reinforcement increases. For the same reason, the strain recorded on the vertical bars shows similar reductions (17.80×10^{-4}, 15.63×10^{-4}, 14.60×10^{-4} and 11.15×10^{-4} respectively) with increase in percentage of vertical reinforcement.

Half-block columns, reinforced with 8 mm ϕ lateral ties and different percentages of vertical reinforcement (0.56%, 1.8%, 3.5% and 5.4%) (**CS4HB**), show increases in the recorded strains over 4-courses of 64.1%, 52.4%, 45.9% and 24.5% respectively, compared to filled unreinforced columns. The strain, recorded on the vertical bars for the same columns, show a similar trend of decreases (17.96×10^{-4}, 14.87×10^{-4}, 17.37×10^{-4} and 13.74×10^{-4} respectively) as the percentage of vertical reinforcement increases. The reason for this is similar to that for the full-block columns (**CS4FB**).

The major conclusions derived from the results of the strain measurements for the full and half-block columns are as follows:

1. All columns, reinforced with hot rolled deformed high yield 8 mm ϕ lateral ties, gave more consistent strain results compared to columns reinforced with 6 and 10 mm ϕ lateral ties.

2. The values of the average strain recorded on the vertical bars for all the columns tested are almost half the yield strain of the vertical bars (see Table 3.6).

3. The values of the average strain recorded on the horizontal ties are small compared to the yield strain recorded in the tensile test of the ties (see Table 3.6).

7.3.2.3 Column strength

Table 7.5 shows the compressive strength of all the unreinforced and the laterally reinforced, full and half-block columns.

The table shows that the compressive strength of the filled unreinforced, full and half-block columns (based on gross area) decreases by 12.9% and 33.5% respectively compared to unfilled columns (based on net area). The explanation for this is similar to the one put forward for the reduction in the compressive strength of the 3-course high full and half-block prisms, namely, the presence of the concrete infill. This was discussed in more detail in chapter 5.

The strength of unfilled, full-block columns on the other hand, shows a decrease of 25.2% compared to the half-block columns. This was caused by differences in the aspect ratio (l/t) (column length-to-thickness) and the mortar

bedded area between the full-block columns (l/t = 2.05) and half-block columns (l/t = 1.0). This was explained in more detail in chapter 6. Small difference in compressive strength was observed between the filled, full and half-block columns.

Table 7.5 also shows that the compressive strength of full-block columns, reinforced with 6 and 8 mm ϕ lateral ties and without vertical bars, (**CS1FB**) increases by 17.7% and 17.6% respectively compared to the filled unreinforced columns. On the other hand, columns reinforced with 10 mm ϕ lateral ties fail at a compressive strength which is 8.3% less than that for filled, unreinforced columns. The increase in column strength can be attributed to the confinement of the concrete infill by the lateral ties. These confinement stresses cause a reduction in the harmful tensile stresses exerted on the block shells by the concrete and are not a result of an increase in the concrete strength. Since as shown in chapter 5, changing the concrete infill strength from 0 to 30 N/mm^2 (prisms with zero concrete strength being the unfilled prisms) has no significant effect on the compressive strength of filled 3-course high, full-block prisms. The decrease in strength of the column reinforced with 10 mm ϕ lateral ties may be due to the premature failure of the column resulting from the high concentration of splitting stresses around the lateral ties, as shown earlier.

On the other hand, the half-block columns (**CS1HB**) show a clear tendency to increase in strength, by 1.7%, 4.4% and 20.5%, with provision of lateral ties of diameter, 6, 8 and 10 mm ϕ respectively.

As with the case of filled, unreinforced columns, no great difference in strength was observed between the laterally reinforced full and half-block columns. The only

anomaly is the full-block column, reinforced with 10 mm ϕ lateral ties, which shows a lower strength than the corresponding half-block column, for the reason mentioned previously.

Table 7.6 gives results for the experimental ultimate loads of columns reinforced with lateral ties and vertical bars.

Full-block columns, reinforced with different percentages of vertical reinforcement (0.42%, 1.7% and 3.4%) and without lateral ties (**CS2FB**), show a decrease of 11.5% and increases of 24.3% and 10.4% respectively for the experimental values of ultimate load of the columns, compared to filled unreinforced columns.

Half-block columns, reinforced with different percentages of vertical reinforcement (0.56%, 1.8% and 3.5%) and without lateral ties (**CS2HB**), show increases of 4.6%, 44.3% and 42.3% respectively for the experimental values of ultimate load of the columns, compared to filled unreinforced columns.

Although the general trend for both columns is an increase in strength with the presence of vertical bars only, the use of such columns in masonry construction should be avoided due to the explosive mode of failure at ultimate load.

To the author's knowledge, no work has been reported so far on the strength and behaviour of blockwork masonry columns reinforced with vertical bars only. In reinforced concrete, the limited work reported by PFISTER[88] showed that columns reinforced with vertical bars only developed ultimate strengths from 6% to 8% less than the calculated values which based on ultimate design theory. PFISTER

reported that those columns exhibited an explosive mode of failure.

Full-block columns, reinforced with the same percentage of vertical reinforcement (1.7%) and different diameters of lateral ties (6, 8 and 10 mm ϕ) (**CS3FB**), show increases of 51.9%, 62.5% and 24.3% respectively in their experimental values of ultimate load, compared to filled unreinforced columns. Similarly, and for the same diameters of lateral tie, full-block columns reinforced with 5.3% vertical bars show increases of 85.6%, 75.3% and 76.8% respectively, compared to filled unreinforced columns.

Half-block columns, reinforced with the same percentage of vertical reinforcement (1.8%) and different diameters of lateral ties (6, 8 and 10 mm ϕ) (**CS3HB**), show increases of 39%, 59.3% and 44.4% respectively in the experimental values of ultimate load, compared to filled unreinforced columns. Similarly, and for the same diameters of lateral tie, half-block columns reinforced with 5.4% vertical bars show increases of 57.8%, 65.4% and 22.8% respectively, compared to filled unreinforced columns.

The above results, for columns reinforced with the same percentage of vertical reinforcement and different diameters of lateral tie, suggests that 8 mm ϕ lateral ties give the most consistent increases in strength, compared to filled unreinforced columns.

Fig. 7.9 shows the effect of changing the percentage of vertical reinforcement on the ultimate load of full and half-block columns reinforced with the same diameter of lateral ties (8 mm ϕ) (**CS4FB** and **CS4HB**). In this figure, columns, reinforced with 8 mm ϕ lateral ties only, were considered as columns with zero percent vertical reinforcement. The relationship between the column ultimate

load, (P_u), and the percentage of vertical reinforcement can be best represented, for full-block columns, by the following formula:

$$P_u = 1590 \ \rho^{0.15} \qquad \ldots(7.10)$$

The ultimate load for half-block columns is given by half the ultimate load from Eqn. 7.10.

The figure also shows that the experimental value of ultimate load of the full-block column, reinforced with a minimum percentage of vertical reinforcement (0.42%), increases by 20.8% compared to the filled unreinforced column. As the percentage of vertical reinforcement increases by 1.7%, 3.4% and 5.3%, the column ultimate load increases correspondingly by 62.5%, 64% and 75.3%.

Similarly, the experimental values of ultimate load for the half-block column, reinforced with the minimum percentage of vertical reinforcement (0.56%), increases by 16.8% compared to the filled unreinforced column. As the percentage of vertical reinforcement increases by 1.3%, 1.8%, 3.5% and 5.4% the column ultimate load increases correspondingly by 35.1%, 59.3%, 58.7% and 65.4%.

The experimental results for columns, reinforced with 8 mm ϕ lateral ties and different percentages of vertical reinforcement, show a steady increase in the column ultimate load, (P_u), as the percentage of vertical reinforcement increases. This behaviour is similar to that for reinforced concrete columns.

Table 7.6 also gives the results of three methods used to predict the ultimate load of all the reinforced blockwork masonry columns tested in this investigation. The first and second methods of calculating the column ultimate load are based on the procedures suggested by BS 5628[21]

and ACI 531R-79[19]. It can be seen that both standards underestimate the ultimate load of the reinforced blockwork masonry columns, even for columns reinforced with vertical bars only. The full-block column, reinforced with a minimum percentage of vertical reinforcement (0.42%) and 8 mm ϕ lateral ties, failed at an ultimate load which was 1.96 times the value estimated using BS 5628 and 6.03 times the value estimated using ACI 531R-79.

Similarly, the half-block column reinforced with a minimum percentage of vertical reinforcement (0.56%) and 8 mm ϕ lateral ties, failed at an ultimate load which was 1.94 times the value estimated using BS 5628 and 5.40 times the value estimated using ACI 531R-79.

The third method of calculating the ultimate load of blockwork columns is based on Eqns 5.4 and 5.5 for the ultimate compressive strength of blockwork masonry, f'_m, as derived in chapter 5 for the 3-course high full and half-block prisms. The contribution of the vertical reinforcement to the strength of blockwork masonry columns is assumed to be based on half the yield strength, (f_y), of the vertical bars, since, as shown above, the vertical bars attain only half their yield strain.

Therefore, the ultimate load of blockwork masonry columns is calculated as follows:

$$P_u = [f'_m (A_g - A_s) + f_y/2 (A_s)]/1000 \qquad ...(7.11)$$

The contribution of the lateral ties, namely 17.6% in the case of full-block columns and 4.4% in the case of half-block columns, was ignored in the calculation.

The reason for the failure of blockwork masonry columns prior to yielding of the vertical bars, may be due

to the outward deformation and failure of the block shells caused by minor buckling of the vertical bars between the lateral ties at ultimate load.

Fig. 7.10 shows the relationship between the ratio of experimental ultimate load and theoretical ultimate load as a percentage, using the proposed method of calculation (P_u (Experimental)/P_u (Theoretical)) and the percentage of vertical reinforcement (A_s/A_g %) for columns reinforced with different percentages of vertical bars and the same lateral ties (8 mm ϕ) (**CS4FB** and **CS4HB**). The figure shows that Eqn. 7.11 gives a good estimation of the ultimate load of the reinforced blockwork masonry columns.

7.4 CONCLUSIONS

1. The presence of lateral ties changes the mode of failure of blockwork masonry columns (**CS1FB** and **CS1HB**) from a sudden explosive failure to a more ductile failure. Columns reinforced with 10 mm ϕ lateral ties show premature splitting of the block side shells and crushing of the concrete cores which may be caused by a high concentration of tensile splitting stresses around the large diameter lateral ties near the block mid-webs.

2. The mode of failure of columns, reinforced with both vertical and lateral ties (**CS3FB**, **CS3HB**, **CS4FB** and **CS4HB**), is dominated by localized block shell crushing and outward deformation at one or two blocks but not throughout the full column height. This was due to the restriction of buckling of the vertical bars to lengths between the lateral ties. The concrete cores remained intact despite the block shells crushing and deforming outward. The failure was more ductile with

no complete collapse at ultimate load. Block shell cracking was observed at 80% to 90% of the ultimate load.

3. A semi-empirical formula (Eqns 7.8 and 7.9) has been suggested to determine the short term static modulus of elasticity of unfilled and filled blockwork masonry.

4. All series of columns, reinforced with hot rolled deformed high yield 8 mm ϕ lateral ties, gave more consistent results for the strain values and for the experimental values of ultimate load compared to columns reinforced with 6 and 10 mm ϕ lateral ties.

5. The strength of filled, full and half-block columns (based on gross area) decreased by 12.9% and 33.5% respectively compared to the unfilled columns (based on net area). The explanation is similar to that used for the reduction in the compressive strength of the 3-course high, full and half-block prisms, namely the presence of the concrete infill.

6. The strength of columns, reinforced with 6 and 8 mm ϕ lateral ties and without vertical bars (**CS1FB**), increased by 17.7% and 17.6% compared to the filled unreinforced columns. On the other hand, columns reinforced with 10 mm ϕ lateral ties failed at loads which were 8.3% less than those for filled unreinforced columns. The increase in column strength results from the confinement of the concrete infill by the lateral ties. These confinement stresses cause a reduction in the harmful tensile stresses exerted on the block shells by the concrete and are not a result of an increase in the concrete strength. The decrease in the strength of columns, reinforced with 10 mm ϕ

lateral ties, may be caused by premature failure of the column due to the high concentration of tensile splitting stresses around the large diameter lateral ties.

On the other hand, the results of the half-block columns (**CS1HB**) show increases in strength of 1.7%, 4.4% and 20.5%, with provision of lateral ties of diameter, 6, 8 and 10 mm ϕ respectively. This tendency of increase in strength is similar to that in reinforced concrete columns.

7. Although, the general trend for the full and half-block columns, reinforced with different percentages of vertical reinforcement and without lateral ties (**CS2FB** and **CS2HB**), is to show an increase in the experimental value of ultimate load of the columns, compared to filled unreinforced columns. The use of such columns in masonry construction should be avoided due to the explosive nature of failure at ultimate load.

8. All the full and half-block columns, reinforced with the same percentage of vertical reinforcement but different diameters of lateral ties (6, 8 and 10 mm ϕ), (**CS3FB**) show an increase in the experimental values of ultimate load of the column, compared to a filled unreinforced columns. The most consistent results for increases in column strength is obtained in columns reinforced with 8 mm ϕ lateral ties.

9. All the full and half-block columns, reinforced with 8 mm ϕ lateral ties and different percentages of vertical reinforcement (**CS4FB** and **CS4HB**), show a uniform increase in the values of ultimate load of the column as the percentage of vertical reinforcement

increases. This relationship is similar to that for reinforced concrete columns.

10. The British and American Masonry Standards underestimate the ultimate load of reinforced blockwork masonry columns, even for columns reinforced with vertical bars only.

11. A new formula (Eqn. 7.11) has been proposed to calculate the ultimate load of blockwork masonry columns based on Eqns 5.4 and 5.5 for the ultimate compressive strength of blockwork masonry f'_m, as derived in chapter 5 for 3-course high full and half-block prisms. The contribution of the vertical reinforcement to the ultimate load of blockwork masonry columns is assumed to be based on half the yield strength (f_y) of the vertical bars, since all the strains recorded on the vertical bars during the investigation were half the yield strain of the vertical bars.

12. The explanation for failure of the blockwork masonry columns prior to yielding of the vertical bars may be due to the outward deformation and failure of the block shells caused by relatively small buckling of vertical bars between the lateral ties at ultimate load.

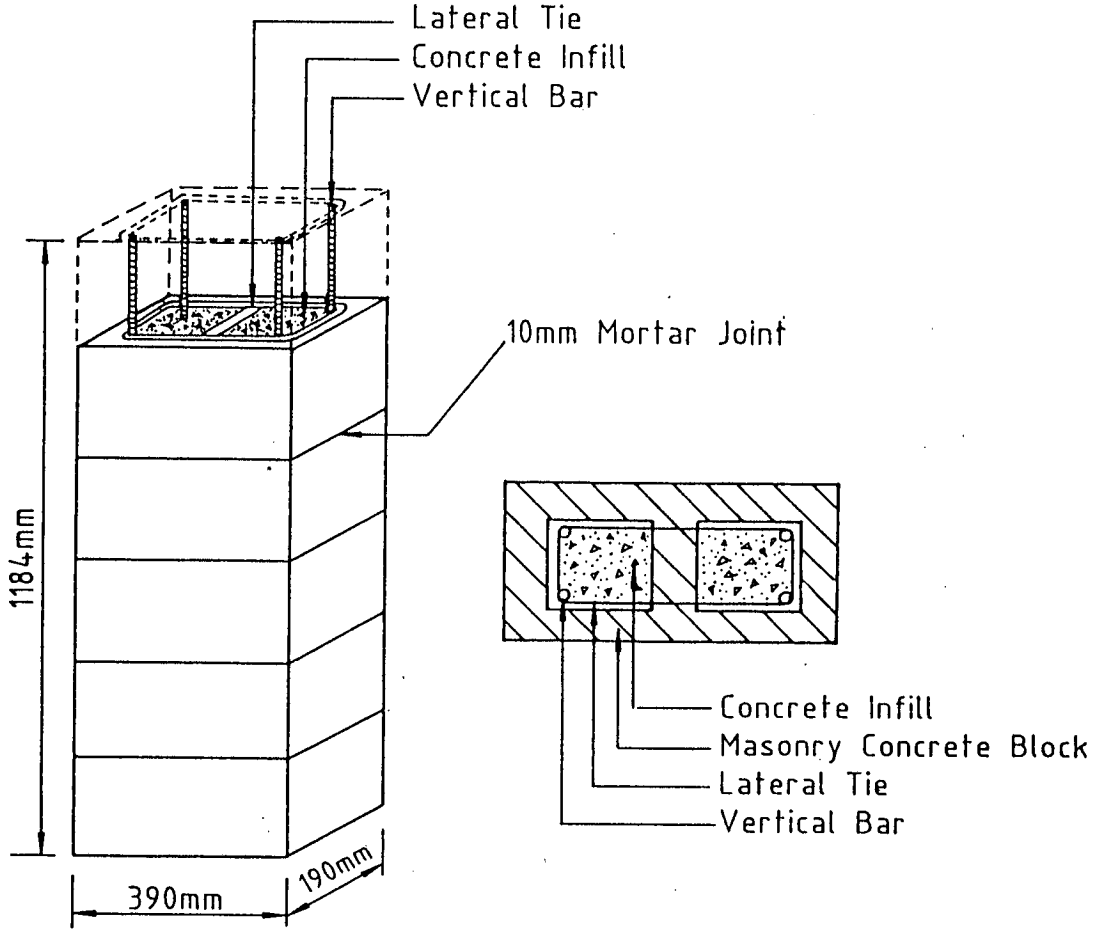

Fig. 7.1 - Details of a typical blockwork masonry column used in the investigation.

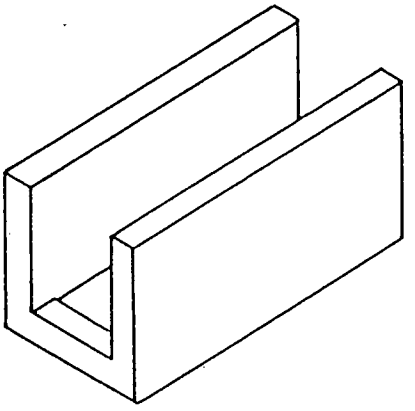

(i) Bond beam
Block

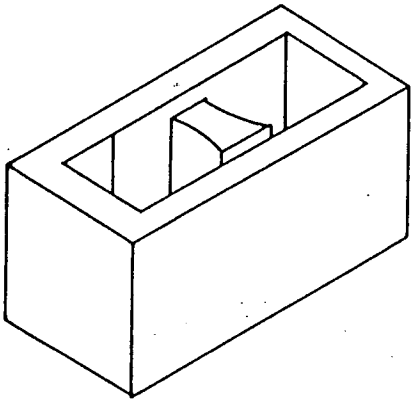

(ii) Standard block
with grooves

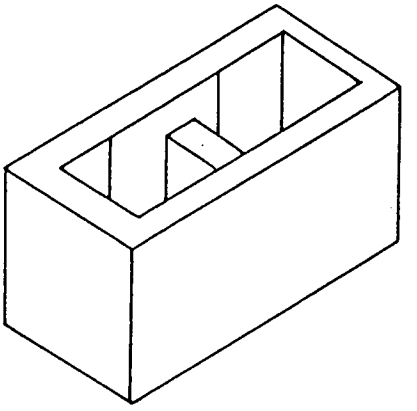

(iii) Standard block
with mid-web dip

Fig. 7.2 - Types of concrete block used in column construction. (i) Bond beam, (ii) Standard, (ii) Standard with mid-web dip.

Table 7.1

Summary of full-block columns details and variables.

Column ♦ type	Vertical Ω reinforcement No. mm ϕ	A_s (mm^2)	f_y * (N/mm^2)	A_s/A_g (%)	f'_m ♀ (N/mm^2)	Material cube comp. ♣ strength (N/mm^2) Mortar (f_{mr})	Infill (f_c)
Unfilled	-	-	-	-	9.99	27.05	-
Filled	-	-	-	-	15.39	27.05	21.59
CS1FB6	-	-	-	-	14.71	28.55	18.27
CS1,4FB8 ♦	-	-	-	-	14.71	28.55	18.27
CS1FB10	-	-	-	-	14.71	28.55	18.27
CS2FB0	4T10	314.16	519.06	0.42	14.80	25.95	19.66
CS2FB0	4T20	1256.64	536.88	1.7	14.80	25.95	19.66
CS2FB0	8T20	2513.28	536.88	3.4	14.80	25.95	19.66
CS3FB6	4T20	1256.64	536.88	1.7	14.71	28.55	18.27
CS3,4FB8	4T20	1256.64	536.88	1.7	14.71	28.55	18.27
CS3FB10	4T20	1256.64	536.88	1.7	14.71	28.55	18.27
CS3FB6	8T25	3926.96	490.28	5.3	14.71	28.55	18.27
CS3,4FB8	8T25	3926.96	490.28	5.3	14.71	28.55	18.27
CS3FB10	8T25	3926.96	490.28	5.3	14.71	28.55	18.27
CS4FB8	4T10	314.16	519.06	0.42	14.71	28.55	18.27
CS4FB8	8T20	2513.28	536.88	3.4	14.71	28.55	18.27

♦ Net area = Area at section (1) = 41700 mm^2. (See Table 3.2).
Gross area = 390 x 190 = 74100 mm^2.

Ω No. of bars Type (mm ϕ).

* 6 mm ϕ lateral tie, f_y = 441.51 N/mm^2.
8 mm ϕ lateral tie, f_y = 527.86 N/mm^2.
10 mm ϕ lateral tie, f_y = 519.06 N/mm^2.

♀ $f'_m = 0.30\ f_b + 0.10\ f_{mr} + 0.25\ f_c$. (See Eqn. 5.4).

♣ Cube compressive strength of block material, f_b = 24.29 N/mm^2.

♦ CS1,4FB8 = Column Series 1 or 4 Full-Block with 8 mm ϕ lateral ties.

Table 7.2

Summary of half-block columns details and variables.

Column ♦ type	Vertical Ω reinforcement No. mm ϕ	A_s (mm^2)	f_y * (N/mm^2)	A_s/A_g (%)	f'_m ♀ (N/mm^2)	Material cube comp. ♦ strength (N/mm^2) Mortar (f_{mr})	Infill (f_c)
Unfilled	-	-	-	-	12.48	25.95	-
Filled	-	-	-	-	17.39	25.95	19.66
CS1HB6	-	-	-	-	17.15	26.91	17.92
CS1,4HB8 ♣	-	-	-	-	17.15	26.91	17.92
CS1HB10	-	-	-	-	17.15	26.91	17.92
CS2HB0	4T8	201.08	527.86	0.56	17.39	25.95	19.66
CS2HB0	4T(8+12)	653.48	507.09	1.8	17.39	25.95	19.66
CS2HB0	4T20	1256.64	536.88	3.5	17.39	25.95	19.66
CS3HB6	4T(8+12)	653.48	507.09	1.8	17.39	25.95	19.66
CS3,4HB8	4T(8+12)	653.48	507.09	1.8	17.39	25.95	19.66
CS3HB10	4T(8+12)	653.48	507.09	1.8	17.39	25.95	19.66
CS3HB6	4T25	1963.48	490.28	5.4	17.39	25.95	19.66
CS3,4HB8	4T25	1963.48	490.28	5.4	17.39	25.95	19.66
CS3HB10	4T25	1963.48	490.28	5.4	17.39	25.95	19.66
CS4HB8	4T8	201.08	527.86	0.56	17.39	25.95	19.66
CS4HB8	4T12	452.40	486.31	1.3	17.39	25.95	19.66
CS4HB8	4T20	1256.64	536.88	3.5	17.39	25.95	19.66

♦ Net area = Area at section (1) = 19900 mm^2. (See Table 3.2).
Gross area = 190 x 190 = 36100 mm^2.

Ω No. of bars Type (mm ϕ).

* 6 mm ϕ lateral tie, f_y = 441.51 N/mm^2.
8 mm ϕ lateral tie, f_y = 527.86 N/mm^2.
10 mm ϕ lateral tie, fy = 519.06 N/mm^2.

♀ $f'_m = 0.30\ f_b + 0.20\ f_{mr} + 0.25\ f_c$. (See Eqn. 5.5).

♦ Cube compressive strength of block material, f_b = 24.29 N/mm^2.

♣ CS1,4HB8 = Column Series 1 or 4 Half-Block with 8 mm ϕ lateral ties.

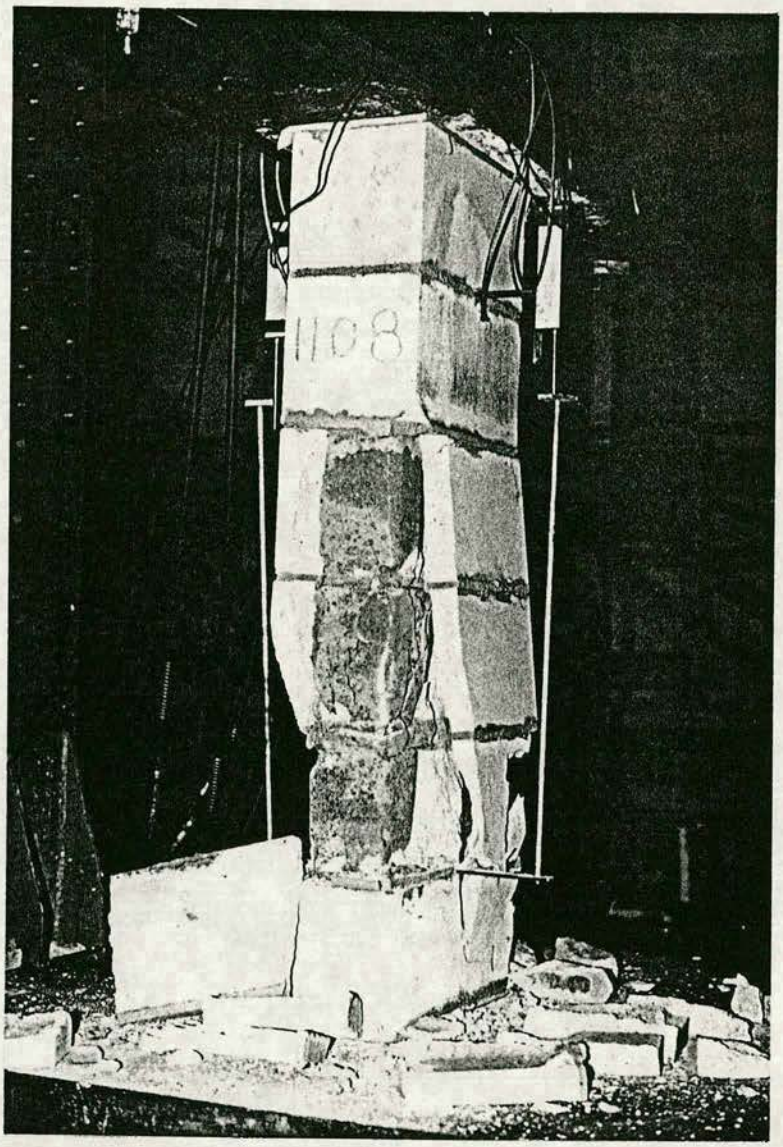

Fig. 7.3 - Mode of failure of full-block masonry column reinforced with 8 mm ϕ lateral ties.

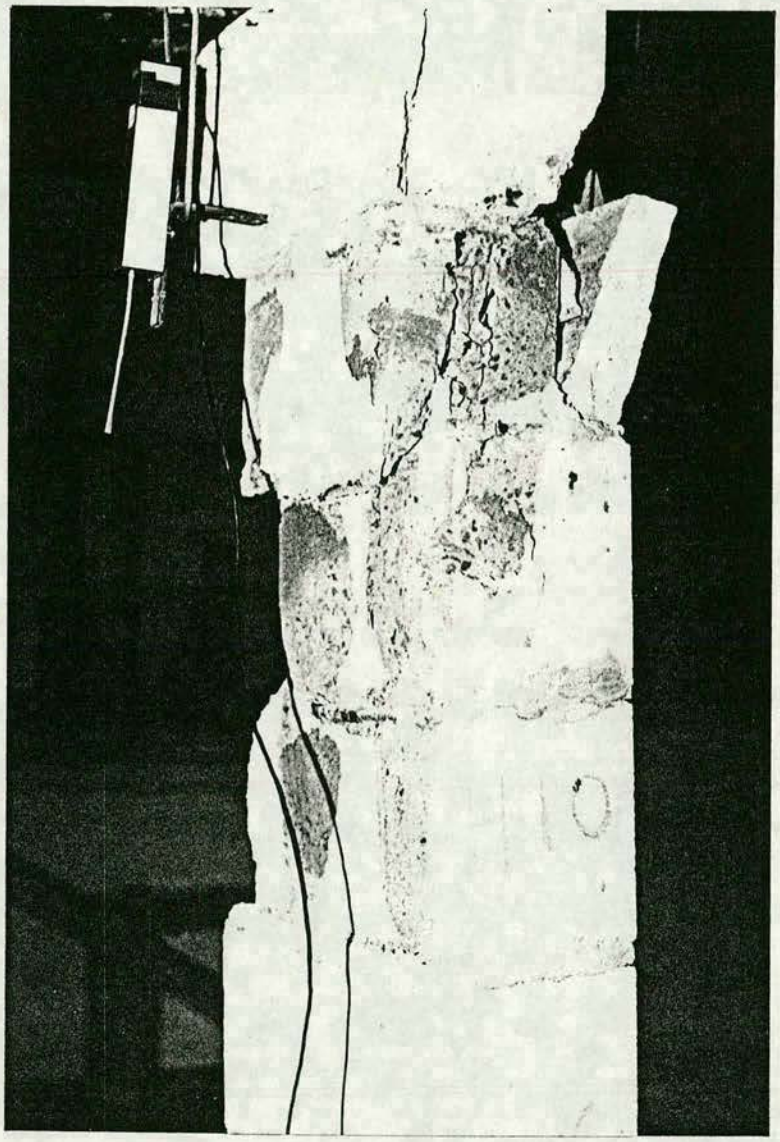

Fig. 7.4 - Mode of failure of full-block masonry column reinforced with 10 mm ϕ lateral ties.

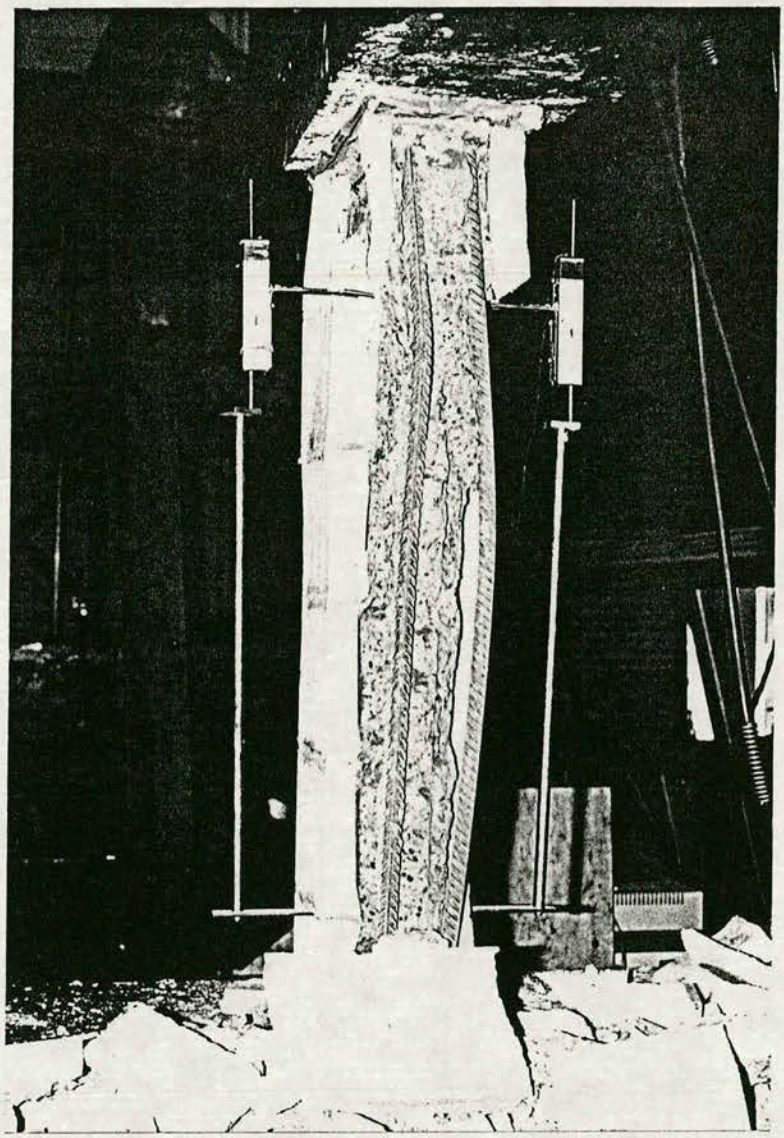

Fig. 7.5 - Typical mode of failure of full-block masonry columns reinforced with vertical bars only.

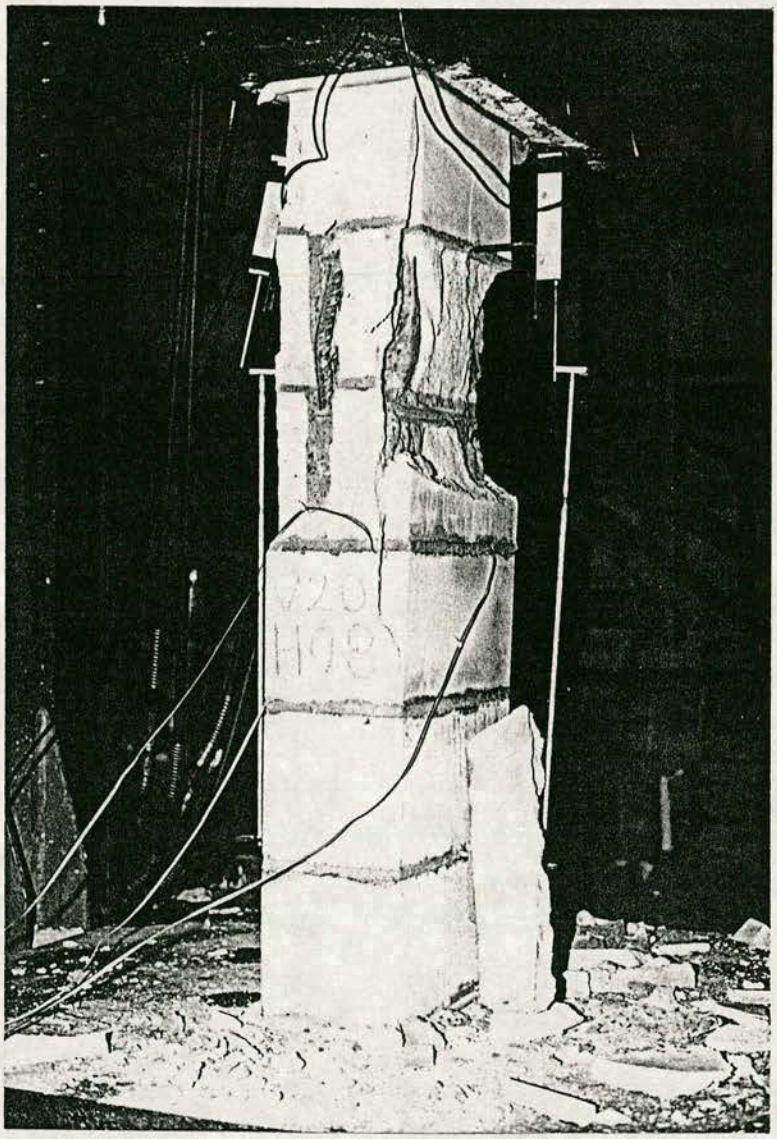

Fig. 7.6 - Typical mode of failure of full-block masonry columns reinforced with lateral ties and vertical bars.

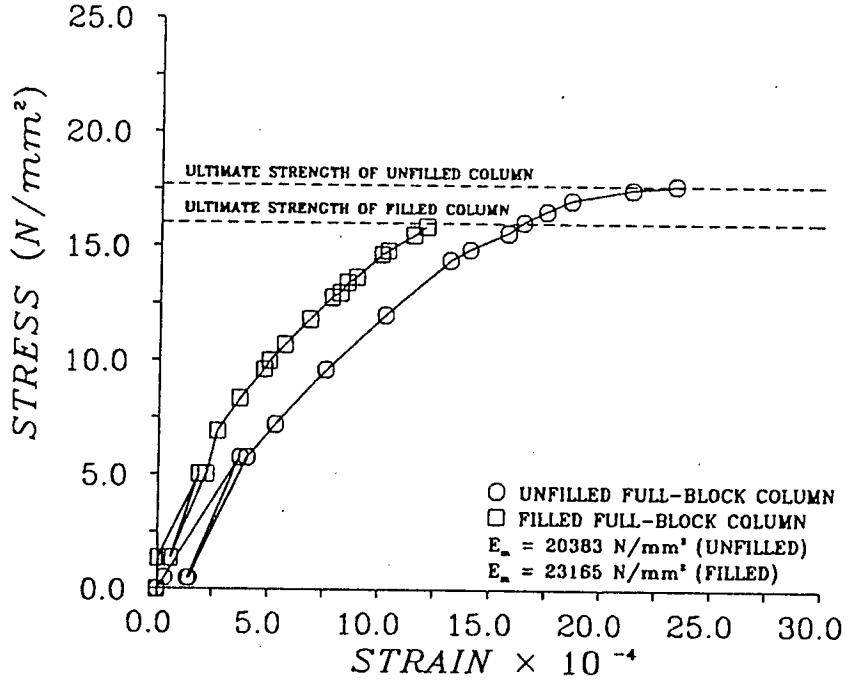

Fig. 7.7 - Typical stress vs strain curves for unfilled and filled unreinforced full-block masonry columns.

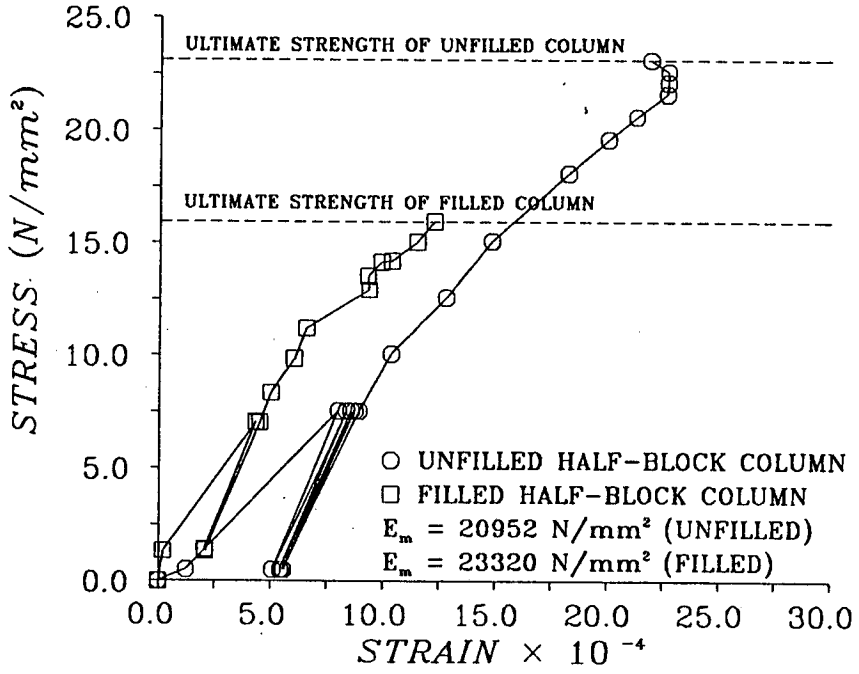

Fig. 7.8 - Typical stress vs strain curves for unfilled and filled unreinforced half-block masonry columns.

Table 7.3

Comparison between experimental and theoretical values of E_m.

Column type	E_m Experimental (N/mm^2)	E_m * Theoretical (N/mm^2)	$\frac{E_m \text{ (Experimental)}}{E_m \text{ (Theoretical)}}$
	Full-block column		
Unfilled	20383	21535	0.95
Filled	23165	24396	0.95
	Half-block column		
Unfilled	20952	21535	0.97
Filled	23320	24396	0.96

* Based on Eqns 7.8 and 7.9

Table 7.4

Strain measurements.

Column type	Vertical Ω reinforcement No. mm ϕ	A_s/A_g (%)	Average transducers strain x 10^{-4}	Average vertical bars strain x 10^{-4}	Average horizontal ties strain x 10^{-4}
			Full-block column		
Unfilled	-	-	23.31	-	-
Filled	-	-	13.10	-	-
CS1FB6	-	-	16.39	-	-5.09
CS1,4FB8 ♦	-	-	15.60	-	-3.25
CS1FB10	-	-	10.86	-	-2.45
CS2FB0	4T10	0.42	16.50	12.75	-
CS2FB0	4T20	1.7	14.21	10.59	-
CS2FB0	8T20	3.4	11.50	8.42	-
CS3FB6	4T20	1.7	22.90	16.65	-3.24
CS3,4FB8	4T20	1.7	19.66	15.63	-3.50
CS3FB10	4T20	1.7	22.32	14.41	-3.27
CS3,4FB8	8T25	5.3	13.24	11.15	-2.50
CS4FB8	4T10	0.42	21.50	17.80	-3.34
CS4FB8	8T20	3.4	14.15	14.60	-2.96
			Half-block column		
Unfilled	-	-	21.91	-	-
Filled	-	-	12.25	-	-
CS1HB6	-	-	17.25	-	-3.09
CS1,4HB8 ♦	-	-	16.56	-	-2.15
CS1HB10	-	-	18.86	-	-3.58
CS2HB0	4T8	0.56	17.25	13.65	-
CS2HB0	4T(8+12)	1.8	15.32	11.29	-
CS2HB0	4T20	3.5	11.85	9.75	-
CS3HB6	4T(8+12)	1.8	17.42	14.86	-3.30
CS3,4HB8	4T(8+12)	1.8	18.67	14.87	-3.26
CS3HB10	4T(8+12)	1.8	16.40	12.84	-2.06
CS3,4HB8	4T25	5.4	15.25	13.74	-4.80
CS4HB8	4T8	0.56	20.10	17.96	-2.60
CS4HB8	4T20	3.5	17.87	17.37	-4.00

Ω No. of bars Type (mm ϕ).

♦ CS1,4FB8 = Column Series 1 or 4 Full-Block with 8 mm ϕ lateral ties.
CS1,4HB8 = Column Series 1 or 4 Half-Block with 8 mm ϕ lateral ties.

-ve Tension.

Table 7.5

Compressive strength of unreinforced and laterally reinforced full and half-block columns.

Column type	Ultimate load (KN)	Average compressive * strength (N/mm^2) Area used: Net	Area used: Gross	S.D. (N/mm^2)
	Unreinforced full-block column ♦			
Unfilled	728.92	17.48	9.84	0.55/0.31
Filled	1128.54	-	15.23	0.92
	Laterally reinforced full-block column ♦			
CS1FB6	1328.68	-	17.93	-
CS1,4FB8 ♣	1327.18	-	17.91	-
CS1FB10	1034.49	-	13.96	-
	Unreinforced half-block column ♀			
Unfilled	465.06	23.37	12.88	0.78/0.43
Filled	561.36	-	15.55	0.96
	Laterally reinforced half-block column ♀			
CS1HB6	570.79	-	15.81	-
CS1,4HB8 ♣	586.03	-	16.23	-
CS1HB10	676.59	-	18.74	-

* Average and S.D. for unreinforced columns are calculated for three specimens.

♦ Net area = Area at section (1) = 41700 mm^2. (See Table 3.2).
Gross area = 390 x 190 = 74100 mm^2.

♣ CS1,4FB8 = Column Series 1 or 4 Full-Block with 8 mm ϕ lateral ties.
CS1,4HB8 = Column Series 1 or 4 Half-Block with 8 mm ϕ lateral ties.

♀ Net area = Area at section (1) = 19900 mm^2. (See Table 3.2).
Gross area = 190 x 190 = 36100 mm^2.

Table 7.6

Ultimate load of laterally and vertically reinforced columns.

Column type	Vertical Ω reinforcement No. mm ϕ	A_s/A_g (%)	P_u Experimental (KN)	P_u * BS 5628 (KN)	P_u ♦ ACI 531R-79 (KN)	P_u ♀ Theoretical (KN)
			Full-block column			
CS2FB0	4T10	0.42	998.45	695.06	226.13	1173.56
CS2FB0	4T20	1.7	1402.30	=	327.83	1415.41
CS2FB0	8T20	3.4	1245.35	=	463.42	1734.15
CS3FB6	4T20	1.7	1713.91	=	327.83	1408.86
CS3,4FB8 ♣	4T20	1.7	1834.20	=	327.83	1408.86
CS3FB10	4T20	1.7	1402.99	=	327.83	1408.86
CS3FB6	8T25	5.3	2094.92	=	615.95	1994.90
CS3,4FB8	8T25	5.3	1978.32	=	615.95	1994.90
CS3FB10	8T25	5.3	1994.67	=	615.95	1994.90
CS4FB8	4T10	0.42	1363.71	=	226.13	1166.92
CS4FB8	8T20	3.4	1850.45	=	463.42	1727.71
			Half-block column			
CS2HB0	4T8	0.56	587.35	338.62	121.20	677.35
CS2HB0	4T(8+12)	1.8	809.96	=	170.01	782.10
CS2HB0	4T20	3.5	798.65	=	235.09	943.26
CS3HB6	4T(8+12)	1.8	780.06	=	170.01	782.10
CS3,4HB8 ♣	4T(8+12)	1.8	894.10	=	170.01	782.10
CS3HB10	4T(8+12)	1.8	810.48	=	170.01	782.10
CS3HB6	4T25	5.4	885.60	=	311.36	1074.96
CS3,4HB8	4T25	5.4	928.67	=	311.36	1074.96
CS3HB10	4T25	5.4	689.35	=	311.36	1074.96
CS4HB8	4T8	0.56	655.63	=	121.20	677.35
CS4HB8	4T12	1.3	758.22	=	148.31	729.92
CS4HB8	4T20	3.5	891.12	=	235.09	943.26

Ω No. of bars Type (mm ϕ).

* BS 5628, $P_u = [f_k A_g]/1000$, $f_k = 9.38$ N/mm^2. (See Table 3.1).

♦ ACI 531R-79, $P_u = [(0.225 f'_m A_g + 0.65 A_s f_s)]/1000$, $f'_m = 11.53$ N/mm^2 (full-block column), $f'_m = 12.25$ N/mm^2 (half-block column), $f_s = 166$ N/mm^2.

♀ $P_u = [(f'_m (A_g - A_s) + f_y/2 A_s)]/1000$.

♣ CS3,4FB8 = Column Series 3 or 4 Full-Block with 8 mm ϕ lateral ties.

CS3,4HB8 = Column Series 3 or 4 Half-Block with 8 mm ϕ lateral ties.

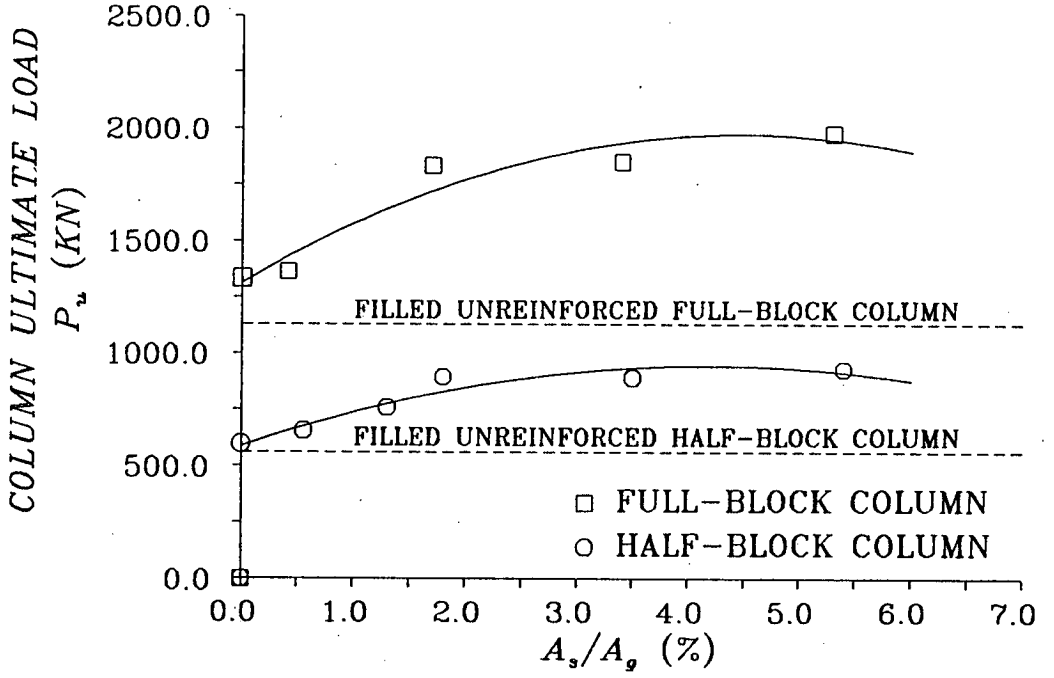

Fig. 7.9 - Effect of changing percentage of vertical reinforcement on ultimate load of masonry columns.

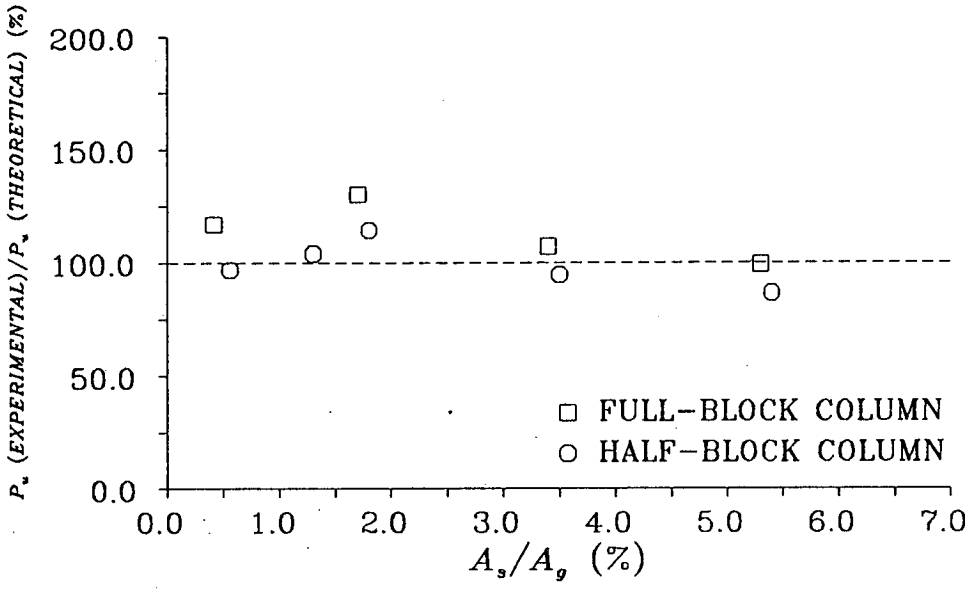

Fig. 7.10 - Comparison between experimental and theoretical values of P_u, for full and half-block columns reinforced with 8 mm ϕ lateral ties and different percentages of vertical bars.

CHAPTER 8

GENERAL SUMMARY AND CONCLUSIONS

8.1 GENERAL SUMMARY

This thesis presents a comprehensive study of blockwork masonry prisms compressed axially in two directions, normal and parallel to the unit bed face. The effects of different factors such as types of mortar, concrete infill strengths, height-to-thickness ratio (h/t), aspect ratio (prism length-to-thickness) (l/t), mortar thickness, shrinkage in 28 days and bond between block and concrete infill affecting the compressive strength and behaviour of blockwork masonry prisms were investigated experimentally and theoretically using the finite element technique. Methods for the determination of the ultimate compressive strength of blockwork masonry f'_m were suggested.

The thesis also presents an extensive study on forty-one axially loaded blockwork masonry short columns. The effects of using different percentages of lateral ties and vertical bars on the ultimate strength and behaviour of reinforced blockwork masonry columns were investigated. A new method of predicting the ultimate load of reinforced blockwork masonry columns subjected to axial compression is proposed.

An introduction to the advantages of using filled hollow concrete blocks in reinforced blockwork masonry and the problems resulting from the masonry non-homogeneity caused by the differences in the mechanical properties of the four component materials (concrete block, mortar, concrete infill and reinforcement) making the masonry assemblage have been described in chapter 1.

Chapter 2 presents a comprehensive literature review of the methods used to determine the ultimate compressive strength of blockwork masonry f'_m and to study the behaviour of blockwork masonry prisms subjected to axial load applied normal and parallel to the unit bed face. Also presented is a review of the work carried out on the strength and behaviour of reinforced brickwork and blockwork masonry columns.

An experimental study of the properties of materials used in this investigation has been reported in chapter 3.

Chapter 4 presents the results of the experimental and theoretical investigations carried out on a two-block masonry prisms compressed in a direction parallel to the unit bed face. On the other hand, chapter 5 has been devoted to the experimental and theoretical investigations of 3-course high stack-bonded blockwork masonry prisms compressed normal to the unit bed face. The theoretical studies in both chapters were carried out using the finite element technique. Based on the experimental and theoretical investigations, methods for the determination of the ultimate compressive strength of blockwork masonry f'_m has been suggested. A new hypotheses for the mechanism of failure of unfilled and filled blockwork masonry prisms compressed parallel and normal to the unit bed face are suggested.

Factors, other than the concrete infill strengths and mortar types, affecting the compressive strength and behaviour of blockwork masonry are discussed in chapter 6. The factors studied were prism height-to-thickness ratio (h/t), aspect ratio (prism length-to-thickness) (l/t), mortar thickness, shrinkage in 28 days and bond between block and concrete infill.

Chapter 7 is devoted to blockwork masonry short columns subjected to axial load. The effect of using different percentages of lateral and vertical reinforcement on the ultimate strength and behaviour of masonry columns are presented. A new method of predicting the ultimate load of reinforced blockwork masonry columns subjected to axial compression is proposed. The new method takes into consideration the specialty of blockwork masonry construction.

8.2 GENERAL CONCLUSIONS

The following conclusions have been reached as a result of the experimental and theoretical investigations presented in this thesis:

1. The ultimate compressive strength for unfilled blockwork masonry, f'_m, in areas where high in-plane horizontal forces are expected, should be determined by one of the following two methods:

   (i) On the basis of the compressive strength of a unit block compressed parallel to the unit bed face and the type of mortar, or by using Eqn. 4.1 for the type of blocks used in this investigation.

   (ii) Tests on two-block masonry prisms made from the same materials as those to be used in the actual construction and compressed parallel to the unit bed face.

2. The ultimate compressive strength for filled blockwork masonry, f'_m, in areas where high in-plane horizontal forces are expected, should be determined by one of

the following methods:

(i) Testing a single-block specimen filled with the same concrete as that used in actual construction, in a direction parallel to the unit bed face, then multiplying the specimen's compressive strength by a reduction factor of 0.75 (Eqn. 4.2), which represents the reduction caused by the presence of the mortar joint.

(ii) Testing two-block masonry prisms built from the same materials as those to be used in the actual construction and compressed parallel to the unit bed face.

3. The presence of the mortar joint in unfilled prisms, compressed parallel to the unit bed face, caused a small reduction in the prism compressive strength compared to unfilled prisms with dental plaster joint. Increasing the mortar strength by at least 166.9% produces an increase of only 6.2% on the compressive strength of unfilled prisms. This was mainly due to the insignificant ratio of the mortar joint thickness to the block height (1/39), and also due to confinement of the mortar by the stiff blocks.

4. Most of the unfilled prisms with a mortar joint, compressed parallel to the unit bed face, failed at a compressive strength higher than the mortar cube strength. This suggests that the mortar strength in a joint is apparently higher than the mortar cube strength. This is due to the relatively small mortar thickness compared to the unit height, and the confinement of the mortar by the stiff concrete blocks.

5. The presence of concrete infill significantly reduced the compressive strength of all the two-block prisms with mortar or with dental plaster joint, compressed parallel to the unit bed face, as compared to unfilled prisms. The best compressive strength result was achieved when the deformational characteristics of the concrete infill matched those of the concrete block.

A stiff concrete infill works as a cleavage forcing the blocks to split before attaining their unfilled block compressive strength. The extent of reduction in strength of all prisms filled with stiff concrete infill is similar to the ones filled with soft concrete infill.

6. The presence of the mortar joint in the filled prisms, compressed parallel to the unit bed face, caused a reduction by a factor of 0.75 in the prism strength as compared to the ones with dental plaster joint. This reduction resulted from the high Poisson's ratio of the mortar near ultimate load, compared to that of the concrete blocks. This was responsible for introducing confinement stresses in the mortar and producing splitting stresses in the blocks.

Increasing the mortar strength by at least 166.9% produces an increase of only 23.9% and 3.8% on the compressive strength of prisms with low and high strength concretes respectively. This was due to the insignificant ratio of mortar joint thickness to height of the block (1/39) and mortar confinement by the stiff blocks.

7. The strength of two-block prisms, compressed parallel to the unit bed face, with a value of h/t = 4.0, are surprisingly, higher than the corresponding single-

block specimens with a value of h/t = 2.0.

8. In the finite element analysis of any masonry element subjected to compressive stress, steel bearing plates should be used to apply the stress to the element. Otherwise excessive high deformation and unacceptable high tensile and shear stresses will results at the location of the applied stress.

9. The finite element analysis shows that the effect of the machine platens is limited to areas near these platens. Thus, using unfilled and filled two-block prisms as a standard specimen to determine f'_m in areas where high in-plane forces are expected is acceptable.

10. Despite the 59.7% increase in the vertical deformation of the unfilled prism from the non-linear analysis, compared to the linear analysis, the increase of 11.2% in the maximum tensile stress in the X-direction and the decrease of 13.5% in shear stress is small compared to the high increase in deformation. This reflects the importance of the materials' non-linearity in the analysis of blockwork masonry assemblage.

11. The ultimate compressive strength for unfilled blockwork masonry, f'_m, in situations where in-plane horizontal forces are not expected to occur, can be determined by one of the following two methods:

    (i) On the basis of the compressive strength of a unit block compressed normal to the unit bed face and the type of mortar, or by using Eqn. 5.4 for the type of blocks used in this investigation.

    (ii) Tests on 3-course high full-block stack-bonded

masonry prisms made from the same materials as those to be used in the actual construction and compressed normal to the unit bed face.

12. The ultimate compressive strength for filled blockwork masonry, f'_m, in situations where in-plane horizontal forces are not expected to occur, can be determined by testing 3-course high full-block stack-bonded masonry prisms, built from the same materials as those used in the actual construction and compressed normal to the unit bed face, or by using Eqn. 5.4 for the type of blocks used in this investigation.

13. Testing unfilled and filled half-block prisms to determine f'_m, in situations where in-plane horizontal forces are not expected to occur, over estimates the actual compressive strength of the blockwork masonry assemblage by 25%. This is due to the difference in values of aspect ratio, as between the full-block prism, (l/t = 2.05), and half-block prism, (l/t = 1.0), and also due to the difference in the mortar bedded area caused by the presence of the mid-web in full-block prism.

14. The presence of a low strength (1:1:6) mortar in the joints of unfilled full-block prisms compressed normal to the unit bed face caused a reduction of 10.2% in the prism strength compared to unfilled prisms with a dental plaster joint. Changing the mortar strength by 188.8% increases the prism strength by 20.1%.

15. The presence of concrete infill significantly reduced the compressive strength of 3-course high prisms with mortar joints or with dental plaster joints. With only one exception, the best compressive strength results were achieved when the deformational characteristics

of the concrete infill matched those of the concrete block. This was achieved by using concrete infill with a cube compressive strength of 45% to 50% higher than that of the concrete block.

16. In filled prisms compressed normal to the unit bed face, the presence of the mortar joints, even though of low strength, are essential to develop the block strength. Their presence, however, caused a further reduction in the prism strength in addition to that caused by the presence of the concrete infill. This reduction resulted from the high plasticity and Poisson's ratio of the mortar, compared to that of the concrete blocks. This was responsible for introducing confinement stresses in the mortar and splitting stresses in the blocks.

17. In filled 3-course high full-block prisms of similar concrete strength, the presence of a low strength (1:1:6) mortar joint, contributed greatly to the strength of the filled prisms. Increasing the mortar strength by 98.2% above this value increased the prism strength by a negligible amount.

18. Empirical formulae (Eqns 5.4 and 5.5) were suggested to determine f'_m, for unfilled and filled, full and half-block prisms taking into account the block, mortar and concrete infill strength. The formulae showed that the strength of the concrete infill is not fully reflected in the strength of prisms compressed normal to the unit bed face.

19. The results of the horizontal deformation from the specific analysis and parametric study FEA, for unfilled and filled **3FBP-MJ** prisms shows incompatibility in the horizontal deformation in the

X- and Z-directions. Due to this incompatibility, the prism end shells will be separated from the rest of the prism and longitudinal cracks will be developed at the line of contact between the end and side prism shells.

20. The distribution of vertical, horizontal, shear and principal stresses resulting from the specific and parametric study non-linear FEA for unfilled and filled **3FBP-MJ** prisms showed that the effect of the steel platens was limited to areas near the platens only. Thus, using the 3-course high prism as a standard specimen to determine f'_m is acceptable.

21. In considering the equilibrium of horizontal stresses at the middle block of the unfilled 3-course high prisms, constructed with high strength (1:0.25:3) mortar, it is better to assume a triangular stress distribution with maximum at the mortar joints and zero at 1/3 of the block height. In the case of the filled prisms, assume the horizontal stresses to be uniformly distributed at the middle block, irrespective of what type of mortar or concrete is used in their construction.

22. A new hypothesis is presented on page 278 for the failure of filled 3-course high prisms, compressed normal to the unit bed face, as a result of the specific non-linear FEA.

23. The strength of the full and half-block prisms, compressed normal to the unit bed face, decreased as the h/t ratio increased from 2.0 to 6.0. This is true for both unfilled and filled prisms. The compressive strength of unfilled and filled, full-block prisms decreased by 29.7% and 9.5% respectively as the h/t

ratio increased from 2.0 to 6.0. The results show that f'_m for unfilled or filled blockwork masonry, in situations where the in-plane horizontal forces are not expected to occur, can be satisfactorily represented by testing an unfilled or filled, 3-course high, full-block prism as a standard specimen.

24. Increasing the mortar thickness from 5 to 20 mm, reduced the strength of both unfilled and filled full-block prisms. This reduction was less for filled, full-block prisms (11.6%) than for unfilled full-block prisms (17.6%).

25. Plastic cracking caused by shrinkage are not a serious problem in concrete filled blockwork masonry. The cracks were usually located near the surface of the prism. Water evaporation from the top surface of specimens was the main reason for these cracks. Fresh concrete surfaces should therefore be covered after casting to reduce shrinkage caused by water evaporation. The crack penetration depth and width increased as the concrete infill slump increased. Prisms filled with high slump concrete infill mixes resulted in unfilled voids caused by the presence of air bubbles and also by the evaporation of the excess water left over after the concrete hardened. Using low slump mixes was also found to be impractical due to the amount of work needed in the compaction process.

26. Breaking the bond completely between blocks and concrete infill in a 3-course high full-block prism, as if there were cracks between the two materials, was found to have no effect on the ultimate compressive strength of blockwork masonry, f'_m.

27. The finite element analysis provided an explanation as

to how differences in aspect ratio (l/t) and mortar bedded area between the full and half-block prisms, compressed normal to the unit bed face, affects the compressive strength and behaviour of unfilled and filled prisms.

Unfilled and filled, full-block prisms, with an aspect ratio of l/t = 2.05 and fully bedded with mortar, suffer incompatibility of deformation between the X- and Z-directions. This will result in the separation of the prism end shells from the rest of the prism and the development of longitudinal cracks at the line of contact between the prism end and side shells.

28. Using FEA, it is possible to create a clear image of how the deformations and stresses in a solid 3-course high prism are distributed. It is also possible to predict the mode of failure and ultimate compressive strength of the prism compared to a filled 3-course high prism. The results show that most of the horizontal tensile stresses in the Z-direction in a solid-block prism are located in the vicinity of the mortar joints. This is not exactly the case for the filled **3FBP-MJ** prisms, where the tensile stresses cover most of the prism height. The predicted mode of failure for the solid **3SBP-MJ** prisms is by separation of the prism end faces from the rest of the prism and the development of tensile splitting cracks along the prism end faces caused by the incompatibility of deformation and high horizontal tensile stresses on this face. The longitudinal cracks, caused by the high horizontal tensile stresses on the prism end faces, will be initiated in the vicinity of the mortar joints, then progress through the solid blocks. The ultimate compressive strength of the solid **3SBP-MJ**

prism, made of the same material as the hollow blocks, should be higher than that for the filled **3FBP-MJ** prisms.

29. Using FEA, it was possible to conduct a parametric study to investigate the effect of changing the aspect ratio (l/t) on the distributions and values of deformation and stress in a solid 3-course high prism.

Changing the aspect ratio from 1.0 to 4.0 resulted in increasing the prism's deformation in the X-direction by 221.4%. This means that prisms with aspect ratios more than 1.0 have a greater incompatibility of deformation between the X- and Z-directions. This in turn, has a weakening effect on the prism compressive strength by causing the separation of the prism end faces from the rest of the prism and the development of longitudinal cracks at the lines of contact between the prisms end and side faces.

Increasing the aspect ratio from 1.0 to 4.0 resulted in an increase in the maximum values of the direct vertical stress and the major principal stress in the block material by 11.2% and 13.7% respectively. It also resulted in an increase in the difference between the horizontal tensile stresses in the block material in X- and Z-directions. The results show that, for prisms with an l/t = 1.0, there is no difference in the horizontal tensile stresses between the X- and Z-directions, but for prisms with an l/t = 4.0, the tensile stresses in the Z-direction are 100% higher than that in the X-direction. The difference in the tensile stresses is even higher, at 116.3%, when determined by comparing the maximum values of the minor principal stresses on the prism end faces (MST2)

with the side faces (MST1).

30. Based on the results of the FEA, the decrease in prisms strength with increases in the aspect ratio (l/t) were calculated as a reduction factor to the strength of solid **3SBP-MJ** prism with an aspect ratio of 1.0.

31. The presence of lateral ties changes the mode of failure of blockwork masonry columns (**CS1FB** and **CS1HB**) from a sudden explosive failure to a more ductile failure. Columns reinforced with 10 mm ϕ lateral ties show premature splitting of the block side shells and crushing of the concrete cores which may be caused by a high concentration of tensile splitting stresses around the large diameter lateral ties near the block mid-webs.

32. The mode of failure of columns, reinforced with both vertical and lateral ties (**CS3FB**, **CS3HB**, **CS4FB** and **CS4HB**), is dominated by localized block shell crushing and outward deformation at one or two blocks but not throughout the full column height. This was due to the restriction of buckling of the vertical bars to lengths between the lateral ties. The concrete cores remained intact despite the block shells crushing and deforming outward. The failure was more ductile with no complete collapse at ultimate load. Block shell cracking was observed at 80% to 90% of the ultimate load.

33. A semi-empirical formula (Eqns 7.8 and 7.9) has been suggested to determine the short term static modulus of elasticity of unfilled and filled blockwork masonry.

34. All series of columns, reinforced with hot rolled deformed high yield 8 mm ϕ lateral ties, gave more consistent results for the strain values and for the experimental values of ultimate load compared to columns reinforced with 6 and 10 mm ϕ lateral ties.

35. The strength of filled, full and half-block columns (based on gross area) decreased by 12.9% and 33.5% respectively compared to the unfilled columns (based on net area). The explanation is similar to that used for the reduction in the compressive strength of the 3-course high, full and half-block prisms, namely the presence of the concrete infill.

36. The strength of columns, reinforced with 6 and 8 mm ϕ lateral ties and without vertical bars (**CS1FB**), increased by 17.7% and 17.6% compared to the filled unreinforced columns. On the other hand, columns reinforced with 10 mm ϕ lateral ties failed at loads which were 8.3% less than those for filled unreinforced columns. The increase in column strength results from the confinement of the concrete infill by the lateral ties. These confinement stresses cause a reduction in the harmful tensile stresses exerted on the block shells by the concrete and are not a result of an increase in the concrete strength. The decrease in the strength of columns, reinforced with 10 mm ϕ lateral ties, may be caused by premature failure of the column due to the high concentration of tensile splitting stresses around the large diameter lateral ties.

On the other hand, the results of the half-block columns (**CS1HB**) show increases in strength of 1.7%, 4.4% and 20.5%, with provision of lateral ties of diameter, 6, 8 and 10 mm ϕ respectively. This tendency

of increase in strength is similar to that in reinforced concrete columns.

37. Although, the general trend for the full and half-block columns, reinforced with different percentages of vertical reinforcement and without lateral ties (**CS2FB** and **CS2HB**), is to show an increase in the experimental value of ultimate load of the columns, compared to filled unreinforced columns. The use of such columns in masonry construction should be avoided due to the explosive nature of failure at ultimate load.

38. All the full and half-block columns, reinforced with the same percentage of vertical reinforcement but different diameters of lateral ties (6, 8 and 10 mm ϕ), (**CS3FB**) show an increase in the experimental values of ultimate load of the column, compared to a filled unreinforced column. The most consistent results for increases in column strength is obtained in columns reinforced with 8 mm ϕ lateral ties.

39. All the full and half-block columns, reinforced with 8 mm ϕ lateral ties and different percentages of vertical reinforcement (**CS4FB** and **CS4HB**), show a uniform increase in the values of ultimate load of the column as the percentage of vertical reinforcement increases. This relationship is similar to that for reinforced concrete columns.

40. The British and American Masonry Standards underestimate the ultimate load of reinforced blockwork masonry columns, even for columns reinforced with vertical bars only.

41. A new formula (Eqn. 7.11) has been proposed to

calculate the ultimate load of blockwork masonry columns based on Eqns 5.4 and 5.5 for the ultimate compressive strength of blockwork masonry f'_m, as derived in chapter 5 for 3-course high full and half-block prisms. The contribution of the vertical reinforcement to the ultimate load of blockwork masonry columns is assumed to be based on half the yield strength (f_y) of the vertical bars, since all the strains recorded on the vertical bars during the investigation were half the yield strain of the vertical bars.

42. The explanation for failure of the blockwork masonry columns prior to yielding of the vertical bars may be due to the outward deformation and failure of the block shells caused by relatively small buckling of vertical bars between the lateral ties at ultimate load.

8.3 SUGGESTIONS FOR FURTHER RESEARCH

In this thesis one type of hollow concrete blocks was used in the experimental and theoretical parts of this investigation. More work is needed one other types of concrete block with different dimensions, strengths, shells thickness and core taper to study the effect of all these variables on the compressive strength and behaviour of blockwork masonry prisms and columns.

All types of blockwork masonry prisms tested in this thesis were fully bedded with mortar and a logical extension to this study would be to test prisms with face-shell bedding as this type of block laying is also used in blockwork construction. Since, all prisms tested in this thesis were built under laboratory control work is needed

to study the effect on compressive strength of field construction.

As mentioned earlier in this thesis one of the reasons for testing prisms in a direction parallel to the unit bed face was to simulate the compression zone in reinforced blockwork masonry beams. As the actual stress distribution in the compression zone of a reinforced masonry beam is parabolic, more work is needed to test prisms under eccentric load to determine the enhancement to compressive strength caused by the strain gradient and also to study the behaviour of blockwork masonry prisms under this type of loading.

More work is needed to study the effects of the shape factor (l/t) ratio (block length-to-thickness) and h/t ratio (block height-to-thickness)) on the compressive strength of the unit and prism made of hollow or solid concrete blocks.

As all the blockwork masonry columns tested in this thesis were axially loaded a logical extension to this study would be to test blockwork masonry columns under eccentric load to establish the axial load-moment interaction diagrams for different eccentricities and percentages of vertical reinforcement.

Hollow concrete blocks provide the advantage of using reinforced concrete filled masonry elements without the need for a frame. Columns with different shapes and configuration can be constructed without the need for complicated framework (Fig. 8.1) which is difficult and more expensive to achieve with normal concrete. Tests are needed to study the strength and behaviour of such columns under axial and eccentric loads.

Blockwork masonry columns can be used in masonry construction as a separate structure by themselves or in association with other load bearing elements such as masonry wall. More work is needed to study the effect of Incorporating the columns into walls on increasing wall stiffness and improving their behaviour.

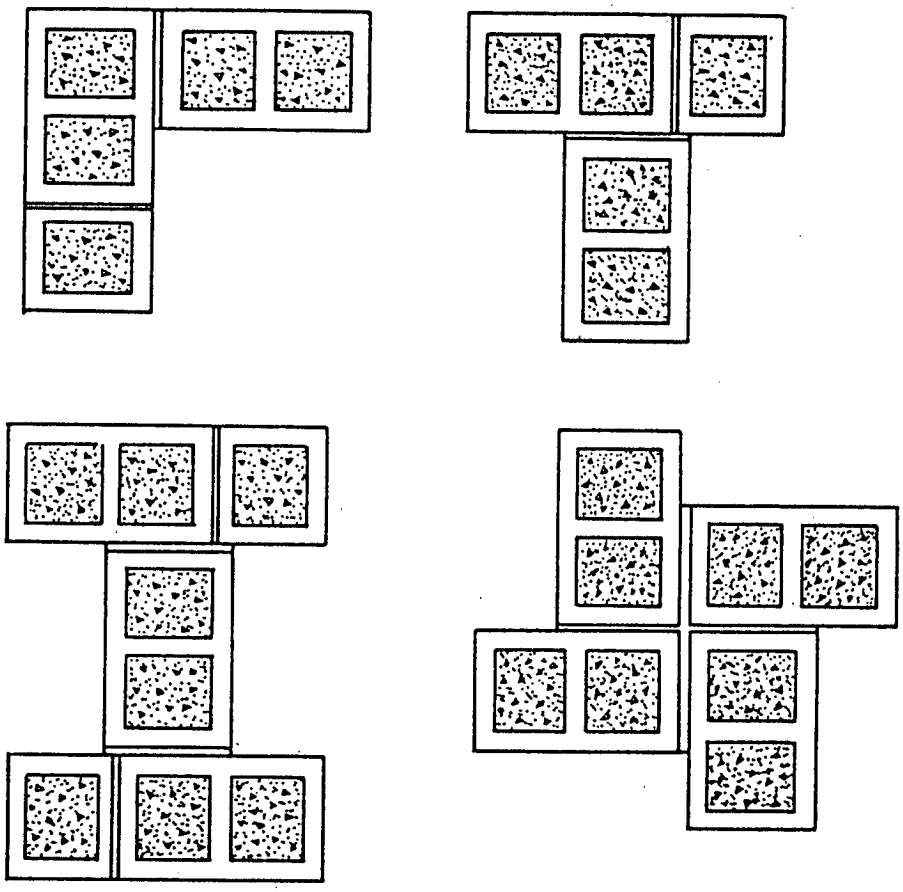

Fig. 8.1 - Methods of constructing blockwork masonry columns with different shapes and configurations.

REFERENCES

1. ROBERTS, J. J., TOVEY, A. K., CRANSTON, W. B. and BEEBY, A. W., "Concrete Masonry Designer's Handbook," Viewpoint Publ., Eyre and Spottiswoode Publ. Ltd., London, 1983, 272 pp.

2. SAHLIN, S., "Structural Masonry," Prentice-Hall Inc., Englewood Cliffs, N. J., 1971, 290 pp.

3. AMRHEIN, J. E., "Reinforced Masonry Engineering Handbook," 3rd Edition, Masonry Institute of America, Los Angeles, 1978, 445 pp.

4. SCHNEIDER, R. R. and DICKEY, W. L., "Reinforced Masonry Design," Prentice-Hall Inc., Englewood Cliffs, N. J., 1980, 619 pp.

5. HASELTINE, B. A. and MOORE, J. F. A., "Handbook to BS 5628: Part 1," Brick Devel. Assoc., Woodside House, Berkshire, 1981, 118 pp.

6. BEALL, C., "Masonry Design and Detailing," Prentice-Hall Inc., London, 1984, 491 pp.

7. ORTON, A., "Structural Design of Masonry," Longman Inc., New York, 1986, 147 pp.

8. ROBERTS, J. J., EDGELL, G. J. and RATHBONE, A. J., "Handbook to BS 5628: Part 2," Viewpoint Publ., Palladian Publ. Ltd., london, 1986, 197 pp.

9. HENDRY, A. W., "Structural Masonry," MacMillan Education Ltd., London, 1990, 284 pp.

10. ROBERTS, J. J., "Concrete Masonry," Cement and Concrete Assoc., London, Publ. No.366 ,1983, 15 pp.

11. ROBERTS, J. J., "Reinforced Concrete Masonry," Cement and Concrete Assoc., London, Publ. No. 410, 1985, 4 pp.

12. ROBERTS, J. J., "Reinforced and Prestressed Masonry," Cement and Concrete Assoc., London, Publ. No. 456, 1986, 8 pp.

13. CRANSTON, W. B. and ROBERTS, J. J., "The Structural Behaviour of Concrete Masonry-Reinforced and Unreinforced," Stru. Eng., Vol. 54, No. 11, 1976, pp. 423-436.

14. TOVEY, A. K. and ROBERTS, J. J., "Interim Design Guide for Reinforced Concrete Blockwork Subject to Lateral

Loading Only," Cement and Concrete Assoc., London, Interim Tech. Note 6, 1980, 44 pp.

15. ROBERTS, J. J., "Further Work on the Behaviour of Reinforced Concrete Blockwork Subject to Lateral Loading," Cement and Concrete Assoc., London, Tech. Report 531, 1980, 43 pp.

16. VEKEY, R. C. and WEST, H. W. H., "The Flexural Strength of Concrete Blockwork," Maga. of Concrete Rese., Vol. 32, No. 113, 1980, pp. 206-218.

17. ROBERTS, J. J., "Further Work on the Behaviour of Reinforced Concrete Blockwork Subject to Lateral Loading," Inter. Jou. of Masonry Const., Vol. 2, No. 1, 1981, pp. 26-38.

18. PLEWES, G. W., "Masonry Bibliography 1900-1977," Inter. Masonry Inst., Washington D. C., 1978, 345 pp.

19. AMERICAN CONCRETE INSTITUTE, "Building Code Requirement for Concrete Masonry Structures," ACI 531R-79, Revised 1981.

20. CANADIAN STANDARDS ASSOCIATION, "Masonry Design and Construction for Buildings," CSA-CAN3-S304, 1978.

21. BRITISH STANDARDS INSTITUTION, "Use of Masonry," BS 5628: Part 1: 1978, Parts 2 and 3: 1985.

22. AUSTRALIAN STANDARD, "SAA Masonry Code," Standards Assoc. of Australia, SAA 3700, 1988.

23. FOSTER, D., "The Potential for Reinforced and Prestressed Brickwork," Presented to Brit. Cera. Soci., Buil. Mate. Section Autumn Meeting, Buxton, November 1982.

24. AMERICAN SOCIETY FOR TESTING AND MATERIALS, "Standard Test Methods for Compressive Strength of Masonry Prisms," ASTM E447-80, 1981.

25. CANADIAN STANDARDS ASSOCIATION, "Method of Test for Compressive Strength of Masonry Prisms," CSA-CAN3-A369.1, 1984.

26. ROBERTS, J. J., "The Effect of Different Test Procedures Upon the Indicated Strength of Concrete Blocks in Compression," Maga. of Concrete Rese., Vol. 25, No. 83, 1973, pp. 87-98.

27. BOULT, B. F., "Concrete Masonry Prism Testing," ACI Jou., Vol. 76, No. 4, 1979, pp. 513-535.

28. DRYSDALE, R. G. and HAMID, A. A., "Behaviour of Concrete Block Masonry Under Axial Compression," ACI Jou., Vol. 76, No. 6, 1979, pp. 707-721.

29. HAMID, A. A. and DRYSDALE, R. G., "Suggested Failure Criteria for Grouted Masonry Under Axial Compression," ACI Jou., Vol. 76, No. 10, 1979, pp. 1047-1061.

30. STURGEON, G. R., LONGWORTH, J. and WARWARUK, J., "An Investigation of Reinforced Concrete Block Masonry Columns," Stru. Eng. Report No.91, Univ. of Alberta, 1980, 355 pp.

31. MAURENBRECHER, A. H. P., "Effect of the Test Procedures on Compressive Strength of Masonry Prisms," Proc. 2nd Canadian Masonry Symp., Ottawa, Canada, 1980, pp. 119-132.

32. CHEEMA, T. S. and KLINGNER, R. E., "Compressive Strength of Concrete Masonry Prisms," ACI Jou., Vol. 83, No. 2, 1986, pp. 88-97.

33. HAMID, A. A. and CHUKWUNENYE A. O., "Compression Behaviour of Concrete Masonry Prisms," Jou. of Stru. Eng., ASCE, Vol. 112, No. 3, 1986, pp. 605-613.

34. KHALAF, F. M., "An Investigation of Flexure in Reinforced Masonry Beams," MSC Thesis, Univ. of Manitoba, Winnipeg, 1981, 262 pp.

35. KHALAF, F. M., "Concrete Blocks Compressed Parallel to the Bed Face: A Theoretical Study," Masonry Inter., Vol. 1, No. 2, 1987, pp. 64-70.

36. KHALAF, F. M., "The Performance of Concrete Blocks Loaded Parallel to the Bed Face," Masonry Inter., Vol. 2, No. 1, 1988, pp. 20-24.

37. NATIONAL CONCRETE MASONRY ASSOCIATION, "Research Investigation of the Properties of Masonry Grout in Concrete Masonry," NCMA Eng. Concrete Masonry Design Committee, NCMA Grout Research Report, 1988, 135 pp.

38. AFSHARI, F. A. and KALDJIAN, M. J., "Finite Element Analysis of Concrete Masonry Prisms," ACI Jou., Vol. 86, No. 5, 1989, pp. 525-530.

39. LYSE, I., "Tests of Reinforced Brick Columns," Jou. Amer. Cera. Soci., Vol. 26, 1933, pp. 584-597.

40. BREBNER, A., "Notes on Reinforced Brickwork," Tech. Pap. 38, Vols 1 and 2, Government of India, 1923.

41. WITHEY, M. O., "Tests on Reinforced Brick Masonry

Columns," Proc. Amer. Soci. Test. Mate., ASTM, Vol. 34, No. 2, 1934, pp. 387-405.

42. DAVEY, N. and THOMAS, F. G., "The Structural Use of Brickwork," Inst. of Civil Eng. Stru. and Buil., Paper No. 24, 1950, pp. 13-66.

43. ANDERSON, D. E. and HOFFMAN, E. S., "Design of Brick Masonry Columns," Inter. Conf. on Masonry Stru. Syst., Univ. of Texas, Austin, 1967, pp. 94-100.

44. BRETTLE, H. J., "Ultimate Strength Design of Reinforced Brickwork Piers in Compression and Biaxial Bending," Civil Eng. Tran. Inst., Eng. Australia, CE 12, (1), No. 49, 1970.

45. ARMSTRONG, A. C. and HENDRY, H. W., "The Compressive Strength of Brickwork with Reinforced Bed Joints," Brit. Cera. Resa. Asso., Tech. Note 209, 1973, 10 pp.

46. OHLER, A. and GOPFERT, N., "The Effect of Lateral Joint Reinforcement on the Strength and Deformation of Brickwork Piers," Proc. 6th IBMAC, Rome, 1982, pp. 677-688.

47. ELTRAIFY, E. A., "Uni-Axial and Bi-Axial Bending of Reinforced Brick Masonry Columns," PhD Thesis, Univ. of Edinburgh, Edinburgh, 1983, 194 pp.

48. EDGELL, G. J. and TEMPLETON, W., "Reinforced Brickwork Columns," Proc. 7th IBMAC, Melbourne, Australia, 1985, pp. 1065-1073.

49. SHANK, J. R. and FOSTER, H. D., "Strength of Concrete Block Pilasters Under Varied Eccentric Loading," Ohio state Univ. Eng. Exper. Station, Bulletin No. 60, 1931.

50. FEEG, C., LONGWORTH, J. and WARWARUK, J., "Effects of Reinforcement Detailing for Concrete Masonry Columns," Stru. Eng. Report No. 76, Civil Eng. Depart., Univ. of Alberta, Edmonton, 1979, 182 pp.

51. SALIM, A. H., "The Effect of Confinement Reinforcement on Load Carrying Capacity of Masonry Prisms," Proc. 2nd Canadian Masonry Symp., Ottawa, Canada, pp. 65-72.

52. AL-SARRAF, S. Z., FAIYADH, F. I. and KHALAF, F. M., "A Study of the Capacity and the Behaviour of Reinforced Short Columns Subjected to Axial Load," Masonry Inter., No. 7, 1986, pp. 3-7.

53. RATHBONE, A. J., "The Behaviour of Reinforced Concrete Blockwork Beams," Cement and Concrete Assoc., Tech.

Report 540, london, 1980, 23 pp.

54. SUTER, G. T. and FENTON, G. A., "Flexural Capacity of Reinforced Masonry Members," ACI Jou., Vol. 83, No. 1, 1986, pp. 127-136.

55. KHALAF, F. M. and HENDRY, A. W., "Effect of Bed-Face Preparation in Compressive Testing of Masonry Units," Proc. 2nd Inter. Masonry Conf., British Masonry Soci., No. 4, 1990, pp. 129-130.

56. NEVILLE, A. M., "Properties of Concrete," 3rd Ed., London, Pitman Books, 1981, 779 pp.

57. BRITISH STANDARDS INSTITUTION, "British Standard Specification for Ordinary and Rapid-Hardening Portland Cement," BS 12: 1978.

58. BRITISH STANDARDS INSTITUTION, "Sampling and Testing of Mineral Aggregates, Sands and Fillers," BS 812: Part 1: 1975.

59. BRITISH STANDARDS INSTITUTION, "Aggregates from Natural Sources for Concrete," BS 882: 1983.

60. BRITISH STANDARDS INSTITUTION, "Testing Concrete: Method for Making Test Cubes from Fresh Concrete," BS 1881: Part 108: 1983.

61. BRITISH STANDARDS INSTITUTION, "Testing Concrete: Method for Making Test Cylinders from Fresh Concrete," BS 1881: Part 110: 1983.

62. AMERICAN SOCIETY FOR TESTING AND MATERIALS, "Standard Methods of Sampling and Testing Grout," ASTM C 1019, 1984.

63. BRITISH STANDARDS INSTITUTION, "Sands for Mortar for Plain and Reinforced Brickwork Blockwalling and Masonry," BS 1200: 1976.

64. BRITISH STANDARDS INSTITUTION, "Specification for Hot Rolled Steel Bars for the Reinforcement of Concrete," BS 4449: 1978.

65. BRITISH STANDARDS INSTITUTION, "Methods for Tensile Testing of Metals," BS 18: Part 2: 1971.

66. BRITISH STANDARDS INSTITUTION, "Precast Concrete Masonry Units," BS 6073: Parts 1 and 2: 1981.

67. BRITISH STANDARDS INSTITUTION, "Testing Concrete: Method for Determination of Tensile Splitting Strength," BS 1881: Part 117: 1983.

68. BRITISH STANDARDS INSTITUTION, "Testing Concrete: Method for Determination of Static Modulus of Elasticity in Compression," BS 1881: Part 121: 1983.

69. BRITISH STANDARDS INSTITUTION, "Structural Use of Concrete: Code of Practice for Special Circumstances," BS 8110: Part 2: 1985.

70. SAENZ, L. P., Discussion of {DESAYI, P. and KRISHNAN, S., "Equation of the Stress - Strain Curve of Concrete," ACI Jou., Vol. 61, 1964, pp. 345-350}, ACI Jou., Vol. 61, 1964, pp. 1229-1235.

71. KHALAF, F. M., "An Investigation into the Capacity and Behaviour of Concrete Block Specimens Loaded Parallel to the Bed Face," Proc. 8th IBMAC, Ireland, 1988, pp. 752-763.

72. KHALAF, F. M., HENDRY, A. W. and FAIRBAIRN D. R., "Compressive Strength of Concrete Block Masonry Prisms Tested Concentrically and Eccentrically Normal and Parallel to the Bed Face," Proc. of the 3rd Inter. Seminar on Struc. Masonry for the Developing Countries, Mauritius, 1990, pp. 123-135.

73. MINITAB, "A General Purpose Data Statistical Analysis system," Minitab Inc., 215 Pond Laboratory, Univ. Park, P. A. 16802, 1985.

74. AMERICAN CONCRETE INSTITUTE, "Building Code Requirements for Reinforced Concrete," ACI 318M-83, 1983.

75. MAHER, A. and DAVID, D., "Mortar Constituent of Concrete in Compression," ACI Jou., Vol. 79, No. 2, 1982, pp. 100-109.

76. HILSDORF, H. K., "Investigation into the Failure Mechanisms of Brick Masonry Loaded in Axial Compression," Designing Eng. and Const. with Masonry Products Ed., JOHNSON, F. B., Houston, Texas, Golf Publ., 1969.

77. HATZINIKOLAS, M., LONGWORTH, J. and WARWARUK, J., "Failure Modes for Eccentrically Loaded Concrete Block Masonry Walls," ACI Jou., Vol. 77, No. 3, 1980, pp. 258-263.

78. THOMAS, F. G., "The Strength of Brickwork," Stru. Eng., Vol. 31, No. 2, 1953, 35 pp.

79. PAGE, A. W., "Finite Element for Masonry," Jou. of Stru. Div., ASCE, Vol. 104, St.8, 1978, pp. 1267-1285.

80. LUSAS, "Finite Element Stress Analysis System," Finite Element Analysis Ltd., Forge House, Kigston Upon Thames, Surrey, 1989.

81. BEECH, D. G., EVERILL, J. B., and WEST, H. W. H., "Effect of Size of Packing Material on Brick Crushing Strength," Proc. Brit. Cera. Soci., No. 21, 1973, pp. 1-6.

82. MORGAN, T. W., "Effect of Specimen Size and Packing Material on Brick Compressive Strength," Jou. of Australian Cera. Soci., Vol. 10, No. 3, 1974.

83. PAGE, A. W. and SHRIVE, N. G., " A Critical Assessment of Compression Tests for Hollow Block Masonry," Masonry Inter., Vol. 2, No. 2, 1988, pp. 64-70.

84. NOLAND, J. L., HANADA, K. T. and FENG, C. C., "The Effect of Slenderness and End Conditions on the Strength of Clay Unit Prisms," Proc. 1st North Amer. Masonry Conf., Boulder, Colorado, 1978.

85. SCRIVENER, J. C. and BAKER, L. R., "Factors Influencing Grouted Masonry Prism Compressive Strength," Proc. 8th IBMAC, Ireland, 1988, pp. 874-883.

86. HATZINIKOLAS, M., LONGWORTH, J. and WARWARUK, J., "Concrete Masonry Walls," Stru. Eng. Report No. 70, Civil Engineering Department, University of Alberta, 1978, 274 pp.

87. HANSEN, T. C., "Creep of Concrete," Swedish Ceme. and Conc. Rese. Inst., Bulletin 33, 1985, pp. 24-33.

88. PFISTER, J. F., "Influence of Ties on the Behaviour of Reinforced Concrete Columns," ACI Jou., Vol. 61, No. 5, 1964, pp. 521-536.

APPENDIX A

Table A.1

Designation of block specimens.

Specimen designation	Specimen description
2BP-MJ	Unfilled and filled 2-Block Prism with Mortar Joint compressed parallel to the unit bed face.
2BP-DPJ	Unfilled and filled 2-Block Prism with Dental Plaster Joint compressed parallel to the unit bed face.
2FBP-MJ	Unfilled and filled 2-course high Full-Block Prism with Mortar Joint compressed normal to the unit bed face.
3FBP-MJ	Unfilled and filled 3-course high Full-Block Prism with Mortar Joints compressed normal to the unit bed face.
6FBP-MJ	Unfilled and filled 6-course high Full-Block Prism with Mortar Joints compressed normal to the unit bed face.
3FBP-DPJ	Unfilled and filled 3-course high Full-Block Prism with Dental Plaster Joints compressed normal to the unit bed face.
3FBP-PJ	Unfilled and filled 3-course high Full-Block Prism with Polystyrene Joints compressed normal to the unit bed face.
2HBP-MJ	Unfilled and filled 2-course high Half-Block Prism with Mortar Joint compressed normal to the unit bed face.
3HBP-MJ	Unfilled and filled 3-course high Half-Block Prism with Mortar Joints compressed normal to the unit bed face.
6HBP-MJ	Unfilled and filled 6-course high Half-Block Prism with Mortar Joints compressed normal to the unit bed face.
3HBP-DPJ	Unfilled and filled 3-course high Half-Block Prism with Dental Plaster Joints compressed normal to the unit bed face.

3HBP-PJ Unfilled and filled 3-course high Half-Block Prism with Polystyrene Joints compressed normal to the unit bed face.

3SBP-MJ 3-course high Solid-Block Prism with Mortar Joints compressed normal to the unit bed face.

CS1FB Column Series 1 Full-Block. Columns with three different diameters of lateral ties (6, 8, 10 mm ϕ), and without vertical reinforcement to study the effect of lateral tie confinement on the strength and behaviour of masonry columns.

CS2FB Column Series 2 Full-Block. Columns reinforced with different percentages of vertical reinforcement (full-block: 0.42%, 1.7%, 3.4% and half-block: 0.56%, 1.8%, 3.5%), and without lateral ties, to study the effect of the absence of lateral ties on the strength and behaviour of masonry columns.

CS3FB Column Series 3 Full-Block. Columns reinforced with the same percentage of vertical reinforcement (full-block: 1.7%, 5.3% and half-block: 0.18%, 5.4%), and with different diameters of lateral ties (6, 8, 10 mm ϕ) to choose the best lateral tie to be used in blockwork masonry columns.

CS4FB Column Series 4 Full-Block. Columns with 8 mm ϕ lateral ties and different percentage of vertical reinforcement (full-block: 0.42%, 1.7%, 3.4%, 5.3%, and half-block: 0.56%, 1.3%, 1.8%, 3.5%, 5.4%) to study the effect of changing the percentage of vertical reinforcement on the strength and behaviour of masonry columns.

CS1HB Column Series 1 Half-Block. Columns with three different diameters of lateral ties (6, 8, 10 mm ϕ), and without vertical reinforcement to study the effect of lateral tie confinement on the strength and behaviour of masonry columns.

CS2HB Column Series 2 Half-Block. Columns reinforced with different percentages of vertical reinforcement (full-block: 0.42%, 1.7%, 3.4% and half-block: 0.56%, 1.8%, 3.5%), and without lateral ties, to study the effect of the absence of lateral ties on the strength and behaviour of masonry columns.

CS3HB Column Series 3 Half-Block. Columns reinforced with the same percentage of vertical reinforcement (full-block: 1.7%, 5.3% and half-block: 1.8%, 5.4%), and with different diameters of lateral ties (6, 8, 10 mm ϕ) to choose the best lateral tie to be used in blockwork masonry columns.

CS4HB Column Series 4 Half-Block. Columns with 8 mm ϕ lateral ties and different percentage of vertical reinforcement (full-block: 0.42%, 1.7%, 3.4%, 5.3%, and half-block: 0.56%, 1.3%, 1.8%, 3.5%, 5.4%) to study the effect of changing the percentage of vertical reinforcement on the strength and behaviour of masonry columns.

CS1, 2, 3, 4FB0, 6, 8, 10: Columns Series 1, 2, 3, 4 Full-Block with 0 (no lateral ties), 6, 8, and 10 mm ϕ lateral ties.

CS1, 2, 3, 4HB0 , 6, 8, 10: Columns Series 1, 2, 3, 4 Half-Block with 0 (no lateral ties), 6, 8 and 10 mm ϕ lateral ties.

APPENDIX B

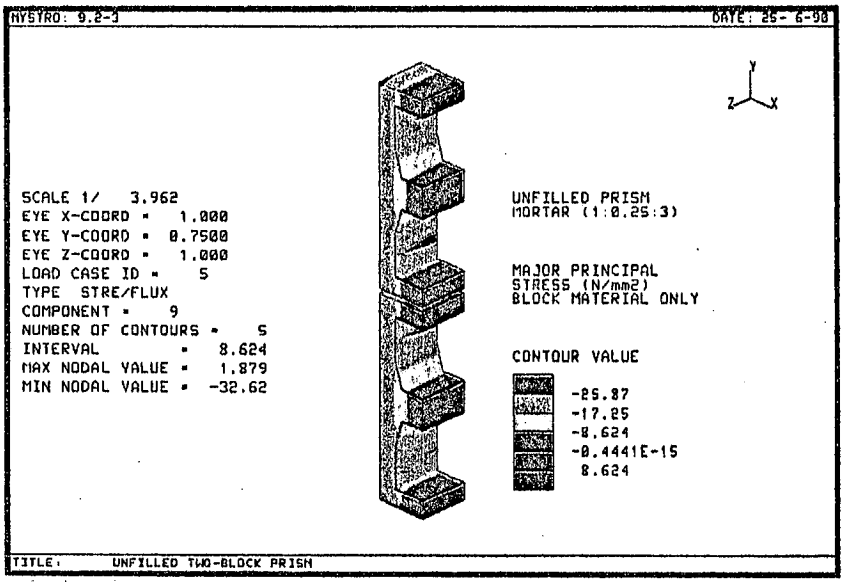

Fig. B.1 - Major principal stress, block material of unfilled 2BP-MJ prism, specific non-linear FEA.

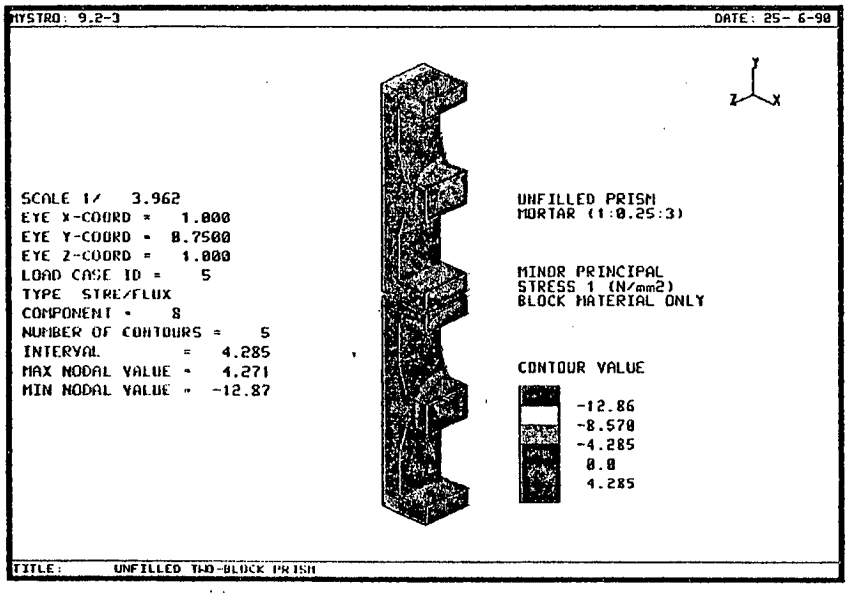

Fig. B.2 - Minor principal stress 1, block material of unfilled 2BP-MJ prism, specific non-linear FEA.

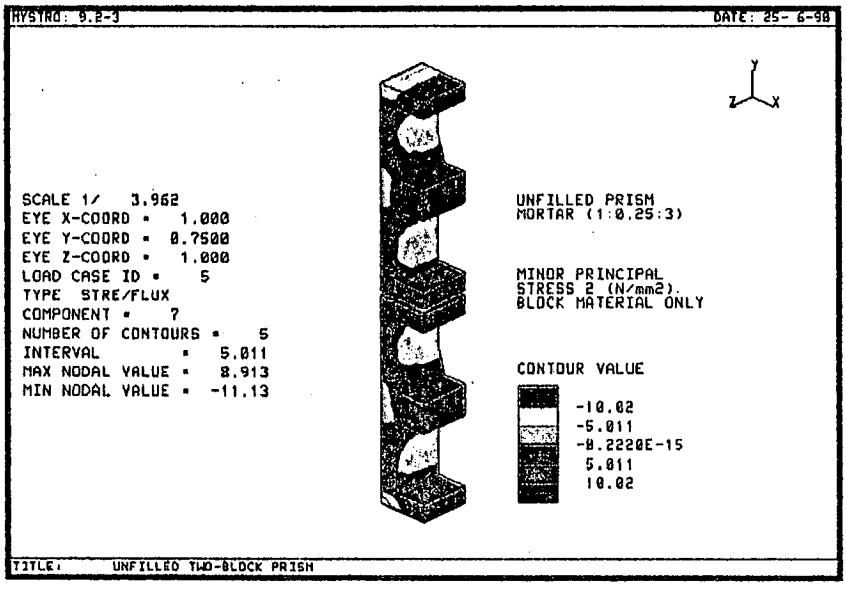

Fig. B.3 - Minor principal stress 2, block material of unfilled 2BP-MJ prism, specific non-linear FEA.

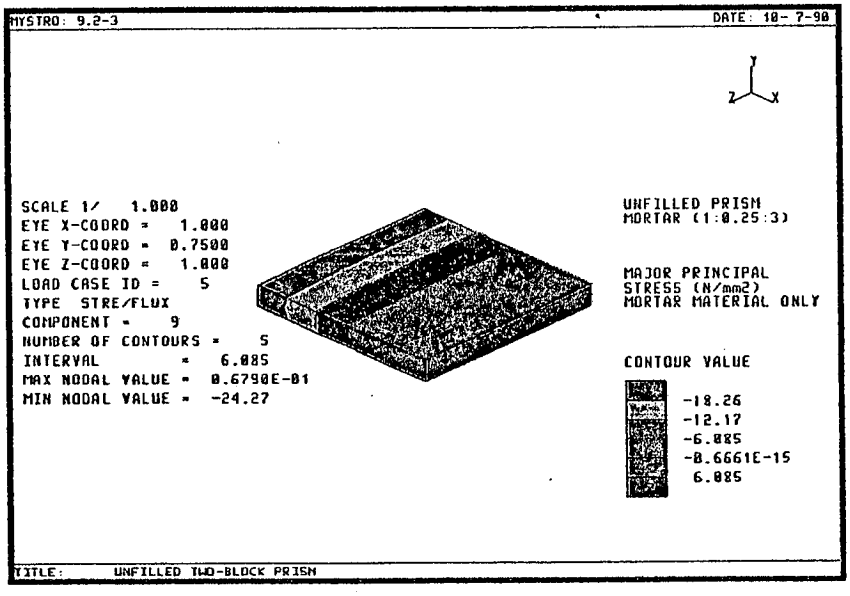

Fig. B.4 - Major principal stress, mortar material of unfilled 2BP-MJ prism, specific non-linear FEA.

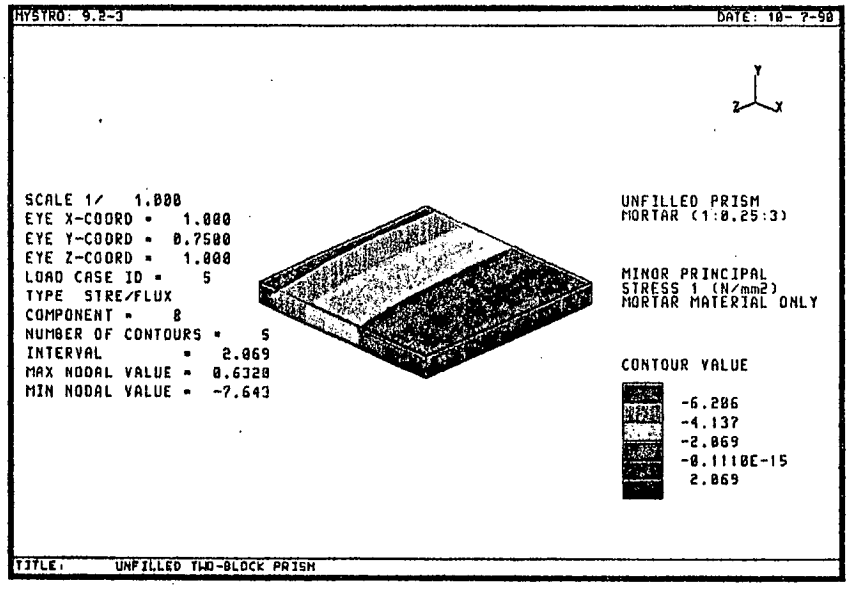

Fig. B.5 - Minor principal stress 1, mortar material of unfilled 2BP-MJ prism, specific non-linear FEA.

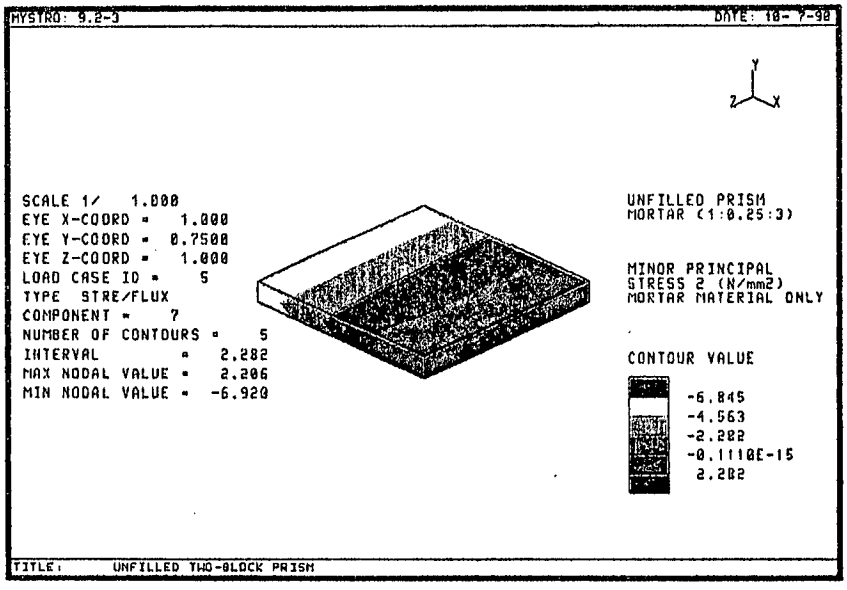

Fig. B.6 - Minor principal stress 2, mortar material of unfilled 2BP-MJ prism, specific non-linear FEA.

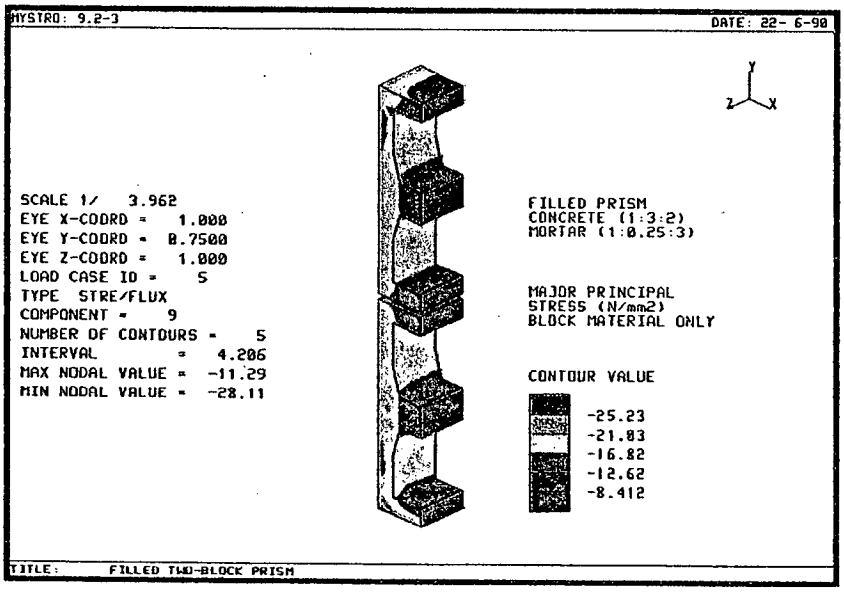

Fig. B.7 - Major principal stress, block material of filled 2BP-MJ prism, specific non-linear FEA.

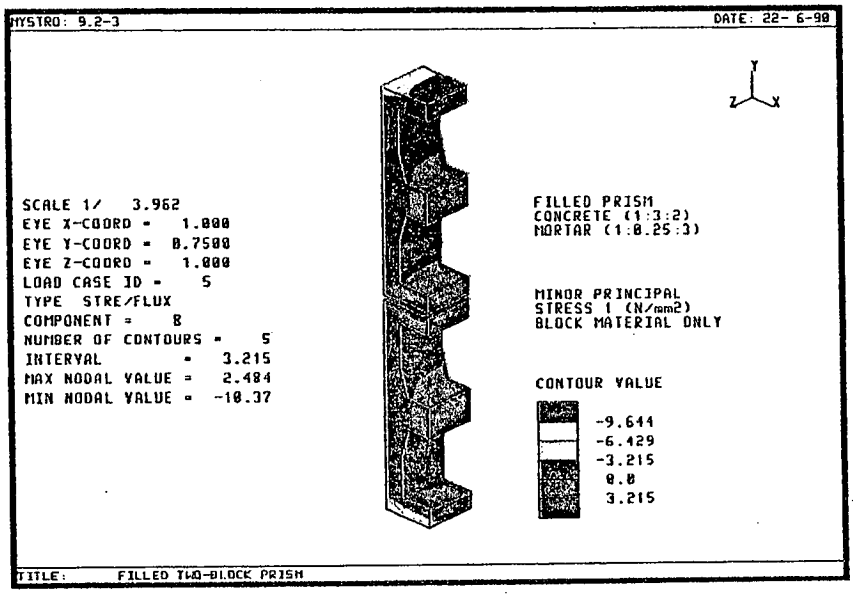

Fig. B.8 - Minor principal stress 1, block material of filled 2BP-MJ prism, specific non-linear FEA.

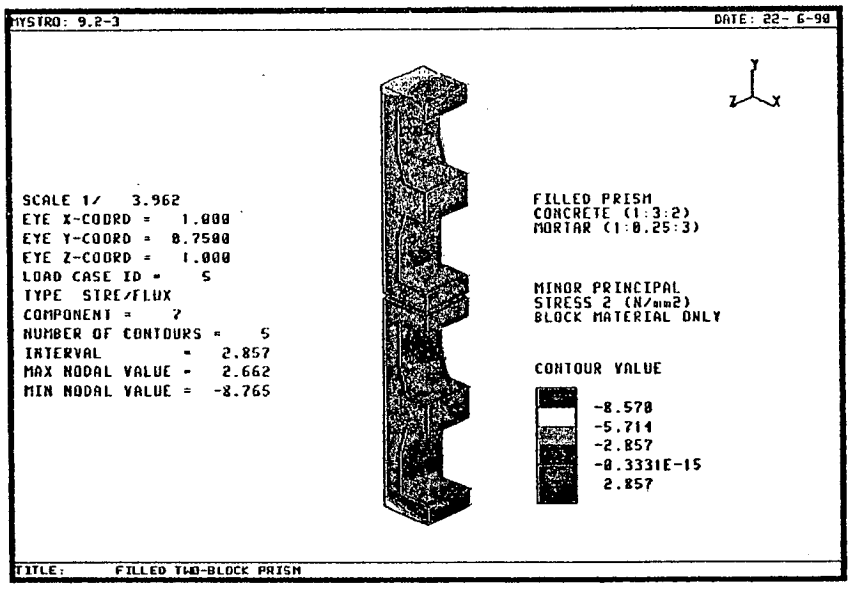

Fig. B.9 - Minor principal stress 2, block material of filled 2BP-MJ prism, specific non-linear FEA.

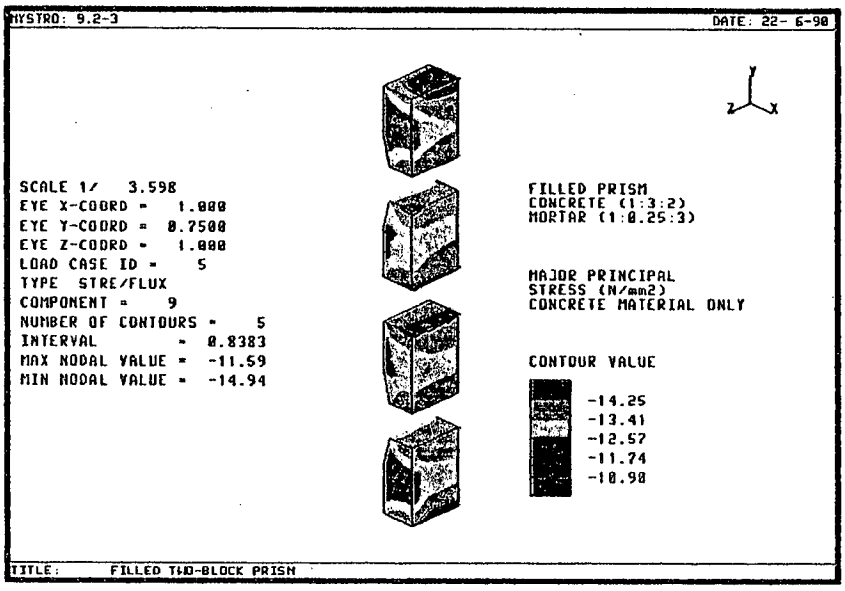

Fig. B.10 - Major principal stress, concrete material of filled 2BP-MJ prism, specific non-linear FEA.

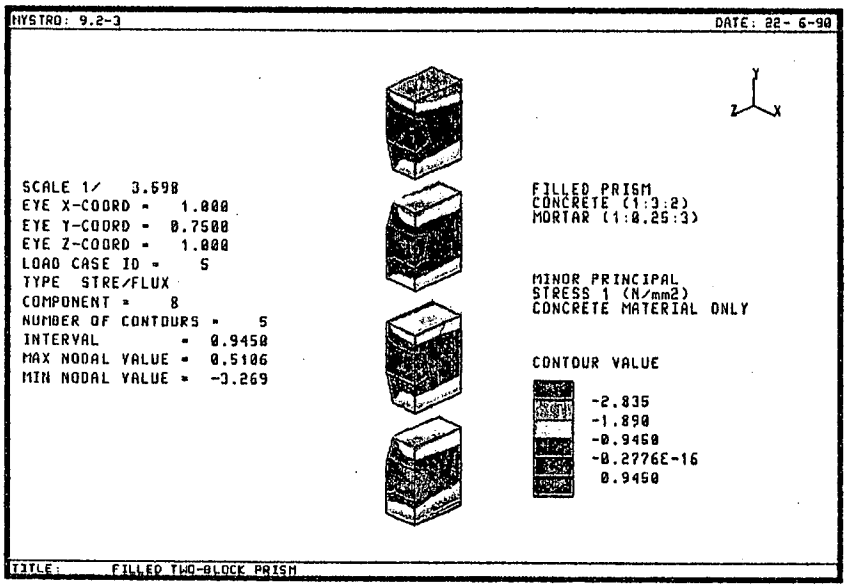

Fig. B.11 - Minor principal stress 1, concrete material of filled 2BP-MJ prism, specific non-linear FEA.

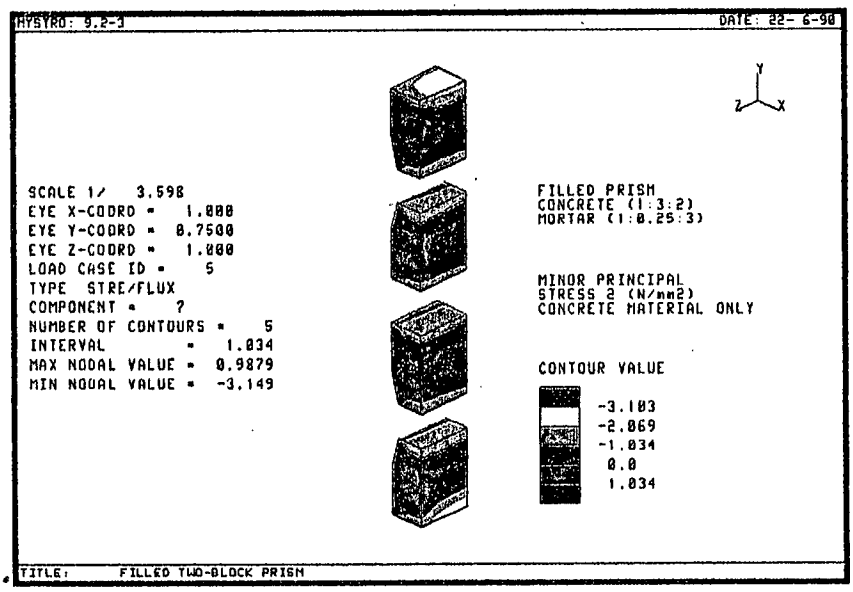

Fig. B.12 - Minor principal stress 2, concrete material of filled 2BP-MJ prism, specific non-linear FEA.

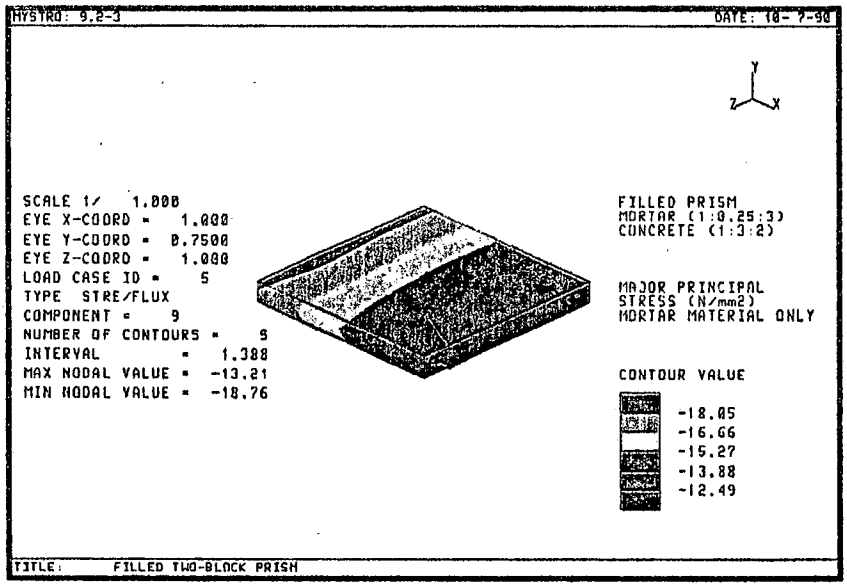

Fig. B.13 - Major principal stress, mortar material of filled 2BP-MJ prism, specific non-linear FEA.

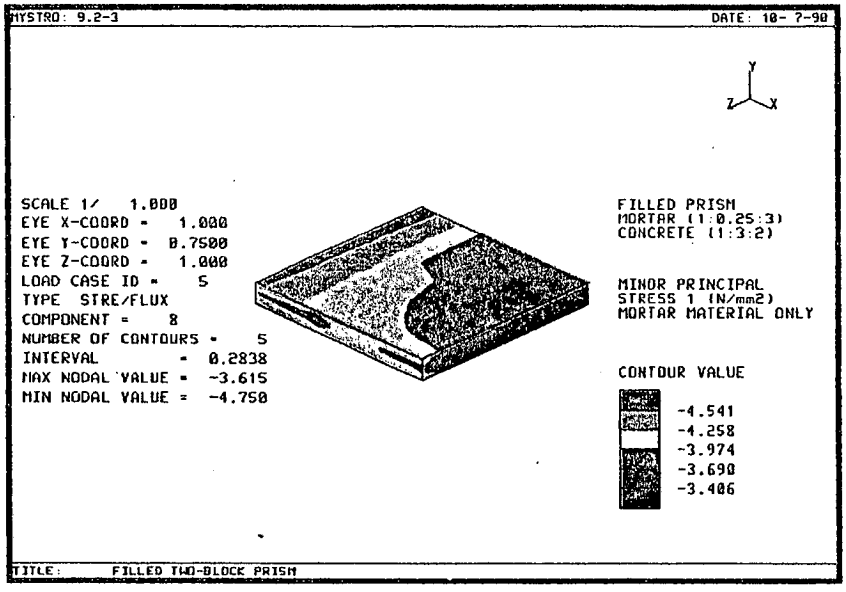

Fig. B.14 - Minor principal stress 1, mortar material of filled 2BP-MJ prism, specific non-linear FEA.

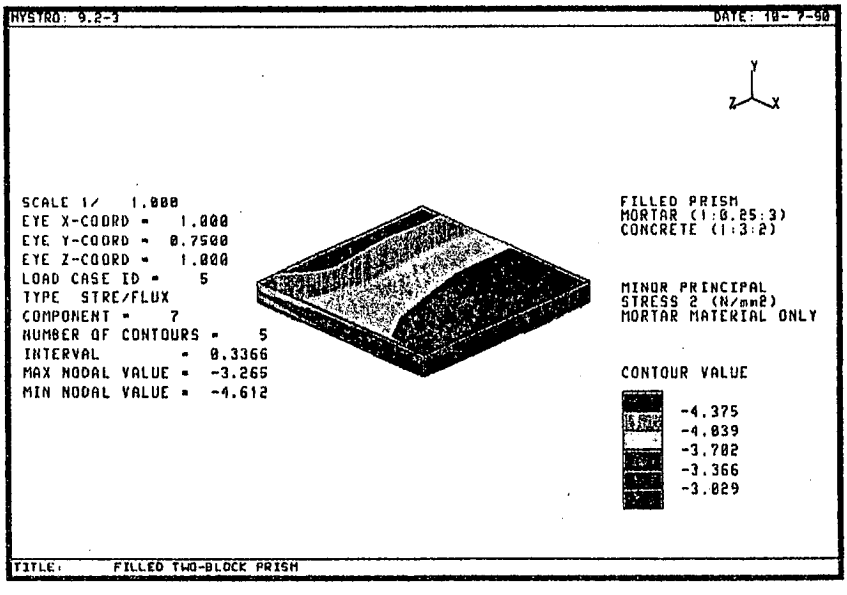

Fig. B.15 - Minor principal stress 2, mortar material of filled 2BP-MJ prism, specific non-linear FEA.

APPENDIX C

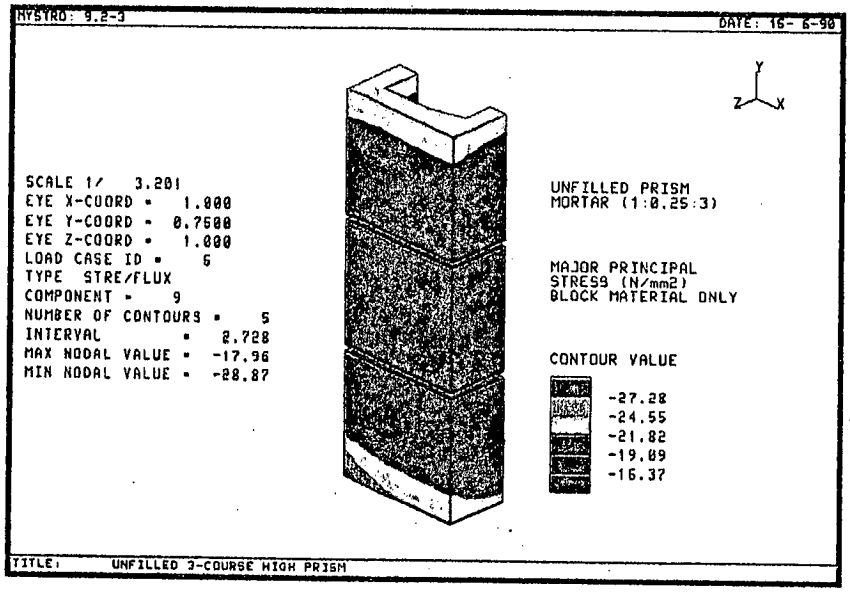

Fig. C.1 - Major principal stress, block material of unfilled 3FBP-MJ prism, specific non-linear FEA.

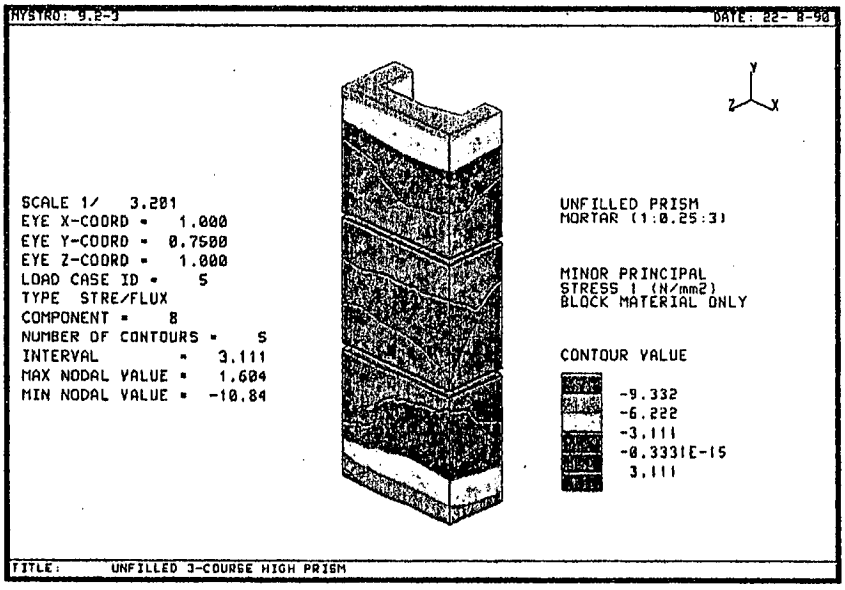

Fig. C.2 - Minor principal stress 1, block material of unfilled 3FBP-MJ prism, specific non-linear FEA.

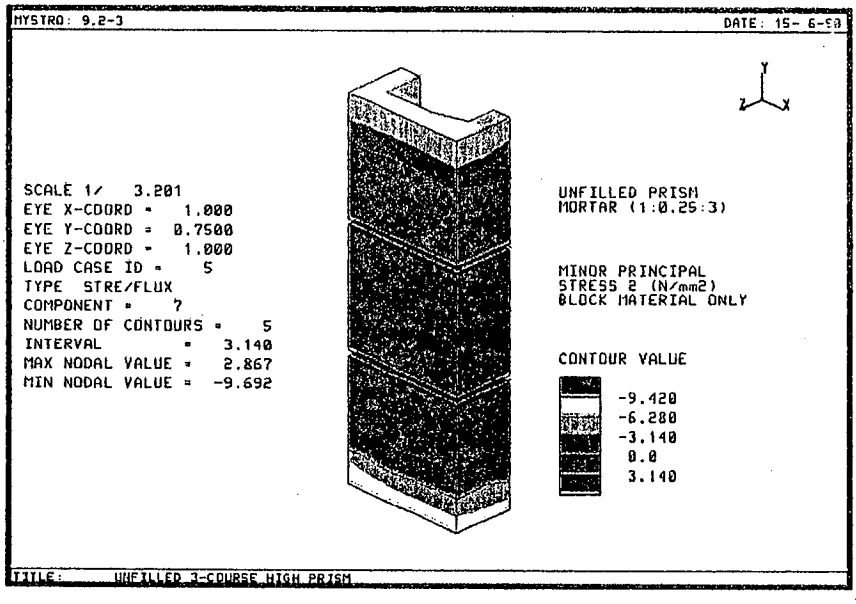

Fig. C.3 - Minor principal stress 2, block material of unfilled 3FBP-MJ prism, specific non-linear FEA.

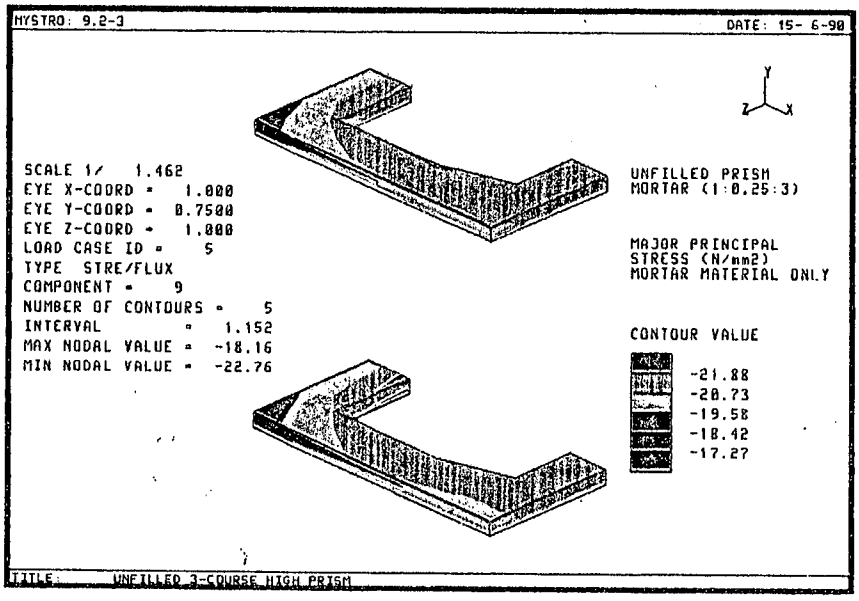

Fig. C.4 - Major principal stress, mortar material of unfilled 3FBP-MJ prism, specific non-linear FEA.

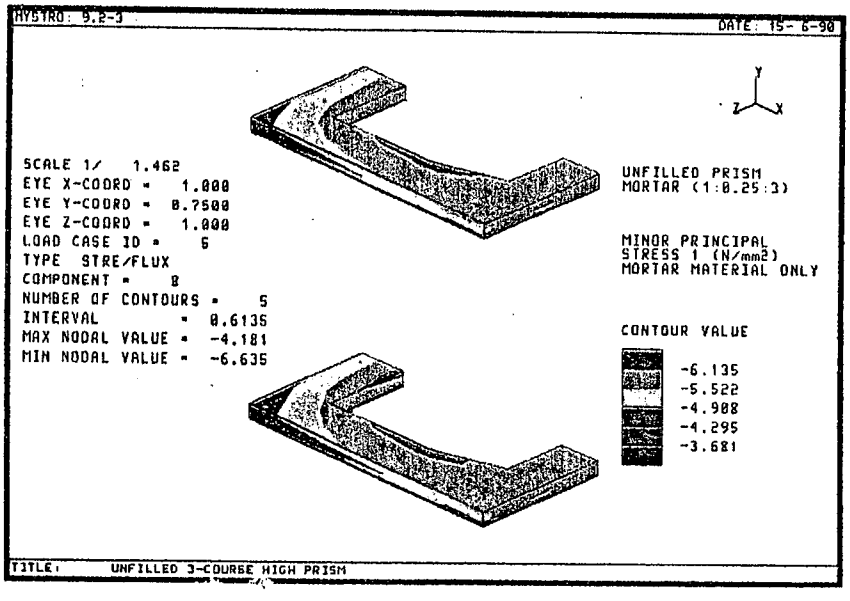

Fig. C.5 - Minor principal stress 1, mortar material of unfilled 3FBP-MJ prism, specific non-linear FEA.

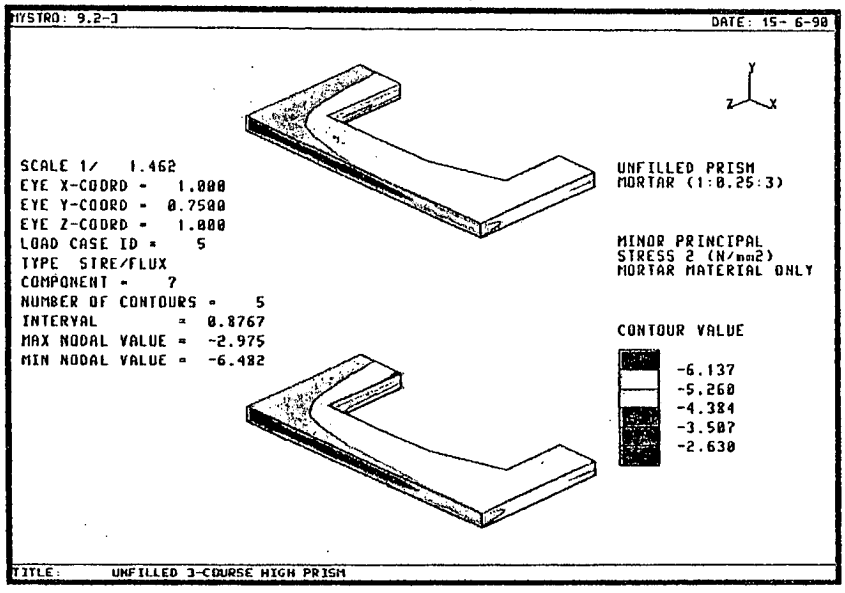

Fig. C.6 - Minor principal stress 2, mortar material of unfilled 3FBP-MJ prism, specific non-linear FEA.

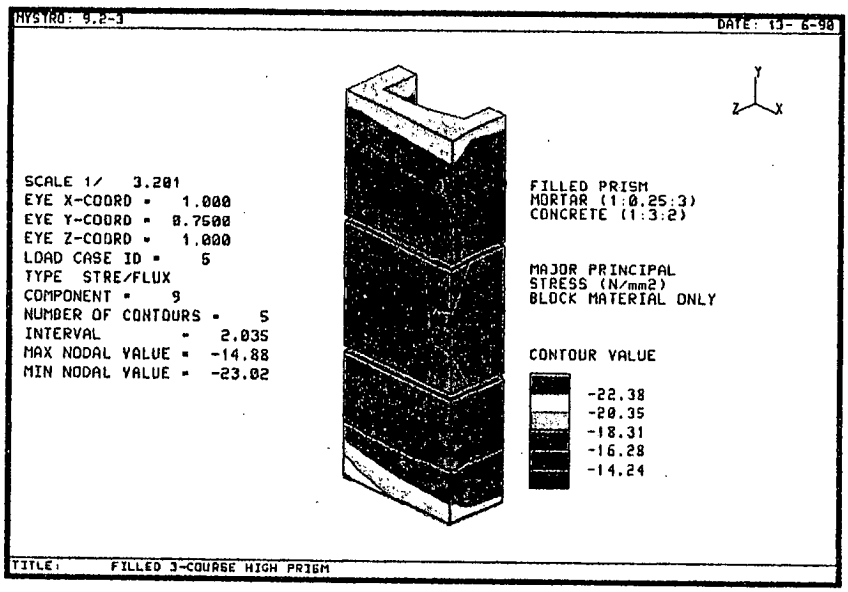

Fig. C.7 - Major principal stress, block material of filled 3FBP-MJ prism, specific non-linear FEA.

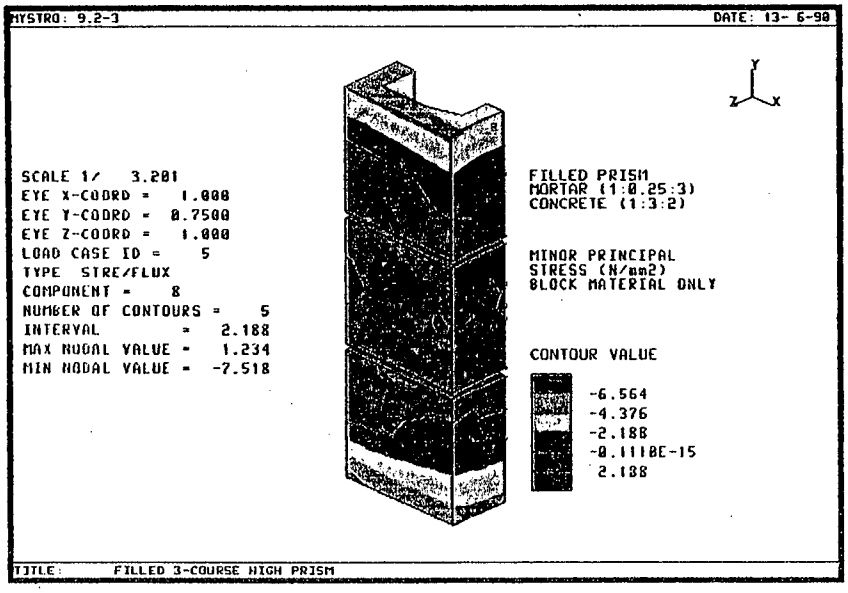

Fig. C.8 - Minor principal stress 1, block material of filled 3FBP-MJ prism, specific non-linear FEA.

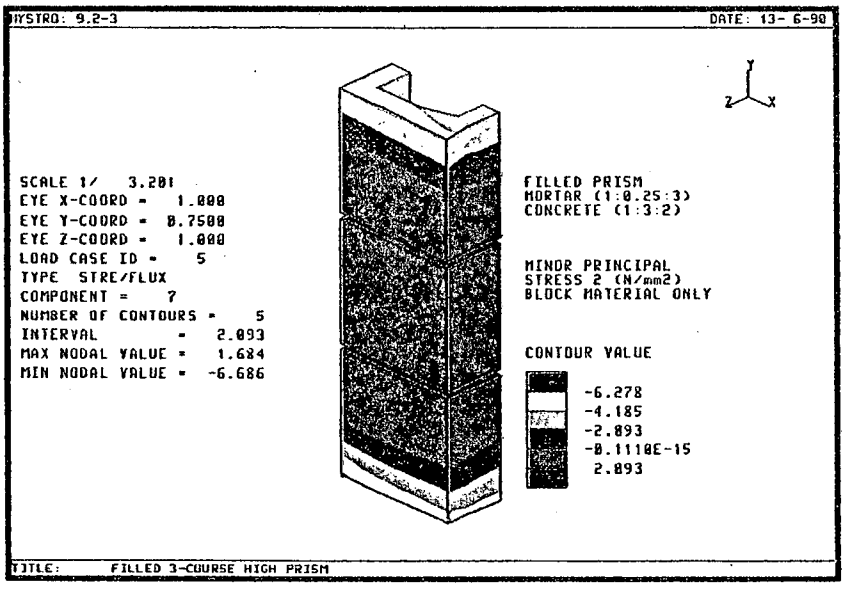

Fig. C.9 - Minor principal stress 2, block material of filled 3FBP-MJ prism, specific non-linear FEA.

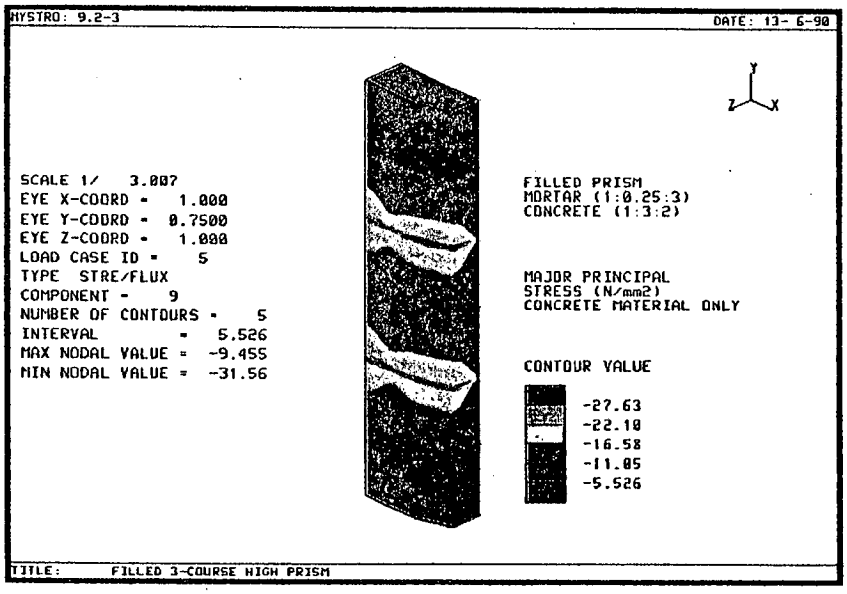

Fig. C.10 - Major principal stress, concrete material of filled 3FBP-MJ prism, specific non-linear FEA.

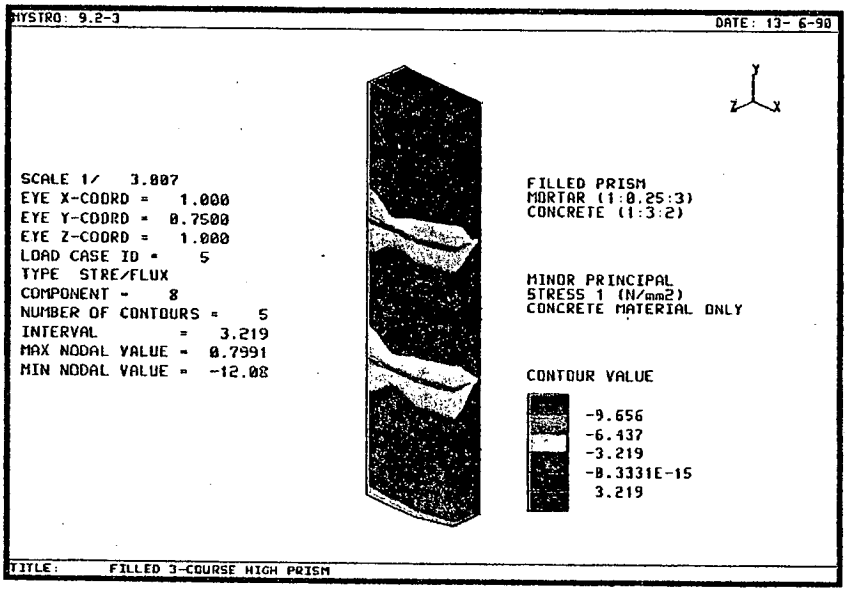

Fig. C.11 - Minor principal stress 1, concrete material of filled 3FBP-MJ prism, specific non-linear FEA.

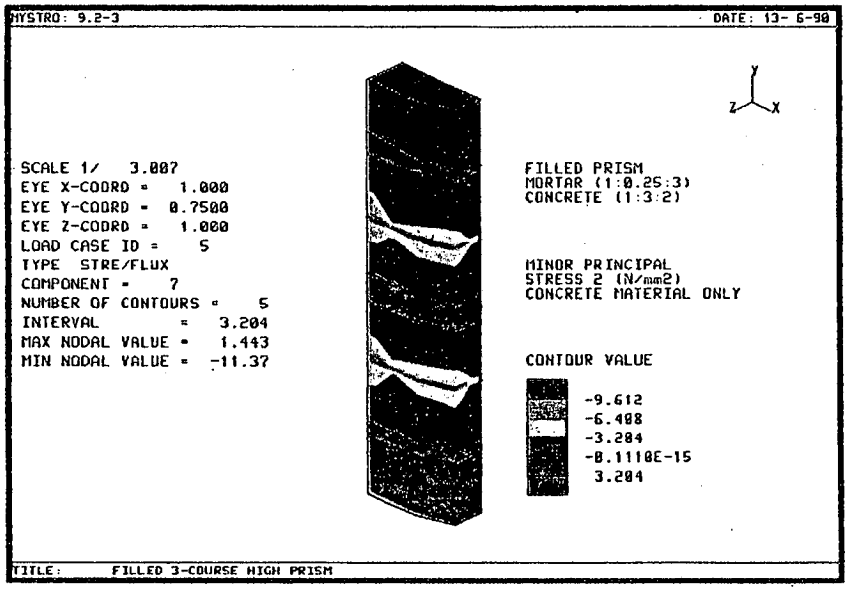

Fig. C.12 - Minor principal stress 2, concrete material of filled 3FBP-MJ prism, specific non-linear FEA.

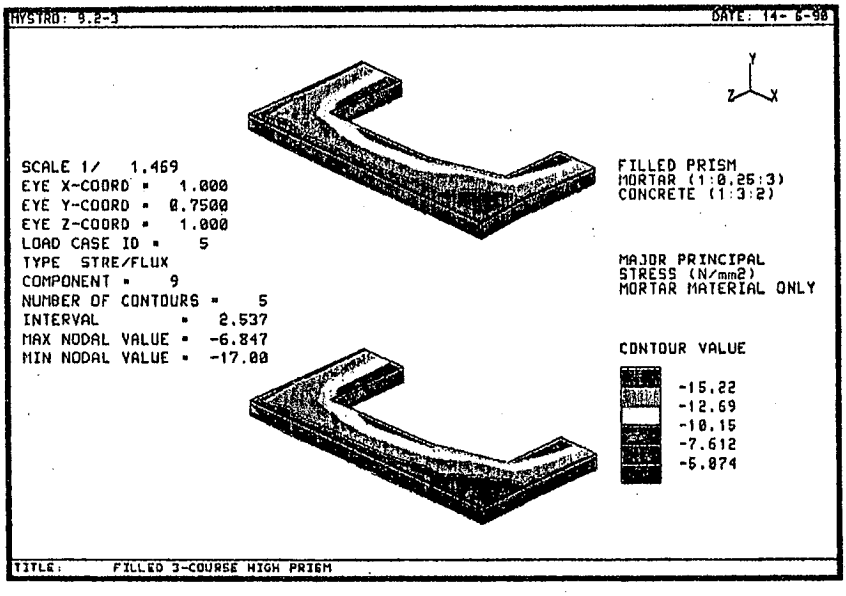

Fig. C.13 - Major principal stress, mortar material of filled 3FBP-MJ prism, specific non-linear FEA.

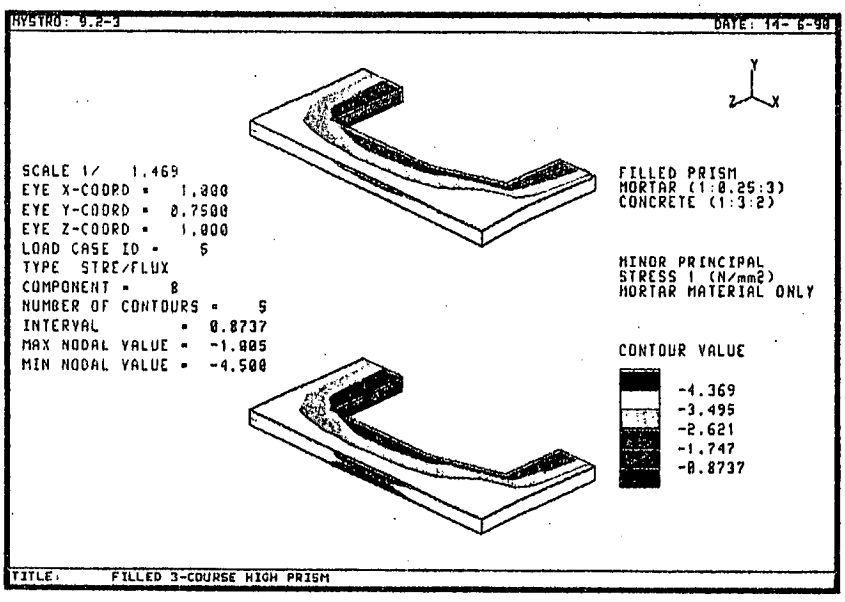

Fig. C.14 - Minor principal stress 1, mortar material of filled 3FBP-MJ prism, specific non-linear FEA.

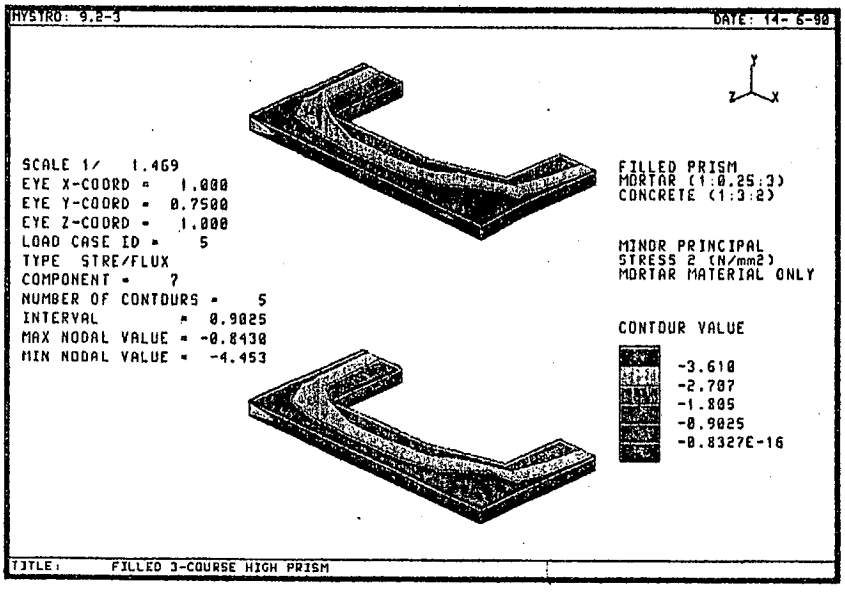

Fig. C.15 - Minor principal stress 2, mortar material of filled 3FBP-MJ prism, specific non-linear FEA.

APPENDIX D

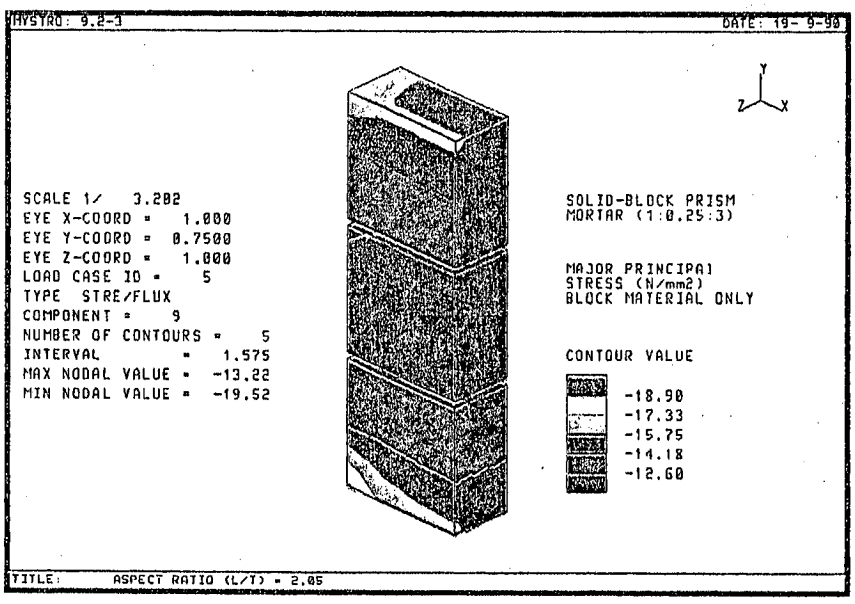

Fig. D.1 - Major principal stress, block material of solid 3SBP-MJ prism, parametric study non-linear FEA.

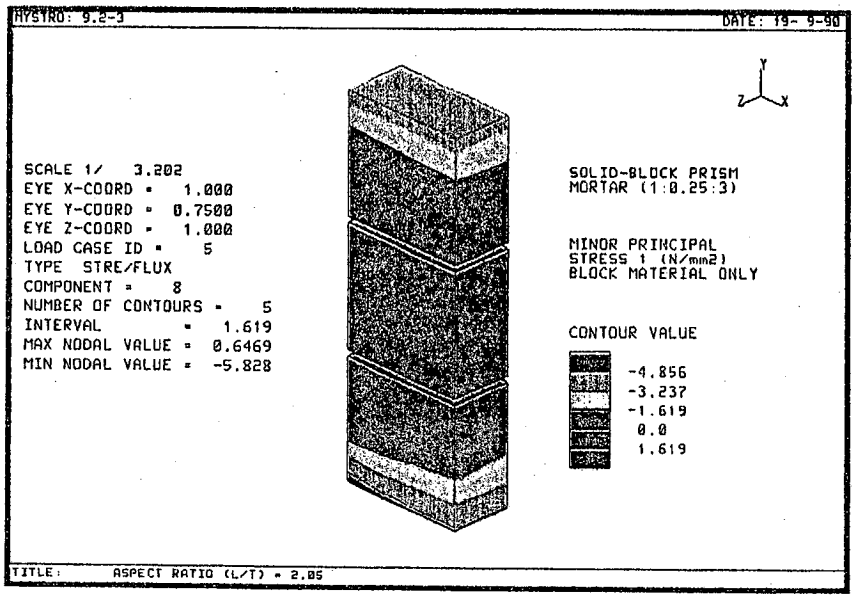

Fig. D.2 - Minor principal stress 1, block material of solid 3SBP-MJ prism, parametric study non-linear FEA.

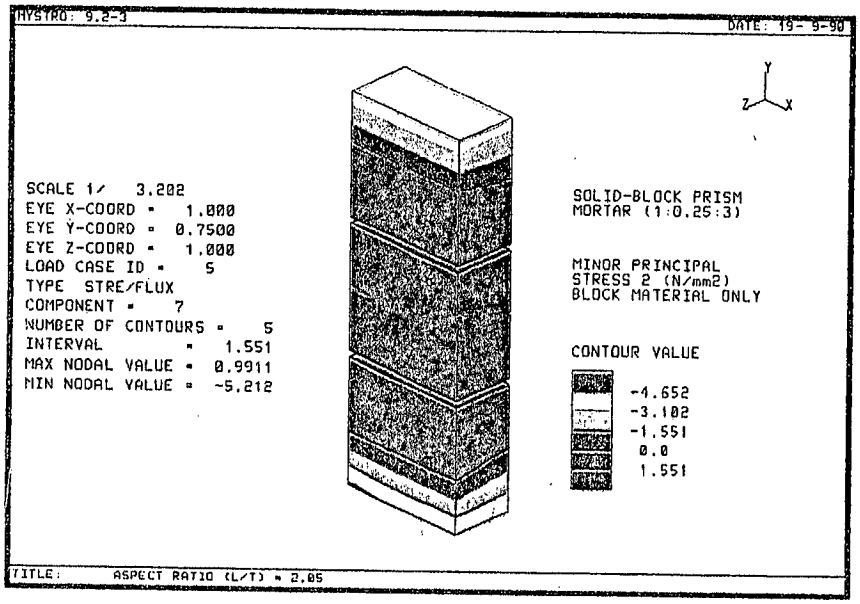

Fig. D.3 - Minor principal stress 2, block material of soiled 3SBP-MJ prism, parametric study non-linear FEA.

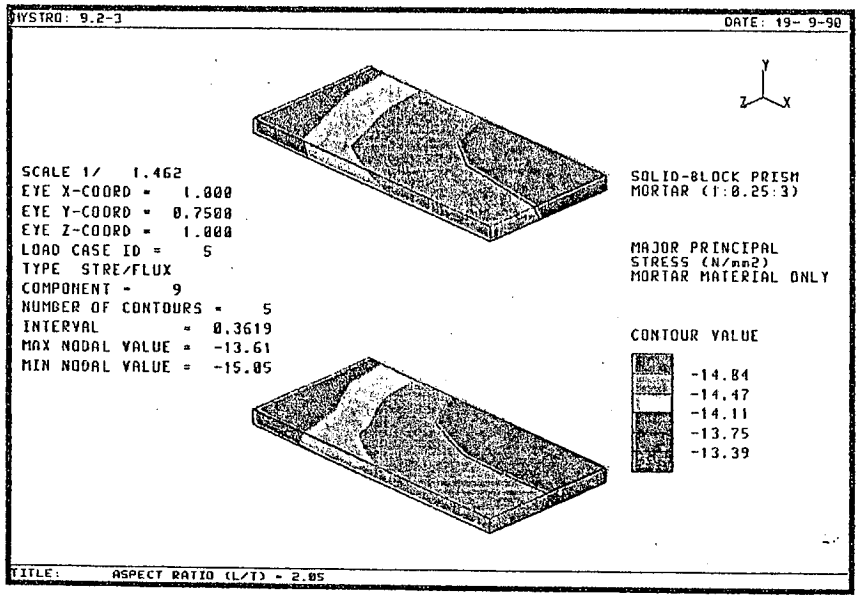

Fig. D.4 - Major principal stress, mortar material of solid 3SBP-MJ prism, parametric study non-linear FEA.

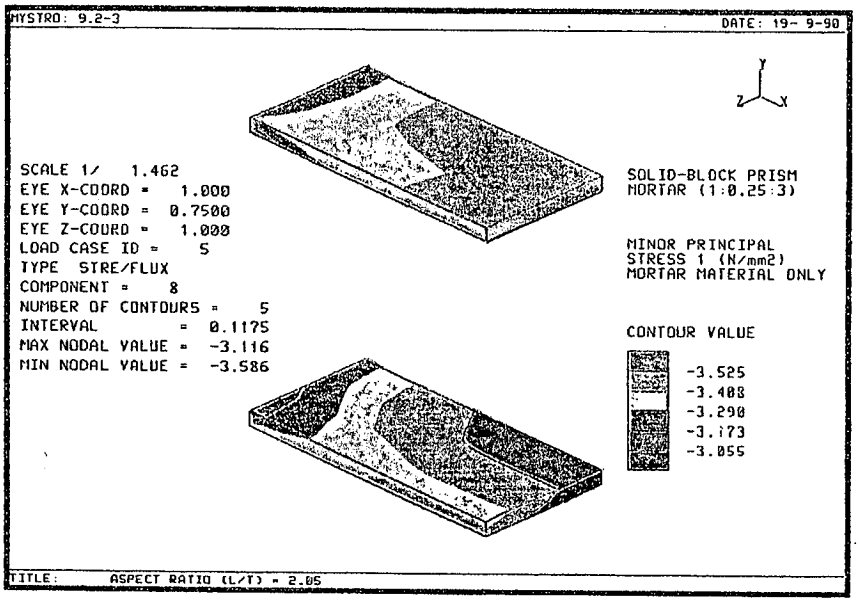

Fig. D.5 - Minor principal stress 1, mortar material of solid 3SBP-MJ prism, parametric study non-linear FEA.

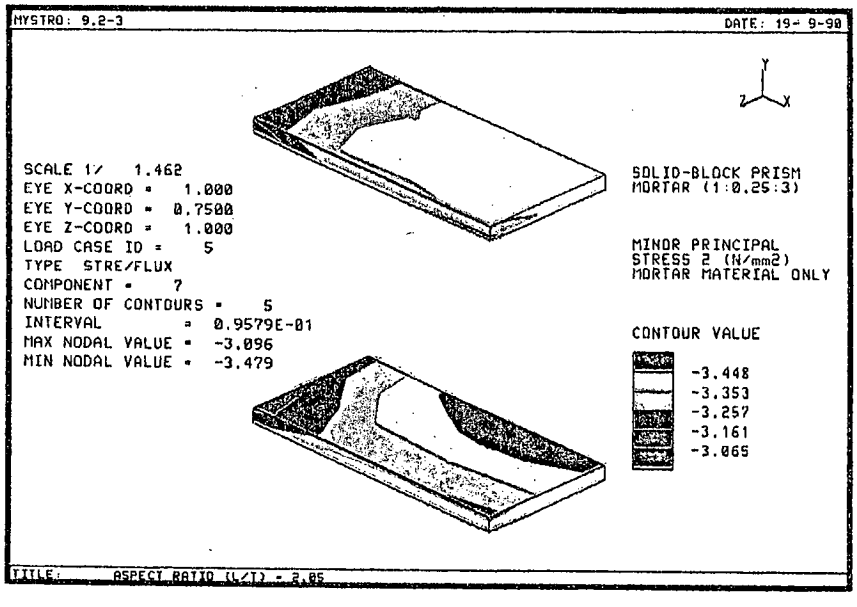

Fig. D.6 - Minor principal stress 2, mortar material of solid 3SBP-MJ prism, parametric study non-linear FEA.